TECHNICAL TRANSACTIONS

CZASOPISMO TECHNICZNE

MECHANICS

MECHANIKA

ISSUE 2-M (3)

ZESZYT 2-M (3)

YEAR 2016 (113)

ROK 2016 (113)

WYDAWNICTWO POLITECHNIKI KRAKOWSKIEJ

TECHNICAL TRANSACTIONS | CZASOPISMO TECHNICZNE

MECHANICS | MECHANIKA

ISSUE 2-M (3) | ZESZYT 2-M (3)
YEAR 2016 (113) | ROK 2016 (113)

Basic version of each Technical Transactions magazine is its online version
Pierwotną wersją każdego zeszytu Czasopisma Technicznego jest jego wersja online
www.ejournals.eu/Czasopismo-Techniczne www.technicaltransactions.com www.czasopismotechniczne.pl

Editorial Board Mechanics

2-M/2016

TECHNICAL TRANSACTIONS | CZASOPISMO TECHNICZNE
MECHANICS | MECHANIKA
2-M/2016

KATARZYNA ADAMOWICZ*, PIOTR SARNA**, WIESŁAW SZATKO

SAFETY IN SUBSEA PETROLEUM PRODUCTION SYSTEMS: SUBSEA CHRISTMAS TREE CASE STUDY

BEZPIECZEŃSTWO W SYSTEMACH DO PODWODNEJ EKSPLOATACJI ZŁÓŻ ROPY NAFTOWEJ NA PRZYKŁADZIE GŁOWICY EKSPLOATACYJNEJ

Abstract

The paper presents an analysis of valves used for closing and opening production tubing, located on the production line. The main safety valves analysed in this work are located in the Christmas Tree and in the Downhole Safety Valve. The analysis was conducted using FMEA; it found that for each basic Christmas Tree's gate valve, the most dangerous failure modes are external leaks and "fail to close" in the open position of the valves. For the Downhole Safety Valve, the most dangerous fault can occur in the open position of the valve. The Downhole Safety Valve and the Christmas Tree complement each other, thus ensuring safety during oil and gas production.

Keywords: safety in subsea petroleum production systems, Christmas Tree's safety valves

Streszczenie

W artykule przedstawiono analizę zaworów przewodu wydobywczego, umiejscowionych w głowicy eksploatacyjnej oraz zawór wgłębny bezpieczeństwa. Analizę przeprowadzono metodą FMEA; stwierdzono, że dla każdego podstawowego zaworu zasuwowego głowicy eksploatacyjnej najgroźniejsze są wycieki zewnętrzne, a także uszkodzenie w pozycji otwartej. Podobnie dla zaworu wgłębnego bezpieczeństwa. Zawór wgłębny bezpieczeństwa i podstawowe zawory zasuwowe uzupełniają się nawzajem gwarantując bezpieczeństwo.

Słowa kluczowe: systemy bezpieczeństwa przy wydobywaniu ropy i gazu, zawory bezpieczeństwa w głowicy eksploatacyjnej

DOI:

* Eng. Katarzyna Adamowicz, DSc. Eng. Wiesław Szatko, Institue of Thermal and Process Engineering, Faculty of Mechanical Engineering, Cracow University of Technology.
** MSc. Eng. Piotr Sarna, Head Energy Cracow, Poland.

1. Introduction

Demand for oil and gas continues to grow, but ground-based hydrocarbon deposits begin to slowly deplete. Therefore, there is expected increase in performed offshore drillings and underwater installations in the coming years. Many wells located in shallow waters are already heavily exploited, so the search for hydrocarbons begins to move into deeper regions of the sea. Today, there are more than 9,000 offshore platforms operating worldwide, serving more than 10,000 wells, and their number will continue to grow [2].

The subsea mining industry puts a strong emphasis on the reliability of equipment. Equipment used in water are typically 5 times more expensive than equipment used for oil and gas extraction on land because all the situations of intervention or repair are associated with high costs. Breakdowns at sea can have additional devastating effects on the environment. An example is the 2010 explosion at the American platform rig Deepwater Horizon in the Gulf of Mexico, which was the cause of the largest oil spill in the world. It is assumed that 780 000 m^3 of oil leaked into the Gulf and the contaminated area consisted of 6,500 to 176,000km^2. Many factors are consisted during safe production of oil and gas from the seabed, but the most important components in the system of subsea production are subsea the Christmas Tree and the Downhole Safety Valve.

2. Christmas Tree

The most important element in the subsea production system is the Christmas Tree (XT). The Christmas Tree is mounted on the wellhead at the seabed. The XT is a set of valves mounted on a specially designed steel block.

Fig. 1. Subsea Christmas Tree [www.gizmodo.com]

The main task of the Christmas Tree is to control the flow of hydrocarbons from the well [5]. Christmas Trees also allow for the injection of various chemicals in order to remove or prevent the formation of hydrocarbon plugs, corrosion, or other prejudicial obstructions having bad influence to the production system. The design of the Christmas Tree also allows for access to the borehole in order to carry out all kinds of maintenance and workovers. The Christmas Tree can also be used for pumping water, gas or other factors to the lode. The Christmas Tree provides additional features, such as pressure and temperature monitoring and flow rate control. The construction of the Christmas Tree may vary depending on the requirements of the project and the area of extraction. The average body weight of a Christmas Tree is from 50 to 70 tonnes. Pressures of exploration for Christmas Trees are standardised and are successively 5,000 psi (35 MPa), 10,000 psi (69 MPa), 15,000 psi (103 MPa) and for ultra-deepwater Christmas Trees: 20,000 psi (138 MPa) [6]. All valves in the Christmas Tree must withstand the same pressure as the Christmas Tree. All equipment is designed to operate at temperatures from 35° to 250°F (2°C to 120°C) [7]. Inside the Christmas Tree, the operating temperature is close to the lode temperature and pressure reservoir decreased by hydrostatic pressure related to the difference between the depth of the lode and the Christmas Tree as well as the linear and local losses. Linear losses derived from friction forces occurring between the elements of the fluid in all its mass and the friction against the walls of the passageway along its length. Take-offs are local obstructions in the flow and changes in the shape of the channel or the velocity of the stream.

Very often, the wells are drilled at depths of 1,500 meters or more. Such depths put high demands on the technical issues; therefore, ultra-deepwater Christmas Trees are used for the exploration of such lodes.

2.1. Safety valves in Christmas Tree

Three valves located in the Christmas Tree were analysed which are important in production of hydrocarbons :

- Production Master Valve (PMV) is the primary and the most important valve in the Christmas Tree. It provides insulation between the borehole and the production tubing, wherein the hydrocarbons flow from the Christmas Tree to the manifold. During the exploitation of the lode, the valve is in the fully open position. The PMV must be strong enough to withstand the pressure prevailing in the well and prevent an uncontrolled leakage of hydrocarbons from the well.
- Production Wing Valve (PWV) is used for closing and opening the XT under normal operating conditions. Just like the Production Master Valve, it is responsible for securing the flow of hydrocarbons from the well.
- Annulus Master Valve (AMV) is the main valve preventing a leak of hydrocarbons from the wellbore to annulus [1].

These valves are fail-safe gate valves. It is a very popular type of valves used in Christmas Trees. This type of valves not only meets the safety function in the event of failure, but also allows for the closure of the valves in the XT without injecting heavy drilling mud into the well in order to eliminate flow from the reservoir into the hole. Closing the valves may be necessary, for example, during pressure and function tests [11].

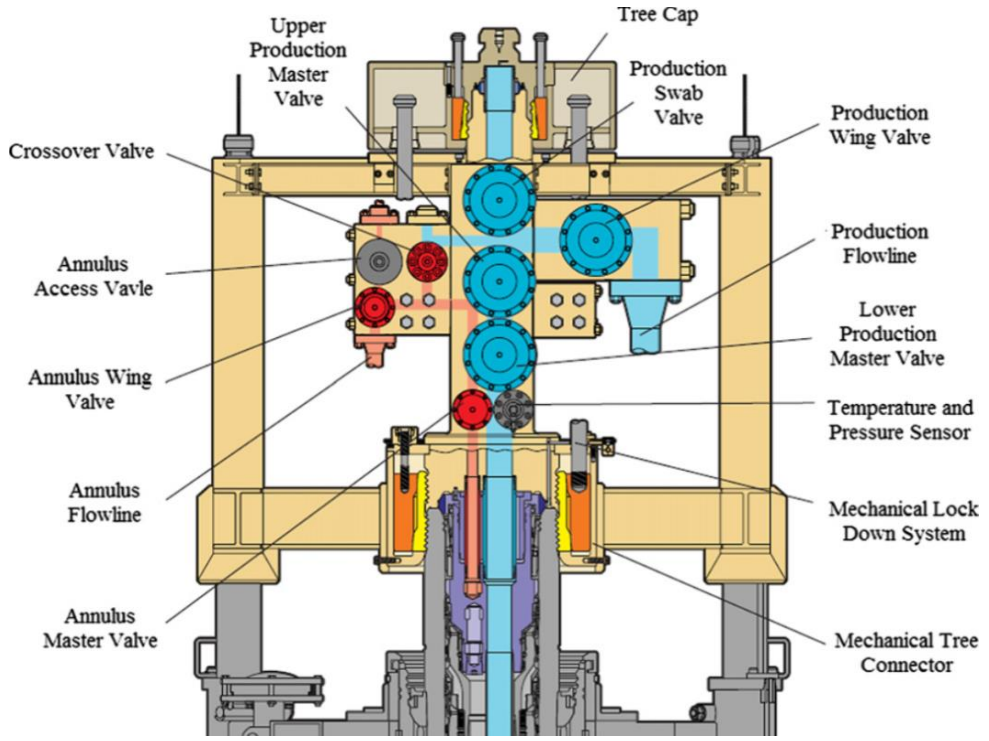

Fig. 2. Valves in Christmas Tree [Dril-Quip]

The valves in the Christmas Tree are controlled via a subsea control module mounted directly on the XT. The subsea control module contains the electronics, hydraulics and instrumentation needed for the safe and effective control of valves in the XT and the Downhole Safety Valve. In addition, the subsea control module is responsible for the distribution of the electric current monitoring signal and for communication with the surface. Modern subsea control modules must have reliability for water depths of up to 3000 meters and pressures of 20,000 psi (138 MPa).

In order to allow for the closing or opening of valves directly and independently of the control system, Christmas Trees are equipped with a panel, which allows for the direct control valve to use the remotely operated vehicle (ROV). Direct control of valves may be necessary for the assembly or disassembly of the XT of maintenance or failure of the control system.

3. Downhole safety valve

A very important valve, which is not located in the Christmas Tree, but it is controlled by it, is the Downhole Safety Valve (DHSV). The DHSV is mounted in a completed wellbore at a depth ranging from 100 to 500 meters below seabed. It is a flap-type valve

and it is intended to prevent the uncontrolled release of hydrocarbons from the lode in the event of an emergency when other valves have failed. The DHSV is controlled with hydraulic fluid by the Christmas Tree.

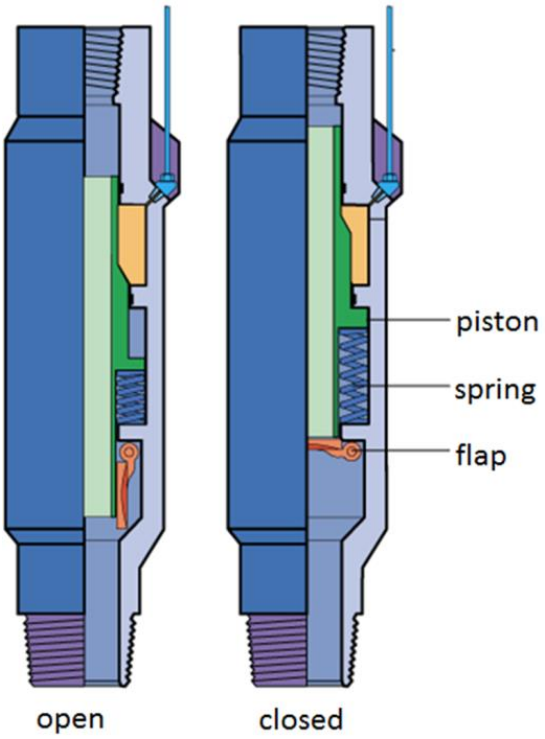

Fig. 3. DHSV valve [www.whcp-oilgas.com]

4. Failure Mode and Effects Analysis

Failure Mode and Effects Analysis (*FMEA*) is a qualitative method, which is used to identify potential errors or defects, and to assess their effects. Many industries require for the FMEA to be used in the design of technical systems and that its sheets to be part of the system documentation. Provisions in the oil industry also require a similar analysis. The analysis uses specific FMEA sheets, in which, inter alia, it distinguishes the failure modes of individual elements or severity of the ranking. Failure mode is a description of a possible malfunction of the element that prevents the required function, which answers the question; how the machine crashes. Modes and causes of damage for the valves depend on the particular design. For a standard subsea gate valve installed in the Christmas Tree, the following typical modes and their corresponding causes as well as mechanisms of damage may be mentioned:

Table 1.

Failure modes and possible causes of it

Failure mode	Possible causes
Fail to close	• Fault control system, • Too high hydraulic pressure in the supply line rod chamber, • Locked return hydraulic line, • Spring failure, • Internal leak.
Fail to open	• Fault control system, • Too low pressure in the hydraulic circuit valve supply, • Damaged piston valve, • Spring failure, • Internal or external leak, • Locked hydraulic return line.
Premature or uncontrolled shutdown	• Fault control system, • External leak.
Internal leak	• Seal failure.
External leak	• Seal failure, • Unsealing the valve body.

4.1. Classification of the severity of fault

The classification of the severity of the effects provides the qualitative dimension of the worst potential consequences of design errors or equipment failures. Each identified failure mode and analysed element is subject to the classification of the severity of the impact. Classification is used in both FMEA and FMECA. The categories are divided into:

- Category I (catastrophic) – failure results in death of workers or huge loss of devices preventing further execution of the planned objectives of the system.
- Category II (critical) – failure causes the degradation of the system beyond acceptable limits, creating a security risk (contributing to the death or injury of employees, if they are no taken steps to combat the risk).
- Category III (severe) – the failure of the system degrades the bounds of safety, but there is a possibility to appropriately counteract the effects.
- Category IV (reduced) – failure does not degrade the whole system performed beyond the acceptable limits of safety, causing one of the various disadvantages of the system.

- Table 2

- **FMEA sheet for PMV**

Description of item: Production Master Valve			**Description of failure**			**Effects of failure**		**Severity**	**Recommended action to reduce the risk**	**Commentary**
Nr	**Function**	**Operating mode**	**Failure mode**	**Potential cause of failur**	**Detection**	**On subsystem**	**On whole system**			
1	It allows on the flow of hydrocarbons from the wellhead; provides isolation between wellhead and production tubing	Valve in open position	Fail to close	Fault control system	D	Is not possible to close valve on demand; continuous flow of hydrocarbons through the valve	The closure of Christmas Tree by the valve is impossible. Other valves on the production line are needed to work	Category II: Critical	Regular inspections and testing of the control system	
				Too high hydraulic pressure in the supply line rod chamber	D				Regular inspections and testing of the hydraulic system	
				Locked hydraulic return line	U				Regular inspections and testing of the hydraulic system	
				Spring failure	U				Proper maintenance	

5. Results

Analysed PMV, PWV, AMV and DHSV. Distinguished two modes of operation: the valve in the open and closed positions and whether the damage is detectable, and each failure mode has been classified according to the classification of the severity of the impact. Table 2 presents an exemplary FMEA sheet that was used while analysing.

The Downhole Safety Valve is the primary barrier and is designed to cut off the Christmas Tree from lodes. For DHSV in the open position, the most dangerous failure mode is "left open the valve," which have been classified in the classification of the severity of fault "leakage through the valve" as a critical fault. Failure mode "fail to close" is extremely dangerous when the situation requires, for example, a fire on the platform. In this case, it is necessary to ensure the proper functioning of the valves in the Christmas Tree. If the secondary barrier does not fulfil its function, the platform will still be transmitting hydrocarbons, which will result in such a situation as an explosion on the surface. Failure mode "leakage through the valve" causing damage to the sealing flap is dangerous due to the fact that the valve does not close the flow of hydrocarbons in the situation required. It is then necessary to activate the valves in the XT, which violates the integrity of the subsea safety at oil and gas production. A major failure mode is uncontrolled shutdown. In this case, there is no assurance that the valve will work and close properly, and on the other hand, there is the possibility that the valve closes spontaneously in normal production, causing downtime and thus financial losses.

The secondary barrier is the Christmas Tree and its main valve is the Production Master Valve. In case of failure, DHSV is the first valve that is designed to cut off the flow of hydrocarbons through the Christmas Tree. This is a very important component of the XT because its failure contributes to an increased risks associated with not closing the whole XT. Failure modes in the basic gate valves of XT are classified from serious to catastrophic consequences. All considered, gate valves (PMV, PWV, AMV) in both operating modes external leak hydrocarbons cause disastrous consequences. In such a situation, it requires keen DHSV or the XT, otherwise it may lead to an ecological catastrophe caused by the contamination of seawater, and thus huge financial losses. If the DHSV works, an ecological catastrophe does not occur, but it is necessary to draw all the XT and replacement of the damaged valve. If the DHSV does not work, but the other valve is closed, it will not be possible to immediately draw the XT. In such a situation, injection of heavy drilling fluid into the wellbore would be needed. Each day of downtime in production is associated with financial losses, but also to draw all the XT generates additional costs. With the exception of an external leak, all failure modes in AMV have serious consequences. Analysing PMV and PWV in operation in the open position failure mode "fail to close" "internal leak" caused damage to the piston seal and the "uncontrolled shutdown" necessitate the activation of other valves, and thus in case of requiring situation increases the probability associated with the failure to close the entire XT. In addition, the occurrence of even one of these failure modes leads to stoppage of the whole production in order to repair the fault. In contrast, the occurrence of leakage caused by damage to the inner piston seal also will stop production because the hydraulic pressure in the chamber, the rod falls, and thus the valve closes. Failure mode "uncontrolled shutdown" is not a dangerous fault because it does not contribute to an increase in the danger of the production of hydrocarbons, but the effects of this mode are felt from the economic side.

The analysis can be concluded that for each basic gate valve of XT, the most dangerous are an external leak and the failure mode "fail to close" in the open position of the valves. Any failure of an individual valve that makes the extraction of hydrocarbons becomes less and less secure. An indispensable component of the safety system of subsea production is the DHSV, the most dangerous defects can occur in the open position of the valve. The DHSV and the Christmas Tree complement each other, thus ensuring the security of oil and gas production.

References

[1] Norsok Standard D-010.
[2] Perrin D., *Well Completion and Servicing*, Technip 1999, 153-156.
[3] Rausand M., *Reliability of Safety-Critical Systems: Theory and Applications*, Wiley 2014, 53-76.
[4] Samir D., *Fundamentals of Oil & Gas Industry for Beginners*, Notion Press Chennai 2015.
[5] Young B., Qiang B., *Subsea Engineering Handbook*, Elsevier, 2010.

TECHNICAL TRANSACTIONS | CZASOPISMO TECHNICZNE
MECHANICS | MECHANIKA
2-M/2016

EUGENE ALEXEEV, BORIS GOLOVUSHKIN,
ALEXANDR LABUTIN, ELENA EROFEEVA*

STUDY OF SYSTEM-WIDE AND STRUCTURAL PROPERTIES AND OPTIMAL CONTROL OF THE PRE-POLYAMIDATION TANK

ANALIZA SYSTEMOWA I STRUKTURALNA WŁAŚCIWOŚCI ORAZ OPTYMALNE STEROWANIE ZBIORNIKIEM DO PRE-POLIAMIDACJI

Abstract

The study on system-wide and structural properties of a prepolyamidation tank were performed by simulation. Control channels were selected. An algorithmical synthesis of a tank optimal control system was performed. A designed control system was simulated.

Key words: chemical tank, controllability, optimal control, control system

Streszczenie

Analizę systemową i strukturalną właściwości zbiornika do pre-poliamidacji przeprowadzono metoda symulacji. Wyznaczono kanały kontrolne, dokonano algorytmicznej syntezy systemu sterowania oraz zamodelowano projektowany system.

Słowa kluczowe: zbiornik, sterowalność, optymalne sterowanie, system sterowania

DOI:

* MSc. Eng. Eugene Alexeev; MSc. Eng. Boris Golovushkin, Prof. PhD. DSc. Eng. Alexandr Labutin, PhD.DSc. Eng. Elena Erofeeva, Department of Technical Cybernetics and Automation, Chemical Engineering and Cybernetics Faculty, Ivanovo State University of Chemistry and Technology.

1. Introduction

At present, the synthetic polymer polycaproamide attracts the attention of many researchers. Thanks to its properties, the polymer is widely used in some industries. Thread for industrial use, composite materials with special properties for medicine and food industry, polymer colour concentrates and thermal stabilisers can be made based on this polymer.

The main industrial method for producing polycaproamide is hydrolytic polymerisation of caprolactam in melt. With an approach to saving energy and resource at our university promising technology, for producing this polymer were developed. Extraction and energetically unfavourable stage regeneration lactam waters were changed by combined drying and removal of the residual monomer in an inert gas process.

In this work, the object is the pre-polyamidation tank in which stage of pre-polyamidation of polyamide-6 in solid phase is existing. Earlier mathematical model of this stage was derived, simulation was performed and the adequacy of the derived model was confirmed.

The aim of this work is to study system-wide and structural properties (connectivity, controllability and observability) of tank and to design an optimal controller by using mathematic and simulation methods.

2. Analysis of system-wide and structural properties

At the present time, researchers widely use simulation methods of technological processes of synthesising synthetic polymers for solving different optimisation and control tasks. It's necessary to create an effective control system for performing the process under the economic or technical point of view's optimal behaviours. The processes are studied as control object for solving this problem.

Analysis of connectivity

Dimensionless transfer coefficients were determined for studying the connectivity degree. Input and output variables were selected after analysing the technological process. Input variables are consumptions of pellets of polymer, nitrogen and heat transfer agent. Output variables are concentrations of caprolactam and water in pellets of polymer and the tank temperature.

Matrix of dimensionless coefficients K has been obtained as follows:

$$K = \begin{pmatrix} 0.388 & 0 & -0.0975 \\ 0.2325 & 0.001875 & 0.041 \\ -0.0855 & 0 & 0.0855 \end{pmatrix} \quad (1)$$

The method using the Bristol matrix which characterises connectivity degree in static, was used for evaluating the degree of system connectivity. Each element of the matrix is a result of the division of two derivatives: the first one is a derivative of steady state open

loop system output under control, the second one is a derivative of steady state closed loop system output under control. The Bristol is as follows:

$$\lambda = K \cdot (K^T)^{-1} \tag{2}$$

where K is a transfer coefficients matrix.

In this work, we have obtained matrix λ as:

$$\begin{aligned} \lambda &= \begin{pmatrix} 0.388 & 0 & -0.0975 \\ 0.2325 & 0.001875 & 0.041 \\ -0.0855 & 0 & 0.0855 \end{pmatrix} \cdot \left(\begin{pmatrix} 0.388 & 0 & -0.0975 \\ 0.2325 & 0.001875 & 0.041 \\ -0.0855 & 0 & 0.0855 \end{pmatrix}^T \right)^{-1} \\ \lambda &= \begin{pmatrix} 0.953 & -114.06 & -0.187 \\ 0.961 & -149.706 & 1.441 \\ 0.041 & -27.892 & 1.041 \end{pmatrix} \end{aligned} \tag{3}$$

After analysing λ, we established that our object is connected. Hence, it's necessary to compensate cross links for controlling the tank.

Analysis of controllability

Before we synthesise the control algorithm, it is necessary to study such properties of object as the stability of free movement, controllability and observability. An analysis of the results of these studies allows us to conclude the ability to control the object. Presentation of the dynamic object in the state-space model is used for this task.

An evaluations of the stability of free movement, controllability and observability are performed in the neighbourhood of operating point. Strong conditions of controllability and stability have been found only for some classes of nonlinear objects. Availability or non-availability of these properties can be established by using linearisation of nonlinear equations describing the object [1]. If the linearised system is controllable in the neighborhood of some steady state, then we may assume that the original nonlinear system is controllable. Consumptions of pellets of polymer, nitrogen and heat transfer agent were previously chosen as control actions. The control task is to fully remove the monomer and water from pellets of polymer and to support the tank temperature at the desired level by changing the control actions.

The original nonlinear model of object with distributed parameters was presented by using its discrete analogue (cell's model). Linearisation of the object in the neighbourhood of the working point was performed in Simulink app «Linear Analysis Tool», MATLAB. Matrix of state **A** (dimension 21×21), matrix of control **B** (dimension 21×3) and matrix of observe **C** (dimension 3×21) were derived.

A study on the stability of the unperturbed system in the state-space model was performed. If all real parts of all eigenvalues α_i of matrix **A** are negative, then the system is stable:

$$\det(\alpha_i \mathbf{I} - \mathbf{A}) = 0 \tag{4}$$

where **I** is identity matrix.

Results show that our object is stable in the neighbourhood of the working point. This way, it has a property of stabilizability [2].

Analyses of the controllability were performed by using the controllability matrix $\mathbf{N_c}$ [1-3]:

$$\mathbf{N}_c = \left[B : AB : A^2B : ... : A^{n-1}B\right] \tag{5}$$

where n is an order of system.

If rank of $\mathbf{N_c}$ is equal to n, then the linear system is fully controllable. If rank of $\mathbf{N_c}$ is smaller than n and bigger than 0, then the system is partly controllable. If rank of $\mathbf{N_c}$ is equal to 0, then the system is non-controllable. The controllability matrix and its rank were derived and calculated by using inbuilt MATLAB functions. The rank of $\mathbf{N_c}$ is 12. It is smaller than the order of the system that equals 21, hence our pre-polyamidation tank is not fully controllable. This way, there are such initial conditions in the phase state when the object cannot be transferred to the specified final condition. Also it was shown that our object is fully controllable in the space of outputs.

Analysis of observability

The observation equation is $\mathbf{y} = \mathbf{C}\cdot\mathrm{x}$, where $\mathbf{y} = (y_1,\ldots,y_m)^{\mathrm{T}}$ is a vector of observation variables, $\mathbf{x} = (x_1,\ldots,x_n)^{\mathrm{T}}$ is vector of the output variables, $\mathbf{C}$ is an observation matrix (dimension $m\times n$). The observability matrix is written as follows [1-3]:

$$N_o = \left[C^T : A^TC^T : (A^T)^2C^T : ... : (A^T)^{n-1}C^T\right] \tag{6}$$

where n is order of system.

The observability matrix and its rank was derived and calculated by using inbuilt MATLAB functions. The rank of N_o is 15. It shows that our object is not fully observable.

The task of controlling the object was solved in next step.

3. Designing the optimal controller

Control of tubular chemical reactors is probably the most difficult among all of reactor systems. It is caused by some technical and design factors.

Controllers using methods of optimal control theory are widely used on tubular reactors. At present, optimal control is one of the perspective direction of automatic control theory development. There are many works about the application of optimal control in some technical and technological objects.

Literature presents a wide range of criteria for the estimation of control quality [1-4]. Among them, criteria of maximum speed and minimum of control error dispersion are widely used. In this work we will use both criteria in dynamics.

Criterion of minimum error dispersion

There is a closed-loop control system (Fig. 1) where stationary centered random signal is used as disturbance. The interference signal is formed by a filter with transfer function $W_f(s)$ from white noise $v(t)$.

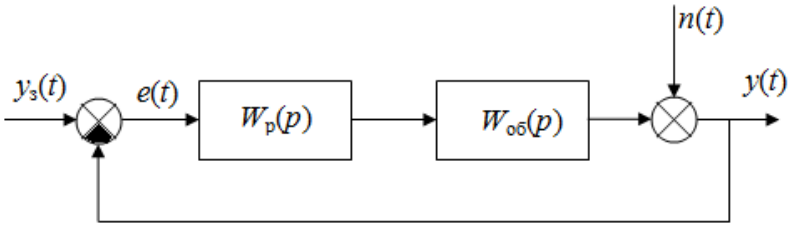

Fig. 1. Closed-loop control system

Dispersion of error can be found as:

$$De = \int_0^\infty \left[k_f(\tau) - k_1(\tau)\right]^2 d\tau \tag{7}$$

where $k_f(\tau)$ is a pulsed transition function of the filter; $k_1(\tau)$ is a pulsed transition function of the system consisting of two dynamic elements:

$$W_1(s) = W_f(s) \cdot F_y(s) \tag{8}$$

where $F_y(s)$ is a transfer function of the closed-loop system on the control channel.

It is necessary to select transfer functions $F_y(s)$ and $W_1(s)$ so that we allow to minimise the expression (4). It is difficult because almost always there is a transport delay in the object. In that cases, the minimum can be achieved only when $k_f(\tau) = k_1(\tau)$ and $\tau > \tau_d$.

Having found the optimal transition function $k_1^{opt}(\tau)$ and $W_1^{opt}(s)$, we can derive the optimal transfer function of the closed-loop system $F_y^{opt}(s)$ from expression (5). The transfer function of the optimal controller can be written as [4]:

$$W_p^{opt}(s) = \frac{F_y^{opt}(s)}{1 - F_y^{opt}(s)} \cdot \frac{1}{W_{об}(s)} \tag{9}$$

It is known that for the system having stationary random signal as a disturbance, the transfer function of the optimal controller is:

$$W_p^{opt}(s) = \frac{e^{-\alpha\tau_d} \cdot e^{-s\tau_d}}{1 - e^{-\alpha\tau_d} \cdot e^{-s\tau_d}} \cdot \frac{1}{W_{об}(s)} \tag{10}$$

where τ_d is the transport delay.

Criterion of the maximum speed

There are many ways to solve the task of seeking optimal control under the criterion of maximum speed. The Hamilton variational calculus, phase space method, Viener optimal control theory are widely used. There are some disadvantages of using these methods. One can distinguish such defects as difficulty of solving equations and their cumbersome, high probability of error, difficulty of expression for computing control actions.

The "Trajectories docking" method [5], based on the Feldbaum theorem, is the simplest method for solving the task of maximum speed. Let's consider it on the object with the transfer function:

$$W_{ob}(s) = \frac{k}{(T_1 \cdot s + 1) \cdot (T_2 \cdot s + 1)} \tag{11}$$

The general solution of the corresponding differential equation is:

$$y(\tau) = c_0 + c_1 \cdot e^{\alpha_1 \tau} + c_2 \cdot e^{\alpha_2 \tau} \tag{12}$$

where α_1 and α_2 are roots of general solution of the homogeneous equation; c_0 is derived from seeking particular solution; c_1 and c_2 are derived from solving the Koshi task.

The entire time interval of changing the control variable and control action is divided into three sectors. The first sector characterises the beginning of the transient process, time interval $[0; \tau_r)$. The control action has a maximum value. The time interval of the second sector is $[\tau_r; \tau_f)$. This sector describes movement of the object to steady state. The control action equals 0. Since $t = \tau_f$ the object is at steady state or finish movement to steady state. The control action at time interval $[\tau_f; \infty)$ has a nominal value.

This way, the optimal control task is to find switching times τ_r and τ_f between maximal, minimal and nominal values of the control action. The system consisting of six nonlinear equations is solved for this. In general, this system may be written as:

$$\begin{cases} c_0 + c_1 \cdot e^{\alpha_1 \tau_0} + c_2 \cdot e^{\alpha_2 \tau_0} = 0, \\ \alpha_1 \cdot c_1 \cdot e^{\alpha_1 \tau_0} + \alpha_2 \cdot c_2 \cdot e^{\alpha_2 \tau_0} = 0, \\ c_{00} + c_{11} \cdot e^{\alpha_1 \tau_f} + c_{22} \cdot e^{\alpha_2 \tau_f} = y_d, \\ \alpha_1 \cdot c_{11} \cdot e^{\alpha_1 \tau_f} + \alpha_2 \cdot c_{22} \cdot e^{\alpha_2 \tau_f} = 0, \\ c_0 + c_1 \cdot e^{\alpha_1 \tau_r} + c_2 \cdot e^{\alpha_2 \tau_r} = c_{00} + c_{11} \cdot e^{\alpha_1 \tau_f} + c_{22} \cdot e^{\alpha_2 \tau_f}, \\ \alpha_1 \cdot c_1 \cdot e^{\alpha_1 \tau_r} + \alpha_2 \cdot c_2 \cdot e^{\alpha_2 \tau_r} = \alpha_1 \cdot c_{11} \cdot e^{\alpha_1 \tau_f} + \alpha_2 \cdot c_{22} \cdot e^{\alpha_2 \tau_f} \end{cases} \tag{13}$$

where y_d is the desired value of the control variable; τ_r and τ_f are switching times; τ_0 is an initial time.

The first two equations of (13) show system condition at an initial time. The next two equations of (13) characterise the system at the steady state. The final equations describe the process of "trajectories docking". So, we may write system (13) as:

$$\begin{cases} ku_m + c_1 + c_2 = 0, \\ \alpha_1 c_1 + \alpha_2 c_2 = 0, \\ c_{11} e^{\alpha_1 \tau_f} + c_{22} e^{\alpha_2 \tau_f} = y_d, \\ \alpha_1 c_{11} e^{\alpha_1 \tau_f} + \alpha_2 c_{22} e^{\alpha_2 \tau_f} = 0, \\ ku_m + c_1 e^{\alpha_1 \tau_r} + c_2 e^{\alpha_2 \tau_r} = c_{11} e^{\alpha_1 \tau_f} + c_{22} e^{\alpha_2 \tau_f}, \\ \alpha_1 c_1 e^{\alpha_1 \tau_r} + \alpha_2 c_2 e^{\alpha_2 \tau_r} = \alpha_1 c_{11} e^{\alpha_1 \tau_f} + \alpha_2 c_{22} e^{\alpha_2 \tau_f} \end{cases} \quad (14)$$

where k is a gain; u_m is a maximal value of the control action.

System (14) can be easily solved by using the numerical method. It should be noted that a description of the method can be used for designing an optimal controller providing the fastest possible shutdown of the process.

Combined system

The control system consisting of two optimal controllers for controlling the tank temperature was designed and presented in figure 2.As we can see, this system has a combined structure.

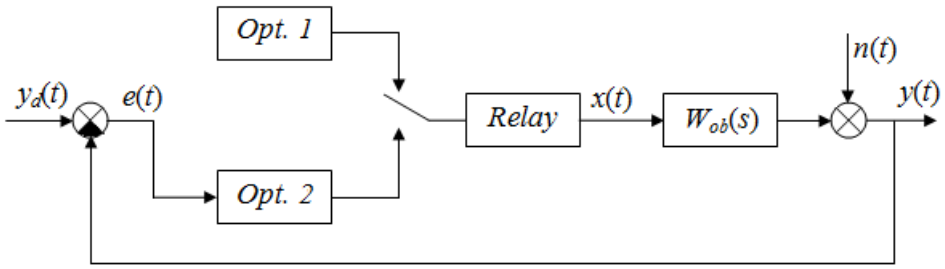

Fig. 2. Combined system for controlling temperature of pellets of polymer

Block *Relay* switches between controllers on the following condition:

$$x(\tau) = \begin{cases} Opt.1, \tau \le \tau_f, \\ Opt.2, \tau > \tau_f \end{cases}$$

For channel “consumption of heat transfer agent – temperature of pellets” transfer function without transport delay is written as follows:

$$W_{ob}(s) = \frac{47502059}{(1200 \cdot s + 1) \cdot (15 \cdot s + 1)} \quad (15)$$

Having solved system (14) with our own parameters, we have found switching times τ_r and τ_f, to equal 703 *s* and 715 *s* respectively.

The transfer function of *Opt*. 2 has the following form (16):

$$W_p^{opt}(s) = \frac{e^{-\alpha\tau_d} \cdot e^{-s\tau_d}}{1 - e^{-\alpha\tau_d} \cdot e^{-s\tau_d}} \cdot \frac{1}{k} \cdot (T_1 \cdot s + 1) \cdot (T_2 \cdot s + 1) \tag{16}$$

Having approximated the autocorrelation function of the disturbance signal formed by the filter from the white noise, we derived parameter α. The filter transfer function was derived.

Optimal controllers for channels “consumption of pellets of polymer – concentration of caprolactam in polymer” and “consumption of nitrogen – concentration of water in polymer” were derived analogically.

4. Conclusion

The carried out evaluation of system-wide and structural properties of pre-polyamidation tank allowed us to choose the control actions and measure the state variables. The problem of structural, algorithmic and parametric synthesis of the control system minimises energy consumption for performing the process synthesis of polyamide-6 was solved.

References

[1] Pupkov K. A., Egupov N. D., *Teoria optimizacii sistem abtomaticeskogo upravlenia*, Izdatelstvo MGTU im. N. E. Baumana 2004.

[2] Gubin G. K., Grebe S. F., Salgado M. E., *Proektirovanie system upravlenia*, BINOM Laboratoria znanij 2004.

[3] Rej U., *Metody upravlenia tehnologiceskimi processami*, Per s angl., Mir 1983.

[4] Besekerskij W. A., Popov E. P., *Teoria system abtomaticeskogo upravlenia*, Spd., Professia 2003.

[5] Golovushkin B., Volynskii V. U., Zaitzev V. A., *Optimal management of the process of convective drying of thin fabric materials*, Shenyang Institute of Chemistry technology, China 2004.

TECHNICAL TRANSACTIONS | CZASOPISMO TECHNICZNE
MECHANICS | MECHANIKA
2-M/2016

VALERIAN BLINICHEV, ANDREY POLANSKI, OLEG CHAGIN*,
JANUSZ KRAWCZYK**

RECTIFICATION COLUMN: CRITERIA OF EFFICIENCY

KRYTERIA OCENY EFEKTYWNOŚCI DZIAŁANIA KOLUMN REKTYFIKACYJNYCH

Abstract

In the paper analysis of the factors influencing the efficiency of the rectification process is provided. The authors show that existing dependences, equivalent to HETP, cannot be used for calculating rectification plate columns and columns with vortex nozzles, in which the coefficients of mass transfer are substantially dependent on the irrigation density and the gas/steam velocity. The dependence of the efficiency of the packet vortex nozzle as a function of the hydrodynamic regimes of the vapour and liquid phases is proposed.

***Keywords**: HETP, efficiency, distillation column, rectification, packing*

Streszczenie

W pracy przedstawiono analizę czynników efektywności procesu rektyfikacji. Autorzy wykazali, że istniejące zależności oparte o WRPT nie mogą być stosowane do kolumn półkowych i z dyszami wirowymi gdzie współczynniki transportu masy są powiązane z wielością zraszania i prędkością gazu/pary. Zaproponowano zależność efektywności dla dysz wirowych jako funkcji parametrów hydrodynamicznych pary i cieczy.

Słowa kluczowe: WRPT, efektywność, kolumny destylacyjne, rektyfikacja wypełnienia

DOI:

* Prof. PhD. DSc. Eng, Valerian Blinichev, MSc Andrey Polanski; PhD. DSc. Eng. Oleg Chagin, Department of Machines and Equipment for Chemical Industry, Faculty of Chemical Engineering and Cybernetics, Ivanovo State University of Chemistry and Technology.

** PhD. DSc. Eng. Janusz Krawczyk, Prof. CUT, Institute of Thermal and Process Engineering. Faculty of Mechanical Engineering. Cracow University of Technology.

1. Introduction

The efficiency of liquid mixture separation, which defines both the quality of the distillate and the size of the column (height), is the most important characteristic for any rectification column. If the diameter of the column is determined through the optimal vapour velocity in the upper and bottom parts of its column, which mainly depends only on the structural design of auxiliaries, then the height (as the most difficult parameter to define) depends on both the heat- and mass-transfer rate on each tray (or height of transfer unit in case of packed column) and the distribution of temperatures along the column length. The heat- and mass-transfer rate on a tray or on the packing is associated with optimal vapour velocity on different column heights, which is usually determined by means of experiments for each type of the mass-transfer devices.

Numerous simulation models exist for batch distillation, but many of these employ theoretical stage models. Some of these models consider tray efficiency, but only as a tuning parameter, obtained by the trial and error method, for matching simulation results with actual experimental data.

The quality of separation of both binary and multicomponent liquid mixtures depends on many factors: the difference between boiling temperatures of the components and the presence of the azeotropic mixtures; reflux flow rates; distribution of temperatures along the column length; structural design of the auxiliaries, which influence not only the quality of separation, but also the column height.

1.1. Factors affecting tray efficiency

The factors affecting the efficiency of a tray include: mechanical design factors (tray type and size, hole size, weir height), operation conditions (liquid and vapour rates) and the characteristics of the mixture on the tray. Some of these factors, which have been considered [1, 2, 3], include outlet weir height, hole size, liquid mixing, entrainment, flow regimes, reflux ratio, composition and surface tension of the components of the mixture.

1.1.1. Hole Size and Outlet Weir Height

The effect of the hole size in sieve trays and weir height (in other trays) on the tray efficiency is usually associated with its holdup characteristics. An investigation [3] of the hole size influence in sieve trays on the tray efficiency showed that smaller holes exhibited higher efficiencies at low vapour rates, but at higher vapour rates, the hole size has not shown any effect. It was suggested that smaller holes at low vapour rates prevented liquid downfall due to the capillary surface tension effects, thus increasing the tray liquid holdup and efficiencies. Smaller flows are issued from smaller holes thus increasing the mass-transfer process.

On the contrary, outlet weir height is used to maintain an appropriate liquid depth (holdup) on the tray and, as it was expected, tray efficiency increases with increasing outlet weir height. Deeper liquid levels on the tray mean that the residence time and mass transfer time of the vapour bubble through the liquid is increased.

1.1.2. Reflux ratio and tray holdup

While studying the reflux ratio effect, Pigford [4] showed that in the presence of appropriate holdup, the effect of the reflux ratio on the sharpness of the separation was less

pronounced than in a column with negligible holdup. Langdon and Keyes [1] however, concluded on the basis of the results obtained from experimental data, using isopropyl-water mixture that changes in reflux ratio had a negligible effect on the tray efficiency. Other researchers [5] have found plate efficiency to vary appreciably with reflux ratio. Ellis and Hardwick's results were based on the results obtained from the distillation of a methylcyclohexane/toluene mixture, but their conclusions did not take into account the effect of concentration on the tray efficiency. The effect of holdup on actual tray efficiency is not reported, but its effect on the sharpness of separation gives an indication to its effect on the distillation operation.

1.1.3. Liquid viscosity

Barker and Choudhury [6] studied the effect of liquid viscosity on the mass transfer and plate efficiency. It was found that with increasing liquid viscosity a reduction in the interfacial area occurs, thus leading to a reduction in the gas-film efficiency. Viscosity can also increase the size of a bubble at bubble formation at the slot or orifice by retarding the rate of closure of the neck of the bubble. This change in bubble size could be detected by liquid holdup measurements for the tray. Liquid holdups decrease with increasing liquid viscosity.

A beneficial effect of liquid viscosity is the reduction of the bubble rise rate through the liquid on the plate, leading to an increased mass transfer. This effect, however, does not appear to be sufficient to balance the decrease in surface area obtained at higher liquid viscosities.

1.1.4. Concentration effects

The effect of concentration on the tray efficiency was demonstrated by Fane and Sawistowski in [2], where they showed a dependence of the benzene-cyclohexane system on the efficiency passing through a maximum. This dependence was found to be strong at medium weir height and at low vapour velocity.

Shilling [7] obtained tray efficiency data for the distillation of ethanol/water mixture (concentration of ethanol was between 0 and 70 mole %). He observed an efficiency maximum in the composition range of 35 to 60 mole percent ethanol with efficiency falling more sharply at the lower ethanol composition range. At very low ethanol concentrations, Murphree efficiency values were observed to exceed 100%, the ones the authors suggested to be erroneous.

2 Packed rectification column: the efficiency of mass-transfer devices

Most of the up-to-date industrial packed beds have very extended surface area. For example, Sulzer AG is currently engaged in the production of packed beds with the specific surface of more than 800 m^2/m^3, and Ingehim Company suggests randomly distributed packing with specific surface in the range of 1000 to 1200 m^2/m^3 [8]. All packing columns, except the vortex ones, certainly work in the film mode, where the nozzle surface area is a mass-transfer surface in case of full flooding. Such columns work in the small operating range for vapour velocities (at vapour velocities less than about 1.5 m/s) and low density irrigation (less than $10 \div 15$ m^3/m^2h). The mass-transfer surfaces in them are to be practically

constant on the whole range of operating vapour/liquid velocities. The only exception is a short range close to the liquid holdup mode, when emulsification arises [9], whereby the value of mass-transfer surface and mass transfer coefficient spontaneously rise.

Inasmuch as this regime is close to the flooding point, its retention is impossible even with the use of modern automation systems. As a result, all the nozzles, except for the ones we studied [10, 11, 12], work as the apparatus with thin-film, which ideally equals the nozzle surface area.

As most packed beds mainly work in the film mode, the main desirable requirements for the packing of distillation columns are: to promote a uniform distribution of gas and liquid, have a large surface area (for greater contact between the liquid and vapour phase) and have an open structure, providing a low resistance to the gas flow. Many types and shapes of packing can satisfactorily meet these requirements [13].

While determining the actual number of trays of mass-transfer apparatus, the concept of theoretical plate is used, where the equilibrium between the vapour and liquid concentration is achieved on a condition that the complete mixing of vapour and liquid phases occurs. On the n-tray, the changing of the light-volatile component from liquid to vapour phase takes place, and semi-volatile component changes from vapour to liquid sate. Such alteration of concentration is named the theoretical step or theoretical plate. Drawing the steps between the tie and equilibrium lines in the given range of operating concentrations, the general number of steps of N_{T} (or number of theoretical plates) is found.

If the number of theoretical trays is known, then the number of actual N_{D} steps of separation is:

$$N_D = \frac{N_T}{\eta_T}, \tag{1}$$

where η_T is the averaged tray efficiency.

As we have noted before [14], many researchers defined the overall tray column efficiency by means of the tray efficiency. The most popular concept for evaluating the height of a packed column is the *HETP* (Height Equivalent to Theoretical Plate), defined by the following equation:

$$Z = HETP \cdot N, \tag{2}$$

where:

Z is a height of the packed bed required for achieving the separation equivalent to the

N – number of theoretical plates [15].

Unfortunately, there are only a few generalised methods available in the open source literature for estimating the *HETP*. These methods are empirical and supported by vendor advice. The performance data published by universities are often obtained while using small columns and with not industrially important packing. When commercial-scale data are published, they usually are not supported by analysis or generalisation. Several correlations and empirical rules have been developed for *HETP* estimation in the last 50

years. Among the empirical methods, there is a rule of thumb for traditional random packing, that says:

$$HETP = \text{Column Diameter}$$

In Caldas's investigation, it has been shown that this rule holds only for small diameter columns.

Lockett [16] has proposed a correlation to estimate *HETP* in columns containing structured packing elements. It was inspired by Bravo's correlation [17] in order to develop an empirical relation between *HETP* and the packing surface area, operating at 80% flooding condition:

$$HETP = \frac{(4.82 \cdot (\rho_L - \rho_G)^{0.5} \mu_r^{-0.06})}{\alpha}, \tag{3}$$

which:

$$\alpha = a_p \cdot \left[\left(1 + 0.78 \cdot e^{0.00058 a_p}\right) \cdot \left(\frac{\rho_G}{\rho_L}\right)^{0.25} \right]^2, \tag{4}$$

where

ρ_G – vapour density, kg/m^3;
a_p – specific surface of the packing, m^2/ m^3;
μ_r – relation between liquid viscosity at the packing bed temperature and viscosity of water at the temperature of 20^{o}C.

According to the Wang studies [18], *HETP* can be evaluated more accurately by the following expression:

$$HETP = \frac{\ln \lambda}{\lambda - 1} \left[\frac{u_{Gs}}{k_G \cdot a_e} + \lambda \cdot \frac{u_{Ls}}{k_L \cdot a_e} \right], \tag{5}$$

where:

λ – inclination ratio between the equilibrium and operation straight;
k_G – gas-phase mass-transfer coefficient;
k_L – liquid-phase mass-transfer coefficient;
a_e – effective interfacial area, m^2/ m^3;
u_{Ls}, u_{Gs} – liquid/gas phase superficial velocity.

Therefore, the precision of *HETP* evaluation by the equation (5) depends on the accuracy of correlations used to predict the effective interfacial area as well as the vapour and liquid mass-transfer coefficients, which are easily defined by the experiments at the known values of the mass-transfer area.

2.1. Murphree vapour phase efficiency

Besides the calculation of height equivalent to a theoretical plate, a number of researchers evaluate that by using the Murphree efficiency. In particular, in Laptev's work [19], the comparison between the efficiencies of diverse packings was provided. Also, it

was shown that “Ingehim” packing has the highest efficiency at the same vapour velocities and reflux ratio.

The equation derived by Murphree is:

$$y_j = y_j^* - M \cdot (y_j^* - y_{j-1}), \tag{6}$$

or in its more familiar form:

$$E_i^{MV} = \frac{y_{i,j} - y_{i,j+1}}{y_{i,j}^* - y_{i,j+1}} \tag{7}$$

where:

E_i^{MV} – is the Murphree vapour phase efficiency,
$y_{i,j}^*$ – equilibrium vapour phase concentration of the volatile component;
j – tray number;
i – component number.

It should be noted that this equation (7) is easily applied to the case where the vapour resistance is negligible in comparison with the liquid film resistance. An equivalent equation for the liquid phase can be also easily derived. However, the given method of calculation of the efficiency just weakly reflects (only through y^*) the real hydrodynamics of the mass-transfer device and it does not give any understanding on the influence of its structural design.

2.2. Description of packed mass-transfer devices

As an objective, Bravo and Fair [17] had the development of a general project model to be applied in packed distillation columns, using a correlation that doesn’t need validation for the different types and sizes of packing. Moreover, the authors did not intend to obtain the dependence on the flooding point, as the model of Bolles and Fair does. For this purpose, the authors used the Onda’s model, with the database of Bolles and Fair, to give a better correlation based on the effective interfacial area for calculating the mass-transfer rate. The better correlation, for all the systems and packing tested, is given by:

$$\frac{a_e}{a_p} = 0.498 \cdot \left(\frac{\sigma^{0.5}}{Z^{0.4}} \right) \cdot (Ca_L \cdot \mathrm{Re}_V)^{0.392}, \tag{8}$$

where:

a_e – effective interfacial area, m^2/ m^3;
a_p – specific surface of the packing, m^2/ m^3;
Ca_L – capillary number;
σ – liquid surface tension, N/m;
Re_V – Reynolds number for vapour phase.

Recently, with the emergence of more modern packing, other correlations predicting the rate of mass-transfer in the packed columns have been studied. Wagner [20], for example,

developed a semi-empirical model, taking into account the effects of pressure drop and holdup in the column for the Nutter rings and IMTP, CMR and Flaximax packing. These packings have a higher efficiency, and therefore they have become more popular for new projects of the packed columns today. However, for the traditional packing, according to the author, only correlations of Cornell [21], Onda [22] and Bravo and Fair [17] can give reliable information for the industrial use in both distillation and absorption processes. The derived theoretical relation is described as:

$$HETP = H_O \cdot \frac{\ln \lambda}{\lambda - 1}, \tag{9}$$

where:

H_O – height of a global mass transfer, m;

λ – inclination ratio between the equilibrium and operation line.

Although the above equation was validated only for the cases of dilute solutions, constant molar flow rates, binary systems and equimolar countercurrent diffusion, it has been applied to systems with very different conditions even for multicomponent systems [5].

Henriques de Brito and his co-workers [23] measured the effective interfacial area of sheet metal structured packings, such as Mellapak 125Y, 250Y and 500Y. Their results have demonstrated that the effective area can be much higher than the packing surface area due to instabilities in liquid flow, such as ripples, waves, etc.

The resulting correlation for all measurements as a function of the Reynolds number for liquid phase is as follows:

$$\frac{a_e}{a_p} = 0.465 \cdot Re_L^{0.3}, \tag{10}$$

where:

Re_L – Reynolds number for liquid phase.

It should be noted that the authors have not checked the correlation with fluids with different densities and viscosities of a liquid. Moreover, none of the aforementioned correlations examined the influence of the vapour flow; consequently, these dependences can be used only at the low velocities of the vapour phase.

3. The difficulties in determination of actual mass-transfer surface

Based on experimental data, many researchers define the mass-transfer coefficients fast enough, inasmuch as, if nozzle surface equals mass-transfer surface, then they present a single unknown in the mass-transfer equations.

$$M = K_V \cdot F_H \cdot \Delta_S, \tag{11}$$

where:

K_V – mass-output coefficient, (kg mol)/(m^2 s);
F_H – packing surface area, m^2;
Δ_s – driving force (an average concentration gradient).

In tray columns and columns with vortex nozzles, while changing both the vapour velocity and the irrigation density, the alteration of two parameters (effective surface area and mass-transfer coefficients) in the mass-transfer equations occurs. Consequently, it is impossible to carry out the tray efficiency calculations by equations 8 and 10, in which we need to know both of the parameters. Thus, the efficiency for these mass-transfer devices is to be calculated either by determining the volumetric mass-transfer coefficients or in the terms of hydrodynamic characteristics of the vapour and liquid phases [19].

$$1-\eta_T = e^{\frac{-K_{oy}\cdot a\cdot f\cdot H}{V}} = e^{-N_{oy}}, \tag{12}$$

where:

f – cross-sectional area, m^2;
N_{oy} – number of transfer units;
H – height of the contact area, m;
($K_{oy}\cdot a$) – volumetric mass-transfer coefficient.

The equation (12) shows that the height of transfer unit can be found, on condition that the value of volumetric mass-transfer coefficient is well-known.

The most interesting approach for determining the efficiency of mass-transfer device has been proposed in the work of Kafarov V. V. [9], where an empirical dependence of overall column efficiency was obtained by means of processing a large amount of data taken from the industrial bubble plate rectification columns.

$$\lg\eta = 1.67 + 0.3\cdot l\cdot g\cdot\left(\frac{L}{V}\right) - 0.25\cdot\lg(\mu_L\cdot\alpha) + 0.3\cdot h_L, \tag{13}$$

where:

L, V – vapour and liquid load, (kg mol)/h;
μ_L – liquid viscosity, (Pa s);
α – relative volatility;
h_L – length from upper end of cut to upper end of weir height plus half length of cut, m.

4. The directions of intensification and energy- and resource conservation of rectification processes

Besides the criteria of efficiency of the packed columns, great interest is presented by the directions of intensification and energy- and resource conservation of rectification processes.

Three directions, which are developed currently by domestic and abroad scientists, should be mentioned:

1. The works concerned with the minimisation of the reflux ratio. These investigations are intensively conducted in Russia under the direction of Serafimov L. A. [24, 25, 26].
2. The researches under Kulov N. N., directed to the development of combined reactive-catalytic processes and distillation processes combined with the processes of crystallisation. The implementation of these processes allows to decrease the external dimensions of equipment and power inputs. The combined processes of catalytic rectification enable to overpass the thermodynamic limitations in equilibrium reactions and to use the heat from exothermic reactions for the separation of the resulting mixtures [27, 28, 29].
3. The works concerned with the development and investigation of the new mass-transfer devices, which allow to essentially increase the rates and accordingly – the mass- and heat-transfer coefficients [8, 10, 11].

This work belongs to the latter direction, as we propose to apply the established by us dependence of transfer unit efficiency of the new packet vortex nozzle on the Reynolds number for the vapour and liquid phases.

The packet bed of this nozzle represents a set of cells combined with each other in the horizontal plane. In contrast with the existing packings, the created nozzle has more developped nonlinear surfaces, which provide the formation of a large quantity of drops on the film surface at vapour velocities of more than 2 m/s. Unlike the packings, which work in the thin-film mode, this nozzle works in the near-emulsive regime, where the mass-transfer surface is much higher than the geometric nozzle surface at the range vapour velocity from 2 to 5.5 m/s and values of the irrigation density of over 120 m^3/m^2s. The vortex nozzle possesses a quality of self-distribution of liquid phase on the column cross section even by feeding by a single jet on the nozzle surface.

The high velocities in the vapour and liquid phases as well as extremely high mass- and heat-transfer coefficients in the volume unit of a nozzle allow essential decreasing of external sizes of rectification columns at a high quality and efficiency of continuous processes.

The processing of experimental data based on the alteration of vapour velocities and flow rates at the column length permitted to derive an explicit form for the efficiency of conditional plate (or packed bed) of the packet vortex nozzle, which depends on the vapour and liquid according to Reynolds criteria; the irrigation density was changed in the range from $0.6 \cdot 10^{-3}$ to $1.4 \cdot 10^{-3}$ m^3/m^2s and the vapour velocity – from 1.2 to 3.5 m/s.

$$\eta_i = 4.5 \cdot 10^{-3} \cdot Re_{iL}^{0.5} \cdot Re_{iV}^{0.72} \tag{14}$$

$$Re_{iL} = \frac{V_{iL} \cdot b \cdot \rho_{iL}}{\mu_{iL}} \tag{15}$$

$$Re_{iV} = \frac{V_{iV} \cdot b \cdot \rho_{iV}}{\mu_{iV}} \tag{16}$$

where:

V – irrigation density, m^3/m^2s;
b – width of a cell in a packet vortex nozzle, m;
ρ_L, ρ_V – vapour and liquid density, kg/m^3;
μ_L, μ_V – vapour and liquid dynamic viscosity, (Pa s);
U_V – vapour velocity, m/s.

5. Conclusion

Literary data analysis shows that the commonly used Murphree efficiency factor can be applied for evaluating the efficiency of the rectification columns with binary mixtures. Besides, it is necessary to know or experimentally determine the concentration of a volatile component on each tray for calculating the Murphree factor.

In turn, for calculating the efficiency of the packed columns, which work in the film mode, knowledge of mass-transfer coefficients and specific contact surface is required. The latter is discussed in a large number of works, in which, according to some foreign studies, the value of the interface area is substantially smaller than the value of the geometric nozzle surface. This is why the calculation of the actual mass-transfer surface is rather difficult even for the nozzles, which work in the film mode.

Due to the fact that for the plate rectification columns and columns with the mass-transfer devices one can't clearly determine the actual mass-transfer surface, the efficiency of the mass transfer devices is to be calculated, either by determining the volumetric mass transfer coefficients or the hydrodynamic characteristics of the vapour and liquid phases, which depend on the structural design of plates or vortex nozzles.

References

[1] Langdon W. M., Keyes D. B., *Vapour-Liquid Equilibrium Data on Ethyl Alcohol–Water and on Isopropyl Alcohol–Water*, Ind. Eng. Chern., vol. 35(4), 1943, 464-469.
[2] Fane A. G., Sawistowski H., *Plate Efficiency in the Foam and Spray Regimes of Sieve plate Distillation*, IChemE Symposium Series №32, 1969, 8-19.
[3] Lockett M. J., Uddin, M. S., *Liquid-phase controlled mass transfer in froths on sieve trays*, Trans. Instn. Chern. Eng., vol. 58(3), 1980, 166-174.
[4] Pigford R. L., Tepe J. B., Garrahan C. J., *Effect of Column Holdup in Batch Distillation*, Ind. Eng. Chern.,vol. 43(11), 1951, 2592-2602.
[5] Ellis S. R. M., Hardwick M. J., *Effect of reflux ratio on plate efficiency*, IChemE Symposium Series №32, 1969, 29-37.
[6] Barker P. E., Choudhury M. H., *Performance of Bubble cap Trays*, British Chemical Engineering, vol. 14, 1959, 348.
[7] Shilling G. D., Beyer G. H., Watson C. C., *Bubble-plate Efficiencies in Ethanol-water Fractionation*, Chern. Engng. Prog. vol. 49(3), 1953, 128-134.

[8] Kagan A. M., Laptev A. G., Pushnov A. S., Farahov M. I., *Contact packings of industrial heat and mass transfer apparatuses*, Otechestvo, Kazan 2013.
[9] Kafarov V. V. *The Foundations of Mass-transfer*, Vysshaja shkola, 1972.
[10] Blinichev V. N., Chagin O. V., Krawczyk J., Kutepov A. M. *Packet vortex nozzle for heat and mass transfer apparatuses*, Patent 2205063 РФ // Б.И. 2003. № 15.
[11] Blinichev V. N., Chagin O. V., Kutepov A. M. *Packet vortex nozzle of nonmetallic materials*, Patent 2130536 РФ // Б.И. 2001. № 11.
[12] Voroshin A. V., Chagin O. V., Blinichev V. N., *Description of the distillation process in the column with packet vortex nozzle*, Proceedings of XXV International Scientific Conference «MMTT», Saratov, 2, 2012, 91.
[13] Henley, E. J., Seader, J. D., *Equilibrium-stage separation*, John Wiley & Sons Inc., New York 1981.
[14] Polanski A. V., Blinichev V. N., Chagin O. V., *Rectification Column: Criteria of Efficiency*, Izvestiya Vysshikh Uchebnykh Zavedeniy, Seriya *Khimiya I Khimicheskaya Tekhnologiya*, tom 59(1), 2016.
[15] Caldas, J. N., de Lacerda, A. I., *Torres Recheadas*, JR Ed. Tecnica, Rio de Janeiro 1988.
[16] Lockett, M. J., *Easily predict structured-packing HETP*, Chemical Engineering Progress, vol. 94(1), 1988, 60.
[17] Bravo, J. L., Fair, J. R., *Generalized correlation for mass transfer in packed distillation columns*, Ind. Eng. Chem. Proc. Des. Dev., vol. 21(1), 1982, 162.
[18] Wang, G. Q., Yuan, X. G., Yu, K., *Review of Mass-Transfer Correlations for Packed Columns*, Ind. Eng. Chem. Res., vol. 44(23), 2005, 8715.
[19] Laptev A. G., Elizarov V. I., Dyakonov S. G. *Determination of volumetric mass transfer coefficients in the gas-liquid layer on the industrial scale contact devices at the transition* (*sieve and jet plates*), Izvestiya Vysshikh Uchebnykh Zavedeniy, Seriya *Khimiya i Khimicheskaya Tekhnologiya*, tom 34(1), 1991.
[20] Wagner, I., Stichlmair, J., Fair, J. R., *Mass transfer in beds of modern, high-efficiency random packings*, Ind. Eng.Chem. Res., vol. 36(1), 1997, 227.
[21] Cornell D., Knapp W. G., Close H. J., Fair J. R., *Mass-transfer efficiency-packed columns*, Chem. Eng. Progr., vol. 56(8), 1960, 48.
[22] Onda K., Takeuchi H., Okumoto Y., *Mass transfer coefficients between gas and liquid phases in packed columns*, J. Chem. Eng. Japan, vol. 1(1), 1968, 56.
[23] Henriques de Brito M., von Stockar U., Menendez Bangerter A., Laso M., *Effective Mass-Transfer Area in a Pilot Plant Column Equipped with Structured Packings and with Ceramic Rings*, Ind. Eng. Chem. Res., vol. 33(3), 1994, 647.
[24] Danilov R. Yu., Petlyuk F. B., Serafimov L. A., *Minimum-reflux regime of simple distillation columns*, Theor. Found. Chem. Eng., vol. 41(4), 2007, 371.
[25] Serafimov L. A., Chelyuskina T. V., Mavletkulova P. O., *Special cases of determination of the minimum reflux ratio for distillation of binary mixtures*, Theor. Found. Chem. Eng., vol. 47(3), 2013, 231.
[26] Serafimov L. A., Chelyuskina T. V., Mavletkulova P. O., *Special distillation regime involving an infinite reflux ratio and an infinite number of separation stages*, Theor. Found. Chem. Eng., vol. 48(1), 2014, 48.
[27] Kulov N. N., *Some problems of separation of mixtures*, Theor. Found. Chem. Eng., vol. 41(1), 2007, 1.

[29] Myasnikov S. K., Uteshinsky A. D., Kulov N. N., *Hybrid separation processes combining vacuum distillation with fractional crystallization, partial melting, and granulation*, Theor. Found.Chem. Eng., vol. 43(3), 2009, 227.
[30] Pavlov O. S., Pavlov S. Yu., Kulov N. N., *New design of reactive distillation processes*, Theor. Found. Chem. Eng., vol. 43(6), 2009, 856.

TECHNICAL TRANSACTIONS | CZASOPISMO TECHNICZNE
MECHANICS | MECHANIKA
2-M/2016

VALERIAN BLINICHEV, IRINA POSTNIKOVA*, JANUSZ KRAWCZYK**

IMPROVEMENT OF THE MASS TRANSFER PROCESSES EFFICIENCY BY MEANS OF MECHANICAL ACTIVATION OF HOMOGENEOUS AND HETEROGENEOUS SYSTEMS

POPRAWA WYDAJNOŚCI PROCESÓW WYMIANY MASY POPRZEZ MECHANICZNĄ AKTYWACJĘ UKŁADÓW JEDNORODNYCH I NIEJEDNORODNYCH

Abstract

In this paper, the ways of intensification of technological processes by means of powerful short pulses of energy in activation machines in solid phase and water systems are considered. The mechanism of accumulation and relaxation of energy for the substances subjected to mechanical activation is shown.

Keywords: intensification, mechanical activation, rotary apparatus, cavitation, accumulation of energy, relaxation.

Streszczenie

W pracy omówione zostały metody intensyfikacji procesów technologicznych w ciałach stałych i cieczach przy użyciu krótkotrwałych impulsów energetycznych. Przedstawiono mechanizmy akumulacji i relaksacji energii w substancjach poddanych mechanicznej aktywacji.

Słowa kluczowe: intensyfikacja, mechaniczna aktywacja, maszyny wirnikowe, kawitacja, akumulacja energii, relaksacja.

DOI:

* Prof. PhD. DSc. Eng. Valerian Blinichev, PhD. DSc. Eng. Irina Postnikova, Department of Machines and Apparatuses of Chemical Productions, Faculty of Chemical Engineering and Cybernetics, Ivanovo State University of Chemistry and Technology.

** PhD. DSc. Eng. Janusz Krawczyk, Prof. CUT, Institute of Thermal and Process Engineering, Faculty of Mechanical Engineering, Cracow University of Technology.

Changes of the physico-chemical properties of solid materials under the influence of mechanical strain had attracted the interest of many researchers from various countries, even at the beginning of the last century.

However, in the sixties and seventies of the last century, a new branch of science – mechanochemistry, appeared, the fundamentals of which were formulated by V. V. Boldyrev, Director of the Novosibirsk Institute of Solid State Chemistry and Mechanochemistry of the Russian Academy of Sciences [1], and by P.U.Butyagin (The Institute of IHF of RAS) [3, 4].

Previously, the tribochemistry concept, developed by P.Tissen and G. Hajnike, preceded the science of "Mechanochemistry" [2].

In the works of P. U. Butyagin and V. V. Boldyrev, it was demonstrated that the new surface formation, when the hard crystalline substances are destructed, is accompanied by a range of physico-chemical phenomena [1, 3, 4], such as:

a) electronic emission of various intensity;
b) luminescence;
c) formation of excess surface energy on the new surfaces and emerging of electric charges and fields due to the bombardment of the surfaces by high-energy electrons;
g) generation of radio waves and x-rays emission;
d) thermo-radiation and accumulation of energy in the form of the elevated temperature of a solid;
e) formation of free radicals on the surface, especially on polymeric materials [10].

It has been previously noted [1, 5, 6, 7] that, as any grinding apparatus or machine is a kind of mechanoactivator, then in order to apply the activated substances for intensifying a particular technology, it is necessary for the amount of accumulated energy in it (before application) to be greater than the energy released in the course of the relaxation process.

Naturally, the greatest effect is achieved when the technological process is carried out in the activating machine.

The list of chemical reactions being carried out in the mills of small dimensions (ball, vibration, ring and centrifugal planetary ones) covers different classes of reactions, which have been studied.

The solid – gas reaction includes synthesis of nitrides, hydrides, and carbonyls [6].

Gases (nitrogen, hydrogen, carbon monoxide) react with metals and oxides.

In the system of Solid 1 + Solid 2, carbides, borides, silicides were synthesised, and a reduction of metals oxides was performed; synthesis of ferrites, catalysts of superconducting ceramics, of new composite construction materials [5, 6, 7] was carried out. Experiments on the mechanochemical process of carbonate decomposition, which stayed for quite a long time in the centrifugal planetary mill, were performed [5].

It should be noted that mechanochemical synthesis was carried out mainly in laboratory high-energy centrifugal planetary ball mills, in which the ratio of centrifugal forces to the force of gravity was: $\Phi = \frac{\omega^2 \cdot r}{g} > 80$

A way for project solution scaling for this types of mills is extremely complex due to large stresses at the machine nodes ($\sigma_{max} > [\sigma]$) when the productivity is $Y_m > 100$ kg/h. So, despite studies relating to the early 70-s of the 20th century, no industrial technology with

their application has yet been implemented, besides of the manufacture of small batches of some products.

In this context, a study of the influence of the strain rate on the intensity of mechanical activation of solids, aimed at further application of the continuously operated machines (mills) with a high speed impact loading, excluding the balls, their grinding and housing fretting, is of great interest. Under these conditions, the activated particles obtain multiple pulse loading, in which the occurring maximum voltages are greater than σ – beyond the limit of their strength.

At ISUCT (Department of Machines and Apparatuses of Chemical Productions), Bobkov S. P. and Blinichev V. N. [11] performed studies on grinding various materials in mills with different constructive designs. The share of energy spent on the formation of a new surface, for releasing thermal energy and for accumulating energy of a grinded body, was measured. These studies revealed that while being ground, the solids accumulate in them significantly greater amount of energy in comparison with the energy spent on the formation of a new surface.

The greatest amount of the accumulated energy (up to 40% of the fed one) was observed in polymer materials, in particular, made of Teflon: the thermal energy was not taken into account – it was measured and then deducted from the total amount of energy absorbed by a solid.

Precise measurement of the surface particles before and after grinding allowed to determine the energy value for a newly formed surface, if the specific surface energy is known (for certain substances). These studies have shown that for the majority of grinded substances (such as NaCl, limestone, Teflon), the value of the accumulated energy is ten times greater than the energy value of the newly formed surface.

It has been established that the amount of energy accumulated by a solid greatly depends on the rate of its strain and can be written as follows [11]:

$$\frac{\mathrm{d}E_{м}}{\mathrm{d}t} = \lambda \cdot \upsilon_{\varepsilon}^{2} \tag{1}$$

where:

$E_{м}$ – is the energy being absorbed;

υ_{ε} – rate of material strain;

λ – (constant) proportionality depending on the physical and mechanical properties of the activated material and on the ability to absorb the energy supplied.

From equation (1), it can be seen that the accumulated energy is proportional to the square of the strain rate.

The kinetics of the active state relaxation is proportional to the quantity of the energy accumulated:

$$\frac{\mathrm{d}E_{м}}{\mathrm{d}t} = -\mathrm{const}E_{м} \tag{2}$$

With multiple pulse loading, such as impact loading, (in collaboration with Bobkov S. P., Padokhin V. A., and Zueva G. A.) the following stochastic equation was derived

by us, which takes into account both the processes of accumulation and dissipation of energy:

$$\frac{\mathrm{d}E(t)}{\mathrm{d}t} = \alpha_c \sum_{i=0}^{i=n} A_i \cdot \delta(t - t_i) + \alpha_c \cdot E(t) \tag{3}$$

where:

$E(t)$ – the accumulated energy;

α_c – a coefficient that depends on the physical and mechanical properties of the material;

t_i – the time of the i-th act of the pulse loading;

A_i – power provided by a single (individual) impact pulse (*amplitude*), which is considered as an independent random variable.

Solution of the differential equation (3), which takes into account the cumulative and relaxation processes occurring when initially provided that $E = E_0$ at $t = 0$, is as follows:

$$E(t) = \alpha_c \cdot \sum_{i=0}^{i=n} A_i \exp\left[-\alpha_c (t - t_1)\right] + E_0 \exp(-\alpha_c \cdot t) \tag{4}$$

The analysis of the given equation demonstrates that between Delta-pulses (i.e. the acts of the particle impact loading) the energy $E(t)$ smoothly exponentially decreases, and at the moment of impact loading with A_1 energy, it rises abruptly at the value of A_i $\alpha_c \cdot A_i$.

Considering a short time lapse between the high-speed impact loadings in multi-staged mills (stress rate is very high, impact loadings are numerous, and the particles stay in a machine for 3.5 ÷ 5 seconds), the quantity of the energy accumulated in these types of mills appeared to be the greatest, despite the fact that the time of staying them in a ball, vibration and centrifugal-planetary mills was 20 minutes.

Therefore, while grinding hard materials, not only an external new active surface is created, but also active centres within the particles in the form of micro- and macrodefects as well as concentration energy centres around them. The latter significantly increase the reactivity of the subsequent relaxation processes.

Given the heavy dependence of the accumulated energy on the stress rate, we performed all the researches on mechanical activation of solids in the installations with multiple impact loading rates ranging from 75 to 180 m/s, depending on the physico-mechanical properties of the activated material, with the productivity of solid material of more than 250 kg/h.

In collaboration with Fedosov S. V., by applying high strain rates, we managed to realise a combined process: grinding and drying of large PVC sintered particles, in a 3-speed mill of impact-radiant type with the following initial parameters: initial humidity – 38%, the terminal one – less than 0.5%; the initial size of the sintered particles – 10 ÷ 50 mm, the final one – 250 microns, the time of staying particles in the mill – 10 seconds, the productivity of a machine in the workshop for PVC production is 250 kg/h.

Our joint studies with Ladaev N. M, aimed at removal of moisture from capillary-porous single particles by the impact with different strain rate, revealed that when the rate of impact loading is more than 45 m/s with a single impact of the particles with a diameter

of 5 mm, and initial humidity is 40%, the particle loses up to 30% per cent of its humidity, even without its destruction, due to inertial forces and waves of the elastic strain.

All these results prove that in cases when it is necessary to obtain dry and fine powder, it is necessary to combine the process of drying and milling, as 70 ÷ 98 % of the supplied energy is converted into thermal energy (internal pulse heat source), and inner diffusion moisture turns into surface moisture, which evaporates easily.

Another example of energy accumulation in polymers in the process of their milling is mechanochemical synthesis of fluorine rubber when Teflon and rubber are jointly milled in our multi-staged impact radiant mill implemented at Saint-Petersburg "Giproplast" plant with the productivity of 250 kg/h.

Totally inert to many PTFE systems, Teflon forms, in the process of joint milling, chemical bonds with rubber due to the energy accumulated in it as microdefects and radicals if a good mixing of the components and multiple impact loadings are provided. Thus, fluorine rubbers were synthesised, which otherwise could not be obtained.

High efficient mechanical activation of solids was achieved by means of their multiple high-rate impact loading in the multi-staged mills of continuous action (Fig. 1) at the Department of “Machines and Apparatuses of Chemical Productions” at ISUCT (with an average time of staying in the mill of less than 10 c) when the process of manufacturing new composite materials based on Teflon and coke was performed, the productivity of the raw materials mixture being 300 ÷ 350 kg/h. Both components were continuously supplied as doses into the mill in the predetermined ratios of fluorine (initial average size of the particles – 1 mm) and coke (average size – 0.25 mm), the ratio of PTFE being: coke – 70:30, 60:40.

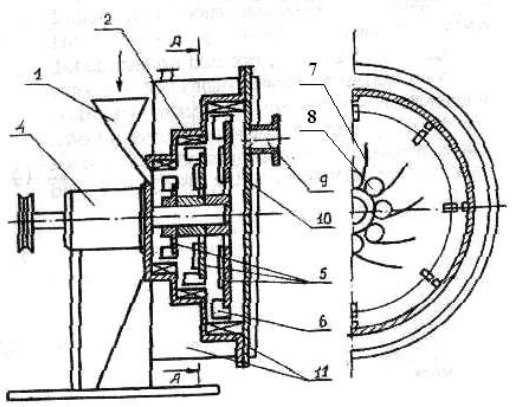

Fig. 1. Multistage continuous mill
1 – loading fitting; 2 – mill housing ; 3 – baffle plates; 4 – shaft; 5 – rotor; 6 – beater; 7 – blades; 8 – holes; 9 – unloading choke; 10 – flange; 11 – cooling jacket

A number of combined processes was carried out in the mill: mixing in powerful turbulent whirlwinds, which were created by the rotor blades and stator bumpers (of a mill housing); the additional pulse milling and mechanical activation of the components. Sintered compositions enabled to create new antifriction materials (FC-30 and FC-40), advantageously differing from the source material (Teflon).

The strength of the new composite materials has increased more than three times (compared with FC-20, which was obtained by means of conventional mixing of powders). Friction coefficient decreased by 2.5 times, and the cost dropped proportionally to the coke content as a cheap raw material.

Technology and equipment were implemented at the Kirovo-Chepetsk chemical plant.

Another example of a large accumulation of energy in repeated high-rate impact loading is ignition of the graphite milled in a multi-staged mill of an impact-radiant type [8].

While testing the optimal operating mode for the impact-radiant separation mill aimed at milling graphite from the Zaval′evsk deposits by means of an industrial machine, designed and constructed by us for Voskressensk Chemical Plant in order to maximise the number of particles of the product with the size less than 1 μm already at the stage of dry grinding, we managed to obtain the product with the particle content 25% less than 1 μm.

Having selected a probe for granulometric composition, we left 30 kg of the product in the cyclone hopper, the temperature in which reached 55^0 C. Within an hour, the product left in the hopper burnt down.

For industrial technology of fine graphite milling by means of CWC, we had to reduce the rate of impact loading in dry grinding mill and to obtain colloidal graphite product with 95% content of particles with dimensions of less than 1μm already in colloid-cavitational wet grinding mill [9], presented in Fig. 2.

Similarly mechanoactivation with pulse energy supply proceeds in liquid media, but only at greater velocity of relaxation processes.

In the works of several authors [12 ÷ 16] and in our works, it has been shown that the greatest effect is observed in water, suspensions and emulsions activation, when they are treated in rotary machines of various constructive design (see Fig. 2) in which a powerful pulse voltage arising because of the burst of cavitation bubbles overlaps with shear stress in a narrow annular gap between the rotor and the stator. Cavitation occurs in the fluid due to pressure pulsations and changes in the fluid flow rate.

Academician Dolynsky A. A. [17, 18], while studying fluid systems activation in rotary-pulsation apparatus, showed that periodic bursts of cavitation bubbles create powerful energetic discrete-pulse energy inputs in fluid systems in the nanoscale, and this process results in significant changes in their structure.

Studies on water and fluid systems activation were conducted by various authors on rotary machines, the basic schemes of which are presented in Fig. 2.

Despite somewhat different constructive features of rotary activators, for all of them, a major trigger factor is the discrete energy input in the form of *cumulative* flow when the cavitation bubbles burst. The frequency of bubbles occurring and bursting depends on constructive features of rotors and stators, as wells on rotors rotation frequency.

In our studies on water treatment of various origin (distilled, tap water and artesian) in rotary cavitators of types (a) and (b) (Fig. 2), it is shown that owing to the number of revolutions in the rotor cavitator and, accordingly, to the intensity of the cavitation impact, only the measured values of redox potential (ORP) increase significantly (Fig. 3); water pH increases insignificantly.

The value of ORP in relaxation process within a few days reduces; however, the level of steady-state values of the AFP remains higher compared to its initial value.

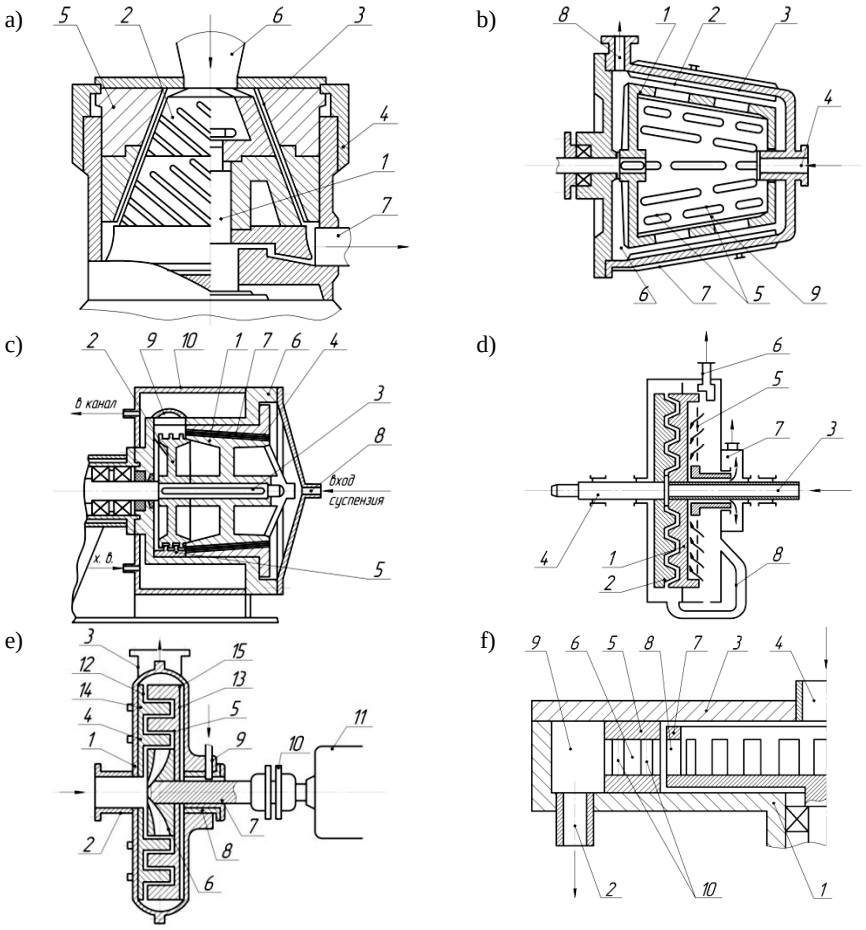

Fig. 2. Scheme of activators

a) Cone Colloid Mill Activator (1 – shaft; 2 – rotor; 3 – ribs; 4 – housing; 5 – stator; 6 – suspension inlet);
b) Colloid Mill Activator with the Perforated Rotor (1 – rotor; 2 – baffles; 3 – housing; 4 – suspension inlet; 5 – perforations; 6 – suspension unloading zone; 7 – jacket ; 8 – suspension outlet);
c) Cavitation-Colloid Mill Activator (1 – rotor; 2 – impact device; 3 – shaft; 4 – stator; 5 – counter-baffles; 6 – housing; 7 – grooves; 8 – suspension inlet; 9 – suspension outlet; 10 – cooling jacket);
d) Colloid Activator with Two Rotating Rotors and Separation of the Activated Solid Phase (1 – rotating hollow shaft rotor; 2 – rotating rotor; 3 – hollow shaft; 4 – shaft; 5 – separator; 6 –outlet of coarse particles; 7 – fine particles outlet);
e) Rotary Hydraulic Mill (1 – housing; 2 – inlet fitting; 3 – suspension outlet fitting; 4 – fixed disc; 5 – movable disc; 6 – rotor; 7 – shaft; 10 – shaft coupling; 11 – coupling drive; 12, 13 – grooves; 14, 15 – protrusions);
f) Rotary RPA Apparatus (1 – housing; 2 – suspension outlet fitting; 3 – cover; 4 – inlet fitting; 5 – stator; 6 – stator channels; 7 – rotor; 8 – rotor channels; 9 – voice camera; 10 – rods).

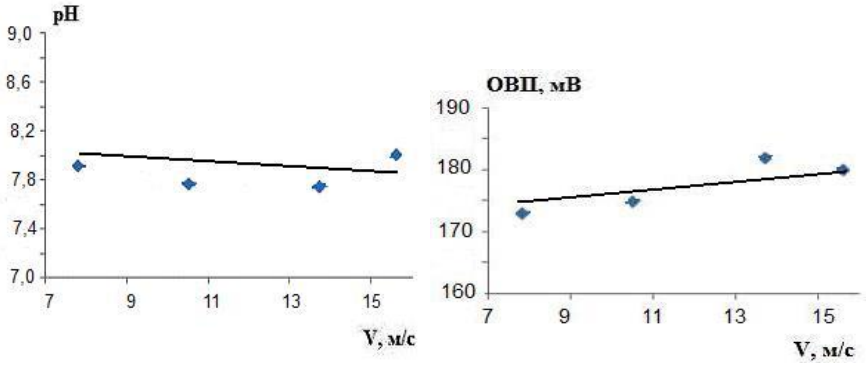

Fig. 3. Dependence of pH and ORP on the linear speed of rotor in the activator

In order to prove that cavitation bubbles do arise and burst in the cavitators, sensors were attached to the housing of the rotor. They allowed to register housing vibration when cavitation bubbles “exploded". Firstly, the housing vibrations of the idle activator operation were registered, and then those in the working mode (see Fig. 4).

From the plot (3) (Fig. 4,) it is clearly seen that when water passes through the activator, high frequency spectrum of additional pressure pulses from the cavitation bubbles bursts appear.

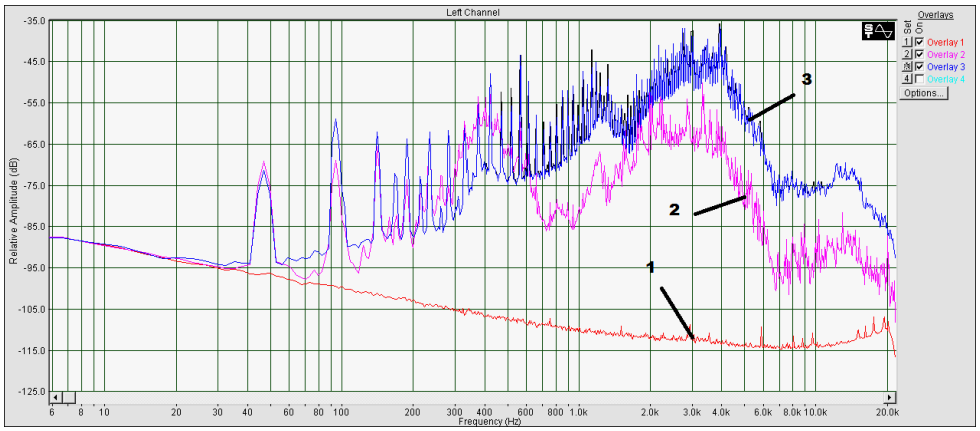

Fig. 4. Fourier spectrum in water treatment (water consumption is 1.44 m^3/h)
1 – background noise, 2 – spectrum of idle mode, 3 – spectrum of fluctuations in operating mode

The same phenomenon is observed when suspension passes through the cavitation device. In earlier works, it has been shown that if the fluid contains solid phase particles, the cavitation bubbles are formed and burst exactly on the moving hard particles.

A powerful pulse of energy, supplied to the hard particles when a bubble bursts, is the very "hammer" which destroys even small particles of solid materials. It is known that the

strength of many materials depends on the particle size, and when the latter reaches a monocrystal size, it increases by two orders of magnitude.

Therefore, when designing the construction of cavitation colloid mill for superfine milling of graphite (95% of the particles should have dimensions less than 1 micron), we have tested about a dozen of different machines constructions with a view of elaborating a cavitator, which would provide the conditions for forming and bursting the maximum number of cavitation bubbles.

The researches that we have jointly conducted with the staff of the Ivanovo Medical Academy and aimed at activation of two licensed drugs for treating diseases of joints (*Tomed and Tomed-Aqua*) in rotary cavitators of type (a) (Fig. 2), showed that death intensity of the various types of bacteria increases significantly, and efficiency of drugs application for treating these diseases (according to medical clinics data for the last 2 years) is growing.

Under the supervision of S. V. Fedosov, T. E. Slizneva (Ivanovo State Polytechnic University) undertook the studies of activation process in rotary-pulsation apparatus in a magnetic field of water solutions of electrolytes [19, 20]. It was shown that their mechano-magnetic treatment contributes to the enhancement of frost resistance of fine-grained concrete for 40 ÷ 50 cycles and provides the increase of the rate of curing at the early stages of hardening and elongation of beginning of setting along with reduction of its finishing, as well as results in enhancing the strength by 15 ÷ 22% compared to the concrete obtained by means of traditional technology. Application of mechano-magnetic activation of liquid mixing allows to save up to 10% of cement.

Mechano-magnetic activation of tempered water containing organic plasticising and water-reducing organic additives promotes mobility of the concrete mixture by up to 100% during 1,5 ÷ 2 hours, i.e. 1.2 ÷ 2.4 times more in comparison with not activated water systems.

Taking into consideration the above-mentioned information, we can conclude that impact pulse loading with a larger momentum energy of solids and water systems allows to intensify significantly many of the heat- and mass-transfer processes, including chemical reactions.

References

[1] Boldyrev W. W., *Eksperimentalnye metody w mehanohimii tberdyh neorganiceskih wescestw*, Nauka, Novosibirsk 1986.

[2] Thiessen P., Meyer K., Heinike Y., *Grundladen der Tribochemie*, Abd. Detsch. Acad. Wiss. Berlin Kl Chem., Ged. Bid., vol. 1, 1966., 194.

[3] Butagin P. U., Kinetika i priroda mehanohimiceskih reakcji, Uspiehi himii, vol. 40, 1971, 1935-1959.

[4] Butagin P. U., Uspiehi himii, vol, 31, 1984, 544-600.

[5] Avvakumov E. G., *Mehaniceskie metody aktivacii himiceskih processov*, Nauka, Novosibirsk 1986.

[6] Avvakumov E. G., Kosova N. U., Senna M., *Magkij mehanohimiceskij sintez – osnova novyh himiceskih tehnologij*, Nauka, Novosibirsk 2000.

[7] Sirokov U. G., *Mehanohimia i tehnologii katalizatorov*, Ivanovo 2005.
[8] Blinicev W. N. and all., *Mnogostupiencataa melnica udarnogo dejstvia*, A.c. № 946651, CCCP 1982.
[9] Blinicev W. N. and all., *Koloidnaa mielnica*, A.c. № 651841, CCCP 1971.
[10] Barambojm N. K., Mehanohimia bysokomolekularnyh soedinenij, Himia, 1971.
[11] Bobkov S. P., Blinicev W. N., Guumdzan P.P., *Wlianie tipa melnicy na energozatraty i mehanohimiceskie avlenia pri tonkom izmelcenii*, Himia i Himic. Tehnologia, vol. 22(3), 1979, 1004-1007.
[12] Balabudkin M. A., *Rotorno-pulsacionnye aparaty v himiko-farmacevticeskoj promyslennosti*, Medicina 1983.
[13] Balabusko A. M., *Rotornye apparaty s modulaciej potoka i ih primenenie v promyslennosti*, Nedra 1992.
[14] Zimin A. I., *Prikladnaa mehanika prerevistyh tecenij*, Foliant 1997.
[15] Promtov M. A., *Pulsacionnye aparaty rotornogo tipa: teoria i praktika*, Masinostroenie, 2001.
[16] Cervakov V. M., Udaev V. F., *Gidrvliceskie i kavitacionnye avlenia v rotornyh apparatah*, Masinostroenie, 2007
[17] Dolinskij A. A., *Nanomasstabnye efekty pri diskretno-impulsnoj transformacii energii*, Inzenerno-fiz. Zurnal, vol. 78(1), 2005, 15-22.
[18] Dolinskij A. A., *Teploobmen i gidrodinamika v parozidkostnyh dipersnyh sredah. Teplofizyceskie osnowy diskretno-impulsnogo vvoda energii*, Nukova dumka, 2008.
[19] Fedosov S. V., Akulova M. V., Slizneva T. E., *Opredelenie tehnologiceskih parametrov mehanomagnitnoj obrabotki vodnyh system s plastifiriuscej dobavkoj*, Stoitelnye materialy, vol. 3, 2010, 49-51.
[20] Fedosov S. V., *Mehanomagnitnaa aktivacia vodnyh rastworov himiceskih dobavok kak sposób modificirovania mielkozernistogo betona*, Himia i Himic. Tehnologia, vol. 57(3), 2014, 111-115.

TECHNICAL TRANSACTIONS | CZASOPISMO TECHNICZNE
MECHANICS | MECHANIKA
2-M/2016

ANETA CELAREK, JAN TALAGA*

A COMPARATIVE ANALYSIS METHODOLOGY OF CALCULATION OF STRENGTH TUBESHEETS BY EUROPEAN STANDARDS AND GUIDELINES FOR UDT

ANALIZA PORÓWNAWCZA METODYKI OBLICZEŃ WYTRZYMAŁOŚCIOWYCH ŚCIAN SITOWYCH WEDŁUG NORM EUROPEJSKICH I WYTYCZNYCH UDT

A b s t r a c t

This paper presents comparison of calculation methods of the required thickness of the tube sheet in the shell and tube heat exchanger compatible with the standards of the European standard PN - EN 13445-3, and the guidelines of the Polish Office of Technical Inspection (UDT). Details of the methods are illustrated by numerical examples – (calculations) for the selected design of the tubesheet.

Keywords: heat exchangers, tubes, tubesheets

S t r e s z c z e n i e

W artykule przedstawiono porównanie metod obliczeniowych wymaganej grubości ściany sitowej w płaszczowo-rurkowym wymienniku ciepła zgodnych ze standardami normy europejskiej PN-EN 13445-3 i wytycznymi polskiego Urzędu Dozoru Technicznego. Szczegóły metod zilustrowano przykładami liczbowymi dla wybranych konstrukcji dna sitowego.

Słowa kluczowe: wymienniki ciepła, rurki, dna sitowe

DOI:

* MSc. Eng. Aneta Celarek, DSc. Eng. Jan Talaga, Institute of Thermal and Process Engineering, Faculty of Mechanical Engineering, Cracow University of Technology.

1. Introduction

The European standard PN-EN 13445-3 shows three primary distinctions in terms of shell and tube heat exchangers. In addition to the above standard PN-EN 13445-3 is Index I, wherein it shows another design solution of a tubesheet. The analysis of strength calculations for the same configurations of tubesheet differs from those described in the Polish guidelines WUDT-UC. Polish guidelines WUDT-UC are treated as mandatory during the design of pressure equipment.

In the norm PN-EN 13445-3: 2002, rules for different types of heat exchangers were shown. According to the norm:

- U-tube heat exchanger (Figure 1);
- Fixed tubesheet heat exchanger (Figure 2);
- Floating head heat exchanger (Figure 3).

Floating head heat exchanger has three different configurations:

a) with an immersed floating head;
b) with an externally sealed floating head;
c) with an internally sealed floating tubesheet [3].

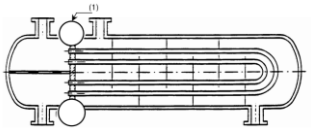

Fig. 1. U-tube heat exchanger [3]

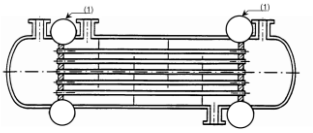

Fig. 2. Fixed tube sheet heat exchanger [3]

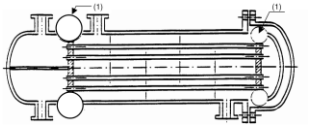

Fig. 3. Floating head heat exchange [3]

Table 1

The characteristic elements in the various types of heat exchangers

Characteristic	U-tube tubesheet heat exchanger	Fixed tubesheet heat exchanger	Floating head heat exchanger
Amount and shape tubesheet	One –flat, circular, uniform thickness	Two – flat, circular and identical (same materials, same connection with shell and channel)	Two – flat, circular, and identical connected by a bundle of straight tubes
Type of tubesheet (moving)	Stationary	Stationary	Stationary attached to the shell and channel Floating
Amount using configurations	6 (see Fig. 4)	6 (see Fig. 4)	6 stationary (Fig. 4) +3 floating (Fig. 5)
Loading conditions	3 cases	7 cases	3 cases
Tubesheet thickness	$e = \frac{D_0}{4\mu(0.8f)}\lvert P_s - P_t \rvert$	$e = \frac{D_0}{4\mu(0.8f)}\lvert P_s - P_t \rvert$	$e = \frac{D_0}{4\mu(0.85f)}\lvert P_e \rvert$

Tab. 1 shows a comparison of the information and characteristics among the types of heat exchangers which are shown in European standards. Tab. 1 also groups the equation on how to calculate the tubesheet thickness and which pressure we have to use in each heat exchanger.

This article shows one of this type – U-tube heat exchanger and different uses of the configurations of tubesheets. According the norm PN-EN 13445-3, the tubesheet may have one of the six configurations (design solutions) shown in Fig 4.

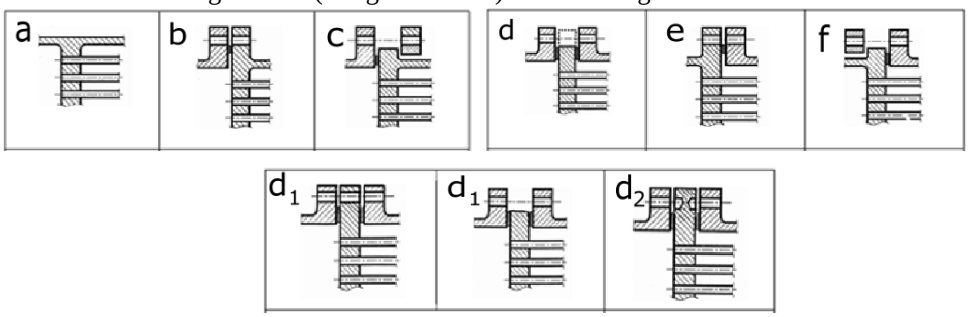

Fig. 4. Various types of configuration tubesheets [3]
a) integral with shell and channel; b) integral with shell and gasketed with channel, extended as a flange; c) integral with shell and gasketed with channel, not extended as a flange; d) gasketed with shell and channel, extended as a flange or not; e) gasketed with shell and integral with channel, extended as a flange; f) gasketed with shell and integral with channel, not extended as a flange

Configuration d covers the cases where the tubesheet is: extended as (d_1 as flange or not d_2)

In the floating tubesheet heat exchangers the floating tubesheet may have one of the 3 configurations shown in Fig 5.

- tubesheet integral (Fig. 5a),
- tubesheet gasketed, extended as a flange (Fig. 5b),
- tubesheet gasketed, not extended as a flange (Fig 5c).

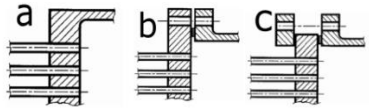

Fig. 5. Various types of configuration floating tubesheets [3]

For each of these types configuration of tubesheet a different method of calculation is used. All of the methods were shown in European standards PE-EN 13445-3.

2. Examples of calculations for U-tube heat exchangers

Below is a numerical example (examples of calculations) of the method of strength calculations for tubesheet contained in European standards PN-EN 13445-3. The calculations were carried out for the tubesheet of configuration b shown in Fig. 6. Tab. 2

presents the type of material and properties which were selected in calculations. The assumed values of tubesheet were shown in Tab. 3 [7, 3].

Table 2

Properties of used material

Tubesheet - material	R_m [MPa]	R_p [MPa]	R_{pt} [MPa]	f [MPa]	f_{20} [MPa]	f_{test} [MPa]	E [MPa]
P280GH (1.0426)	460	280	225	150	186.67	266.67	198610

Table 3

Input date of tubesheet

Input date	Value	Units	Description
e_n	100	mm	Nominal thickness of tubesheet (assume)
c_t	3	mm	Tubesheet corrosion allowance on the tube -side
c_s	3	mm	Tubesheet corrosion allowance on the shell - side
p	34	mm	Tube pitch
d_t	25	mm	Nominal outside diameter of tubes
$l_{t,x}$	80	mm	Expanded length of tube in tubesheet
e_a	94	mm	Analysis thickness
e_t	2.3	mm	Nominal tube wall thickness
E_t	$1.9861 \cdot 10^5$	MPa	Elastic modulus of tube material at design temperature
E	198610	MPa	Elastic modulus of tubesheet material at design temperature
f_t	111.33	MPa	Nominal design stress of tube material at design temperature
f	150	MPa	Nominal design stress of tubesheet material at design temperature
S	178000	mm^2	Total unperforated area of tubesheet
D_0	1163.4	mm	Equivalent diameter of outer tube limit circle
G_S	1255	mm	Diameter of shell gasket load reaction
G_c	1255	mm	Diameter of channel gasket load reaction
W_S	181026	kN	Shell flange design bolt load for the assembly condition
W_c	1097.94	kN	Channel flange design bolt load for the assembly condition

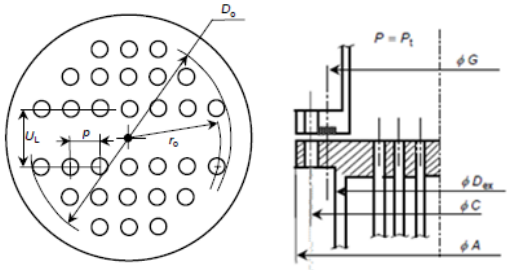

Fig. 6. Tubesheet design for b configuration [3]

The results of calculations on the thickness of the tubesheet are shown in Tab. 4. At this state of calculations, there are no differences in the method of calculation. Despite the following example of the various assumed operating pressures of the tubesheet, the calculation is carried out in the same way [3].

Table 4

The method of calculations concerning size of tubesheet

Equation	Results/ value	Units	Description
$e_a = e_n - c_t - c_s$	94	mm	Analyses thickness tubesheet (initial)
$\mu = \frac{p^* - d^*}{p^*}$	0.2647	–	The basic ligament efficiency for shear
$\rho = \frac{l_{t,x}}{e}$	0.8511	–	The tube expansion depth ratio ($0 \le \rho \le 1$)
$d^* = \max\left\{\begin{bmatrix} d_t - 2\cdot e_t \cdot \left(\frac{E_t}{E}\right)\cdot\left(\frac{f_t}{f}\right)\cdot\rho; \\ [d_t - 2\cdot e_t] \end{bmatrix}\right\}$	22.09	mm	The effective tube hole diameter
$p^* = \frac{p}{\sqrt{1 - 4\frac{\min[(S);(4\cdot D_0\cdot p)]}{\pi\cdot D_0^{\,2}}}}$	36.85	mm	The effective tube pitch
$\mu^* = \frac{p^* - d^*}{p^*}$	0.4005	–	The effective ligament efficiency of perforated tubesheet for bending
$\frac{E^*}{E} = \alpha_0 + \alpha_1\cdot\mu^* + \alpha_2\cdot\mu^{*2} + \alpha_3\cdot\mu^{*3} + \alpha_4\cdot\mu^{*4}$	0.414	–	Determination of the graph
$E^* = E\cdot 0414$	82227.64	MPa	The effective elastic modulus of the tubesheet at design temperature
$\vartheta^* = \beta_0 + \beta_1\cdot\mu^* + \beta_2\cdot\mu^{*2} + \beta_3\cdot\mu^{*3} + \beta_4\cdot\mu^{*4}$	0.3106	–	The effective Poisson's ratio of tubesheet (Determination of the graph)
$D^* = \frac{E^*\cdot e^3}{12\cdot(1-\vartheta^{*2})}$	$6.2993\cdot10^9$	Nmm	The equivalent bending rigidity of tubesheet
$\rho_s = \frac{G_s}{D_0}$	1.0787	–	The shell diameter ratio
$\rho_c = \frac{G_c}{D_0}$	1.0787	–	The channel diameter ratio
$K = \frac{A}{D_0}$	1.1174	–	The tubesheet diameter ratio
$F = \frac{1-\vartheta^*}{E^*}\cdot(E\cdot\ln K)$	0.1848	–	The coefficient
$W_{\max} = \max[W_s; W_c]$	181026	kN	The maximum flange design bolt load for the assembly condition

After this stage, for future calculations, pressures operating at the side shell and tube should be selected. In this example, calculations of three types of pressures were carried out. Values of the operating pressure were assumed.

In first load case, the analysed negative pressure operated on the shell – side. In the second load case, the analysed negative pressure operated on the tube – side. In the third case, the negative pressure operating on the shell or the tube side was not taken into consideration.

Table 5

Load cases used in design

ID	Load Case 1	LC2	LC3	Units	Description
P_s	-0.1	1	1	MPa	Shell – Side Pressure
P_t	0.6	-1	0.6	MPa	Tube – Side Pressure

Below, Tab. 6 shows the procedure and the results of calculations carried out of the different load cases described in Tab. 5.

Table 6

Calculation the moment acting at different part of tubesheet [3]

Equation	LC 1	LC 2	LC 3	Units	Description
$M_{TS} = \frac{D_0^2}{16} \cdot [(\rho_s - 1) \cdot (\rho_s^2 + 1) \cdot P_s - (\rho_c - 1) \cdot (\rho_c^2 + 1) \cdot P_c]$	-10087.73	28822.08	5764.42	Nmm	The moment due to pressures P_s and P_t acting on the unperforated tubesheet rim
$M^* = M_{TS} + \frac{W_{\max}(G_c - G_s)}{2 \cdot \pi \cdot D_0}$	-10087.73	28822.08	5764.42	Nmm	The moment acting on the unperforated tubesheet rim
$M_P = \frac{M^* - \frac{D_0^2}{32} \cdot F \cdot (P_s - P_t)}{1 + F}$	-3894.83	11128.08	2225.62	Nmm	the moment acting at periphery of tubesheet
$M_0 = M_P + \frac{D_0^2}{64} \cdot (3 + \vartheta^*) \cdot (P_s - P_t)$	-52905.35	151160	30231.63	Nmm	The moment acting at centre of tubesheet
$M = \max[\lvert M_P \rvert ; \lvert M_0 \rvert]$	52905.35	151160	30231.63	Nmm	The maximum moment acting of tubesheet
$\sigma = \frac{6 \cdot M}{\mu^* \cdot (e_a - h_g')^2}$	97.86	279.59	55.92	MPa	The calculated stress in a component
$\tau = \left(\frac{1}{4 \cdot \mu}\right) \cdot \left(\frac{D_0}{e}\right) \cdot \lvert P_s - P_t \rvert$	-8.18	23.28	4.6756	MPa	The calculated shear stress in a component

Depending on the applied pressure, different torques were obtained. In any case, the strength conditions of the maximum radial bending stress in the tubesheet and the maximum shear stress in the tubesheet have been fulfilled. The designed tubesheet fulfilled strength conditions for pressures assumed in Tab. 5. The material and size of the tubesheet were well selected.

3. Example of calculation for U-tube heat exchanger tubesheet extended as a flange

This section shows a comparison of the results of calculations performed in accordance with the WUDT-UC [2, 4, 8] and European standards. Tab. 7. shows input dates of strength parameters for the material used in the calculations [7, 6]. Tables 9, 10 and 11 were shown the selected results of these calculations. The calculations were carried out for tubesheet extended as a flange [4, 8].

Table 7

Properties of used material

Tubesheet – material	R_m [MPa]	R_p [MPa]	R_{pt} [MPa]	E [MPa]
S235JRG2 (1.0038)	410	235	210	205000

Tab. 8 contains basic information about the value assumed during the design of tubesheet. The input dates of tubesheet were selected from the Polish standards for this project [1, 5].

Table 8

The dimensions and the results of the calculated thickness of the tubesheets depending on the area

WUDT-UC	PN-EN 13445-3	Units	Description
$d_z = 25$	$d_t = 25$	mm	The nominal outer diameter of the pipe
$t = 32$	$p = 32$	mm	The tube pitch
$g = 12$	–	mm	Initial thickness
$l_0 = 12$	$l_{t,x} = 12$	mm	The expanded length of tube in tubesheet
–	$U_L = 32$	mm	The large centre- to- centre distance between adjust tube rows
$f = 533.126$	$S = 533.126$	mm^2	The total unperforated area of tubesheet

Tab. 9 and 10 show the results of calculating assembly and operating the bolts loads, necessary for the appropriate operation of the flange connection.

Table 9

The results of calculations for the assembly in the event of a tubesheet used in connection flange -screw

WUDT-UC	PN-EN 13445-3	Units	Description
D_1 = 1400	d_1 = 1400	mm	The nominal diameter of the tubesheet
D_w = 1426	B = 1426	mm	The inside diameter of the contact face between loose and stub flanges in a lap joint
D_u = 1481	G = 1504.3	mm	The diameter of gasket load reaction
–	b_0 = 26	mm	The basic gasket or joint seating width
U = 54.5	w = *52*	mm	The contact width of gasket or joint seating pressure
U_{cz}= 25.61	b = 12.85	mm	The effective gasket or joint seating width
σ_m = 18.3	y = 26.20	MPa	The minimum required gasket or joint seating pressure
N_{m1} = 2502000	W_A = 104694	**N**	The minimum required bolt load for assembly condition
C = 1.4	–	–	The correction coefficient use in WUDT-UC
N_{m2} = 5618000	–	N	The minimum required bolt load for assembly condition – used correction coefficient

Table 10

The results of calculations for operating in the event of a tubesheet used in connection flange – screw

WUDT-UC	PN-EN 13445-3	Units	Description
D_u = 1481	G = 1504.3	mm	The inside diameter of the contact face between loose and stub flanges in a lap joint
p_0 = 1.6	P = 1.6	MPa	Design pressure
b = 1.5	–	–	The coefficient of hedging against a decline in the strength S as a result of creep
σ_r = 4.8	mP = 2.4	MPa	The pressure on the gasket to guarantee tightness of the joint in the operating conditions
U_{cz} = 26.61	b = 12.85	mm	The effective gasket or joint seating width
P = 2754000	H = 2843667	N	The total hydrostatic end force
S = 953200	H_G = 22684	N	The compression load on gasket to ensure tight joint
N_r = 4013000	W_{op} = 2866351	N	The minimum required bolt load for operating condition

Tab. 11 shows the final results for the calculation of the bottom sieve according to WUDT-UC and European standards.

Table 11

Comparison of the results of calculated thickness of the tubesheet

The calculated thickness of the tubesheet	WUDT-UC g_o mm	PN-EN 13445-3 e mm
1. Precinct flange connection	26	32
2. Precinct bundle of tubes	20	12
3. Outside the bundle of tubes	34	12
The thickness of whole tubesheet *	34	32

* Industry seeks to standardise the thickness of the tube sheet for each of its area

4. Conclusion

The European standard PN-EN 13445-3 has procedures for the calculation of tubesheet for more structural solutions than Polish guidelines WUDT-UC. The calculations are dependent on the heat exchanger and the type of tubesheets.

In the case of guidelines WUDT-UC, the amount of these solutions is very limited and reduced to a few cases. However, this greatly facilitates carrying out the calculations. All the values in the design are known.

Large difference were noted when comparing the two methods of calculating algorithms. For calculation algorithm strength WUDT-UC as the minimum thickness of the tube sheet assumes a value equal to 12 mm, regardless of the material from which the tube sheet and the diameter of the heat exchanger and the load applied pressure.

In the European standard PN-EN 13445-3, there is no requirement specifying the minimum size of the tubesheet. The calculation is carried out for the assumed thickness of the tubesheet. It is important only for the thickness to fulfil strength requirements. If these conditions are not fulfilled, the calculations must be repeated by increasing the thickness of the tubesheet.

When comparing the results of calculation for tubesheet extended as a flange, conducted for both of these documents, large differences are noted. The same situation occurs in the event of comparing the dimensions of sealing solutions for the flange connection. They relate to the average diameter of the seal D_u and the inside diameter of the contact face between loose and stub flanges in a lap joint G.

According to the algorithm calculations WUDT-UC thickness of the tubesheet meets the conditions adopted in the project in the precinct flange connection and it is 26 mm. However, according to European standard PN-EN 13445-3, this value is higher, at 32 mm. In the precinct bundle of tubes, higher values in the calculation were obtained for the guidance WUDT-UC equal 20 mm. In the case of the European standard, this value was 12 mm. For the region outside the bundle of tubes, a similar situation was noted. For the European standard PN-EN 13445-3 there was a higher value – 32 mm than for the guidelines WUDT-UC – 12 mm.

Finally, the thickness of tubesheet for European standard PN-EN 13345-3 was equal to 34 mm. The calculations that were carried out for guidelines WUDT-UC amounted to 32 mm.

It was found that the calculations performed according to the European standards PN-EN 13445-3 are more accurate and increase the strength of the structure. Due to the greater thickness of the tubesheet heat exchanger, it meets the requirements of safety and allows safe operation of the device.

In the analysed examples, an analogy on the section of the tubesheet into different areas was noted. Equation determination of tubesheet thickness have been summarised in below Tab. 12.

Table 12

Comparison of formulas used to determine the thickness of the tube sheet in each of its region

Region / Standards	Precinct flange connection	Outside the bundle of tubes	Precinct bundle of tubes
WUDT-UC	$D_z = D_w + 2 \cdot g_s$: - assembly conditions: $\sigma_{km} = 2 \cdot N_m \cdot \frac{D_0 - D_w - 2 \cdot g_s}{\pi \cdot (D_{zk} - 2 \cdot d_0) \cdot h^2}$ - operating conditions: $\sigma_{kr} = 2 \cdot N_r \cdot \frac{D_0 - D_w - 2 \cdot g_s}{\pi \cdot (D_{zk} - 2 \cdot d_0) \cdot h^2}$	$g_0 = 0.45 \cdot \delta \cdot \sqrt{\frac{p_0}{k}}$	$g = \frac{q_{\min}}{m}$
PN-EN 13445-3	- assembly conditions: $e_{fl,a} = \sqrt{\frac{12}{\pi \cdot D_{ex} \cdot \left[(1+\vartheta) + (1-\vartheta) \cdot \left(\frac{D_{ex}}{A} \right)^2 \right]} \cdot \frac{M_A}{f_A}}$ - operating conditions: $e_{fl,op} = \sqrt{\frac{12}{\pi \cdot D_{ex} \cdot \left[(1+\vartheta) + (1-\vartheta) \cdot \left(\frac{D_{ex}}{A} \right)^2 \right]} \cdot \frac{M_{op}}{f}}$	Assumed in the project, checked under the strength conditions and corrected when are not complied.	Assumed in the project, checked under the strength conditions and corrected when are not complied.

References

[1] Pikoń J, *Podstawy konstrukcji aparatury chemicznej. Cz II. Elementy aparatury chemicznej*, PWN, Warszawa 1979.

[2] Warunki Urzędu Dozoru Technicznego, *Urządzenia Ciśnieniowe*, Wydanie 10.2003.

[3] Norma PN-EN 13445-3:2002.

[4] Talaga J, Felkowski Ł, *Obliczenia połączeń kołnierzowych w świetle norm PN-EN 13445 i specyfikacji technicznej WUDT-UC*, Inżynieria i Aparatura Chemiczna, 50, nr 6, 2011, 5-8.
[5] Pikoń J, *Podstawy konstrukcji aparatury chemicznej. Cz I. Tworzywa konstrukcyjne*, PWN, Warszawa 1979.
[6] Materiały firmy Spetech (15.05.2016): http://www.spetech.com.pl.
[7] Norma PN-EN 13445-2:2002.
[8] Celarek A, *Analiza porównawcza metodyki obliczeń wytrzymałościowych ścian sitowych według Norm Europejskich i wytycznych UDT*, Praca magisterska, Politechnika Krakowska, Kraków 2015.

TECHNICAL TRANSACTIONS | CZASOPISMO TECHNICZNE
MECHANICS | MECHANIKA
2-M/2016

PAVEL DITL, ALEXANDER FERNANDO*

SIMULATION OF PROCESS LINES IN MICROSOFT EXCEL - NITRIC ACID PRODUCTION

SYMULACJA LINII TECHNOLOGICZNYCH W PROGRAMIE MICROSOFT EXCEL – PRODUKCJA KWASU AZOTOWEGO

A b s t r a c t

In this contribution, it is explained in the detail how useful Microsoft EXCEL could be for the simulation of process lines. The report contains a manual flowsheet as well as a tutorial case and the results of its application for Nitric acid production can be gained.

Keywords: program Microsoft EXCEL, simulation

S t r e s z c z e n i e

W artykule szczegółowo przedstawiono jak użytecznym narzędziem do symulacji linii procesowych może być program Microsoft EXCEL. Praca zawiera indywidualne arkusze danych, poradniki przydatne w szczególnych przypadkach (tutoriale) oraz wyniki ich zastosowania w produkcji kwasu azotowego.

Słowa kluczowe: program Microsoft EXCEL, symulacja

DOI:

* Prof. PhD. DSc. Eng. Pavel Ditl, MSc. Eng. Alexander Fernando, Department of Process Engineering, Faculty of Mechanical Engineering, Czech Technical University in Prague.

1. Introduction

I already introduced the usage of Microsoft Excel for process line simulation at the 2012 conference in Berlin.

Now, I would like to explain the main principles of this method on the „Boiler“ example, which demonstrates both enthalpy and mass balances.

First of all, we need to understand the basic principles, which are shortly described in this presentation:

1.1. Decision-making

Experience and practice have made us realise that mass and material balances represent effective tools for decision-making. The concept of decision-making shall include the following spheres of action:

- Sizing lines and individual apparatus in designing.
- Adjusting a line to the modified composition of materials.
- Adjusting a line to the modified requirements for quality (composition) of a product.
- Diagnosing failures of operation of lines and locating causes of failure.
- Checking or substituting measured quantities by calculating those quantities and taking advantage of this principle to ensure easier control or to carry out process, or guarantee measurements.
- Optimising operation of a line and searching for alternatives of operation using the method: “What will happen if.....?”
- Training and teaching operating personnel.

This enumeration is certainly not complete; however, it gives us an idea of the content of the concept of decision-making.

1.2. Working tools for decision-making

Decision-making that involves any process requires a quantitative model. This decision-making shall mean either proposing a new process, or modifying a process, or controlling an existing process. Such a model should give us an opportunity to study the behaviour of the system if the initial conditions change. In other words, the model should enable one to study changes of the system behaviour after modifying initial conditions, that is to search for an answer to the question: What will happen if…? Such a model constitutes a prerequisite for an objective quantitative economic analysis of the system. It is necessary to bear in mind at all times that the quantitative model should be exact. This means we receive one and only solution for the selected values of the designating parameters. When using empirical coefficients, such as efficiency, yield, or adjustable constants guaranteed by the provider of the equipment, maximum attention must be paid in order to define these coefficients accurately. The use of empirical coefficients is thus limited to cases where those coefficients include deviations from the ideal behaviour, express efficiency of the process, or adjust the theory to the real behaviour of the equipment. These adjustable parameters often constitute the subject of know-how. In any case, however, exact mass and enthalpy balances constitute the basis of the model. Thereby, a quantitative model of a

process establishes a reliable foundation of the system's economic model, which is the final tool for the management in making decisions.

The law of conservation of mass and the law of conservation of energy can be used as an exact model for processes accompanied by a chemical reaction and heat exchange. On the basis of this model, mass and enthalpy balances can be drawn up for the process in question, and subsequently, complete system characteristic can be acquired.

1.3. Complete system characteristic

Material balances are used for obtaining a complete characteristic for all streams that are present in the process flow chart. This information is essential both for a designer and for the operation control itself. A complete characteristic contains the following details:

- Where the stream comes from and where it goes – that defines the direction of the stream, i.e. its orientation.
- Size of the stream, expressed as weight per time unit ($kg \cdot s^{-1}$) or moles per time unit ($kmol \cdot s^{-1}$).
- What components the stream contains and their part, expressed as a weight or mole fraction of the component in the stream in question. The method of expressing the composition of the stream should be invariant to temperature and pressure.
- Temperature and pressure for each stream are added to the above-mentioned in the case of enthalpy balance.

2. Basic concepts

If we know the composition, temperature and pressure for a stream, we are able to determine:

- any intensive physical property of the stream – such as density, viscosity, or surface tension,
- whether the stream consists of one or more phases and what these phases consist of.

In general, we can say that all intensive physical properties represent a function of composition, temperature and pressure. With liquid and solid phases, the effect of pressure on the value of intensive properties is mostly negligible. As to ideal gases, the change of enthalpy with pressure is null. A more noticeable dependence of enthalpy on pressure is encountered only with streams, the position of which is in the proximity of a two-phase range. This leads to the following conclusions:

- The composition of the stream must serve the purpose of mass balance.
- The temperature of the stream must serve the purpose of enthalpy balance.
- The pressure of the stream does not constitute the object of balance calculations. If we need to know its value (for instance, in order to calculate in what phase the stream is – whether in a gaseous or liquid phase), its value must be determined.

2.1. What is flowsheeting?

Flowsheeting consists of a flow sheet of the process being analysed and the complete system characteristic. It includes neither the dimensions and the structural design of the apparatus, nor the planning of the piping system. Flowsheeting consists in the following steps:

- Drawing up a process flow sheet
- Defining components in individual streams
- Establishing balance equations

By working them out, we obtain the missing information for complete system characteristic. Flowsheeting is a working tool for decision-making.

2.2. What is a balance?

Any extensive property – a property, the numerical value of which changes with the size of the system – can be balanced. This class includes mass, volume, internal energy, entropy, and so forth. On the contrary, intensive properties are properties with their value being independent of the size of the system, such as density, temperature, viscosity, specific heat, colour, hardness, and so forth.

Within the defined boundaries of the system being balanced and the limited time for which the balancing is being performed, the following balance relation holds good for the extensive property being balanced:

$$Accumulation = Input - Output + Source$$

- Input is the quantity of the extensive property being balanced that passes into the system through the balanced system boundaries within the limited time for which the balance is being performed.
- Source is the quantity of the extensive property being balanced that is generated within the system boundaries in the course of the balanced period. Disappearance of the extensive property is expressed as a source with a negative sign.
- Output is the quantity of the extensive property being balanced that gets out of the system through the balanced system boundaries within the limited time, for which the balance is being performed.
- Accumulation is the change in the quantity of the extensive property being balanced within the balanced system boundaries in the course of the balanced period.

The introduction of a source element enables us to balance all extensive properties, even those properties to which the law of conservation does not apply (for instance, entropy, exergy, component subject to a chemical reaction, and so forth). In order to apply a balance relation, it is still necessary to define in greater detail the concepts involved in the balance relation.

At the start of each balancing, three concepts must be defined clearly:

- *Extensive property being balanced*
- *Balanced system boundaries*
- *Limited time for which the balance is being performed*.

2.3. What is a component?

An extensive property being balanced will be hereinafter referred to as a component. Components can be:

- pure chemical compounds, such as methane, sulphuric acid, water, oxygen, to which a specific molar mass can be attributed,
- polymers – chemically pure substances, whose molar mass is not clearly defined,
- substances representing a group of chemical compounds, such as fats, R_2O_3, silicates, hydrocarbons C_{4+},
- substances that cannot be specified chemically, such as water-insoluble residue, substances with density lower than water, substrate in bioreactors.

When defining a component, it is necessary to define in a precise manner the method through which the component is determined. Differences in methods used for determining a component can lead to significant discrepancies. For instance, it is not enough to define a component as water content in a solid phase, it being loose material. Water can be on the surface of particles; in the case of porous particles, it can be bound through adsorption to the inner surface of particles; it can be water of crystallisation if the particles are of crystalline nature, and in the case of some substances it can be chemically bound water. Based on the method of determining the water content, results can differ even in the order of magnitude.

This applies also to a component defined as a particle size. If we determine the proportion of particles of a specific dimension by measuring the particle's largest dimension under the microscope, by separating on sieves, or by measuring the distribution of the particles using the settling method, we will arrive at different results.

2.4. What is a balanced system boundary?

A boundary of the system being balanced must be defined in order so that a component can enter or get out of the system only by crossing the system's boundaries. System boundaries do not have to be identical with the apparatus housing. A system can also be an imaginary volume defined within the apparatus. This method is very often used to define differential volume, it being the system with dx, dy and dz dimensions in rectangular coordinates. Then, the balance relation for the component leads to a partial differential equation.

The system being balanced does not have to be identical with the individual units of apparatus. Units of apparatus can be combined for the purposes of balancing. Admittedly, this reduces the number of input data, required for the performance of the balance calculation, but the possibility of acquiring further information is thereby lost. For instance, if we link, for the purposes of balancing, an evaporating apparatus and crystalliser, we lose the information about the properties of the concentrated solution entering the crystalliser, which is an information necessary for the structural design of the evaporating apparatus. An opposite approach is possible as well. For instance, instead of balancing the whole distillation column, individual levels can be balanced.

2.5. What is a limited time of balance?

If we divide all elements of the balance relation by the limited time of balance, we will obtain the component's quantity per unit of time. This quantity can be termed as stream. Then, the balance relation for any one component can be posted as follows:

Rate of Accumulation = Input Stream -Output Stream + Source per Unit of Time

Source of component per unit of time (rate of source) can be seen as an imaginary (fictive) stream that enters into the system; however, it does not cross its boundaries at the same time. It can have both positive – a component is formed – and negative – a component disappears – value.

Accumulation per unit of time can be designated as the rate of accumulation; it is the change in quantity of the balanced component in the system with time. Therefore, the final form of the balance relation reads as follows:

Input Stream of Component + Fictive Stream of Component = Output Stream of Component + Accumulation Rate of Component.

2.6. What is an amount of component?

In order to substitute into the above-mentioned relation, we need to know the stream of the component, which is the quantity of the component per unit of time. However, we do not usually have the opportunity to measure the component stream directly. In most cases, we measure the overall stream and its composition. The component stream can be calculated from these two pieces of information.

If the component is a differential particle size, the size of the stream of this component can be calculated by multiplying the overall flow of particles by the relative frequency of occurrence of the particles within the monitored interval. When reducing the interval of the particle size to zero, we get a differential and integral description known in literature as population balance.

The numerical value of the flow of the component is required to be invariant to temperature and pressure. This requirement excludes the overall stream to be expressed as volume per unit of time. There remains the possibility of expressing the flows of components as mass or amount (number of pieces) – kilograms of flour and number of eggs per unit of time.

Furthermore, it is required to have the opportunity to convert mass to amount (number of pieces) and vice versa. For it is common practice to weigh small screws instead of counting our thousands of pieces. The approach is accurate only if every piece has exactly the same mass as the other ones. This requirement is satisfied strictly only with molecules. Molecules are too small to be counted out. However, we know that one kmol of any substance contains the same number of molecules, corresponding to the Avogadro's number, which is $6.0221367 \cdot 10^{26}$ $kmol^{-1}$. If we know the molar mass for a component ($kg \cdot kmol^{-1}$), we can convert the amount of substance (kmol) to mass (kg) and vice versa. If a component cannot be attributed molar mass, its quantity can be expressed only as mass in kg.

Consequently, we shall express the fraction of the component present in the stream only as a weight fraction or a mole fraction, depending on whether the overall stream is expressed in $kmol \cdot s^{-1}$ or $kg \cdot s^{-1}$.

2.7. What is a continuous process?

The accumulation of a component in the system is the change in the quantity of the property being balanced (hold-up). If a process is run continuously in a steady state, the change in hold-up and its composition with time is null, and therefore, the rate of accumulation is also null.

The accumulation of mass is usually applied in batch systems. If we choose a limited time of balance exceeding the time of a batch process cycle by a long way, we can accept the assumption of a zero rate of accumulation. If we choose no matter how long balance period, the system accumulation will be given by the level of the system hold-up at the end of the balance period minus the system hold-up at the start of the balance period. This can be the difference between the maximum and the minimum hold-up at the most. If we choose the balance period to be just as long so that the maximum accumulation possible is negligible compared with the input and output streams for the balance period, we can regard also the periodical batch processes to be continuous and deem the rate of accumulation to be zero.

Complete system characteristic does not say anything about the dimensions of individual pieces of equipment, and therefore, the relations we use for balancing do not contain any parameters of the equipment. However, in order to calculate the rate of accumulation, it is necessary to know the hold-up, which constitutes a parameter of the equipment. Therefore, our concern will be focused on continuous and periodical batch processes, where the accumulation rate can be ignored.

2.8. What is a source stream of reaction?

Just as in the case of accumulation, it is necessary to know the hold-up of the equipment in which the chemical reaction takes place in order to calculate the source of a component directly. The rate of generation of the component being balanced is the amount of component generated at the given place in the unit of capacity of the system per unit of time. That means that an intensive property is involved. Since the source in balances is an extensive property, we have to integrate the intensive property through the capacity of the system being balanced. In the case of an ideal stirred tank, where composition and temperature do not constitute functions of the place, we simply multiply the mentioned intensive property by the capacity of the hold-up, which is, however, a parameter of the equipment. In order to avoid this difficulty, we can substitute the source by a fictive stream of reaction.

For every independent reaction, there will be one fictive stream, which will be denominated as nr_k for balances of amount of substance and as mr_k for mass balances, where k is the serial number of reaction in case that more independent reactions are taking place in the block being balanced.

Instead of posting mole and/or weight fractions into the fictive stream column in the specification table for k, we:

- enter the component's stoichiometric coefficient into the component's row, with a positive sign if the component is a product of the reaction (second term on the right side of the stoichiometric equation), or with a negative sign if the component

is a reactant (first term on the left side of the stoichiometric equation) in the case of material balance;

- multiply, in addition, the stoichiometric coefficient (with the appropriate sign) by the component's molar mass in the case of mass balance.

Tutorial Problem:

If we take the stoichiometric equation of formation of sodium hydrogen carbonate in manufacturing soda

$$NaCl + NH_3 + CO_2 + H_2O = NaHCO_3 + NH_4Cl$$

as an example, the column for the fictive stream will read as follows:

Table 1

Stoichiometric coefficients and molecular weight

		for molar balance in kmols/sec	for mass balance in kg/sec
	components	Nr	Mr
1	H_2O	-1	-18.02
2	NaCl	-1	-58.44
3	CO_2	-1	-44.01
4	NH_3	-1	-17.03
5	$NaHCO_3$	1	84.01
6	NH_4Cl	1	53.49

2.9. Why enthalpy balance and not heat balance?

The change in energy of 1 kg of water upon being heated by 0.5°C corresponds to the change in the mass flow rate of the same by 65 $m \cdot s^{-1}$ or raising by 213 m. Such changes in kinetic and potential energy can be hardly encountered in a chemical plant, the exception thereof being power-producing machinery (turbines). For the purposes of balancing, we can therefore ignore potential and kinetic energy of streams and substitute heat balance by enthalpy balance.

This has the same advantage as disregarding the accumulation rate. In order to calculate kinetic and potential energy of a stream at the given place, we need to know the diameter of the piping and its height above the ground, which are parameters of equipment that do not belong into the system characteristic. We do not need this information to calculate the enthalpy of a stream, and therefore, we replace the overall heat balance by enthalpy balance. The mistake that can be thereby caused is negligible in the absolute majority of cases.

2.10. What is the difference between material balance and enthalpy balance?

For a continuous process or a batch process occurring periodically, material balance of a component has the following form:

Accumulation Rate of Component = Input Stream of Component – Output Stream of Component+ Source.

This applies to every component, which means that for a balanced system, we have as many material balances as there are components present in the system.

The dimension of individual parts of the balance equation is $kg \cdot s^{-1}$, or $kmol \cdot s^{-1}$.
The system being balanced can interchange energy with the surroundings not only through the material streams, but also through the exchange across the system boundaries – heat exchangers, or stirrers as the case may be, and so forth.

In this case, the enthalpy balance for a continuous process or a batch process occurring periodically will have the following form:

Enthalpy Accumulation = Input Stream Enthalpy -Output Stream Enthalpy + Interchange of Energy with Surroundings + Source

Individual parts of the balance equation are expressed in kW.
Removal of energy into the surroundings has a plus sign, while power supply has a negative sign. The system in which the interchange of energy with the surroundings is zero, is called *adiabatic*.

Only one enthalpy balance holds good for the balanced block.

2.11. Enthalpy balance

To draw up an enthalpy balance, physical and chemical data of individual components must be available. Various databases can serve as sources of data. Data from individual databases may not be quite consistent, and therefore, it is practical to use only one database if possible and not to take data for various components from different databases. A database adapted for Excel from the book by R.C. Reid, J.M. Prausnitz, and T.K. Sherwood – The Properties of gases and liquids (Mc Graw Hill 1982) is used for the purposes of teaching at the Czech Technical University.

The database of the National Bureau of Standards or the DECHEMA database can be recommended for industrial applications. The respective Internet addresses are provided at the end.

2.12. Formulation of the problem being solved

In order to comply with the law of conservation of mass and enthalpy, the following equations must hold true for every block of the flow sheet:

- material balance for every one component (in order words, the number of balance equations agreeing with the number of different components present in the streams, which pass into or get out of the given block – we take into account both real and fictive streams);
- summation equations for every one stream (in other words, the total of weight or mole fractions of all components in the given stream must equal one);
- other equations, if any, follow from the laws that determine the relations among the composition, pressure, and temperature of individual streams. These are the laws of thermodynamics, chemical and phase balance, or laws of kinetics of processes. These relations are almost always non-linear;

- other equations issue from specifications given by technological regulations (such as yield, selectivity) or in data provided by the producer of the equipment (such as efficiency of machines);
- in the case of changes in temperature, one enthalpy balance is added.

The first two groups form a system of linear equations.
Enthalpy balance is non-linear, which is given by the fact that molar heats represent functions of temperature.

This set of equations forms a mathematical model, for which methods of solving must be established.

2.13. How many equations define the system behaviour in full?

A system is defined in full if the sum of balance equations, summation equations, equations for physical laws, specification equations, and enthalpy balance is equal to the number of unknowns in the equations.

2.14. Solving possibilities of the governing equations

The issue of simplicity of information transmission plays an important role with the model used. There is specialised software available for these models, such as CHEMCAD, PRO, or MAX. In addition, advantage can be taken of mathematical software, such as MATLAB, Mathematica, MATHCAD, and so forth.

This software has two big disadvantages – firstly, it is very expensive, and secondly, to become proficient in the software requires great efforts and a lot of time. It is necessary to bear in mind that a model set up by means of certain software will be used from a certain level of management upwards. At this level, it is possible to encounter the willingness to sacrifice the financial means to buy the software; however, it is an absolute illusion to expect that someone would be willing to sacrifice the time needed in order to become familiar with the software.
However, there is software available with the following advantages:

- It is installed on every computer in an enterprise – one can assume that Microsoft Office is installed on every PC.
- Almost everyone, who is able to use a computer, has a good command of it. And if the manager is not willing to communicate with a computer, his secretary is bound to have a good command of this programme.
- Operating records and source data are stored by means of this programme. Transmitting source data into our model is therefore possible without even one number being retyped using a keyboard.
- All and any economic and statistical analyses are performed by means of this programme. Transferring data for these analyses is also performed through floppy disks, over the net and through other channels, but not by typing the data on the keyboard.
- Tables and diagrams obtained using this programme can be, without the slightest difficulty, transferred into the most widespread Word processor.

We are talking about Excel. Working with Excel may not be as elegant as working with special programmes, but the above-mentioned advantages are significant to such an extent that, for the time being, Excel cannot be replaced with any other tool – exception perhaps being Lotus II, but it is fully compatible with Excel.

3. Methods of setting up and solving a model

The methods of solving have been drawn up to be generally valid and uniform for all types of balance cases. Exactly the same procedure is used for all cases, ranging from the problem of what ratio to use to mix two streams of water with different temperatures so that the resulting stream can have the temperature required, to systems containing dozens of blocks and streams.

These uniform methods have facilitated the elaboration of an exact method of solving, which is available to the engineering public at large, and which consists of the following steps:

The following are required for any process we wish to balance:

1. Process basis and data available with respect thereto.
2. Process flow sheet and definition of balance blocks, incidence matrix.
3. List of components in streams and their definitions.
4. Basis of calculation and conversion of specified flows and compositions.
5. Chemical reactions, determination of number of independent chemical reactions.
6. Specification table and matrix of coefficients.
7. Formulation of additional relations.
8. Conditions of system solvability.
9. Solution of a system of equations using methods of linear algebra, with the advantage of using excel.
10. Table of solutions containing complete system characteristic.

3.1. Solving a system of equations – a model

In general, tasks are not noticeably complicated from the mathematical point of view. Solving a system of equations, most of which are linear, is always involved.

It is important to solve the essential question of whether the system has been overdetermined, that is whether also data that should be the result of the calculation are available for the system characteristic, or whether the system has been determined insufficiently, that means that not enough information is available to enable us to determine the complete system characteristic.

The method of how to proceed from process description to solvable mathematical model has certain logic, which must be adhered to when computing with a calculator as well as when using programmes, such as PRO, MAX, or CHEMCAD. The mentioned programmes obtain the required information from the user using various menus. Formation of and recording in what is known as a specification table is, in fact, making a list of all equations that are available to us to solve the problem.

The methods for EXCEL have exactly the same logical structure as the mentioned programmes, with the difference consisting in that we know exactly why we take the respective steps. Although this method is more laborious, we know the logic and subject-matter of the procedure, and therefore, we are able to eliminate any contingent mistake or error in the specification right at the beginning.

A system can be solved using a calculator only in the cases where it is possible to apply the solution through iterative method by means of substitution.

The following part demonstrates in detail on sample problems the application of the general methods discussed above. Stress is put on the uniform procedure, which must be unconditionally observed for success of the solution to be guaranteed.

3.2. General information

In describing the methods, we will proceed by providing the reader with a standard text and with a solution of the problem being described in EXCEL. This file has been provided with quite a detailed description and numerous commentaries, so that the standard text can serve, after the initial working through, only as reference. In addition, series of problems solved in EXCEL have been attached so that the user can review the methods on other problems as well. This file contains problems ranging from the most simple to the larger-scale ones. Commentaries on these problems do not constitute part of the standard text anymore; the commentary, with which the EXCEL file has been provided, should be sufficient for the user.

Let's discuss the individual phases of the procedure in detail. For example we use problem **Boiler**:

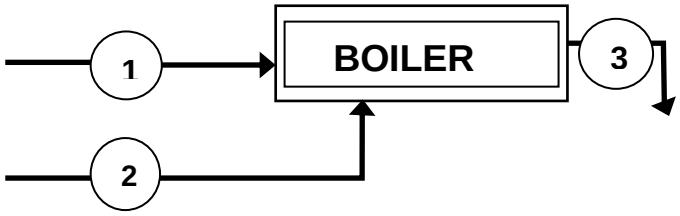

Fig. 1. Input and output flows in a boiler

A pipe oven serves as a source of energy for heating a family house, where power-gas is mixed with air and burned. We assume that power-gas is pure CH_4.
The process of combustion runs according to the following stoichiometric equation

$$CH_4 + 2O_2 = CO_2 + 2H_2O$$

Dry air comes into the oven in surplus compared with the stoichiometry of the process. Combustion occurs under an oxygen surplus and the flue gas contains traces of unburned power-gas.

1. **Process input parameters:**
   R = 8,314 kW·s·Kmol^{-1}·K^{-1}
   T = 273,15 K
   Q = 20 kW
   C_{CH4} in flue gas = 0,004 kmol/∑kmol

C_{O2} in air = 0,21 kmol/∑kmol
Air surplus = 25%
$T_{stream\ 1}$ = 5°C, $T_{stream\ 2}$ = - 15°C, $T_{stream\ 3}$ = 150°C

2. List of components ,streams and process units:
CH_4 = 16,04 kg/kmol
O_2 = 32 kg/kmol
N_2 = 28,01 kg/kmol
CO_2 = 44,01 kg/kmol
H_2O = 18,02 kg/kmol

3. Common basis:
mol flow kg/kmol

4. Reference stream & component flows:
Q = 20 kW

5. Recalculations:
Component concentration in Stream:
Stream 3, Component 4
$C_{3,4}$ = 0,004 kmol/∑kmol
Relation between two Component Flows:
Stream 2, Component 2
$n_{2,2} = 2{,}5 \cdot n_{1,1}$

6. Chemical reactions:
Reactants = Products
$CH_4 + 2\ O_2 = 2\ H_2O + CO_2$
Stoichiometric Coefficients:

Stoichiometric coefficients are defined in the following way:

A) stoichiometric coefficients of reactants have a minus sign and reaction products have a plus sign.
B) stoichiometric coefficients of reactants have a minus sign and reaction products have a plus sign.
C) single stoichiometric coefficients are used in mol balances.
D) In the case of mass balances, we must multiply the stoichiometric coefficients by the corresponding mol masses.

Table 2

Stoichiometric coefficients (S.C)

	Element	S.C	Mass [kg/kmol]	Thermodata indexes
1	CH_4	-1	-16,043	63
2	O_2	-2	-64	34
3	N_2	0	0	31
4	CO_2	1	44,01	48
5	H_2O	2	36,03	22

For the calculation of molar enthalpies of individual components, as a function of temperature, we will use a suitable data-base where we could find the necessary information. For our purposes, we will use the data-base Thermodata.

Now, we have to arrange available data into a suitable form.
As the first step, we put down the **basic parameters.**

Table 3

Basic parameters

number of streams	3
number of chemical reactions	1
number of process units	1
number of components	5

Respecting the recommended form, we put down the **IM** matrix (incidence matrix) and the **TD** matrix (data table):

Table 4

IM

process unit	streams			reactions
	1	2	3	r1
1. Boiler	1	1	-1	1

Table 5

TD

	process unit	streams			reactions
	1. Boiler	1	2	3	r1
1	CH_4	1	0	1	-1
2	O_2	0	1	1	-2
3	N_2	0	1	1	0
4	CO_2	0	0	1	1
5	H_2O	0	0	1	2

Number of unknown parameters:

Scalar product of the matrix TD + number of reactions gives the number of unknowns (**nUKN**):

nUKN = SUMMPRODUCT(TD) + 1

Table 6

Number of mass balance equations can be calculated as the product of TD x IM matrixes

		Number of balances for **Boiler** for each element
1	CH_4	2
2	O_2	2
3	N_2	2
4	CO_2	1
5	H_2O	1

Balance equations = number of non zero elements.

Table 7

Enthalpy of components [kJ/mol], using Termodata.xls:

index values	components	streams			reactions
		1	2	3	r1
63	CH_4	1	0	1	-1
34	O_2	0	1	1	-2
31	N_2	0	1	1	0
48	CO_2	0	0	1	1
22	H_2O	0	0	1	2
T	°C	5	-15	150	Hr1

Table 8

Enthalpy table

index values	components	streams			reactions
		1	2	3	r1
63	CH_4	-0,69989	0	4,88453	74,90181
34	O_2	0	-1,1691	3,73545	0
31	N_2	0	-1,1680	3,65165	0
48	CO_2	0	9	4,96869	-393,768
22	H_2O	0	0	4,26865	-483,99
T	°C	5	-15	150	Hr1
					-802,86

Table 9

Matrix of coefficients “A” and vector of right sides “B”

Element	Process unit	No. of element	Stream; element									
			1	2	2	3	3	3	3	3		
			1	2	3	1	2	3	4	5		
			n1; 1	n2; 2	n2;3	n3; 1	n3; 2	n3; 3	n3; 4	n3; 5	r1	B
CH_4	1	1	1	0	0	-1	0	0	0	0	-1	0
O_2	1	2	0	1	0	0	-1	0	0	0	-2	0
N_2	1	3	0	0	1	0	0	-1	0	0	0	0
CO_2	1	4	0	0	0	0	0	0	-1	0	1	0
H_2O	1	5	0	0	0	0	0	0	0	-1	2	0
	Enthalpy Balance		-0.699	-1.169	-1.168	-4.884	-3.735	-3.651	-4.968	-4.268	802.86	20
	Conc. O_2 in stream 2		0	-0.79	0.21	0	0	0	0	0	0	0
	Conc. CH_4 in stream 3		0	0	0	-0.996	0.004	0.004	0.004	0.004	0	0
	O_2 overflow		2.5	-1	0	0	0	0	0	0	0	0

After, we need to calculate the determinant of Matrix A (blue area) to control if it is solvable

Det A	146,402

And finally, we calculate the mol flows for each stream (vector "**X**") , because $A \cdot X = B$ => $X = B \cdot A^{-1}$

4. Results

Stream	n1,1	n2,2	n2,3	n3,1	n3,2	n3,3	n3,4	n3,5	r1
Flowrate [kmol/sec]	0,028688	0,07172	0,269805	0,001481	0,017306	0,269805	0,027207	0,054414	0,027207

In the same way, we applied this method for simulation of Nitric acid production, where the situation was much more complicated. The matrix of coefficients is the matrix 145 × 145. A block-diagram is shown in the Fig. 2 and a simulation Excel-file can be sent on request- ditl@centrum.cz

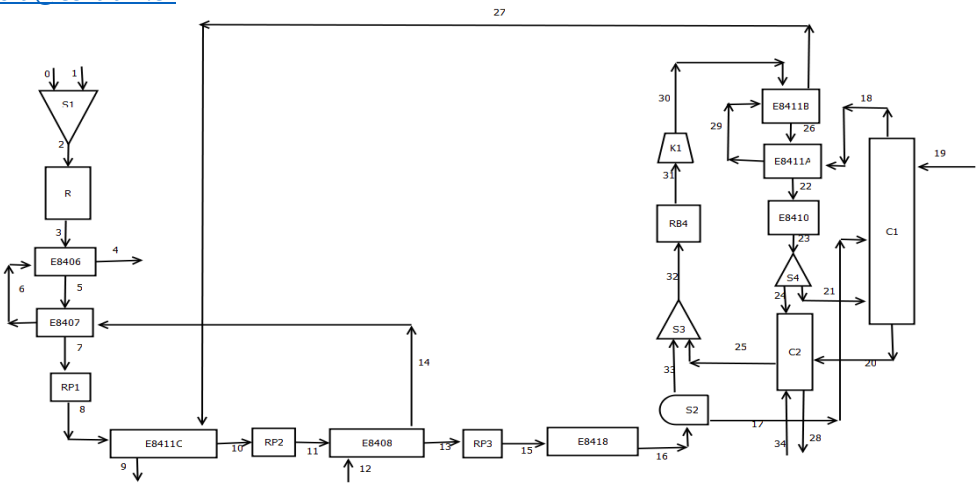

Fig. 2. Block diagram of nitric acid production

For those who are more deeply interested in the methodology we can provide the manual "Flowsheeting in EXCEL" (In Russian, English, German or Czech).

References

[1] http://www.i-programmer.info/ebooks/automating-excel/1264-getting-started.html
[2] https://studium.fs.cvut.cz/studium/u12118/DITL/PPP/ (access only for staff and students, having university ID)
[3] http://4excel.ru/index.php?id=excelbasic

TECHNICAL TRANSACTIONS | CZASOPISMO TECHNICZNE
MECHANICS | MECHANIKA
2-M/2016

EWA DŁUSKA, AGNIESZKA MARKOWSKA-RADOMSKA, AGATA METERA*

MULTIFUNCTIONAL EMULSION STRUCTURES FOR ENCAPSULATION AND MODIFIED RELEASE OF ACTIVE INGREDIENTS

WIELOFUNKCYJNE STRUKTURY EMULSYJNE DO ENKAPSULACJI I MODYFIKOWANEGO UWALNIANIA SKŁADNIKÓW AKTYWNYCH

Abstract

The paper presents the results of encapsulation of biologically and chemically active ingredients, such as living cells and drugs within multiple emulsions and release co-encapsulated drugs with the rate controlled by physicochemical properties of emulsions. The influence of process parameters in a Couette-Taylor flow bioreactor on the obtained emulsions structures, rate and mechanisms of release and the possibility to modify the release profiles have been discussed and presented.

Keywords: multiple emulsions, encapsulation process, release rate and mechanism

Streszczenie

Praca dotyczy wyników badań enkapsulacji substancji biologicznie i chemicznie czynnych takich jak leki i żywe komórki w emulsjach wielokrotnych oraz procesu ko-uwalniania z szybkością kontrolowaną parametrami fizykochemicznymi emulsji. W pracy przedyskutowano wpływ parametrów procesowych w bioreaktorze z przepływem Couette'a-Taylora na otrzymywane struktury emulsji oraz szybkość i mechanizm procesu uwalniania oraz możliwość modyfikacji krzywych uwalniania.

Słowa kluczowe: emulsje wielokrotne, proces enkapsulacji, szybkość i mechanizm uwalniania

DOI:

* PhD. DSc. Ewa Dłuska, PhD. Agnieszka Markowska-Radomska, MSc. Agata Metera, Faculty of Chemical and Process Engineering, Warsaw University of Technology.

1. Introduction

Multiple emulsions are defined as dispersed systems having structures of droplets in a drop (Fig. 1). The smaller droplets of one liquid (internal phase) within larger drops of a second immiscible liquid (membrane phase) are themselves dispersed in a continuous phase, which has the same composition as the smaller droplet, or a different one. Due to their compartmentalised internal structure, multiple emulsions present many advantages over simple O/W or W/O emulsions for encapsulation, such as the ability to carry both polar and non-polar molecules, and better control in releasing therapeutic molecules [1-5]. They combine the properties of both types of simple emulsions and have the potential to encapsulate a large number of different ingredients e.g. cosmetics, drugs, living cells and incompatible materials, and protect active substances from the environment [1, 4, 6]. These dispersed systems offer a wide range of possible applications for cosmetics, food or the pharmaceutical industries, especially for the encapsulation and controlled release of active ingredients. Double emulsions ($F_1/F_2/F_3$) represent the simplest structures among multiple emulsions, Fig. 1.

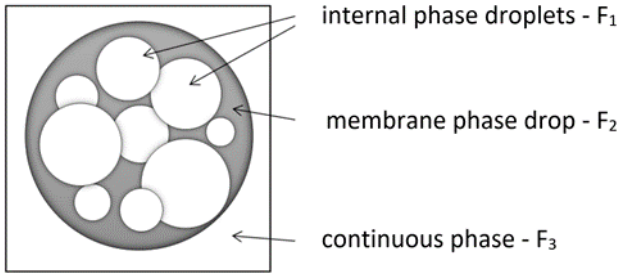

Fig. 1. The structure of double emulsion $F_1/F_2/F_3$

Encapsulation is the process of entrapping biologically/chemically active substances or in general particles of solid or droplets of liquid material or bubbles of gas within a protective membrane to produce capsules/drops in the micro/nanometre to millimetre range. There are two encapsulation processes, matrix in case dispersing active substances within membrane material or core shell when surrounding/coating with a continuous film of polymeric material is considering. The matrix particle allows a manufacturer to encapsulate more than one active ingredient within one particle, while the core shell is ideal for protecting an active ingredient where humidity and moisture or aggressive agents are present. The method of encapsulation can be divided into chemical, physiochemical, electrostatic and mechanical processes. Chemical processes include the interfacial and *in situ* polymerisation methods. Physiochemical processes include coacervation phase separation, multiple emulsion, meltable dispersion and powder bed methods. Mechanical processes include the air-suspension method, pan coating, and spray drying, spray congealing, micro-orifice system and the rotary fluidisation bed granulator method. Material or materials closed can be released for a specified time at a predetermined rate, depending on the process conditions for release-controlled or modified release.

Systems with a modified release of active agents are defined as systems providing a modify rate, profile or place where the release occurs, in comparison to conventional dosage forms of drugs administered through the same route [1, 4, 6]. The main objective of applying modified release systems is to achieve a constant concentration of active ingredients over a therapeutic time. Among systems with a modified profile of release, the following types can be distinguished: delayed, sustained and pulsatile release. The most widespread presentations of modified release drugs include oral, parenteral and transdermal dosage forms. Oral dosage forms are the most commonly used by patients due to their convenient administration. Obtaining drugs with a modified profile of an active agent release involves employing different settings concerning dispersed systems like suspensions, emulsions, aerosols, liposomes or micellar/lamellar structures. However, micro/nanoparticles that have undergone coating or incorporation are most frequently applied to a modified release profile.

Multiple emulsions are an example of a dispersed system applied in the modified release of an active agent. There are two main mechanisms of release: simple or facilitated diffusion or fragmentation of multiple emulsion, i.e. breakage of multiple drops and formation of simple emulsion [6]. In addition, the release process can be controlled by both of the mentioned mechanisms. In majority of drug release systems, the release is limited by mechanisms like dissolution, osmosis, diffusion or chemical reaction [1]. They can take place simultaneously or at different stages of the release process.

A literature overview has shown that the issue of the simultaneous encapsulation of two or more different active ingredients in the multiple emulsion, and their release has not been fully reported and explained yet.

The purpose of the work was to investigate a simultaneous encapsulation of two active ingredients, such as two drugs or living cells within double emulsions and process of release of co-encapsulated drugs.

2. Emulsification and encapsulation process in a Couette-Taylor flow biocontactor

The aim of the experimental research was to examine the process of biological and chemical ingredients encapsulation in double emulsions. Methods: Double emulsions of two types $W_1/O/W_2$ and $O_1/W/O_2$ were prepared by simultaneous emulsification and encapsulation in liquid-liquid Couette-Taylor flow (CTF) bioreactor/biocontactor, Fig. 2 (annular gap width of 1.5 and 2,5 mm and length of 400 mm).

$W_1/O/W_2$ emulsions consisted of alginic acid aqueous solution (inner phase) with living cells (Human Embryonic Kidney – HEK) and a cryoprotectant (sucrose), paraffin (membrane phase), distilled water (outer continuous phase) with appropriate surfactants (Tween and Span) added to each phase. The process parameters included: the rotational frequency of the inner cylinder of the CTF biocontactor: 540 rpm, an annular gap width of 2.5, the ratio of the volumetric flow rates of phases: internal to continuous: 0.25÷0.5 and internal to membrane: 0.5÷1.0, concentration of living cells: one million cells per cm^3.

$O_1/W/O_2$ emulsions contained liquid paraffin as oil phases with an addition of two model active agents (phenyl salicylate and benzoic acid) to inner oil phase and aqueous gelatine solution as a membrane water phase. The process of emulsification and co-

encapsulation of model drugs into $O_1/W/O_2$ has been successfully carried out under conditions corresponding to the rotational frequency of the inner cylinder of the CTF contactor: 1550÷1900 rpm, an annular gap width of 1.5, the ratio of the volumetric flow rates of phases: internal to continuous: 0.1÷0.5 and internal to membrane: 0.2÷0.5, concentration of drugs in the inlet stream for phenyl salicylate: 9.25 and 10 wt%, for benzoic acid: $2 \div 9.1 \cdot 10^{-3}$ wt%.

The details of the preparation technique of multiple emulsions in the CTF contactor and micro-encapsulation procedure were discussed in our earlier publications [6, 7]. The CTF contactor creates suitable hydrodynamic conditions for conducting mass transfer processes in multiphase systems (high interfacial area and mass transfer coefficients) [7÷9].

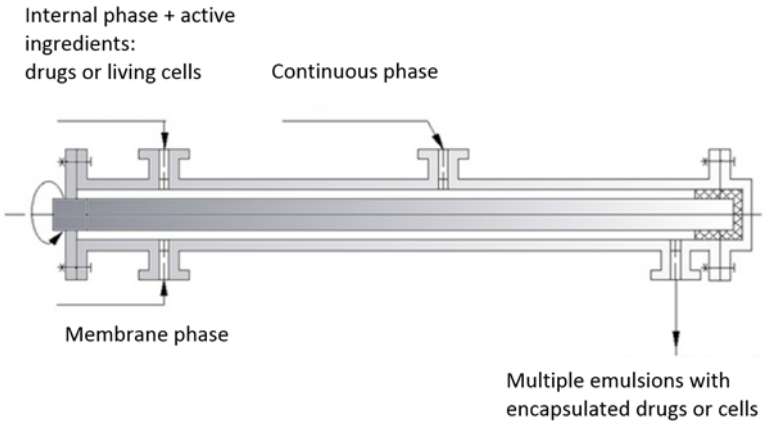

Fig. 2. Liquid-liquid Couette-Taylor flow biocontactor/bioreactor for forming double emulsion $W_1/O/W_2$ and $O_1/W/O_2$ and encapsulating of active ingredients

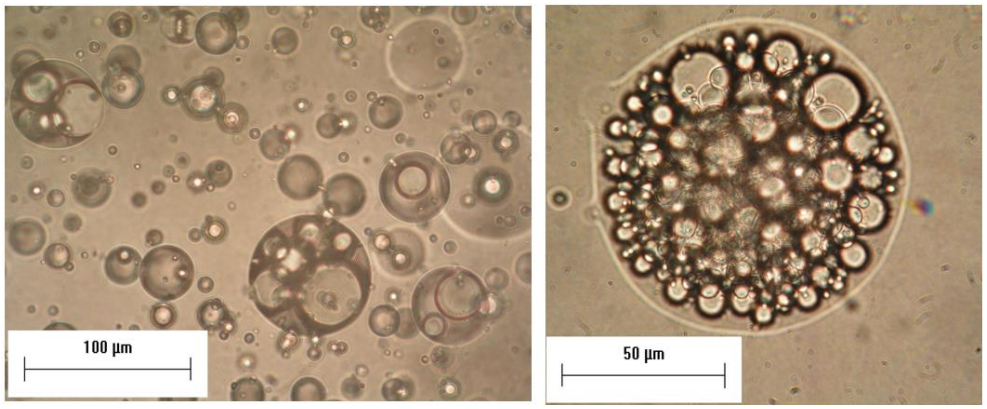

Fig. 3. The representative photos of multiple emulsions $O_1/W/O_2$ with co-encapsulated of two hydrophobic drugs (phenyl salicylate and benzoic acid) within internal paraffin droplets: phenyl salicylate (9.25 wt%) and benzoic acid $2.68 \cdot 10^{-3}$ wt%: left – at time $t = 0$, right – at $t = 46.22$ h.

Hydrodynamic conditions in the CTF biocontactor: rotational frequency of inner cylinder: 1622 rpm; flow rates of the liquid phases: internal/membrane/continuous = 50 /15 /100 cm^3/min

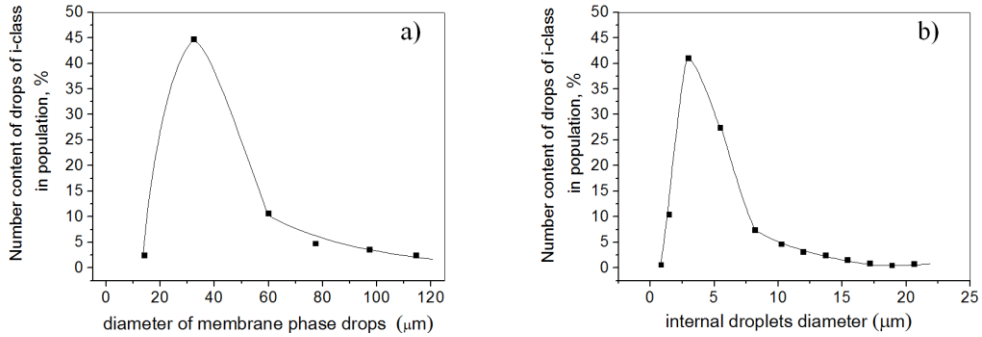

Fig. 4. The drop size distribution of double emulsions $O_1/W/O_2$ with two hydrophobic drugs encapsulated presented in Fig. 3: a) membrane phase drops, b) internal droplets

The shear stresses in a Couette-Taylor Flow apparatus are reduced by one to two orders of magnitude compared to a stirred tank with similar power input per unit volume and stirrer diameter being equal to the rotor of CTF [7]. This is a result of an increase in the area subjected to a constant maximum shear defined by friction drag on the larger surface of cylinder in the CTF device.

The structures of double emulsions with two hydrophobic drugs being encapsulated into internal droplets and drop size distribution are presented in Figs. 3 and 4.

The structures of double emulsions with living cells encapsulated within the internal droplets and the drop size distribution are shown in Figs. 5 and 6.

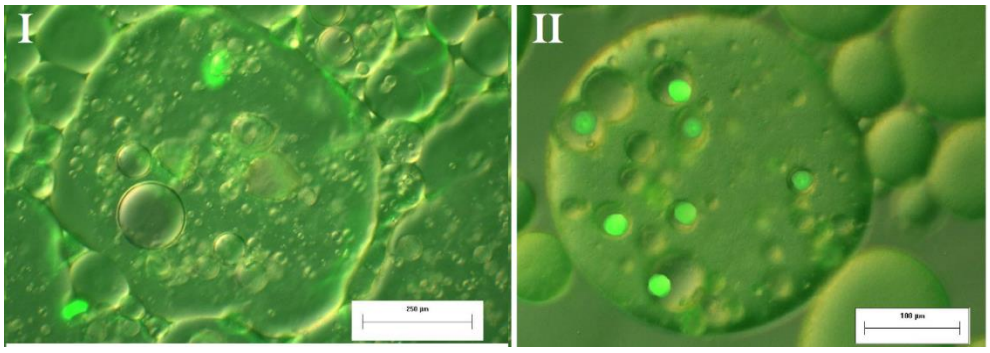

Fig. 5. The fluorescence microscope photos of multiple emulsions $W_1/O/W_2$ with encapsulated of living cells (HEK- Human Embryonic Kidney) within internal alginate droplets – I and additionally with sucrose as a cryoprotectant in the internal droplets – II:
Hydrodynamic conditions in the CTF biocontactor: rotational frequency of inner cylinder: 540 rpm; flow rates of the liquid phases: internal/membrane/continuous = 30 /30 /60 cm^3/min

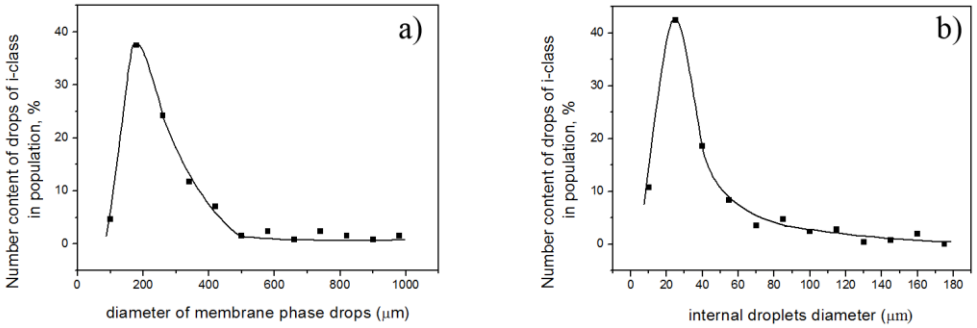

Fig. 6. The drop size distribution of double emulsions $W_1/O/W_2$ with living cells (HEK) encapsulated within internal alginate droplets shown in Fig. 5: a) membrane phase drops, b) internal droplets

3. The rate and mechanism of simultaneous release of two active ingredients

The experimental release study involved the influence of parameters of the emulsification and encapsulation process in a CTF biocontactor and the conditions of the release process (mixing intensity) on the release rates of two entrapped model active agents from internal paraffin droplets to the external paraffin phase of emulsions. The release experiments have been carried out in the stirred tank under a stirring frequency of 150 and 250 rpm at a temperature of 37°C.

The process of simultaneous encapsulation of phenyl salicylate and benzoic acid in the internal phase of $O_1/W/O_2$ double emulsions in the CTF contactor has shown an ability to create modified release by forming different structures of emulsions. The best double emulsions have been those obtained from a solution of drug concentration: 10 wt % of phenyl salicylate and $2.91 \cdot 10^{-3}$ wt % of benzoic acid in a contactor with an internal cylinder frequency of 1802 rpm [10]. These double emulsions $O_1/W/O_2$ with co-encapsulated hydrophobic have been characterised by a high encapsulation efficiency, the highest stability of internal and membrane phase drops and a two-step release profile of phenyl salicylate. The influence of preparation conditions in the CTF contactor, an initial concentration of benzoic acid and the conditions in the release environment on the kinetics of release process are demonstrated in Figs. 7 ÷ 9. The release profiles have been presented in the form of a dependence of cumulative mass fraction of the released ingredient on time.

Simultaneous release of both active substances from double emulsions (prepared under different hydrodynamic and process conditions in the CTF contactor) has shown that the release process occurring in the stirred tank is governed by a diffusion mechanism. The release mechanism has been verified during experiments performed in the stirred tank by comparing change in the drop size using microscopic image analysis. Since the diameter of the membrane phase drops and internal droplets remain unchanged, consequently, the basic release mechanism responsible for the release was unchanged too.

The comparison of the release profiles of emulsions with one (phenyl salicylate) and two (phenyl salicylate + benzoic acid) active agents has shown that the modified pattern, i.e. two-step release kinetics of phenyl salicylate has been a result of the presence of the second ingredient (Figs. 7, 8).

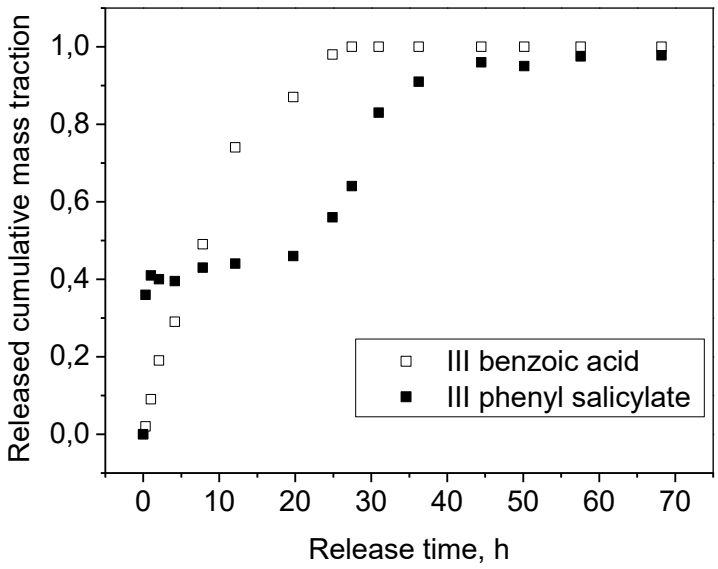

Fig. 7. Release profiles of both encapsulated drugs: benzoic acid and phenyl salicylate from double emulsions III formed under conditions in the CTF contactor: rotational frequency of inner cylinder 1802 rpm, initial concentration of benzoic acid: $9.09 \cdot 10^{-3}$ wt% and phenyl salicylate 10 wt%

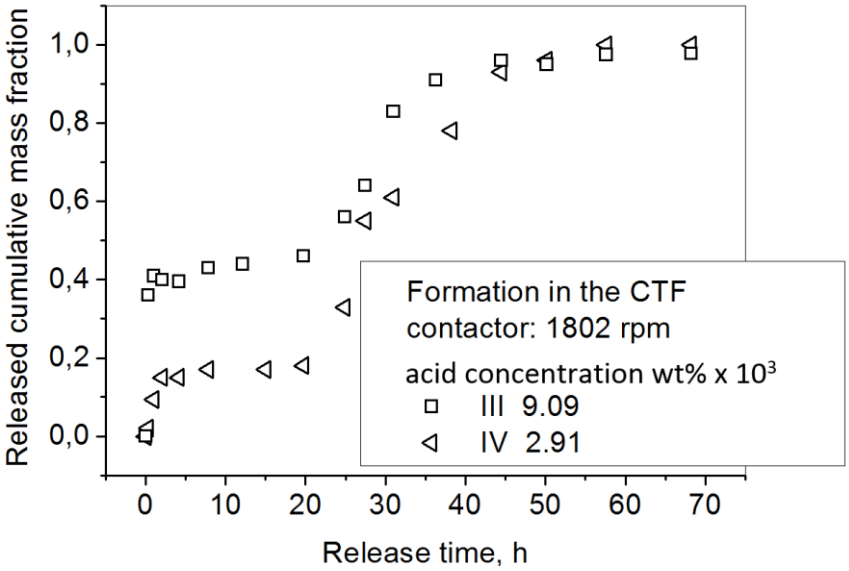

Fig. 8. The influence of an initial benzoic acid concentration on the release rate of phenyl salicylate from double emulsions III and IV formed in the CTF contactor

Addition of the second ingredient affects the time required to completely release the basic encapsulated ingredient, i.e. phenyl salicylate. The longest period of time required for a complete release of phenyl salicylate was observed for emulsions, which have been prepared under the highest rotational frequency of inner cylinder in the CTF contactor. Increasing the mixing intensity of the release medium caused a faster release of the encapsulated drugs (Fig. 9).

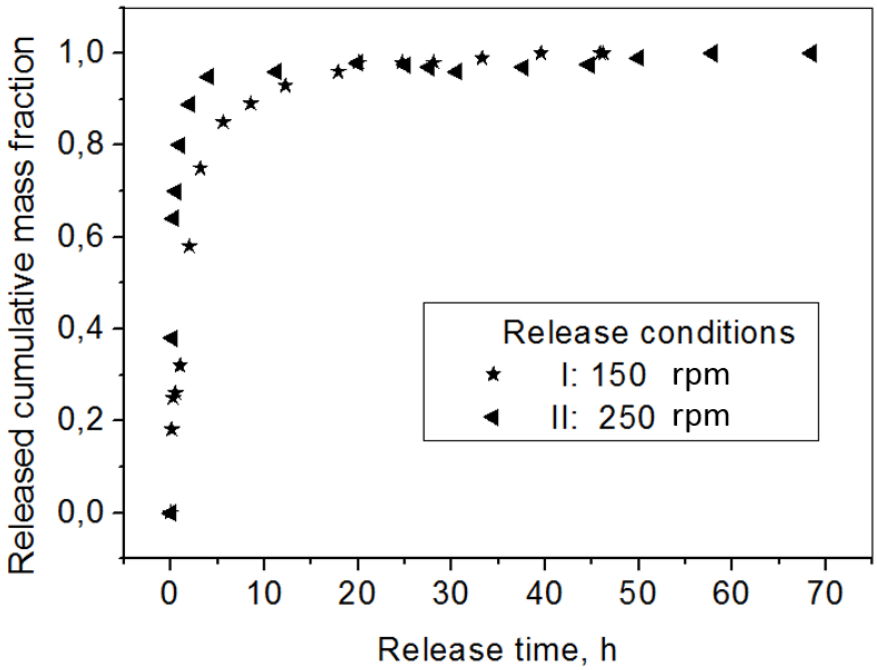

Fig. 9. The influence of the mixing intensity of environment on the release rate of phenyl salicylate from double emulsions I and II formed under conditions in the CTF contactor: rotational frequency of inner cylinder: 1622 rpm; initial concentration of benzoic acid: $2.68 \cdot 10^{-3}$ wt% and phenyl salicylate: 9.25 wt% – emulsions I, initial concentration of benzoic acid: $9.09 \cdot 10^{-3}$ wt% and phenyl salicylate 10 wt% – emulsions II

4. Summary

The study showed that it is possible to encapsulate biologically and chemically active ingredients, such as living cells and two different drugs in double emulsion $W_1/O/W_2$ or $O_1/W/O_2$ using the CTF contactor. Multiple emulsions with living cells can be further considered as carriers of biological material and a microenvironment for banking and storing cells for therapeutic purposes.

The release study involved the simultaneous release of two entrapped model active ingredients (two hydrophobic drugs) from the internal droplets to the external continuous phase of emulsions of

different structures proved that it is possible to modify the release kinetics, i.e. the rate and type of release profiles. The release of active ingredients from multiple emulsions can be controlled through the physicochemical parameters of emulsions and the size of internal droplets and drops forming a liquid-permeable membrane separating the internal droplets from the external environment. A desirable modified type of the release profile would be achieved by adding a few active ingredients into the internal droplets.

Research on simultaneous encapsulation and release of a few substances that have been made until now demonstrates new potential applications of multiple emulsions as systems for controlled/modified drugs release in targeted therapies. However, the issue of simultaneous release of a few active agents from multiple emulsions requires an extension of experimental investigations and mathematical modelling of the process.

References

[1] Aserin A., *Multiple emulsions: Technology and Applications*, J. Wiley & Sons, USA 2008.

[2] Wilson J. L., McDevitt, T. C., *Stem cell microencapsulation for phenotypic control, bioprocessing, and transplantation,* Biotechnology and bioengineering vol. 110(3), 2013, 667-682.

[3] Khopade A. J., Jain N. K., *Concanavalin-A conjugated fine-multiple emulsion loaded with 6-mercaptopurine.*, Drug Delivery, vol. 7(2), 2000, 105-112.

[4] Siepmann J., Siegel R. A., Rathbone M. J. (Eds.), *Fundamentals and applications of controlled release drug delivery*, Springer Science & Business Media, USA 2011.

[5] Hino T., Kawashima Y., Shimabayashi S., *Basic study for stabilization of w/o/w emulsion and its application to transcatheter arterial embolization therapy*, Advanced drug delivery reviews, vol. 45(1), 2000, 27-45.

[6] Markowska-Radomska A., Dluska E., *An evaluation of a mass transfer rate at the boundary of different release mechanisms in complex liquid dispersion,* Chemical Engineering and Processing: Process Intensification, 101, 201656-71.

[7] Dluska E., Markowska-Radomska A., *Regimes of multiple emulsions of W1/O/W2 and O1/W/O2 type in the continuous Couette-Taylor flow contactor*, Chemical Engineering and Technology, vol. 33(1), 2010, 113-120.

[8] Curran S. J., Black R. A., *Oxygen transport and cell viability in an annular flow bioreactor: Comparison of laminar Couette and Taylor-vortex flow regime,* Biotechnology and bioengineering, vol. 89(7), 2005, 766-774.

[9] Dluska E., Hubacz R., *Mass transfer in the two-phase helicoidal contactor,* Inżynieria chemiczna i procesowa, vol. 21(1), 2000, 103-113.

[10] Metera A., *Wytwarzanie aktywnych emulsji wielokrotnych metodą enkapsulacji w przepływie helikoidalnym*, Praca dyplomowa magisterska, Politechnika Warszawska, 2014.

Acknowledgments

The authors would like to thank the National Science Centre – Poland for supporting the part of the research regarding the drugs encapsulation and co-release under grant number 2014/13/B/ST8/04274.

TECHNICAL TRANSACTIONS | CZASOPISMO TECHNICZNE
MECHANICS | MECHANIKA
2-M/2016

ANDRZEJ DUDA, JERZY KAMIEŃSKI*

THE CIRCULATION OF LIQUID IN THE MIXING VESSEL EQUIPPED WITH DIFFERENT DUAL IMPELLERS

CYRKULACJA CIECZY W APARACIE Z DWOMA RÓŻNYMI MIESZADŁAMI

A b s t r a c t

The aim of the article was the analysis of liquid flow of radial-axial circulation in the mixing vessel equipped with a dual impeller set, of which the lower impeller induces radial-axial liquid stream, while the upper is turbine disc impeller with vertical blades, ejecting the liquid radially. On the basis of measurements of the liquid instantaneous velocity, the circulation flow rate was evaluated and supplemented with the exchange flow rate – occurring between adjacent compartments. The usage of a CMA model allows to describe the cycle of liquid transport.

Keywords: mixing, circulation of liquid,

S t r e s z c z e n i e

W artykule analizowano przepływy strumieni cieczy cyrkulacji promieniowo-osiowej w zbiorniku z dwoma mieszadłami na wale, z których dolne wytwarza promieniowo-osiowy strumień cieczy, górnym zaś jest mieszadło turbinowe tarczowe, z pionowymi łopatkami, wyrzucającymi ciecz promieniowo. W oparciu o pomiary chwilowej prędkości cieczy wyznaczono wydatek jej przepływu cyrkulacyjnego, uzupełniony o przepływy między obszarami cyrkulacyjnymi. Korzystając z modelu CMA opisano cykl przenoszenia cieczy.

Słowa kluczowe: mieszanie, curkulacja cieczy

DOI:

* MSc. Eng. Andrzej Duda, Firma Doradczo-Inżynieryjna EDA, Wieliczka, Prof. PhD. DSc. Eng. Jerzy Kamieński, Institute of Thermal and Process Engineering, Faculty of Mechanical Engineering, Cracow University of Technology.

1. Introduction

This study is dedicated to the flows of liquid streams of the radial-axial circulation in a mixing vessel equipped with different dual impeller sets. In each dual set, the lower impeller induces radial-axial liquid stream, while the upper is a turbine disc impeller with vertical blades, ejecting the liquid radially.

The impellers, rotating in the liquid, spin it as a stream of primary circulation. Whereas the centrifugal force acting on the spinning liquid induces secondary circulation in the entire volume of the vessel. This secondary circulation is known as radial-axial circulation and is related to the pumping process of the impellers. This circulation is crucial for proper and efficient mixing.

In order to achieve the required intensity of the mixing process, two impellers are often assembled on a common drive shaft. Such solution is often used in the mixing of a multiphase systems.

The paper presents the study on three dual impeller sets, located on a common single shaft, at several different distances from each other. During the experiments, the values of the instantaneous velocity of liquid were measured (radial and axial component of the velocity). Then, on the basis of the mean velocities, the circulation flow rate of the liquid was determined.

In the study, the Compartment Model Approach (CMA) was used. The total flow rate values were supplemented by the exchange flow rate of the liquid occurring between circulation compartments. This additional flow rates are caused by fluctuations of liquid velocity. Based on the CMA model, the two-dimensional chart of liquid transport in an apparatus was described. Further use of this model enabled to describe the cycle of liquid transport in an apparatus, the duration of which was related to the mixing time, and could be a measure of the mixing process efficiency when considered it together with energy consumption.

2. Experimental set-up and methodology

The measurements of the instantaneous velocities of liquid were performed using two-channel laser Doppler anemometer (LDA, delivered by the DANTEC Company), operating in the backscattering mode [6]. The experiments were carried out in a cylindrical vessel, with the inner diameter of D = 0.286 m, equipped with four flat baffles, each with the standard width of $0.1 \cdot D$. The cylindrical vessel was built in the rectangular jacket. Both of them were made of the same material, a borosilicate glass of the DURAN type. To eliminate an error of the refraction effect, occurring when the laser beams pass through different materials, the dimethyl sulfoxide, fully transparent liquid, having the same refractive index as DURAN glass, was employed in the experiments. The temperature of the liquid and vessels' walls was controlled by the thermostatic system; the measurements were carried out at the temperature of 22.5°C, wherein the density of the dimethyl sulfoxide was 1100 kg/m^3 and the dynamic viscosity coefficient – of 2.3 mPa.

As the seeding particles, the hollow glass spheres with a silver plated outer surface (trade symbol S-HGS) were used in the experiments. The mean diameter of the particles

was 10 μm, and their average density was 1150 kg/m^3. Both the vessel and the jacket were filled up with liquid to the height of 1.258*D*.

Three different dual impeller sets were examined. The upper impeller was in each case the disc turbine, equipped with six vertical, flat blades – TR-6. The lower impeller was exchanged by three different types: the turbine with six blades inclined at 45° (Pitched Blade Turbine, PBT-6 type), the hydrofoil Chemineer HE-3 impeller [4] and the hydrofoil Lightnin A-315 impeller [12]. The diameter of all examined impellers was of $d = D/3$. The lower impeller was in each case located at the distance of $h = 0.5 \cdot d$ from the vessel's bottom and the value of the impeller spacing Δh was changed in the range of $(0.5 \div 2) \cdot d$.

The liquid velocities were measured in the selected points, located at the vertical middle plane of the vessel, placed between two successive baffles and forming a regular, rectangular grid. The measurement points were spaced by 0.005 m along the radius of the vessel and its height. The two components of the instantaneous velocity of liquid were measured: the radial $u_r(t)$ and the axial $u_z(t)$.

The experiments were carried out within the turbulent flow regime of liquid, at a constant rotational frequency of impellers of 5 [s^{-1}], which corresponded to the Reynolds number for a mixing process, $Re \approx 2.16 \cdot 10^4$. The power consumption was an additional magnitude measured during the experiments.

3. Experimental results

3.1. Mean velocities of liquid

The values of the velocity components: mean $\bar{u}$ and fluctuating u', were calculated on the basis of prior measurement data of the instantaneous velocities, benefiting from the FLOware software.

The components of mean velocity $\bar{u}_i$ were calculated as the weighted averages, with weights corresponding to the residence time $\Delta t_{i,j}$ of seeding particles in the measurement volume [6, 11]:

$$\bar{u}_i = \frac{\sum_{i=1}^{N} u_{i,j} \cdot \Delta t_{i,j}}{\sum_{i=1}^{N} \Delta t_{i,j}} \tag{1}$$

The shape and intensity of the mean flow of liquid in the mixing vessel is determined by the distributions of velocity components and their local values. The primary circulation of liquid, induced during the mixing process by rotating impellers, is partly being converted to the secondary, related to the radial-axial flow. This flow is also directly related to the components of mean velocity: radial and axial.

These radial-axial flows of liquid, occurring in the mixing vessel, depend on the design of applied impellers and their mutual position. They were illustrated in Figs. 1÷3, as distributions of the resultants of mean velocities in the radial and axial direction. They were drawn at the vertical middle plane located between two baffles in the vessel.

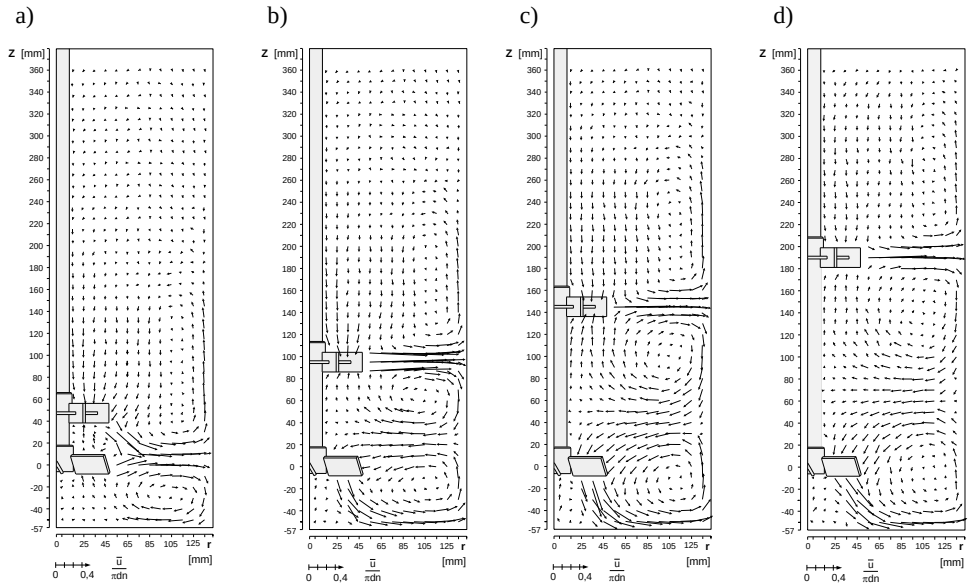

Fig. 1. The distribution of the resultants of mean liquid velocities in the radial and axial direction, in the dual mixing vessel equipped with the upper disc turbine TR-6 and the lower impeller pitched blade turbine PBT-6. The impeller spacing:a) $\Delta h = 0.5d$, b) $\Delta h = d$, c) $\Delta h = 1.5d$, d) $\Delta h = 2d$ [5]

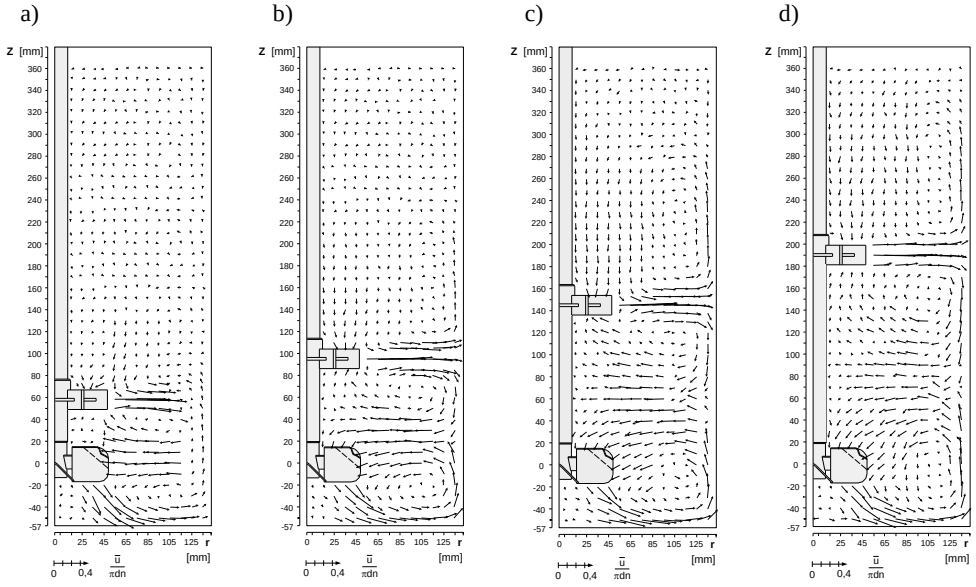

Fig. 2. The distribution of the resultants of mean liquid velocities in the radial and axial direction, in the dual mixing vessel equipped with the upper disc turbine TR-6 and the lower A-315 impeller; the impeller spacing: a) $\Delta h = 0.6d$, b) $\Delta h = d$, c) $\Delta h = 1.5d$, d) $\Delta h = 2d$ [5]

All examined dual impeller sets induce an advantageous structure of the liquid flow in the mixing vessel. When the impellers are at sufficient distance, the flow of liquid is expanded in the entire volume and is sufficiently intense. The flow structure is then composed of several compartments, close to the model structure of a multistage mixing [1, 15, 18]. The circulation flows in the mixing vessel are similar; however, they differ from each other quantitatively, depending on the design of the lower impeller.

The adjacent circulation loops interact only at certain distances between the impellers. If these distances are too small or too large, then the interaction completely disappears. At small values of the spacing, the adjacent circulation loops induced by the upper and the lower impeller coalesce into one common. The shapes of these loops are determined by the resultant streams of the liquid flow, pumped through both of the impellers.

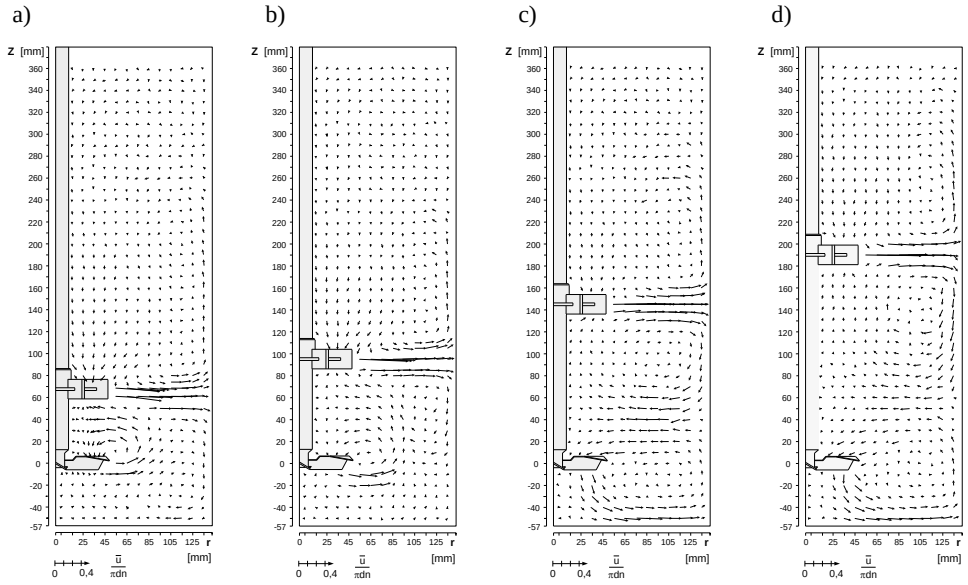

Fig. 3. The distribution of the resultants of mean liquid velocities in the radial and axial direction, in the dual mixing vessel equipped with the upper disc turbine TR-6 and the lower HE-3 Impeller; the impeller spacing: a) $\Delta h = 0.7d$, b) $\Delta h = d$, c) $\Delta h = 1.5d$, d) $\Delta h = 2d$ [5]

It was clearly shown in Figs. 1a, 2a and 3a, illustrating the flows in the mixing vessel equipped with two impellers located at the spacing of $\Delta h = (0.5 \div 0.7) \cdot d$.

In case of dual impeller sets with the lower PBT-6 or HE-3 impeller, the impact of the upper disc turbine is so intense that the lower impeller ejects the liquid radially towards the vessel's wall. While it should induce an axial flow of liquid, taking into consideration its position inside the mixing vessel. In the case of HE-3 impeller, this trend also occurs at greater spacing. It is evident even when $\Delta h = d$. It is different, however, in case of the set with lower A-315 impeller, which induces an intensive axial flow of liquid, directed towards the bottom of the tank, even at a position close to the upper impeller. When the impeller spacing is being increased, a gradual loss of the interaction between the adjacent

liquid streams can be observed, with simultaneous change of the geometry of circulation loops. In case the lower impeller is PBT-6 turbine or A-315, the loops are being spread along the height of the vessel, and for the dual set with the lower impeller of HE-3 type, additionally, a complete change of the geometry of loops and their position in the tank can be noticed.

3.2. Circulation flow rate of liquid

The liquid flow rate Q_C refers to the motion of liquid in the entire volume of the mixing vessel. It is defined as the stream of liquid flowing through the surface, which is located at any cross-section in the tank. Whereby it is considered, both the axial flow rate Q_z, occurring at the horizontal section plane of the tank, at the height of z_i and the radial flow rate Q_r – present at the vertical section plane, at the radius of r_i. Moreover, assuming the circular symmetry of the flow, they are defined as [9]:

$$Q_z(z_i) = \iint_{S_{z_i}} (\bar{u}_z)_{z_i} \, \mathrm{d}S_{z_i} \tag{2}$$

$$Q_r(r_i) = \iint_{S_{r_i}} (\bar{u}_r)_{r_i} \, \mathrm{d}S_{r_i} \tag{3}$$

Furthermore, assuming axial symmetry, the circulation flow rate of liquid in the mixing vessel, Q_C is equal to the maximum value of the flow rates Q_z and Q_r [10]:

$$Q_C = \max\{|Q_z|, |Q_r|\} \tag{4}$$

The circulation flow rate was calculated on the basis of the components of mean velocity of liquid, evaluated at selected measurement points (Figs. 1÷3).

The quantity and limits of the circulation zones were evaluated on the basis of distributions of resultants of the mean velocity components: radial and axial. The analysis of directions and senses of the mean velocity resultants allowed to evaluate the limits of each zone, by determining the value of z_o height, in around which the real limit of zone can be found. It is exemplified in Fig. 4, where the limits of the respective zones are defined as $z_{o1\text{-}2}$, $z_{o2\text{-}3}$ and $z_{o3\text{-}4}$. The values of the axial components of the mean liquid velocity, measured at the points located the closest to the height coordinate of z_o, just below and above it, were then approximated using a continuous function. Next, it was found by means of standard mathematical procedure that the z value of the height at which this velocity component changed its sign reaching zero.

Thus, the z_g coordinate value of the point on the limit line was obtained, corresponding to a given radius of r. This procedure was repeated for each group of points corresponding to different values of the radius, which was changed every 5 mm. The determination of the limit line, described by the $z_{og} = f(r)$, was based on the approximation of the evaluated z_g values, with usage of the continuous function.

In case the centres of loops (restricted in the respective circulation zones) did not coincide the one straight line corresponding to a certain radius value and parallel to the vessel's axis, it was not possible to evaluate the position of the points of limits, based on

the $\bar{u}_z = f(z)$ function. The vectors of the axial component of the mean velocity took the same sense, near the limit of adjacent circulation zones. In such cases, the points of limit were evaluated using the $\bar{u}_r = f(r)$ function and searching for its zero value corresponding to a certain r argument. This function describes alterations of the radial component of the mean velocity versus the radius, at different heights. Then, the points of the circulation zone limit were described using the *rog* radius, which differed depending on the height in the mixing vessel, replacing the dependency of $z_{og} = f(r)$ – with the $r_{og} = f(z)$ function. The circulation flow rate of liquid was evaluated within the limits of each such determined zone. The equations (2), (3) were converted to following form:

$$Q_z(z_i) = 2\pi \int_{r_1}^{r_2} (\bar{u}_z)_{z_i} \, r \, \mathrm{d}r \tag{5}$$

$$Q_r(r_i) = 2\pi r_i \int_{z_{og1}}^{z_{og2}} (\bar{u}_r)_{r_i} \, \mathrm{d}z \tag{6}$$

The procedure described above was illustrated in Fig. 4a. The profiles of $\bar{u}_r$ velocity component drawn along the vessel's height are marked in this figure, for the four selected radiuses, against the real limits of the considered liquid circulation zone. The area covered by this zone is also marked in Fig. 4b, illustrating the mean radial-axial flow of liquid.
In this case, the $\bar{u}_r$ velocity profiles were integrated using the equation (6), within the limits of zone of $|z_{og1\text{-}2}, z_{og2\text{-}3}|$ corresponding to a given radius of the vessel. The liquid flow within the circulation zone was assumed as in closed-circuit. For each velocity profile, there is some part of it in accordance with the direction of coordinate system ($\bar{u}_r^{(+)}$), and its remaining part is opposite of the coordinate system ($\bar{u}_r^{(-)}$). Thus, the two integrals: $Q_r^{(+)}$ and $Q_r^{(-)}$ were calculated. This procedure was repeated for the further values of *ri* radius, and next, all of obtained values were approximated at the end with usage of the continuous function. Similarly, the procedure was carried out using the equation (5). The maximum of these values was the wanted circulation flow rate Q_{Ci}, of the *i*-th zone in the vessel. The liquid flow rate circulating in the total volume of the vessel was evaluated as the sum of the *n* – flow rates from the respective *n*-zones of circulation, which form the total structure of the flow:

$$Q_{C\,\mathrm{sum}} = \sum_{i=1}^{n} Q_{Ci} \tag{7}$$

Finally, it was presented in the form of a dimensionless circulation flow number, of which values were collected in Table 1 and shown in Fig. 5:

$$K_C = \frac{Q_{C\,\mathrm{sum}}}{n \cdot d^3} \tag{8}$$

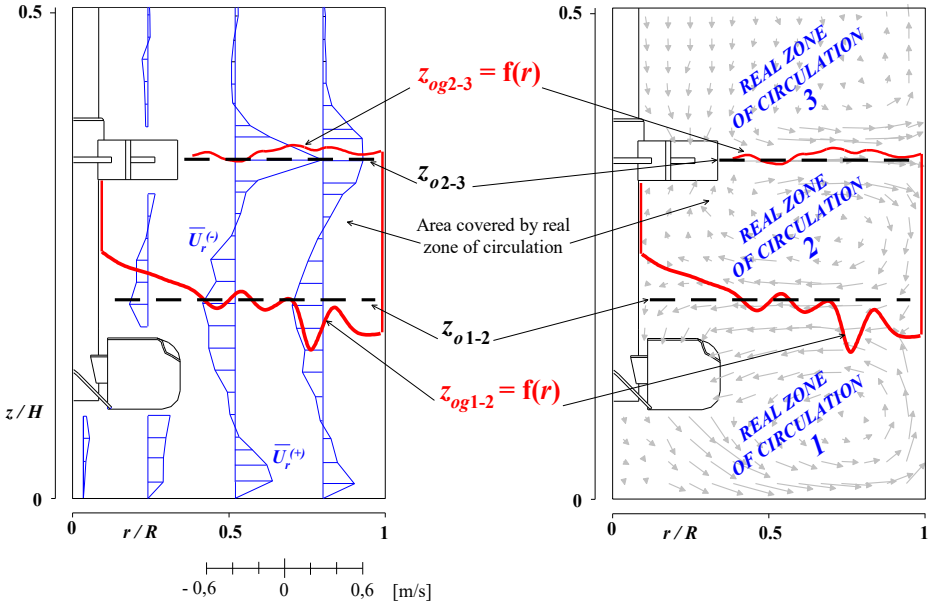

Fig. 4. The location of points of limit z_{og} along the radius of tank. The z_o heights and the real limiting lines of the circulation zones, determined by the procedure of approximation of points z_{og}. The dual impeller set: TR-6 and A-315, $\Delta h = d$

The greatest values of the circulation flow number can be found for the dual set with A-315 impeller. The set with a pitched blade turbine can induce even a more efficient circulation only at the greatest possible impeller spacing. For the values of $\Delta h \geq d$, the least intense circulation is always induced by the set of lower HE-3 impeller. For each of the examined pair of impellers, the circulation flow rate of liquid takes the greatest values when the impellers are spaced by $\Delta h = 1.5d$.

Table 1

The circulation flow numbers of liquid K_C and $K_{C\,calk}$ for the examined dual impellers, with the upper TR-6 disc turbine

Lower impeller:	PTB-6		A-315		HE-3	
	K_C	$K_{C\,calk}$	K_C	$K_{C\,calk}$	K_C	$K_{C\,calk}$
$\Delta h \cong 0.5d$	2.12	2.93	2.28	3.13	2.15	3.00
$\Delta h = d$	3.09	4.69	3.21	4.53	1.93	3.00
$\Delta h = 1.5d$	3.58	5.19	3.63	4.96	3.08	3.98
$\Delta h = 2d$	3.42	4.57	3.22	4.50	2.83	3.88

The analysis of the flow structure was carried out using the Compartment Model Approach (CMA) [7, 8, 13]. For the flow modelling purposes, the real circulation flows of liquid, determined by the radial and axial components of the mean velocity, were replaced

with the contractual circulation compartments: of the first order - situated above and below each impeller, of the second order – in other zones of the vessel. Thus, the zones of liquid circulation (illustrated in Figs. 1÷3) could be presented in the form of contractual, two-dimensional and rectangular compartments specified in the vertical section of the vessel and located cascaded – one above the other. The compartments illustrate the secondary radial-axial circulation flow of liquid in the dual mixing vessel [7, 17, 18]. The limits of these compartments result from the real limits of the circulation zones, z_{og}. The liquid flow inside the compartment is determined by the Q_{Ci} flow rate. The momentum exchange between adjacent compartments takes place at their limiting line, only in the axial direction. It is correlated to the exchange flow rate, induced by the axial component of fluctuation velocity. This component was determined at the points located on the limiting line of the adjacent circulation zones. The values of u'_z, measured at the points located at certain radius coordinate and at several height coordinates, the closest to the corresponding point of the limiting line, z_g, were compiled as a function of the vessel's height and approximated using the continuous function $u'_z = f(z)$. When this function was known, the value of $u'_{zg} = f(z = z_g)$ could be determined. The RMS values, referred to the axial components of fluctuations of the instantaneous velocity, were assumed in place of the u_z' and u_{zg}'. The RMS values were directly obtained from the LDA measurements.

Then, the liquid velocity components, as a function of radius in the vessel, were processed by another approximation using the $u_{zg}' = f(r)$ relationship. This was carried out in the total volume of the dual mixing vessel, at all of the limits which separate corresponding compartments of the circulation flows. The Q_{Ei} flow rate between the adjacent circulation compartments of liquid was determined by the integration process of the $u_{zg}' = f(r)$ function, within the range of r_g radius values. Due to the symmetry of structure and the continuity of flow, it is assumed that the exchange flow occurs in both directions and is equal from both sides as is:

$$Q_{Ei} = 0.5\left[2\pi \int_{r_{g1}}^{r_{g2}} \left[u'_{zg}(r)\right] r \, \mathrm{d}r\right] \tag{9}$$

The total exchange flow rate $Q_{E\ sum}$ was then defined as a sum of all flows determined on the limiting lines between respective compartments of the circulating liquid:

$$Q_{E\,sum} = \sum_{i=1}^{n} Q_{Ei} \tag{10}$$

Thus, the total, corrected liquid flow rate in the dual mixing vessel $Q_{C\ calk}$ was defined as:

$$Q_{C\,cala} = Q_{C\,\mathrm{sum}} + Q_{E\,\mathrm{sum}} \tag{11}$$

and was presented in the dimensionless form, as the corrected, total flow rate number $K_{c\ calk}$:

$$K_{C\,calk} = \frac{Q_{C\,sum} + Q_{E\,sum}}{n\,d^3} \tag{12}$$

Its values, obtained for the examined dual impeller sets, are collected in Table 1 and shown in Fig. 5.

The corrected flow rate of liquid includes the mean flows within the limits of its circulation compartments, as well as the fluctuation flows – between them. It describes the liquid flow, as if it was an averaged inside each compartment, but considered as instantaneous at its limits. The exchange flows cause quantitative increase of the total flow rate of liquid in the vessel, depending on the total value of flow rate – $Q_{E\,sum}$. This value of flow rate is as various as miscellaneous are the flow structures, in dual mixing vessel.

The results indicate that for the impeller spacing of $\Delta h \geq d$ the greatest values of flow rate number $K_{C\,calk}$ can be found if the lower is pitched blade turbine (PBT-6). Slightly less value (by 1÷4%) can be found if it is A-315 impeller. On the other hand, $K_{C\,calk}$ reaches by far the lowest values in case of HE-3 impeller. The situation is different at close location of the impellers ($\Delta h = d$). Then, the $K_{C\,calk}$ number takes the greatest value for the set of lower A-315 impeller, and is of a few percent lower in case of the rest of examined sets.

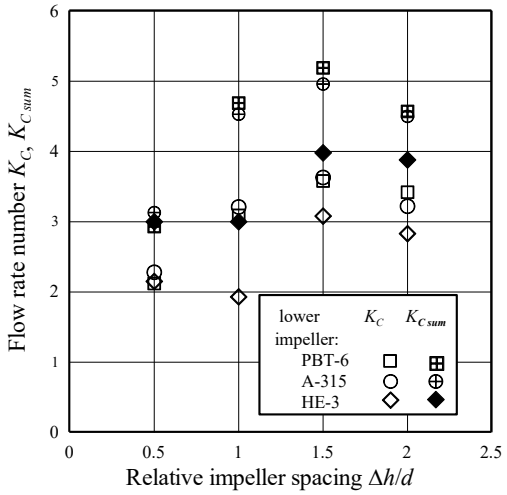

Fig. 5. The flow rate numbers of liquid, K_C and $K_{C\,calk}$ in the dual mixing vessel, versus the relative value of impeller spacing

3.3. Cycle of liquid transport

The flow of liquid is a crucial problem for its mixing. It is related to the transport of liquid elements along the vessel's height, towards the liquid level and reversely. It is possible to describe the liquid transport phenomena in a dual mixing vessel using the assumptions of the CMA model, in the context of momentum exchange within the compartments and between them. The liquid element is successively being moved through the circulation compartments with the velocities of $\bar{u}_r$ and $\bar{u}_z$, and while crossing the compartments' limits, is moving with the velocities of u'_z. An exemplary chart of the trajectories of liquid element is presented in Fig. 6.

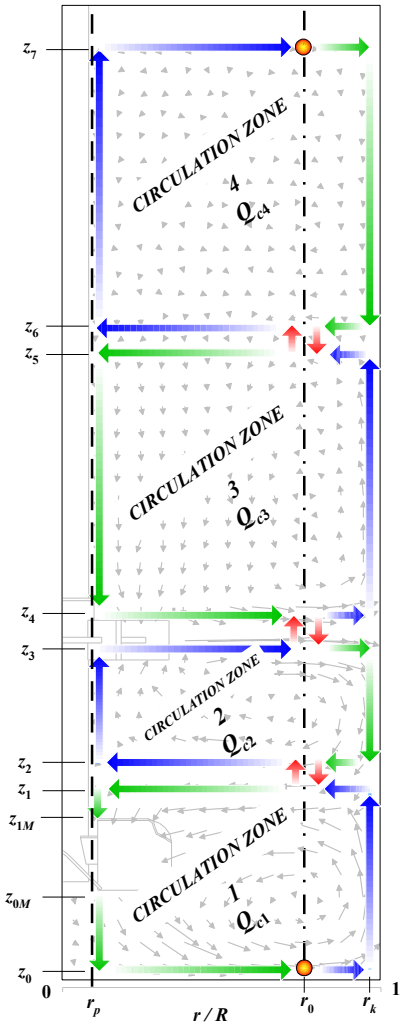

Fig. 6. The chart of liquid element transport in the dual mixing vessel with the lower A-315 impeller and four circulation zones, at $\Delta h = 1d$

Let us assume that the liquid element flows rectilinearly through each length. This element begins its move at the point of coordinates of (r_0, z_0) and flows upward, in the range of [z_0, z_7] and of [r_p, r_k], along the height and radius of the vessel. Once the element reaches one of the above limit coordinates, it changes its direction. Within the compartment, the liquid element flows on the horizontal lengths with the velocity of $\bar{u}_r$, while on the vertical lengths – with the velocity of $\bar{u}_z$. The liquid element traverses each length with different mean velocities. The lengths of element trajectories are set so that they coincide the lines of measurement points, at the middle vertical plane of the vessel. The liquid element crosses the limits of compartments at the points of radial coordinate of r_0, in

which the centres of circulation loops are also located. The crossing velocity of liquid element at these points is u'_z. The calculations were performed for the sets of impellers spaced at $\Delta h = 2d$. The flow structure induced in the mixing vessel, presented in Fig. 6, consists of three compartments of the first order and the fourth – of the second order. The mean velocity values, obtained at the measurement points, were compiled and described with continuous functions, within the respective range: from r_p to r_k and from z_0 to z_7, determining the trajectory of the liquid element. These functions were obtained by the interpolation of discrete values of the velocity, using the MATLAB software and selecting the spline type functions. Thus, to obtain the total transport time of liquid element at the certain length, the numerical integration of the formulas of inversed velocity was performed, according to the equations (13) and (14):

$$\vartheta_j = \int_r \frac{1}{\mathrm{f}_j(r)}\,\mathrm{d}r \tag{13}$$

$$\vartheta_j = \int_z \frac{1}{\mathrm{f}_j(z)}\,\mathrm{d}z \tag{14}$$

where the j-th index refers to the serial number of function, as shown in Table 2.

Table 2

The summary of the functions of liquid element velocity and their intervals of validity (domains)

Lp.	$\bar{u}_i$	r, z
1	$\mathrm{f}_1 = \bar{u}_r(r)$	$r \in \{[r_0, r_k]\} z_0$
2	$\mathrm{f}_2 = \bar{u}_z(z)$	$z \in \{[z_0, z_1]\} r_k$
3	$\mathrm{f}_3 = \bar{u}_r(r)$	$r \in \{[r_k, r_0]\} z_1$
4	$\mathrm{f}_4 = u'_{z1\text{-}2}(z)$	$z \in \{[z_1, z_2]\} r_0$
5	$\mathrm{f}_5 = \bar{u}_r(r)$	$r \in \{[r_0, r_p]\} z_2$
6	$\mathrm{f}_6 = \bar{u}_z(z)$	$z \in \{[z_2, z_3]\} r_p$
7	$\mathrm{f}_7 = \bar{u}_r(r)$	$r \in \{[r_p, r_0]\} z_3$
8	$\mathrm{f}_8 = u'_{z\,2\text{-}3}(z)$	$z \in \{[z_3, z_4]\} r_0$
9	$\mathrm{f}_9 = \bar{u}_r(r)$	$r \in \{[r_0, r_k]\} z_4$
10	$\mathrm{f}_{10} = \bar{u}_z(z)$	$z \in \{[z_4, z_5]\} r_k$
11	$\mathrm{f}_{11} = \bar{u}_r(r)$	$r \in \{[r_k, r_0]\} z_5$
12	$\mathrm{f}_{12} = u'_{z\,3\text{-}4}(z)$	$z \in \{[z_5, z_6]\} r_0$
13	$\mathrm{f}_{13} = \bar{u}_r(r)$	$r \in \{[r_0, r_p]\} z_6$
14	$\mathrm{f}_{14} = \bar{u}_z(z)$	$z \in \{[z_6, z_7]\} r_p$
15	$\mathrm{f}_{15} = \bar{u}_r(r)$	$r \in \{[r_p, r_0]\} z_7$

The numerical integration was performed using the Gaussian quadrature method, and next based on the Newton-Cotes formulas, yielding thereby an exact result of calculations. This way, the functions describing alterations of the radial and axial component of the mean velocity depending on the radius – $\bar{u}_r(r)$ and the vessel's height – $\bar{u}_z(z)$ were obtained. These functions and their intervals were shown in Table 2.

In case the liquid element flowed through the compartments with the velocity values of u'_z, expressed by f_4, f_8 and f_{12} functions, it was assumed that the lengths of $|z_1, z_2|$, $|z_3, z_4|$, $|z_5, z_6|$ were close to zero because the horizontal lengths of the element's trajectory should be located as close to the limits of the adjacent compartments. Therefore, the liquid transport on these lengths could be approximately considered as a pulsing movement, occurring on an infinitely short path, and therefore f_4, f_8, f_{12} functions can be expressed using the limit of a function:

$$\vartheta_j = \lim \frac{z}{\mathrm{f}\left(u'_z\right)} \tag{15}$$

These intervals were evaluated considering the most adverse case, the greatest vertical and horizontal flow lengths of the liquid element. Thus, it was stated that the values of r_p and r_k were located as close to the impeller's shaft and the vessel's wall, but far enough, so that neither the boundary layer nor the rotation of the shaft influenced the velocity of the liquid element. Similarly, the values of z_0 and z_7 of height were located as close to the vessel's bottom and to the liquid level, so that the boundary layer and the disturbances on a free liquid surface did not influence the element's velocity.

The duration of cycle of liquid transport was expressed as: $\sum_{j=1}^{m} \vartheta_j$, or in the dimensionless form, as:

$$\Theta = \left(\sum_{j=1}^{m} \vartheta_j \right) \cdot n \tag{16}$$

where m – superscript is the number of lengths (the intervals of integration), which were being traversed by the liquid element while transporting in the tank, wherein: $\{\vartheta_4, \vartheta_8, \vartheta_{12}\} \approx 0$. The results were summarised in Table 3. The energy consumption E during the cycle was also added there.

Table 3

The magnitudes relating to the cycle of liquid transport for the examined dual impeller sets

Lower impeller:	PTB-6			A-315			HE-3		
	$\sum_{j=1}^{m} \vartheta_j$ s	Θ –	E J	$\sum_{j=1}^{m} \vartheta_j$ s	Θ –	E J	$\sum_{j=1}^{m} \vartheta_j$ s	Θ –	E J
$\Delta h = 2 \cdot d$	19.32	96.6	138.1	21.67	108.4	153.4	37.20	186.0	199.8

4. Conclusions and final remarks

If taking into account the mean liquid flow, the application of the disc turbine combined with the axial impeller yields the beneficial effect of mixing. However, it depends on the design of the lower impeller.

The liquid flow rate in the mixing vessel varies, depending on the relative location of the impellers. The change of the impeller spacing affects the change in the flow structure, which can take different transitional forms as well as thoroughly deformed shapes. In such cases, local reinforcing or suppressing of the liquid streams can occur. It can be seen by an increase or decrease of the K_{ccalk} number. There is the exchange flow rate, occurring on the limit of the respective, adjacent compartments. It was expressed as a function of the axial component of fluctuating velocity. The greatest intensity of the induced liquid flow and beneficial energy consumption can be found for the set of the lower PBT-6 turbine. This magnitude is only slightly lower for the set of A-315 impeller. The situation becomes reversed only at a very close position of the impellers.

Nomenclature

d – impeller diameter, m;
D – vessel diameter, m;
H – lower impeller's clearance in vessel, m;
Δh – impeller spacing, m;
K_C – circulation flow number in total liquid volume;
$K_{C\,calk}$ – corrected flow rate number;
n – rotation frequency of impellers, s^{-1};
Q_C – liquid flow rate general, m^3/s;
$Q_{C\,sum}$ – liquid flow rate in total volume of vessel, m^3/s;
$Q_{C\,calk}$ – liquid flow rate corrected, m^3/s;
Q_E – exchange flow rate of liquid in mixing vessel, general, m^3/s;
$Q_{E\,sum}$ – exchange flow rate of liquid in mixing vessel, total, m^3/s;
Q_r – circulation flow rate in radial direction, within circulation zone, m^3/s;
Q_z – circulation flow rate in axial direction, within circulation zone, m^3/s;
r – radius coordinate, m;
R – vessel diameter, m;
Re – Reynolds number for mixing, –;
R – variable and radial coordinate in vessel, m;
Δt – time residence of liquid in the measuring, s;
u'_{zg} – axial component of fluctuation velocity, at point on limiting line, z_{og}, m/s;
$\bar{u}$, $\bar{u}(t)$ – mean liquid velocity, m/s;
Z – variable and axial coordinate in vessel, m;
z – axial coordinate, m;
z_g – real height of points of limit between compartments, height of point of limit, m;
z_o – estimated height of limits between circulation zones, m;
z_{og} – real limit between compartments (circulation zones), m;
ϑ – transport time of liquid element through certain length, s;

Subscripts

i – general index of component, index of summation;
j – index of summation;
r – index of radial component;
z – index of axial component;

Superscripts

(+) – just drawdown;
(–) – refers to the gas-liquid system conditions;

References

[1] Alves S. S., Maia C. I., Vasconcelos J. M. T., *Experimental and modelling study of gas dispersion in a double turbine stirred tank*, Chemical Engineering Science, vol. 57, 2002, 487-496.

[2] Aubin J., Mavros P., Fletcher D. F., Xuereb C., Bertrand J., *Effect of axial agitator configuration (up-pumping, down-pumping, reverse rotation) on flow patterns generated in stirred vessels*, Transactions of the Institution of Chemical Engineers, vol. 79(A8), 2001, 845-856.

[3] Bader F. G., *Modelling mass transfer and agitator performance in multiturbine fermentors*, Biotechnology and Bioengineering, vol. 30(1), 1987, 37-51.

[4] *Chemineer Bulletin*, Nr 710, homepage: http://www.chemineer.com (date of access: 2008-02-10).

[5] Duda A., *Hydrodynamika mieszania cieczy w aparacie z dwoma mieszadłami*, Rozprawa doktorska, Politechnika Krakowska 2015.

[6] Elsner J. W., Drobniak S., *Metrologia turbulencji przepływów*. *Maszyny Przepływowe*, vol. 18, Wydawnictwo PAN, Wrocław-Warszawa-Kraków 1995.

[7] Fajner D., Magelli F., Pasquali G., *Modelling of non-standard mixers stirred with multiple impellers*, Chemical Engineering Communication, vol. 17, 1982, 285-295.

[8] Jahoda M., Machoň V., *Homogenization of liquids in tanks stirred by multiple impellers*, Chemical Engineering & Technology, vol. 17, 1994, 95-101.

[9] Jaworski Z., Nienow A. W., Koutsakos E., Dyster K. W., Bujalski W., *An LDA study of turbulent flow in a baffled vessel agitated by a pitched blade turbine*, Transactions of the Institution of Chemical Engineers, vol. 69, Part A, 1991, 313-320.

[10] Jaworski Z., Nienow A. W., Dyster K. W., *An LDA study of the turbulent flow field in a baffled vessel agitated by an axial, down-pumping hydrofoil impeller*, Canadian Journal of Chemical Engineering, vol. 74, 1996, 3-15.

[11] Johnson R. W., The *handbook of fluid dynamics*, CRC Press LLC, Boca-Raton, USA, 2000.

[12] *Lightnin Bulletin*, Nr E-120 09/01, homepage: http://www.lightninmixers.com (date of access: 2008-02-15).

[13] Manfredini R. Cavallera V., Marini L., Donati G., *Mixing and oxygen transfer in conventional stirred fermenters*, Biotechnology and Bioengineering, vol. 25(12), 1983, 3115-3131.
[14] MATLAB *Online Documentation*, homepage: http://www.mathworks.com/help/matlab (date of access: 2014-08-03).
[15] Saito F., Nienow A. W., Chatwin S., Moore J. T. J., *Power gas dispersion and homogenisation characteristics of Scaba SRGT and Rushton turbine impellers*, Chemical Engineering Japan, vol. 25(3), 1992, 281-287.
[16] Takenaka K., Takahashi K., Bujalski W., Nienow A. W., Paolini S., Paglianti A., Etchells A. W., *Mixing time for different diameters of impeller at a high solid concentration in an agitated vessel*, Journal of Chemical Engineering of Japan, vol. 38(5), 2005, 309-315.
[17] Vasconcelos J. M. T., Alves S. S., Barata J. M., *Mixing in gas-liquid contractors agitated by multiple turbines*, Chemical Engineering Science, vol. 50(14), 1995, 2343-2354.
[18] Vrábel P., van der Lans R. G. J. M., Luyben K. Ch. A. M., Boon L., Nienow A. W., *Mixing in large-scale vessels stirred with multiple radial or radial and axial up-pumping impellers: modelling and measurements*, Chemical Engineering Science, vol. 55, 2000, 5881-5896.

TECHNICAL TRANSACTIONS | CZASOPISMO TECHNICZNE
MECHANICS | MECHANIKA
2-M/2016

ZYGMUNT DZIECHCIOWSKI, ANDRZEJ CZERWIŃSKI*

NOISE ANALYSIS OF THE LONGITUDINAL PAPER CUTTING MACHINE IN THE CONTEXT OF DECLARATION OF COMPLIANCE OF THE MACHINERY

ANALIZA HAŁASU MASZYNY DO WZDŁUŻNEGO CIĘCIA PAPIERU W KONTEKŚCIE DEKLARACJI ZGODNOŚCI MASZYNOWEJ

Abstract

The paper summarises the noise measurements of a bobbin cutting machine, also referred to as a longitudinal paper cutter machine, taken as a part of the procedure involved in the declaration of compliance of the machinery. Noise measurements were taken with a view to improve the conditions in the work environment. Due to the machine operation, noise level conditions were determined by testing the impulse response inside the machine room. Calculations were carried out in an attempt to improve the working conditions for machine operators.

Keywords: noise analysis, declaration of compliance of machinery, acoustic adjustment

Streszczenie

W artykule przedstawiono wyniki pomiarów i analiz bobiniarki, tj. maszyny do wzdłużnego cięcia roli papieru. Pomiary te były częścią prac związanych ze spełnieniem przez badaną maszynę wymagań deklaracji zgodności maszynowej. W ramach pracy wykonano pomiary hałasu i analizy, których celem była poprawa warunków pracy na stanowisku pracy poddanym ocenie. W ramach pomiarów przeprowadzono tak ocenę warunków akustycznych wywołanych pracą maszyny jak i określono odpowiedź impulsową pomieszczenia, w którym maszyna się znajduje. Wykonano również obliczenia w aspekcie poprawy warunków pracy.

Słowa kluczowe: analiza hałasu, deklaracja zgodności maszynowej, adaptacja akustyczna

DOI:

* DSc. Eng. Zygmunt Dziechciowski, DSc. Eng. Andrzej Czerwiński, Institute of Machine Design, Faculty of Mechanical Engineering, Cracow University of Technology.

1. Introduction

In the context of EU regulations aimed to ensure work safety for machine operators, it is required that all machines designed, manufactured, launched and put to use should ensure the highest possible safety levels. Employers are obligated to ensure that machines are used for what they are intended, in accordance with the manufacturer's recommendations and that all further steps and measures are taken when necessary to improve safety features [1]. This approach is pursued in two basic groups of EU directives on work safety. The first group of documents are those having relevance to design, manufacturing, launching and use of machines and other products, issued to ensure the best safety levels possible. Among those documents, the Directive on Machinery is now of key importance [2]. The other group of EU directives are those specifying the minimum requirements that need to be satisfied when arranging the operators' work and the work environment, such as [3, 4, 5].

The respective requirements as to health and safety and work are applicable as long as the machine operated in the manner specified by the manufacturer still poses a real occupational hazard addressed by the relevant standard requirements, including those relating to noise and mechanical vibration control.

The group of machines covered by the Directive on Machinery [2] includes machines used in the paper industry and the printing industry, for example bobbin cutting machines, which produce high-level acoustic emission when in service. This is caused by the structural design of the machine and its interactions with additional equipment, which are necessary for the process.

As mentioned above, the technological process used in the paper industry and the printing industry makes that they are characterised by the production of high-level acoustic emission when in service. Because of this, they should often be subjected to acoustical adaptation. This adaptation should be preceded by computer simulations. The articles [6] [7, 8, 9] concern the issues of improving the acoustical conditions in the workplace inside of a printing house. In these articles are described, inter alia, the identification process of noise sources, the measurement methodology of acoustic properties of a room (production hall), as well as the results of digital simulation for the selected configuration of acoustic protections.

The purpose of the present study was to determine the potentials of noise reduction in areas in the vicinity of paper cutting machines such that the requirements set forth in the Directive on Machinery should be complied with. Digital simulation procedures were performed to assess the potential benefits of applying a variety of noise reduction strategies (reducing the level of noise produced by machine components, improving the noise absorption capacity of the machine room). The parameters of the calculation model were determined based on sound level measurement data.

2. Test object

The test object was a bobbin cutting machine, i.e. a machine for longitudinal paper cutting. During the cutting process, the roll of paper is spread on the rewinding cylinders, rewound on the roller set and cut longitudinally with circular cutters, followed by winding

of the paper sheet. The machine is located in a room of 12 m in length, 5.7 in width and 3.27/2.88 in height, the ceiling in the room is sloping. The walls and the ceiling are plastered. Up to about 2 m in height, the walls are coated with enamel, and above that- painted with an emulsion paint. The ceiling is painted with an emulsion paint, too. The floor is made of ground concrete. There are two windows in the room (approximately 1 m × 2 m in size) and two gates 2.75 m × 2.75 m. The gates are locked by a sliding door. The layout of the room is shown in Fig 1.

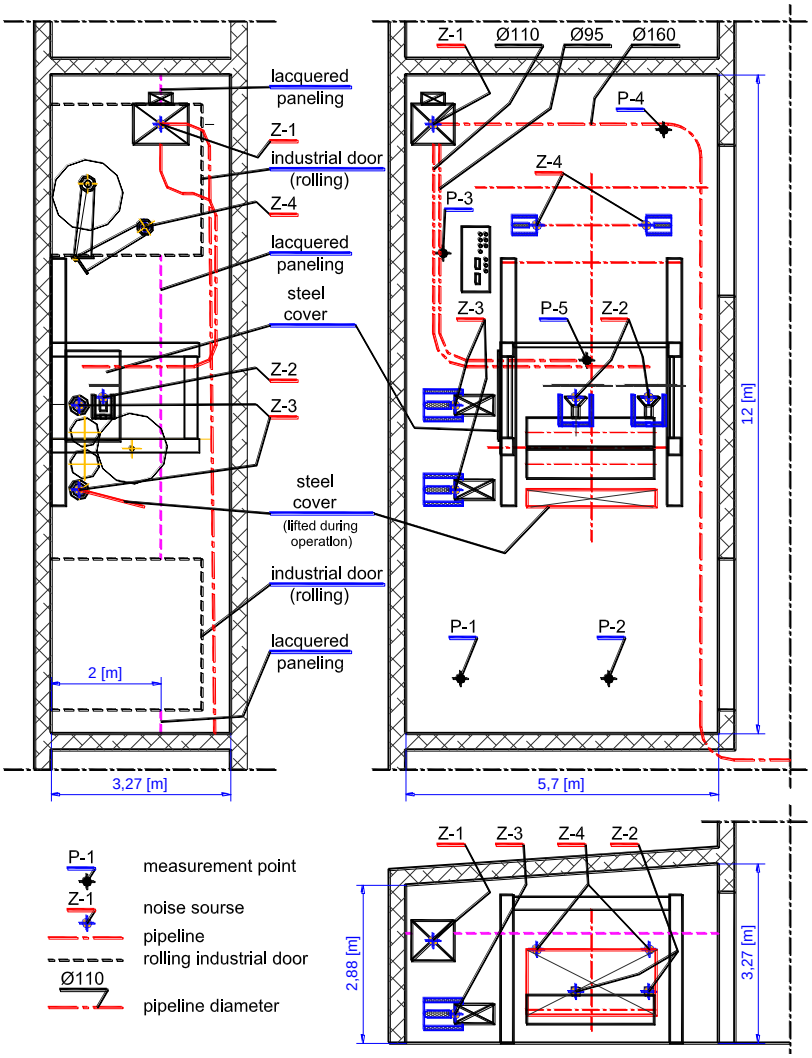

Fig. 1. Test object- position of the bobbin cutting machine inside the room

The bobbin cutting machine has two integral components: the machine for cutting paper sheets on the winding and rewinding end plus the cutting tools and the exhaust system (an exhaust fan with the pipeline, suction nozzles). Key machine components are shown in Fig 1.

Major sources of noise in the investigated area include:

- an exhaust fan (designated as Z-1 in Fig. 1),
- suction nozzles (designated as Z-2 in Fig. 1),
- unwinding cylinder drives (designated as Z-3 in Fig. 1),
- an unwinding roll drive (designated as Z-4 in Fig. 1).

3. The maintenance zone of the operator

When the bobbin cutting machine is in operation, machine operators spend most of their time in zones shown in Fig. 2 and listed in Table 1. During the analyses, attention should mainly be paid to these zones.

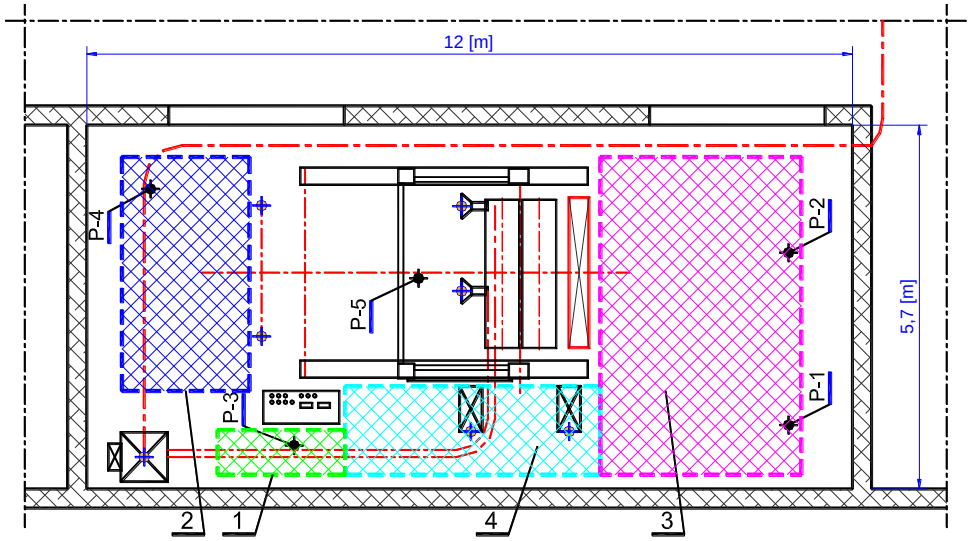

Fig. 2. Investigated area- the workplace operation zones

Table 1

Designation of workplace operation zones (see Fig. 1)

Name of zone	Number of area according to Fig. 2
The operating desktop zone	1
Loading the paper roll zone	2
Receiving the paper roll zone	3
The maintenance zone along the machine	4

4. Results of sound level measurements in workplace operation zones

Sound level measurements were taken to determine the noise levels in particular workplace operation zones (as shown in Fig. 2).

Results of measurements taken in the existing conditions are summarised in Table 2, revealing the exceeded values of equivalent noise levels in relation to the admissible levels during the 8 hours' noise exposure for humans ($L_{EX\ 8h\ perm}$ = 85 dB [10]). Measurements were taken in accordance with the procedure specified in [11, 12].

Table 2

Variability range of the equivalent noise levels in investigated zones- present conditions

Measurement area in accord. with Fig. 2 and Table 2	Mean value for the area $L_{Aeq\ meas\ av}$ [dB]	Exceeding the permissible noise level value for 8 hours' exposure ($L_{EX\ 8h\ perm}$ = 85 dB) $L_{Aeq\ meas\ av} - L_{EX\ 8h\ perm}$ [dB]
[1]	[2]	[3]
1	85.3	0.3
2	87.0	2.0
3	87.1	2.1
4	87.0	2.0

5. Identification of noise sources

To identify the major noise sources inside the machine, sound analyses were performed for various modes of machine operation. Measurements were taken at five points, indicated in Fig 1 and in the vicinity of the selected sources. Specificity of machine operations and processes involved precluded separate measurements of each individual source. Therefore, measurements were repeated for as large as possible number of configurations of operating noise sources.

Table 3

Operating configurations- designations and description

Configuration number	Designation area in accord. with Fig. 3	Description of configuration area in accord. with Fig. 2
Config. No. 1	K-1	Machine stopped; working only source Z-4
Config. No. 2	K-2	Machine stopped; work only noise sources Z-1, Z-2, Z-4
Config. No. 3	K-3	Machine is running; work of sources Z-3, Z-4; without of noise source Z-1, Z-2
Config. No. 4	K-4	Machine is running; work of sources Z-1, Z-3, Z-4; without of noise source Z-2
Config. No. 5	K-5	Machine is running (full operating); work of sources Z-1, Z-2, Z-3, Z-4
Config. No. 6	K-6	Machine stopped; the background noise

Results of 1/3 octave band analysis of the noise levels as given in Fig. 3 as averaged values from 5 measurement points. Plots represent particular configurations of contributing noise sources (summarised in Table 3). Fig. 3 also plots the background noise curve (K-6 curve) and the K-5 curve obtained for all noise sources working, including the cutting process). In Fig. 3 are placed also the summated values of noise level A for the entire frequency band. These values are given in frames where the frame colour and edge pattern correspond to relevant plots.

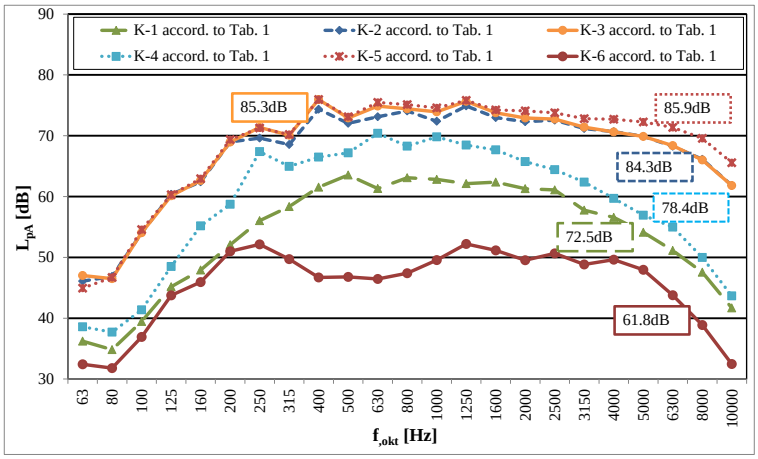

Fig. 3. 1/3 octave band analysis of sound level for the given configuration of operating noise sources – averaged values from 3 measurement points

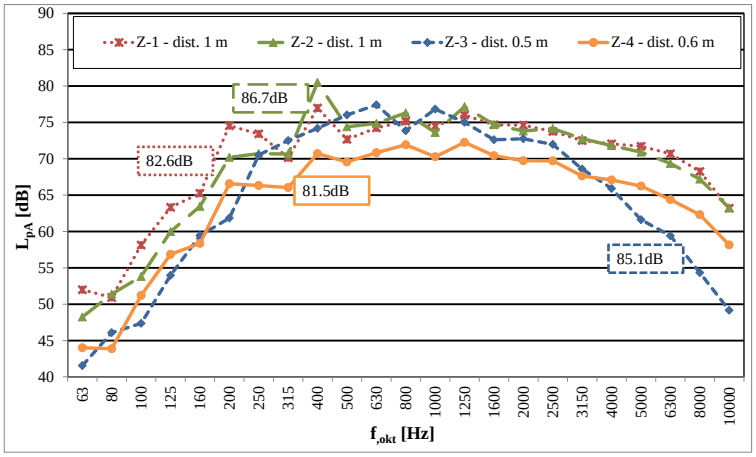

Fig.4. 1/3 octave band analysis of sounds from individual noise sources (Z-1, Z-2, Z-3, Z-4) – near-field measurements

For selected sources, measurements of sound levels were also taken in their close vicinity. Measurement data are summarised in Fig. 4, listing the source number and the distance at which the measurement was taken.

Basing on noise level measurements at selected points near the machine and for various configurations of noise sources, the numerical simulation procedure was applied to identify the sources and establish their sound power levels. To account for sounds reflected in the room, the reverberation time was measured, in accordance with the procedure set forth in [13].

The reverberation time measurement process was also described in [9]. In the room in question, the reverberation time was determined on the basis of the measurement of impulse responses in several points located at a height of 1.2 m above the floor on its overall area. To perform the measurements, measuring equipment shown in Fig. 5 was employed.

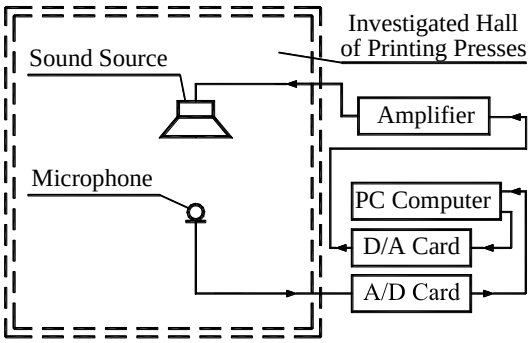

Fig. 5. Measuring equipment

Measured reverberation times are summarised in Fig. 6.

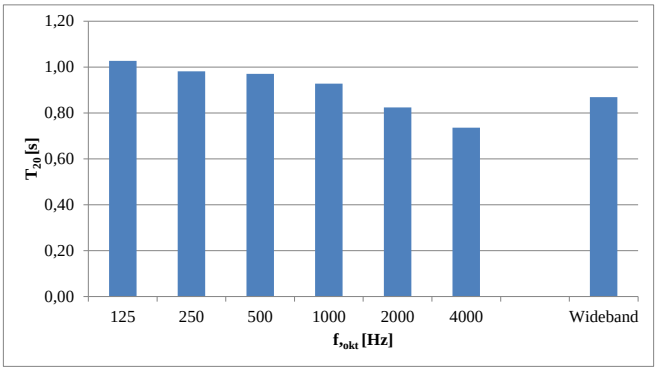

Fig. 6. Values of reverberation time inside the room

Finally, estimated values of sound power level L_{WA} of particular noise sources are summarised in Table 4. The sound power level L_{WA} values were estimated in accordance with the procedure given in [14].

Table 4

Estimated values of sound level L_{WA} from the noise sources

The noise source	Designation in Fig. 1	The number of noise sources	Sound power level L_{WA} [dB]
Exhaust fan	Z-1	1	90
Suction nozzles of paper scrap	Z-2	2	89
Drive of a unwinding cylinders	Z-3	2	86
Drive of a roll unwinding	Z-4	2	79
Pipeline (as a total one)	–	–	71

6. The effects of acoustic adjustments and control on noise distribution in the workplace operation zone

The analysis was conducted to determine the effects of specific sound control and adjustment solutions on the noise levels in the workplace operation zones.

The calculation procedure was applied addressing three aspects: first - adjustments of noise sources, designated with "I", second – acoustic design and adaptation of the room's interior, designated with "II" and third – improvement of working conditions at the control desk, designated with "III". As regards the adjustments of noise sources, several solutions were considered that were aimed at reducing noise emissions to acceptable levels (four options were considered, indicated by numbers 1÷4). In the calculation procedure associated with potential modifications of the machine room, two solutions were considered (II.1, II.2). Further combinations of measures taken to reduce the sound levels were considered too (enhancing the sound absorption capacity of the room and providing a screen near the control desk- designated as "I.4+II.2"), thus yielding 8 options to be handled in calculations.

These options are summarised in Table 5.

Options (I) (designated with "I" in the calculation procedure) involve the modification or adjustments of noise sources, such as fans or driving systems. Four combinations of noise sources were considered (I.1 to I.4), listed in Table 6.

Further calculations were performed to find out how the improvement of sound absorption capacity of the machine room should affect the noise levels. It is suggested that sound absorption capacity of one wall (the wall near the exhaust fan) and of the ceiling should be improved. Average values of the sound absorption coefficients for the walls and the ceiling in the room in the present conditions are taken to be $\alpha = 0.13$ (walls) and $\alpha = 0.11$ (ceiling). The sound absorption coefficient of the used sound absorbent material is $\alpha = 0.5$ [15].

Table 5

Configurations of noise control measures in the considered variants

		Noise control measures						
		Acoustic adjustments of the noise sources in the machine				Acoustic design and adaptation of the machine room		Modification of the control desk
		Exhaust fan Z-1	Suction nozzles of paper scrap Z-2	Drive of a unwinding cylinders Z-3	Drive of a roll unwinding Z-4	Ceiling	Back wall	Screen of a desktop
	Designation	[1]	[2]	[3]	[4]	[5]	[6]	[7]
Variant of calculations	I.1	**x**	**x**					
	I.2	**x**	**x**		**x**			
	I.3	**x**	**x**	**x**				
	I.4	**x**	**x**	**x**	**x**			
	II.1					**x**		
	II.2					**x**	**x**	
	I.4+II.2	**x**	**x**	**x**	**x**	**x**	**x**	
	I.4+III	**x**	**x**	**x**	**x**			**x**

Table 6

Solution options involving adjustment/ no adjustment of selected noise sources

		Characteristics of the calculation variants			
Noise sources	Designation in Fig. 1	I.1	I.2	I.3	I.4
Exhaust fan	Z-1	acoustical adaptation (9 dB) L_{WA} = 81 dB	acoustical adaptation (9 dB) L_{WA} = 81 dB	acoustical adaptation (9 dB) L_{WA} = 81 dB	acoustical adaptation (9 dB) L_{WA} = 81 dB
Suction nozzles of paper scrap	Z-2	a partial acoustic enclosure – absorber R = 15 dB	a partial acoustic enclosure – absorber R = 15 dB	a partial acoustic enclosure – absorber R = 15 dB	a partial acoustic enclosure – absorber R = 15 dB
Drive of a unwinding cylinders	Z-3	Without adaptation L_{WA} = 86 dB	Without adaptation L_{WA} = 86 dB	acoustical adaptation (5 dB) L_{WA} = 81 dB	acoustical adaptation (5 dB) L_{WA} = 81 dB
Drive of a roll unwinding	Z-4	Without adaptation L_{WA} = 79 dB	acoustical adaptation (5 dB) L_{WA} = 74 dB	Without adaptation L_{WA} = 79 dB	acoustical adaptation (5 dB) L_{WA} = 74 dB

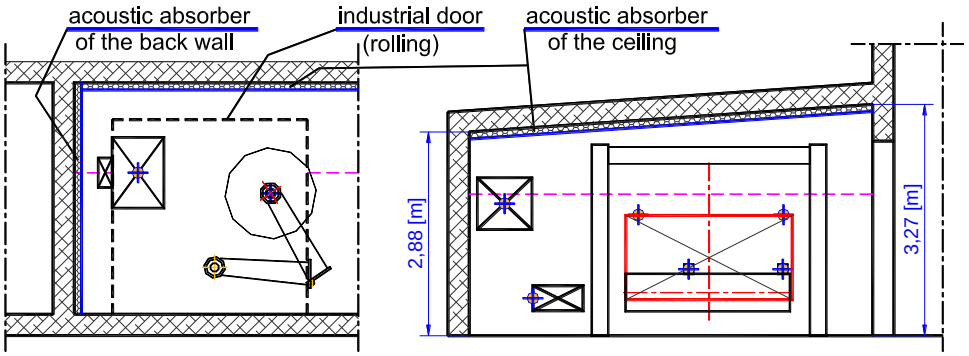

Fig. 7. Positions of acoustical absorbers on the back wall and on the ceiling

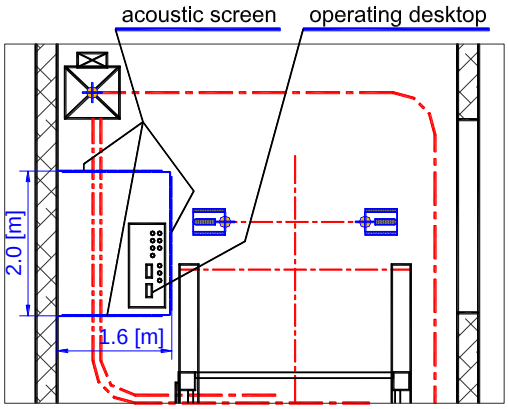

Fig. 8. Position of an acoustic screen protecting the control desk

Surfaces subjected to acoustical adaptation are shown in Fig. 7.

Calculations were also performed to account for the case when a screen was provided to protect the operator from acoustic wave emissions when monitoring the machine. The acoustic screen shall be made of PVC baffles, its position with respect to the control desk is shown in Fig. 8.

Other solutions considered in the procedure were combinations of several sound control measures. Calculations were performed to determine the effectiveness of these sound control measures in relation to particular noise sources (i.e. variant I.4 in Table 3) and to establish the effectiveness of the two sound absorbers (variant II.2 in Table 3). This variant is designated as “I.4+II.2” in Table 3. The effects of acoustic adjustment of all sources and providing the protective screen near the control desk are estimated in the solution variant labelled as “I.4+III”.

7. Calculation results

Measurement data were utilised in computer simulations to investigate both the existing conditions and the 8 variants listed in section 6. Calculation data are presented in the form of sound level distribution maps.

Fig. 9 plots the results obtained in the present conditions. Figs. 10 and 11 show the sound pressure distribution maps for selected variants of room adaptations, illustrating the effectiveness of noise control measures involved in particular solutions.

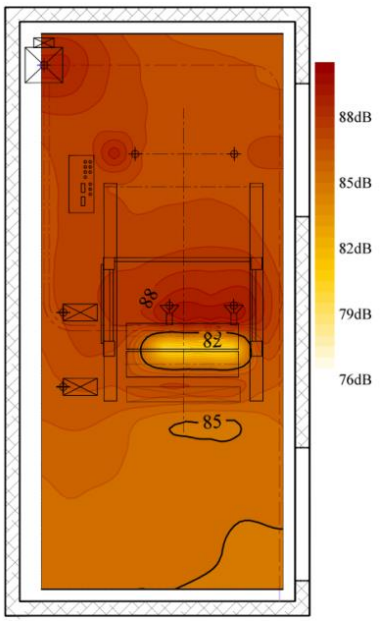

Fig. 9. Sound pressure level distribution inside the room- present state

Analysis of a map in Fig. 9 reveals that among the workplace operation areas, the highest noise levels are registered in the vicinity of sources Z-1 and Z-2, and near the control desk. The sound level registered in these zone approaches 87÷86 dB. Near the point where the paper roll is set, the sound level is as high as 85 dB.

Fig. 10 plots the results obtained when the acoustic adjustments and modifications are made to control the noise level near the major sources (variant I.4). Fig. 10a shows a map of noise distribution around the bobbin cutting machine and the effects of using the noise control measures listed in Fig. 6 are illustrated in Fig. 10b. It is readily apparent that adjustment measures provided in variant I.4 lead to a reduction of sound pressure by 4 or 5 dB.

Noise reduction is more significant when sound absorbers are placed on the wall (variant II.2), which is shown in the map in Fig. 10c. The map plotting the sound pressure reduction levels (Fig. 10d) reveals that in the workplace operation zone, the noise reduction effect is less significant than in the variant I.4 (by 1 or 2 dB).

The effects of simultaneous adjustments and modifications near the major noise sources (I.4) and adaptation and acoustic re-design of selected walls (II.2) are illustrated in Fig. 10a and 10b. In the operation zones the noise level may be reduced by 8÷9 dB.

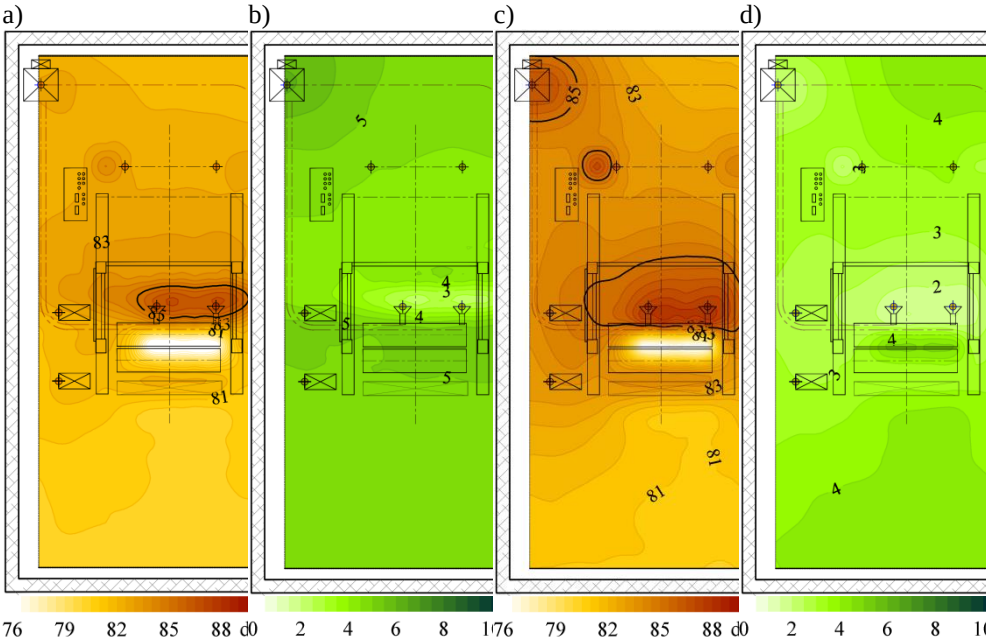

Fig. 10. Calculation results: a) sound pressure level for variant I.4; b) noise reduction for variant I.4; c) sound pressure level for variant II.2; d) noise reduction in variant II.2

Figs. 11a and 11c plot the calculation data obtained for the specific case when the major noise sources were controlled (I.4) and, at the same time, a screen was provided to isolate the control desk zone (III). Noise reduction by 5÷7 dB is sufficient to ensure that the noise levels experienced by the machine operator should be reduced to acceptable levels in the work environment. Distribution of noise reduction values inside the room is presented in Figs. 11c and 11d.

The analysis of results allows for evaluating the potential noise reduction strategies to be implemented in the operation zones (Fig. 2), enabling a preliminary cost analysis of such solutions.

Application of the protective measures listed in variants I.4 (see Table 6), involving the adaptation of the major noise sources and the fan. Providing a transparent screen made of PVC (variant “I.4+III”) leads to further noise reduction in the zone I (see Fig. 2).

In order that the noise levels in the workshop operation zones should fall within the admissible limits, it is required that additional flat sound absorbers should be installed on selected walls and on the ceiling (variant “I.4+II.2”). One has to bear in mind, however, that the costs of additional absorbers will be rather high.

Table 7 summarises the estimated noise reduction levels in the zones 1, 2, 3, 4 (see Fig. 2), for the specific solution variants.

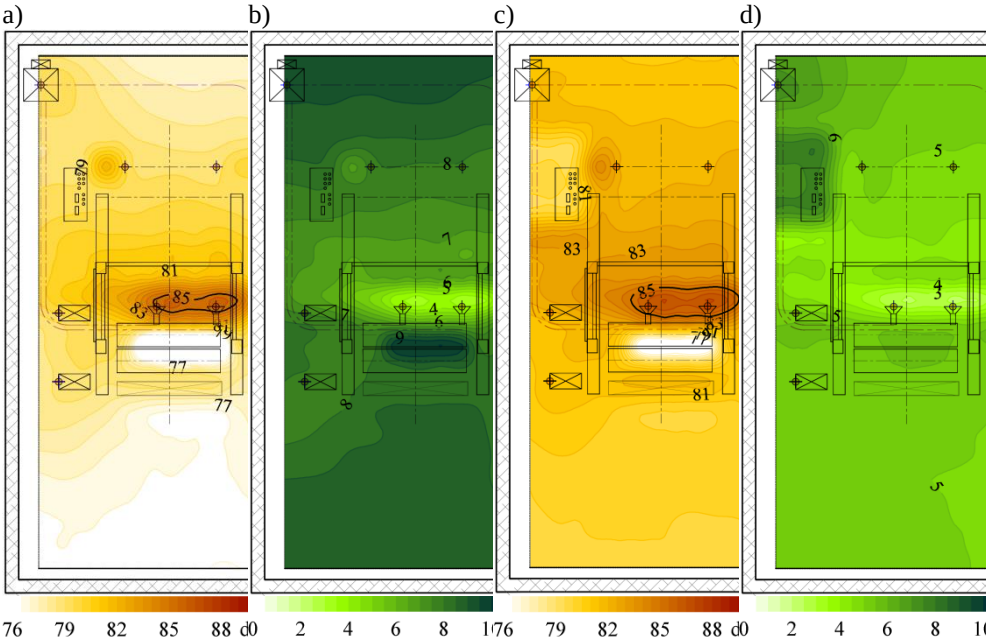

Fig. 11. Calculation results: a) sound pressure level for variant "I.4+II.2"; b) noise reduction for variant "I.4+II.2"; c) sound pressure level for variant "I.4+III"; d) noise reduction in variant "I.4+III"

Table 7

Predicted noise reduction in the workshop operation zone for analysed solutions in relation to the average measured sound level $L_{Aeq\ meas\ av}$ in the area

		Predicted noise reduction in the workshop operation zone for analysed solutions in relation to the average measured sound level $L_{Aeq\ meas\ av}$ in the area $\Delta L_{red\ av}$ [dB] = $L_{Aeq\ meas\ av}$ - $L_{Aeq\ zone\ av}$							
Zone number area in accord. with Fig. 2	Current state Average measured sound level $L_{Aeq\ meas\ av}$ [dB]	I.1	I.2	I.3	I.4	II.1	II.2	I.4+II.2	I.4+III
[1]	[2]	[3]	[4]	[5]	[6]	[7]	[8]	[9]	[10]
1	85.3	2.6	2.8	4.4	4.7	3.3	3.9	8.5	5.1
2	87.0	2.4	2.6	4.2	4.5	2.3	2.9	7.2	4.8
3	87.1	3.1	3.4	4.4	4.8	2.4	3.2	8.2	7.4
4	87.0	3.2	3.7	4.2	4.8	2.6	3.5	8.5	5.4

8. Conclusions

The purpose of the present study was to estimate the effectiveness of the proposed modifications and acoustic adjustments aimed to reduce the noise level in the bobbin machine operation zone. The investigations were undertaken as part of the project aimed to ensure that all relevant requirements set forth in the Directive on Machinery should be complied with [2]. The study considers all potential noise control measures: modification and acoustic adjustment of machine components, re-design and adaptation of the acoustic features of the machine room and providing a transparent screen, made of PVC, around the control desk. Various configurations of sound control measures were duly evaluated. The list of applied noise control measures is given in section 6 and specific options (8) are summarised in Table 5.

The analysis identified the solutions that proved most effective.

The most effective noise reduction in operation zones was registered for the variants "I.4+II.2" and "I.4+III", which involve full adjustment of the noise sources and adaptation (increase the sound absorption coefficient) of the walls and ceiling in the machine room, as well as full acoustic adjustment of major sources of noise plus the screen provided around the control desk. Acoustical adaptation (increase the sound absorption coefficient) of walls and ceiling in the machine rooms with the use of sound absorbers is an expensive solution and found not to be cost-effective despite its excellent performance.

The effectiveness of variant I.4 in noise control is high, too. Even though not in all workshop operation zones could the noise levels be reduced to the admissible levels specified in normative references (below 85 dB), the effectiveness of noise control was found to be satisfactory. This view is fully justified since the normative value involves not only the actual noise level in the zone, but to exposure time as well.

Investigations show that in certain cases the requirements set forth in the Directive on Machinery [2] cannot be fully met through acoustic adjustments of the machine itself (or its components). In many cases, the machine and the machine room have to be treated as one system. Acoustic adjustments of machine components alongside the improvement of acoustic parameters of the machine room will lead to required results. One has to bear in mind the cost-effectiveness of the proposed solutions, which in many cases becomes the major criterion in decision-making.

References

[1] *Ensuring compliance of machinery with the essential requirements in the field of health and safety. Guidelines for producers, suppliers and users of machinery* (in Polish), Centralny Instytut Ochrony Pracy – Państwowy Instytut Badawczy, www.ciop.pl, Warszawa 2010.

[2] Directive 2006/42/EC of the European Parliament and of the Council of 17 May 2006 on machinery.

[3] Directive 89/391/EEC – COUNCIL DIRECTIVE of 12 June 1989 on the *introduction of measures to encourage improvements in the safety and health of workers at work.*

[4] Directive 2009/104/EC – use of work equipment of 16 September 2009 concerning *the minimum safety and health requirements for the use of work equipment by workers at work* (second individual Directive within the meaning of Article 16(1) of Directive 89/391/EEC).
[5] Directive 89/655/EEC - COUNCIL DIRECTIVE of 30 November 1989 concerning the minimum safety and health requirements for the use of work equipment by workers at work (second individual Directive within the meaning of Article 16 (1) of Directive 89/391/EEC).
[6] Czerwiński A., Dziechciowski Z., Krawczyk J., *The concept of reduction of the sound level at workplaces in the printing industry* (in Polish), in: *Teoreticieskie osnowy eniergoriesursosbieriegajuścich priocesow, oborudowania i ekołogicieski biezopasnych proizbodctw*, ISBN 978-5-9616-0377-4, Goubno ИГХТУ (IGChTU), Iwanowo – Rosja, 2010.
[7] Borkowska-Czarnecka K., Czerwiński A., Dziechciowski Z., *Analysis of influence of new printing press installation on a acoustic climate in a press room of a printing house* (in Polish), Czasopismo Techniczne „Mechanika", vol. 2-M, 2012, 55-62.
[8] Czerwiński A., Dziechciowski Z., *Acoustic parameters verification of enclosures of high-performance printing presses* (in Polish), Czasopismo Techniczne „Mechanika", vol. 2-M, 2012, 63-72.
[9] Dziechciowski Z.; Czerwiński A., *Concepts of noise reduction in workplace areas of roll unwinding operators of printing offset press*, Meždunarodnaâ Naučno-Tehničeskaâ Konferenciâ *Problemy resurso- i energosberegaûŝih tehnologij v promyšlennosti i APK* (PRET-2014), monografiâ, Ivanovskij Gosudarstvennyj Himiko-Tehnologičeskij Universitet, tom 2, 2014, 100-113.
[10] Regulation of the Minister of Labour and Social Policy of 6 June 2014 on Maximum Permissible Concentration and Intensity of Agents Harmful to Health in the Working Environment, Journal of Laws of 2014, item 817.
[11] PN-94/N-01307, *Noise – Permissible values of noise in the workplace – Requirements relating to measurements*.
[12] PN EN ISO 9612:2009, *Acoustics – Determination of Occupational Noise Exposure – Engineering Method*.
[13] PN EN ISO 3382-2:2010, *Acoustics – Measurement of Room Acoustic Parameters*, Part 2: *Reverberation Time In Ordinary Rooms*.
[14] PN-EN ISO 3746:2011, *Acoustics – Determination of sound power levels of noise sources using sound pressure – Survey method using an enveloping measurement surface over a reflecting plane*.
[15] Engel Z., *Environmental Noise and Vibration Protection* (in Polish), PWN, Warszawa 1993.

TECHNICAL TRANSACTIONS | CZASOPISMO TECHNICZNE
MECHANICS | MECHANIKA
2-M/2016

TOMÁŠ JIROUT, FRANTIŠEK RIEGER*

MIXING WASTE GYPSUM SUSPENSIONS

MIESZANIE ODPADOWYCH ZAWIESIN GIPSOWYCH

A b s t r a c t

The paper deals with experimental research of the waste suspensions mixing from the energy industry. Mixing experiments were carried out in a transparent baffled vessel with a diameter of 290 mm. Standard pitched six-blade turbine and folded four-blade turbine with diameters of 100 mm in two relative distances from bottom H_2/d = 1 and 0.5 were used in experiments. Measurements were carried out with three volumetric concentrations of suspensions: 16, 31.5 and 47%.

Keywords: m*ixing, suspension, gypsum*

S t r e s z c z e n i e

W pracy przedstawiono badania eksperymentalne mieszania odpadowych zawiesin gipsowych powstających w energetyce. Badania prowadzono w przezroczystym zbiorniku o średnicy 290 mm, z przegrodami. W badaniach stosowano mieszadła osiowe o średnicy 100 mm: standardowe mieszadło sześciołopatkowe oraz mieszadło czterołopatkowe, zakrzywione dla dwóch odległości od dna zbiornika H_2/d = 1 i 0.5. Badania przeprowadzono dla trzech stężeń objętościowych zawiesiny 16, 31.5 i 47%.

Słowa kluczowe: mieszanie, zawiesina, gips

DOI:

* Prof. DSc. Eng. Tomáš Jirout, Prof. PhD. Eng. František Rieger, Department of Process Engineering, Faculty of Mechanical Engineering, Czech Technical University in Prague.

1. Introduction

This paper reports on an experimental study of the waste suspensions mixing from the energy industry. The sedimentation and the rheological behaviour of these suspensions were described in our recent paper [1]. Figs. 1 and 2, reproduced from that paper, show that the settling velocity decreases and the viscosity of these suspensions increases rapidly with increasing particle concentration.

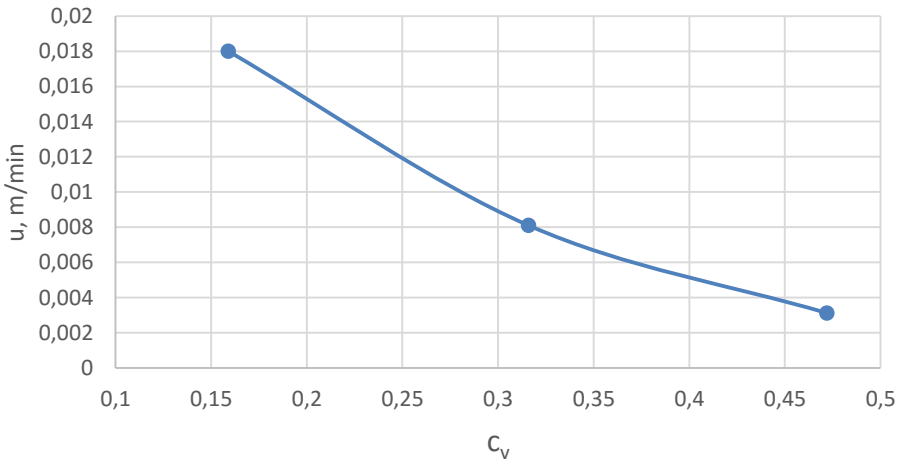

Fig. 1. Dependence of sedimentation velocity on concentration

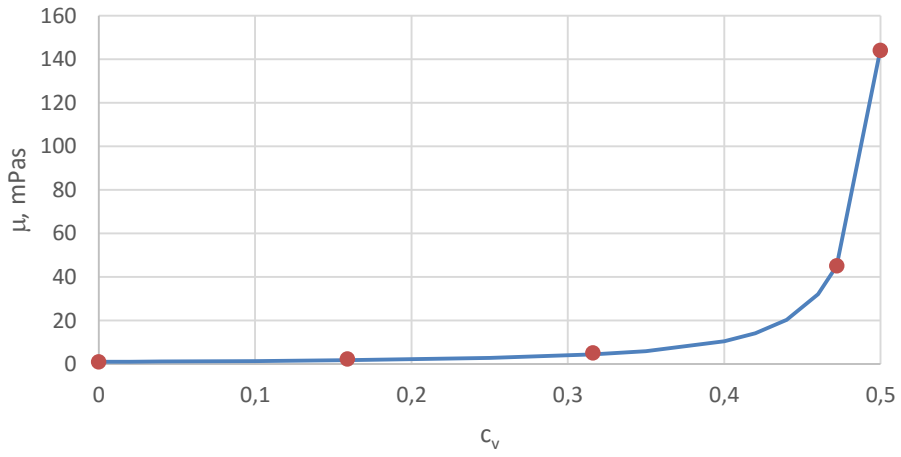

Fig. 2. Dependence of viscosity on volumetric concentration

2. Experimental

Mixing experiments were carried out in a transparent baffled vessel (see Fig. 3) 290 mm in diameter.

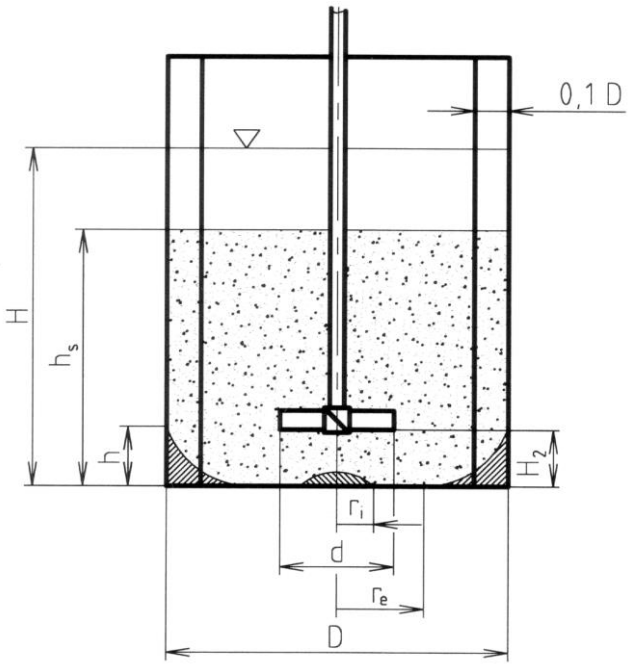

Fig. 3. Experimental vessel, $H/D = 1$

A standard pitched six-blade turbine (6SL45) and a diagonally folded four-blade turbine (4RLL) 100 mm in diameter, as shown in Fig. 4, at two relative distances from the bottom, $H_2/d = 1$, 0.75, and 0.5, were used in the experiments. Measurements were carried out with three volumetric concentrations of the suspensions: 16%, 31.5% and 47%.

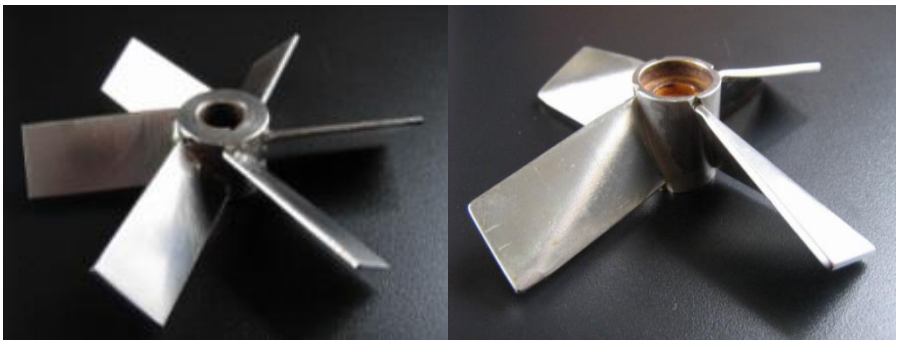

Fig. 4. Agitators used in the experiments

The just suspension speed of the agitator was stated as the speed at which the height of the particle layer h in the bottom corner was zero. The height of the suspension layer h_s and the concentration distribution at the suspension speed were also measured. The concentration distribution was stated on the basis of an analysis of samples taken from the wall of the vessel at various distances from the bottom of the vessel, see Fig. 5. Samples were taken at just-suspension speed and at the speed at which the height of the interface between the suspension and clear water $h_s = H$. An analysette A22 laser analyser was used for sample analysis. The distances z of the places at which samples were taken are specified in Table 1.

Fig. 5. Experimental vessel

Table 1

Sampling point	**1**	**2**	**3**	**4**	**5**	**6**
z [mm]	48	73	97	145	193	242
z/H	0.17	0.25	0.33	0.50	0.67	0.83

3. Experimental results

Analyses of the samples were carried out for a standard pitched six-bade turbine at the lowest concentration of 16%, at which the settling velocity is highest (see Fig. 1). The results for the agitator speed at which $h_s = H$ (see Fig. 5, second photo) are shown in Fig. 6. The results for just-suspension speed (see Fig. 5, third photo) are shown in Figs. 7 and 8. It follows from the results shown in Fig. 6 that at $h_s = H$ there is homogeneity and the particle

size distribution is uniform. From Figs. 7 and 8, when $h_s < H$ at z = 48 mm the concentration is higher, and near the interface at z = 242 mm the concentration is smaller and the particle size distribution is not uniform (the suspension contains only the smallest particles). At the other sampling points (2-5), the suspension is uniform.

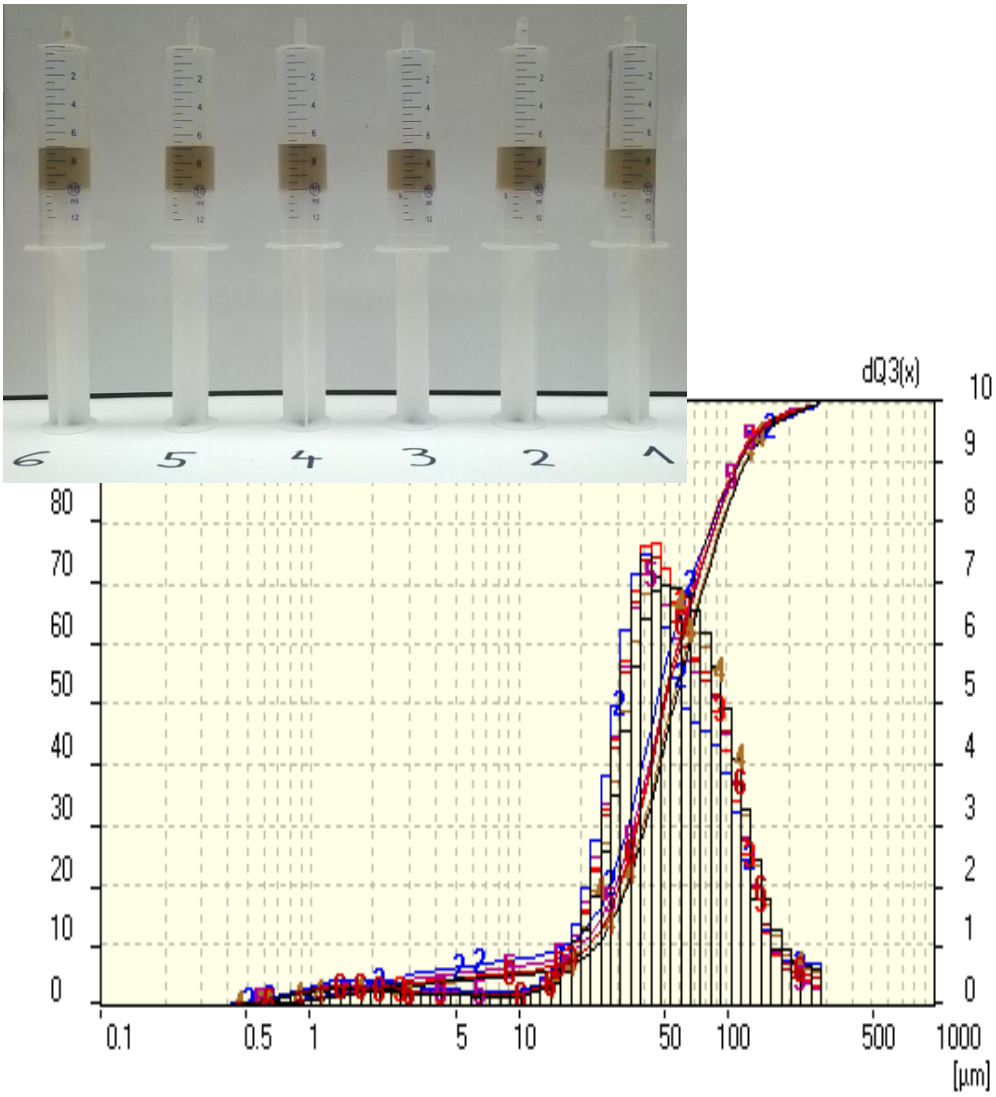

Fig. 6. Analysis of the concentration profile and the particle size distribution at $h_s = H$ (c_v = 16%, pitched blade turbine: H_2/d = 1, n_h = 502 min^{-1})

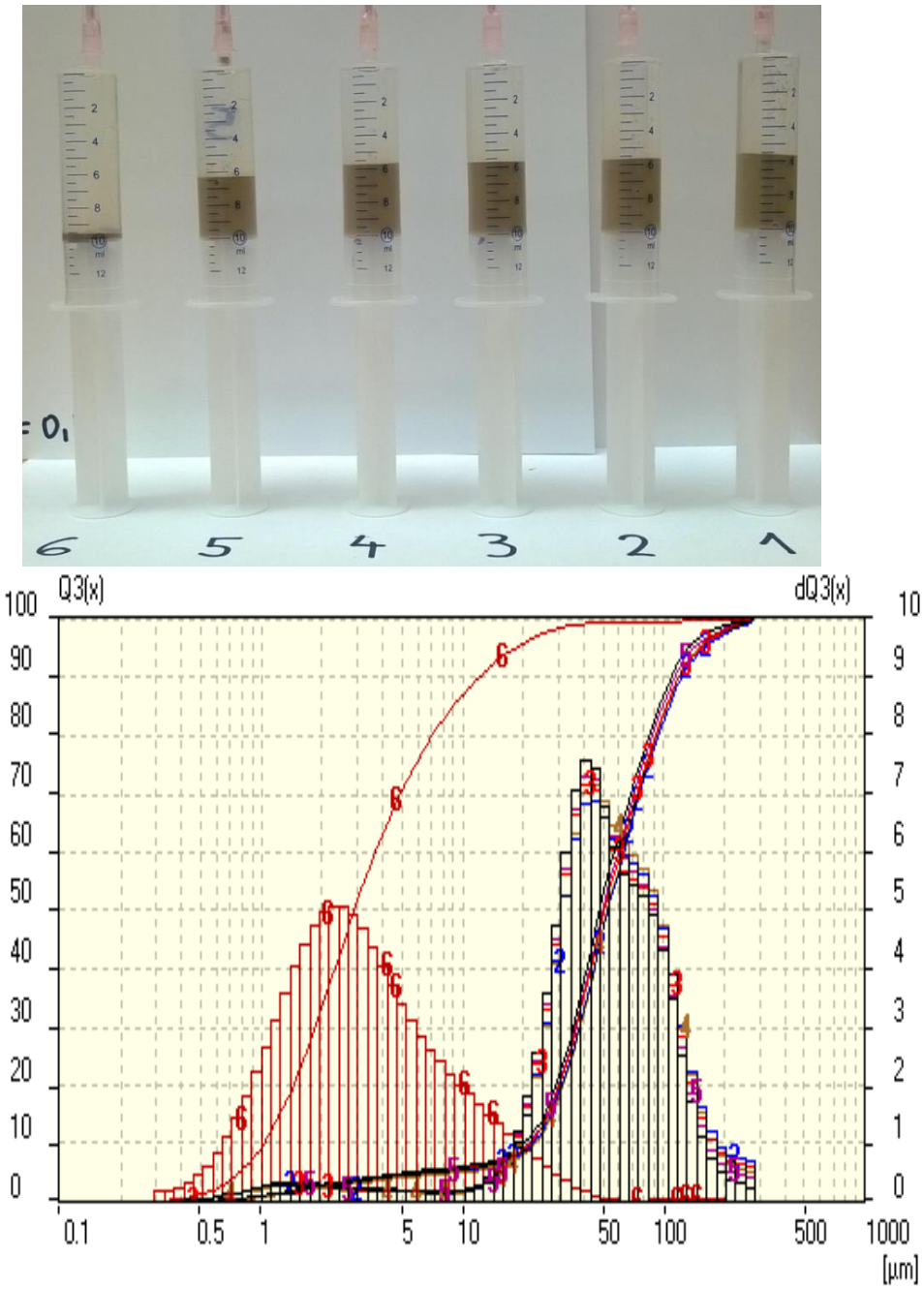

Fig. 7. Analysis of the concentration profile and the particle size distribution at just-suspension speed (c_v = 16%, pitched blade turbine: H_2/d = 0.5, n_{cr} = 226 min^{-1}, h_s/H = 0.724)

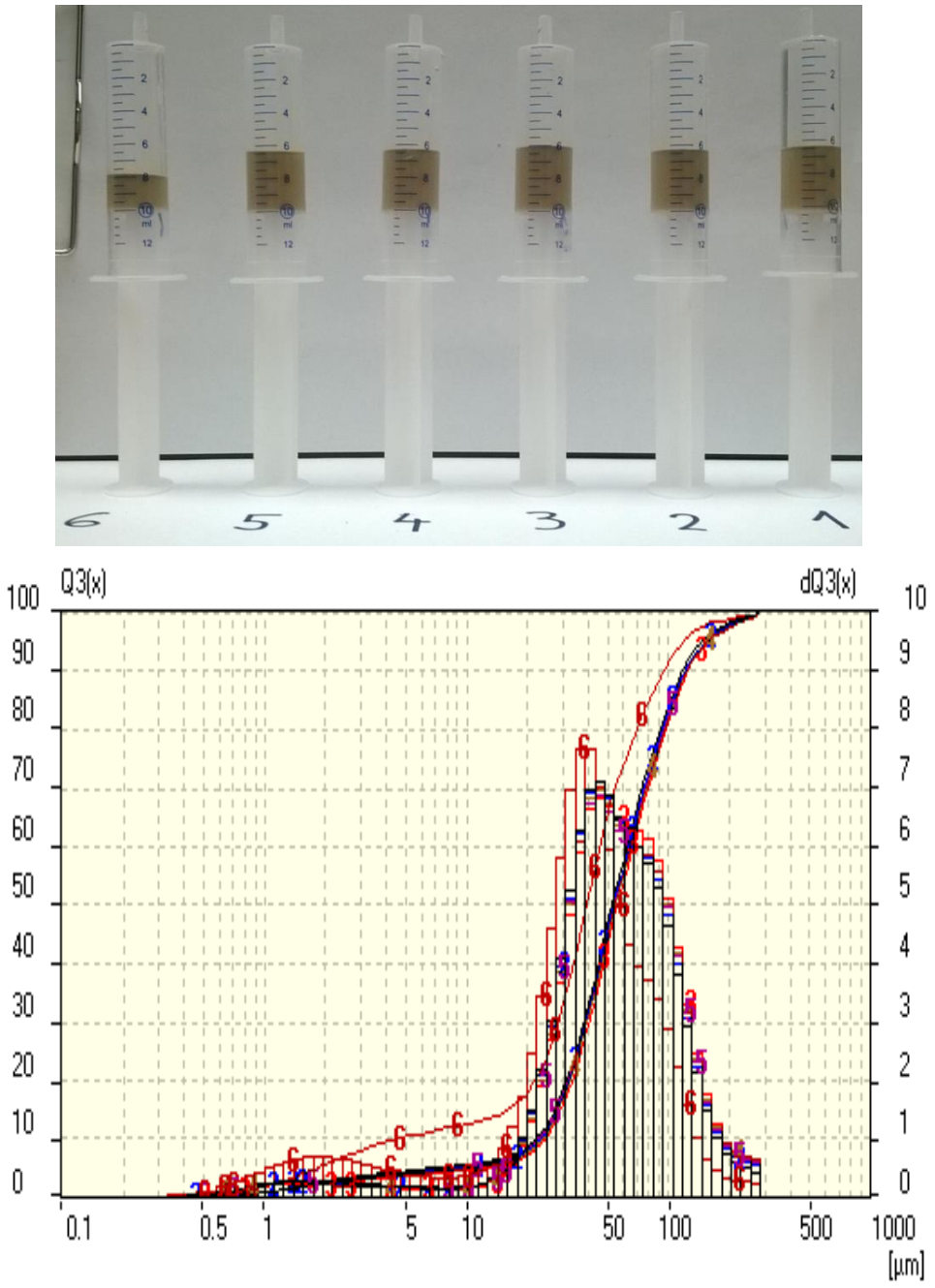

Fig. 8. Analysis of the concentration profile and the particle size distribution at just-suspension speed (c_v =16%, pitched blade turbine: H_2/d = 1, n_{cr} = 330 min^{-1}, h_s/H = 0.879)

The experimental values of just-suspension speed and agitator speed at $h_s = H$ are presented in tables 2 and 3. These tables also contain values for the power consumption and for specific power, calculated from the power number values presented in [2].

Table 2

Values obtained at just-suspension speed

Volumetric particle concentration	*Agitator*	H_2/d	n_{cr} [min^{-1}]	h_s [mm]	h_s/H	*Po*	*P* [W]	ε [$W \cdot m^{-3}$]
16 %	**6SL45**	1	330	255	0.879	1.66	3.31	173
		0.5	226	210	0.724	1.81	1.16	61
	4RLL	1	302	215	0.741	0.78	1.19	62
		0.5	260	195	0.672	0.99	0.97	50
31.5 %	**6SL45**	1	349	270	0.931	1.66	4.57	239
		0.5	245	245	0.845	1.81	1.73	90
	4RLL	1	345	240	0.828	0.78	2.08	108
		0.75	290	240	0.828	0.80	1.26	66
		0.5	280	230	0.793	0.99	1.41	74
47 %	**6SL45**	1	430	290	1.000	1.66	8.55	447
		0.5	390	290	1.000	1.81	6.96	363
	4RLL	1	508	290	1.000	0.78	6.63	346
		0.75	500	285	0.983	0.80	6.48	338
		0.5	480	290	1.000	0.99	7.10	370

Table 3

Values obtained at $h_s = H$

Volumetric particle concentration	*Agitator*	H_2/d	n_h [min^{-1}]	h_s [mm]	h_s/H	*Po*	*P* [W]	ε [$W \cdot m^{-3}$]
16 %	**6SL45**	1	502	290	1	1.66	11.67	609
		0.5	483	290	1	1.81	11.33	592
	4RLL	1	580	290	1	0.78	8.45	441
		0.5	505	290	1	0.99	7.08	370
31.5 %	**6SL45**	1	510	290	1	1.66	14.27	745
		0.5	470	290	1	1.81	12.18	636
	4RLL	1	539	290	1	0.78	7.92	413
		0.75	490	290	1	0.80	6.10	318
		0.5	485	290	1	0.99	7.32	382

It follows from the results presented here that at just-suspension speed for concentrations of 16% and 31.5% $h_s < H$, and for a concentration of 47% $h_s = H$. The just-suspension speeds at the maximum concentration of 47% are significantly higher than at lower concentrations. A comparison of the power consumption shows that a folded blade turbine needs less power than a standard pitched blade turbine.

A comparison of the experimental just-suspension speed values with the values calculated from the relations presented in [3] is shown in Fig. 9. It follows from this figure that there is no significant difference between the experimental values and the calculated values at concentrations of 16% and 31.5%. The experimental values obtained at the maximum concentration of 47% are significantly higher than the calculated values. This is due to the high viscosity of the suspension and the transitional flow in the vessel (the relations presented in [3] hold only for turbulent flow).

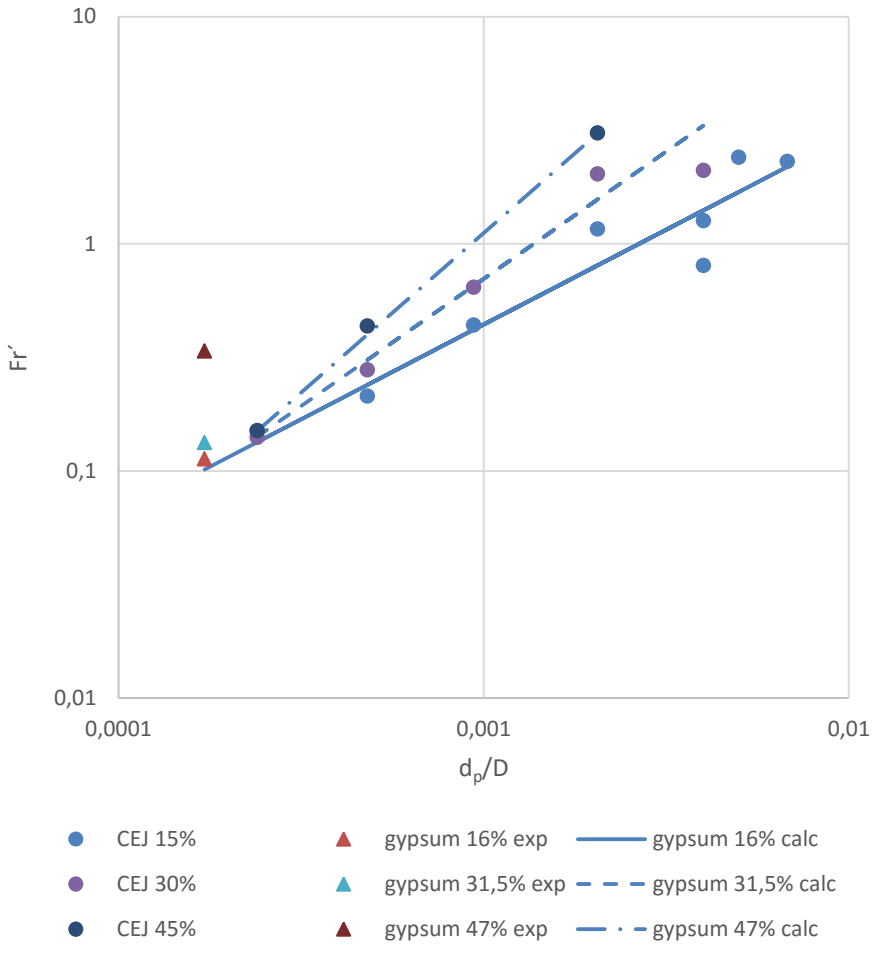

Fig. 9. Comparison of experimental values with results from [3]

List of symbols

c_v – mean volumetric particle concentration
d – agitator diameter
D – vessel diameter
d_p – particle diameter
Fr' – modified Froude number $Fr'=n^2d\rho/g\Delta\rho$
g – gravity acceleration
h – sediment height
h_s – height of interface between suspension and clear liquid
H – batch height
H_2 – distance between agitator and bottom
n – agitator speed
n_{cr} – just-suspension agitator speed
n_h – agitator speed at which $h_s = H$
$r_{i,e}$ – radii of sediment layer
u – settling velocity
z – distance of sampling point
μ – dynamic viscosity
ρ – suspension density

References

[1] Moravec J., Rieger F., Jirout T., *Viscosity measurements of gypsuzm suspensions*, Proceedings of 22nd Polish Conference of Chemical and Process Engineering, Spala, 5-9 September 2016.
[2] Medek J., *Power characteristics of agitators with flat inclined blades*, Int. Chem. Eng., vol. 20, 1980, 665-672.
[3] Rieger F., *Effect of particle content on agitator speed for off-bottom suspension*, Chem. Eng. J., vol. 79, 2000, 171-175.

TECHNICAL TRANSACTIONS | CZASOPISMO TECHNICZNE
MECHANICS | MECHANIKA
2-M/2016

EVGENY KALININ, SERGEY ERSHOV, SERGEY KOZHEVNIKOV*

REGENERATION AND UTILISATION ROTARY SYSTEMS OF WASTE TECHNOLOGICAL LIQUIDS

WYKORZYSTANIE UKŁADÓW WIRUJĄCYCH DO REGENARACJI ZANIECZYSZCZONYCH PŁYNÓW TECHNOLOGICZNYCH

Abstract

The article shows prospects of using regeneration and utilisation rotary systems of waste technological liquids in enclosed local water systems.

Keywords: local water systems, waste technological liquids, filtration of disperse solutions.

Streszczenie

W pracy przedstawiono perspektywy wykorzystania układów wirujących do regeneracji zanieczyszczonych płynów technologicznych w zamkniętych, lokalnych systemach

Słowa kluczowe: lokalne systemy wodne, zanieczyszczone płyny technologiczne, filtracja zdyspergowanych roztworów

DOI:

* Prof. PhD. DSc. Eng. Evgeny Kalinin, PhD. DSc. Eng. Sergey Ershov, PhD. DSc. Eng. Sergey Kozhevnikov, Department of Ground Vehicles and Technological Machines, Faculty of Mechanics and Automations, Ivanovo State Polytechnic University.

1. Introduction

In industry, wastewater is formed in treatment processes of different materials in aqueous media, and its quantitative and qualitative composition significantly varies, depending on the purpose of the implemented process.

When using wastewater as a heat carrier, a decisive influence on the efficiency of the heat recovery is had by such features as its pollution, heat capacity and the volume of abduction. Therefore, an analysis of the above wastewater characteristics in different liquid processes is appropriate.

The problem of material resources reusing, for example, in the manufacture of textile finishing industry is of great importance both from the technical and economic point of view, and to ensure optimal production of ecological interaction with the environment. At the same time, the complex problem is solving not only for the regeneration of waste material of technological solutions, but also for the problem of secondary recovery environments with a significant energy potential, by creating technologies and systems operating in a closed loop.

2. Methods

2.1. Local methods of a wastewater treatment

Numerous studies have shown that the wastewater treatment in chemicals and other types of industries is most effective if they are processing directly in the field of contaminants formation before mixing in wastewater sewers. Wastewater technological equipments for the same type of purposes usually contain a significant amount of the same quality contaminants, whose removal can be performed by one method or by combining them, which is economically efficient for cleaning mixtures. A number of pollutions in the wastewater individual equipment can be so large that their discharge into the sewers and further works general constructions is impossible without special pre-treatment means. Thus, local wastewater treatment uses various mechanical, chemical and physico-chemical methods, and the circulating local sewage systems in a number of cases should be a part of an industrial complex.

2.2. Choice of a local method of a wastewater treatment

A local treatment of concentrated effluents allows to recycle valuable components. However, a prerequisite wastewater before entering it into the overall transportation system for biological treatment facilities should consider the necessity of pre-cleaning and preparation at local wastewater treatment plants. Creating reliable automatic quality control systems largely contributes to the execution of the conditions.

Separating the waste water treatment systems plant-wide and locally eliminates the need for costly construction of long-distance pipelines, reservoirs diameters are reduced, simplified communications and water ways post-treatment.

Concentrated waste water after finishing processes advisable to clean by means of various chemicals and oxidation methods extracting from the wastewater components -

extraction, electrochemical, flotation methods, adsorption, filtration, ultrafiltration. Recent methods on the technological characteristics are the most advanced and promising in terms of both the quality of ultrafiltration and capital, and energy costs for wastewater treatment.

The complex technological scheme of wastewater treatment is based on the following principles:

- creation of independent (local) water circulating in each production system with the necessary local treatment facilities and the subsequent use of treated wastewater in the process;
- separation and disposal of waste liquid technological environments, which may be used in a recycling water management;
- construction of facilities for the advanced treatment of biochemical effluent with the return of all recycled water in the production working cycle.

Concentrated wastewater cleared on local technological units can be taken to the biochemical adsorption or filtration systems for the fullest cleaning and then return to the system of water consumption.

Filtration is one of the methods for separating suspended solids from liquids and gases by means of porous walls or special centrifuges.

3. Decisions

3.1. New trends

Today, the development of a membrane filtration unit, in which in order to create the working pressure, a centrifugal force field will be applied, is the most urgent task. This is caused by the fact that besides installing baromembrane, the membrane elements should include: the pump unit, pre-treatment equipment, tanks for feed solution, the permeate and the concentrate, sensors and automatic control and monitoring devices, connection and control valves, frame elements, etc. Centrifugal filtration units, with the diaphragm, have the following advantages: tens of times less power consumption; considerably less space requirements; mobility in mind the small size; relatively low operating pressures due to low contamination of separation surfaces.

It gives even more advantages to bring together multiple stages of membrane separation into one centrifugal set – the combination of macro and micro-filtration process with ultrafiltration. Therefore, expansion of the application scope of membrane technology can only be achieved at the expense of development work on the creation of new and improved existing spacer elements and devices.

The main objective of the developed local treatment systems and the recycling of technological water is to prevent the discharge of waste water into the environment (into the surrounding water). No less important is the problem of collecting valuable chemical components contained in waste solutions with a view to their re-use.

Creating a multi-stage cleaning system running on the wastewater of the whole enterprise requires significant capital expenditures. In this case, mixing sewage processing equipment after different purposes (different from the chemistry of the process) makes it impossible to extract expensive components from working solutions. These components are

irretrievably lost, and in addition to damage to the environment, they increase the costs for companies to resume raw materials.

Saving technological water and preventing the discharge of waste water to a large extent can be achieved through the use of membrane technology. With it, you can select valuable components from spent wash water and send them for recycling. This method allows to avoid a chemical degradation of component molecules in contrast to the method of evaporation and brought to a state in which it becomes possible to reuse by increasing the concentration.

The most promising is using ultrafiltration membranes that provided a high-speed shared solution on its surface, which leads to the possibility of long-term operation of the filtration equipment without intermediate cleaning. Centrifugal devices, in this case, are a key element to create a local waste treatment system of liquid media technology.

A centrifugal membrane device (Fig. 1), as a part of the system, contains three separate levels: macro, microfiltration and ultrafiltration [1]. Performance of the centrifugal membrane device, according to the starting solution, may be chosen in the installation via separation factor value in accordance with the rotor speed. This scheme provides for the recovery and recycling of chemical components process with sufficiently high concentration, and returns to the washing process line the hot cleaned water, which reduces the cost of heat for its subsequent display.

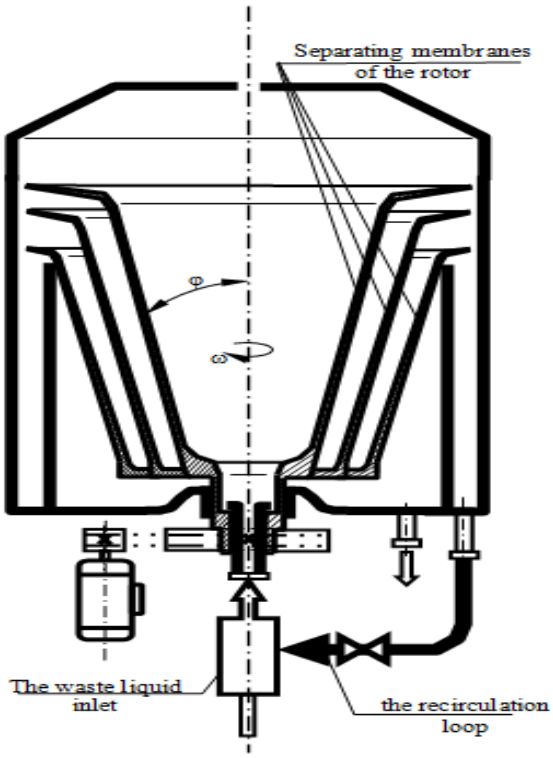

Fig. 1. The design concept of a centrifugal membrane device (CMD)

Equipment of circulating water local system is located directly next to the main process equipment and requires the use of long pipelines and large amounts of storage volume.

Local water recycling system, for example, as a part of the dyeing and drying line, allows achieving the following technical and economic indicators:

- saving technological water, no more than, m^3/h – 6.0;
- saving thermal energy for heating water, no more, Gcal/h (1.3 t/h of normal Pair) – 0.7
- volume reduction of wastewater containing a dye no more than 0.3...0.5 g/l, m^3/h – 6.0.

Thus, the local system of closed water consumption, which included applied centrifugal membrane device, allows to return the purified water effectively into the technological cycle.

3.2. Complete solution

Wastewater of textiles has a high value and high concentration of adsorbed organic halogen compounds as well as intense colour and a significant salt content. Approximately 60% of wastewater in the application of the purification method can be recycled into the production water circulation. The remaining wastewater is treated to such a degree that it can be discharged into the surface water body.

The flow part of the recycled water is desalted by reverse osmosis. Additional demand for industrial water covered by make-up the system of pre-prepared fresh water.

Membrane filtration processes, in particular ultrafiltration and microfiltration, are the separation processes, which take place under pressure using polymeric or porous inorganic materials.

Basic filtration systems consist of two kinds of the same products – filtration devices and filtration modules, which differ mainly by their large-scale indicators (size and weight).

The prospect of the application of multi-stage wastewater treatment system, which comprises: the first stage – pre-cleaning method of macro microfiltration; at the next stage – ultrafiltration separation, realised at higher separation factors (Fig. 2) [2, 3].

4. Conclusions

The possibility of combining all the steps into one system, realised in a centrifugal filtration apparatus, makes it possible to create a highly economical method, implemented on space-saving type of equipment for local systems of circulating water use of technological production.

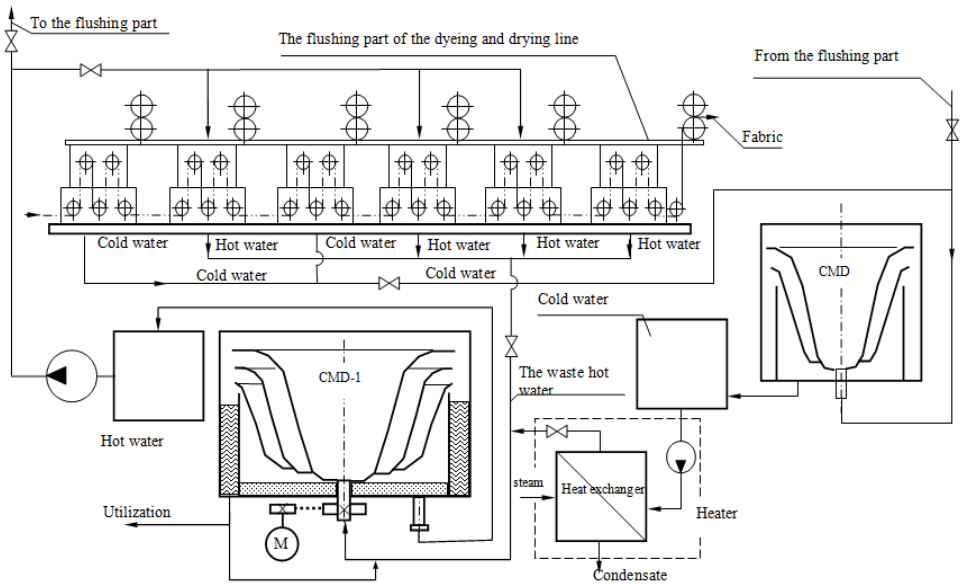

Fig. 2. Technological scheme of the circulating water local system for a dyeing and drying line

References

[1] Ganichev I. V., Kalinin E. N., Kozlov V. V., *The centrifugal device for cleaning the fluid from dispersed impurities: a patent*, Russia, №2226419.

[2] Ganichev I. V., Kalinin E. N., Kozlov V. V., *Experimental and analytical research of centrifugal filtration parameters*, Proceedings of the universities, Technology of textile industry, vol. 6, 2003.

[3] Ganichev I. V., Kalinin E. N., *Identification of the vortex motion dynamic model of membrane fluid flow*, Proceedings of the universities, Technology of textile industry, vol. 2, 2004.

TECHNICAL TRANSACTIONS | CZASOPISMO TECHNICZNE
MECHANICS | MECHANIKA
2-M/2016

RYSZARD KANTOR*, PIOTR SEWERYN**

DYNAMIC MODELING OF OPERATION OF CONTROLLED SOLAR HEATING SYSTEM IN ECOSIMPRO

DYNAMICZNE MODELOWANIE DZIAŁANIA STEROWANEGO GRZEWCZEGO UKŁADU SOLARNEGO W PROGRAMIE ECOSIMPRO

Abstract

The article describes the structure and operation of virtual one-dimensional dynamic model of the solar heating system using components from the libraries of the EcosimPro program. The model is based on a fragment of a real hybrid sorption-compressor refrigeration system, designed and built in the Laboratory of Thermodynamics and Thermal Machines Measurements at the Faculty of Mechanical Engineering of the Cracow University of Technology. In the second part of the paper, the results of the dynamic simulation are shown along with their comparison to the actual measurement data recorded during one day (and night).

Keywords: dynamic modelling, solar heating system, EcosimPro

Streszczenie

Prezentowany artykuł zawiera opis struktury i działania wirtualnego jednowymiarowego dynamicznego modelu solarnego systemu grzewczego przy użyciu komponentów z bibliotek programu EcosimPro. Model oparty jest na fragmencie rzeczywistego hybrydowego sorpcyjno-sprężarkowego systemu ziębniczego, zaprojektowanego i zbudowanego w Laboratorium Termodynamiki i Pomiarów Maszyn Cieplnych na Wydziale Mechanicznym Politechniki Krakowskiej. W drugiej części artykułu pokazano wyniki dynamicznej symulacji i ich porównanie do rzeczywistych danych pomiarowych, zarejestrowanych w ciągu jednej doby.

Słowa kluczowe: modelowanie dynamiczne, system ogrzewania słonecznego, EcosimPro

DOI:

* DSc. Eng. Ryszard Kantor, Institute of Thermal and Process Engineering, Faculty of Mechanical Engineering, Cracow University of Technology.
** Piotr Seweryn, Faculty of Mechanical Engineering, Cracow University of Technology.

1. Introduction

In the laboratory of Institute of Thermal and Process Engineering seated at the Faculty of Mechanical Engineering of the Cracow University of Technology, there has been designed and assembled a prototype of a two stage hybrid adsorption-compression cooling system [1]. The high temperature stage component of the system is the adsorption chiller driven by the heat generated by the solar collectors. The adsorption chiller works during the summer period as a chiller rejecting the heat from the condenser of the low temperature compressor stage with CO_2 as the cooling agent. Generally, all heating systems driven by solar collectors are characterised by periodic operation and unstable availability of a heat source. This enforces the use of heat accumulators to store the surplus of the heat generated during day and use it during periods of low solar operation (e.g. at nights). The excessive solar heat load to the system may cause a rise of the temperature above limits, thus an additional safety protection system is necessary. There are two possible solutions: a heat rejection system (e.g. by using a cooling tower) or thermally controlled solar blinds blocking the solar radiation.

In the present paper, the structure and operation of a virtual one-dimensional dynamic model of the solar heating system is shown. The model built in the EcosimPro software is based on a fragment of the above-mentioned hybrid refrigeration system.

2. Hybrid sorption-compressor refrigeration system

In Figure 2.1, a general scheme of the hybrid cooling system is shown.

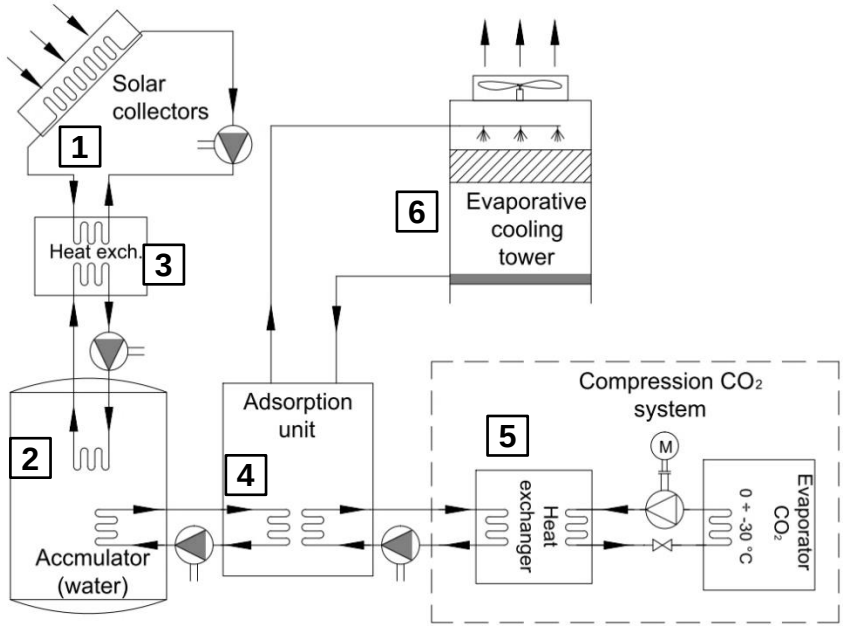

Fig. 2.1. General diagram of the system

The system consists of four main subsystems:

- solar collectors (1) with accumulator (2) coupled by the heat exchanger (3),
- adsorption chiller (4),
- compression CO2 system (5),
- cooling tower (6).

The aim of the present paper is to build a virtual model of one complete subsystem comprising of a set of solar collectors (1), an accumulator (2) and the heat exchanger (3). The model allows to simulate a dynamic behaviour of the solar heating subsystem during a period of several days. A detailed diagram of the solar heating subsystem is shown in Figure 2.2.

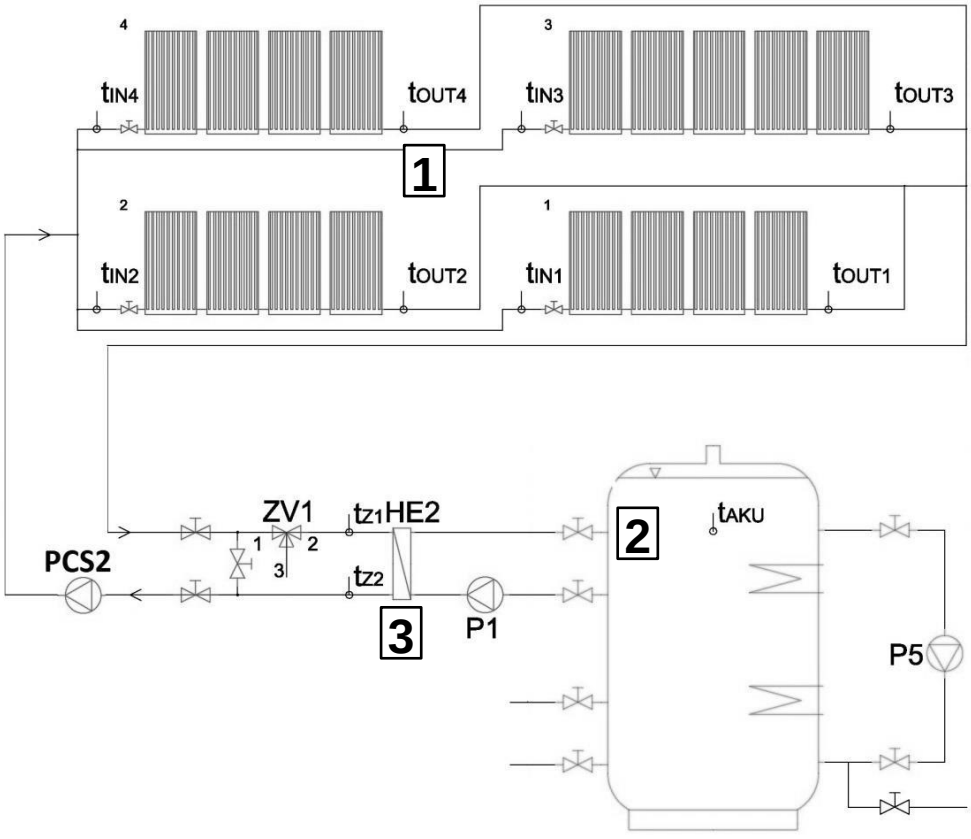

Fig. 2.2. General diagram of the system [2]

3. One-dimensional dynamic modelling in EcosimPro

EcosimPro is a modelling and simulation tool developed by Empresarios Agrupados and used, among others, by ESA[1] and CERN[2]. It allows to build mathematical models of 0D or 1D multidisciplinary continuous-discrete systems and any kind of systems based on differential-algebraic equations (DAE) and discrete events [3].

Models can be created with predefined components from multiple libraries or custom objects written in EL (EcosimPro Language). In order to simulate a schematic model, a mathematical model called partition has to be created. For each partition, the user can define experiments, which contain information about simulation settings, such as time or file name, to save results, initial and boundary conditions.

The greatest advantage of EcosimPro is the possibility of reusing models outside of the software environment in several forms, e.g. standalone C^{++} application. This feature guarantees model reusability by others and further development possibilities like dedicated applications for operator's training, testing models with control programs from real PLC device etc.

The model described below has been created with EcosimPro 5.2.0 by using major components from embedded libraries: Fluidapro, Control, Thermal. The Control and Thermal libraries are standard and free to use, the Fluidapro is a separate library that requires an additional, extra paid, license.

3.1. Virtual model description

In Figure 3.1, a diagram of the created model of solar heating system with the heat storage is shown. The model presents one of the optional states of the system – the heat generated by solar collectors (1) is stored by the accumulator (2).

Fluidapro elements like pipes, tees, valves, volume, heat exchanger, tank and temperature sensors can be distinguished by their symbol shapes. The *Working Fluid* abstract elements (WF) define the working medium (e.g. water). The real pumps are virtually modelled by a simplified component (PCS2, P1).

Elements, which serve to model solar irradiance (G), temperature outside (T_OUT) and mass flow (QM), are imported from the Control library. There are also two Thermal components to simulate the impact of environmental temperature on heat storage.

SolarCollectors element represents a sub-model, which is separately defined in a different file, in order to clarify the scheme view. The *Psolar* element is used to calculate the power gained by solar collectors with given inputs, where the temperature sensor T_MIX registers the current working medium temperature.

In the current *Psolar* model, the measuring point of controlling (feedback) temperature is located after the solar collectors because all solar collectors are identical and thus all are characterised by the same parameters. This workaround simplifies the computational effort and also improves the scheme view. Further simplifications are discussed in the next chapter.

---

[1] European Space Agency

[2] European Organization for Nuclear Research

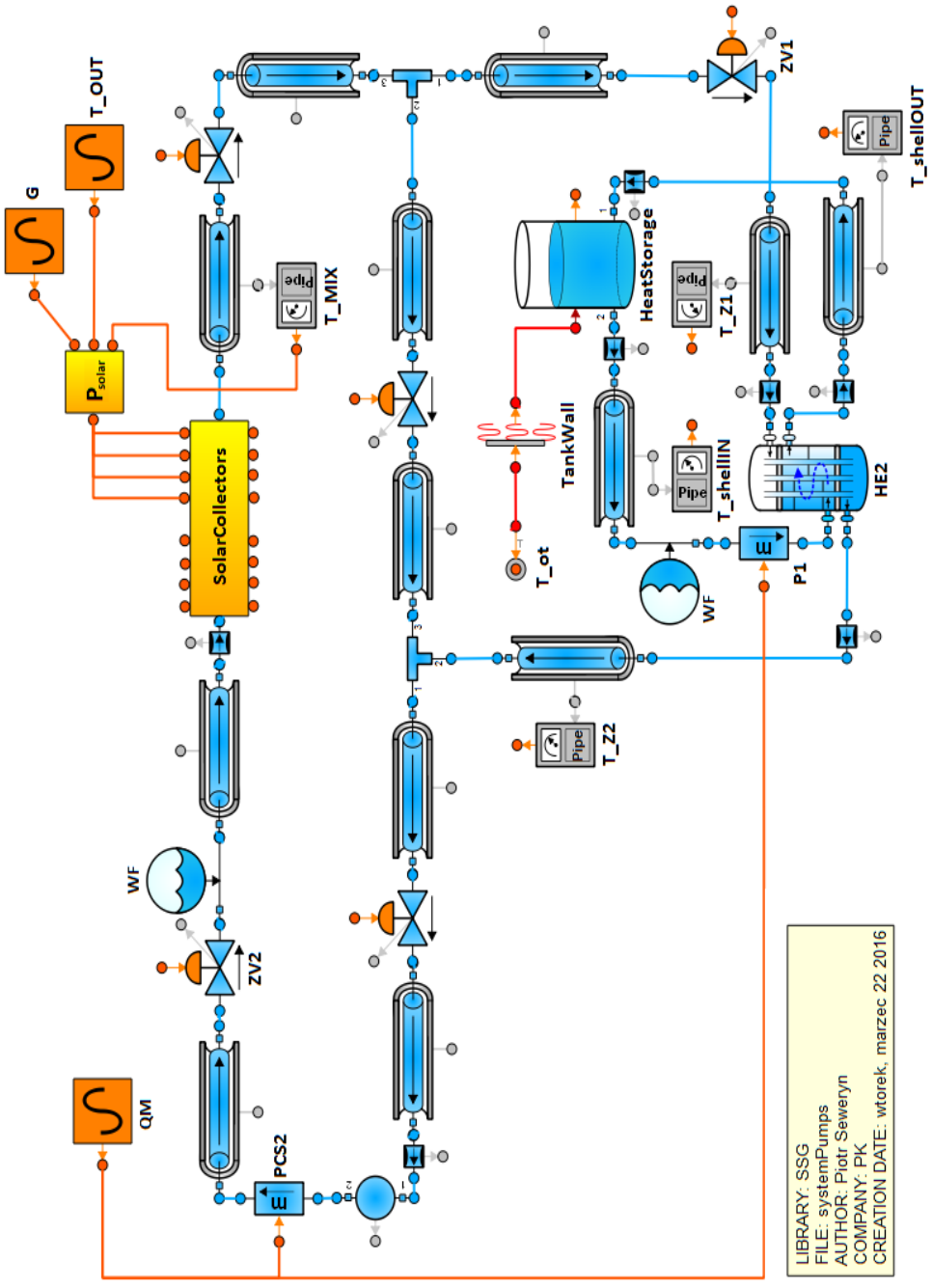

Figure 3.1. Schematic model of solar heating system created in EcosimPro

3.2. Major components of the model

Default parameters of each component have been modified according to the real objects in order to provide as accurate results as possible. The parameters are, e.g. geometrical dimensions, heat exchange coefficients, applied materials etc.

The model of solar heating system in EcosimPro includes some simplifications:

- In order to simplify calculation process, internal boundary conditions (PCS2, P1) are used instead of pumps.
- Working fluid is water instead of glycol mixture, which is not defined in a properties library. It is possible to add it manually in the future.
- In the real solar heating system the brazed plate heat exchangers are used. Due to lack of that element in the library and complexity in custom modelling, a shell-tube heat exchanger (HE2) with appropriately tuned parameters is used instead.

Solar collectors are wrapped in an additional custom component to clarify the scheme view. In Figure 3.2, the model of solar collectors with its distribution pipes, valves and temperature sensors is shown. Heat load from the solar radiation to tube elements is modelled by a heater element from the Thermal library.

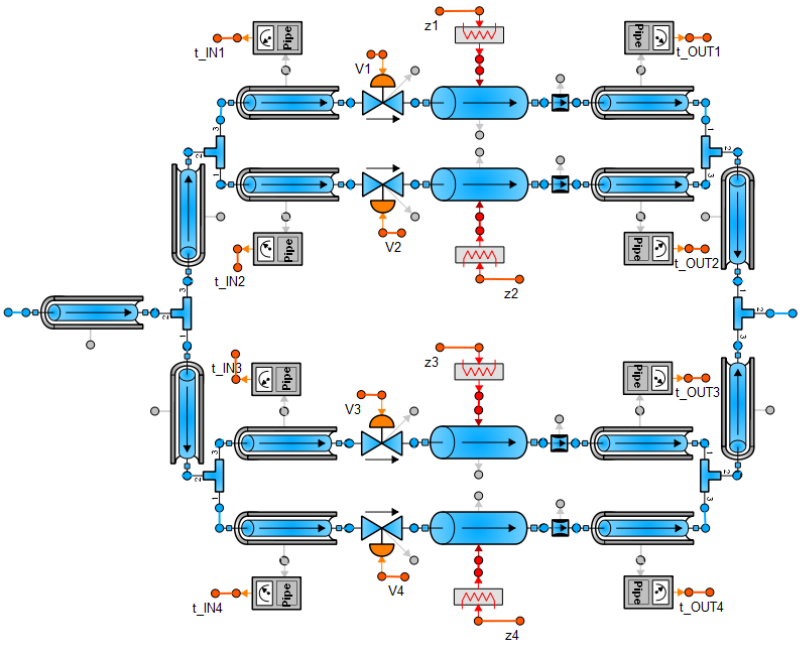

Fig. 3.2. Schematic model of solar collectors

The *Psolar* is a user defined and arranged component that calculates the solar power. It takes into account solar irradiance, ambient temperature and working fluid temperature. It uses the following formula [4]:

$$P = S \cdot (\eta_0 \cdot G - a_1 \cdot (T_m - T_a) - a_2 \cdot (T_m - T_a)^2)$$

where:

S – total aperture area of the collector array, m^2,
η_0 – collector optical efficiency, – ,
G – solar irradiance, W/m^2,
T_m – collector operating temperature (T_MIX), K,
T_a – ambient temperature (T_OUT), K,
a_1, a_2 – temperature difference loss coefficients, W/m^2K, W/m^2K^2 [4].

3.3. Simulation strategy and boundary conditions

In order to carry out the simulation, it is necessary to provide simulation settings, initial and boundary conditions. They are all defined in an experiment file, which is a script written in EL. Regarding initial and boundary conditions, which default values are suggested by the program in each new experiment file, the user may change them by modifying partition file.

All results, presented in the following chapter, have been acquired with the following conditions:

- Initial conditions for the temperature impact on the solar collector's tubes objects are 293.15 K.
- Boundary conditions regarding not fully constrained components are:
  - all valves, except for bypass, are in open state,
  - ambient temperature of heat storage room is 293 K.

Some boundary conditions remain in default values due to their constant character, e.g. gravity acceleration or lack of need to use them in this particular model.

3.4. Simulation results

EcosimPro allows to present and save the simulation results in two ways. The first option is to use an additional application called Monitor to display the results and then save them as images or data files. Another way is to use in the experiment file a function that defines the target file and variables to save in it and then use of acquired data to draw plots in a different application, e.g. Microsoft Excel.

In Figure 3.3, simulation results of the presented model with already defined initial and boundary conditions are shown. The first plot presents a simulated temperature of water in the accumulator (T_AKU) and in the piping located after the solar collectors (T_MIX) and also the ambient temperature T_OUT. The second plot shows the solar irradiance G, with assumption of a warm, sunny and cloudless day in Krakow. Results registered within temperature plots are consistent with preliminary calculations.

The temperature T_AKU of water inside of the heat accumulator (2) is rising consequently, but day by day less effectively. Moreover, during nights, the temperature drops are registered. To reduce this effect, a more complex model with a controlled pump shall be worked out. Switching off the pump during nights and speed control is highly recommended.

In the real system, the collected heat is used not only to charge the heat accumulator (2), but also to drive the adsorption unit (4). Moreover, for safety reason, the wet cooling tower (6) is used for rapid cool down of the overheated working fluid. The presented simplified

model does not include the mentioned safety solutions and in result the overheating (T_MIX above limit of 373 K) of the working fluid is registered during the time of maximal sun irradiation.

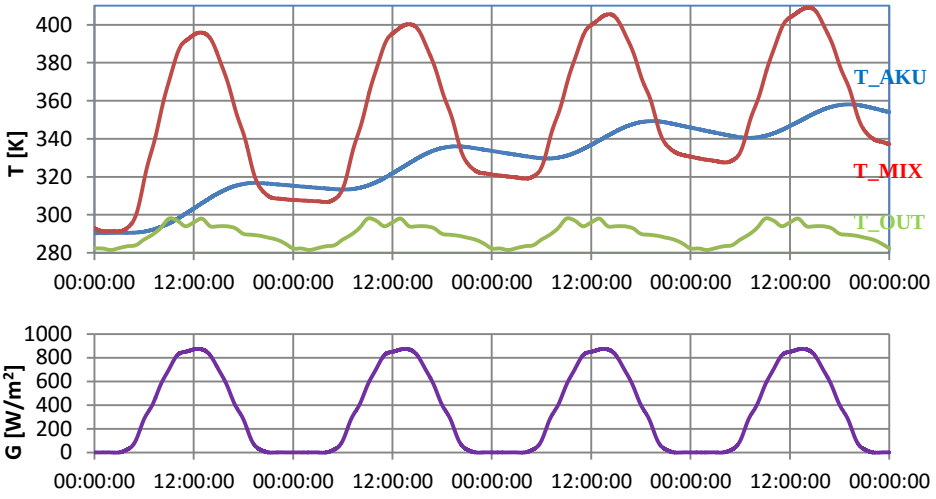

Fig. 3.3. Simulation results – temperature characteristics T_AKU, T_MIX, T_OUT and solar irradiance G

There are two possible solutions to keep the temperature of the working fluid below the limit. The first is a heat rejection system by using a cooling tower, applied in a real installation. The second is a thermally controlled solar blind system, blocking the solar irradiation. For the aim of the present paper, the solar blind system has been modelled. The blinds are being closed on temperature 368 K or above and remain closed until temperature drops to 335 K.

Registered results of the simulation (24 hours) are shown in Figure 3.4. The T_MIX temperature saw-shaped characteristics shows that this is a very efficient method of maximum temperature controlling. The temperature fluctuation span can be narrowed, but in result, this will increase the frequency of the open-close cycle of the solar blind system.

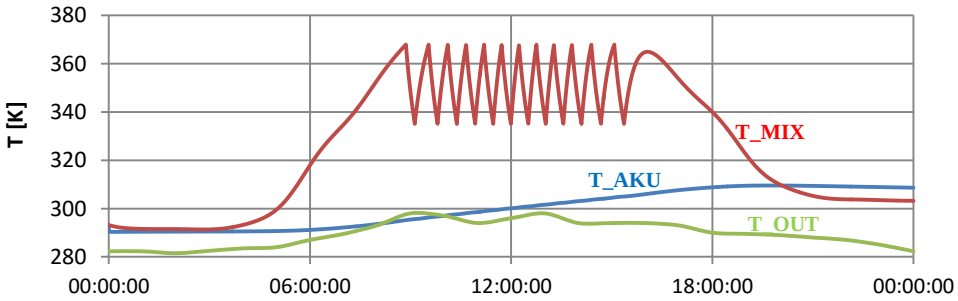

Fig. 3.4. Simulation results for a model with solar collectors covers

4. Experimental verification of the virtual model

The virtual model is based on the real system and there is a certain possibility to compare selected results of the simulation with measurements on the real object in real conditions. It allows to verify the model, performance and effectiveness in comparison to the real installation. However, it is a rare phenomenon characterised by several days of clear unclouded sky, during which one could register quasi-optimal system parameters and the theoretical solar irradiance (Figure 3.3).

4.1. Verification points and parameters

The selected temperatures, presented in Figure 4.1, were registered on 16.06.2015 in the existing system during operation. The temperatures were registered during a sunny day with small rare clouds. It is noticeable on the T_OUT plot that the weather deteriorates from 9 a.m. till 12 a.m. Moreover, during considered time of the year – June, heat accumulator (2) was already charged (T_AKU) and in a stand-by mode. The plot of temperature T_MIX clearly shows the heating process broken by cloudy sky periods. This effect is similar to the mechanical operation of blocking out the solar collectors by the solar blinds during the sunny period of the day.

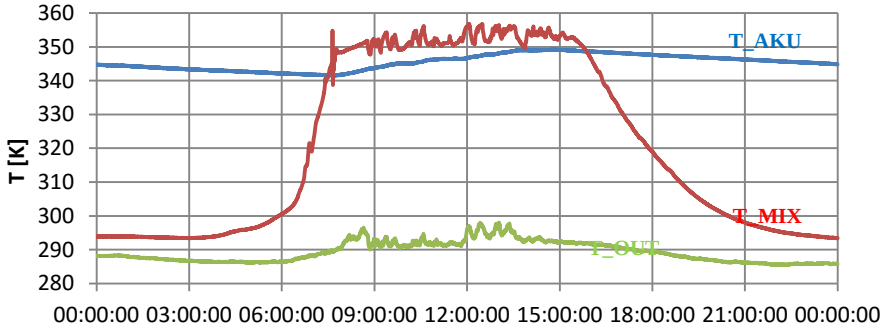

Fig. 4.1. Selected measurements in the real conditions – 16.06.2015 (by courtesy of Roman Duda, Institute of Thermal and Process Engineering)

4.2. Results discussion

In spite of the above-mentioned differences, it is a valuable comparison, showing the performance of the system with both solutions of the maximum temperature control. Although the currently used system is thermally effective, it requires a circulating pump to be frequently switched on during rapid cooling of the overheated working fluid. It is much more effective to use the controlled solar blind system together with the controlled heating medium flow rate (pump speed).

Results of measurements partially resemble those from the simulation. The visible oscillations are the result of cloudy weather. On the other hand, the working fluid temperature measured that day is from 10 to 20 K smaller than on the virtual model with solar blinds, which is mostly caused by ideal solar irradiance applied to the model.

Regarding the heat storage temperature, it is increasing and decreasing in a similar way in all 3 cases and measurements results confirm that during heating process each next day charging is less effective, which mainly is caused by a smaller temperature difference between liquids in the heat exchanger (3).

5. Conclusions

Simulation software, like EcosimPro, is widely used in a modern and innovative industry. It is mostly due to the possibilities of analysing and simulating conceptual solutions without incurring costs of physical implementation. Moreover, it also can be used with existing installations for the purpose of testing new modifications, e.g. the mentioned in this paper system with implemented solar collector blinds.

The virtual model of solar heating system presented in this paper is only a fragment of the much larger and more complex cooling system and any physical difference between the real and the virtual system can have an influence on the results.

The simulation effort allows to save money and time by simulating the virtual experiment. Although to obtain reliable results, it is often required to precisely define the whole system and all of its components.

References

[1] Cyklis P., Kantor R., Ryncarz T., Górski B., *The hybrid compression-sorption system for thermal energy transformation*, 3rd International Conference: Low Temperature and Waste Heat Use in Communal and Industrial Energy Supply Systems. Theory and Practice, October 25th & 26th, 2012, Bremen, Germany, 2012, 44-51.

[2] Cyklis P., Duda R., *Computer driven automatic control of the hybrid two stage refrigeration cycle*, Czasopismo Techniczne. Mechanika, vol. 112(7), 2-M, 2015.

[3] *EcosimPro, system modeling and simulation software*, Empresarios Agrupados [Online: *http://www.ecosimpro.com/products/ecosimpro/*].

[4] *Próżniowy czy płaski - jaki wybrać kolektor słoneczny?*, Hewalex [Online: *http://www.hewalex.pl/pliki/jaki_kolektor.pdf/*].

TECHNICAL TRANSACTIONS | CZASOPISMO TECHNICZNE
MECHANICS | MECHANIKA
2-M/2016

ANN KAPRANOVA, ANTON LEBEDEV, SERGEY SOLOPOV*,
ALEXANDER MELTSER**

THE APPLICATION PROCESS OF THE ORNSTEIN-ULENBEK TO THE FORMATION OF CAVITATION BUBBLES

ZASTOSOWANIE PROCESU ORNSTEIN'A-ULENBEK'A DO OPISU POWSTAWANIA PĘCHERZY KAWITACYJNYCH

A b s t r a c t

In this paper we propose the process of formation of cavitation bubbles in the pilot valve, considered as the steady and homogeneous Markov process.

Keywords: cavitation, formation of bubbles, the Fokker-Planck equation

S t r e s z c z e n i e

W pracy przedstawiono proces powstawania pęcherzy kawitacyjnych w zaworze sterującym jako stabilny i homogeniczny proces Markowa.

Słowa kluczowe: kawitacja, powstawanie pęcherzy, równanie Fokker'a-Planck'a

DOI:

* Prof. DSc. Ann B. Kapranova, Associate Professor DSc. Anton E. Lebedev, MSc Sergey A. Solopov, Mechanical engineering Department, Yaroslavl State Technical University.
** General Director Alexander M. Meltser, ZAO NPO «Regulyator», Yaroslavl.

1. Introduction

The use of regulatory bodies in piping systems allows to perform different technological operations – mixing of liquid streams, maintaining pressure and preventing reverse leakage, etc. The success of the design or modernisation of the elements of the valves depends on the effectiveness of the chosen method of combating undesirable effects of cavitation [1]. To its initial stage in the valves is the formation of bubbles filled with gas and a condensable vapour, arising due to tearing of the liquid in the case of flow in conditions of sharp falling pressure in the flow path of the device.

Application of the stochastic approach for the description of the initial stage of hydrodynamic cavitation as a rule boils down to one of three types of models of education of the nucleons (steam germ) in a liquid environment. In the absence of impurities, an equitable model of homogeneous type [2, 3], and in the presence of suspended particles on or near the surfaces with cracks – heterogeneous type [4, 5]. In addition, the known modifications of the first method of modelling the introduction of an additional coefficient for the number of Gibbs [6], which takes into account the effect of heterogeneity of the environment. However, despite known attempts, the postulation of the relevant law of the distribution of heterogeneous nuclei [7], as shown by the analysis of literary sources [8], the question of the formation of the distribution functions of the cavitation bubbles according to their sizes remains open.

2. The application of the Fokker-Planck equation for the process of formation of cavitation bubbles

In this paper, the process of formation of cavitation bubbles in the regulatory valve, considered as steady and homogeneous Markov process, is presented. In the case when the description of the probability distribution of events, the stationarity implies the possibility of shifting the origin of time, and the uniformity is dependent on time intervals. Note that the main feature of the given random process is that the transition to the subsequent state of the system is determined by its instantaneous condition.

Modelling the process of formation of cavitation bubbles is a stochastic way, including in the formalism of a process of Ornstein-Ulenbek when this bubble macro system is energetically closed from the Gibbs ensemble. Microscopic parameters of this ensemble can serve as the selected coordinates and impulses of Hamilton for each of the similar subsystems, for example, cavitation bubbles are spherical. In the process, the principle of maximum entropy runs, which is in its growth for closed macrosystem and then saving at equilibrium condition [9, 10]. For the process of bubble formation in the conditions of hydrodynamic cavitation will set in the phase space a set of variables, consisting of two variables: the radius of the spherical bubble r, and the velocity of its centre of mass v. The Fokker-Planck equation with drift and diffusion terms of the types corresponding to the process of the Ornstein-Ulenbek is recorded relative to the equilibrium distribution function condition generated spherical cavitation bubbles

$$\frac{\partial F(t,r,v)}{\partial t} = D_1 \frac{\partial^2 F}{\partial r^2} + D_2 \frac{\partial^2 F}{\partial v^2} + \varepsilon_1 \frac{\partial (rF)}{\partial r} + \varepsilon_2 \frac{\partial (vF)}{\partial v} \tag{1}$$

where in the set of phase space coordinates r and velocity v

D_1, D_2 – the diffusion coefficients,
ε_1, ε_2 – the frequency of bubble formation,
F – the equilibrium distribution function of the system condition.

3. Description of stochastic cavitation energy sphere

It is believed that when cavities formed after the rupture of liquids under conditions of rapid pressure drop are filled with gas and a condensable vapour, there is an internal vortex motion in the cavitation bubbles. Then, according to [10], the element dΩ of the phase space is defined as

$$\mathrm{d}\Omega = v\,\mathrm{d}v\,\mathrm{d}r \tag{2}$$

Description of stochastic cavitation bubble energy E with respect to its radius r and the speed of the centre of mass of v implies taking into account the kinetic energies of motion of the bubble in the liquid flow and the internal motion of the system of gas-steam, the energies of formation of the free surface and cavity fill energy due to the condensation of vapour, energy of the hydrodynamic interaction of bubble and liquid. Consequently, introducing coefficients c_1 and c_2

$$c_1 = q_1 \cdot \bar{r}^3 + q_2 \cdot \bar{r}^{-1} \tag{3}$$

$$c_2 = \frac{5 \cdot q_1 \cdot M^2 \cdot \bar{r}^{-7}}{8} + q_3 \cdot \bar{r} + q_4 \tag{4}$$

depending on the structural and regime parameters of flow area control valve and physico-mechanical characteristics of the transported medium, the simulated stochastic energy takes the form

$$E = c_1 \cdot r^2 + c_2 \cdot v^2 \tag{5}$$

where

$\bar{r}$ – the average value of the radius of the bubble,
M – the random component of angular momentum.

Expression (3) and (4) contain the constants q_i, $i = \overline{1,4}$ when asked by the formulas

$$q_1 = \frac{2 \cdot \pi \cdot (\alpha_g \cdot \rho_g + \alpha_s \cdot \rho_s)}{3} \tag{6}$$

$$q_2 = \frac{k_\varsigma \cdot \varsigma_{12} \rho_1}{4}, \quad q_3 = \frac{8 \cdot \pi \cdot P_s}{3} \tag{7}$$

$$q_4 = 4 \cdot \pi \cdot \sigma \tag{8}$$

where

α_g, α_s – the volume fraction of filling bladder with gas and steam,

ρ_g, ρ_s, ρ_l – the density of the gas, steam and liquids,

k_ς – the parameter of proportionality in the expression for the energy of hydrodynamic interaction $E_{hi} = k_\varsigma \cdot \Delta P/(2 \cdot r)$ when calculating the pressure drop in the valve by the formula of Weisbach $\Delta P = \zeta_{12} \cdot \rho_i \cdot v^2/2$,

ζ_{12} – the coefficient of hydraulic resistance of the transition zone for movement of liquid medium, which corresponds to the limit of variation of the Reynolds number $10 < Re < 10^4$, according to [1],

P_s – the saturated vapour pressure,

σ – e surface tension of the liquid.

Note that the value of ζ_{12} is determined by the sum of the coefficients of hydraulic resistance for two zones of laminar and turbulent flows of fluids in the flow part of the valve, which are calculated according to the principle of superpositions of local losses taking into account design and operating parameters of the regulating device and the physical properties of the surfaces of the channels. For example, such parameters include: the diameters of conditional passes and various sections of the spool, the length of the straight channels and the throttle passages, a square cross-section entrance of the (conditional, before and after sudden expansion), gap width of the throttle passage, the degree of roughness of the internal surfaces of the valve, etc.

4. Representation of the kinetic equation of the equilibrium process in the formalism of stochastic energy of the cavitation bubble

The representation (1) of the kinetic equation for $F(t, r, v)$ is the sought distribution function over the States relative to one set of variables (time, radius, velocity the centre of mass of the bubble) to the Fokker-Planck equation with a different set of (stochastic time and energy bubble from the expression (5)) when $\tilde{F}(t, E)$

$$\frac{\partial \tilde{F}(t, E)}{\partial t} = \frac{\mathrm{d}E_0}{\mathrm{d}t} \cdot \left(E \cdot \frac{\partial^2 \tilde{F}}{\partial E^2} + \frac{\partial \tilde{F}}{\partial E} \right) + \frac{1}{E_0} \cdot \frac{\mathrm{d}E_0}{\mathrm{d}t} \cdot \left(E \cdot \frac{\partial \tilde{F}}{\partial E} + \tilde{F} \right) \tag{9}$$

where

E_0 – the energy of the system at the time of stochastic according to [9, 10].

In particular, during the transition from the representation (1) to the form (9) for a given kinetic equation the equilibrium state of the system, it is assumed that the ratios are

$$c_1 \cdot D_1 = c_2 \cdot D_2 \tag{10}$$

$$\varepsilon_1 = \varepsilon_2 \tag{11}$$

where

c_1, c_2 – the coefficients of the expressions (3).

Then taking into account (5) the energy of the system at the time of stochastic E_0 and its flow $\mathrm{d}E_0/\mathrm{d}t$ when $j = \overline{1,2}$ can be specified in the form

$$E_0 = \left(2 \cdot \varepsilon_j\right)^{-1} \frac{\mathrm{d}E_0}{\mathrm{d}t} \tag{12}$$

$$\frac{\mathrm{d}E_0}{\mathrm{d}t} = 4 \cdot c_j \cdot D_j \tag{13}$$

Therefore, taking into account the expressions (3) and (12), we obtain

$$\varepsilon_1 = \varepsilon_2 = \left(2 \cdot E_0\right)^{-1} \frac{\mathrm{d}E_0}{\mathrm{d}t} \tag{14}$$

$$D_1 = \left[4 \cdot \left(q_1 \cdot \bar{r}^3 + q_2 \cdot \bar{r}^{-1}\right)\right]^{-1} \frac{\mathrm{d}E_0}{\mathrm{d}t} \tag{15}$$

$$D_2 = \left[4 \cdot \left(\frac{5 \cdot q_1 \cdot M^2 \cdot \bar{r}^{-7}}{8} + q_3 \cdot \bar{r} + q_4\right)\right]^{-1} \frac{\mathrm{d}E_0}{\mathrm{d}t} \tag{16}$$

where

q_i – constants defined by formulas (6 ÷ 8) when $i = \overline{1,4}$.

The Fokker-Planck equation (6) has a reduced representation [9]

$$\frac{\partial \tilde{F}(t,E)}{\partial t} = \frac{\mathrm{d}E_0}{\mathrm{d}t}\left[\frac{\partial}{\partial E}\left(E\frac{\partial \tilde{F}}{\partial E}\right) + \frac{1}{E_0}\frac{\partial\left(E\tilde{F}\right)}{\partial E}\right] \tag{17}$$

with the solution according to the described way of modelling a stochastic energy of the cavitation bubble (5) in the form of the representation of the equilibrium distribution function on the system condition

$$\tilde{F}\left(t, E(t,r,v)\right) = A \cdot \exp\left[-\frac{E(t,r,v)}{E_0}\right] \tag{18}$$

where

A – normalisation constant, defined with an input element of the phase space $d\Omega$ according to (2) from the relation

$$\int_{\Omega} \widetilde{F}\left(t, E\left(t, r, v\right)\right) d\Omega = 1 \tag{19}$$

5. The main results and conclusions

Thus, this operation of transition from the representation of the kinetic equation (1) to the form (9) for the equilibrium state of the system leads to the relations (14 ÷ 16) for connection between the diffusion coefficients D_1, D_2, the frequency of formation of cavitation bubbles ε_1, ε_2 and the energy of the system at the time of randomisation E_0.

Note that the General form of the obtained expressions (12) for the energy characteristics of the process of bubble formation coincides with the given parameters for the process of disintegration of the liquid jet from the work [10]. The equilibrium distribution function for the states of the system in the form (18) with normalisation of the ratio (19) and formed of stochastic energy of the cavitation bubble (5) can be used to determine the differential distribution function of bubbles on radiuses.

References

[1] Arzumanov E. S., *Cavitation in local hydraulic resistances*, Energy, Moscow, 1978.

[2] Frenkel J. I., *Kinetic theory of liquids*, Nauka, Leningrad 1959.

[3] Lienhard J H., Karimi A., *Homogeneous nucleation and the spinodal line*, Journal of Heat Transfer, vol. 103(1), 1981, 61-64.

[4] Shin T .S., Jones O. C., *Nucleation and flashing in nozzles-1. A distributed nucleation model*, Int. J. Multiphase Flow, vol. 19(6), 1993, 943-964.

[5] Hsu Y. Y., *On the size range of active nucleation cavities on a heating surface*, Journal of Heat Transfer, vol. 94, 1962, 207–212.

[6] Ellas E., Chambre P. L., *Bubble transport in flashing flow*, Int J. Multiphase Flow, vol. 26, 2000, 191-206.

[7] Kumzerova E. J., Schmidt A. A., *Numerical modeling of nucleation and bubble dynamics with the rapid loss of fluid pressure*, Journal of Engineering. Physics, vol. 2(7), 2002, 36-40.

[8] Kapranova A. B., Lebedev A. E., Melzer A. M., Nekludov S. V., Serov E. M., *On the methods of modeling the main stages of development of hydrodynamic cavitation*, Fundamental Research, vol. 3(2), 2016, 268-273.

[9] Klimontovich Y. L., *Turbulent motion and structure of Chaos: A new approach to the statistical theory of open systems*, LENAND, Moscow 2014.

[10] Zaitsev A. I., Bytev D. O., *Impact processes in the dispersion-film systems*, Chemistry, Moscow 1994.

TECHNICAL TRANSACTIONS | CZASOPISMO TECHNICZNE
MECHANICS | MECHANIKA
2-M/2016

ANN KAPRANOVA, IVAN VERLOKA, ANTON LEBEDEV, ANATOLIJ ZAITSEV*

THE MODEL OF DISPERSION OF PARTICLES DURING THEIR FLOW FROM CHIPPING THE SURFACE

MODELOWANIE ROZKŁADU WIELKOŚCI CZĄSTEK PO UDERZENIU O PŁASZCZYZNĘ

Abstract

We propose a method for forming differential of the distribution functions of the number of particles of bulk materials on the angle of reflection from bumper (baffle) plate.

Keywords: mixing, brush elements, the bumper, the granular mixture, model

Streszczenie

Zaproponowano metodę wyznaczania różniczkowych funkcji rozkładu wielkości cząstek stałych w zależności od kąta odbicia od płaszczyzny.

Słowa kluczowe: mieszanie, elementy szczotkowe, zderzak, mieszanina cząstek, model

DOI:

* Prof. DSc. Ann B. Kapranova, MSc. Ivan I. Verloka, Associate Professor DSc. Anton E. Lebedev, PhD. DSc. Anatolij I. Zaitsev, Mechanical Engineering Department, Yaroslavl State Technical University.

1. Introduction

The problem of obtaining a homogeneous particle mixture containing unequal volume fractions of particulate components, for example, in routine ratio 1:10 or more, remains relevant and can be successfully achieved using a gravity type mixer [1]. In the designed device of special purpose for the formation sparse streams offered to apply mixing drums with brush elements above the tray, which serves the working materials. In order to improve the quality of the granular mixture obtained in the gravity apparatus, bumper plates (baffle plates) may be used, which are established after drums with brush elements. Shock interaction between the baffle plate and the arrive flows of loose components that are gripped by end of brush elements, resulting in the formation of reflected flow of mixture, which is sliding on the tray located under the drum.

The development of engineering methods of calculating gravity mixer involves choosing the most efficient ranges for changing its design and operational parameters. In connection with this, a special interest is had in the evaluation of the angles of reflection streams of loose components, which are formed after the shock interaction with the flat baffle plate. It is believed that these reflection angles are angles in which the average speed of particle of i-th component (i = 1, ..., n_k) is directed perpendicular to the plane of impingement. Such modelling of the dispersion of particles in the process of reflection stream of i-th material from the baffle plate can be made on the basis of a stochastic approach [2, 3].

2. Geometric features of ways of moving sparse flows of loose components in the working volume of a gravity mixer

The tray, which is under the mixing drum (with brush elements) and on which there are vertically fed n_k particle ingredients in a volume ratio that given by the technological regulations, is at an angle μ_0 to the vertical direction. In the gap, which is had by the height h_0, between this tray and rotating drum, there is a deformation of brush elements and gripping by them portions of layers working loose materials. The number of deformed brush elements – n_b. Baffle plate is located behind the drum at an angle ψ to it tray. Arrive on the baffle plate, flow of bulk component i formed after gripping of particles by brush elements (j = 1, ..., n_b), mounted on a cylindrical surface of the mixing drum along helical lines in opposite directions, starting from its ends. Step of helical winding –h_s; Length of brush element – l_b; the radius and the length of the mixing drum – r_b and L_b; the angular speed of rotation ω. The expressions for the relationship between constructive-regime parameters of the mixing drum and characteristic angles λ_{ij}, α_{ij}, φ_{ij}, β_{ij} and averaged by the number of deformed brush elements values λ_i, α_i, φ_i, β_i for the arriving on the baffle plate flow of i-th component after gripping by brush element j according to [4] are of the form

$$\lambda_{ij} = \alpha_{ij} + \varphi_{ij} - \beta_{ij}, \quad \lambda_i = \frac{\alpha_i}{n_b} + \varphi_i - \beta_i, \quad \alpha_i \equiv \sum_{j=1}^{n_b} \alpha_{ij} \tag{1}$$

$$\beta_{ij} = \operatorname{arctg}\left[\frac{2\cdot h_s\cdot\left(l_b - h_0\right)}{L_b\left\{r_b + h_0 + \left(l_b - h_0\right)\cdot\left[1 - \frac{2\cdot h_s\cdot\left(\alpha_{ij} + \varphi_{ij}\right)}{L_b}\right]\right\}}\right], \quad \beta_i \equiv n_b^{-1}\sum_{j=1}^{n_b}\beta_j \tag{2}$$

$$\varphi_{ij} = \frac{\pi}{2} + \alpha_{ij} - \frac{\arcsin\left(\left\{\left(r_b\cdot\sin\sigma_{ij}\right)^2 + \left(r_b + h_0\right)^2\right\}\cdot\dfrac{\cos\sigma_{ij}}{r_b + h_0}\right)}{1 + \dfrac{d_0\cdot\left\{2\cdot h_s\cdot\left(l_b - h_0\right)/L_b\right\}^2}{d_1^{1/2}}}, \quad \varphi_i \equiv n_b^{-1}\sum_{j=1}^{n_b}\varphi_{ij} \tag{3}$$

where

λ_{ij}, α_{ij} – angle spreading by brush element j for material *i*, respectively, from the vertical and the horizontal directions;

φ_{ij} – central angle relative to the drum rotation axis, describing the bending of brush element that have number *j* depending on the position on it occupied portions of component *i*;

β_{ij} – characteristic angle between the direction of the material flow rate *i* and vector tangent to the helical path of end of brush element *j* in section plane of the drum*;*

σ_{ij}, d_0, d_1 – constants depending on the values of these parameters of the mixing element.

By introducing the concept of the coefficient of restitution ($k_{Vi} = \sin\gamma_{1i} / (\sin\gamma_{2i})$) for the average velocities of the move of arriving on the baffle plate, loose flow of *i*-th component and reflected from it respectively at angles γ_{1i} and γ_{2i}, can similarly [5] to obtain the functional dependence $k_{Vi} = f_i$ (μ, ψ, L_i, h_i), where μ – characteristic angle between the perpendiculars to the baffle plate and to the tray under the mixing drum; ψ – angle between the tray and the baffle plate; L_i – spreading width of the *i*-th material along a tray; h_i – height between tray and baffle plate to shock point for average speed of arriving flow of component *i*. Then, the average value of spreading angle α by the number of deformed brush elements from (1) with considering (2) and (3) and the expression $\psi = \psi_1 + \mu_0 - \pi/2$ takes the form of functional dependence

$$\alpha_i\left(\gamma_{2i}\right) = n_b\cdot\left\{\pi - \left[\frac{\psi_1 + \mu_0 + \gamma_{2i}}{f_i\left(\mu, \psi, L_i, h_i\right)}\right] - \varphi_i + \beta_i\right\} \tag{4}$$

where

ψ_1 – the angle between baffle plate and horizontal direction;

μ_0 – the angle of the tray under the drum to the vertical direction.

3. Determination of differential distributions of particles of flow reflected from baffle plate depending on the angle of reflection

Stochastic modelling of process dispersion of particles of mixed components after reflection from the rectilinear baffle plate inclined at a predetermined angle to the vertical can be accomplished using complete differential distribution function of particles of each material on the angle of spreading after interaction with brush elements [6]

$$S_i^{(np)}\left(\alpha_{ij}\right)=\prod_{j=1}^{n_b} S_{ij}^{(np)}\left(\alpha_{ij}\right) \tag{5}$$

$$\begin{aligned} S_{ij}^{(np)}\left(\alpha_{ij}\right)=\varsigma_{ij}\cdot\left\{\left[\operatorname{erf}\left(\frac{\eta_{ij}\left(\tilde{\alpha}_{ij}\right)\cdot\left[1+\varepsilon_0\cdot\varepsilon_{3i}\cdot\left(\alpha_{ij}+\varphi_{ij}\right)\right]^2}{\varepsilon_{3i}}\right)-\operatorname{erf}\left(\frac{\eta_{ij}\left(\tilde{\alpha}_{ij}\right)}{\varepsilon_{3i}}\right)\right]\times\right. \\ \left.\times\left[\eta_{ij}\left(\tilde{\alpha}_{ij}\right)\right]^{-1}\cdot\exp\left\{-\frac{\left[\eta_{ij}\left(\tilde{\alpha}_{ij}\right)\right]^2\cdot\varepsilon_4\cdot\varepsilon_0{}^2\cdot\left(\alpha_{ij}+\varphi_{ij}\right)^2}{\varepsilon_{1i}\cdot\varepsilon_{2i}}\right\}\right\} \end{aligned} \tag{6}$$

These functions are non-equilibrium and correspond to the kinetic equations for the energetically open macrosystem with macroscale fluctuations of states [1] caused by the influx of outside material (energy) and leading to the ordering of macrosystem in unstable conditions. For example, such as fluctuations in [6] are collisions between particles arriving streams of loose components, which are formed after the gripping by symmetrically arranged brush elements in the form of helical winding with different ends of the mixing drum. Wherein this modelling of stochastic energy $E_{ij}^{(np)}$ for a particle i of bulk material when gripped by brush element j, which is part of the expression to determine the number of particles of component i

$$\mathrm{d}N_{ij}^{(np)}=A_{ij}^{(np)}\cdot\exp\left[-\frac{E_{ij}^{(np)}}{E_{0ij}^{(np)}}+\frac{\left(E_{ij}^{(np)}\right)^2}{2\cdot E_{fij}{}^2}\right]\mathrm{d}\Omega_{ij} \tag{7}$$

in the element of phase volume $\mathrm{d}\Omega_{ij} = -\omega^2 r_{ij}\mathrm{d}r_{ij}\mathrm{d}\Theta_{ij}$ for polar coordinate system in the cross-section of the drum with centre on its axis of rotation allows for translational movement of bulk materials particles, the random nature of their angular momentum when gripping by deformed brush element j and the interaction with the brush element having angular stiffness. Parameters $E_{0ij}^{(np)}$ and $E_{fij}^{(np)}$ included in the expression (7) have the meaning, respectively, of a macrosystem energy at the moment of its randomisation and the energy loss of the macrosystem at macroscale fluctuations of its condition; $A_{ij}^{(np)}$ – normalization parameter.

Geometric relationship (1) in (4) between the angles of spreading flows of particles arriving on the baffle plate and the angle of inclination according to expressions (5) and (6) allows to create full differential distribution function of particles of loose components $\chi_{ij}^{(np)}(\gamma_{2i})$ on the angle of reflection from the baffle surface taking into account the coefficient of restitution $k_V = k_V(\gamma_{2i})$

$$\chi_i^{(np)}(\gamma_{2i}) = \prod_{j=1}^{n_b} \xi_{ij}^{(np)}(\gamma_{2i}) \tag{8}$$

$$\xi_{ij}^{(np)}(\gamma_{2i}) = \varsigma_{ij} \cdot \left\{ \left[\operatorname{erf}\left(\frac{\eta_{ij}(\tilde{\alpha}_{ij}) \cdot \left\{ 1 + \varepsilon_0 \cdot \varepsilon_{3i} \cdot \left[\alpha(\gamma_{2i}) + \varphi_{ij} \right] \right\}^2}{\varepsilon_{3i}} \right) - \operatorname{erf}\left(\frac{\eta_{ij}(\tilde{\alpha}_{ij})}{\varepsilon_{3i}} \right) \right] \times \right.$$
$$\left. \times \left[\eta_{ij}(\tilde{\alpha}_{ij}) \right]^{-1} \cdot \exp\left\{ - \frac{\left[\eta_{ij}(\tilde{\alpha}_{ij}) \right]^2 \cdot \varepsilon_4 \cdot \varepsilon_0^{\,2} \cdot \left[\alpha(\gamma_{2i}) + \varphi_{ij} \right]^2}{\varepsilon_{1i} \cdot \varepsilon_{2i}} \right\} \right\} \tag{9}$$

where the functional dependence of $\alpha_i(\gamma_{2i})$ has the following form

$$\alpha_i(\gamma_{2i}) = n_b \cdot \left(\beta - \varphi_i + \frac{B_1 \cdot B_3 - B_2 + \left[(B_1 \cdot B_3 + B_2)^2 - 4 \cdot B_3 \cdot \gamma_{2i} \right]^{1/2}}{2 \cdot B_3} \right) \tag{10}$$

$$B_1 = \frac{\pi}{2} - \psi + \mu_0, \quad B_2 = P_{1i} \cdot \left[(\pi - \psi) \cdot \cos\mu - P_{2i} \right], \quad B_3 = (\pi - \psi) \cdot P_{1i} \cdot \sin\mu \tag{11}$$

$$P_{1i} = \frac{1 - (\pi - \psi) \cdot \left(\frac{L_i}{h_i} - \operatorname{ctg}\psi \right)}{2 \cdot \left(\frac{L_i}{h_i} - \operatorname{ctg}\psi \right) \cdot \left(1 + \frac{L_i}{h_i} - \operatorname{ctg}\psi \right)}, \quad P_{2i} = \left(\pi - \psi + \frac{L_i}{h_i} - \operatorname{ctg}\psi \right) \cdot \operatorname{ctg}\psi \tag{12}$$

4. The main results of modelling and conclusions

We illustrate the results obtained for functions $\chi ij^{(np)}(\gamma_{2i})$ and $\xi_{ij}^{(np)}(\gamma_{2i})$ from expressions (8) and (9) on the example of the reflection natural sand GOST 8736-93 (i = 1) from the baffle plate. The dependence presented by the graphs in Fig. 1 allow us to estimate the maximum value of the reflection angle γ_{21} of the flow of loose ingredient (i = 1), after interaction with brush elements j = 1, 2, 3. In particular, the sparse stream of particles arriving on the baffle plate, formed after gripping of natural sand by brush elements, which first was captured by the layers of material from the clearance with the tray (Fig. 1, curve *3*, j = 3, with n_b = 3), is discarded from the baffle plate on angle greater by 2.6 times than a similar flow formed after interaction with brush elements (Fig. 1, curve *1*, j = 1), which came out of the gap tray-drum last. The maximum value of the angle of reflection that characterises the dispersion of the full arriving flow of natural sand flow after hitting the baffle plate (Fig. 1, curve 4), close to the value of the angle for the flow relating to gripping by brush elements with a number j = 2 (Fig. 1, curve 2).

Thus, hereinafter depending $\chi_{ij}^{(np)}(\gamma_{2i})$ and $\xi_{ij}^{(np)}(\gamma_{2i})$ from the expressions (8) and (9) may be used for calculating the weight fraction of the mixed components of the resulting mixture, and for assessing it quality for selected criteria.

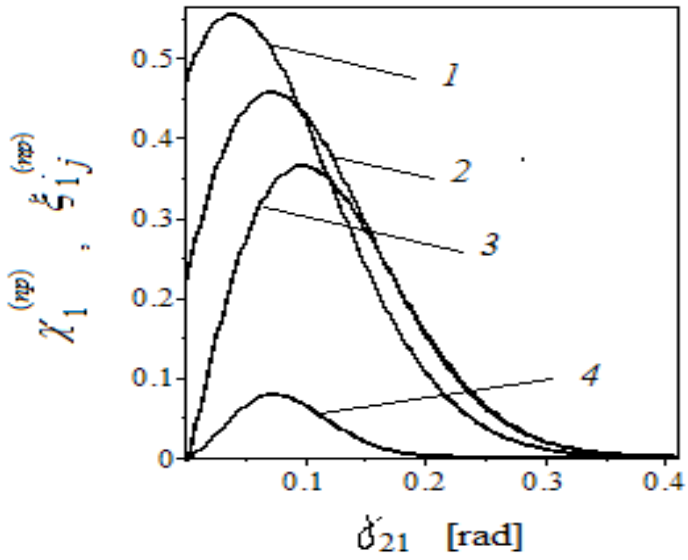

Fig. 1. Dependencies $\chi_1^{(np)}(\gamma_{21})$ and $\xi_{1j}^{(np)}(\gamma_{21})$ for differential non-equilibrium distribution functions of the number of particles of natural sand GOST R 8736-93 ($i = 1$) in the angle of reflection γ_{21} from the baffle plate: $L_b = 1{,}85\ 10^{-2}$ m; $l_b = 4{,}5 \cdot 10^{-2}$ m; $r_b = 3{,}0 \cdot 10^{-2}$ m; $h_s = 1{,}6 \cdot 10^{-2}$ m; $h_0 = 3{,}0 \cdot 10^{-2}$ m; $\omega = 52{,}36\ s^{-1}$; $n_b = 3$; $\mu_0 = 1{,}3089$ rad; $\Psi_1 = 0{,}9599$ rad; $\mu = 0{,}7071$ rad; $L_1 = 2{,}8 \cdot 10^{-1}$ m; $h_1 = 8{,}0 \cdot 10^{-2}$ m; 1-3 – $\xi_{1j}^{(np)}(\gamma_{21})$; 1 – $j = 1$; 2 – $j = 2$; 3 – $j = 3$; 4 – $\chi_{1(}^{np)}(\gamma_{21})$

References

[1] Kapranova A. B., Bakin M. N., Verloka I. I., Zaitsev A. I., *Ways to describe the motion of the solid dispersed mediums in different planes for the cross sections of the mixing drum*, Transactions of the TSTU, vol. 21(2), 2015, 296-304.

[2] Klimontovich Y. L., *Turbulent motion and structure of Chaos: A new approach to the statistical theory of open systems*, LENAND, Moscow 2014.

[3] Zaitsev A. I., Bytev D. O., Impact processes in the dispersion-film systems, Chemistry, Moscow, 1994.

[4] Bakin M. N., Kapranova A. B., Verloka I. I., *Investigation of the distribution of bulk components in the working volume of the drum-ribbon mixer*, Fundamental Research, vol. 5(5), 2014, 928-933.

[5] Kapranova A. B., Bakin M. N., Lebedev A. E., Zaitsev A. I., *Parameter estimation of recovery shock interacting streams of particulate media with a sloping baffle plate*, Chemistry and Chemical Technology, vol. 56 (8), 2013, 111-113.

[6] Kapranova A. B., Verloka I. I., Zaitsev A. I., *Comparative analysis of equilibrium and nonequilibrium distribution functions of granular media mix*, XXVIII – International Scientific Conference on Mathematical Methods in Technics and Technologies - MMTT- 28, Yaroslavl, Russia, 2 – 4 june 2015, 223-227.

TECHNICAL TRANSACTIONS | CZASOPISMO TECHNICZNE
MECHANICS | MECHANIKA
2-M/2016

TADEUSZ KOMOROWICZ*, KONRAD NERING, STANISŁAW WALCZAK**

ANALYSIS OF THE FLOW OF CRYSTALLISING WATER SLURRIES IN PIPELINES

ANALIZA PRZEPŁYWU SZLAMÓW WODNYCH KRYSTALIZUJĄCYCH W RUROCIĄGACH

Abstract

The paper presents a method for monitoring the flow conditions in pipelines in the case of transport of crystallising water slurries forming scale. The method's core is the ability to calculate the equivalent pipeline diameter under varying flow conditions in industrial practice. The method was successfully tested in the laboratory and employed in an industrial plant.

Keywords: hydrotransport, formation of scale in pipelines, flow monitoring

Streszczenie

W artykule przedstawiono metodę monitorowania warunków przepływu w rurociągach w przypadku transportu krystalizujących szlamów wodnych tworzących osady. Sedno metody to przedstawienie sposobu obliczania średnicy zastępczej rurociągu w warunkach zmiennego przepływu w praktyce przemysłowej. Metoda została z powodzeniem przetestowana w laboratorium i wdrożona w jednym z zakładów przemysłowych.

Słowa kluczowe: hydrotransport, tworzenie się osadów w rurociągach, monitoring przepływu

DOI:

* DSc. Eng. Tadeusz Komorowicz, Chair of Chemical and Process Engineering, Faculty of Chemical Engineering and Technology, Cracow University of Technology.
** DSc. Eng. Konrad Nering, DSc. Eng. Stanisław Walczak, Institute of Thermal and Process Engineering, Faculty of Mechanical Engineering, Cracow University of Technology

1. Introduction

Many branches of industry employ long distance pipeline hydraulic transport of waste powder solids. Because of a complex chemical composition of the transported solids, a partial solubility in water of individual components of the mixture, possible chemical reactions between them in the water environment and varying transport conditions caused by the weather, scale on the internal pipeline surface grows as a result of the crystallisation effect (Fig. 1). The problem of solid's deposition in pipelines is also discussed in the literature [1, 2, 3].

Fig. 1. A view of a pipeline cross-section – the formed scale decreases the free cross sectional area

As a result of the scale formation, the pipeline throughput decreases. In order to keep the flow rate of slurry at a constant level, it is necessary to gradually raise the inlet pressure generated by the pumps by increasing their rotational speed. In order to do this, a problem of gradual increase of the current intensity and a simultaneously higher consumption of power by pumps appears. It results in higher operational costs. Because of this, a lot of effort is put in industry to prevent the crystallisation and formation of scale in pipelines by adding carefully selected chemical agents.

In order to prove the effectiveness of the applied chemical additives, it is necessary to develop a continuous method for monitoring the flow conditions. But in industrial practice, the streams of transported slurries often vary in time intervals, which results in difficulties in making an appraisal. The authors made an effort to find a parameter to appraise the flow conditions in pipelines, i.e. an actual diameter, independent of the stream quantity. As a result of the investigations, an equivalent pipeline diameter derived on the basis of the Darcy-Weisbach equation has been introduced.

2. Analysis of flow conditions in an industrial plant

The analysis was carried out in an industrial hydrotransport plant susceptible to scale formation. The analysing operational parameters were:

- the discharge pressure values at the inlets to individual pipelines,
- the current intensity values received by pumps,
- the volume flow rate values of pumped slurry.

The analysis was based on a large range of data. They were systemised and averaged to cause their clarity.

The exemplary plots of pressure vs. time in a selected pipeline inlet, and the current intensity consumed by pumps vs. the time to keep a constant pump capacity in time in this pipeline are presented respectively in Figs. 2-4.

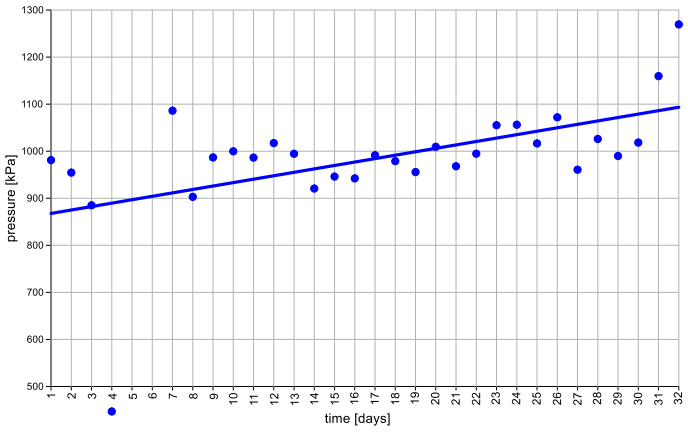

Fig. 2. Pressure vs. time for a selected pipeline

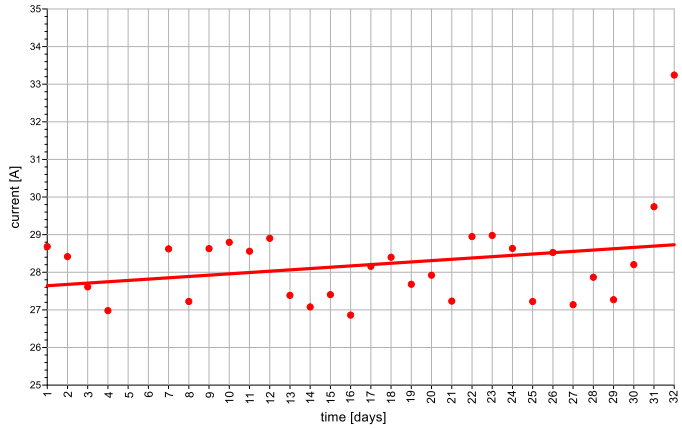

Fig. 3. Current intensity vs. time for a selected pipeline

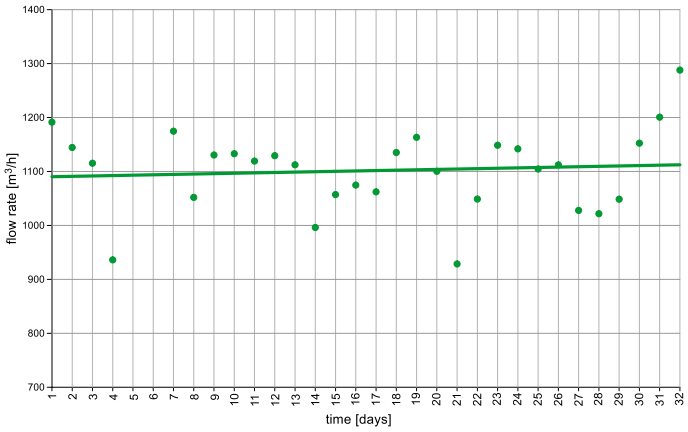

Fig. 4. Pump capacity vs. time for a selected pipeline

3. Rheological studies of examined slurry

Monitoring the hydrotransport pipeline, especially under conditions of various flow rates, demands the determination of the parameter unambiguously describing the pipeline's state, regardless of the flow conditions, such as the flow rate and the pressure drop. This parameter could be the dimensionless equivalent pipeline diameter.

To determine the dimensionless equivalent pipeline diameter using the Darcy-Weisbach equation, it is necessary to identify the rheological parameters of the flowing slurry, including the curves describing the flow resistance [4].

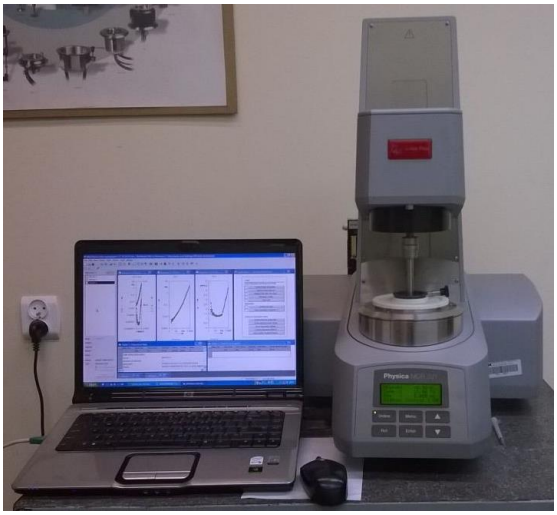

Technical Data	Unit	MCR 302
Bearing		Air
EC motor		Yes
Maximum torque	mNm	200
Min. torque, rotation	nNm	1
Min. torque, oscillation	nNm	0.5
Angular deflection (set value)	µrad	0.05 to ∞
Min. angular velocity	rad/s	10^{-9}
Max. angular velocity	rad/s	314
Max. speed	1/min	3000
Min. angular frequency	rad/s	10^{-7}
Max. angular frequency	rad/s	628
Normal force range	N	0.005-50
Normal force resolution	mN	0.5

Fig. 5. MCR301 rheometer with basic technical data

In order to identify the rheological parameters of the flowing slurry, the rheological studies were carried out with the application of a rotational rheometer (MCR 301 type) available at the Department of Fluid Mechanics. The rheometer and its basic technical data are presented in Fig. 5.

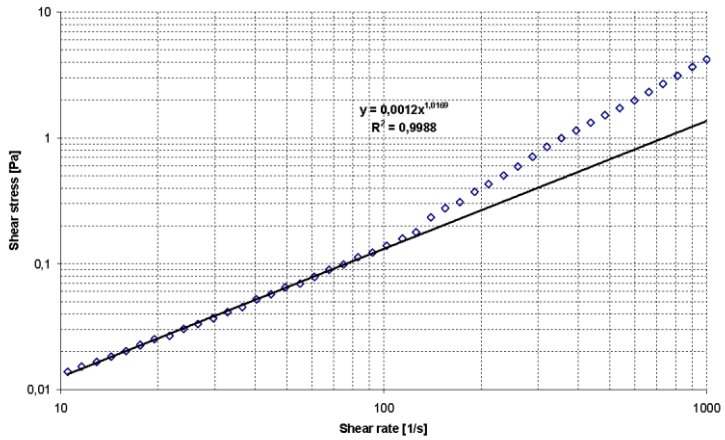

Fig. 6. Flow curve of slurry flowing through the examined pipeline

The prepared slurry was subjected to a preliminary rheological examination in order to determine the characteristics of its rheological parameters. The resulting flow curve with regression is shown in Fig. 6. This curve describes a relationship between the tangential stress and the shear rate. The values of the flow behaviour index *n* and the flow consistency index *K* according to Ostwald - de Waele rheological model were determined by linear regression of the experimental data and presented in the logarithmic scale.

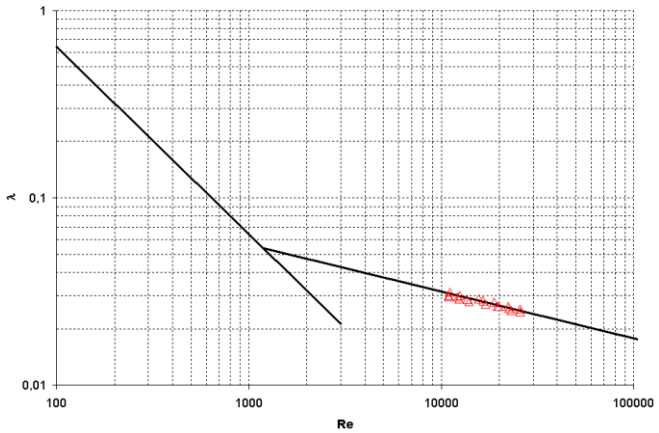

Fig. 7. Comparison of friction factor λ (measured – red, Blasius formula – black) in turbulent flow using a capillary-pipe rheometer

The obtained results of the flow behaviour index *n* for the tested slurry are close to 1, so the tested slurry can be treated as a Newtonian liquid and the flow resistance can be presented in classic Reynolds number (*Re*)-lambda (λ) layout.

The aim of further research was to determine the curve of flow resistance of the slurry flowing through the examined pipeline. The studies were carried out in a tube of an inner diameter D = 13.04 mm. The measurements were made with the application of a capillary-pipe rheometer built at the Division of Fluid Mechanics [5]. This setup allows to conduct a comprehensive identification of the rheological properties of complex rheological fluids in the laboratory. The test results are shown in Fig. 5.

4. Derivation of formula for calculating the equivalent pipeline diameter

The formula for calculating the dimensionless equivalent pipeline diameter can be derived on the basis of the Reynolds number formula and the Darcy-Weisbach equation:

$$Re = \frac{D \cdot u}{\nu} \tag{1}$$

$$\lambda = \frac{D \cdot \Delta p}{2 \cdot \rho \cdot u^2 \cdot L} \tag{2}$$

where

D – the nominal pipeline diameter,
u – the mean flow velocity,
ρ – the density of slurry,
ν – the kinematic viscosity coefficient of the slurry,
Δp – the pressure drop in the pipeline,
L – the pipeline length.

Basing on the resistance curve, it can be found that the Darcy friction factor λ in the turbulent flow can be approximated with the Blasius formula:

$$\lambda = \frac{0.3164}{\sqrt[4]{\frac{D \cdot u}{\nu}}} = \frac{0.3164}{\sqrt[4]{\frac{4 \cdot Q}{\pi \cdot D \cdot \nu}}} \tag{3}$$

where

Q – the volume flow rate.

When replacing the mean velocity with the volume flow rate, the Darcy-Weisbach equation can be written as follows:

$$\Delta p = \lambda \cdot \frac{8 \cdot L}{D^5} \cdot \frac{\rho \cdot Q^2}{\pi^2} \tag{4}$$

Then, the friction factor λ can be described by the relation:

$$\lambda = \frac{\pi^2 \cdot \Delta p}{8 \cdot L \cdot \rho} \cdot \frac{\cdot d^5}{Q^2} \tag{5}$$

where

d – the actual pipeline diameter related to the free cross-sectional area.

When equalising (3) and (5) and taking into account the actual diameter, a following relation can be obtained:

$$d = \left(3.398 \cdot 10^{-3} \cdot L^4 \cdot \rho^4 \cdot \nu \cdot \frac{Q^7}{\Delta p^4} \right)^{\frac{1}{19}} \tag{6}$$

For a fluid flowing through a pipeline, it can be assumed that the values in equation (6) are constant, except for the volume flow rate Q and the pressure drop Δp. Hence, the dependence (6) can be represented as:

$$d = B \cdot \left(\frac{Q^7}{\Delta p^4} \right)^{\frac{1}{19}} \tag{7}$$

where

B – the constant describing the liquid and the pipeline parameters.

The dimensionless equivalent pipeline diameter d_e has been defined as a ratio of the actual pipeline diameter d to the nominal pipeline diameter D (it is a relative quantity):

$$d_e = \frac{d}{D} \tag{8}$$

5. Results and discussion

The developed method for determining the dimensionless equivalent pipeline diameter has been applied for monitoring the bore of a selected industrial pipeline. An additional object of monitoring was a verification of the effectiveness of the action of chemical additive preventing crystallisation and scale deposition in the pipeline. The composition of the chemical additive is confidential. Earlier, during the hydrotransport, the examined pipeline grew over with scale and it was necessary to clean it periodically.

The tests proved the correctness of the developed method of pipeline monitoring: it indicated a gradual decrease of the dimensionless equivalent pipeline diameter (Fig. 6 left – a declined line with time) in normal operation. The application of the mentioned chemical additive caused a set-back of the crystallisation and scale deposition in the pipeline (Fig. 6 right – the horizontal line, a constant value of the dimensionless equivalent pipeline diameter).

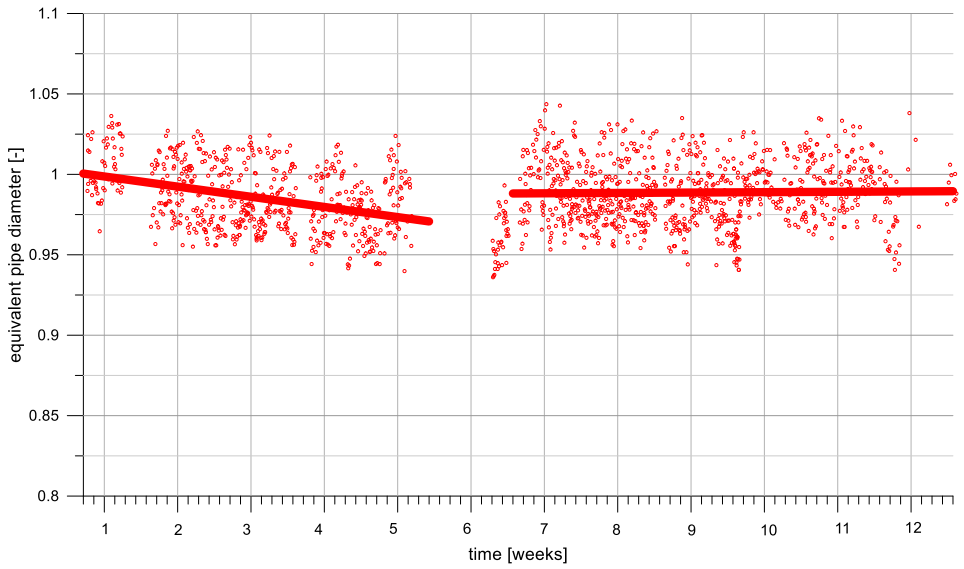

Fig. 6. The results of tests of the hydrotransport pipeline dimensionless equivalent diameter (a linear approximation)

The presented method can be applied in industrial practice for monitoring the bores ofpipelines in case of varying flow rates.

References

[1] Kaushai D. R., *Solids concentration profiles and pressure drop in pipeline flow of multisized particulate slurries*, International Journal of Multiphase Flow, vol. 28(10), 2002, 1697-1717.

[2] Kaushai D. R., *Concentration at the pipe bottom at deposition velocity for transportation of commercial slurries through pipeline*, Powder Technology, vol. 125(1), 2002, 89-101.

[3] Bednarski S., Komorowicz T., Pabiś A., *Sposób hydraulicznego transportu na duże odległości materiałów poliziarnistych i urządzenie do wyprowadzania frakcji grubej z rurociągu hydrotransportu*, Patent RP Nr 205676 z dn. 31.05.2010 (WUP 05/10)

[4] Matras Z., *Metoda identyfikacji reologicznej cieczy*, Inżynieria i Aparatura Chemiczna, Nr 4-5, 2007, 83-86.

[5] Matras Z., Walczak S., *Reometr kapilarno-rurowy*, Czasopismo Techniczne, Z. 5-M, 2003, 359-370.

TECHNICAL TRANSACTIONS | CZASOPISMO TECHNICZNE
MECHANICS | MECHANIKA
2-M/2016

JANUSZ KRAWCZYK*, ANDRZEJ HERYAN, ŁUKASZ WAWSZCZAK**

ENVIRONMENTAL INTERACTION ASSESSMENT OF VOC'S EMISSION FROM PRINTING PLANT HOT ROTARY HEAT-SET

OCENA ODDZIAŁYWANIA NA ŚRODOWISKO EMISJI LZO W PROCESIE DRUKU GORĄCY OFFSET ROTACYJNY (HEAT-SET)

Abstract

The paper presents an analysis of gaseous emissions arising from the operations of printing using a printing process hot offset rotary. The first part presents the general characteristics of the process and the paint used. The following part shows the results of modelling the emission of pollutants according to the efficiency of the cleaning system, as well as depending on other parameters influencing the dispersion process impurities.

Keywords: modelling of emissions, printing industry, rotary offset (heat-set)

Streszczenie

W pracy przedstawiono analizę emisji zanieczyszczeń (LZO) powstających w wyniku działalności zakładu poligraficznego wykorzystującego w procesie druku gorący offset rotacyjny. Część pierwsza prezentuje ogólną charakterystykę procesu oraz wykorzystywanych farb. W dalszej części przedstawiono wyniki modelowanie emisji zanieczyszczeń w zależności od sprawności układu oczyszczającego, a także w zależności od innych parametrów wpływających na proces dyspersji zanieczyszczeń.

Słowa kluczowe: modelowanie emisji zanieczyszczeń, gorący offset rotacyjny

DOI:

* PhD. DSc. Eng. Janusz Krawczyk, prof. CUT, Institute of Thermal and Process Engineering, Faculty of Mechanical Engineering, Cracow University of Technology.

** DSc. Andrzej Heryan, MSc. Łukasz Wawszczak, Department of Scientific Research "Eko-Hera", Cracow.

1. Introduction

From the time of Johannes Gutenberg, who is considered to be one of the precursors of industrial printing method, printing processes have undergone many changes and modifications. Constant competition forces the use of ever newer solutions to optimise printing costs, while maintaining appropriate quality parameters. In the case of multi-format printing, a frequently used technique is the process of printing by hot rotary heat-set, which enables to print significant amounts of paper in a relatively short time. Multi-format printing implies the use of the equipment of printing machines that are significant sources of emissions of dust and gas pollutants, mainly organic compounds.

The paper presents an analysis of the emission of dust and gas emitted by modern offset printing, in which a large part of printing is done on automatic thermoforming machines.

2. Analysis of the sample printing offset in the context of emissions of dust and gas into the atmosphere

2.1. The object of the study

The object of the analysed company is printing activity.

The printing plant prints colour magazines, newspapers, advertising catalogues and leaflets, etc. A flat indirect (offset) printing technique with the fixation of paint at elevated temperature (*heat-set*) applies in the production process.

The printing plant is located in one of the outlying districts of the city in an area planned for the activities of production and services. The immediate surroundings of the plant are the lands used for the purposes of business production and service.

2.2. Printing technology

Web offset printing is a relatively cheap and quick way to obtain a large number of prints. Lightweight aluminium matrix formed on the drum printing sends an image on an intermediate drum with a rubber coating, which in turn transfers the image to paper. Hence, there is the second important definition of this technique – *indirect* print. This printing unit is capable of rotation at high speed.

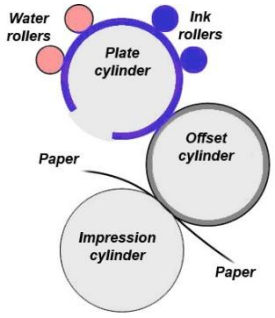

Fig. 1. Offset printing

Common use of colour web offset printing in addition to speed arises from the variety of possible use of media, i.e.: from coated paper (*non-absorbent* surface), the newsprint to cardboard (substrate *absorbent*).

2.3. Raw materials used in the printing process

Due to the volume of raw materials, which are used and the characteristics of the fusing mechanisms of printing inks in the process of web offset printing, determination of the characteristics of used inks is essential in order to assess the impact of the installation on the atmospheric air. Fusing mechanisms of inks of the type of *heat-set* occur due to the influence of the delivery of significant amounts of heat (blow heat, drying tunnels, which are heated by gas burning, etc.). Depending on the drying system, the paper has a temperature ranging from 90 to 150°C, which corresponds to a temperature of 200÷300°C of the drying agent. At these high temperatures, it evaporates mineral oil, which is a solvent for paints of *heat-set* type and water (moisture) from paper and wetting agents.

For the production of *heat-set* paints, adhesives containing the composition of phenol-formaldehyde resins and alkyd resins, polymerised linseed oil, mineral oil (fraction with a boiling point of 240÷300°C), colorants, tinters and excipients are used. Mineral oils used for the production of paints of the type *heat-set* are special species usually of naphthenic mineral oils. They are refined in such a way that they are almost odourless and colourless. Depending on the distillation, the boiling point is in the range of 240÷270°C, 260÷290 and 270÷300°C. In the *halftone* paints, mineral oils vary in their boiling points because paints of different colours are to be traversed in the printing path of different distances. Therefore, a black colour which has the longest distance to go, has in its composition an oil having the lowest volatility. The yellow ink goes in turn the shortest possible route and, therefore, contains mineral oil with high volatility [1].

2.4. Characteristics of emerging emissions

For the production of *heat-set* paints, mineral oils containing aromatic compounds are used. In addition, wetting agents containing alcohol, iso-propyl or organic alternatives are used in the printing process. Depending on the drying system, it evaporates mineral oil, in varying amounts, which is a solvent of *heat-set* paint and water (moisture) from paper and wetting agents. The main pollution are therefore volatile organic compounds (VOCs) emitted in the installation in the amount of approx. 30 kg/h of VOC.

Furthermore, due to the demand on the substantial amount of thermal energy for the drying process of the paper, the fuel is typically used for natural gas, in which the products of combustion (mainly nitrogen oxides, carbon monoxide, carbon dioxide) also flow to the atmosphere.

2.5. Legal requirements relating to the issue of emerging contaminants

Legal requirements for environmental protection regulate the Framework Law of 27 April 2001. Environmental Protection Law (Polish Journal of Laws of 2013 item. 1232, as amended.) and implementing acts to the above Law. According to the Regulation of the Minister of Environment of 26 January 2010 on reference values for certain substances in the air (Polish Journal of Laws of 2010 no. 16 item. 87) [2] plant, which leads pollution in

an organised manner to the atmosphere is obliged to use solutions that will not exceed the permissible reference value, ice. appropriate normative values concerning excess emissions will be saved.

Moreover, in the case of large printing plants, which consume large quantities of raw materials (this translates into considerable use of VOC), additional requirements apply for the protection of atmospheric air as defined in the Regulation of the Minister of Environment of 4 November 2014 on emission standards for certain types of installations, combustion plants and equipment incineration or co-incineration of waste [3]. The processes carried out in the system used in this printing plant include (in accordance with Annex 7 to the above regulation to hot offset rotary process, which identified the following emission standards (Annex 8 point 1):

For VOC usage> 25 Mg / year
S1 = 20 mg / m^3 VOC
(counted on organic carbon).

2.5. Methods of reducing emissions of pollutants

Systems of injecting air containing solvents are usually designed to maintain an adequate atmosphere within the workspaces and equipment significantly below the permissible concentrations of pollutants. Deriving solvents from the key sources can lead to disposal system of waste gases because of the need to comply with regulations on environmental protection. When designing injecting systems, some things must be taken into account:

- the amount of the discharged air,
- level of solvent,
- type of utilisation, its cost-effectiveness and impact on the environment,
- number of working hours per year.

When injecting a large amount of air relative to the solvent increases the size of reduction system, and may increase the amount of energy required as drive, which supports combustion. In the case of large printing plants using web offset printing generally used methods are based on oxidation of pollutants through the use of thermal afterburners. In certain cases, it is reasonable to use catalytic afterburners, which through the use of a catalyst operate at lower temperatures than thermal afterburners (this translates into energy savings).

Moreover, in the case of large printing plants, there are also solutions in which every single print line may have a dedicated system of waste gas treatment. For example, if it is integrated into the dryer(s), the system allows for easy use of heat or exhaust gases for heating the air in the dryer. Printing presses in such a case depend on the central system of waste gases.

2.6. Sources of emissions in the tested offset printing plant

When injecting pollutants into the air is related to the functioning of the basic technological processes (sources of emissions from the production equipment). Vapours produced during drying of the printed paper web are extracted on machines and routed to a

thermal afterburner, which reduces pollution. Burners with the installed thermal capacity in the range 850÷1600 kW function for particular drying tunnels of web offset printing machines for drying the printed paper.

2.7. Maps of the distribution of concentrations of selected pollutants around the premises

Simulations of the changes of individual pollutants concentrations in the atmosphere were made using modelling software a steady-state Gaussian plume model on the basis of measurements of pollutants emissions carried out by an accredited laboratory according to Polish reference methodology [2]. The resulting simulations are expressed as map of spatial concentration distribution and demonstrated in Figs. 2 a and b to show the greatest concentration of major pollutants in the vicinity of the plant.

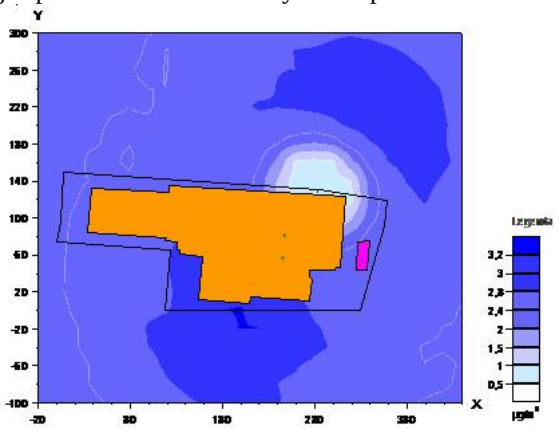

Fig. 2a. The map showing isolines of the peak concentrations of selected pollutants (aromatic hydrocarbons)

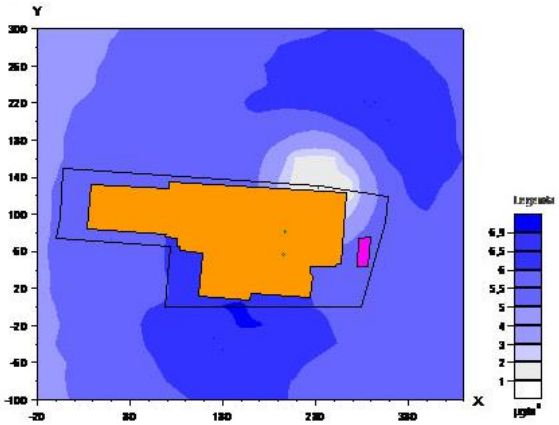

Fig. 2b. The map showing isolines of the peak concentrations of selected pollutants (aliphatic hydrocarbons)

3. Calculation of the concentrations of dust and gas pollutants emitted into the atmosphere depending on changes of selected technical parameters of the installation

According to the measurements carried out by the accredited laboratory, the afterburner efficiency in the test plant is approx. 99% of VOC. The tables 1 and 2 show how the change in volume would have affected the maximum concentration of emitted pollutants (VOC) by using afterburner with a different efficiency, as well the change of peak levels when choosing the other technical characteristics of the emitter (height, diameter) was presented.

This simulation was performed to investigate whether the use of relatively cheap and fast to carry out technical solutions (change in height or diameter of the emitter) instead of afterburners with extremely high efficiency, can significantly reduce the impact of printing plant on the atmospheric air.

Table 1

The average increase in the concentrations of pollutants compared to the actual afterburner efficiency

Pollution	**Maximum concentration of impurities (depending on the efficiency of the afterburner) [mg/m^3]**				
	95%	**96%**	**97%**	**98%**	**99%**
Benzene [1]	2.03	1.84	1.64	1.44	1.24
Xylene [2]	2.08	1.74	1.39	1.04	0.69
Styrene[3]	1.09	0.90	0.70	0.50	0.30
Toluene [4]	1.69	1.41	1.12	0.84	0.56
Aromatic hydrocarbons [5]	14.42	11.71	8.99	6.28	3.57
Ethylbenzene [6]	1.21	1.02	0.82	0.62	0.42
Aliphatic hydrocarbons [7]	31.34	25.43	19.53	13.63	7.72
The average increase in the concentrations of pollutants compared to the actual afterburner efficiency [%]	+ 218.28	+ 163.67	+ 109.10	+ 54.52	–

When changing the performance of an afterburner from 99% to 95%, we can observe up to 218% average increase in the concentration of pollutants in the air. Even in the case of restriction of performance of afterburner from 99% to 98% we can observe up to 50% average increase in peak concentrations in the atmosphere. A summary of calculation results is also presented graphically in the chart below:

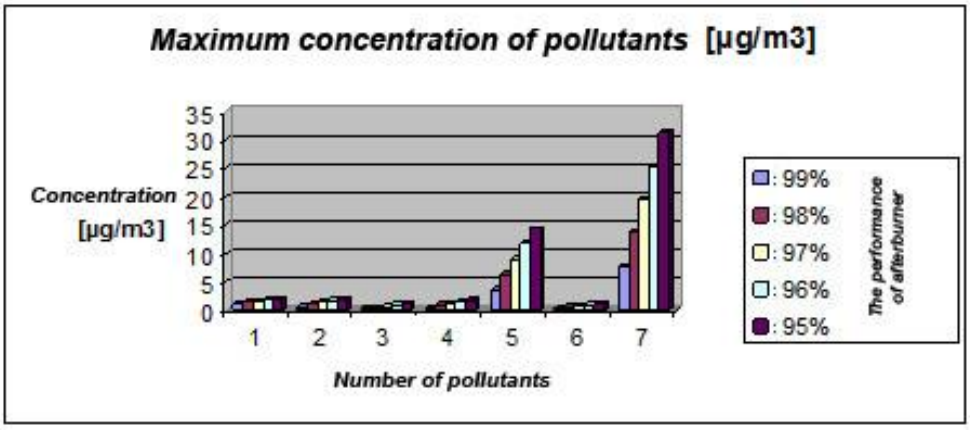

Fig. 3. A graph showing maximum concentration of selected impurities depending on the performance of afterburner

The change of the height of the emitter can affect the concentration pollutants as follows:

Table 2

The average decrease in the concentrations of pollutants depending on the height of emitter of afterburner

	Maximum concentration of impurities (depending on the amount of boost emitter) [m]				
	14	**16**	**18**	**20**	**22**
The average decrease in the concentrations of pollutants depending on the height of emitter of afterburner [%]	–	- 6.05	- 11.32	- 14.36	- 18.31

When changing the diameter of the emitter, concentrations of pollutants can achieve the values as follows:

Table 3

The average decrease in the concentrations of pollutants depending on the diameter of emitter of afterburner

	Maximum concentration of impurities (depending on the diameter of emitter) [m]				
	1,4	**1,3**	**1,2**	**1,1**	**1,0**
The average decrease in the concentrations of pollutants depending on the diameter of emitter of afterburner [%]	–	- 2.46	- 4.96	- 6.30	- 9.18

4. Conclusions

- From the presented analysis of emissions (VOC) resulting from the operations of the printing plant using hot offset, in a printing process, we can conclude that the concentrations of VOCs are within the range of permissible emission standards.
- Change of the performance of afterburner to a varying degrees results in the maximum concentration of each pollutant.
- Change of performance of afterburner from 99% to 98% causes – according to modelling, which was carried out – more than 50% increase in peak concentrations of impurities.
- Change of the diameter of the emitter by about 0.2÷0.4 meter or change of the height of the emitter by 2 to 6 meters allows for a reduction of the maximum concentrations of pollutants by approx. 5 to 15%.
- In the case of small deviations from the normative reference values of pollutants in ambient air can be considered as a method to reduce nuisance on a change of parameters of emitter (height, diameter).

References

[1] Jakucewicz S., *Farby drukowe*, Michael Huber Polska Sp. z o.o., Wrocław 2001.
[2] Regulation of the Minister of Environment of 26 January 2010 on *reference values for certain substances in the air*, Polish Journal of Laws of 2010, no. 16, item 87.
[3] Regulation of the Minister of Environment of 4 November 2014 on *emission standards for certain types of installations, combustion plants and equipment incineration or co-incineration of waste*, Polish Journal of Laws of 2014, vol. 1, item 1546.

TECHNICAL TRANSACTIONS | CZASOPISMO TECHNICZNE
MECHANICS | MECHANIKA
2-M/2016

ANDREY A. LIPIN, ALEKSANDR G. LIPIN*, RYSZARD WÓJTOWICZ**

MODELLING THE COMBINED POLYMERISATION AND DRYING OF POLYACRYLAMIDE PREPOLYMER

MODELOWANIE ŁĄCZONEGO PROCESU POLIMERYZACJI I SUSZENIA DLA PREPOLIMERU POLIAKRYLOAMIDOWEGO

Abstract

In the paper, the mathematical model of combined polymerisation and drying of polyacrylamide prepolymer is presented. It allows to predict the change of monomer conversion degree, polymer moisture content, the temperatures of gas and polymer in the dryer as well as dryer sizes. Using a developed model, values of technological parameters were established, providing faster polymerisation than in the case of drying.

Keywords: *acrylamide, polyacrylamide, polymerization, aqua solution, drying, combined process, mathematical model, belt dryer*

Streszczenie

W ramach pracy stworzono model matematyczny dla łączonego procesu polimeryzacji i suszenia prepolimeru poliakryloamidowego. Proponowany model umożliwia wyznaczenie zmiany stopnia konwersji monomeru, zawartość wilgoci polimeru, temperatury gazu i polimeru w suszarce oraz wymiary suszarki. Z użyciem modelu wyznaczono wartości parametrów technologicznych procesu, umożliwiając szybszy proces polimeryzacji w porównaniu z suszeniem w aparacie.

S*łowa kluczowe:* *akryloamid, poliakryloamid, polimeryzacja, roztwór wodny, suszenie, proces łączony, model matematyczny, suszarka taśmowa*

DOI:

* PhD. DSc. Eng. Andrey A. Lipin, DSc. Eng. Aleksandr G. Lipin, Faculty of Chemical Engineering and Cybernetics, Ivanovo State University of Chemistry and Technology.

** DSc. Eng. Ryszard Wójtowicz, Institute of Thermal and Process Engineering, Faculty of Mechanical Engineering, Cracow University of Technology.

1. Introduction

Polyacrylamide is a water soluble polymer. Owing to the unique combination of properties, it is widely used as thickener, film former, stabiliser of suspensions, sizing agent in the textile industry, coagulant and flocculant, agent reducing of hydraulic resistance, soil builder as well as protective reagent in the drilling technique [1]. This necessitates a significant increase in the production efficiency of polyacrylamide.

One way of improving polyacrylamide production technology is to combine prepolymer polymerisation to high conversion degree with drying [2]. In the laboratory scale, this process was implemented in the belt drier with radiation-convective heat supply. For industrial production of polyacrylamide with the use of this method, it is necessary to design the apparatus of industrial-scale. A suitable tool for the calculation and prediction of technological and constructional parameters of industrial-scale apparatus is the mathematical modelling method. Therefore, developing a mathematical model of the combined polymerisation and drying is an important goal.

2. Mathematical model

The combined process of polymerisation and drying of polyacrylamide prepolymer is carried out in a belt drier with radiation-convective heat supply. Infrared drying is used because it allows to provide high values of the specific heat flow. It is necessary due to a high moisture content of prepolymer (about 60%). As a source of infrared radiation, it is advisable to use gas-fired panels. Flue gases move inside these panels, heating them. Air serves to remove water vapour and it moves in the dryer by natural convection. The prepolymer is fed into the dryer as a gel. It moves by belt countercurrent to air. The diagram of dryer is shown in Fig. 1.

The mathematical model of the combined process includes a system of equations (1 - 5), complemented by equations of chemical kinetics (6 - 10) with closing relations (11 - 19).

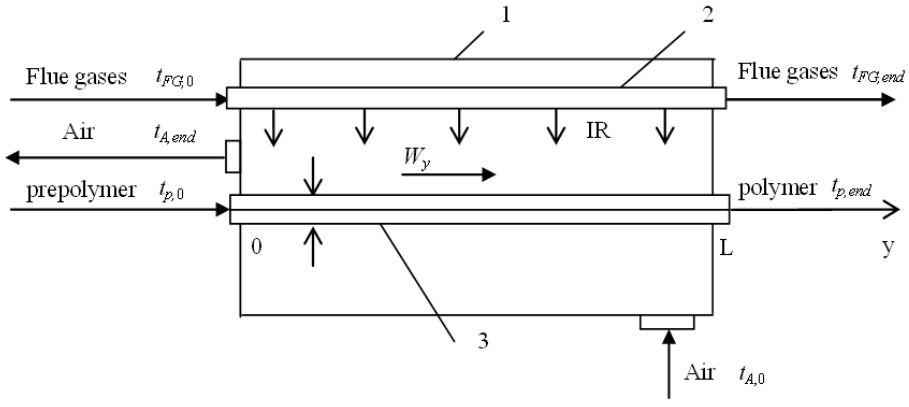

Fig.1. The diagram of dryer: 1 – the shell; 2 – heat-radiating panel; 3 – material

Changes of heat-radiating panel temperature T_{IR}, flue gases temperature T_{FG}, moisture content U and drying polymer temperature T_p upon the dryer length are calculated by solving the system of equations (1 - 5).

$$\alpha_{FG}\left(T_{FG}-T_{IR}\right)=c_{12}\left[\left(\frac{T_{IR}}{100}\right)^4-\left(\frac{T_p}{100}\right)^4\right] \tag{1}$$

$$\frac{\mathrm{d}t_{FG}}{\mathrm{d}y}=-\frac{\alpha_{FG}\cdot B\cdot\left(t_{FG}-t_{IR}\right)}{G_{FG}\cdot c_{FG}} \tag{2}$$

$$\frac{\mathrm{d}t_p}{\mathrm{d}y}=\frac{c_{12}\cdot\left[\left(\frac{T_{IR}}{100}\right)^4-\left(\frac{T_p}{100}\right)^4\right]\cdot B+r^*\frac{\mathrm{d}U}{\mathrm{d}y}\cdot G_p+\alpha_A\cdot\left(t_A-t_p\right)\cdot B+\Delta H\cdot\left(\frac{\mathrm{d}C_M}{\mathrm{d}y}\right)\cdot W_y\cdot B\cdot h}{G_p\cdot\left(c_p+c_w\cdot U\right)} \tag{3}$$

$$\frac{\mathrm{d}U}{\mathrm{d}y}=\frac{\beta\cdot B\cdot\left(p_p-p_A\right)}{G_p} \tag{4}$$

$$p_p=p_s\left(t_p\right)\cdot\psi\left(U\right) \tag{5}$$

where: $\psi(U)$ – empirical coefficient considering reduction of water vapour partial pressure by reducing the moisture content of the prepolymer.

Initial conditions for equations (2)-(4) are as follows: $t_{FG}(0) = t_{FG,0}$, $t_p(0) = t_{p,0}$, $U(0)=U_0$.

The polymerisation kinetics was described in [3]. Free radical-forming reaction, growth and chain termination reactions were considered having simulated of the acrylamide radical polymerisation kinetics, initiated by a redox system.

The system of kinetic equations for concentrations of redox system compounds (oxidant and reductant), monomer concentration, and initial moments of the molecular weight distribution of both active and inactive chains, is as follows:

$$\frac{\mathrm{d}I}{\mathrm{d}y}=-\frac{a\cdot k_i\cdot I^a\cdot J^b}{W_y} \tag{6}$$

$$\frac{\mathrm{d}J}{\mathrm{d}y}=\frac{-b\cdot k_i\cdot I^a\cdot J^b}{W_y} \tag{7}$$

$$\frac{\mathrm{d}C_M}{\mathrm{d}y}=\frac{-k_p\cdot C_M\cdot\mu_0}{W_y} \tag{8}$$

$$\frac{d\mu_0}{dy} = \frac{f_i \cdot k_i \cdot I^a \cdot J^b - k_{td} \cdot \mu_0^{\,2}}{W_y} \tag{9}$$

$$\frac{d\lambda_0}{dy} = \frac{k_{td} \cdot \mu_0^{\,2}}{W_y} \tag{10}$$

Initial conditions for the system of differential equations (6 - 10) are as follows: $\mu_0(0) = \lambda_0(0) = 0$, $C_M(0) = C_{M,0}$, $I(0) = I_0$, $J(0) = J_0$.
The average value of the polymer molecular weight was predicted by:

$$\overline{M}\ n = \frac{M_M \cdot \left(C_{M,0} - C_M\right)}{\mu_0 + \lambda_0} \tag{11}$$

Constants of elementary reactions rates were calculated by following equations:

$$k_i = 1.039 \cdot 10^8 \cdot \exp\left(-\frac{42000}{R \cdot T}\right) \tag{12}$$

$$k_p = 0.8 \cdot 10^7 \cdot \exp\left(-\frac{11700}{R \cdot T}\right) \tag{13}$$

$$k_{td}^0 = 6.8 \cdot 10^{11} \cdot \exp\left(-\frac{11700}{R \cdot T}\right) \tag{14}$$

Laws of change of growth and chain termination rate constants with conversion increasing are approximated by the following dependencies:

$$\frac{k_{td}}{k_{td}^0} = \frac{1}{1 + 122.2 \cdot X^2} \tag{15}$$

$$\frac{f_i}{f_i^0} = \frac{1}{1 + s \cdot X^m} \tag{16}$$

$$m = 4 + 0.2 \cdot t \tag{17}$$

$$s = 121767 + 0.395 \cdot t^3 - 23202 \cdot t^{0.5} + 7.418 \cdot 10^{14} \cdot e^{-t} \tag{18}$$

$$X = 1 - \frac{C_M}{C_{M,0}} \tag{19}$$

The system of equations (1 - 19) was solved numerically by means of the Mathcad software. Runge-Kutta 4th order numerical method was used. Mesh with step Δy = 0.001 m was used along the dryer length.

Proposed model has been practically validated. In the laboratory scale experiments two technological parameters were measured: the temperature and moisture content of the polymer. The relative error for temperature was 5.5%, for moisture content it was 7%. The relative error in both cases did not exceed 10%, so we can make a conclusion about the adequacy of the proposed mathematical model.

3. Results and discussion

Computation of the dryer was performed using the developed mathematical model. Initial conditions of the processes occurring in the prepolymer for the drying step are characteristic of the reaction mass obtained under isothermal conditions at temperature of 30°C. The initial moisture content is 1 kg/kg, degree of conversion is 50%. Calculations were performed for a 2 mm thickness of the prepolymer layer.

Figure 2 presents the change of prepolymer temperature t, air temperature t_A, heat-radiating panel temperature t_{IR} and flue-gases temperature t_{FG} along the dryer length. The model considers the inconstancy of flue gases temperature t_{FG} inside of heat-radiating panels. Flue gases move inside these panels heating them; therefore, the temperature of radiation surface t_{IR} changes also. The prepolymer is heated by a stream of infrared radiation. Its temperature changes from 25°C to 95°C. The air moves counter current to prepolymer and heats from 20°C till 93°C (Fig. 2).

Figure 3 shows the change of prepolymer moisture content U and the degree of monomer conversion X during time of combined polymerisation and drying processes. The initial stage of the process is characterised by rapid growth of the prepolymer temperature (see curve 1 in Fig. 2), which leads to a reduction of diffusion limitations on the initiation reaction and chain growth reaction, and hence to an increase of the polymerisation rate. Water is a required component of the reaction mass. The prepolymer moisture content decreases rapidly, but it is sufficient to complete the polymerisation. Thus, at a conversion of 99%, the polymer moisture content is about 0.2 kg/kg. Figure 3 shows that the monomer conversion increases rapidly and achieves 99.5% conversion degree on the 2/3 of dryer length. It corresponds to 4 meters. The prepolymer moisture content reaches the required value only at 6 meters. So, we can conclude that for the chosen range of parameters, the

polymerisation proceeds faster than drying. This is achieved due to drying being carried out by natural air convection. Heating the material is provided by IR radiation sources.

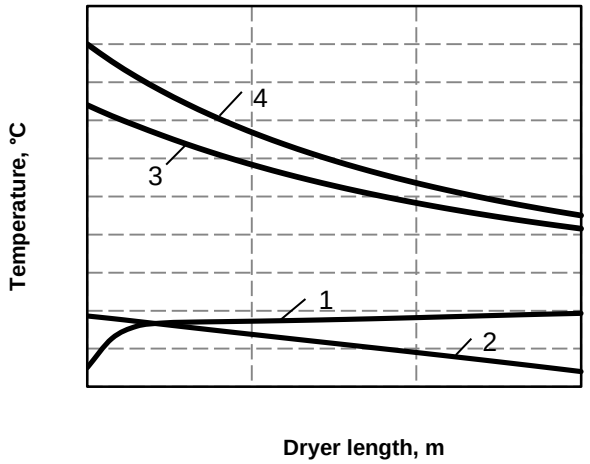

Fig. 2. The temperature upon the dryer length
1 – polymer temperature; 2 – air temperature; 3 – heat-radiating panel temperature; 4 – flue gases temperature

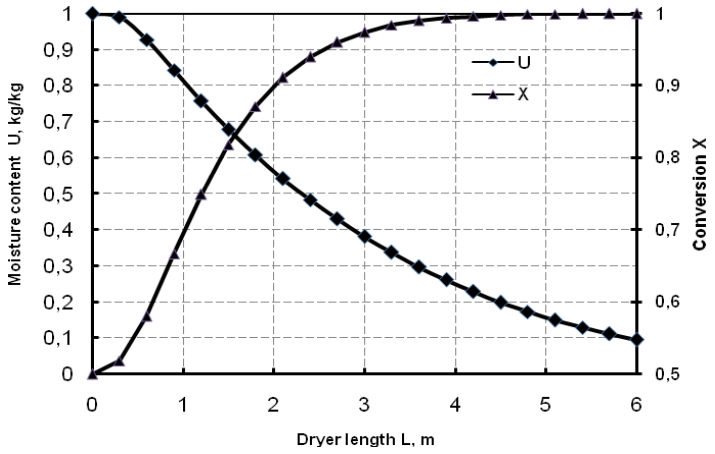

Fig. 3. The polymer moisture content *U* and monomer conversion *X* upon the dryer length *L*

Thus, the developed mathematical model describes the kinetic laws of combined polymerisation and drying as well as the influence of polymerisation kinetics on the heat and mass transfer. It allows to predict the change of monomer conversion degree, moisture content of polymer, temperatures of gas and polymer in the dryer as well as dryer sizes.

In a practical industrial scale application the combined polymerisation and drying of polyacrylamide prepolymer can be carried out in existing commercial IR dryers. But these dryers should be upgraded for new product.

Nomenclature

- a, b – stoichiometric factors, – ;
- B – belt length, m;
- c_{12} – mutual emissivity coefficient, W m^{-2} K^{-4};
- C_M – monomer concentration, [mole l^{-1};
- c – heat capacity, J kg^{-1} K^{-1};
- f_i – initiation efficiency, – ;
- G – mass flow, kg s^{-1};
- h – gel layer thickness, m;
- I – oxidant concentration, mole l^{-1};
- J – reductant concentration, mole l^{-1};
- k_p – chain growth rate constant, l $mole^{-1}$ s^{-1};
- k_{td} – chain termination rate constant, l $mole^{-1}$ s^{-1};
- k_i – initiation rate constant, l^{a+b-1} $mole^{1-a-b}$ s^{-1};
- m – empirical coefficient, – ;
- p – pressure, [Pa;
- R – universal gas constant, J $mole^{-1}$ K^{-1};
- r^* – vaporisation heat, J kg^{-1};
- s – empirical coefficient – ;
- t – temperature, °C;
- T – temperature, °K;
- U – moisture content, kg kg^{-1};
- W_y – velocity of the prepolymer, m s^{-1};
- X – degree of monomer conversion, – ;
- y – coordinate along the dryer length, m;
- α_{FG} – heat-transfer coefficient from flue gases to heat radiating panel, W m^{-2} K^{-1};
- α_A – heat-transfer coefficient from polymer to air, W m^{-2} K^{-1};
- β – mass transfer coefficient, kg m^{-2} s^{-1} Pa^{-1};
- ΔH – heat of reaction, J $mole^{-1}$;
- μ_0 – initial moment of the molecular weight distribution of active chains, mole l^{-1};
- λ_0 – initial moment of the molecular weight distribution of inactive chains, mole l^{-1};

Subscripts

- A – air
- FG – flue gases

IR – infrared radiation
w – water
0 – initial value
end – end value

References

[1] Abramova L. I., *Polyacrylamide*, Khimiya, Moscow 1992.
[2] Lipin A. A., Lipin A. G., Shibashov A. V. *Polyacrylamide synthesis using polymerisation-desorption process*, Izv. Vyssh. Uchebn. Zaved. Khim., Khim. Tekhnol. 2015. Vol. 58(1), 2015, 51-53.
[3] Lipin A. A., Shibashov A. V., Lipin A. G. *Modelling of acrylamide polymerization in the concentrated water solutions*, Izv. Vyssh. Uchebn. Zaved. Khim., Khim. Tekhnol., vol. 57(12), 2014, 85-87.

TECHNICAL TRANSACTIONS | CZASOPISMO TECHNICZNE
MECHANICS | MECHANIKA
2-M/2016

ZBIGNIEW MATRAS, BARTOSZ KOPICZAK*

THE POLYMER-MICELLAR AGGREGATES AS AN EFFICIENT REDUCER OF THE ENERGY LOSSES IN PIPE FLOW

AGREGATY POLIMEROWO-MICELARNE JAKO EFEKTYWNY REDUKTOR STRAT ENERGETYCZNYCH W PRZEPŁYWACH RUROWYCH

Abstract

The paper presents polymer-micellar aggregates as efficient drag reducers of the energy losses in straight pipe flow. A small amount of high molecular polymers: Polyethylene Oxide, Cetyltrimetyl Ammonium Bromide surfactant and Sodium Salicylate salt additives, are applied to obtain polymer-micellar aggregates formation. An analysis of how polymer-micellar additives influence the shape and character of flow resistance curves has been performed. It is documented that for polymer-micellar solutions the stable transitional zone between, the laminar and the turbulent flows are **extended** toward higher values of the Reynolds number. Occurrence of the third turbulent zone of drag reduction is also observed.

Keywords: Energy losses, pipe flow, flow laminarisation, aggregate

Streszczenie

W artykule przedstawiono agregaty polimerowo-micelarne jako efektywny reduktor strat energetycznych w przepływach rurowych. Do procesu formowania agregatów wykorzystano niewielkie ilości wielkocząsteczkowego politlenku etylenu i substancji powierzchniowo czynnej bromku heksadecylotrójmetyloamoniowego z dodatkiem salicylanu sodu. Dokonano analizy wpływu roztworu polimerowo-micelarnego na kształt i charakter krzywych oporów przepływu. Dla analizowanych roztworów zaobserwowano rozszerzenie stabilnej strefy przejściowej w kierunku większych wartości liczby Reynoldsa. Zaobserwowano również trzecią, turbulentną strefę redukcji oporów przepływu.

Słowa kluczowe: Straty energetyczne, przepływ rurowy, laminaryzacja przepływu, agregat

DOI:

* Prof. PhD. DSc. Eng. Zbigniew Matras, MSc. Eng. Bartosz Kopiczak, Institute of Thermal and Process Engineering, Faculty of Mechanical Engineering, Cracow University of Technology.

1. Introduction

Drag reducers have been widely investigated for more than 60 years, since the first observations of drag reduction in turbulent flows was documented by Toms [1] and Mysels [2]. Since then, the abnormal flow drag reduction by surfactant or polymer additives has been intensively examined and described in the subject literature [3, 4, 5, 6, 7, 8]. This phenomenon allows for a significant increase of the flow rate without increasing power demand, or vice versa – to reduce power demand, while maintaining a constant flow rate. It provides large potential possibilities for the application of this effect in different industry branches, particularly in the oil industry [7, 9] or in heating [8], firefighting [10], transport of slurries [7], sludge and brines [8, 11]. Causes of the described drag reduction have been perceived in the existence of a new internal solution structure, which is formulated at the moment when the special additives are introduced into the solution. Addition of high molecular weight polymer agents into the solvent results in macromolecule formation, which has a crucial influence on turbulence structure in the flow [4, 7, 12, 13,]). Although, there is still strong debate on whether a single polymer molecule or clusters of polymer molecules are responsible for the drag reduction effect, experimental results clearly prove that even a dozen of the ppm polymer concentration in solvent induces an efficient drag reduction effect in turbulent range of flow [7, 8, 14].

In case of application of surfactants as drag reducing additives, formation of micelle structures is observed [8, 12]. In order to improve the micellarisation process effectiveness in a surfactant solution, small amounts of electrolytes are applied (e.g. sodium salicylate or sodium bromide). At no motion condition, the mentioned structures are chaotic. Only during fluid flow shearing do both macromolecules and micelles start to arrange in a characteristic orientation, in accordance with the principle of minimum resistance. In both surfactant and polymer induced experiments on the drag reduction effect, a hypothetical mechanism of the phenomenon is widely accepted to be found in the interaction between polymer or surfactant molecules with the flow turbulence structure. On the basis of advanced measurement techniques, such as Particle Image Velocimetry (PIV), it is observed that the analysed polymer additives can lead to reduction or elimination of the ejections of low-momentum fluid from the wall region to the outer velocity region [14]. It is also observed that the presence of polymers leads to a decrease in the frequency and the intensity of large-scale ejections when compared to a Newtonian solvent and to the reduction of the magnitude and frequency of the small-scale eddies [15]. Usually, elongational viscosity or elasticity of polymer chain [5, 7] are proposed to explain hypothetical polymer drag reduction mechanics. On the other hand, for a surfactant aqueous solution, which reveals neither viscoelastic properties nor presence of elongational viscosity is observed [8, 13], a local shear-thickening hypothesis is proposed [8, 16].

The novel and poorly recognised effect is a phenomenon of fluid flow drag reduction by the simultaneous addition into the solvent of both high molecular polymer and surfactant with salt. In the published works related to this subject [17, 18, 19], the internal structure formation and chemical reaction process in polymer-micellar solutions are mainly highlighted. First attempts at experimental examination of turbulent wall shear stress and drag reduction effect have been performed [20, 21, 22, 23, 24, 25]. The results confirmed that simultaneous addition into the solvent of the analysed additives combines and intensifies positive features of their purely polymer and micellar analogues, providing

additional extension of drag reduction zones. Moreover, the researchers indicate that this new effect requires a comprehensive experimental study to gain a deeper knowledge of this phenomenon.

Presence of polymer macromolecules in the surfactant solution enhances micelles structures formation ability. It leads to the formation of micellar structure at a lower concentration. The newly formed macromolecules are called aggregates [21, 24]. Adding a slight amount of salt (e.g. NaCl or NaSal) to the high molecular polymer and surfactant solution causes micelles size growth. The number of micelles linked with polymer chains also increases. Furthermore, the addition of the salt can increase the solution viscosity.

The aim of this paper is to perform an analysis of the drag reduction efficiency by simultaneous addition to the solvent both surfactants and high molecular polymer, comparing to the drag reduction effect obtained by addition of pure polymer or pure surfactant agents. The paper presents polymer-micellar aggregates as efficient drag reducers of the energy losses in straight pipe flow

2. Characteristic of polymer-micellar solution aggregates structure

A simultaneous addition of small amounts of polymer and surfactant additives to the solvent triggers an initiation of the micellarisation process at much a lower concentration, comparing to the critical micelle concentration (CMC) [8, 25, 27]. This concentration at which micelles formation initiation occurs in the presence of polymer macromolecules is called the critical aggregation concentration (CAC). Most of experimental studies have shown that a simultaneous addition of small amounts of polymer and surfactant agents to the solvent cause initiation of the micellarisation process at lower concentration, compared to CMC [18, 21]. The newly formed polymer-micelle macromolecules are called aggregates [21, 26, 27]. Upon the experimental study of polymer-micellar aqueous solutions [21, 24, 26], the mechanism of aggregates formation process can be described. Initially, polymer and surfactants molecules occur in the solution independently. The situation significantly changes when a small amount of salt is introduced into the solution. According to the [17, 18, 21, 27], as a result of electrostatic or hydrophobic interaction, the micelles are combined with the polymer chains by coiling around them. The final state of the mixture has single threadlike micelles with a part of polymer macromolecule chain coiled around rigid micelles, forming aggregates.

Consequently, it increases the solution's viscosity values. It should be pointed out that salt additive causes a significant viscosity decrease. It is justified by the more intensive interaction between polymer chains.

3. Material and measurments set-up

Having analysed the level of difficulty of the planned experimental tests and taking into account the type of physical quantities to be measured, the experiment was performed using a modern capillary-pipe rheometer, designed and constructed in the Division of Fluid Mechanics laboratory at the Cracow University of Technology [28]. The device allows the

operator to conduct a comprehensive identification of rheological characteristics of the examined liquid in laboratory conditions.

The versatility of the described capillary-pipe rheometer allows the operator to assign not only classical experimental flow curves in the laminar range of flow, but also to examine and interpret properly the flow characteristics of fluids, which behave differently when compared with purely viscous non-Newtonian fluids in the turbulent flow region. This applies primarily to the solutions of polymers and surfactants, which are the subject of research in this work, as well as to the fluids, which can be considered on the border between the physical continuum and multi-phase system, e.g. rheostable (purely viscous) or viscoelastic suspensions. A schematic diagram of the capillary-pipe rheometer is illustrated in Figure 1.

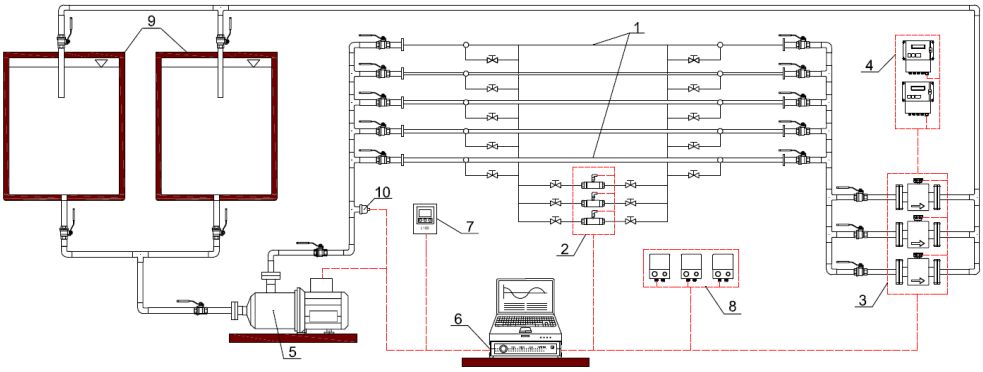

Fig. 1. Diagram of the multifunction capillary-pipe rheometer:
1 – straight capillaries and pipes with circular cross-section; 2 – differential pressure drop sensors PD1 and PDF, 3 – electromagnetic flowmeters; 4 – flowmeter controllers; 5 – Multistage rotodynamic pumps with triple-phase electrical engine; 6 – data acquisition system; 7 – microprocessor frequency converter L100; 8 – amplifiers WP-01A; 9 – tanks; 10 – temperature sensors PT 100

The basic elements of the device are straight copper and stainless steel capillaries and pipes with a circular cross-section (1). They are used for the measurement of fluid flow pressure loss at pipe distance L. Static pressure holes were spotted at distances $L_{inl} = L_{out} \approx 150d$ from the pipe inlet and outlet. This ensures stable flow conditions and eliminates the influence of the so-called "entrance effect."

The fluid flow in the capillary-pipe rheometer is forced by hermetic multistage rotodynamic pumps (5), which suck in the fluid from one of the tanks (9) and then pump it into one of the eight horizontal pipes of different diameters (1). After passing through the electromagnetic flowmeters (3), the fluid returns to the storage tank. The measurements of the pressure losses were performed using PD1 or PDF differential pressure drop sensors (2).

For the current temperature control (possibility of maintaining a constant temperature in the measuring system was provided), a resistive temperature sensor (10) was placed in the fluid supply pipe.

Pumps can work in either series or parallel arrangements, depending on the required flow rate or pressure loss value. This allows the operator to obtain a wide range of Reynolds number reaching the value of 3×10^5 for the measurement system pressure value up to 10 bar, without the loss of fluid continuity (no foaming of the solution or air bubbles).

A microprocessor frequency converter (7) was used to control the pump frequency and consequently the volumetric flow rate. The main element supporting the action of the capillary-pipe rheometer is a multi-channel data acquisition system SPIDER 8 (Hottinger Baldwin Messtechnik), arranged to measure the electrical signals from the different sensors (tension, force, pressure, displacement, acceleration and temperature sensors).

Additionally, large volume tanks (1 m^3) were used to eliminate the effect of foaming of micellar and polymer-micellar solutions and to minimise the influence of the unavoidable degradation of the polymer-micellar aggregates or macromolecular structures on measurement results.

During the preparation of the polymer-surfactant solutions, pH of the chosen drag reducing additives should be particularly considered. Incorrect selection of pH may result in an undesired chemical reaction.

Anionic surfactants cannot be used, while aqueous solutions of certain polymers can have an acidic reaction. Cationic and anionic surfactants can be combined with non-ionic polymer solutions.

After the preliminary study, the following drag reducers have been used for the experimental analysis:

- Poly(ethylene oxide) $[CH_2\ CH_2\ O]_n$ (PEO) – non-ionic polymer with viscosity-based high molecular weight given by the manufacturer equal to $8\cdot10^6$ g/mol^{-1}, purchased from Sigma-Aldrich, Inc.
- Cetyltrimetyl ammonium bromide $[CH_3(CH_2)i_5N(CH_3)_3]+Br\sim$ (CTAB) – cationic surfactant purchased from Sigma-Aldrich, Inc.

In order to lower the CAC value, salt $C_7H_5NaO_3$ (NaSal) sodium salicylate has been used. Different compositions of polymer, surfactant and salt mass fraction in solvent were used in order to analyse the chemical additive concentration effect. Distilled water was used as a solvent. Polna, Inc. Electrical Distillatory Type DE20 was used to purify tap water. The conductivity of the solvent was of the order of 1μS/cm.

After the addition of the appropriate drag reducers to the solvent, the solutions were mixed gently so as not to cause mechanical degradation of polymer chains. The first mixing was performed in cylindrical vessels, by the use of our own designed roller mixer with very a low rotational speed equal to 1÷5 rpm. Then, the solution was diluted in the main tanks. Before measurements, the mixtures were left to rest for 24 hours.

Adiabatic steady flow of homogenous solutions was examined in 8 different straight pipes with diameters between 1.8mm and 21mm, all with a temperature of 27˚C.

4. Rheological characteristics and flow resistance measurements results

In order to identify the rheological characteristics of the analysed solutions, each of the experimental/pipe flow curves have been drawn in form of functional relationship described by the Equation (1):

$$\tau_w = f(\Gamma) \tag{1}$$

where: $\tau_w = \frac{D\Delta P}{4L}$ – shear stress on pipe wall,

$\Gamma = \frac{8v_m}{D}$ – pipe shear rate (value of shear rate on pipe wall).

An interpretation of experimental results presented in form of function (1) indicates that the analysed solutions can be successfully approximated with the Ostwald de Waele power-law fluid model. Representative rheological characteristics in form of experimental/pipe flow curves are illustrated in Figure 2.

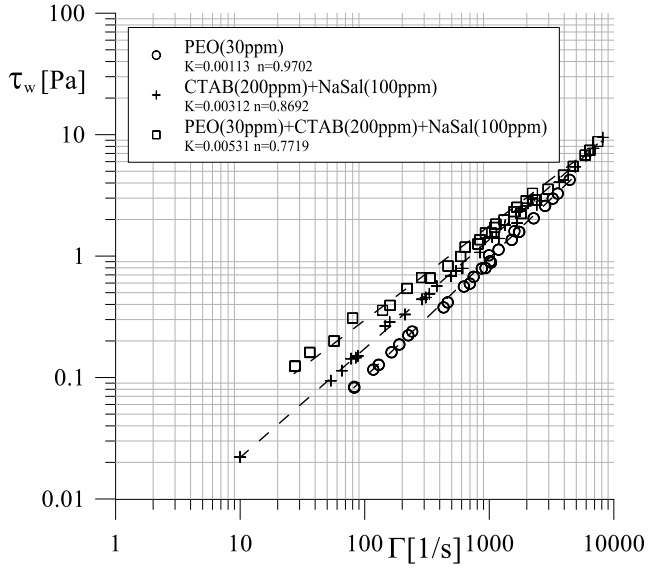

Fig. 2. Representative experimental flow curves for polymer, surfactant and polymer-surfactant solutions

Additionally, representative diagram of the shear viscosity curves vs. shear rate for the analysed solutions, which correspond to Figure 2, are presented in Figure 3.

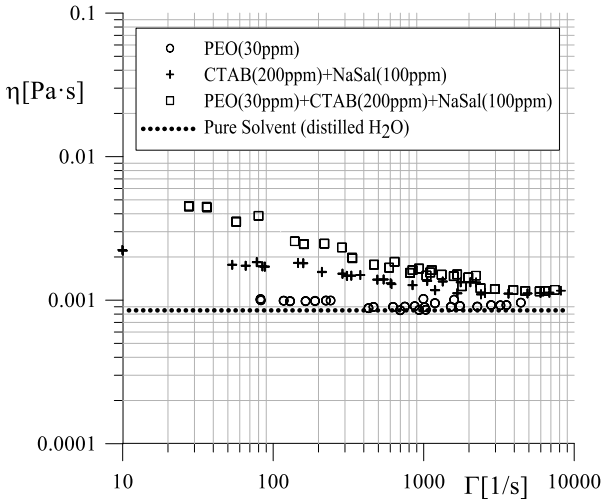

Fig. 3. Representative shear viscosity curves as a function of shear rate for polymer, surfactant and polymer-surfactant solutions

The mass fraction of individual additives, composing rheologically complex polymer-micellar solution, affects the value of the n flow index. This parameter characterises non-Newtonian properties of a fluid. There is no way to predict a priori, its value for a solution composed is arbitrarily and having different mass frictions of particular drag reducers. It was only observed that the increase of both CTAB and NaSal concentration in the examined solution having a constant polymer concentration leads to the intensification of non-Newtonian properties of the fluid, i.e. to the increase of the value of fluid consistency constant K and the decrease of the n flow index.

The interpretation of experimental data and the assessment of the respective solution additives' influence on the increase or reduction of the flow resistance and the shape and location of resistance curves depend significantly on the adopted coordinate system in which these data is presented. Firstly, experimental results of flow resistance are presented in the classical system of dimensionless numbers [Re_s, c_f] described by formulas (2) and (3):

$$Re_S = \frac{\nu_m \cdot \rho_S \cdot d}{\eta_S} \tag{2}$$

$$c_f = \frac{d \cdot D \cdot P}{2 \cdot r \cdot \nu_m^{\,2} \cdot L} \tag{3}$$

and additionally, in the form of drag reduction coefficient *DR*, defined as a function of the Reynolds number (2), and described in percentage term:

$$DR = \left(1 - \frac{c_f}{c_{fS}}\right) \cdot 100\% \tag{4}$$

Figure 4 presents the flow resistance curves of polymer, surfactant and polymer-surfactant water solutions, defined in the system of dimensionless numbers (2) and (3).

Analyses of flow resistance curves reveal that in any of analysed flow ranges measurement points do not correspond to the theoretical functions, which describe Newtonian fluid flow. The simultaneous addition of even small amounts of high molecular polymers and surfactants causes an increase of flow resistance in the laminar range of flow.

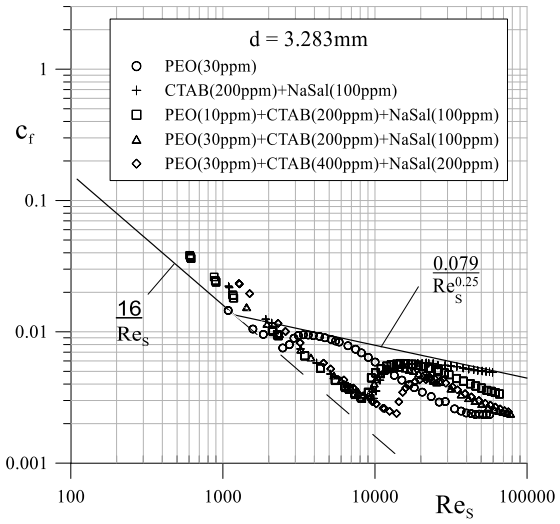

Fig. 4. The flow resistance curves of polymer, surfactant and polymer-micellar water solutions, defined in the system of dimensionless numbers (2) and (3)

The drag reduction coefficient curves (4) are illustrated in Figure 5. It is observed that in case of the turbulent flow simultaneous application of analysed chemical additives produces the drag reduction effect.

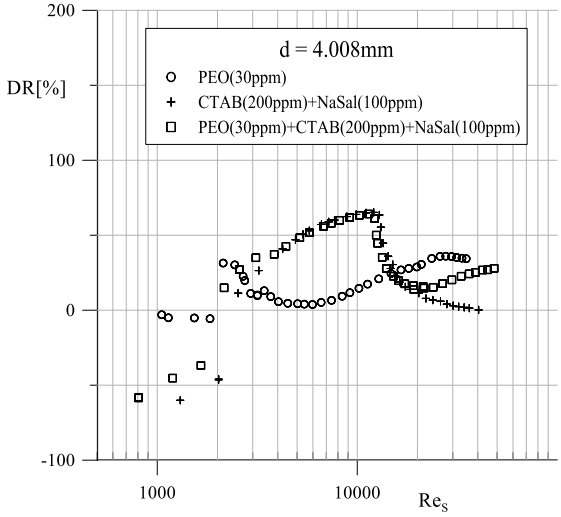

Fig. 5. The drag reduction coefficient curves *DR* = *f*(*Re*)

Due to the difficulty in unambiguous determination of the critical value the Reynolds number Re_s, the *DR* values presented in Figure 5 are calculated in such a way that it was assumed that $c_{fs} = 16/Re_s$ in the range of the Reynolds number $Re_s < 2100$, whereas the formula $c_{fs} = 0.079/Re_s^{-0.25}$ was used in the range of Reynolds number $Re_s \geq 2100$. Therefore, a sharp increase of the DR value observed in the transition zone, particularly in the polymer solution (see in Figure 5), does not reflect the actual degree of drag reduction in this range of flow. In case of the polymer solution flow, in the initial stage of the turbulent flow, no noticeable reduction of flow resistance is observed. Only after exceeding certain characteristic Reynolds number $Re_s \approx 1.5 \cdot 10^4$, the onset of the drag reduction effect occurs and the phenomenon increases with the increase in the value of the Reynolds number. A similar increase in the reduction of the shear resistance in rotating disc apparatus for the turbulent flow range, induced with PEO additive, was observed in the drag reduction effect obtained by the use of a rotating-disk apparatus [22].

Furthermore, the value of the critical Reynolds number, for which transition from the laminar flow to the turbulent flow is observed, takes various values, which depend on pipes' diameters, type and concentration of chemical additives introduced to the solvent.

A better interpretation of the simultaneous addition of the polymer and surfactant with salt effect on drag reduction, in comparison with adequate addition of pure polymer or pure surfactant with salt, can be achieved by presentation of the same measurement date in modified system of "pseudorheostable" numbers [Re_M, c_{fM}]. The modified system on dimensionless numbers used in the analysis is described correspondingly by formulas (5) and (6):

$$Re_M = \frac{d^n \cdot v_m^{2-n} \cdot \rho_S}{K \cdot \left(\frac{3 \cdot n + 1}{4 \cdot n}\right) 8^{n-1}} \cdot \left[\frac{2 \cdot (n+1)}{3 \cdot n + 1}\right]^{-2,5} \tag{5}$$

$$c_{fM} = \frac{d \cdot \Delta P}{2 \cdot \rho_S \cdot v_m^2 \cdot L} \cdot \left[\frac{2 \cdot (n+1)}{3 \cdot n + 1}\right]^{2,5} \tag{6}$$

As one knows [5], in such defined dimensionless numbers system flow resistance curves of rheostable (purely viscous) non-Newtonian fluids are transformed to a single curve – in the whole range of modified Reynolds numbers (5) – identical to the classical Newtonian curve described in the laminar range by Fanning equation and in the turbulent flow by Blasius formula. Selection of such a coordinate system was dictated additionally by the fact that it facilitates identification and description of the characteristic drag reduction flow zones. In this modified system of pseudorheostable dimensionless numbers [Re_M, c_{fM}], each deviation of experimental flow resistance curve, which indicates abnormal drag reduction from pseudorheostable Blasius curve, allows for the identification of the influence of specific additives (polymers or/and surfactants with salt) on the range of analysed drag reduction effect. Figure 6 presents comparison of flow resistance curves in the modified dimensionless number system (5) and (6) for 3 types of solutions with different internal structures.

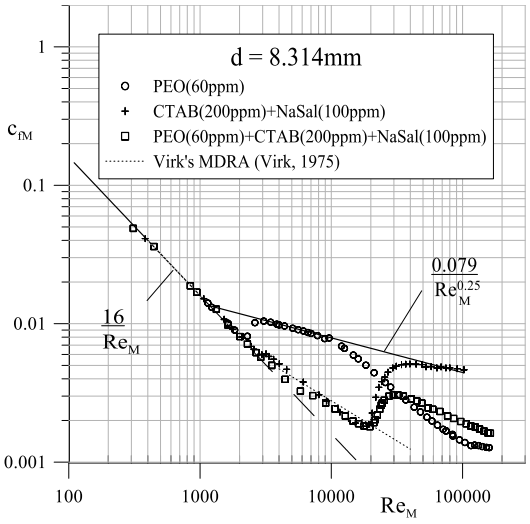

Fig. 6. The flow resistance curves of polymer, surfactant and polymer-surfactant water solutions, defined in the system of cardinal numbers (5) and (6).

The results of experimental data analysis indicate that polymer-surfactant-salt additives cause significant drag reduction in a wider range of flow in comparison with pure polymer or pure surfactant-salt solutions. Surfactant and salt additives (micellar solution) induce appearance of the stable transitional zone B (compare Figure 6 and Figure7), in which spectacular reduction of flow resistance is observed – usually greater when compared to the same effect achieved with polymer additives.

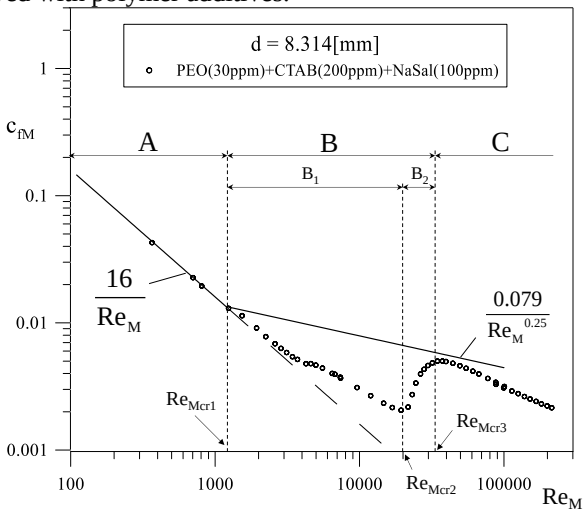

Fig. 7. The scheme of characteristic flow resistance curve zones for representative polymer-micellar solution: A – laminar zone, B – extended transitional zone (B_1 – stable transitional zone, B_2 – unstable transitional zone), C – turbulent zone.

It is observed that in the stable transitional zone B_1, the loss of the stability of the laminar flow increases very softly when the Reynolds number values grow. In this range, relative drag reduction is the greatest. Beyond a certain second critical value of the Reynolds number Re_{Mcr2} the occurrence of an unstable transitional zone B_2 is observed. It is especially well-illustrated in Figure 7. In this range of flow, a rapid loss of drag reduction effect occurs.

From Figure 6, it is documented that for polymer-micellar solutions, beyond a certain third critical value of the Reynolds number Re_{Mcr3}, the fluid starts to behave like a classical rheostable non-Newtonian fluid.

However, in comparison with pure micellar solution, an additional abnormal drag reduction zone C (see Figure 7) in the turbulent range of flow is observed in case of analysed polymer-micellar solution. The viscoelastic properties of the solution are a dominant factor in this zone of flow. This effect is also well-illustrated in Figure 8.

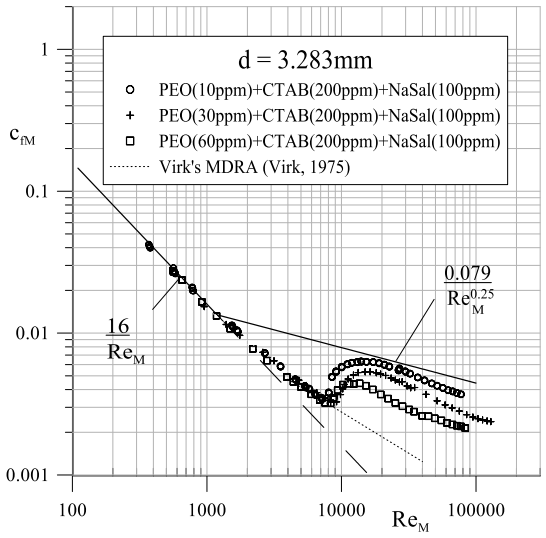

Fig. 8. Polymer concentration effect on the flow resistance curves of polymer-surfactant aqueous solutions

It should also be pointed out that addition to the micellar solution of even small amounts of high molecular weight polymer (about 10 ppm) causes a reduction of the non-Newtonian properties of the solution.

Experiment results indicate the influence of NaSal additive on drag reduction effect. Figure 9 presents a comparison of flow resistance curves of the pure polymer solution, the polymer-surfactant solution and the polymer-surfactant-salt solution.

It is clearly evident that with the addition of a small amount of electrolytes (e.g. salts or alcohols), a reformation of spherical micelles into threadlike micelles must proceeded. It leads to significant extension of the transitional zone B_1. Efficient drag reduction effect is observed within this zone of flow

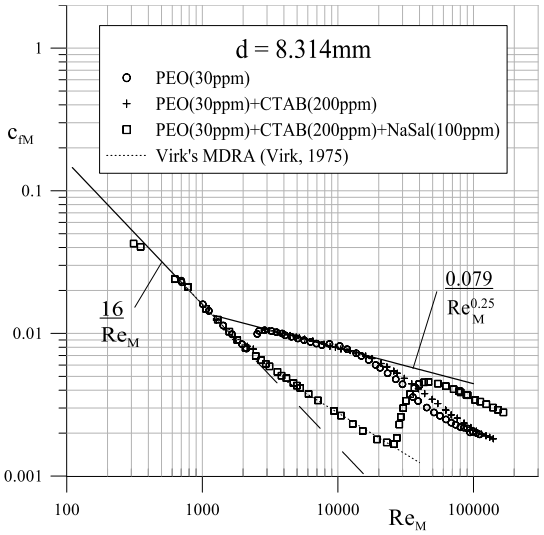

Fig. 9. The effect of NaSal additive on polymer-surfactant flow resistance curve

The results of drag reduction measurements analysis indicate the effect of pipe diameter influence on the drag reduction efficiency. Figure 10 illustrates the pipe diameter effect on the flow resistance curves of polymer-surfactant aqueous solutions.

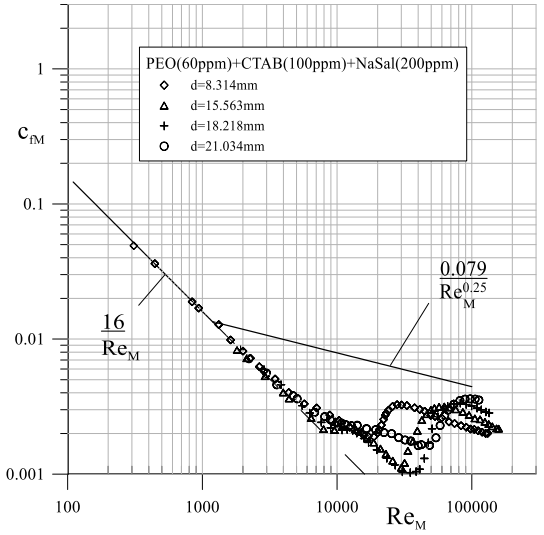

Fig. 10. Pipe diameter effect on the flow resistance curves of polymer-surfactant aqueous solutions

Increasing the pipe diameter d results in a clear extension of the stable transitional zone B_1 towards higher values of the Reynolds number. Moreover, decreasing the pipe diameter

value d results in an increase of the drag reduction effect in the third additional turbulent range of flow C.

The experimental results reveal that polymer-micellar solution can be characterised by a lower susceptibility to mechanical degradation during flow or that its degradation can be almost unnoticeable in the analysed range of flow. Figure 11 illustrates a shift of the collapse of drag reduction effect toward greater values of Reynolds number caused by application of polymer and polymer-surfactant additives.

A pure PEO solution degrades very fast when it goes under high shearing conditions. A collapse of the drag reduction is gradually observed in such a case. Experimental results show a considerable increase of the Reynolds number value for which mechanical degradation of polymer and collapse of DR effect is observed in polymer-micellar solution.

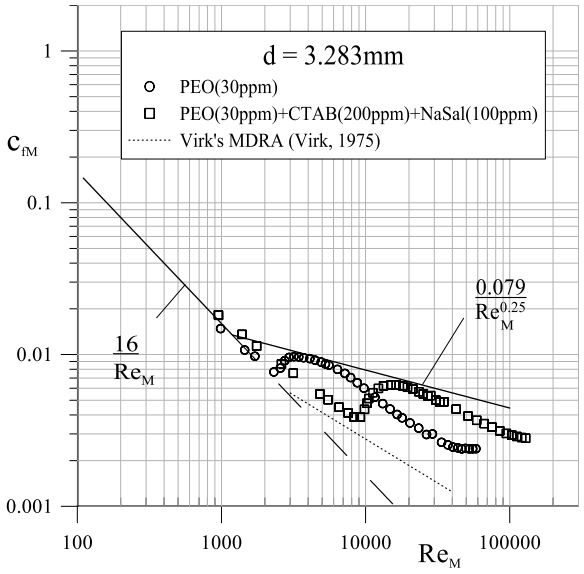

Fig. 11. Shift of the collapse of drag reduction effect toward greater values of Reynolds number caused by application of polymer and polymer-surfactant additives

5. Conclusions

Experimental study of drag reduction process induced by co-addition of polymer and surfactant with salt indicates that polymer-micellar aggregates are efficient drag reducers of the energy losses in straight pipe flow. Analyses of experimental data document that the simultaneous addition of surfactants and salt, together with high molecular polymers, causes a minor increase of flow resistance in the laminar range of flow compared to the analogue flow of pure solvent. It produces, however, a significant extension of the stable transitional zone between the laminar flow and the turbulent flow. The surfactant with salt additives has a major influence on the efficiency of the drag reduction in this zone.

Experimental results prove that the simultaneous addition of surfactant, salt and high molecular polymer leads to the occurrence of third significantly extended drag reduction zone in the turbulent range of flow. The dominant factors in that zone are the viscoelastic properties of the solution caused by the presence of polymer macromolecules, wherein an increase of the mass fraction of the polymer additive increases the efficiency of the drag reduction effect only in the turbulent range of flow.

The performed comparative studies presented that the analysed polymer-micellar solutions combine and intensify positive features of their purely polymer or purely micellar analogues, providing a more efficient drag reduction effect in a wider range of flow.

Under the experimental data, it can be hypothesised that aggregates, subjected to the shear stress, take orientation consistent with the aforementioned principle of minimum resistance. With an increasing value of the Reynolds number, internal friction forces stretch and extend the aggregates, leading to the laminarisation of the initial phase of the turbulent flow.

Therefore, it can be presumed that the rigid rod like/threadlike micelles, which create the core of the aggregates, are responsible for reducing the flow resistance in the extended transitional zone between the laminar and the turbulent flow.

The aggregates and micelles are responsible for the transmission of internal friction within the liquid. The value of the critical Reynolds number for which the transition to the turbulent zone is observed is greater for polymer-micellar solutions. This means that the stable transition zone is extended. The reason for such behaviour can be the partial disintegration of aggregates to original forms, i.e. micelles (formed from the surfactant) and macromolecules (formed from the polymer) due to a significant increase of the shear rate. From this moment, both micelles and macromolecules interact separately on the transported solution, causing a further drag reduction effect. Passing further in the turbulent range of flow micelles lose their orientation and no longer have a major impact on the drag reduction. A key role in this zone is played by the polymer. Not having undergone an earlier degradation, the polymer macromolecules still cause the flow reduction.

In drag reduction caused by the use of polymer-micellar solution, one cannot talk about the so-called *collapse of the drag reduction.* It occurs permanently over a wide range of Reynolds numbers. Nevertheless, in the turbulent zone, polymer macromolecules undergo a certain mechanical degradation. Decreasing the shear rate leads to the reconstruction of the internal structure of the solution. As a result of electrostatic or hydrophobic interaction, the recreated micelles are combined with the polymer chains by coiling around them. These chains are somewhat shorter and such newly created aggregates do not have the same rheological properties as the original ones. This results in a slight increase of the flow resistance in comparison with a freshly prepared solution.

Thee presented experimental results of the drag reduction effect are consistent in terms of qualitative analysis with proposed hypothesis, and confirm the described mechanism of the phenomenon in an indirect way.

References

[1] Toms, B. A., *Some Observations on the flow of linear polymer solutions through straight tubes at large Reynolds numbers*. Proceedings of the International Congress of Rheology, Holland, North-Holland, Amsterdam, Section II, 1948, 135-141.

[2] Mysels, K. J., *Flow of thickened fluid*. December 27, US Patent 2, 492:173, 1949.

[3] Virk P. S., *Drag reduction fundamentals*, AIChE Journal, vol. 21, Issue 4, 1975, 625-656.

[4] Sellin, R. H. J., Hoyt, J. W., Poliert, J., Scrivener, O., *The effect of drag reducing additives on fluid flows and there industrial applications part II: present applications and futures proposals*. Journal of Hydraulic Research, vol. 20, 1982, 235-292.

[5] Matras Z., *Przepływ cieczy Tomsa w przewodach kołowych*, Politechnika Krakowska, Monografia 29, 1984.

[6] Gyr A., Bewersdorff H. W., *Drag reduction of turbulent flows by additives*, vol. 32, Kluwer Academic Publishers, P.O. Box 17, 3300 AA, 1995.

[7] White, C. M., Mungal, M. G., *Mechanics and Predictions of Turbulent Drag Reduction with Polymer Additives*, Annular Review of Fluid Mechanics, no. 40, 2008, 235-256.

[8] Wang Y., Yu B., Zakin J. L., Shi H., *Review on Drag reduction and Its Heat Transfer by Additives*, Advances in Mechanical Engineering, no. 10,2011, 17.

[9] Dujmovich T. and Gallegos A., *Drag reducers improve throughput, cut costs*, Offshore, vol. 65, no. 12, 2005, 55-58.

[10] Fabula, A. G., *Fire-fighting benefits of polymeric friction reduction*. Trans ASME J Basic Engng, 1971, 93-453.

[11] Motier, J. F., Chou L. C., Kommareddi N. S., *Commercial drag reduction: past, present, and future*, Proceedings of the ASME Fluids Engineering Division Summer Meeting, San Diego, Calif, USA 1996.

[12] Tamano S., Ito M., Kato K. and Yokota K., *Turbulent drag reduction in nonionic surfactant solutions*, Physics of Fluids, vol. 22(5), 2010, 055102.

[13] Cai S.-P., *Drag reduction of a cationic surfactant solution and its shear stress relaxation*, Jurnal of Hydrodynamics, vol. 24(2), 2012, 202-206.

[14] Warholic M. D., Heist D. K., Katcher M., Hanratty T. J., *A study with particle- image velocimetry of the influence of drag-reducing polymers on the structure of turbulence*, Exp. Fluids, vol. 31, 2001, 474-483.

[15] Liberatore M. W., Baik S., Mchugh A. J., Hanratty T. J., *Turbulent drag reduction of polyacrylamide solutions: effect of degradation on molecular weight distribution*. J. Non-Newtonian Fluid Mech., vol. 123, 2004, 175-183.

[16] Hadri F., Besq A., Guillou S., Makhloufi R., *Drag reduction with an aqueous solution of CTAC-NaSal: Study of the wall slip with a Couette geometry*, Comptes Rendus Mécanique, vol. 338, Issue 3, 2010, 152-157, ISSN 1631-0721.

[17] Minatti E., Zanette D., *Salt effects on the interaction of poly(ethylene oxide) and sodium dodecyl sulfate measured by conductivity*, Colloids Surfaces A: Phisicochem Eng Aspects, 1996, 113:237.

[18] Hou Z., Li Z., Wang H., *Interaction between poly(ethylene oxide) and sodium dodecyl sulfonate as studied by surface tension, conductivity, viscosity, electron spin resonance and nuclear magnetic resonance*, Colloid Polym. Sci., vol. 277, 1999, 1011-1018.
[19] Goddard E. D., *Polymer/Surfactant Interaction: Interfacial Aspects*, Journal of Colloid and Interface Science, vol. 256, 2002, 228-235.
[20] Suksamranchit S., Sirivat A., Jamieson A. M., *Polymer–surfactant complex formation and its effect on turbulent wall shear stress*, Journal of Colloid and Interface Science, vol. 294, Issue 1, 2006, 212-221, ISSN 0021-9797.
[21] Matras Z., Malcher T., Gzyl-Malcher B., *The influence of polymer-surfactant aggregates on drag reduction*, Thin Solids Films, vol. 516, 2008, 8848-8851.
[22] Kim J. T., Kim C. A., Zhang K., Jang C. H., Choi H. J, *Effect of polymer–surfactant interaction on its turbulent drag reduction*, Colloids and Surfaces A: Physicochemical and Engineering Aspects, vol. 391, Issues 1-3, 2011, 125-129, ISSN 0927-7757.
[23] Mohsenipour A. A., Pal R., *The Role of Surfactants in Mechanical Degradation of Drag-Reducing* Polymers, Ind. Eng. Chem. Res., vol. 52 (3), 2013, 1291-1302.
[24] Mohsenipour A. A., Pal R., Prajapati K., *Effect of cationic surfactant addition on the drag reduction behaviour of anionic polymer solutions*, The Canadian Journal of Chemical Engineering, vol. 91, Issue 1, 2013, 181-189.
[25] Matras Z. and Kopiczak B., *Intensification of drag reduction effect by simultaneous addition of ,surfactant and high molecular polymer into the solvent,* Chemical Engineering Research and Design, vol. 96, 2015, 35-42.
[26] Jönsson B., Lindman B., Holmberg K., Kronberg B., *Surfactants and polymers in aqueous solution*, John Wiley & Sons, Chichester, UK 1998.
[27] Diamant H., Andelman D., *Onset of self-assembly in polymer-surfactant systems*, Europhysics Letters, vol. 48(2), 1999, 170-176.
[28] Matras Z., Walczak S., *The capillary-pipe rheometer for the identification of complex properties of multiphase non-Newtonian fluids*, Inżynieria i Aparatura Chemiczna, No. 6,2006, 150-151.

TECHNICAL TRANSACTIONS | CZASOPISMO TECHNICZNE
MECHANICS | MECHANIKA
2-M/2016

MATEUSZ MUSIK*, JAN TALAGA**

INVESTIGATION OF FLUID DYNAMICS IN AN UNBAFFLED STIRRED VESSEL WITH AN ECCENTRICALLY LOCATED RUSHTON TURBINE

BADANIA HYDRODYNAMIKI MIESZANIA W MIESZALNIKU BEZ PRZEGRÓD Z NIECENTRYCZNIE USYTUOWANYM MIESZADŁEM TURBINOWYM

Abstract

The paper presents the results of experimental investigation of the hydrodynamics in unbaffled stirred vessel with eccentric Rushton turbine configuration. Basing on flow visualisation. the main flow features were determined. Laser Doppler Anemometry measurements provided radial and axial components of the mean flow velocity vectors. The obtained data of power consumption allowed to determine the impact of the impeller eccentricity ratio *e*/*R* on the power number *Ne*.

Keywords: agitation, eccentrically located impeller, unbaffled vessel, LDA measurements

Streszczenie

W artykule przedstawiono wyniki badań doświadczalnych hydrodynamiki mieszania w zbiorniku bez przegród z niecentrycznie usytuowanym mieszadłem turbinowym tarczowym. Dokonano wizualizacji przepływu. W oparciu o wyniki pomiarów z wykorzystaniem anemometru laserowego wyznaczono rozkłady promieniowej i osiowej składowej średniej prędkości przepływu cieczy. Określono doświadczalnie wpływ niecentryczności *e*/*R* usytuowania mieszadła na liczbę mocy mieszania *Ne*.

Słowa kluczowe: mieszanie, niecentryczne mieszadło, mieszalnik bez przegród, pomiary LDA

DOI:

* MSc. Eng. Mateusz Musik, Avio Aero GE Aviation business, Turbine Unit Department, Bielsko-Biała, Poland.

** DSc. Eng. Jan Talaga, Institute of Thermal and Process Engineering, Faculty of Mechanical Engineering, Cracow University of Technology.

1. Introduction

Mechanical mixing is commonly used in many processes in chemical, food, pharmaceutical or biotechnology industries. A typical design solution of stirred tank is a vertical vessel with a centrically located shaft. Most often, the stirred tank is equipped with four vertical baffles, fixed to the vessel wall, which deter vortex formation and intensify mixing by increasing the axial flow rate [1]. However, in some processes, baffles may cause an undesired effect creating dead zones behind baffles where sludge can accumulate. It can occur especially in stirred tanks with a flat bottom and during multiphase fluid mixing [2]. In such case, it is an alternative solution as unbaffled mixing [3, 4] with eccentrically located impeller. What is more, the design also eliminates unfavourable central vortex formation.

This paper presents an experimental investigation of hydrodynamics and power consumption of mixing in unbaffled stirred tank with eccentrically located Rushton impeller.

2. Experimental

Research was performed in a vertical tank (Fig. 1a) made of *Duran* glass with inside diameter D = 0,286 m and flat bottom. Liquid level were equal to tank inside diameter ($H = D$). The standard Rushton turbine was used. The impeller diameter was $d = 1/3D$ and the blade thickness to diameter ratio was 0,01. The off-bottom clearance was $h = d$. Dimethyl sulfoxide (DMSO) (η = 0,0023 Pa·s, ρ = 1100 kg/m^3) was used as the working fluid.

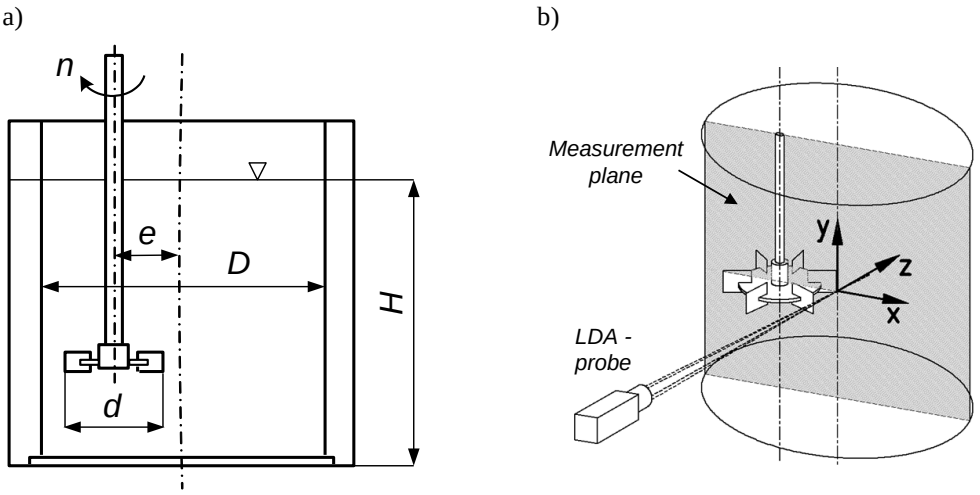

Fig. 1. Stirred vessel with an eccentrically located Rushton turbine;
a) geometric characteristics of stirred vessel, b) scheme of measuring system

The hydrodynamics investigation involved a visualisation of the liquid flow in the stirred tank and an analysis of the components of the mean flow velocity vectors. Temporary flow velocity measurements were carried out using two-component Laser Doppler Anemometry (LDA) operating in back scatter mode [5]. Argon-Ion laser provided a pair of blue beams with λ = 488 nm and a pair of green beams with λ = 514,5 nm. The obtained measurement data were processed by a *Dantec Burst Spectrum Analyser*. The working fluid was seeded with silver coated hollow glass spheres with a mean diameter of 10 μm and a density of 1150 kg/m^3. Liquid flow visualisation was carried out using a digital camera.

The power consumption ($P = M \cdot 2\pi n$) was determined from torque measurements M performed on the shaft using torquemeter (*Vibrometer)*. At the same time, the impeller rotational speed n had been measured.

Research was performed for 3 different positions of the impeller shaft from the tank axis: central position *(*e = 0) and two off-axis positions (e = 0,25R, e = 0,5R*)*, where $R = D/2$.

The flow velocity measurements were performed in plane through tank axis and impeller shaft axis (Fig. 1b). The mixing intensity was controlled by impeller rotational speed changes, and ranged from 200 to 600 *rpm*, corresponding to full turbulent flow in stirred tank and impeller Reynolds number $Re = (1{,}44 \div 4{,}32) \cdot 10^4$.

3. Results and discussion

Fig. 2 shows an example of the impact of the impeller's shaft eccentricity on the liquid flow in an unbaffled stirred tank for a rotational impeller speed of n = 250 rpm. When the impeller is located in the axis of the tank (e = 0, Fig. 1a), one centrically vortex can be observed. The vortex depth increases with the impeller rotational speed increase. For n = 502 rpm, the vortex departs from the top of the vessel above the impeller. From that moment, some air from above the liquid surface starts to be entrained into the flow. The air was dispersed in the tank by the impeller blades. Displacement of the shaft from tank axis towards the wall causes the formation of the vortex in the field between tank wall and impeller shaft (Fig. 2b). Low rotational speed characterises the presence of a vortex in the upper part of the tank, bellow the liquid surface. With a rotational speed increase, the vortex reaches more into the bottom of the tank and at a sufficiently rate of rotation, it reaches the impeller blades. The formation of that vortex in the stirred vessel with eccentrically located impeller were also documented in experimental studies [6, 7], as well as in CFD simulations [2]. Authors of the study [6] also observed the creation of the second vortex departing from the impeller blades towards the vessel bottom. In this paper, such results were not observed. The difference can be explained by the fact that in [6], the stirred tank was equipped with an cover, which was located just above the liquid level and prevented air to be entrained into the flow from the above of liquid surface.

The increase of eccentricity changes the location of the forming vortex, which moves toward the tank wall. Equally higher eccentricity corresponds to a higher vortex inclination to the vertical axis of the tank. For e = 0,5R eccentricity, inclination is 29°±4°. A similar observation has been found in other studies. In paper [6], the upper vortex was inclined by

15°, whereas paper [7] presents an inclination between 16° and 23°. For [7], the root cause of these differences may be explained by a different impeller off-bottom clearance (where $h = 0{,}5D$), and in case of [6], providing closing cover. No changes of the vortex inclination due to rotational speed were observed.

a) b) c)

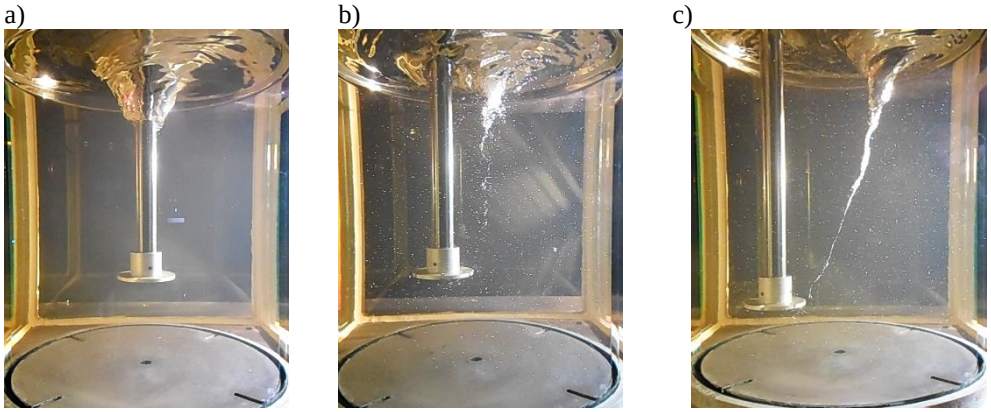

Fig. 2. Flow visualisations with the impeller rotational speed n = 250 rpm for various eccentricity; a) $e = 0$, b) $e = 0{,}25R$, c) $e = 0{,}5R$

a) b)

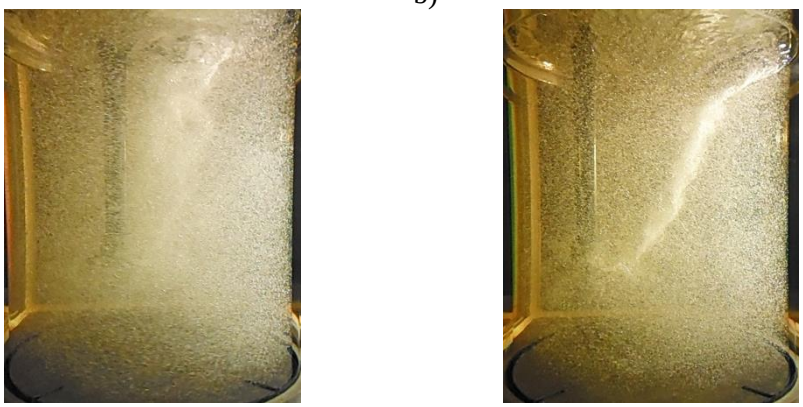

Fig. 3. Air dissipation throughout the volume of the vessel; a) $e = 0{,}25R$ and n = 354 rpm, b) $e = 0{,}5R$ and n = 302 rpm

The vortex created by the eccentrical location of the impeller causes entraining of the gas from the surface into the flow. The intensity of that phenomenon strengthens with an increase of the impeller rotational speed increase and the eccentricity. Fig. 3 shows an example of gas dissipation throughout the volume of the tank for two different e values. For $e = 0{,}25R$ eccentricity, such effect is achieved at rotational speed n = 354 rpm (Fig. 3a), and for $e = 0{,}5R$ eccentricity at lower rotational speed n = 302 rpm (Fig. 3b).

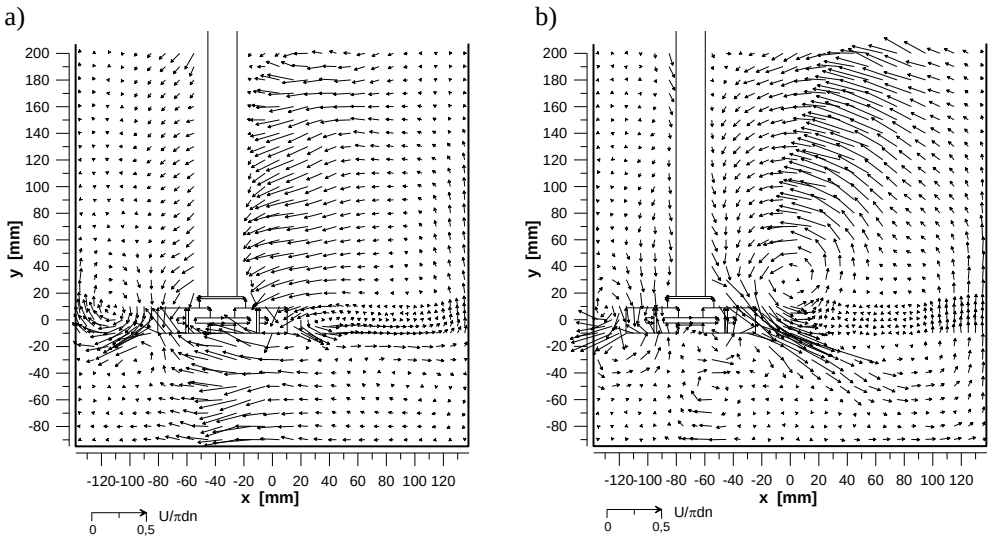

Fig. 4. Vector plot of liquid flow in a stirred vessel with an eccentrically positioned Rushton turbine for various impeller eccentricity: a) $e = 0{,}25R$, b) $e = 0{,}5R$

Fig. 4 shows the results of the measurement of the radial and axial components of the mean flow velocity for two different eccentricities: $e = 0{,}25R$ (Fig. 4a) and $e = 0{,}5R$ (Fig. 4b). Fig. 1b presents the measuring plane. Velocity data determined during mixing with rotational speed $n = 225$ rpm are presented in dimensionless form, i.e. normalised with respect to the impeller blade tip velocity, $(U/\pi \cdot d \cdot n)$. Based on the results, it can be stated that for mixing with eccentrically positioned impeller, the flow pattern is not axisymmetric as it is for central position of the impeller [8]. For the eccentricity $e = 0{,}25R$ (Fig. 4a), the largest values of the radial component occur in the vortex area from impeller blades towards the top of the vessel. Large radial component values are also observed under Rushton turbine. For the eccentricity $e = 0{,}5R$ (Fig. 4b), velocities are much lower, while in the vortex area values of radial velocity components increase. Higher eccentricity also causes significant variation of velocity profiles in the impeller discharge stream. In $e = 0{,}5R$ (Fig. 4b) case, the formed vortex affects the flow of the pumped by impeller blades liquid. It results in a significant increase of the radial component of velocity at the side where the distance between the impeller and the tank wall is the largest. In this case, maximum radial velocities are about 2 ÷ 2,5 larger in comparison with $e = 0{,}25R$ case. The axial components also increase, which cause the flow stream to be pumped towards the vessel bottom. At the area where the impeller is closest to the vessel wall, the velocity profile changes due to the impeller discharge stream-wall interaction.

The measurement of the power consumption for the stirred vessel without baffles is presented in Fig. 5 as the power characteristic $Ne = f(Re)$ for different eccentricities e/R of the impeller shaft. All power characteristics $Ne = f(Re)$ are found to be independent of the Re number for the range of the performed experiments. The similar independence was found in [9] for impellers type HE 3 and for propeller stirrer. Marked in Fig 5 by dashed line decrease of power number Ne for large Reynolds numbers Re, for eccentric impeller

position, is the result of the increase of aeration of mixing liquid caused by formed in the stirred vessel vortex. The aeration of the liquid increases with the impeller rotational speed increase, which results in mixing liquid density decrease, and therefore, with a decrease of the power number.

The results of the experimental analysis allow to conclude that for the liquid stirring in the unbaffled tank with an eccentrically located impeller, the power number is always larger than for the stirring with centrically located impeller (e = 0). Fig. 5 presents also power numbers *Ne* for the conventional stirring with four baffles (J = 4) and centrically located Rushton turbine (e = 0). According to analysis of changes in eccentricity (e = 0 ÷ 0,5R) it can be concluded that power number *Ne* for mixing with eccentrically located impeller in the unbaffled stirred tank is always larger than for centric agitation (*Ne* = 0,74) and always lower than for conventional stirred vessel with baffles (*Ne* = 3,75).

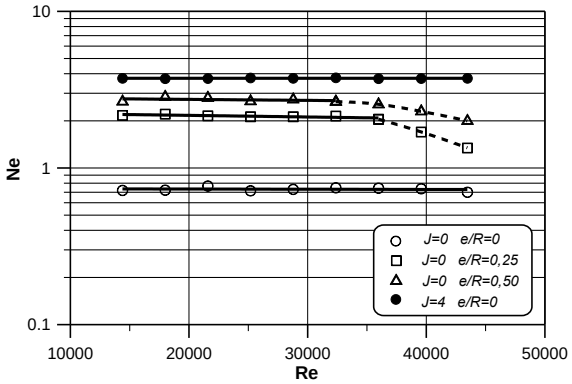

Fig. 5. Power characteristics *Ne = f (Re)* for the stirred tank with the Rushton turbine: J = 0 and e/R = 0; 0,25; 0,5 or J = 4 and e/R = 0

The experimentally proven effect of the stirrer eccentricity ratio e/R on the power number *Ne* in the stirred tank without baffles and with the Rushton turbine is depicted in Fig. 6. The obtained results of the measurements were described mathematically and were approximated by the following correlation:

$$Ne = 0{,}74 \cdot \left[-6{,}89 \cdot \left(\frac{e}{R} \right)^2 + 9{,}04 \cdot \left(\frac{e}{R} \right) + 1 \right] \tag{1}$$

with the maximal relative error ±5,6%, within the ranges of the $Re \in \langle 1{,}44 \cdot 10^4; 4.32 \cdot 10^4 \rangle$ and eccentricity $e/R \in \langle 0; 0{,}6 \rangle$.

Equation (1) describes the evaluated impact of impeller eccentricity e/R as a quadratic function, which is in agreement with experimental results for Rushton turbine, which were reported in [8, 10]. In [9], the linear relationship $Ne = f(e/R)$ was estimated; however, it concerned different impeller types (HE 3 and propeller stirrer), which operate as axial pumping impellers. As the conclusion, it can be estimated that the impact of eccentricity on the power number can be presented as a quadratic function for radial pumping impellers, such as the Rushton turbine, and as a linear function for axial pumping impellers.

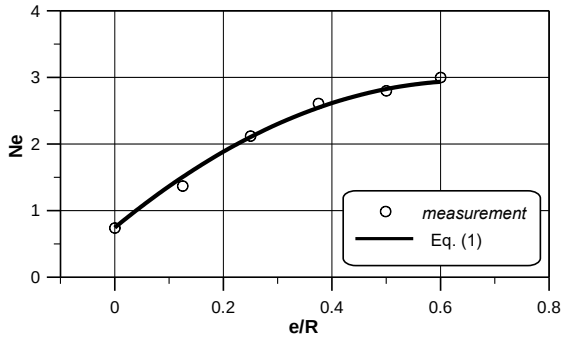

Fig. 6. The dependence $Ne = f(e/R)$ for the unbaffled stirred tank with the Rushton turbine

4. Conclusions

Displacement of the shaft from tank axis towards the wall causes the formation of the vortex in the field between tank wall and the impeller shaft (Fig. 2b). Low rotational speed characterises the presence of vortex in the upper part of the tank, bellow the liquid surface. With a rotational speed increase, the vortex reaches closer into the bottom of the tank and at a sufficiently rate of rotation reaches the impeller blades. The increase of eccentricity changes the location of the forming vortex, which moves toward the tank wall. Equally, higher eccentricity corresponds to a higher vortex inclination to the vertical axis of the tank. For $e = 0{,}5R$ eccentricity, the inclination is 29°±4°. No changes of the vortex inclination due to rotational speed were observed.

Based on the results of the measurement of the mean flow velocity, it can be stated that for mixing with eccentrically positioned impeller, the flow pattern is not axisymmetric as it is for central position of the impeller. The largest values of the radial component occur in the vortex area from impeller blades towards the top of the vessel. At the area where the impeller is closest to the vessel wall, the velocity profile changes due to the impeller discharge stream-wall interaction.

According to analysis of changes in eccentricity ($e = 0 \div 0{,}5R$), it can be concluded that the power number Ne for mixing with eccentrically located impeller in the unbaffled stirred tank is always larger than for centric agitation ($Ne = 0{,}74$) and always lower than for conventional stirred vessel with baffles ($Ne = 3{,}75$).

The experimentally determined effect of the stirrer eccentricity ratio e/R on the power number Ne in the stirred tank without baffles and with the Rushton turbine describes equation (1). That correlation estimates that for radial pumping impeller, the impact of eccentricity on power number is a quadratic dependence.

S y m b o l s

d	impeller diameter, m,
D	tank inner diameter, m,

e	eccentricity, i.e., distance of the shaft from the vessel axis, m,
h	off-bottom clearance of the stirrer, m,
H	liquid height in the tank, m,
M	torque, N·m,
n	impeller rotational speed, s^{-1},
P	power consumption, W,
R	radius of the stirred tank, $R = D/2$, m,
U	mean velocity, $m \cdot s^{-1}$,
Ne	power number, $Ne = P/(n^3 d^5 \rho)$, –,
Re	impeller Reynolds number, $Re = (n \cdot d^{2} \rho)/\eta$, –,
η	dynamic viscosity of the liquid, Pa·s,
ρ	liquid density, $kg \cdot m^{-3}$.

References

[1] Kamieński J., *Mixing of multiphase systems*, WNT, Warszawa 2004 (in Polish).

[2] Wójtowicz R., Lipin A. A., *The computational-fluid-dynamics study of an unbaffled stirred vessel with eccentrically positioned impeller*, Technical Transactions, series Chemistry, vol. 17(1), 2015, 99-108.

[3] Rieger F., Ditl P., Novák V., *Vortex depth in mixed unbaffled vessels*, Chemical Engineering Science, vol. 34, 1979, 397-403.

[4] Ciofalo M., Brucato A., Grisafi F., Torraca N., *Turbulent flow in closed and free-surface unbaffled tanks stirred by radial impellers*, Chemical Engineering Science., vol. 51, 1996, 3557-3573.

[5] Talaga J., *Measurements of tutbulent-flow parametres in a stirred mixer*, Chemical and Process Engineering, vol. 22, 3E, 2001, 1387-1392 (in Polish).

[6] Galletti C., Brunazzi E., *On the main flow features and instabilities in an unbaffled vessel agitated with an eccentrically located impeller*, Chemical Engineering Science, vol. 63, 2008, 4494-4505.

[7] Montante G., Bakker A., Paglianti A., Magelli F., *Effect of the shaft eccentricity on the hydrodynamics of unbaffled stirred tanks*, Chemical Engineering Science, vol. 61, 2006, 2807-2814.

[8] Galleti C., Pintus S. Brunazzi E., *Effect of shaft eccentricity and impeller blade thickenes on the vortices features in an unbaffled vessel*, Chemical Engineering Research and Design, vol. 87, 2009, 391-400.

[9] Karcz J., Cudak M., Szoplik J., *Stirring of a liquid in a stirred tank with an eccentrically located impeller*, Chemical Engineering Science, vol. 60, 2005, 2369-2380.

[10] Karcz J., Cudak M., *An effect of the type of an eccentrically located impeller on the efficiency of heat transfer process*, In Proceedings of the 12th European Conference on Mixing, 27-30 June 2006, Bologna, Italy, 727-734.

TECHNICAL TRANSACTIONS | CZASOPISMO TECHNICZNE
MECHANICS | MECHANIKA
2-M/2016

STANISLAV RUDOBASHTA[*], GALINA ZUEVA[**], VJACHESLAV DMITRIEV[***]

THEORETICAL AND EXPERIMENTAL BACKGROUNDS OF OSCILLATING INFRARED DRYING DISPERSED MATERIALS

TEORETYCZNE I EKSPERYMENTALNE PODSTAWY OSCYLACYJNEGO SUSZENIA PROMIENNIKOWEGO MATERIAŁÓW SYPKICH

Abstract

The research on the influence of the initial moisture content of seeds, of the duration of IR drying, of temperature regime on the effect of stimulation and keeping the effect with time, was carried out. A mathematical model for the dynamics of heating a seed layer, taking into account the moisture evaporation, is developed. Paper presents experimental data on mass conductivity properties for a dried layer of seeds, the recommendations for process equipment design are given.

Keywords: drying, kinetic calculation, zone method, dispersed materials

Streszczenie

W pracy analizowano wpływ początkowej zawartości wilgoci w nasionach, czasu trwania suszenia IR oraz zakresu temperatur na stymulację jakości nasion oraz utrzymywanie efektu stymulacji. Zaproponowano model matematyczny dynamiki ogrzewania warstwy nasion uwzgledniający odparowanie wilgoci. Przedstawiono dane eksperymentalne przewodności masowej dla warstw suszonych nasion oraz wytyczne projektowania urządzeń.

Słowa kluczowe: suszenie, obliczenia kinetyczne, metoda strefowa, materiały sypkie

DOI:

[*] Prof. PhD. Stanislav Rudobashta, Department of Heat Engineering, Hydraulics and Enterprises Energy Supply, Russian State Agrarian University.

[**] Prof. PhD. Galina Zueva, Department of Higher and Applied Mathematics, Ivanovo State University of Chemistry and Technology.

[***] Prof. PhD. Vjacheslav Dmitriev, Department of Security and Legal Order, Tambov State Technical University.

1. Introduction

Infrared drying of various materials is frequently used in practice [1-4], thus for drying heat-sensitive materials in order to prevent overheating, an oscillating mode in temperature must be used. It was found in [5] that the oscillating IR drying of the vegetable seeds carried out under conditions of the temperature range from t_{min} = 34°C till t_{max} = 40°C causes significant seeds stimulation. Research on the influence of the initial moisture content of seeds, of the duration of the IR drying on the effect of stimulation, were carried out in [6], as well as the research on keeping with time the stimulating effect. The mathematical model, which allows to calculate the dynamics of the heating material layer irradiated by an oscillating electromagnetic field – taking into account the evaporation of moisture from it is developed in [7], numerical experiments to study on the basis of the model the influence of technological parameters on the dynamics of layer heating are carried out in [8, 9]. They showed the possibility of the model in the organisation of the drying process. The calculations have been done in [8, 9] for a monolayer of seeds, but with mass conductivity data for isolated seeds. However, to reduce the size of the dryer for oscillating IR drying, the seeds must be dried in the bed. There are no data on mass conductivity of seeds in a layer, so the aim of this work is to obtain experimental data on mass conductivity of seeds in a layer, to describe these data with a function of moisture content and temperature of material, to compare the results for a layer with the data on mass conductivity of individual seeds, to develop an engineering method for calculating the kinetics of seeds oscillating infrared drying using these data and to calculate the industrial machine on its base.

2. Experimental study of seed layer mass conductivity

The mass conductivity of a seed layer was investigated with the zonal method – by receiving the drying curves with the exclusion of external diffusion resistance, and their processing by the method of splitting into a number of concentration zones and defining the value of mass conductivity coefficient for each of them by the solution of a linear differential equation of mass conductivity in a regular process mode. Drying curves were obtained when the drying agent (air) at velocity of 5 m/s had three different temperatures: 40, 50 and 60°C. As the object of the study "Stuttgarter Risen" onion seeds have been chosen because there are data on mass conductivity for a single seed, which could be compared to the results of the research.

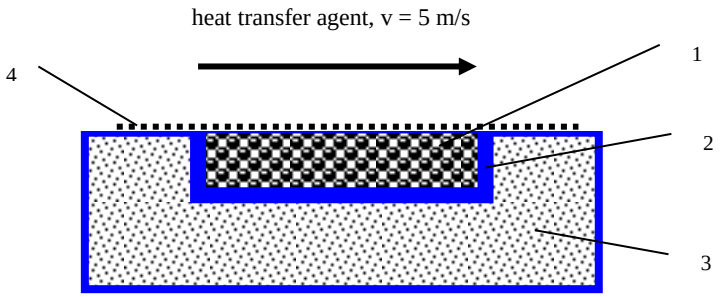

Fig. 1. Measuring cell for studying the kinetics of drying the seed layer
1 – layer of seeds; 2 – cell; 3 – thermal insulation; 4 – mesh

The measuring cell was designed as a cell filled with seeds, 5 mm high and 50 mm in diameter, situated in a substrate of foamed polyurethane (Fig.1).

The top layer was covered with a thin brass mesh (wire thickness of 0.12 mm, cell size of 1.5 mm), which prevents seeds from being blown-off by the air flow. A single "Stuttgarter Risen" onion seed is a limited cylinder with a diameter d = 1.7 mm and a length l = 0.9 mm (equivalent diameter d_{eq} = 1.57 mm). Thermocouples HC with 0.08 mm diameter electrodes were placed into three seeds, which measure the changes in seeds' temperature while drying. The seeds with embedded thermocouples were placed in three basic layers: the upper, middle and lower (bottom layer) (Figure 2.).

A measuring cell was placed into a working chamber of a dryer (Fig. 1), which was an air thermostat with air circulating inside it and driven by a fan. Air in the thermostat is dried by means of silica gel, which allowed to maintain a low moisture content that is close to zero. The set-up was equipped with an electric air heater, with TRM202 temperature regulators working HC with thermocouple. The air temperature was measured and maintained with an accuracy of ±0.1°C. A layer weight in the drying process was measured by AB 210-01 EDO electronic balance with accuracy of 1 mg cell without extraction of cell with seeds from a drying chamber, measuring time should not exceed 10 seconds.

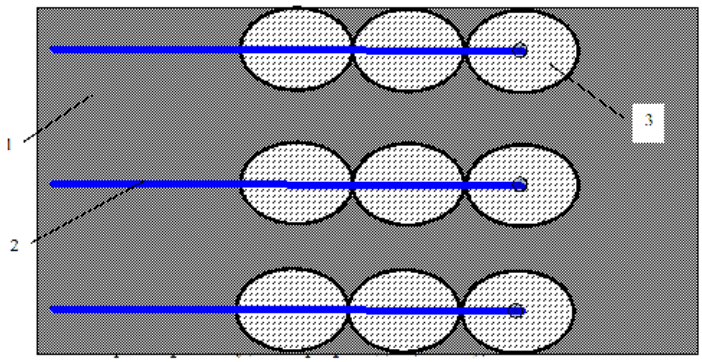

Fig. 2. The layout of thermocouples in the layer of seeds:
1 – a layer of seeds; 2 – thermocouple; 3 – seed

The analysis of drying curves of onion seed layer, obtained at different air velocities, showed that at velocity of 5 m/s external diffusion resistance is completely eliminated and the drying process is limited by the internal diffusion resistance, which makes it possible to determine the dependence of the mass conductivity ratio on the seeds' moisture content from drying curve by zonal method [10].

Fig. 3 illustrates the drying curves obtained when the velocity of the drying agent is 5 m/s, and Fig. 4 shows the experimental heating thermogram of elementary layers of seeds, obtained for drying agent at 50°C (at other temperatures of the drying agent, they have a similar form).

Consideration of the thermograms allows to come to two conclusions: 1) the temperature in each layer varies throughout the process of drying, so the drying is characterised by non-isothermal internal mass transfer; 2) heating curves for different

elementary layers of a material, despite the small thickness of the entire layer (5 mm), differ substantially. The values of mass conductivity coefficient k, m^2s^{-1} according to each concentration zone were calculated by a zonal method using drying curves, shown in Fig. 3 [10]. The changes in the value of the mass conductivity coefficient during the process calculated by zones are shown in Fig. 5.

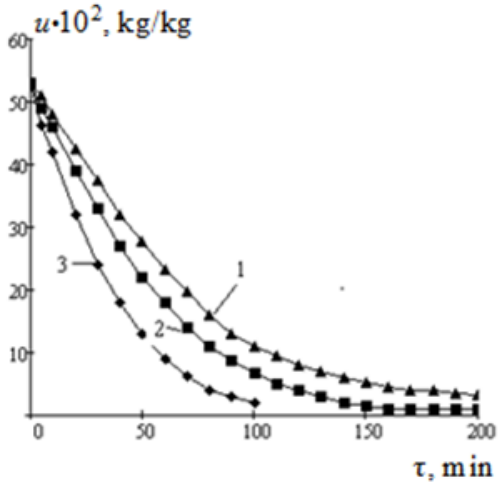

Fig. 3. The convective drying curves of a wet dense layer of "Stuttgarter Risen" onion seeds $u \cdot 10^2$, kg/kg (air velocity 5 m/s; 1 – $t_{d.a}$ = 40°C; 2 – $t_{d.a}$ = 50°C; 3 – $t_{d.a}$ = 60°C)

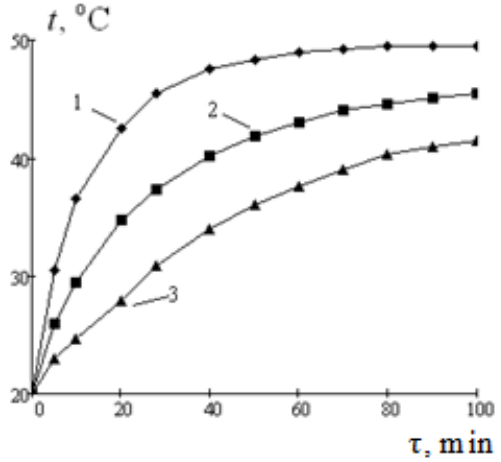

Fig. 4. Heating thermograms of elementary seeds layers at $t_{d.a}$ = 50°C:
1 – top layer; 2 – middle layer; 3 – bottom layer

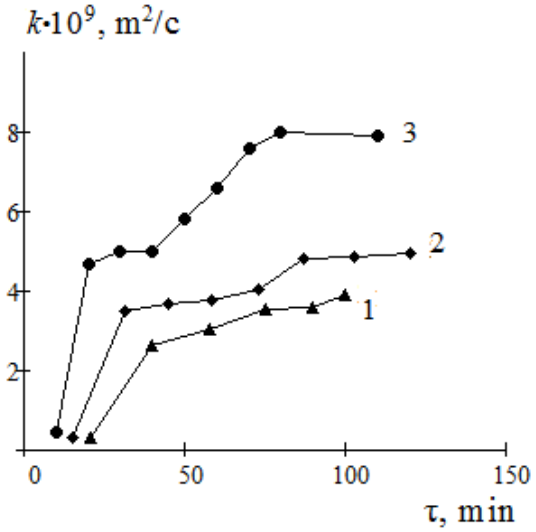

Fig. 5. Changing with time mass conductivity ratio while drying at air temperature:
1 – 40°C; 2 – 50°C; 3 – 60°C

3. The analysis and mathematical processing the data obtained

Examination of Fig. 5 allows to conclude the following: 1) the mass conductivity coefficient *k* changes significantly during drying, thus the calculation of drying kinetics at a constant value of *k* would result in significant errors in the determination of the drying time (estimation error arising from negligence of the change is given in [10]); 2) change in the coefficient k in the investigated drying process is due to its dependence on both moisture content and the temperature, but the effect of temperature on the coefficient k prevails over the effect of moisture, so the mass conductivity coefficient increases as the temperature of the seeds rises while drying; 3) coefficient *k* has the order of 10^{-9}, while its order is equal to 10^{-11} in drying single seed [11]. The difference in orders of mass conductivity coefficient while drying a unit seed and a seed layer is caused by the fact that during drying, a layer of vapour diffusion in areas between individual seeds plays an important role, while in a unit seed drying, vapour diffusion in spaces between individual seeds as a type of mass transfer is absent.

Since the mass conductivity coefficient *k* as the physical parameter is a function of the moisture content and temperature of the material $k = f(u,t)$, it is advisable in experimental data obtained for this coefficient to untie affecting parameters, thus it gives an opportunity to present this coefficient as a physical quantity, and not as a regime parameter, and to use it for engineering calculations. This problem was solved with the use of multidimensional (two-dimensional) function approximation procedures using the Cobb-Douglas model in the MATHCAD system [12]. As a result, the following functional dependence of the mass conductivity on the moisture content and temperature of the material was obtained, which

can be used in the calculation of convective drying kinetics of a dense layer of "Stuttgarter Risen" onion seeds, blown over the surface

$$k = a_0 \cdot u^{a1} \cdot t^{a2} \cdot f(t_{d.a}/50), \tag{1}$$

where

$$a_0 = 4.12 \cdot 10^{-15};\ a_1 = 6.19 \cdot 10^{-2};\ a_2 = 3.73;$$

$$f(t_{d.a}/50) = 9.59 - 15.15 \cdot (t_{d.a}/50) + 6.50 \cdot (t_{d.a}/50)^2;$$

t – temperature of the material, °C,

$t_{d.a}$ – temperature of drying agent, °C,

U – local moisture content, kg/(kg of dry material).

Equation (1) was used to calculate the drying kinetics of onion seed layer during oscillating IR drying at layer thickness h = 5 mm, at oscillation of seeds' temperature between t_{min} = 34°C to t_{max} = 40°C, at continuous blowing of the seeds' surface by atmospheric air with temperature $t_{d.a}$ = 20°C. The calculation is performed under the condition that the temperature of the material to be dried is constant and equal to $t = (t_{min} + t_{max})/2 = (34° + 40°)/2 = 37°C$. The results of calculation and their comparison with experimental drying curve are shown in Fig. 6.

As it can be seen in the figure, the calculation of the drying curve using data on mass conductivity described by equation (1) gives a satisfactory agreement with the experiment. The same figure shows the comparison between experimental and calculated drying curves for a monolayer of onion seeds, in this calculations data on mass conductivity for individual seeds, shown in [11] are used. In this case, the calculated and experimental drying curves have satisfactory agreement, and the drying curve for a monolayer of seeds passes, as would be expected, more steeply than for the layer.

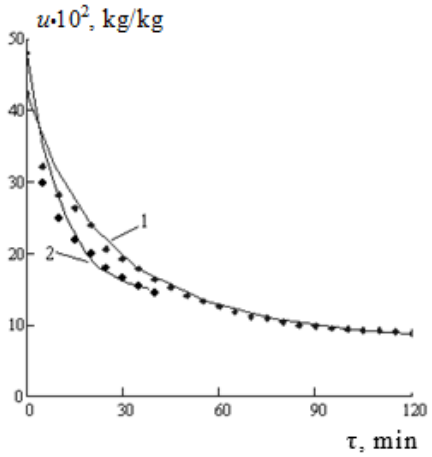

Fig. 6. Comparison of experimental and calculated drying curves of "Shtutgarer Risen" onion seeds at oscillating infrared energy supply (the line – calculation, points - experiment):
1 – dense blown layer; 2 – monolayer; t_{min} = 34°C; t_{max} = 40°C, $t_{d.a}$ = 20°C.

4. Recommendations for hardware design of oscillating infrared seeds drying and kinetic calculation of the process

The studies performed have shown that the data on mass conductivity of seeds in a layer are reliable and can be used for calculating drying kinetics. The absence of oscillations in the moisture content of seeds on the drying curve in the oscillating seeds layer IR drying, carried out in the temperature range of the material t_{min} = 34°C ... t_{max} = 40°C (Fig. 6), suggest the possibility of calculating the kinetics of this process on the basis of the solution of mass conductivity differential equation written for layer blown up on the surface, under appropriate boundary conditions of the problem – using the data in terms of mass conductivity for a layer. The calculation methods are described in [10]. To implement this method in practice, is necessary to obtain data on the mass conductivity of dried seeds, which can be obtained in the same way as it was done in this work for onion seeds.

The infrared dryer for continuous oscillating infrared drying can be carried out on the basis of a typical conveyor dryer with IR emitters located over the dried material (e.g. based on a commercial IR dryer, such as an infrared belt dryer of Russian production model UTZ-4). Equipping a corresponding dryer by automatic control system will implement an oscillating mode of infrared drying. The technique of engineering kinetic calculation has been proposed for the apparatus of this type on the basis of a developed mathematical model, using the data of mass conductivity coefficient for a layer. The aim of the calculation is to determine the necessary residence time for the seeds in the apparatus, thus providing the specified productivity, and at the same time, it allows to find the device dimensions on the stage of its design.

References

[1] Ratti C., Mujumdar A. S., *Infrared drying*, in *Handbook of Industrial Drying*, 3-rd edition. A. S. Mujumdar (Ed), CRC Press, Boca Raton, FL. 2007.

[2] Mujumdar A. S. (Ed)., *Drying'92*, Proceedings of 8-th International Drying Symposium, Elsevier, Amsterdam, 1992, 667-729.

[3] Supmoon N., Noomhorm, A. *Influence of combined hot air impingement and infrared drying on drying kinetics and physical properties of potato chips*, Drying Technology, vol. 31(1), 2013, 24-31.

[4] Bon J., Kudra T,. *Enthalpy-driven optimization of intermittent drying*, Drying Technology, vol. 25 (4), 2007, 523-532.

[5] Rudobashta S. P., Grigoriev I. V., *Impulse infrared drying the seeds of vegetables, nontraditional and rare plants*, Industrial Heat Engineering, vol. 33 (8), 2011, 85-90 (in Russian).

[6] Rudobashta S. P., Zueva G. A.; Zuev N. A., S*eeds stimulation by oscillating infrared heat treatment*, Industrial Heat Engineering, vol. 35 (7), 2013, 218-222 (in Russian).

[7] Rudobashta S. P., Kartashov E. M., Zuev N. A., *Heat-and Mass Transfer in Drying in an Oscillating Electromagnetic Field*, Theoretical Foundations of Chemical Engineering, vol. 45 (6), 2011, 830-837.
[8] Rudobashta, S., Zueva G., Zuev N., *Mathematical Modelling and Numerical*, Analysis of Oscillating Infrared Seeds Drying Process, XIII Polish Drying Symposium, Kołobrzeg, 5-6 September, 2013, 1-6.
[9] Rudobashta, S., Zueva G., Zuev N., *Mathematical modeling and numerical simulation of seeds drying under oscillating infrared irradiation*, Drying Technology, vol. 32 (11), 2014, 1352-1359.
[10] Rudobashta, S. P., *Mass transfer in the solid phase systems*, Chemistry, Moscow 1980 (in Russian).
[11] Rudobashta S. P., Zueva G. A., Dmitriev V. M., Zuev N. A., *Mass conductivity when drying colloidal capillary-porous materials*, Proceedings of the Higher Educational Institutions. Chemistry and Chemical Engineering, vol. 57 (1), 2014, 103-107 (in Russian).
[12] Ohorzin V. A., *Applied mathematics in MATHCAD system*: Schoolbook, Lany, St. Petersburg 2009 (in Russian).

TECHNICAL TRANSACTIONS | CZASOPISMO TECHNICZNE
MECHANICS | MECHANIKA
2-M/2016

WIESŁAW SZATKO*, ŁUKASZ WAWSZCZAK**

WORK SAFETY INTERACTION ASSESSMENT OF VOC'S EMISSION UNDER EMERGENCY WORK OF IPPC INSTALLATION

OCENA ODDZIAŁYWANIA NA ŚRODOWISKO PRACY EMISJI LZO W WARUNKACH AWARYJNEJ PRACY INSTALACJI IPPC

Abstract

The study evaluated the impact of emissions (VOCs) as a result of the operation of the printing of plant at working positions of those performing their tasks outdoors or in buildings next door. The first part of the paper presents the general characteristics of the process and materials used for printing. The further part shows the results of the modelling of emissions, depending on the operating state of purification (emission in normal conditions and emission in failure state of the afterburner).

Keywords: *modelling of emissions, printing industry, heat-set rotary offset, working under emergency conditions, failure of afterburner*

Streszczenie

W pracy oceniono wpływ emisji zanieczyszczeń (LZO) przez zakład poligraficzny na stanowiskach pracy usytuowanych na wolnym powietrzu lub w budynkach sąsiadujących. Część pierwsza prezentuje charakterystykę procesu oraz materiałów wykorzystywanych do druku. W dalszej części przedstawiono wyniki modelowania emisji zanieczyszczeń w zależności od stanu pracy układu oczyszczającego (normalna praca oraz awaria dopalacza).

Słowa kluczowe: *modelowanie emisji zanieczyszczeń, przemysł poligraficzny, gorący offset rotacyjny (heat-set), praca w warunkach awaryjnych, awaria dopalacza*

DOI:

* Dr Wiesław Szatko, Institute of Thermal and Process Engineering, Faculty of Mechanical Engineering, Cracow University of Technology.
** MSc. Eng. Łukasz Wawszczak, Eco-HERA, Cracow.

1. Introduction

As part of this work, concentrations of pollutants in ambient air emitted during technological processes were calculated (based on the measurements of emissions of pollutants):

a) under normal conditions (operation of all equipment is compatible with the assumptions of technological process and the conditions, which are set out in the applicable decision – permission for the introduction of pollutants into the air (i.e. the integrated and sectoral permission)
b) during fault conditions of the thermal afterburner and emissions of emitters of emergency in accordance with the conditions, which are set out in the applicable decision – permission for the introduction of pollutants into the air (i.e. the integrated permission):
   - in the case of "normal weather conditions";
   - in the case of "very unfavourable weather conditions".

The publication presents a comparison of the calculated concentrations of pollutants in the air to the limit values for specific workplaces by the applicable Ordinance of the Minister of Labour and Social Policy with the maximum concentrations of pollutants.

2. The analysis in the context of emissions of dust and gas in various operating conditions of the flue gas purification

2.1. Research object

The object of the analysed company is printing activity. The installation that is classified as an IPPC installation (web offset machines) is covered by an integrated permission defined in the Regulation of the Minister of the Environment of the 27th of August 2014 on the types of installations, which may cause significant pollution of individual elements of nature or the environment as a whole (Journal of Laws of 2014 item 1169), i.e. installation for offset printing, classified as an installation for the surface treatment of substances, objects or products using organic solvents, solvent consumption of 150 kg per hour or more than 200 tonnes per year.

The plant area has an approximately rectangular shape with dimensions of 340×120 m. Other industrial plants outweigh in the vicinity of the plant. Wastelands, fields, meadows, groves, etc. prevail from the northern side. The nearest residential buildings (low, dispersed buildings) are located approximately 500 meters from the plant.

2.2. Emission of contaminants

Emission is the act of an operation, which involves the transfer of any element to its surroundings. Emission of contaminants to the environment involves the introduction of pollution (the products of human activity) to the environment, and in particular:

- substances (e.g. solid contaminants, liquid or gaseous contaminants),
- energy (e.g. noise, vibration, electromagnetic fields) to the air, water, soil or earth.

The definition of emission in ecological importance is given in the Act of the 27th of April 2001 on Environmental Protection Law. By emissions, legislator determines the introduction, directly or indirectly, of substances or energy, such as heat, noise, vibration and electromagnetic fields to the air, water, soil or earth as a result of human activity. Importantly, substances are chemical elements and their compounds, mixtures or solutions appearing in the environment or elements, which are the results of human activity. A hazardous substance is one or more substances or mixtures of substances, which, because of their chemical, biological or radioactive characteristics, in the event of improper handling, cause risk to the life or health of humans or the environment; a hazardous substance may be a raw material, product, intermediate waste, as well as a substance, which arises as a result of a failure.

The type and quantity of the introduced substances or energy at a given time and the concentration or levels of substances or energy, in particular in waste gases, sewage and waste generated, is defined as the amount of emissions.

In this paper, we analysed the emissions of solid, liquid and gas contaminants into the air. Emission unit is kg/h (or their derivatives – mg/s, Mg/year).

As a result of the emission of pollutants, the concentration of the pollutant increases in the air. This concentration is dependent on the amount of emissions, characteristics of the emitted gases, the emission process and mainly on the meteorological conditions. Distribution of concentrations of the contaminants in the air is called immission pollution, and the area under study – immission field. The unit of immission is $\mu g/m^3$, determined for the following conditions (temperature 293 K, pressure 101.3 kPa).

Table 1

The list of pollutants emitted into the atmosphere

No	Pollution
1	Benzene
2	Methylethylketon
3	Nitrogen dioxide
4	Sulphur dioxide
5	Ethylbenzene
6	Xylene
7	Sulphuric acid
8	entire dust
9	PM10 dust
10	PM2.5 dust
11	Styrene
12	Carbon monoxide
13	Toluene
14	aliphatic hydrocarbons
15	aromatic hydrocarbons

2.3. Types of emitted pollutants

All the pollution associated with both the functioning of the basic technological processes, as well as the auxiliary processes, were taken into account. The table below lists

all the contaminants identified in the measurements of emissions performed by specialised companies dealing with the measurement of emissions, as well as listed in material safety data sheets of used raw materials.

2.4. Legal requirements relating to the issue of emerging contaminants

The permissible concentrations of pollutants on the health requirements defined in the Regulation of the Minister of Labour and Social Policy of the 6th of June 2014 on the maximum permissible concentration and intensity of harmful factors in the work environment (Journal of Laws 2014/817 of the 23rd of June 2014) according to the above Regulation pursuant to Art. 228 § 3 of the Act of the 26th of June 1974 – Labour Code (Journal of Laws of 1998. No. 21, item 94, as amended):

§ 1.1. The values of maximum concentrations of chemicals and dust of harmful factors in the work environment are specified in the list attached as Annex 1 to the Regulation.

§ 2. The values referred to in § 1.1, determine the maximum permissible concentrations of harmful factors, determined as:

1) The maximum allowable concentration (MAC) – the value weighted average concentration, the impact on the employee during an 8-hour daily and average weekly working time, as defined in the Act of the 26th of June 1974 – the Labour Code, the period of its activity should not cause negative changes in the state of health and the health of the future generations;

2) The maximum instantaneous concentration (MIC) – average value of concentration, which should not cause negative changes in the health of the worker, whether in the workplace no longer than 15 minutes and not more than 2 times during a work shift, at an interval of less than 1 hour;

3) maximum threshold concentration (MTC) – the concentration that due to the risk of health or life of the employee cannot be exceeded in the work environment at any time.

Note the differences in the definition of pollution in the environmental protection legislation and the regulations on permitted values of contamination at workplaces.

2.5. Assumptions about the calculations of the spread of contamination

To realise this objective work, three variants (variant I variant IIA and IIB variant) were established, for which the analysis of the spread of pollutants was performed:

- Variant I – normal operation of all installations and equipment reducing emissions. In this variant of pollution, arising printing presses are collected in one conduit and carried to catalytic afterburner where they are burned. The purified exhaust gas is emitted into the atmosphere.
- Variant II – failure of the catalytic afterburner. In this variant of pollution, the arising printing presses are discharged by the individual emergency emitters to the atmosphere. There is no purification of impurities.

Due to the fact that the aim of the study was to determine the concentrations of pollutants in the grid of receptors and in free points, and as we know, this concentration

will be a function of the emission and meteorological conditions, two variants: IIA and IIB variant were separated for the second variant.

- Variant IIA is characterised by normal meteorological conditions.
- Variant IIB is characterised by very bad weather.

Thus, the size of the air pollution will vary discretely;

- the lowest contamination to the conditions described in Option I, which will occur approximately 75% of the time during the year,
- high contamination for conditions described in Variant IIA, which will be present to 7.5% of the time during the year,
- very high contamination for conditions described in the variant IIB, which will occur to 2.5% of the time during the year,
- lack of contamination, when the system does not work – about 15% per year.

Normal meteorological conditions mean meteorological data containing meteorological statistics for given area and the different seasons (winter, summer and year).

The nuisance of sources of emissions to the environment depends, to a large extent, on meteorological parameters, of which the most important are: speed and wind direction, the equilibrium of the atmosphere, the air temperature and precipitation. Factors affecting speed and intensity of the spread of contamination are: atmospheric stability conditions characterised by the possibility of atmospheric diffusion and the frequency and speed of the winds. There are 6 classes of atmospheric stability, and 36 found in the atmosphere of a combination of equilibrium states and wind speed.

- Class I – highly unstable,
- Class II – moderately unstable,
- Class III – weak instability,
- Class IV – indifferent balance,
- Class V – poor durability,
- Class VI – constant and firmly fixed equilibrium,

The occurrence of class balance I ÷ III proves favourable dispersion (taking out the emissions outside the region of their emittance). The occurrence of states V and VI proves unfavourable spread of contamination and the possibility of their concentration in the area of emissions.

Class IV is an indifferent class, but its occurrence while large wind speed favours a beneficial spread of contamination.

Due to the fact that computer programs used for modelling the emission calculate the distribution of contaminants for the annual meteorological values, there was no possibility to introduce in the program the conditions, which occurred in the small amount of time (about several to several tens of hours). For this reason, when trying to grasp the impact of very adverse weather conditions, after a full analysis of the data resulting from our own research and literature data, it was found that it is possible to do this indirectly by increasing the size of the emission with the ratio, which presents the hindered spread of pollutants in the air.

2.6. Tables of distribution of concentrations of selected pollutants around the premises

Distribution maps of concentrations of individual pollutants (according to Polish reference methodology for performing the analysis) were made on the basis of knowledge of the emission of pollutants (developed on the basis of measurements carried out by an accredited laboratory). The results in the following tables allow you to determine where the greatest concentration of major pollutants is in the vicinity of the plant and to compare them with the maximum concentrations of pollutants in the workplace:

Working conditions in offices

Table 2

Working conditions – normal operation of afterburner

No	No*	Pollution	MAC µg/m^3	STEL µg/m^3	Maximum concentration µg/m^3	The ratio of maximum concentration to MAC
1.	1	The dust containing free silica >50 % inhalable fraction	**2 000**	**---**	***8,175*** **11,443**	***0,0041*** **0,0057**
2	1	The dust containing free silica >50 % respirable fraction	**300**	**---**	***8,175*** **11,443**	***0,0272*** **0,0381**
3	37	Benzene	**1600**	**---**	***1,817*** **1,650**	0,0011 **0,0010**
4	448	Styrene	**50 000**	**100 000**	***0,871*** **0,780**	***0,0001*** **0,0001**
5	67	Methylethylketon	**450 000**	**900 000**	***9,918*** **17,021**	***0,0001*** **0,0001**
6	220	Ethylbenzene	**200 000**	**400 000**	***0,919*** **0,841**	***0,0001*** **0,0001**
7	301	Xylene	**100 000**	**---**	***1,530*** **1,412**	***0,0001*** **0,0001**
8	479	Toluene	**100 000**	**200 000**	***1,282*** **1,174**	***0,0001*** **0,0001**
9	188	Nitrogen dioxide	**700**	**1500**	***68,840*** **157,177**	***0,0983*** **0,2245**
10	190	Sulphur dioxide	**1300**	**2700**	***8,925*** **6,902**	***0,0069*** **0,0053**
11	320	Sulphuric acid	**50**	**---**	***0,110*** **0,074**	***0,0022*** **0,0015**
12	475	Carbon monoxide	**23 000**	**117 000**	***202,712*** **172,499**	***0,0088*** **0,0075**
13	---	aliphatic hydrocarbons	---	---	***24,586*** **21,915**	---
14	---	aromatic hydrocarbons	---	---	***11,277*** **10,055**	---

Table 3

Operating conditions: failure of afterburner – favourable weather conditions

No	No*	Pollution	MAC µg/m^3	STEL µg/m^3	Maximum concentration µg/m^3	The ratio of maximum concentration to MAC
1.	1	The dust containing free silica >50 % inhalable fraction	**2 000**	---	***8,194*** **9,706**	***0,0041*** **0,0048**
2	1	The dust containing free silica >50 % respirable fraction	**300**	---	***8,194*** **9,706**	***0,0273*** **0,0323**
3	37	Benzene	**1600**	---	***22,951*** **16,859**	***0,0143*** **0,0105**
4	448	Styrene	**50 000**	**100 000**	***24,305*** **17,868**	***0,0005*** **0,0004**
5	67	Methylethylketon	**450 000**	**900 000**	***9,938*** **17,221**	***0,0001*** **0,0001**
6	220	Ethylobenzene	**200 000**	**400 000**	***24,337*** **17,911**	***0,0001*** **0,0001**
7	301	Xylene	**100 000**	---	***40,406*** **29,585**	***0,0004*** **0,0003**
8	479	Toluene	**100 000**	**200 000**	***34,174*** **25,020**	***0,0004*** **0,0003**
9	188	Nitrogen dioxide	**700**	**1500**	***146,415*** **236,042**	***0,2092*** **0,3372**
10	190	Sulphur dioxide	**1300**	**2700**	***10,987*** **8,799**	***0,0084*** **0,0068**
11	320	Sulphuric acid	**50**	---	***0,110*** **0,074**	***0,0022*** **0,0015**
12	475	Carbon monoxide	**23 000**	**117 000**	***210,548*** **180,460**	***0,0091*** **0,0078**
13	---	aliphatic hydrocarbons	---	---	***700,524*** **514,828**	---
14	---	aromatic hydrocarbons	---	---	***321,060*** **235,955**	---

Table 4

Operating conditions: failure of afterburner – adverse weather conditions

No	No*	Pollution	MAC µg/m^3	STEL µg/m^3	Maximum concentration µg/m^3	The ratio of maximum concentration to MAC
1.	1	The dust containing free silica >50 % inhalable fraction	**2 000**	---	*8,220* **9,709**	*0,0041* **0,0048**
2	1	The dust containing free silica >50 % respirable fraction	**300**	---	*8,220* **9,709**	*0,0274* **0,0323**
3	37	Benzene	**1600**	---	*78,976* **50,401**	*0,0494* **0,0315**
4	448	Styrene	**50 000**	**100 000**	*84,308* **53,688**	*0,0017* **0,0011**
5	67	Methylethylketon	**450 000**	**900 000**	*9,952* **17,454**	*0,0001* **0,0001**
6	220	Ethylobenzene	**200 000**	**400 000**	*84,340* **53,714**	*0,0001* **0,0001**
7	301	Xylene	**100 000**	---	*140,024* **89,177**	*0,0014* **0,0009**
8	479	Toluene	**100 000**	**200 000**	*118,450* **75,438**	*0,0012* **0,0007**
9	188	Nitrogen dioxide	**700**	**1500**	*429,360* **361,463**	*0,6134* **0,5164**
10	190	Sulphur dioxide	**1300**	**2700**	*17,298* **11,643**	*0,0133* **0,0090**
11	320	Sulphuric acid	**50**	---	*0,124* **0,086**	*0,0025* **0,0017**
12	475	Carbon monoxide	**23 000**	**117 000**	*218,732* **189,409**	*0,0095* **0,0082**
13	---	aliphatic hydrocarbons	---	---	*2430,695* **1547,808**	---
14	---	aromatic hydrocarbons	---	---	*1114,013* **709,378**	---

The results for office space in the building number 1 are presented by the green colour (italics), while the results for office space in building number 2 are presented by the blue colour.

3. Conclusion

1. The amount of pollutant concentrations at workplaces (points free) is dependent on the emission of pollutants.
2. An increase in the concentrations of pollutants, which are burnt by the afterburner in the event of a failure of the afterburner and adverse weather conditions, is 10,000% (assuming normal operation of the afterburner for 100%).
3. The size of the concentrations in free points is the smallest at the normal operation of the afterburner and the largest in the failure of afterburner and adverse weather conditions,
4. The volume of concentrations in free points is the lowest for the level of an area ($Z = 0$) and increases with the increasing Z and reaches maximum values at $Z = 11$ m.
5. The analysed work of the plant does not pose a threat to life and health of office workers; however during the failure of the afterburner, temporarily onerous conditions may occur, but they are not harmful.
6. It should be noted that the exposure limits for the workplace environment are about 1,000 times higher than those resulting from environmental regulations. For this reason, the STEL and TWA are expressed in mg/m^3, while the reference values are set out in the environmental protection legislation in $\mu g/m^3$.

TECHNICAL TRANSACTIONS | CZASOPISMO TECHNICZNE
MECHANICS | MECHANIKA
2-M/2016

MAŁGORZATA ŚRODULSKA-KRAWCZYK[*], JERZY ROSIŃSKI[**]

WET DUST COLLECTION IN SUB-ZERO TEMPERATURES

ODPYLANIE MOKRE W TEMPERATURACH UJEMNYCH

Abstract

The results of experimental studies confirm the suitability of non-freezing liquids for use as dust collecting liquids in equipment working at low temperatures. Based on the completed studies, the hypothesis regarding the impact of liquid viscosity on the effect of releasing the surface collecting the dust particles and, therefore, on the efficiency of the dust collection process cannot be clearly verified. Decreasing the efficiency of dust collection correlated with the increase of liquid viscosity is likely an effect of changing the conditions for the formation of liquid dust collectors.

Keywords: wet dedusting, dedusting efficiency, dedusting in sub-zero temperatures

Streszczenie

Wyniki badań eksperymentalnych potwierdzają przydatność płynów niezamarzających do wykorzystania urządzeniach pracujących w niskich temperaturach. Hipoteza dotycząca wpływu lepkości cieczy na uwolnienie powierzchni wychwytu cząstek pyłu, a w związku z tym skuteczność procesu odpylania nie może być jednoznacznie zweryfikowana. Zmniejszenie skuteczności odpylania związane ze wzrostem lepkości cieczy może być efektem zmiany warunków tworzenia ciekłych kolektorów.

Słowa kluczowe: mokre odpylanie, skuteczność odpylania, odpylanie w temperaturach ujemnych

DOI:

[*] Chair of Chemical and Process Engineering, Faculty of Chemical Engineering and Technology, Cracow University of Technology.

[**] Department of Industrial Apparatus, Institute of Thermal and Process Engineering, Cracow University of Technology.

The operation of wet dust collection equipment, especially periodic operation, in sub-zero temperatures is problematic and expensive. It requires the use of additional equipment, maintaining an above-zero temperature within the unit or the use of non-freezing liquids for dust collection. The literature regarding wet dust collection lacks the assessment of possibilities and results of tests in the field of dust collection from gas using non-freezing liquids. Despite the fact that the proposed method is expensive, it should be mentioned that in certain conditions, it may be the only solution available. This pertains in particular to the equipment located outside buildings and operating in winter conditions. This equipment, frequently for the lack of indoor installation, operates directly adjacent to industrial systems. Often, their function is a short-term, periodic operation in case of system failure. It is, therefore, vital to maintain their permanent stand-by status by the use of types of liquids, which do not freeze in sub-zero outdoor temperatures as the dust collecting liquid.

In the process of operation, the temperature of the collection liquid can be changed in the course of direct contact heat exchange inside the unit. Temperature changes are accompanied by alterations in the physical properties of the dust collection liquid, in particular – viscosity.

There are no descriptions of theoretical or experimental studies determining the effect of the viscosity of the dust collection liquid on the efficiency of the dust collection process. The reason seems to be the fact that water is the most prominent dust collection liquid and the units most frequently operate in stable temperature conditions.

Discussions substantiating the possibility of the effect of liquid viscosity on the efficiency of the dust collection process can be related both to the analysis of basic mechanisms affecting the deposition of particles on liquid collectors and the conditions of generating said collectors. The transmission of dust particles from gas to the liquid occurs for the most part as a result of inertial effects, catching effect and diffusion. Dust particles are separated in liquid collectors – depending on the type of the wet dust collector: droplets of liquid moving in a stream of aerosol, layers of liquid formed in the unit, surfaces of gas bubbles formed in the barbotage process or wet surfaces of the walls of the unit. One of the tendencies in the development of wet dust collection systems is the introduction of intensive operation units with a large gas phase flow capacity, which would entail an advantageous decrease in the size of the units. In these cases, due to the high relative velocity of the gas and liquid phases, the inertial and direct catching mechanisms have a decisive impact on the dust collection process.

The Warych's monograph [1] contains an extensive description of individual mechanisms on the dust particles deposition on liquid collectors. Descriptions of the mechanisms and their impact on the efficiency of the dust collection process can be found in virtually all monographs, e.g. Warych's [2] or Löffler's [3] addressing the issues of wet dust collection from gas. The literature assigns less significance to the description of the conditions of the generation of liquid collectors and their impact on the efficiency of the dust collection process.

When discussing the mechanism of inertial effects independent from the dust collector, it is generally assumed that in the case of hydrophilic dusts, dust contact with the surface of the liquid is equal to immediate absorption of the dust by the liquid and therefore – immediate release and renewal of the liquid surface for further collisions. In the case of hydrophobic (poor wettability) dusts, the time required for the absorption of the particle by

the liquid may be longer than the time after which the next particle comes into contact with the surface of the liquid. The reduction of the dust collection capacity of the liquid is therefore probable – due to the deflection of the particle approaching the surface of the liquid from the deposited particle. This effect can be considered particularly probable because, in the wet dust collection conditions, more dust collides with each liquid surface element than is required to coat the surface once. Therefore, the rate of particle absorption can be critical in the efficiency of the dust collection process [4]. The rate of particle absorption can be affected not only by the energy required to overcome the surface tension forces, but also the velocity of the particle in a liquid medium, depending on its viscosity.

The efficiency of the dust collection process can be correlated [4] with the rate of binding of dust and liquid, defined as the mass m_s penetrating the liquid surface unit A into the liquid as a result of the collision of dust particles with the surface in a unit of time:

$$r = \frac{m_s}{A \cdot \tau} \tag{1}$$

The rate of binding of dust and liquid depends on the physical and chemical properties of the dust and its susceptibility to wetting, physical and chemical properties of the gas and the dust collection liquid as well as the concentration of the aerosol. In order to verify his hypothesis, Kabsch [4] carried out studies regarding the effect of aerosol concentration on the rate of binding of dust and liquid. The increase in the concentration of dust in gas resulted in an increase of the rate of binding; however, to a lesser degree than would result from linear relationship.

The hypothesis that wettability is significant in the case of inertial particle deposition and rate of penetration of the liquid seems to be justified. The confirmation is the Weber's experiment [5] – shooting 1 mm water droplets with glass and silicone balls. Wettable dust balls immediately penetrated inside the droplets, silicone balls accumulated on the surface.

The analysis of basic wet dust collection models by Semrau, Barth and Calvert [3], no effect of the viscosity of the suspension on the dust collection process was found. Pemberton [6] found that in the case of deposition of particles with poor wettability on droplets, their penetration inside the liquid is necessary and their movement in the liquid is determined by Stokes' law. The rate of movement depends on the medium resistance coefficient and also the dynamic liquid viscosity index. The efficiency of dust particles deposition on droplets as a result of the simultaneous effects of three mechanisms – inertial, impaction, interception and diffusion – is described by a semi-empirical Slinn's formula [7], taking into account the relation between liquid viscosity and gas viscosity.

It is generally believed that there is a specific droplet diameter [8], for which optimum conditions are achieved for the deposition of specific size dust particles, and the efficiency of dust particles deposition on the droplet quickly decreases together with the decrease in particle size.

Upon their analysis of the circulating dust collector operation, Jarzębski and Głowiak [9] found that the inertial dust collision with water droplets is key to the dust collection process. The efficiency of dust particles deposition decreases with the increase in the size of droplets generated in the deposition area. In the case of droplet population with compressed air, the size of the droplets is determined by the Nukijama and Tanasawa formula [10], which indicates that droplet size is positively correlated with the viscosity of the liquid

phase. An increase in the viscosity can therefore result in a decrease of the dust collection efficiency.

The height of the dynamic foam layer created in the dust collection at a given relative difference between the gas and liquid phase velocities is reduced with the increase in the liquid viscosity [11], resulting in decreasing effectiveness of the dust collection system.

It should follow that a similar effect also applies to the layer of intensive barbotage and the droplet–splash layer often occurring in dust collection systems.

In summary, it can be said that the literature describes cases, which could warrant conclusions regarding the effect of liquid viscosity on the efficiency of the dust collection process. This effect can be observed when considering the inertial effects as well as variables, together with the change in viscosity, generation conditions and sizes of the created collectors.

Since, in the case of wet dust collection in intensive operation units, the inertial mechanism is key to the efficiency of the process, it was decided to conduct model tests on a modified circulating system. The construction of the model unit was simplified compared to classic circulating dust collectors. The two-chamber structure was abandoned, the "dirty" chamber was included in the guide channel. In this case, all dust particles are captured in one unit volume. The separation of dust particles in the unit occurs on droplets generated in the guide, in the intensive barbotage zone formed near the aerosol outlet from the guide, on the wetted surfaces of the guise, in the layer of liquid flowing from the guide (water curtain) and in the droplet-splash layer. In the conditions of developed unit operation, there is a possibility of generating almost all types of liquid collectors occurring in wet dust collection processes.

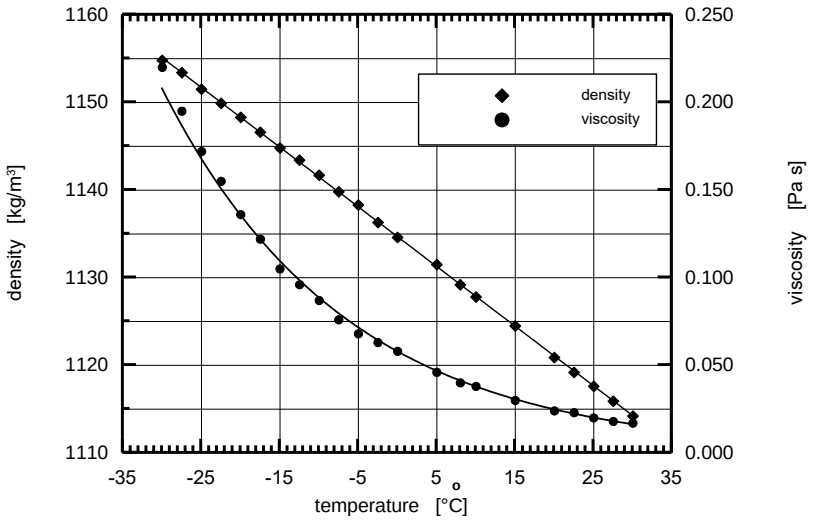

Fig. 1. Relationship between density / non-freezing liquid dynamic viscosity index and temperature

The tests were conducted using a non-freezing liquid with viscosity strongly reacting to changes in the temperature. The relationship between density / non-freezing liquid dynamic

viscosity index and the temperature is presented in the diagram – figure 1. Due to the high dynamic viscosity, the liquid was mixed with water in a 1:1 ratio. This decreased the dynamic viscosity of the solution, which in the temperature range of: - 10°C to 15°C changed between 0.004 and 0.00081 Pa·s. At this concentration, the crystallisation temperature for the liquid is - 37°C, which is important for use in actual industrial conditions.

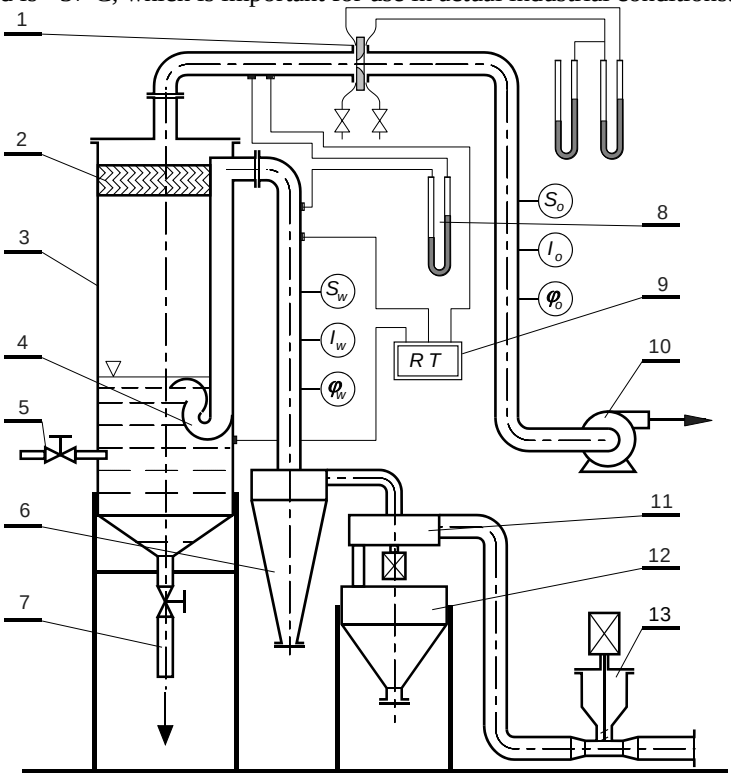

Fig. 2. Testing unit setup
1 – measuring orifice, 2 – liquid trap, 3 – rotoclone, 4 – guide, 5 – water supply, 6 – sorter discharge cyclone, 7 – suspension discharge from the rotoclone, 8 – measurement of the pressure drop on the rotoclone, 9 – thermometer, 10 – exhaust fan, 11 – sorter, 12 – tank for oversize particles separated in the sorter, 13 – dust batcher, S_w, S_o – dust concentration measurement system, I_w, I_o – grade composition measurement system, φ_w, φ_o – gas moisture content measurement system

A testing unit presented in figure 2 was constructed in order to conduct the tests. The main component of the unit is the rotoclone–type circulating dust collector /3/. The aerosol was created by introducing dust to the inlet pipeline with a batcher /13/. The application of a batcher with efficiency adjustment enabled the creation of the desired dust concentration on the dust collector inlet. Since talc was used as test dust, a pneumatic sorter /11/ was installed on the inlet pipeline to stop dust grades over 20 μm. The dusty gas travelled via the inlet pipeline through the guide /4/ into the process area of the unit. From there, purified gas was exhausted by the outlet pipeline, through the liquid trap /2/. The flow of the gas

was generated by the exhaust fan /10/, its expenditure was measured by a quadrant measuring orifice /1/. The expenditure of the gas flowing through the system was adjusted by changing the amount of "false" air introduced to the pipeline directly before the exhaust fan. A pressure gauge /8/ enabled the measurement of the drop in the pressure of gas flowing through the unit and the thermometer /9/ indicated the temperatures of gas in inlet and outlet pipelines as well as the temperature of liquid in the unit. Similar system for the measurement of dust concentration /S_w, S_o/, grade composition /I_w, I_o/ and gas moisture content /φ_w, φ_o/.

The overall efficiency of the dust collection process was calculated based on the measurements of dust concentrations in specific cross-sections of the inlet and outlet pipelines. The concentrations both in the inlet and outlet pipelines were determined based on the collected gas samples from which the dust was separated through filtration.

In order to determine the grade-based efficiency of the dust collection process for the tested unit, the grade composition of the aerosol was measured before and behind the dust collector. Cascade impactors [12] were used to determine the grade composition. This method enabled measurements by sampling the aerosol directly from the pipeline, without the need to separate the required amount of liquid beforehand.

The results of talc collection tests using non-freezing liquid, i.e. the overall efficiency and grade-based efficiency, are presented as a table and on diagrams – figures 4 and 5. Testing was conducted at three temperatures: t = -10°C, t = 0°C and t = 15°C, with the corresponding viscosities of: μ = 0.004 Pa·s, μ = 0.0056 Pa·s, μ = 0.0081 Pa·s.

Table 1

Changes in dust collection liquid viscosity and overall efficiency in relation to temperature measurement

measurement temperature	dynamic viscosity coefficient	overall efficiency
°C	Pa·s	%
- 10	0.0081	97.8
0	0.0056	98.8
15	0.0040	99.5

Very high overall talc collection efficiencies of 97.8%, 98.8% and 99.5% were obtained in testing conditions. The achieved efficiencies of talc separation in ambient temperatures were higher than in the case of dust collection with the use of pure water only [13]. It can be said that the high efficiency was a result of low, compared to water, surface tension of the liquid of $61.4 \cdot 10^{-3}$ N/m in t = 15°C. As the temperature rises, the viscosity of the liquid and its surface tension decrease. The assessment of the effects of individual physical and chemical properties on the dust collection process efficiency was impossible. An instrument capable of measuring the surface tension of liquids in sub-zero temperatures was not available. According to table data, the surface tension for water changes by $4 \cdot 10^{-3}$ N/m when the temperature changes by 20°C. Based on that, it can be expected that the effect of temperature on the surface tension of the liquid applied in the tests would be rather minor –

this, unfortunately, was not confirmed with an experiment. Following this assumption, obtaining such minute changes in overall efficiency with doubling the dynamic viscosity index questions the previously stated hypothesis regarding the effect of viscosity on the efficiency of particle absorption inside collectors and releases their surface. Also small are the changes in the efficiency of capturing particles smaller than 2 micrometres in the efficiency range of 97.1% to 85.6% as presented in figures 4 and 5. Decreasing the efficiency of dust collection correlated with the increase of liquid viscosity is likely an effect of changing the hydrodynamic conditions of the system, which affects the formation of liquid dust collectors. The hypothesis, however, applied to particles with poor dynamic wettability and the wettability properties of dust could have improved together with the decrease in the surface tension of the liquid.

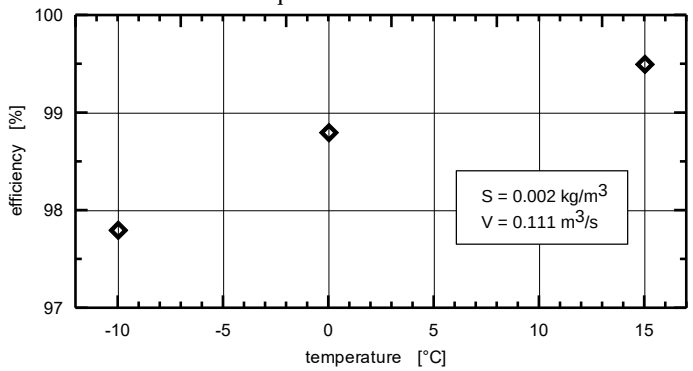

Fig. 4. Relationship between the overall efficiency of the dust collection process in non-freezing liquid and temperature

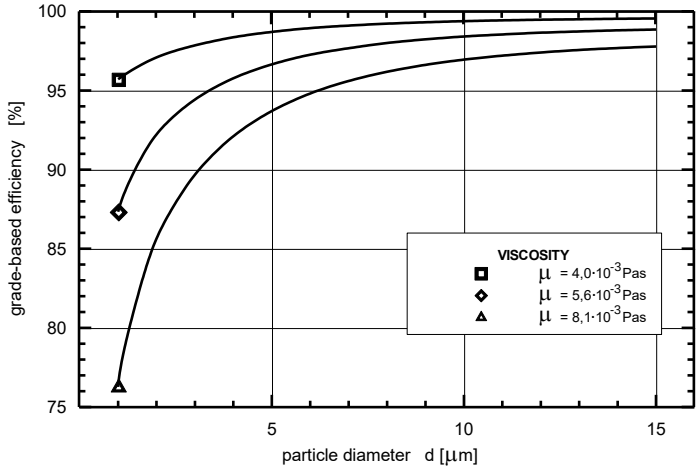

Fig. 5. Relationship between the grade-based efficiency of the dust collection process in non-freezing liquid and temperature

Therefore, based on the completed studies, the hypothesis regarding the impact of liquid viscosity on the effect of releasing the surface collecting the dust particles and, therefore, on the efficiency of the dust collection process cannot be clearly verified. The results confirm the suitability of non-freezing liquids for use as dust collecting liquids in equipment working at low temperatures.

References

[1] Warych J., *Odpylanie gazów metodami mokrymi*, Warsaw, WNT, 1979.
[2] Warych J., *Oczyszczanie przemysłowych gazów odlotowych*, WNT, Warszawa 1994.
[3] Löffler F., *Staubabscheiden*, Georg Thieme Verlag, Stuttgart, New York, 1988.
[4] Kabsch M., *Metody badania zwilżalności pyłów*, Prace naukowe Instytutu Inżynierii Ochrony Środowiska, nr 28 (7), Wrocław 1976.
[5] Weber E., Broche W., *Aparate und Ferfahren der industriellen Gasreinigung*, Oldenbourg – Verlag, 1973.
[6] Pemberton C. S., *Scavening Action of Rain on Non – Wettable Particle Matter Suspended in the Atmosphere*, Aerodynamic Capture of Particles, Pergamon Press 1960.
[7] Slinn W., Water, Air and Soil Poll., vol. 7, 1977, 513.
[8] Wicke M., *Aufbau, Leistung und Betriebsverhalten von Naßentstaubern Fortschritt*, Berichte der VDI, v. 3, nr 33.
[9] Jarzębski L., Głowiak B., Arch. Ochrony Środ., nr 1, 1977, 11.
[10] Hobler T., *Dyfuzyjny ruch masy i absorbery*, WNT, Warszawa 1976.
[11] Użow B. N., Waldberg A. Y., *Oczistka gazow mokrymi filtrami*, Himiâ, Moscow 1972.
[12] Dyląg M., Maszek L., Roszak Z., Rosiński J., *Impaktory kaskadowe – przegląd oraz podstawy konstrukcji*, Mat. konf. *Rozdzielanie zawiesin ciał stałych w płynach*, Warszawa 1990.
[13] Kasz J., Krawczyk J., Filtration and Separation, Nov/Dec. 1988.

TECHNICAL TRANSACTIONS | CZASOPISMO TECHNICZNE
MECHANICS | MECHANIKA
2-M/2016

JUSTYNA WIŚNIOWSKA*, STANISŁAW WITCZAK, MARCIN PIETRZAK**

MULTI-PHASE FLOW MIXTURE THROUGH A SUDDEN CHANGE IN CHANNEL CROSS-SECTION

PRZEPŁYW MIESZANINY WIELOFAZOWEJ PRZEZ NAGŁĄ ZMIANĘ PRZEKROJU KANAŁU

Abstract

The paper presents the results of a study involving the impact of sudden change of cross-sectional area on the flow patterns and local pressure drops for flow of multi-phase mixture. The experiment was conducted in the conditions of a horizontal and vertical flow through a measuring channel. Pressure drops calculated on the basis Kawahara and Lottes methods are compared with experimental data. A system of two interconnected pipes with internal diameters of 40 and 22 mm as well as 46 and 16 mm and a total length of 7 m formed the measurement channel. The experiments involved air, water and oil.

Keywords: multi-phase flow, contraction, expansion, flow patterns, pressure drops

Streszczenie

W pracy przedstawiono wyniki badań dotyczących wpływu gwałtownej zmiany pola przekroju poprzecznego kanału na struktury przepływu oraz miejscowe straty ciśnienia w przepływie mieszaniny wielofazowej. Porównano spadki ciśnienia obliczone na podstawie metod Kawahary i Lottesa z wartościami eksperymentalnymi. Badania prowadzono w warunkach poziomego i pionowego przepływu przez kanał pomiarowy z przeszkodą lokalną. Kanał pomiarowy stanowił układ dwóch rur o średnicach wewnętrznych 40 i 22 mm oraz 46 i 16 mm i całkowitej długości 7 m. Fazę gazową stanowiło powietrze, a fazę ciekłą olej maszynowy i woda.

Słowa kluczowe: przepływ wielofazowy, przewężenie, rozszerzenie, struktury przepływu, opory przepływu

DOI:

* Justyna Wiśniowska, Wakro Sp. z o.o.

** Prof. PhD. DSc. Eng. Stanisław Witczak, DSc. Eng. Marcin Pietrzak, Department of Chemical and Process Engineering, Faculty of Mechanical Engineering, Opole University of Technology.

1. Introduction

Multi-phase flow of gas-liquid mixtures takes place in a variety of installations in the chemical, oil, gas, or food industries, to mention just a few. The local obstacles, such as sudden expansions and contractions of the pipe, are inherent components in a number of flow-through systems. As pressure, volume fraction and flow pattern regimes are considerably affected by the design of such systems, it is important to understand the impact of existing elements on the parameters of multi-phase flow. The knowledge of the type of multi-phase flow patterns plays a fundamental role in the calculations of flow parameters [1]. However, the ability to forecast the type of flow pattern is very difficult due to the very nature of multi-phase flow. An additional difficulty is associated with the existence of certain areas of flow pattern disturbance caused by a change in the cross-section of the pipe.

Despite the bulk of research into multi-phase flow in straight channels reported to this date, there is a scarcity of works concerned with the subject of multi-phase flow in the channels including a sudden contraction or expansion of the cross sectional area of a pipe. Only a few methods for calculating the local pressure drop of two-phase flow through a sudden contraction and expansion are available in the literature. However, even the existing methods do not account for all parameters that affect the value of the pressure drop during such flow including, in particular, a study of the impact of flow pattern disturbances. For this reason, experimental research was carried out and is reported by the authors.

To complement and expand the description of the phenomena of the gas-liquid flow resulting from a sudden change in the diameter of a channel, new experiments and studies work were carried out.

2. Experiment

The experimental setup was designed and built according to recommendations available in the literature. For clarification purposes, the diagram presents the design of the flow-through system for the case of horizontal flow in Figure 1. The main element of the installation was a measurement channel, which consisted of two interconnected pipes with two internal diameters of D = 40 mm and d = 22 mm in a horizontal layout and a total length of 7 m. An experiment involving flow through a sudden expansion or contraction of the channel was conducted for this purpose. The pipes were made of transparent PMMA, as it enabled the authors to visually assess two-phase flow patterns and their disturbance areas. The length of these areas was determined using a millimetre scale placed along the pipes.

Multi-phase mixture consisted of a mixture of water or low viscosity oil and air. The volumetric flow rates of phases were measured by flowmeters of oil, water and air (V_{oil} = 5.0÷20.0 dm^3/min, V_{water} = 2.0÷20.0 dm^3/min and V_{air} = 1.6÷509.0 dm^3/min). The observations of the flow patterns were performed on a 1 m test section, which was located at a distance of 50 diameters from the inlet to the test section. This made it certain that the flow structure is fully developed and it is not affected by the installation of a local obstacle. In addition, the flow patterns were also observed directly before and after the local obstacle. A series of pressure transducers were installed behind the control section, used for the

measurement of the pressure drops due to the existence of a sudden pipe contraction or expansion. The system of pressure transducers locations used for the measurement along the pipe is the same before and after a local obstacle. The data regarding the local pressure drops was collected by a measurement card, coupled with a computer, which recorded data at a high frequency (i.e. 100 measurements per 1 second) followed by averaging the measured values over time.

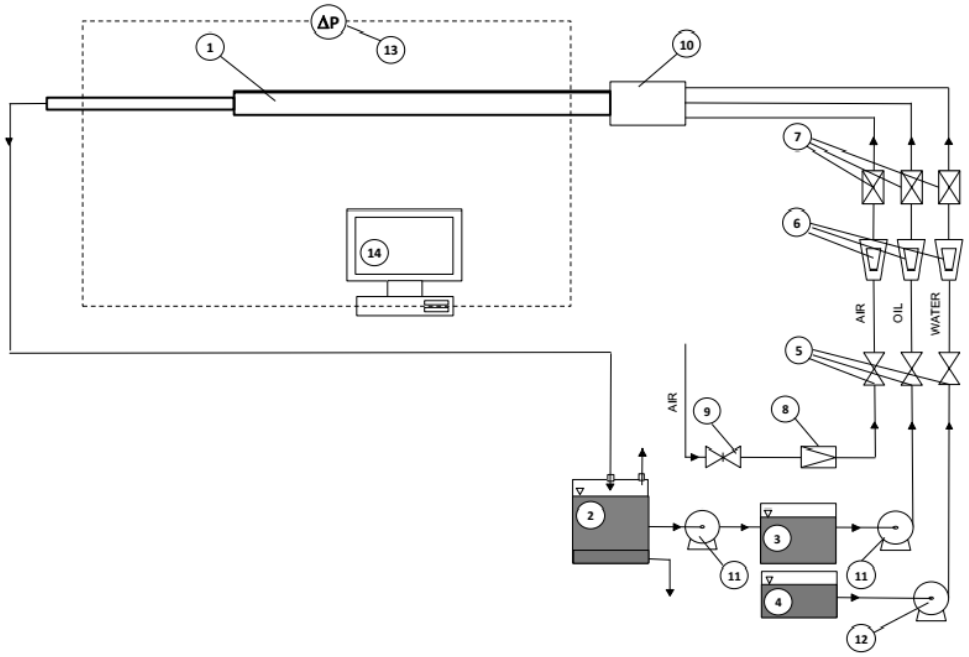

Fig. 1. Experimental set-up
1 – measurement channel with sudden expansion, 2 – separator, 3 – oil tank, 4 – water tank, 5 – shut-off valves, 6 – flowmeter of oil, water, air, 7 – one-way valves, 8 – pressure regulation valve, 9 – air control valve, 10 – agitator, 11 – oil pump, 12 – water pump, 13 – pressure transducers, 14 – measurement card coupled with a computer

3. Results

During the next stage of research, flow conditions corresponding to the two-phase flow patterns identified during the experiment were subsequently compared with the areas of these patterns found in the flow pattern map created by Ulbrich and Troniewski [1] (Fig. 2). Figure A shows the flow pattern map for a pipe before the local obstacle (D = 40 mm) where the types of flow patterns were marked. In Figure B, the type of flow pattern was marked for the smaller pipe diameter (d = 22 mm).

The figures show that in both cases the observed flow patterns were approximately in conformity with the corresponding areas shown in the Troniewski and Ulbrich map.

However, it was observed that the decrease of the pipe diameter during the flow of gas – liquid results in a change in the flow pattern.

For demonstration purposes, figure 3 shows several photographs taken during the experiment involving oil-air and air-water flow through a sudden expansion. Figure 4 shows several photographs taken during the experiment involving oil-air and air-water flow through a sudden contraction. As can be seen, the presence of a local obstacle always leads to a change in the flow patterns both before and after the pipe contraction. The photographs found above indicate the changes in the flow patterns caused by a sudden increase in pipe diameter. The distances where the flow pattern was not fully developed can be clearly discerned there. Such a length, also known as the length of the disturbance area, is defined here as the distance from an obstacle to the location where a uniform flow pattern is formed again. Beyond this area, the mean square root of the deviation of the local void fraction profile is constant and less than 5%, as reported by the authors of the study in [2].

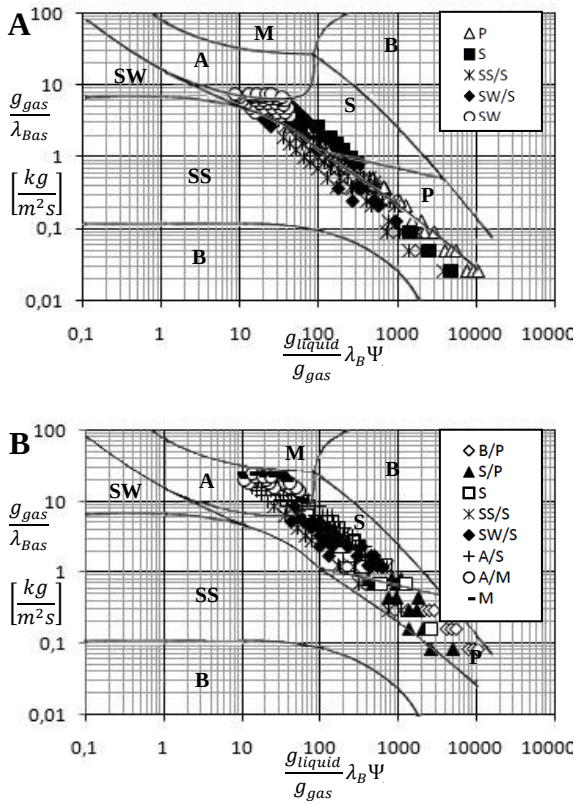

Fig. 2. The flow patterns observed in a pipe before the contraction (A) and after the contraction (B): B – bubble flow, P – plug flow, S – slug flow, SS – stratified flow, SW – stratified-wavy flow, A – annular flow, M – mist flow.

Figure 5 shows one example of the measured change of pressure in two-phase oil-air and water-air flow along the measuring channel. Pressure profiles in the case of flow through a sudden expansion of the channel may vary significantly due to the length of the disturbance zone of flow patterns followed by the area in which the system can recover pressure to its initial value. The pressure recovery due to the sudden expansion is defined as the difference in the pressure when the fully developed pressure gradient lines upstream and downstream of the expansion are extrapolated to a point where a change in the area occurs[3].

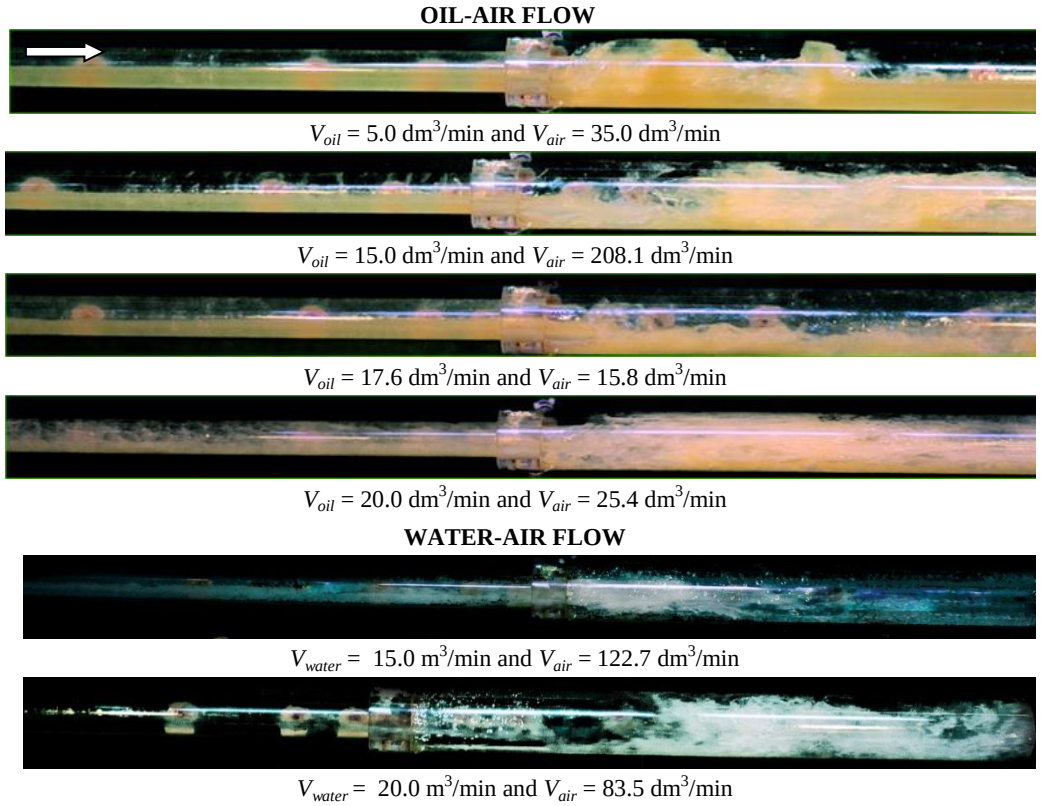

Fig. 3. Flow pattern development during flow of oil-air and water-air mixtures through a sudden expansion

The graphs above (Fig. 6) show the flow patterns developing along the pipe after its sudden expansion. The analysis of the resulting images clearly indicates that the correlations used for calculating the disturbance zones should take into account both the parameters of the liquid phase and the gas phase. If the impact of any of them is disregarded, an adequate assessment of the length of these zones for the sudden expansion will not be possible [4].

On the other hand, during the two-phase flow through sudden contraction of the pipe immediately before this obstacle, the local static pressure decreases due to a sudden acceleration of the flow. After the sudden contraction, the pressure in the pipe gains its minimum value and then increases slightly to the point where a fully developed gradient line of the pressure is achieved. The pressure drop during flow through a sudden contraction is defined as the difference in the pressure in the local obstacle, based on the fully developed pressure gradients upstream and downstream of the contraction.

Figure 7 contains several photographs derived from the research of the characteristics of two-phase oil-air flow through a sudden contraction. Figure 8 is meant to show the areas of flow pattern disturbance in the channel before the contraction.

By analogy to two-phase flows, the pressure drop noted during the three-phase flow is relative to the relations between the volume rates of the components in the flow. On the basis of the data shown in Fig. 9, we can see that an increase in pressure drop occurs for a constant volumetric flow rate of the air accompanied by an increase in volume flow rate of liquid.

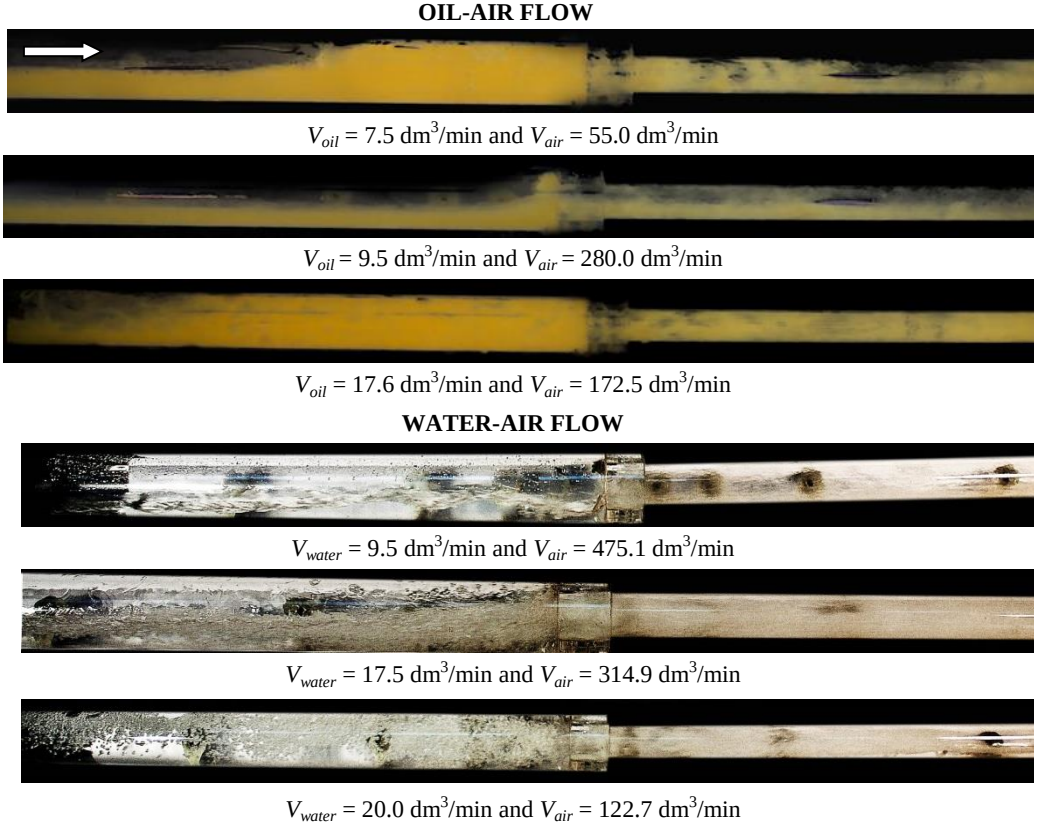

Fig. 4. Changes of flow patterns of oil-air and water-air flow through a sudden contraction

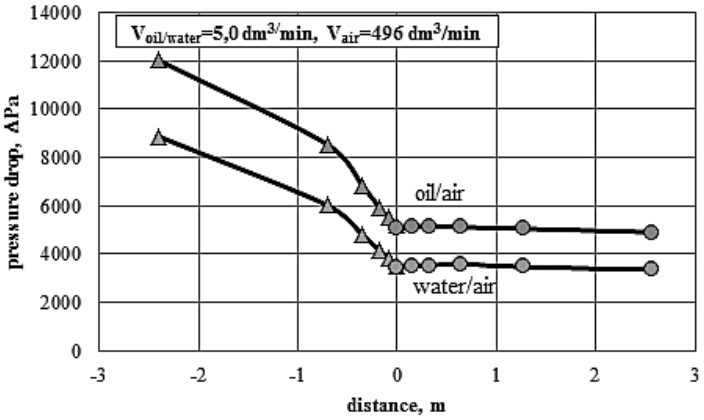

Fig. 5. Pressure drop profiles during the two-phase gas-liquid flow through a sudden expansion

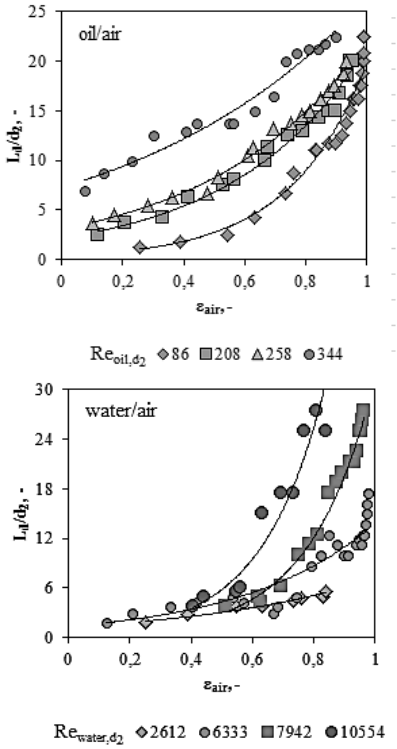

Fig. 6. Developing lengths of flow patterns in the pipe after a sudden expansion

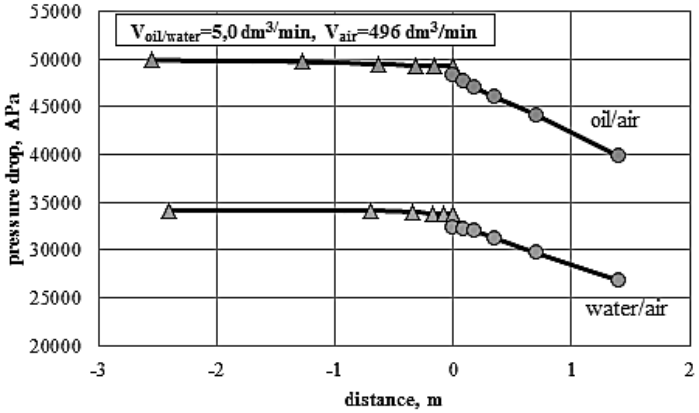

Fig.7. Pressure profiles during the two-phase gas-liquid flow across the channel with a sudden contraction

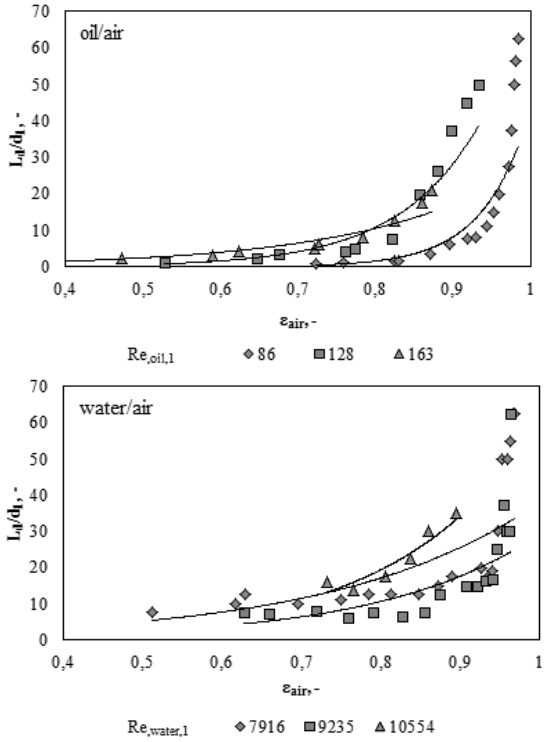

Fig. 8. Developing lengths of flow patterns in the pipe before a sudden contraction

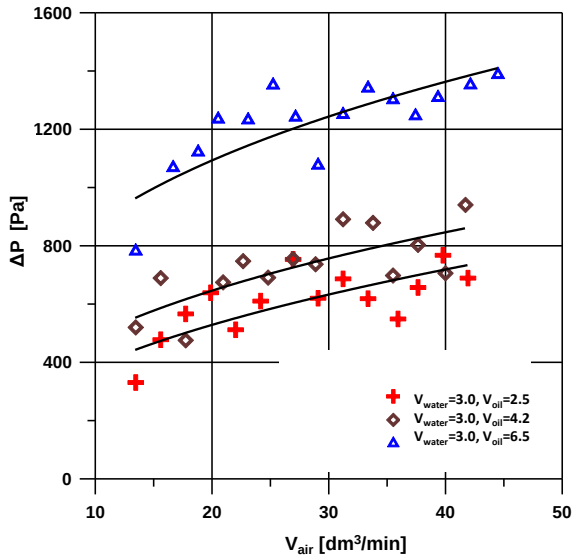

Fig. 9. Pressure drop profiles during gas-liquid-liquid three-phase flow through a sudden contraction

4. Calculation of pressure drops in air-water-oil three-phase flow

The results of statistical tests indicate that the pressure drops for the sudden contraction should be calculated by the use of the Kawahara [5] method, to be equal to:

$$\Delta P_T = \frac{g_T^2}{2 \cdot \rho_{liquid}} \cdot \left[\left(\frac{1}{C_c} - 1 \right)^2 + 1 - \sigma_A^2 \right] \cdot \left[1 + x \cdot \left(\frac{\rho_{liquid}}{\rho_{air}} - 1 \right) \right] \tag{1}$$

$$\rho_{liquid} = \rho_{water} \cdot \alpha_{water} + \rho_{oil} \cdot \alpha_{oil} \tag{2}$$

$$\alpha_{water} = (\varepsilon_{water})^{0.8} \tag{3}$$

$$\alpha_{oil} = 1 - \alpha_{water} \tag{4}$$

$$C_c = \frac{1}{0.639 \cdot (1 - \sigma_A)^{0,5} + 1} \tag{5}$$

$$\sigma_A = \left(\frac{d}{D} \right)^2 \tag{6}$$

where:

ΔP_T – total pressure drop, Pa
g_T – total mass flux density, kg/(m^{2}s)
ρ_{liquid} – liquid density, kg/m^3
ρ_{air} – gas density, kg/m^3
x – mass quality, -
α_{water} – water volume fraction, -
α_{oil} – oil volume fraction, -
σ_A – area ratio, -
ρ_{water} – water density, kg/m^3
ρ_{oil} – oil density, kg/m^3
d, D – internal diameter (contraction, expansion), m.

For gas-liquid flow conditions through expansion, the highest accuracy ensured by application of the Lottes [6] method:

$$\Delta P_T = \frac{g_T^2}{2 \cdot \rho_{liquid}} \cdot \frac{\sigma_A \cdot (1-\sigma_A)}{(1-\alpha_{air})^2} \tag{7}$$

$$\alpha_{air} = \frac{\varepsilon_{air}^{0.37}}{1+\left(\frac{1}{\varepsilon_{air}}-1\right)^{0.5}} \cdot \left(\frac{1-\varepsilon_{water}}{1+\varepsilon_{oil}}\right)^{0.43} \tag{8}$$

$$\varepsilon_{air} = \frac{V_{air}}{V_{air}+V_{water}+V_{oil}}, \tag{9}$$

$$\varepsilon_{water} = \frac{V_{water}}{V_{air}+V_{water}+V_{oil}} \tag{10}$$

$$\varepsilon_{oil} = \frac{V_{oil}}{V_{air}+V_{water}+V_{oil}} \tag{11}$$

where:

α_{air} – mean real void fraction, -
ε_{air} – inlet void fraction, -
ε_{water} – inlet water volume fraction, -
ε_{oil} – inlet oil volume fraction, -.

The values obtained on the basis of calculations were compared with data obtained in experimental studies, as shown in Figures 10 and 11. The result of less than ±40% of relative error was obtained for both correlations.

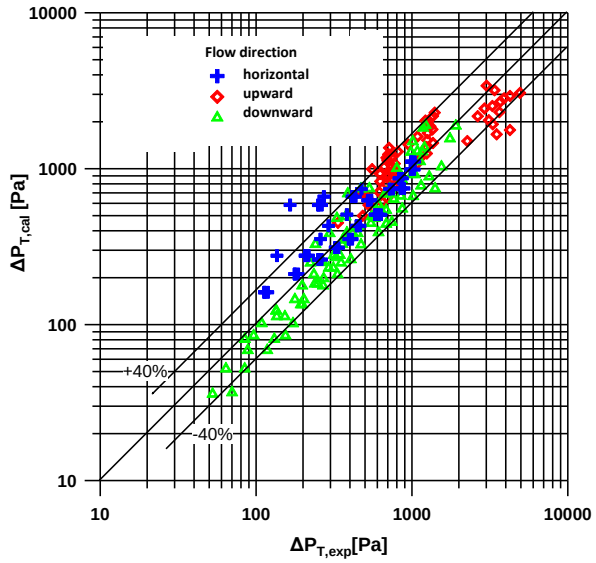

Fig. 10. Comparison of measured pressure drop $\Delta P_{T,exp}$ of three-phase flow with the calculated value $\Delta P_{T,cal}$ on the basis of the Kawahara method (1)

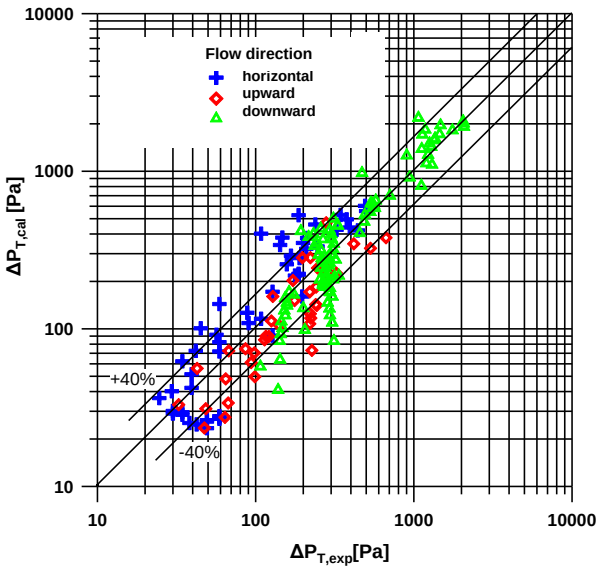

Fig. 11. Comparison of measured pressure drop $\Delta P_{T,exp}$ of three-phase flow with the ones calculated $\Delta P_{T,cal}$ on the basis of the Lottes method (4)

5. Conclusions

The following general conclusions could be derived from the analysis of the results and review of the literature:

1. Flow pattern disturbances of a multi-phase mixture occur during flow through a sudden change in the cross-section of the pipe.
2. The disturbances of flow pattern form the reason for the local change in the void fraction of the phases, and consequently, properties of the mixture are affected by them.
3. Due to the presence of local disturbances caused by the change in the cross-section of pipe, local pressure drop, it is difficult to calculate the local pressure drop.
4. The current methods of calculating the developing lengths in the two-phase flow of gas-liquid mixture through sudden expansion of the channel are not always effective as they do not enable all flow parameters to be taken into account.
5. Further analysis of the results should be aimed at the development of a mathematical equation used to describe the impact of the length of disturbance of flow pattern on the pressure drop in the multi-phase flow in a channel with a sudden change in the cross sectional area.

References

[1] Dziubiński M., *Hydrodynamika mieszanin dwufazowych ciecz-gaz*, Wyd. Politechniki Łódzkiej, Łódź 2005.
[2] Ahmed W. H., Ching C. Y., Shoukri M., International Journal of Heat and Fluid Flow, vol. 29, 2008, 194-206.
[3] Ahmed W. H., Ching C. Y., Shoukri M., International Journal of Multi-phase Flow, vol. 33, 2007, 575-594.
[4] Wiśniowska J, Zeszyty Naukowe Politechniki Opolskiej, seria: Mechanika z. 98, nr 341, 2011, 97-98.
[5] Kawahara, A., Chung, P., Kawaji, M.: *Investigation of two-phase flow pattern, void fraction and pressure drop in a microchannel*, International Journal of Multi-phase Flow, vol. 28, 2002, 1411-1435.
[6] Lottes P. A., *Expansion losses in two-phase flow*, Nuclear Science Engineering, vol. 9, 1961, 26-31.

TECHNICAL TRANSACTIONS | CZASOPISMO TECHNICZNE
MECHANICS | MECHANIKA
2-M/2016

RYSZARD WÓJTOWICZ*, PAWEŁ WOLAK**

PERFORMANCE OF A CYCLONE WITH AN ASLANT SHAPED INLET

ANALIZA PRACY ODPYLACZA CYKLONOWEGO Z UKOŚNIE UKSZTAŁTOWANYM KANAŁEM WLOTOWYM

Abstract

This paper presents an analysis of selected operating parameters of a cyclone with a modified inlet. The modification consisted in an angular arrangement of an inlet channel wall. This can result – in view of previously conducted experiments – in a faster insertion of a dusty gas into a swirl motion, an improvement of particles separation process. The analysis was carried out using numeric CFD simulations. The results were compared to those obtained from simulations and lab-measurements for a cyclone with standard inlet.

Keywords: dedusting, cyclone, pressure drop, dedusting efficiency, CFD simulations

Streszczenie

W pracy przedstawiono analizę wybranych parametrów pracy odpylacza cyklonowego ze zmodyfikowanym wlotem. Modyfikacja polegała na kątowym usytuowaniu ścianki kanału wlotowego, co – w świetle prowadzonych wcześniej badań własnych – może skutkować szybszym wprowadzeniem strumienia zapylonego gazu w ruch wirowy i w jego efekcie poprawą efektywności procesu separacji cząstek. Analizę przeprowadzono wykonując symulacje numeryczne CFD. Uzyskane wyniki porównano z wynikami symulacji i pomiarów laboratoryjnych wykonanymi dla cyklonu ze standardowym wlotem.

Słowa kluczowe: odpylanie, odpylacz cyklonowy, spadek ciśnienia, skuteczność odpylania, symulacje CFD

DOI:

* DSc. Eng. Ryszard Wójtowicz, Institute of Thermal and Process Engineering, Faculty of Mechanical Engineering, Cracow University of Technology.
** M.Sc. Eng. Paweł Wolak, Mechanical Equipment Department, Air Liquide Global E&C Solutions Poland S.A.

1. Introduction

The cyclones are commonly used in industry, process engineering and environmental protection for separation of solid particles from dusty gases, and also as a separation device in pneumatic transport systems [1, 2]. It is worth noting that apparatuses of this kind – despite a seemingly simple design – are characterised by complex and difficult-to-describe gas flow, resulting from simultaneously coexistence two opposite directed gas streams. The performance of a cyclone (its dedusting efficiency, pressure drop, reliability, etc.) is strongly influenced by its geometry and dimensions. Even a slight change of these parameters may result in a change of the dedusting efficiency and the creation of undesirable phenomena, e.g. a gas flow directly from an inlet channel to the outlet (short circuit) or unfavourable for dust removal process transferring of gas motion to a dust chamber.

A useful tool for cyclone design and optimisation seem to be simulation packages, based on codes of Computational Fluid Dynamics (CFD) [3]. They allow preliminary quick analysis of gas flow inside a cyclone and easy modification of its dimensions and geometry, without having to build costly prototypes and to conduct time-consuming experimental investigations.

This work verifies an idea [4] concerning the improvement of cyclone performance by an angular arrangement of a wall of the inlet channel. It should result in directing the dusty gas stream closer to a cyclone wall, putting it faster in a swirl motion, reduction of particles bouncing from a wall and unfavourable particles entrainment by a clean gas in an outflow. Analysis was carried out using CFD modelling. The results were compared to those obtained from simulations and lab-measurements for a cyclone with a standard inlet.

2. Experimental

Cyclones used in numerical investigations are shown in Figure 1. The diameter of the cylindrical part was always D = 0.192 m and the total height of the cyclone H = 0.745 m. The height of the cylindrical part was h = 0.242 m. The diameter and length of the vortex finder were D_e = 0.09 m and s = 0.140 m, respectively. The diameter of the cyclone at the end of the conical part was chosen to be B = 0.045 m. Three different gas inlets were tested. One of them was a standard, square cross-sectional with dimensions $a = b$ = 0.042 m (Fig. 1b), two modified by an angular arrange of the inlet channel wall at an angle $\alpha = 2°$ (Fig. 1c) and $\alpha = 4°$ (Fig. 1d). Other cyclones dimensions are presented in Fig.1. Gas flowing through the cyclone was air (ρ_c = 1.225 kg/m^3, $\mu_c = 1.7894 \cdot 10^{-5}$ Pa·s). Its velocity at the inlet of the cyclone was u = 15 m/s. The density of solid particles was ρ_s = 2700 kg/m^3. The dispersed phase volume fraction was relatively low, less than 5%. During simulations, it was assumed that particle size distribution is characterised by the Rosin-Rammler theoretical distribution. The analysis of flow was performed based on results of numerical modelling, using as a pre-processor the mesh generator *Gambit 2.4* and as a solver *Ansys Fluent 14.0*. Turbulent gas flow in the cyclone was described using the Navier-Stokes equations of mass and momentum transport, averaged by Reynolds method (RANS) [5]. As a closing method, the RNG (Renormalisation Group) [3, 6] k-ε turbulence

model was selected with an additional option of the Swirl Modification [7], taking into account a vorticity nature of flow inside the cyclone. To simulate the motion of the discrete phase (particles), the Euler-Lagrange (EL) [8] approach was used.

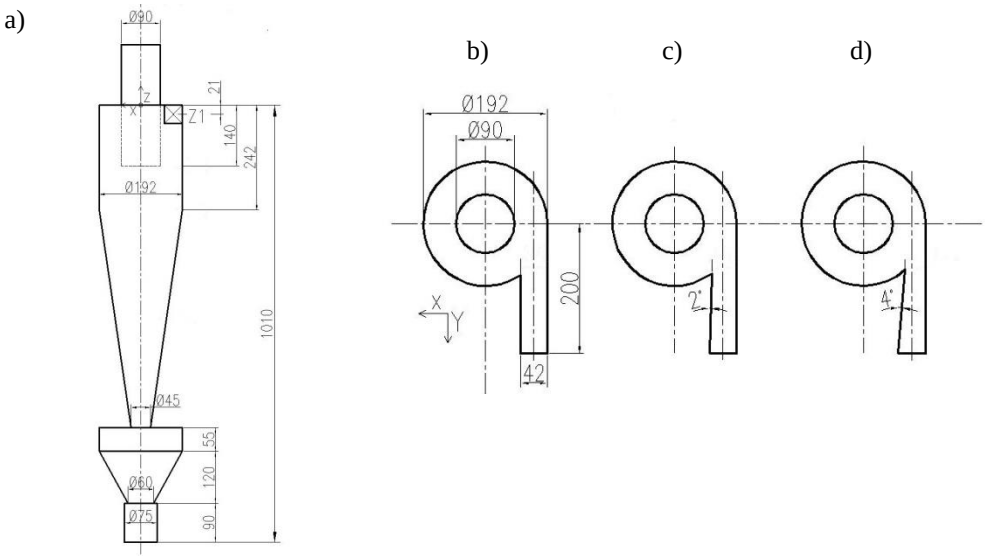

Fig. 1. The cyclone examined a) a view, b) standard inlet $\alpha = 0°$, c) modified inlet $\alpha = 2°$, d) modified inlet $\alpha = 4°$

Detailed information on the cyclone design and methodology of simulations is presented elsewhere [9, 10]. These papers also present comparisons of the standard cyclone simulations with theoretical models and measurements, which confirm that the used numerical model is correct.

3. Results and discussion

Figure 2 presents contour and vector maps of the flow pattern in the cyclone. An angular arrangement of a cyclone inlet makes that a gas delivered is inclined toward a cyclone wall with a sudden narrowing of a stream. Dusty gas starts to rotate with high tangential velocities, of which maximum values for an inlet channel angle $\alpha = 0°$ (Fig. 2a), $\alpha = 2°$ (Fig.2b) and $\alpha = 4°$ (Fig.2c) are higher in comparison with an inlet velocity (u = 15 m/s) by 30%, 42% and 65%, respectively. This tendency observed already in a cyclone with a standard inlet [9, 10] is significantly intensified by an angular arrangement of an inlet. It can cause an increase of cyclone dedusting efficiency. Besides, in a cyclone with an aslant shaped inlet, solid particles are supplied closer to the cyclone wall and they are faster introduced into rotational motion. It largely reduces their bouncing from a wall and eliminates their flow directly to the gas outlet stream.

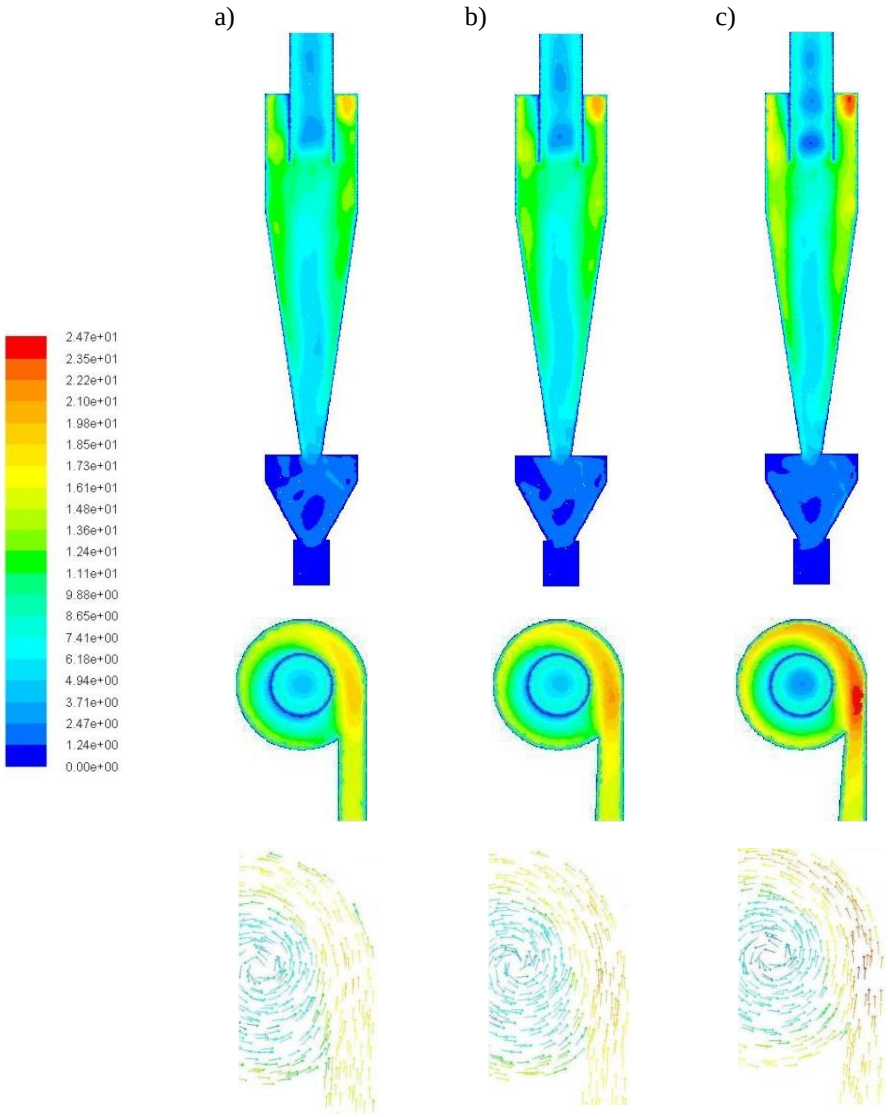

Fig. 2. Contour and vector maps of flow pattern: a) standard inlet $\alpha = 0°$, b) modified inlet $\alpha = 2°$, c) modified inlet $\alpha = 4°$

Figure 3 presents the trajectory of the selected particle (d_p = 2 μm), which is supplied to the cyclone with a dusty gas stream. In the cyclone with a standard inlet (Fig. 3a), a particle of this size will not be dedusted. After several rotations in a swirl gas stream, a particle enters an outflow and leaves the cyclone. In cyclones with modified inlets (Fig. 3b and Fig. 3c), trajectories of particle in the cyclone upper part are larger in diameter. Polluted gas in this part has a proper velocity and particles are separated.

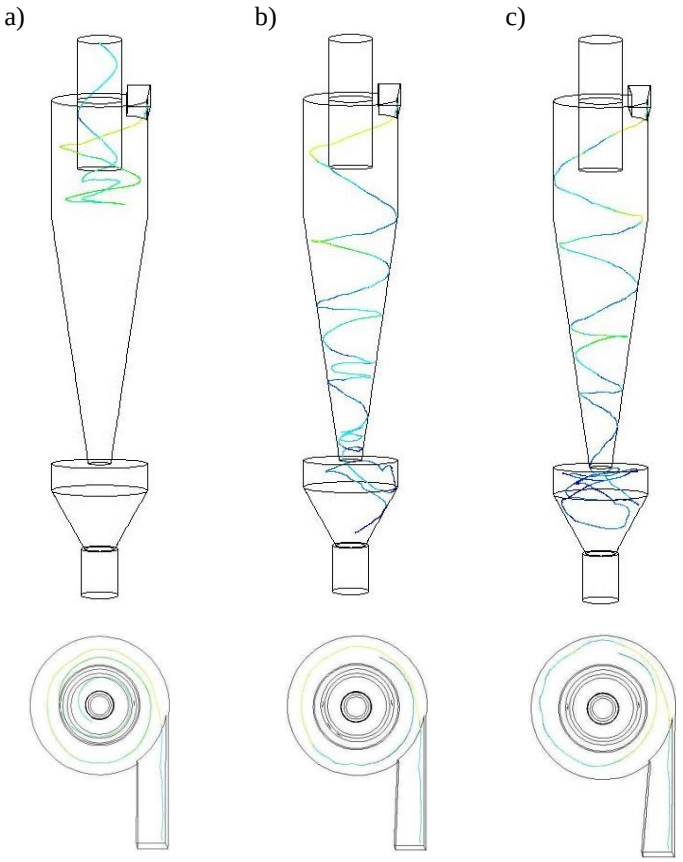

Fig. 3. Trajectories of a dust particle (d_p = 2 μm): a) standard inlet α = 0°, b) modified inlet α = 2°, c) modified inlet α = 4°

The above-described phenomena and mechanisms are confirmed by data presented in Table 1. Predicted cyclone efficiency, estimated on the basis of a classic relation:

$$\eta = \frac{m_s}{m_i} \cdot 100\% \tag{1}$$

(m_s is a mass dedusted (collected) particles, and m_i is the mass of all particles supplied to a cyclone with a polluted gas) increases for both modified inlets (α = 2° and α = 4°) by 1.3 % and 3% respectively.

On the other hand, it should be noted that for cyclone performance estimation, a second parameter – the pressure drop – should be taken into account. This parameter, in addition to efficiency, also decides on the cost-effectiveness of the process and its expenditures. In Table 1, predicted pressure drops are also presented. With respect to the cyclone with a standard inlet, they increase by 20 % (α = 2°) and 32.6% (α = 4°).

Table 1

Pressure drop and dedusting efficiency for examined cyclones

Cyclone	Pressure drop [Pa]	Dedusting efficiency [%]
Standard inlet ($\alpha = 0°$)	313	86.3
Modified inlet ($\alpha = 2°$)	376	87.4
Modified inlet ($\alpha = 4°$)	415	88.9

In the literature, there are not any uniform criterion linking these two parameters and evaluating of cyclone efficiency together. In general, the leading parameter determining the cyclone choice is the dedusting efficiency. These CFD simulations show that modification of a cyclone inlet by an angular arrangement of its wall is fully justified.

References

[1] Hoffmann A. C., Stein L. E., *Gas cyclones and swirl tubes – principles, design and operation*, Springer - Verlag, Berlin 2008.

[2] Warych J., *Gas cleaning*, WNT, Warsaw 1998 (in Polish).

[3] Jaworski Z., *Computational fluid dynamics in chemical engineering*, Exit, Warsaw 2005 (in Polish).

[4] Mieszkowski A., Roszak Z., *Environment protection systems*, Cracow University of Technology, Cracow 2010 (in Polish).

[5] Pope S.B., *Turbulent flows*, Cambridge University Press, Cambridge 2013.

[6] Wójtowicz R., Lipin A.A., Talaga J., *On the possibility of using of different turbulence models for modeling flow hydrodynamics and power consumption in mixing vessels with turbine impellers*, Theoretical Foundations of Chemical Engineering, 48, (4), 2014, 360-375. DOI: 10.1134/S0040579514020146

[7] Ansys Inc., Ansys Fluent theory guide, Canonsburg 2011.

[8] Andersson B., Andersson R., Hakansson L., Mortensen M., Sudiyo R., van Wachem B., *Computational fluid dynamics for engineers*, Cambridge University Press, Cambridge 2012.

[9] Wójtowicz R., Wolak P., *Identification of multiphase flow in a cyclone separator*, International Scientific and Technical Conference "Problems of Resources and Energy Saving Technologies in the Industry and Agricultural Complex (PRET-2014)" (Monograph, W.N. Bliniczew, edt.), ISUCT, Iwanowo, Russia 2014, p. 252-264 (ISBN 978-5-9616-0494-8).

[10] Wójtowicz R., Wolak P., *An example of the use of computational-fluid-dynamics analysis for simulation of two-phase flow in a cyclone with a tangential inlet*, Environment Protection Engineering, 4, 2016 (in press).

CONTENTS

TREŚĆ

Editorial Board Mechanics

2-M/2016

TECHNICAL TRANSACTIONS | CZASOPISMO TECHNICZNE
MECHANICS | MECHANIKA
2-M/2016

KATARZYNA ADAMOWICZ*, PIOTR SARNA**, WIESŁAW SZATKO

SAFETY IN SUBSEA PETROLEUM PRODUCTION SYSTEMS: SUBSEA CHRISTMAS TREE CASE STUDY

BEZPIECZEŃSTWO W SYSTEMACH DO PODWODNEJ EKSPLOATACJI ZŁÓŻ ROPY NAFTOWEJ NA PRZYKŁADZIE GŁOWICY EKSPLOATACYJNEJ

Abstract

The paper presents an analysis of valves used for closing and opening production tubing, located on the production line. The main safety valves analysed in this work are located in the Christmas Tree and in the Downhole Safety Valve. The analysis was conducted using FMEA; it found that for each basic Christmas Tree's gate valve, the most dangerous failure modes are external leaks and "fail to close" in the open position of the valves. For the Downhole Safety Valve, the most dangerous fault can occur in the open position of the valve. The Downhole Safety Valve and the Christmas Tree complement each other, thus ensuring safety during oil and gas production.

Keywords: safety in subsea petroleum production systems, Christmas Tree's safety valves

Streszczenie

W artykule przedstawiono analizę zaworów przewodu wydobywczego, umiejscowionych w głowicy eksploatacyjnej oraz zawór wgłębny bezpieczeństwa. Analizę przeprowadzono metodą FMEA; stwierdzono, że dla każdego podstawowego zaworu zasuwowego głowicy eksploatacyjnej najgroźniejsze są wycieki zewnętrzne, a także uszkodzenie w pozycji otwartej. Podobnie dla zaworu wgłębnego bezpieczeństwa. Zawór wgłębny bezpieczeństwa i podstawowe zawory zasuwowe uzupełniają się nawzajem gwarantując bezpieczeństwo.

Słowa kluczowe: systemy bezpieczeństwa przy wydobywaniu ropy i gazu, zawory bezpieczeństwa w głowicy eksploatacyjnej

DOI:

* Eng. Katarzyna Adamowicz, DSc. Eng. Wiesław Szatko, Institue of Thermal and Process Engineering, Faculty of Mechanical Engineering, Cracow University of Technology.
** MSc. Eng. Piotr Sarna, Head Energy Cracow, Poland.

1. Introduction

Demand for oil and gas continues to grow, but ground-based hydrocarbon deposits begin to slowly deplete. Therefore, there is expected increase in performed offshore drillings and underwater installations in the coming years. Many wells located in shallow waters are already heavily exploited, so the search for hydrocarbons begins to move into deeper regions of the sea. Today, there are more than 9,000 offshore platforms operating worldwide, serving more than 10,000 wells, and their number will continue to grow [2].

The subsea mining industry puts a strong emphasis on the reliability of equipment. Equipment used in water are typically 5 times more expensive than equipment used for oil and gas extraction on land because all the situations of intervention or repair are associated with high costs. Breakdowns at sea can have additional devastating effects on the environment. An example is the 2010 explosion at the American platform rig Deepwater Horizon in the Gulf of Mexico, which was the cause of the largest oil spill in the world. It is assumed that 780 000 m^3 of oil leaked into the Gulf and the contaminated area consisted of 6,500 to 176,000km^2. Many factors are consisted during safe production of oil and gas from the seabed, but the most important components in the system of subsea production are subsea the Christmas Tree and the Downhole Safety Valve.

2. Christmas Tree

The most important element in the subsea production system is the Christmas Tree (XT). The Christmas Tree is mounted on the wellhead at the seabed. The XT is a set of valves mounted on a specially designed steel block.

Fig. 1. Subsea Christmas Tree [www.gizmodo.com]

The main task of the Christmas Tree is to control the flow of hydrocarbons from the well [5]. Christmas Trees also allow for the injection of various chemicals in order to remove or prevent the formation of hydrocarbon plugs, corrosion, or other prejudicial obstructions having bad influence to the production system. The design of the Christmas Tree also allows for access to the borehole in order to carry out all kinds of maintenance and workovers. The Christmas Tree can also be used for pumping water, gas or other factors to the lode. The Christmas Tree provides additional features, such as pressure and temperature monitoring and flow rate control. The construction of the Christmas Tree may vary depending on the requirements of the project and the area of extraction. The average body weight of a Christmas Tree is from 50 to 70 tonnes. Pressures of exploration for Christmas Trees are standardised and are successively 5,000 psi (35 MPa), 10,000 psi (69 MPa), 15,000 psi (103 MPa) and for ultra-deepwater Christmas Trees: 20,000 psi (138 MPa) [6]. All valves in the Christmas Tree must withstand the same pressure as the Christmas Tree. All equipment is designed to operate at temperatures from 35° to 250°F (2°C to 120°C) [7]. Inside the Christmas Tree, the operating temperature is close to the lode temperature and pressure reservoir decreased by hydrostatic pressure related to the difference between the depth of the lode and the Christmas Tree as well as the linear and local losses. Linear losses derived from friction forces occurring between the elements of the fluid in all its mass and the friction against the walls of the passageway along its length. Take-offs are local obstructions in the flow and changes in the shape of the channel or the velocity of the stream.

Very often, the wells are drilled at depths of 1,500 meters or more. Such depths put high demands on the technical issues; therefore, ultra-deepwater Christmas Trees are used for the exploration of such lodes.

2.1. Safety valves in Christmas Tree

Three valves located in the Christmas Tree were analysed which are important in production of hydrocarbons :

- Production Master Valve (PMV) is the primary and the most important valve in the Christmas Tree. It provides insulation between the borehole and the production tubing, wherein the hydrocarbons flow from the Christmas Tree to the manifold. During the exploitation of the lode, the valve is in the fully open position. The PMV must be strong enough to withstand the pressure prevailing in the well and prevent an uncontrolled leakage of hydrocarbons from the well.
- Production Wing Valve (PWV) is used for closing and opening the XT under normal operating conditions. Just like the Production Master Valve, it is responsible for securing the flow of hydrocarbons from the well.
- Annulus Master Valve (AMV) is the main valve preventing a leak of hydrocarbons from the wellbore to annulus [1].

These valves are fail-safe gate valves. It is a very popular type of valves used in Christmas Trees. This type of valves not only meets the safety function in the event of failure, but also allows for the closure of the valves in the XT without injecting heavy drilling mud into the well in order to eliminate flow from the reservoir into the hole. Closing the valves may be necessary, for example, during pressure and function tests [11].

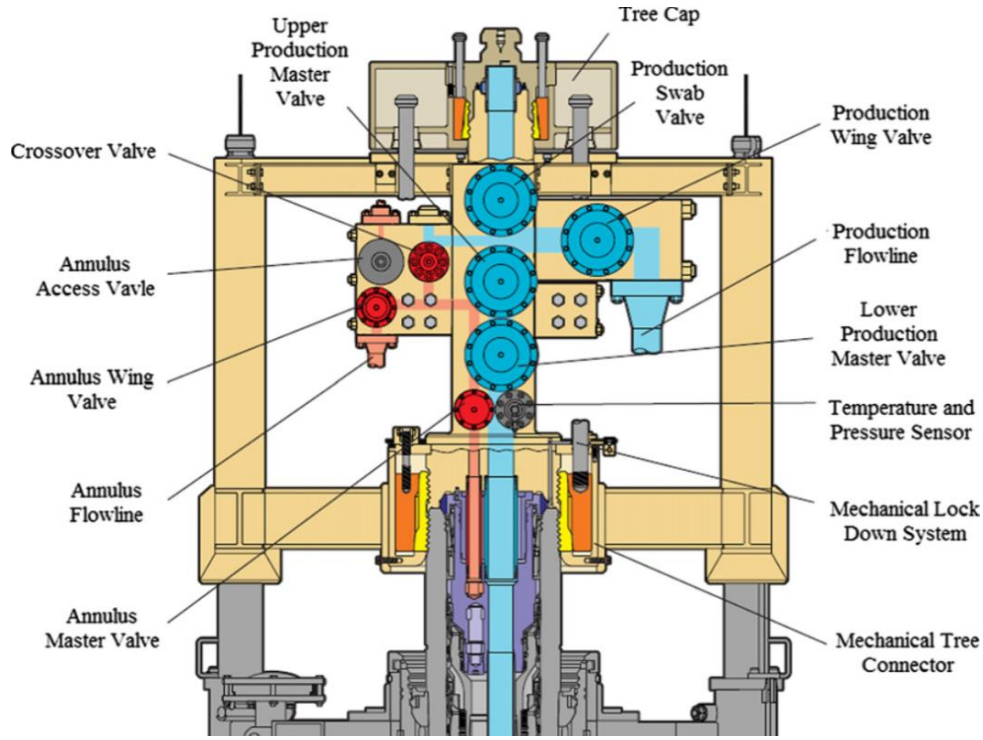

Fig. 2. Valves in Christmas Tree [Dril-Quip]

The valves in the Christmas Tree are controlled via a subsea control module mounted directly on the XT. The subsea control module contains the electronics, hydraulics and instrumentation needed for the safe and effective control of valves in the XT and the Downhole Safety Valve. In addition, the subsea control module is responsible for the distribution of the electric current monitoring signal and for communication with the surface. Modern subsea control modules must have reliability for water depths of up to 3000 meters and pressures of 20,000 psi (138 MPa).

In order to allow for the closing or opening of valves directly and independently of the control system, Christmas Trees are equipped with a panel, which allows for the direct control valve to use the remotely operated vehicle (ROV). Direct control of valves may be necessary for the assembly or disassembly of the XT of maintenance or failure of the control system.

3. Downhole safety valve

A very important valve, which is not located in the Christmas Tree, but it is controlled by it, is the Downhole Safety Valve (DHSV). The DHSV is mounted in a completed wellbore at a depth ranging from 100 to 500 meters below seabed. It is a flap-type valve

and it is intended to prevent the uncontrolled release of hydrocarbons from the lode in the event of an emergency when other valves have failed. The DHSV is controlled with hydraulic fluid by the Christmas Tree.

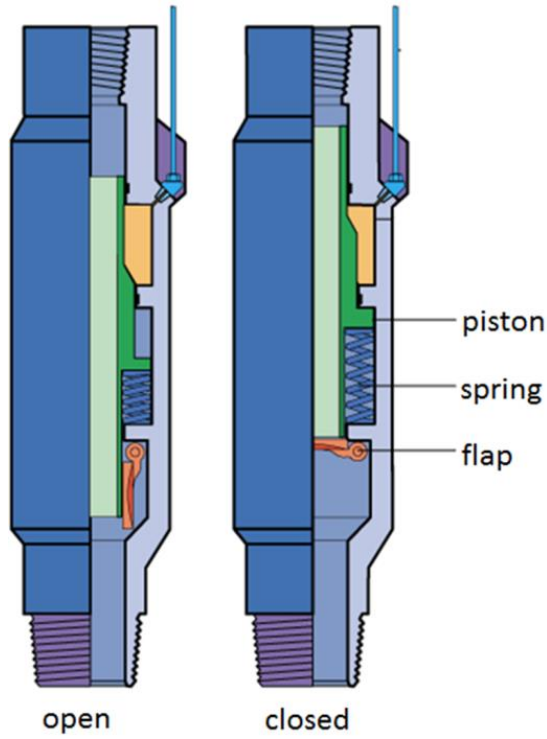

Fig. 3. DHSV valve [www.whcp-oilgas.com]

4. Failure Mode and Effects Analysis

Failure Mode and Effects Analysis (*FMEA*) is a qualitative method, which is used to identify potential errors or defects, and to assess their effects. Many industries require for the FMEA to be used in the design of technical systems and that its sheets to be part of the system documentation. Provisions in the oil industry also require a similar analysis. The analysis uses specific FMEA sheets, in which, inter alia, it distinguishes the failure modes of individual elements or severity of the ranking. Failure mode is a description of a possible malfunction of the element that prevents the required function, which answers the question; how the machine crashes. Modes and causes of damage for the valves depend on the particular design. For a standard subsea gate valve installed in the Christmas Tree, the following typical modes and their corresponding causes as well as mechanisms of damage may be mentioned:

Table 1.

Failure modes and possible causes of it

Failure mode	Possible causes
Fail to close	• Fault control system, • Too high hydraulic pressure in the supply line rod chamber, • Locked return hydraulic line, • Spring failure, • Internal leak.
Fail to open	• Fault control system, • Too low pressure in the hydraulic circuit valve supply, • Damaged piston valve, • Spring failure, • Internal or external leak, • Locked hydraulic return line.
Premature or uncontrolled shutdown	• Fault control system, • External leak.
Internal leak	• Seal failure.
External leak	• Seal failure, • Unsealing the valve body.

4.1. Classification of the severity of fault

The classification of the severity of the effects provides the qualitative dimension of the worst potential consequences of design errors or equipment failures. Each identified failure mode and analysed element is subject to the classification of the severity of the impact. Classification is used in both FMEA and FMECA. The categories are divided into:

- Category I (catastrophic) – failure results in death of workers or huge loss of devices preventing further execution of the planned objectives of the system.
- Category II (critical) – failure causes the degradation of the system beyond acceptable limits, creating a security risk (contributing to the death or injury of employees, if they are no taken steps to combat the risk).
- Category III (severe) – the failure of the system degrades the bounds of safety, but there is a possibility to appropriately counteract the effects.
- Category IV (reduced) – failure does not degrade the whole system performed beyond the acceptable limits of safety, causing one of the various disadvantages of the system.

- Table 2

- **FMEA sheet for PMV**

Description of item: Production Master Valve			**Description of failure**			**Effects of failure**		**Severity**	**Recommended action to reduce the risk**	**Commentary**
Nr	**Function**	**Operating mode**	**Failure mode**	**Potential cause of failur**	**Detection**	**On subsystem**	**On whole system**			
1	It allows on the flow of hydrocarbons from the wellhead; provides isolation between wellhead and production tubing	Valve in open position	Fail to close	Fault control system	D	Is not possible to close valve on demand; continuous flow of hydrocarbons through the valve	The closure of Christmas Tree by the valve is impossible. Other valves on the production line are needed to work	Category II: Critical	Regular inspections and testing of the control system	
				Too high hydraulic pressure in the supply line rod chamber	D				Regular inspections and testing of the hydraulic system	
				Locked hydraulic return line	U				Regular inspections and testing of the hydraulic system	
				Spring failure	U				Proper maintenance	

5. Results

Analysed PMV, PWV, AMV and DHSV. Distinguished two modes of operation: the valve in the open and closed positions and whether the damage is detectable, and each failure mode has been classified according to the classification of the severity of the impact. Table 2 presents an exemplary FMEA sheet that was used while analysing.

The Downhole Safety Valve is the primary barrier and is designed to cut off the Christmas Tree from lodes. For DHSV in the open position, the most dangerous failure mode is "left open the valve," which have been classified in the classification of the severity of fault "leakage through the valve" as a critical fault. Failure mode "fail to close" is extremely dangerous when the situation requires, for example, a fire on the platform. In this case, it is necessary to ensure the proper functioning of the valves in the Christmas Tree. If the secondary barrier does not fulfil its function, the platform will still be transmitting hydrocarbons, which will result in such a situation as an explosion on the surface. Failure mode "leakage through the valve" causing damage to the sealing flap is dangerous due to the fact that the valve does not close the flow of hydrocarbons in the situation required. It is then necessary to activate the valves in the XT, which violates the integrity of the subsea safety at oil and gas production. A major failure mode is uncontrolled shutdown. In this case, there is no assurance that the valve will work and close properly, and on the other hand, there is the possibility that the valve closes spontaneously in normal production, causing downtime and thus financial losses.

The secondary barrier is the Christmas Tree and its main valve is the Production Master Valve. In case of failure, DHSV is the first valve that is designed to cut off the flow of hydrocarbons through the Christmas Tree. This is a very important component of the XT because its failure contributes to an increased risks associated with not closing the whole XT. Failure modes in the basic gate valves of XT are classified from serious to catastrophic consequences. All considered, gate valves (PMV, PWV, AMV) in both operating modes external leak hydrocarbons cause disastrous consequences. In such a situation, it requires keen DHSV or the XT, otherwise it may lead to an ecological catastrophe caused by the contamination of seawater, and thus huge financial losses. If the DHSV works, an ecological catastrophe does not occur, but it is necessary to draw all the XT and replacement of the damaged valve. If the DHSV does not work, but the other valve is closed, it will not be possible to immediately draw the XT. In such a situation, injection of heavy drilling fluid into the wellbore would be needed. Each day of downtime in production is associated with financial losses, but also to draw all the XT generates additional costs. With the exception of an external leak, all failure modes in AMV have serious consequences. Analysing PMV and PWV in operation in the open position failure mode "fail to close" "internal leak" caused damage to the piston seal and the "uncontrolled shutdown" necessitate the activation of other valves, and thus in case of requiring situation increases the probability associated with the failure to close the entire XT. In addition, the occurrence of even one of these failure modes leads to stoppage of the whole production in order to repair the fault. In contrast, the occurrence of leakage caused by damage to the inner piston seal also will stop production because the hydraulic pressure in the chamber, the rod falls, and thus the valve closes. Failure mode "uncontrolled shutdown" is not a dangerous fault because it does not contribute to an increase in the danger of the production of hydrocarbons, but the effects of this mode are felt from the economic side.

The analysis can be concluded that for each basic gate valve of XT, the most dangerous are an external leak and the failure mode "fail to close" in the open position of the valves. Any failure of an individual valve that makes the extraction of hydrocarbons becomes less and less secure. An indispensable component of the safety system of subsea production is the DHSV, the most dangerous defects can occur in the open position of the valve. The DHSV and the Christmas Tree complement each other, thus ensuring the security of oil and gas production.

References

[1] Norsok Standard D-010.
[2] Perrin D., *Well Completion and Servicing*, Technip 1999, 153-156.
[3] Rausand M., *Reliability of Safety-Critical Systems: Theory and Applications*, Wiley 2014, 53-76.
[4] Samir D., *Fundamentals of Oil & Gas Industry for Beginners*, Notion Press Chennai 2015.
[5] Young B., Qiang B., *Subsea Engineering Handbook*, Elsevier, 2010.

TECHNICAL TRANSACTIONS | CZASOPISMO TECHNICZNE
MECHANICS | MECHANIKA
2-M/2016

EUGENE ALEXEEV, BORIS GOLOVUSHKIN,
ALEXANDR LABUTIN, ELENA EROFEEVA*

STUDY OF SYSTEM-WIDE AND STRUCTURAL PROPERTIES AND OPTIMAL CONTROL OF THE PRE-POLYAMIDATION TANK

ANALIZA SYSTEMOWA I STRUKTURALNA WŁAŚCIWOŚCI ORAZ OPTYMALNE STEROWANIE ZBIORNIKIEM DO PRE-POLIAMIDACJI

A b s t r a c t

The study on system-wide and structural properties of a prepolyamidation tank were performed by simulation. Control channels were selected. An algorithmical synthesis of a tank optimal control system was performed. A designed control system was simulated.

Key words: chemical tank, controllability, optimal control, control system

S t r e s z c z e n i e

Analizę systemową i strukturalną właściwości zbiornika do pre-poliamidacji przeprowadzono metoda symulacji. Wyznaczono kanały kontrolne, dokonano algorytmicznej syntezy systemu sterowania oraz zamodelowano projektowany system.

Słowa kluczowe: zbiornik, sterowalność, optymalne sterowanie, system sterowania

DOI:

* MSc. Eng. Eugene Alexeev; MSc. Eng. Boris Golovushkin, Prof. PhD. DSc. Eng. Alexandr Labutin, PhD.DSc. Eng. Elena Erofeeva, Department of Technical Cybernetics and Automation, Chemical Engineering and Cybernetics Faculty, Ivanovo State University of Chemistry and Technology.

1. Introduction

At present, the synthetic polymer polycaproamide attracts the attention of many researchers. Thanks to its properties, the polymer is widely used in some industries. Thread for industrial use, composite materials with special properties for medicine and food industry, polymer colour concentrates and thermal stabilisers can be made based on this polymer.

The main industrial method for producing polycaproamide is hydrolytic polymerisation of caprolactam in melt. With an approach to saving energy and resource at our university promising technology, for producing this polymer were developed. Extraction and energetically unfavourable stage regeneration lactam waters were changed by combined drying and removal of the residual monomer in an inert gas process.

In this work, the object is the pre-polyamidation tank in which stage of pre-polyamidation of polyamide-6 in solid phase is existing. Earlier mathematical model of this stage was derived, simulation was performed and the adequacy of the derived model was confirmed.

The aim of this work is to study system-wide and structural properties (connectivity, controllability and observability) of tank and to design an optimal controller by using mathematic and simulation methods.

2. Analysis of system-wide and structural properties

At the present time, researchers widely use simulation methods of technological processes of synthesising synthetic polymers for solving different optimisation and control tasks. It's necessary to create an effective control system for performing the process under the economic or technical point of view's optimal behaviours. The processes are studied as control object for solving this problem.

Analysis of connectivity

Dimensionless transfer coefficients were determined for studying the connectivity degree. Input and output variables were selected after analysing the technological process. Input variables are consumptions of pellets of polymer, nitrogen and heat transfer agent. Output variables are concentrations of caprolactam and water in pellets of polymer and the tank temperature.

Matrix of dimensionless coefficients K has been obtained as follows:

$$K = \begin{pmatrix} 0.388 & 0 & -0.0975 \\ 0.2325 & 0.001875 & 0.041 \\ -0.0855 & 0 & 0.0855 \end{pmatrix} \quad (1)$$

The method using the Bristol matrix which characterises connectivity degree in static, was used for evaluating the degree of system connectivity. Each element of the matrix is a result of the division of two derivatives: the first one is a derivative of steady state open

loop system output under control, the second one is a derivative of steady state closed loop system output under control. The Bristol is as follows:

$$\lambda = K \cdot (K^T)^{-1} \tag{2}$$

where K is a transfer coefficients matrix.

In this work, we have obtained matrix λ as:

$$\lambda = \begin{pmatrix} 0.388 & 0 & -0.0975 \\ 0.2325 & 0.001875 & 0.041 \\ -0.0855 & 0 & 0.0855 \end{pmatrix} \cdot \left(\begin{pmatrix} 0.388 & 0 & -0.0975 \\ 0.2325 & 0.001875 & 0.041 \\ -0.0855 & 0 & 0.0855 \end{pmatrix}^T \right)^{-1}$$
$$\lambda = \begin{pmatrix} 0.953 & -114.06 & -0.187 \\ 0.961 & -149.706 & 1.441 \\ 0.041 & -27.892 & 1.041 \end{pmatrix} \tag{3}$$

After analysing λ, we established that our object is connected. Hence, it's necessary to compensate cross links for controlling the tank.

Analysis of controllability

Before we synthesise the control algorithm, it is necessary to study such properties of object as the stability of free movement, controllability and observability. An analysis of the results of these studies allows us to conclude the ability to control the object. Presentation of the dynamic object in the state-space model is used for this task.

An evaluations of the stability of free movement, controllability and observability are performed in the neighbourhood of operating point. Strong conditions of controllability and stability have been found only for some classes of nonlinear objects. Availability or non-availability of these properties can be established by using linearisation of nonlinear equations describing the object [1]. If the linearised system is controllable in the neighborhood of some steady state, then we may assume that the original nonlinear system is controllable. Consumptions of pellets of polymer, nitrogen and heat transfer agent were previously chosen as control actions. The control task is to fully remove the monomer and water from pellets of polymer and to support the tank temperature at the desired level by changing the control actions.

The original nonlinear model of object with distributed parameters was presented by using its discrete analogue (cell's model). Linearisation of the object in the neighbourhood of the working point was performed in Simulink app «Linear Analysis Tool», MATLAB. Matrix of state **A** (dimension 21×21), matrix of control **B** (dimension 21×3) and matrix of observe **C** (dimension 3×21) were derived.

A study on the stability of the unperturbed system in the state-space model was performed. If all real parts of all eigenvalues α_i of matrix **A** are negative, then the system is stable:

$$\det(\alpha_i \mathbf{I} - \mathbf{A}) = 0 \tag{4}$$

where **I** is identity matrix.

Results show that our object is stable in the neighbourhood of the working point. This way, it has a property of stabilizability [2].

Analyses of the controllability were performed by using the controllability matrix $\mathbf{N_c}$ [1-3]:

$$\mathbf{N}_\mathbf{c} = \left[B : AB : A^2B : \ldots : A^{n-1}B\right] \tag{5}$$

where n is an order of system.

If rank of $\mathbf{N_c}$ is equal to n, then the linear system is fully controllable. If rank of $\mathbf{N_c}$ is smaller than n and bigger than 0, then the system is partly controllable. If rank of $\mathbf{N_c}$ is equal to 0, then the system is non-controllable. The controllability matrix and its rank were derived and calculated by using inbuilt MATLAB functions. The rank of $\mathbf{N_c}$ is 12. It is smaller than the order of the system that equals 21, hence our pre-polyamidation tank is not fully controllable. This way, there are such initial conditions in the phase state when the object cannot be transferred to the specified final condition. Also it was shown that our object is fully controllable in the space of outputs.

Analysis of observability

The observation equation is $\mathbf{y} = \mathbf{C}\cdot\mathrm{x}$, where $\mathbf{y} = (y_1,\ldots,y_m)^{\mathrm{T}}$ is a vector of observation variables, $\mathbf{x} = (x_1,\ldots,x_n)^{\mathrm{T}}$ is vector of the output variables, **C** is an observation matrix (dimension $m\times n$). The observability matrix is written as follows [1-3]:

$$N_o = \left[C^T : A^TC^T : (A^T)^2C^T : \ldots : (A^T)^{n-1}C^T\right] \tag{6}$$

where n is order of system.

The observability matrix and its rank was derived and calculated by using inbuilt MATLAB functions. The rank of N_o is 15. It shows that our object is not fully observable.

The task of controlling the object was solved in next step.

3. Designing the optimal controller

Control of tubular chemical reactors is probably the most difficult among all of reactor systems. It is caused by some technical and design factors.

Controllers using methods of optimal control theory are widely used on tubular reactors. At present, optimal control is one of the perspective direction of automatic control theory development. There are many works about the application of optimal control in some technical and technological objects.

Literature presents a wide range of criteria for the estimation of control quality [1-4]. Among them, criteria of maximum speed and minimum of control error dispersion are widely used. In this work we will use both criteria in dynamics.

Criterion of minimum error dispersion

There is a closed-loop control system (Fig. 1) where stationary centered random signal is used as disturbance. The interference signal is formed by a filter with transfer function $W_f(s)$ from white noise $v(t)$.

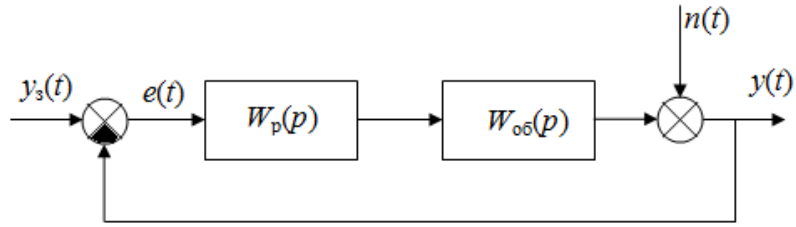

Fig. 1. Closed-loop control system

Dispersion of error can be found as:

$$De = \int_0^\infty \left[k_f(\tau) - k_1(\tau)\right]^2 d\tau \tag{7}$$

where $k_f(\tau)$ is a pulsed transition function of the filter; $k_1(\tau)$ is a pulsed transition function of the system consisting of two dynamic elements:

$$W_1(s) = W_f(s) \cdot F_y(s) \tag{8}$$

where $F_y(s)$ is a transfer function of the closed-loop system on the control channel.

It is necessary to select transfer functions $F_y(s)$ and $W_1(s)$ so that we allow to minimise the expression (4). It is difficult because almost always there is a transport delay in the object. In that cases, the minimum can be achieved only when $k_f(\tau) = k_1(\tau)$ and $\tau > \tau_d$.

Having found the optimal transition function $k_1^{opt}(\tau)$ and $W_1^{opt}(s)$, we can derive the optimal transfer function of the closed-loop system $F_y^{opt}(s)$ from expression (5). The transfer function of the optimal controller can be written as [4]:

$$W_p^{opt}(s) = \frac{F_y^{opt}(s)}{1 - F_y^{opt}(s)} \cdot \frac{1}{W_{об}(s)} \tag{9}$$

It is known that for the system having stationary random signal as a disturbance, the transfer function of the optimal controller is:

$$W_p^{opt}(s) = \frac{e^{-\alpha\tau_d} \cdot e^{-s\tau_d}}{1 - e^{-\alpha\tau_d} \cdot e^{-s\tau_d}} \cdot \frac{1}{W_{об}(s)} \tag{10}$$

where τ_d is the transport delay.

Criterion of the maximum speed

There are many ways to solve the task of seeking optimal control under the criterion of maximum speed. The Hamilton variational calculus, phase space method, Viener optimal control theory are widely used. There are some disadvantages of using these methods. One can distinguish such defects as difficulty of solving equations and their cumbersome, high probability of error, difficulty of expression for computing control actions.

The "Trajectories docking" method [5], based on the Feldbaum theorem, is the simplest method for solving the task of maximum speed. Let's consider it on the object with the transfer function:

$$W_{ob}(s) = \frac{k}{(T_1 \cdot s + 1) \cdot (T_2 \cdot s + 1)} \tag{11}$$

The general solution of the corresponding differential equation is:

$$y(\tau) = c_0 + c_1 \cdot e^{\alpha_1 \tau} + c_2 \cdot e^{\alpha_2 \tau} \tag{12}$$

where α_1 and α_2 are roots of general solution of the homogeneous equation; c_0 is derived from seeking particular solution; c_1 and c_2 are derived from solving the Koshi task.

The entire time interval of changing the control variable and control action is divided into three sectors. The first sector characterises the beginning of the transient process, time interval $[0; \tau_r)$. The control action has a maximum value. The time interval of the second sector is $[\tau_r; \tau_f)$. This sector describes movement of the object to steady state. The control action equals 0. Since $t = \tau_f$ the object is at steady state or finish movement to steady state. The control action at time interval $[\tau_f; \infty)$ has a nominal value.

This way, the optimal control task is to find switching times τ_r and τ_f between maximal, minimal and nominal values of the control action. The system consisting of six nonlinear equations is solved for this. In general, this system may be written as:

$$\begin{cases} c_0 + c_1 \cdot e^{\alpha_1 \tau_0} + c_2 \cdot e^{\alpha_2 \tau_0} = 0, \\ \alpha_1 \cdot c_1 \cdot e^{\alpha_1 \tau_0} + \alpha_2 \cdot c_2 \cdot e^{\alpha_2 \tau_0} = 0, \\ c_{00} + c_{11} \cdot e^{\alpha_1 \tau_f} + c_{22} \cdot e^{\alpha_2 \tau_f} = y_d, \\ \alpha_1 \cdot c_{11} \cdot e^{\alpha_1 \tau_f} + \alpha_2 \cdot c_{22} \cdot e^{\alpha_2 \tau_f} = 0, \\ c_0 + c_1 \cdot e^{\alpha_1 \tau_r} + c_2 \cdot e^{\alpha_2 \tau_r} = c_{00} + c_{11} \cdot e^{\alpha_1 \tau_f} + c_{22} \cdot e^{\alpha_2 \tau_f}, \\ \alpha_1 \cdot c_1 \cdot e^{\alpha_1 \tau_r} + \alpha_2 \cdot c_2 \cdot e^{\alpha_2 \tau_r} = \alpha_1 \cdot c_{11} \cdot e^{\alpha_1 \tau_f} + \alpha_2 \cdot c_{22} \cdot e^{\alpha_2 \tau_f} \end{cases} \tag{13}$$

where y_d is the desired value of the control variable; τ_r and τ_f are switching times; τ_0 is an initial time.

The first two equations of (13) show system condition at an initial time. The next two equations of (13) characterise the system at the steady state. The final equations describe the process of "trajectories docking". So, we may write system (13) as:

$$\begin{cases} ku_m + c_1 + c_2 = 0, \\ \alpha_1 c_1 + \alpha_2 c_2 = 0, \\ c_{11} e^{\alpha_1 \tau_f} + c_{22} e^{\alpha_2 \tau_f} = y_d, \\ \alpha_1 c_{11} e^{\alpha_1 \tau_f} + \alpha_2 c_{22} e^{\alpha_2 \tau_f} = 0, \\ ku_m + c_1 e^{\alpha_1 \tau_r} + c_2 e^{\alpha_2 \tau_r} = c_{11} e^{\alpha_1 \tau_f} + c_{22} e^{\alpha_2 \tau_f}, \\ \alpha_1 c_1 e^{\alpha_1 \tau_r} + \alpha_2 c_2 e^{\alpha_2 \tau_r} = \alpha_1 c_{11} e^{\alpha_1 \tau_f} + \alpha_2 c_{22} e^{\alpha_2 \tau_f} \end{cases} \quad (14)$$

where k is a gain; u_m is a maximal value of the control action.

System (14) can be easily solved by using the numerical method. It should be noted that a description of the method can be used for designing an optimal controller providing the fastest possible shutdown of the process.

Combined system

The control system consisting of two optimal controllers for controlling the tank temperature was designed and presented in figure 2.As we can see, this system has a combined structure.

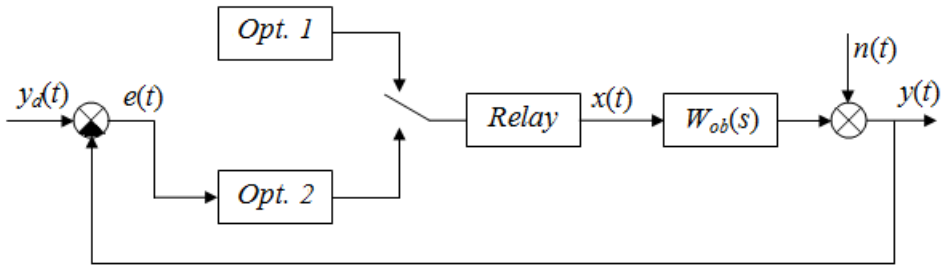

Fig. 2. Combined system for controlling temperature of pellets of polymer

Block *Relay* switches between controllers on the following condition:

$$x(\tau) = \begin{cases} Opt.1, \tau \le \tau_f, \\ Opt.2, \tau > \tau_f \end{cases}$$

For channel “consumption of heat transfer agent – temperature of pellets” transfer function without transport delay is written as follows:

$$W_{ob}(s) = \frac{47502059}{(1200 \cdot s + 1) \cdot (15 \cdot s + 1)} \quad (15)$$

Having solved system (14) with our own parameters, we have found switching times τ_r and τ_f, to equal 703 *s* and 715 *s* respectively.

The transfer function of *Opt*. 2 has the following form (16):

$$W_p^{opt}(s) = \frac{e^{-\alpha\tau_d} \cdot e^{-s\tau_d}}{1 - e^{-\alpha\tau_d} \cdot e^{-s\tau_d}} \cdot \frac{1}{k} \cdot (T_1 \cdot s + 1) \cdot (T_2 \cdot s + 1) \tag{16}$$

Having approximated the autocorrelation function of the disturbance signal formed by the filter from the white noise, we derived parameter α. The filter transfer function was derived.

Optimal controllers for channels "consumption of pellets of polymer – concentration of caprolactam in polymer" and "consumption of nitrogen – concentration of water in polymer" were derived analogically.

4. Conclusion

The carried out evaluation of system-wide and structural properties of pre-polyamidation tank allowed us to choose the control actions and measure the state variables. The problem of structural, algorithmic and parametric synthesis of the control system minimises energy consumption for performing the process synthesis of polyamide-6 was solved.

References

[1] Pupkov K. A., Egupov N. D., *Teoria optimizacii sistem abtomaticeskogo upravlenia*, Izdatelstvo MGTU im. N. E. Baumana 2004.

[2] Gubin G. K., Grebe S. F., Salgado M. E., *Proektirovanie system upravlenia*, BINOM Laboratoria znanij 2004.

[3] Rej U., *Metody upravlenia tehnologiceskimi processami*, Per s angl., Mir 1983.

[4] Besekerskij W. A., Popov E. P., *Teoria system abtomaticeskogo upravlenia*, Spd., Professia 2003.

[5] Golovushkin B., Volynskii V. U., Zaitzev V. A., *Optimal management of the process of convective drying of thin fabric materials*, Shenyang Institute of Chemistry technology, China 2004.

TECHNICAL TRANSACTIONS | CZASOPISMO TECHNICZNE
MECHANICS | MECHANIKA
2-M/2016

VALERIAN BLINICHEV, ANDREY POLANSKI, OLEG CHAGIN*,
JANUSZ KRAWCZYK**

RECTIFICATION COLUMN: CRITERIA OF EFFICIENCY

KRYTERIA OCENY EFEKTYWNOŚCI DZIAŁANIA KOLUMN REKTYFIKACYJNYCH

Abstract

In the paper analysis of the factors influencing the efficiency of the rectification process is provided. The authors show that existing dependences, equivalent to HETP, cannot be used for calculating rectification plate columns and columns with vortex nozzles, in which the coefficients of mass transfer are substantially dependent on the irrigation density and the gas/steam velocity. The dependence of the efficiency of the packet vortex nozzle as a function of the hydrodynamic regimes of the vapour and liquid phases is proposed.

***Keywords**: HETP, efficiency, distillation column, rectification, packing*

Streszczenie

W pracy przedstawiono analizę czynników efektywności procesu rektyfikacji. Autorzy wykazali, że istniejące zależności oparte o WRPT nie mogą być stosowane do kolumn półkowych i z dyszami wirowymi gdzie współczynniki transportu masy są powiązane z wielością zraszania i prędkością gazu/pary. Zaproponowano zależność efektywności dla dysz wirowych jako funkcji parametrów hydrodynamicznych pary i cieczy.

Słowa kluczowe: WRPT, efektywność, kolumny destylacyjne, rektyfikacja wypełnienia

DOI:

* Prof. PhD. DSc. Eng, Valerian Blinichev, MSc Andrey Polanski; PhD. DSc. Eng. Oleg Chagin, Department of Machines and Equipment for Chemical Industry, Faculty of Chemical Engineering and Cybernetics, Ivanovo State University of Chemistry and Technology.

** PhD. DSc. Eng. Janusz Krawczyk, Prof. CUT, Institute of Thermal and Process Engineering. Faculty of Mechanical Engineering. Cracow University of Technology.

1. Introduction

The efficiency of liquid mixture separation, which defines both the quality of the distillate and the size of the column (height), is the most important characteristic for any rectification column. If the diameter of the column is determined through the optimal vapour velocity in the upper and bottom parts of its column, which mainly depends only on the structural design of auxiliaries, then the height (as the most difficult parameter to define) depends on both the heat- and mass-transfer rate on each tray (or height of transfer unit in case of packed column) and the distribution of temperatures along the column length. The heat- and mass-transfer rate on a tray or on the packing is associated with optimal vapour velocity on different column heights, which is usually determined by means of experiments for each type of the mass-transfer devices.

Numerous simulation models exist for batch distillation, but many of these employ theoretical stage models. Some of these models consider tray efficiency, but only as a tuning parameter, obtained by the trial and error method, for matching simulation results with actual experimental data.

The quality of separation of both binary and multicomponent liquid mixtures depends on many factors: the difference between boiling temperatures of the components and the presence of the azeotropic mixtures; reflux flow rates; distribution of temperatures along the column length; structural design of the auxiliaries, which influence not only the quality of separation, but also the column height.

1.1. Factors affecting tray efficiency

The factors affecting the efficiency of a tray include: mechanical design factors (tray type and size, hole size, weir height), operation conditions (liquid and vapour rates) and the characteristics of the mixture on the tray. Some of these factors, which have been considered [1, 2, 3], include outlet weir height, hole size, liquid mixing, entrainment, flow regimes, reflux ratio, composition and surface tension of the components of the mixture.

1.1.1. Hole Size and Outlet Weir Height

The effect of the hole size in sieve trays and weir height (in other trays) on the tray efficiency is usually associated with its holdup characteristics. An investigation [3] of the hole size influence in sieve trays on the tray efficiency showed that smaller holes exhibited higher efficiencies at low vapour rates, but at higher vapour rates, the hole size has not shown any effect. It was suggested that smaller holes at low vapour rates prevented liquid downfall due to the capillary surface tension effects, thus increasing the tray liquid holdup and efficiencies. Smaller flows are issued from smaller holes thus increasing the mass-transfer process.

On the contrary, outlet weir height is used to maintain an appropriate liquid depth (holdup) on the tray and, as it was expected, tray efficiency increases with increasing outlet weir height. Deeper liquid levels on the tray mean that the residence time and mass transfer time of the vapour bubble through the liquid is increased.

1.1.2. Reflux ratio and tray holdup

While studying the reflux ratio effect, Pigford [4] showed that in the presence of appropriate holdup, the effect of the reflux ratio on the sharpness of the separation was less

pronounced than in a column with negligible holdup. Langdon and Keyes [1] however, concluded on the basis of the results obtained from experimental data, using isopropyl-water mixture that changes in reflux ratio had a negligible effect on the tray efficiency. Other researchers [5] have found plate efficiency to vary appreciably with reflux ratio. Ellis and Hardwick's results were based on the results obtained from the distillation of a methylcyclohexane/toluene mixture, but their conclusions did not take into account the effect of concentration on the tray efficiency. The effect of holdup on actual tray efficiency is not reported, but its effect on the sharpness of separation gives an indication to its effect on the distillation operation.

1.1.3. Liquid viscosity

Barker and Choudhury [6] studied the effect of liquid viscosity on the mass transfer and plate efficiency. It was found that with increasing liquid viscosity a reduction in the interfacial area occurs, thus leading to a reduction in the gas-film efficiency. Viscosity can also increase the size of a bubble at bubble formation at the slot or orifice by retarding the rate of closure of the neck of the bubble. This change in bubble size could be detected by liquid holdup measurements for the tray. Liquid holdups decrease with increasing liquid viscosity.

A beneficial effect of liquid viscosity is the reduction of the bubble rise rate through the liquid on the plate, leading to an increased mass transfer. This effect, however, does not appear to be sufficient to balance the decrease in surface area obtained at higher liquid viscosities.

1.1.4. Concentration effects

The effect of concentration on the tray efficiency was demonstrated by Fane and Sawistowski in [2], where they showed a dependence of the benzene-cyclohexane system on the efficiency passing through a maximum. This dependence was found to be strong at medium weir height and at low vapour velocity.

Shilling [7] obtained tray efficiency data for the distillation of ethanol/water mixture (concentration of ethanol was between 0 and 70 mole %). He observed an efficiency maximum in the composition range of 35 to 60 mole percent ethanol with efficiency falling more sharply at the lower ethanol composition range. At very low ethanol concentrations, Murphree efficiency values were observed to exceed 100%, the ones the authors suggested to be erroneous.

2 Packed rectification column: the efficiency of mass-transfer devices

Most of the up-to-date industrial packed beds have very extended surface area. For example, Sulzer AG is currently engaged in the production of packed beds with the specific surface of more than 800 m^2/m^3, and Ingehim Company suggests randomly distributed packing with specific surface in the range of 1000 to 1200 m^2/m^3 [8]. All packing columns, except the vortex ones, certainly work in the film mode, where the nozzle surface area is a mass-transfer surface in case of full flooding. Such columns work in the small operating range for vapour velocities (at vapour velocities less than about 1.5 m/s) and low density irrigation (less than $10 \div 15$ m^3/m^2h). The mass-transfer surfaces in them are to be practically

constant on the whole range of operating vapour/liquid velocities. The only exception is a short range close to the liquid holdup mode, when emulsification arises [9], whereby the value of mass-transfer surface and mass transfer coefficient spontaneously rise.

Inasmuch as this regime is close to the flooding point, its retention is impossible even with the use of modern automation systems. As a result, all the nozzles, except for the ones we studied [10, 11, 12], work as the apparatus with thin-film, which ideally equals the nozzle surface area.

As most packed beds mainly work in the film mode, the main desirable requirements for the packing of distillation columns are: to promote a uniform distribution of gas and liquid, have a large surface area (for greater contact between the liquid and vapour phase) and have an open structure, providing a low resistance to the gas flow. Many types and shapes of packing can satisfactorily meet these requirements [13].

While determining the actual number of trays of mass-transfer apparatus, the concept of theoretical plate is used, where the equilibrium between the vapour and liquid concentration is achieved on a condition that the complete mixing of vapour and liquid phases occurs. On the n-tray, the changing of the light-volatile component from liquid to vapour phase takes place, and semi-volatile component changes from vapour to liquid sate. Such alteration of concentration is named the theoretical step or theoretical plate. Drawing the steps between the tie and equilibrium lines in the given range of operating concentrations, the general number of steps of N_{T} (or number of theoretical plates) is found.

If the number of theoretical trays is known, then the number of actual N_{D} steps of separation is:

$$N_D = \frac{N_T}{\eta_T}, \tag{1}$$

where η_T is the averaged tray efficiency.

As we have noted before [14], many researchers defined the overall tray column efficiency by means of the tray efficiency. The most popular concept for evaluating the height of a packed column is the *HETP* (Height Equivalent to Theoretical Plate), defined by the following equation:

$$Z = HETP \cdot N, \tag{2}$$

where:

Z is a height of the packed bed required for achieving the separation equivalent to the N – number of theoretical plates [15].

Unfortunately, there are only a few generalised methods available in the open source literature for estimating the *HETP*. These methods are empirical and supported by vendor advice. The performance data published by universities are often obtained while using small columns and with not industrially important packing. When commercial-scale data are published, they usually are not supported by analysis or generalisation. Several correlations and empirical rules have been developed for *HETP* estimation in the last 50

years. Among the empirical methods, there is a rule of thumb for traditional random packing, that says:

$$HETP = \text{Column Diameter}$$

In Caldas's investigation, it has been shown that this rule holds only for small diameter columns.

Lockett [16] has proposed a correlation to estimate *HETP* in columns containing structured packing elements. It was inspired by Bravo's correlation [17] in order to develop an empirical relation between *HETP* and the packing surface area, operating at 80% flooding condition:

$$HETP = \frac{(4.82 \cdot (\rho_L - \rho_G)^{0.5} \mu_r^{-0.06})}{\alpha}, \tag{3}$$

which:

$$\alpha = a_p \cdot \left[\left(1 + 0.78 \cdot e^{0.00058 a_p}\right) \cdot \left(\frac{\rho_G}{\rho_L}\right)^{0.25} \right]^2, \tag{4}$$

where

ρ_G – vapour density, kg/m^3;
a_p – specific surface of the packing, m^2/ m^3;
μ_r – relation between liquid viscosity at the packing bed temperature and viscosity of water at the temperature of 20^{o}C.

According to the Wang studies [18], *HETP* can be evaluated more accurately by the following expression:

$$HETP = \frac{\ln \lambda}{\lambda - 1} \left[\frac{u_{Gs}}{k_G \cdot a_e} + \lambda \cdot \frac{u_{Ls}}{k_L \cdot a_e} \right], \tag{5}$$

where:

λ – inclination ratio between the equilibrium and operation straight;
k_G – gas-phase mass-transfer coefficient;
k_L – liquid-phase mass-transfer coefficient;
a_e – effective interfacial area, m^2/ m^3;
u_{Ls}, u_{Gs} – liquid/gas phase superficial velocity.

Therefore, the precision of *HETP* evaluation by the equation (5) depends on the accuracy of correlations used to predict the effective interfacial area as well as the vapour and liquid mass-transfer coefficients, which are easily defined by the experiments at the known values of the mass-transfer area.

2.1. Murphree vapour phase efficiency

Besides the calculation of height equivalent to a theoretical plate, a number of researchers evaluate that by using the Murphree efficiency. In particular, in Laptev's work [19], the comparison between the efficiencies of diverse packings was provided. Also, it

was shown that “Ingehim” packing has the highest efficiency at the same vapour velocities and reflux ratio.

The equation derived by Murphree is:

$$y_j = y_j^* - M \cdot (y_j^* - y_{j-1}), \tag{6}$$

or in its more familiar form:

$$E_i^{MV} = \frac{y_{i,j} - y_{i,j+1}}{y_{i,j}^* - y_{i,j+1}} \tag{7}$$

where:

E_i^{MV} – is the Murphree vapour phase efficiency,
$y_{i,j}^*$ – equilibrium vapour phase concentration of the volatile component;
j – tray number;
i – component number.

It should be noted that this equation (7) is easily applied to the case where the vapour resistance is negligible in comparison with the liquid film resistance. An equivalent equation for the liquid phase can be also easily derived. However, the given method of calculation of the efficiency just weakly reflects (only through y^*) the real hydrodynamics of the mass-transfer device and it does not give any understanding on the influence of its structural design.

2.2. Description of packed mass-transfer devices

As an objective, Bravo and Fair [17] had the development of a general project model to be applied in packed distillation columns, using a correlation that doesn’t need validation for the different types and sizes of packing. Moreover, the authors did not intend to obtain the dependence on the flooding point, as the model of Bolles and Fair does. For this purpose, the authors used the Onda’s model, with the database of Bolles and Fair, to give a better correlation based on the effective interfacial area for calculating the mass-transfer rate. The better correlation, for all the systems and packing tested, is given by:

$$\frac{a_e}{a_p} = 0.498 \cdot \left(\frac{\sigma^{0.5}}{Z^{0.4}} \right) \cdot (Ca_L \cdot \mathrm{Re}_V)^{0.392}, \tag{8}$$

where:

a_e – effective interfacial area, m^2/m^3;
a_p – specific surface of the packing, m^2/m^3;
Ca_L – capillary number;
σ – liquid surface tension, N/m;
Re_V – Reynolds number for vapour phase.

Recently, with the emergence of more modern packing, other correlations predicting the rate of mass-transfer in the packed columns have been studied. Wagner [20], for example,

developed a semi-empirical model, taking into account the effects of pressure drop and holdup in the column for the Nutter rings and IMTP, CMR and Flaximax packing. These packings have a higher efficiency, and therefore they have become more popular for new projects of the packed columns today. However, for the traditional packing, according to the author, only correlations of Cornell [21], Onda [22] and Bravo and Fair [17] can give reliable information for the industrial use in both distillation and absorption processes. The derived theoretical relation is described as:

$$HETP = H_O \cdot \frac{\ln \lambda}{\lambda - 1}, \tag{9}$$

where:

H_O – height of a global mass transfer, m;
λ – inclination ratio between the equilibrium and operation line.

Although the above equation was validated only for the cases of dilute solutions, constant molar flow rates, binary systems and equimolar countercurrent diffusion, it has been applied to systems with very different conditions even for multicomponent systems [5].

Henriques de Brito and his co-workers [23] measured the effective interfacial area of sheet metal structured packings, such as Mellapak 125Y, 250Y and 500Y. Their results have demonstrated that the effective area can be much higher than the packing surface area due to instabilities in liquid flow, such as ripples, waves, etc.

The resulting correlation for all measurements as a function of the Reynolds number for liquid phase is as follows:

$$\frac{a_e}{a_p} = 0.465 \cdot Re_L^{0.3}, \tag{10}$$

where:

Re_L – Reynolds number for liquid phase.

It should be noted that the authors have not checked the correlation with fluids with different densities and viscosities of a liquid. Moreover, none of the aforementioned correlations examined the influence of the vapour flow; consequently, these dependences can be used only at the low velocities of the vapour phase.

3. The difficulties in determination of actual mass-transfer surface

Based on experimental data, many researchers define the mass-transfer coefficients fast enough, inasmuch as, if nozzle surface equals mass-transfer surface, then they present a single unknown in the mass-transfer equations.

$$M = K_V \cdot F_H \cdot \Delta_S, \tag{11}$$

where:

K_V – mass-output coefficient, (kg mol)/(m^2 s);
F_H – packing surface area, m^2;
Δ_s – driving force (an average concentration gradient).

In tray columns and columns with vortex nozzles, while changing both the vapour velocity and the irrigation density, the alteration of two parameters (effective surface area and mass-transfer coefficients) in the mass-transfer equations occurs. Consequently, it is impossible to carry out the tray efficiency calculations by equations 8 and 10, in which we need to know both of the parameters. Thus, the efficiency for these mass-transfer devices is to be calculated either by determining the volumetric mass-transfer coefficients or in the terms of hydrodynamic characteristics of the vapour and liquid phases [19].

$$1-\eta_T = e^{\frac{-K_{oy}\cdot a\cdot f\cdot H}{V}} = e^{-N_{oy}}, \tag{12}$$

where:

f – cross-sectional area, m^2;
N_{oy} – number of transfer units;
H – height of the contact area, m;
$(K_{oy}\cdot a)$ – volumetric mass-transfer coefficient.

The equation (12) shows that the height of transfer unit can be found, on condition that the value of volumetric mass-transfer coefficient is well-known.

The most interesting approach for determining the efficiency of mass-transfer device has been proposed in the work of Kafarov V. V. [9], where an empirical dependence of overall column efficiency was obtained by means of processing a large amount of data taken from the industrial bubble plate rectification columns.

$$\lg\eta = 1.67 + 0.3\cdot l\cdot g\cdot\left(\frac{L}{V}\right) - 0.25\cdot\lg(\mu_L\cdot\alpha) + 0.3\cdot h_L, \tag{13}$$

where:

L, V – vapour and liquid load, (kg mol)/h;
μ_L – liquid viscosity, (Pa s);
α – relative volatility;
h_L – length from upper end of cut to upper end of weir height plus half length of cut, m.

4. The directions of intensification and energy- and resource conservation of rectification processes

Besides the criteria of efficiency of the packed columns, great interest is presented by the directions of intensification and energy- and resource conservation of rectification processes.

Three directions, which are developed currently by domestic and abroad scientists, should be mentioned:

1. The works concerned with the minimisation of the reflux ratio. These investigations are intensively conducted in Russia under the direction of Serafimov L. A. [24, 25, 26].
2. The researches under Kulov N. N., directed to the development of combined reactive-catalytic processes and distillation processes combined with the processes of crystallisation. The implementation of these processes allows to decrease the external dimensions of equipment and power inputs. The combined processes of catalytic rectification enable to overpass the thermodynamic limitations in equilibrium reactions and to use the heat from exothermic reactions for the separation of the resulting mixtures [27, 28, 29].
3. The works concerned with the development and investigation of the new mass-transfer devices, which allow to essentially increase the rates and accordingly – the mass- and heat-transfer coefficients [8, 10, 11].

This work belongs to the latter direction, as we propose to apply the established by us dependence of transfer unit efficiency of the new packet vortex nozzle on the Reynolds number for the vapour and liquid phases.

The packet bed of this nozzle represents a set of cells combined with each other in the horizontal plane. In contrast with the existing packings, the created nozzle has more developped nonlinear surfaces, which provide the formation of a large quantity of drops on the film surface at vapour velocities of more than 2 m/s. Unlike the packings, which work in the thin-film mode, this nozzle works in the near-emulsive regime, where the mass-transfer surface is much higher than the geometric nozzle surface at the range vapour velocity from 2 to 5.5 m/s and values of the irrigation density of over 120 m^3/m^2s. The vortex nozzle possesses a quality of self-distribution of liquid phase on the column cross section even by feeding by a single jet on the nozzle surface.

The high velocities in the vapour and liquid phases as well as extremely high mass- and heat-transfer coefficients in the volume unit of a nozzle allow essential decreasing of external sizes of rectification columns at a high quality and efficiency of continuous processes.

The processing of experimental data based on the alteration of vapour velocities and flow rates at the column length permitted to derive an explicit form for the efficiency of conditional plate (or packed bed) of the packet vortex nozzle, which depends on the vapour and liquid according to Reynolds criteria; the irrigation density was changed in the range from $0.6\cdot10^{-3}$ to $1.4\cdot10^{-3}$ m^3/m^2s and the vapour velocity – from 1.2 to 3.5 m/s.

$$\eta_i = 4.5\cdot10^{-3}\cdot Re_{iL}^{0.5}\cdot Re_{iV}^{0.72} \tag{14}$$

$$Re_{iL} = \frac{V_{iL}\cdot b\cdot \rho_{iL}}{\mu_{iL}} \tag{15}$$

$$Re_{iV} = \frac{V_{iV}\cdot b\cdot \rho_{iV}}{\mu_{iV}} \tag{16}$$

where:

V – irrigation density, m^3/m^2s;
b – width of a cell in a packet vortex nozzle, m;
ρ_L, ρ_V – vapour and liquid density, kg/m^3;
μ_L, μ_V – vapour and liquid dynamic viscosity, (Pa s);
U_V – vapour velocity, m/s.

5. Conclusion

Literary data analysis shows that the commonly used Murphree efficiency factor can be applied for evaluating the efficiency of the rectification columns with binary mixtures. Besides, it is necessary to know or experimentally determine the concentration of a volatile component on each tray for calculating the Murphree factor.

In turn, for calculating the efficiency of the packed columns, which work in the film mode, knowledge of mass-transfer coefficients and specific contact surface is required. The latter is discussed in a large number of works, in which, according to some foreign studies, the value of the interface area is substantially smaller than the value of the geometric nozzle surface. This is why the calculation of the actual mass-transfer surface is rather difficult even for the nozzles, which work in the film mode.

Due to the fact that for the plate rectification columns and columns with the mass-transfer devices one can't clearly determine the actual mass-transfer surface, the efficiency of the mass transfer devices is to be calculated, either by determining the volumetric mass transfer coefficients or the hydrodynamic characteristics of the vapour and liquid phases, which depend on the structural design of plates or vortex nozzles.

References

[1] Langdon W. M., Keyes D. B., *Vapour-Liquid Equilibrium Data on Ethyl Alcohol–Water and on Isopropyl Alcohol–Water*, Ind. Eng. Chern., vol. 35(4), 1943, 464-469.

[2] Fane A. G., Sawistowski H., *Plate Efficiency in the Foam and Spray Regimes of Sieve plate Distillation*, IChemE Symposium Series №32, 1969, 8-19.

[3] Lockett M. J., Uddin, M. S., *Liquid-phase controlled mass transfer in froths on sieve trays*, Trans. Instn. Chern. Eng., vol. 58(3), 1980, 166-174.

[4] Pigford R. L., Tepe J. B., Garrahan C. J., *Effect of Column Holdup in Batch Distillation*, Ind. Eng. Chern.,vol. 43(11), 1951, 2592-2602.

[5] Ellis S. R. M., Hardwick M. J., *Effect of reflux ratio on plate efficiency*, IChemE Symposium Series №32, 1969, 29-37.

[6] Barker P. E., Choudhury M. H., *Performance of Bubble cap Trays*, British Chemical Engineering, vol. 14, 1959, 348.

[7] Shilling G. D., Beyer G. H., Watson C. C., *Bubble-plate Efficiencies in Ethanol-water Fractionation*, Chern. Engng. Prog. vol. 49(3), 1953, 128-134.

[8] Kagan A. M., Laptev A. G., Pushnov A. S., Farahov M. I., *Contact packings of industrial heat and mass transfer apparatuses*, Otechestvo, Kazan 2013.
[9] Kafarov V. V. *The Foundations of Mass-transfer*, Vysshaja shkola, 1972.
[10] Blinichev V. N., Chagin O. V., Krawczyk J., Kutepov A. M. *Packet vortex nozzle for heat and mass transfer apparatuses*, Patent 2205063 РФ // Б.И. 2003. № 15.
[11] Blinichev V. N., Chagin O. V., Kutepov A. M. *Packet vortex nozzle of nonmetallic materials*, Patent 2130536 РФ // Б.И. 2001. № 11.
[12] Voroshin A. V., Chagin O. V., Blinichev V. N., *Description of the distillation process in the column with packet vortex nozzle*, Proceedings of XXV International Scientific Conference «MMTT», Saratov, 2, 2012, 91.
[13] Henley, E. J., Seader, J. D., *Equilibrium-stage separation*, John Wiley & Sons Inc., New York 1981.
[14] Polanski A. V., Blinichev V. N., Chagin O. V., *Rectification Column: Criteria of Efficiency*, Izvestiya Vysshikh Uchebnykh Zavedeniy, Seriya *Khimiya I Khimicheskaya Tekhnologiya*, tom 59(1), 2016.
[15] Caldas, J. N., de Lacerda, A. I., *Torres Recheadas*, JR Ed. Tecnica, Rio de Janeiro 1988.
[16] Lockett, M. J., *Easily predict structured-packing HETP*, Chemical Engineering Progress, vol. 94(1), 1988, 60.
[17] Bravo, J. L., Fair, J. R., *Generalized correlation for mass transfer in packed distillation columns*, Ind. Eng. Chem. Proc. Des. Dev., vol. 21(1), 1982, 162.
[18] Wang, G. Q., Yuan, X. G., Yu, K., *Review of Mass-Transfer Correlations for Packed Columns*, Ind. Eng. Chem. Res., vol. 44(23), 2005, 8715.
[19] Laptev A. G., Elizarov V. I., Dyakonov S. G. *Determination of volumetric mass transfer coefficients in the gas-liquid layer on the industrial scale contact devices at the transition* (*sieve and jet plates*), Izvestiya Vysshikh Uchebnykh Zavedeniy, Seriya *Khimiya i Khimicheskaya Tekhnologiya*, tom 34(1), 1991.
[20] Wagner, I., Stichlmair, J., Fair, J. R., *Mass transfer in beds of modern, high-efficiency random packings*, Ind. Eng.Chem. Res., vol. 36(1), 1997, 227.
[21] Cornell D., Knapp W. G., Close H. J., Fair J. R., *Mass-transfer efficiency-packed columns*, Chem. Eng. Progr., vol. 56(8), 1960, 48.
[22] Onda K., Takeuchi H., Okumoto Y., *Mass transfer coefficients between gas and liquid phases in packed columns*, J. Chem. Eng. Japan, vol. 1(1), 1968, 56.
[23] Henriques de Brito M., von Stockar U., Menendez Bangerter A., Laso M., *Effective Mass-Transfer Area in a Pilot Plant Column Equipped with Structured Packings and with Ceramic Rings*, Ind. Eng. Chem. Res., vol. 33(3), 1994, 647.
[24] Danilov R. Yu., Petlyuk F. B., Serafimov L. A., *Minimum-reflux regime of simple distillation columns*, Theor. Found. Chem. Eng., vol. 41(4), 2007, 371.
[25] Serafimov L. A., Chelyuskina T. V., Mavletkulova P. O., *Special cases of determination of the minimum reflux ratio for distillation of binary mixtures*, Theor. Found. Chem. Eng., vol. 47(3), 2013, 231.
[26] Serafimov L. A., Chelyuskina T. V., Mavletkulova P. O., *Special distillation regime involving an infinite reflux ratio and an infinite number of separation stages*, Theor. Found. Chem. Eng., vol. 48(1), 2014, 48.
[27] Kulov N. N., *Some problems of separation of mixtures*, Theor. Found. Chem. Eng., vol. 41(1), 2007, 1.

[29] Myasnikov S. K., Uteshinsky A. D., Kulov N. N., *Hybrid separation processes combining vacuum distillation with fractional crystallization, partial melting, and granulation*, Theor. Found.Chem. Eng., vol. 43(3), 2009, 227.
[30] Pavlov O. S., Pavlov S. Yu., Kulov N. N., *New design of reactive distillation processes*, Theor. Found. Chem. Eng., vol. 43(6), 2009, 856.

TECHNICAL TRANSACTIONS | CZASOPISMO TECHNICZNE
MECHANICS | MECHANIKA
2-M/2016

VALERIAN BLINICHEV, IRINA POSTNIKOVA*, JANUSZ KRAWCZYK**

IMPROVEMENT OF THE MASS TRANSFER PROCESSES EFFICIENCY BY MEANS OF MECHANICAL ACTIVATION OF HOMOGENEOUS AND HETEROGENEOUS SYSTEMS

POPRAWA WYDAJNOŚCI PROCESÓW WYMIANY MASY POPRZEZ MECHANICZNĄ AKTYWACJĘ UKŁADÓW JEDNORODNYCH I NIEJEDNORODNYCH

Abstract

In this paper, the ways of intensification of technological processes by means of powerful short pulses of energy in activation machines in solid phase and water systems are considered. The mechanism of accumulation and relaxation of energy for the substances subjected to mechanical activation is shown.

Keywords: intensification, mechanical activation, rotary apparatus, cavitation, accumulation of energy, relaxation.

Streszczenie

W pracy omówione zostały metody intensyfikacji procesów technologicznych w ciałach stałych i cieczach przy użyciu krótkotrwałych impulsów energetycznych. Przedstawiono mechanizmy akumulacji i relaksacji energii w substancjach poddanych mechanicznej aktywacji.

Słowa kluczowe: intensyfikacja, mechaniczna aktywacja, maszyny wirnikowe, kawitacja, akumulacja energii, relaksacja.

DOI:

* Prof. PhD. DSc. Eng. Valerian Blinichev, PhD. DSc. Eng. Irina Postnikova, Department of Machines and Apparatuses of Chemical Productions, Faculty of Chemical Engineering and Cybernetics, Ivanovo State University of Chemistry and Technology.

** PhD. DSc. Eng. Janusz Krawczyk, Prof. CUT, Institute of Thermal and Process Engineering, Faculty of Mechanical Engineering, Cracow University of Technology.

Changes of the physico-chemical properties of solid materials under the influence of mechanical strain had attracted the interest of many researchers from various countries, even at the beginning of the last century.

However, in the sixties and seventies of the last century, a new branch of science – mechanochemistry, appeared, the fundamentals of which were formulated by V. V. Boldyrev, Director of the Novosibirsk Institute of Solid State Chemistry and Mechanochemistry of the Russian Academy of Sciences [1], and by P.U.Butyagin (The Institute of IHF of RAS) [3, 4].

Previously, the tribochemistry concept, developed by P.Tissen and G. Hajnike, preceded the science of "Mechanochemistry" [2].

In the works of P. U. Butyagin and V. V. Boldyrev, it was demonstrated that the new surface formation, when the hard crystalline substances are destructed, is accompanied by a range of physico-chemical phenomena [1, 3, 4], such as:

a) electronic emission of various intensity;
b) luminescence;
c) formation of excess surface energy on the new surfaces and emerging of electric charges and fields due to the bombardment of the surfaces by high-energy electrons;
g) generation of radio waves and x-rays emission;
d) thermo-radiation and accumulation of energy in the form of the elevated temperature of a solid;
e) formation of free radicals on the surface, especially on polymeric materials [10].

It has been previously noted [1, 5, 6, 7] that, as any grinding apparatus or machine is a kind of mechanoactivator, then in order to apply the activated substances for intensifying a particular technology, it is necessary for the amount of accumulated energy in it (before application) to be greater than the energy released in the course of the relaxation process.

Naturally, the greatest effect is achieved when the technological process is carried out in the activating machine.

The list of chemical reactions being carried out in the mills of small dimensions (ball, vibration, ring and centrifugal planetary ones) covers different classes of reactions, which have been studied.

The solid – gas reaction includes synthesis of nitrides, hydrides, and carbonyls [6].

Gases (nitrogen, hydrogen, carbon monoxide) react with metals and oxides.

In the system of Solid 1 + Solid 2, carbides, borides, silicides were synthesised, and a reduction of metals oxides was performed; synthesis of ferrites, catalysts of superconducting ceramics, of new composite construction materials [5, 6, 7] was carried out. Experiments on the mechanochemical process of carbonate decomposition, which stayed for quite a long time in the centrifugal planetary mill, were performed [5].

It should be noted that mechanochemical synthesis was carried out mainly in laboratory high-energy centrifugal planetary ball mills, in which the ratio of centrifugal forces to the force of gravity was: $\Phi = \frac{\omega^2 \cdot r}{g} > 80$

A way for project solution scaling for this types of mills is extremely complex due to large stresses at the machine nodes ($\sigma_{max} > [\sigma]$) when the productivity is $Y_m > 100$ kg/h. So, despite studies relating to the early 70-s of the 20th century, no industrial technology with

their application has yet been implemented, besides of the manufacture of small batches of some products.

In this context, a study of the influence of the strain rate on the intensity of mechanical activation of solids, aimed at further application of the continuously operated machines (mills) with a high speed impact loading, excluding the balls, their grinding and housing fretting, is of great interest. Under these conditions, the activated particles obtain multiple pulse loading, in which the occurring maximum voltages are greater than σ – beyond the limit of their strength.

At ISUCT (Department of Machines and Apparatuses of Chemical Productions), Bobkov S. P. and Blinichev V. N. [11] performed studies on grinding various materials in mills with different constructive designs. The share of energy spent on the formation of a new surface, for releasing thermal energy and for accumulating energy of a grinded body, was measured. These studies revealed that while being ground, the solids accumulate in them significantly greater amount of energy in comparison with the energy spent on the formation of a new surface.

The greatest amount of the accumulated energy (up to 40% of the fed one) was observed in polymer materials, in particular, made of Teflon: the thermal energy was not taken into account – it was measured and then deducted from the total amount of energy absorbed by a solid.

Precise measurement of the surface particles before and after grinding allowed to determine the energy value for a newly formed surface, if the specific surface energy is known (for certain substances). These studies have shown that for the majority of grinded substances (such as NaCl, limestone, Teflon), the value of the accumulated energy is ten times greater than the energy value of the newly formed surface.

It has been established that the amount of energy accumulated by a solid greatly depends on the rate of its strain and can be written as follows [11]:

$$\frac{\mathrm{d}E_{м}}{\mathrm{d}t} = \lambda \cdot \upsilon_{\varepsilon}^{2} \tag{1}$$

where:

$E_{м}$ – is the energy being absorbed;

υ_{ε} – rate of material strain;

λ – (constant) proportionality depending on the physical and mechanical properties of the activated material and on the ability to absorb the energy supplied.

From equation (1), it can be seen that the accumulated energy is proportional to the square of the strain rate.

The kinetics of the active state relaxation is proportional to the quantity of the energy accumulated:

$$\frac{\mathrm{d}E_{м}}{\mathrm{d}t} = -\mathrm{const}E_{м} \tag{2}$$

With multiple pulse loading, such as impact loading, (in collaboration with Bobkov S. P., Padokhin V. A., and Zueva G. A.) the following stochastic equation was derived

by us, which takes into account both the processes of accumulation and dissipation of energy:

$$\frac{\mathrm{d}E(t)}{\mathrm{d}t} = \alpha_c \sum_{i=0}^{i=n} A_i \cdot \delta(t - t_i) + \alpha_c \cdot E(t) \tag{3}$$

where:

$E(t)$ – the accumulated energy;

α_c – a coefficient that depends on the physical and mechanical properties of the material;

t_i – the time of the i-th act of the pulse loading;

A_i – power provided by a single (individual) impact pulse (*amplitude*), which is considered as an independent random variable.

Solution of the differential equation (3), which takes into account the cumulative and relaxation processes occurring when initially provided that $E = E_0$ at $t = 0$, is as follows:

$$E(t) = \alpha_c \cdot \sum_{i=0}^{i=n} A_i \exp\left[-\alpha_c (t - t_1)\right] + E_0 \exp(-\alpha_c \cdot t) \tag{4}$$

The analysis of the given equation demonstrates that between Delta-pulses (i.e. the acts of the particle impact loading) the energy $E(t)$ smoothly exponentially decreases, and at the moment of impact loading with A_1 energy, it rises abruptly at the value of A_i $\alpha_c \cdot A_i$.

Considering a short time lapse between the high-speed impact loadings in multi-staged mills (stress rate is very high, impact loadings are numerous, and the particles stay in a machine for 3.5 ÷ 5 seconds), the quantity of the energy accumulated in these types of mills appeared to be the greatest, despite the fact that the time of staying them in a ball, vibration and centrifugal-planetary mills was 20 minutes.

Therefore, while grinding hard materials, not only an external new active surface is created, but also active centres within the particles in the form of micro- and macrodefects as well as concentration energy centres around them. The latter significantly increase the reactivity of the subsequent relaxation processes.

Given the heavy dependence of the accumulated energy on the stress rate, we performed all the researches on mechanical activation of solids in the installations with multiple impact loading rates ranging from 75 to 180 m/s, depending on the physico-mechanical properties of the activated material, with the productivity of solid material of more than 250 kg/h.

In collaboration with Fedosov S. V., by applying high strain rates, we managed to realise a combined process: grinding and drying of large PVC sintered particles, in a 3-speed mill of impact-radiant type with the following initial parameters: initial humidity – 38%, the terminal one – less than 0.5%; the initial size of the sintered particles – 10 ÷ 50 mm, the final one – 250 microns, the time of staying particles in the mill – 10 seconds, the productivity of a machine in the workshop for PVC production is 250 kg/h.

Our joint studies with Ladaev N. M, aimed at removal of moisture from capillary-porous single particles by the impact with different strain rate, revealed that when the rate of impact loading is more than 45 m/s with a single impact of the particles with a diameter

of 5 mm, and initial humidity is 40%, the particle loses up to 30% per cent of its humidity, even without its destruction, due to inertial forces and waves of the elastic strain.

All these results prove that in cases when it is necessary to obtain dry and fine powder, it is necessary to combine the process of drying and milling, as 70 ÷ 98 % of the supplied energy is converted into thermal energy (internal pulse heat source), and inner diffusion moisture turns into surface moisture, which evaporates easily.

Another example of energy accumulation in polymers in the process of their milling is mechanochemical synthesis of fluorine rubber when Teflon and rubber are jointly milled in our multi-staged impact radiant mill implemented at Saint-Petersburg "Giproplast" plant with the productivity of 250 kg/h.

Totally inert to many PTFE systems, Teflon forms, in the process of joint milling, chemical bonds with rubber due to the energy accumulated in it as microdefects and radicals if a good mixing of the components and multiple impact loadings are provided. Thus, fluorine rubbers were synthesised, which otherwise could not be obtained.

High efficient mechanical activation of solids was achieved by means of their multiple high-rate impact loading in the multi-staged mills of continuous action (Fig. 1) at the Department of “Machines and Apparatuses of Chemical Productions” at ISUCT (with an average time of staying in the mill of less than 10 c) when the process of manufacturing new composite materials based on Teflon and coke was performed, the productivity of the raw materials mixture being 300 ÷ 350 kg/h. Both components were continuously supplied as doses into the mill in the predetermined ratios of fluorine (initial average size of the particles – 1 mm) and coke (average size – 0.25 mm), the ratio of PTFE being: coke – 70:30, 60:40.

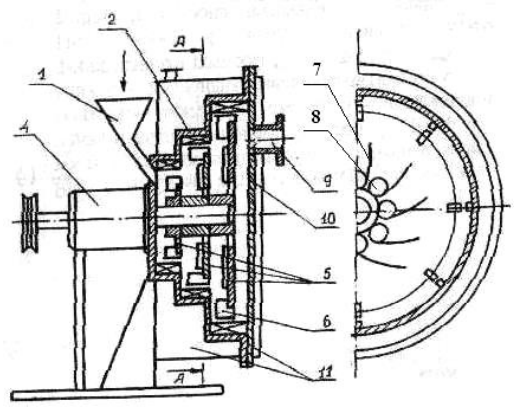

Fig. 1. Multistage continuous mill
1 – loading fitting; 2 – mill housing ; 3 – baffle plates; 4 – shaft; 5 – rotor; 6 – beater; 7 – blades; 8 – holes; 9 – unloading choke; 10 – flange; 11 – cooling jacket

A number of combined processes was carried out in the mill: mixing in powerful turbulent whirlwinds, which were created by the rotor blades and stator bumpers (of a mill housing); the additional pulse milling and mechanical activation of the components. Sintered compositions enabled to create new antifriction materials (FC-30 and FC-40), advantageously differing from the source material (Teflon).

The strength of the new composite materials has increased more than three times (compared with FC-20, which was obtained by means of conventional mixing of powders). Friction coefficient decreased by 2.5 times, and the cost dropped proportionally to the coke content as a cheap raw material.

Technology and equipment were implemented at the Kirovo-Chepetsk chemical plant.

Another example of a large accumulation of energy in repeated high-rate impact loading is ignition of the graphite milled in a multi-staged mill of an impact-radiant type [8].

While testing the optimal operating mode for the impact-radiant separation mill aimed at milling graphite from the Zaval′evsk deposits by means of an industrial machine, designed and constructed by us for Voskressensk Chemical Plant in order to maximise the number of particles of the product with the size less than 1 μm already at the stage of dry grinding, we managed to obtain the product with the particle content 25% less than 1 μm.

Having selected a probe for granulometric composition, we left 30 kg of the product in the cyclone hopper, the temperature in which reached 55^0 C. Within an hour, the product left in the hopper burnt down.

For industrial technology of fine graphite milling by means of CWC, we had to reduce the rate of impact loading in dry grinding mill and to obtain colloidal graphite product with 95% content of particles with dimensions of less than 1μm already in colloid-cavitational wet grinding mill [9], presented in Fig. 2.

Similarly mechanoactivation with pulse energy supply proceeds in liquid media, but only at greater velocity of relaxation processes.

In the works of several authors [12 ÷ 16] and in our works, it has been shown that the greatest effect is observed in water, suspensions and emulsions activation, when they are treated in rotary machines of various constructive design (see Fig. 2) in which a powerful pulse voltage arising because of the burst of cavitation bubbles overlaps with shear stress in a narrow annular gap between the rotor and the stator. Cavitation occurs in the fluid due to pressure pulsations and changes in the fluid flow rate.

Academician Dolynsky A. A. [17, 18], while studying fluid systems activation in rotary-pulsation apparatus, showed that periodic bursts of cavitation bubbles create powerful energetic discrete-pulse energy inputs in fluid systems in the nanoscale, and this process results in significant changes in their structure.

Studies on water and fluid systems activation were conducted by various authors on rotary machines, the basic schemes of which are presented in Fig. 2.

Despite somewhat different constructive features of rotary activators, for all of them, a major trigger factor is the discrete energy input in the form of *cumulative* flow when the cavitation bubbles burst. The frequency of bubbles occurring and bursting depends on constructive features of rotors and stators, as wells on rotors rotation frequency.

In our studies on water treatment of various origin (distilled, tap water and artesian) in rotary cavitators of types (a) and (b) (Fig. 2), it is shown that owing to the number of revolutions in the rotor cavitator and, accordingly, to the intensity of the cavitation impact, only the measured values of redox potential (ORP) increase significantly (Fig. 3); water pH increases insignificantly.

The value of ORP in relaxation process within a few days reduces; however, the level of steady-state values of the AFP remains higher compared to its initial value.

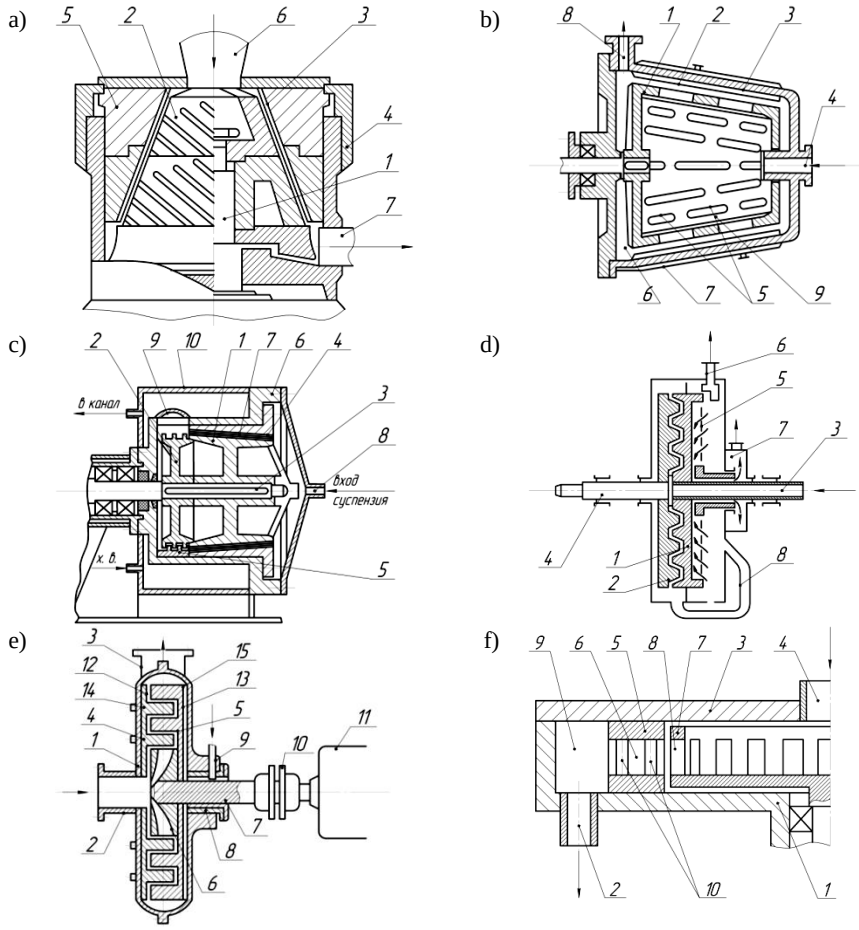

Fig. 2. Scheme of activators

a) Cone Colloid Mill Activator (1 – shaft; 2 – rotor; 3 – ribs; 4 – housing; 5 – stator; 6 – suspension inlet);
b) Colloid Mill Activator with the Perforated Rotor (1 – rotor; 2 – baffles; 3 – housing; 4 – suspension inlet; 5 – perforations; 6 – suspension unloading zone; 7 – jacket ; 8 – suspension outlet);
c) Cavitation-Colloid Mill Activator (1 – rotor; 2 – impact device; 3 – shaft; 4 – stator; 5 – counter-baffles; 6 – housing; 7 – grooves; 8 – suspension inlet; 9 – suspension outlet; 10 – cooling jacket);
d) Colloid Activator with Two Rotating Rotors and Separation of the Activated Solid Phase (1 – rotating hollow shaft rotor; 2 – rotating rotor; 3 – hollow shaft; 4 – shaft; 5 – separator; 6 –outlet of coarse particles; 7 – fine particles outlet);
e) Rotary Hydraulic Mill (1 – housing; 2 – inlet fitting; 3 – suspension outlet fitting; 4 – fixed disc; 5 – movable disc; 6 – rotor; 7 – shaft; 10 – shaft coupling; 11 – coupling drive; 12, 13 – grooves; 14, 15 – protrusions);
f) Rotary RPA Apparatus (1 – housing; 2 – suspension outlet fitting; 3 – cover; 4 – inlet fitting; 5 – stator; 6 – stator channels; 7 – rotor; 8 – rotor channels; 9 – voice camera; 10 – rods).

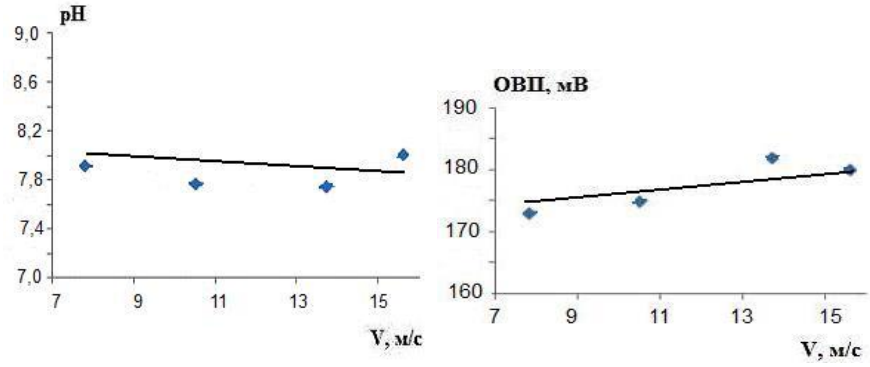

Fig. 3. Dependence of pH and ORP on the linear speed of rotor in the activator

In order to prove that cavitation bubbles do arise and burst in the cavitators, sensors were attached to the housing of the rotor. They allowed to register housing vibration when cavitation bubbles “exploded". Firstly, the housing vibrations of the idle activator operation were registered, and then those in the working mode (see Fig. 4).

From the plot (3) (Fig. 4,) it is clearly seen that when water passes through the activator, high frequency spectrum of additional pressure pulses from the cavitation bubbles bursts appear.

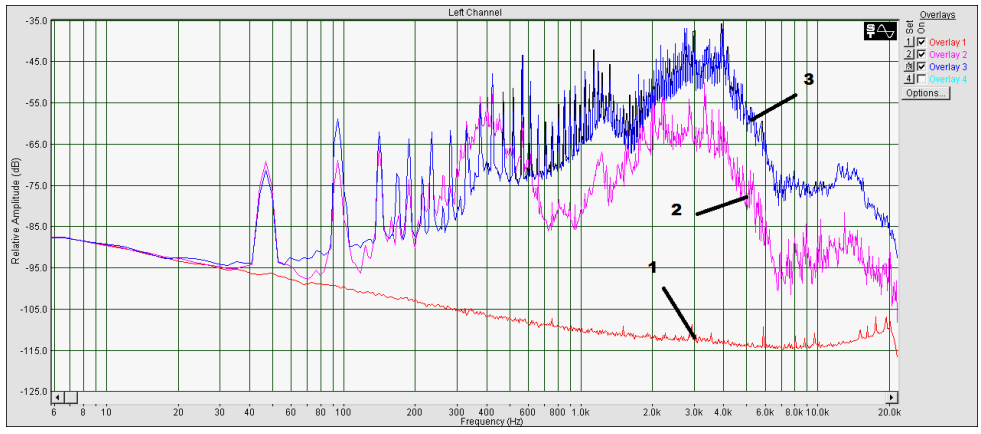

Fig. 4. Fourier spectrum in water treatment (water consumption is 1.44 m^3/h)
1 – background noise, 2 – spectrum of idle mode, 3 – spectrum of fluctuations in operating mode

The same phenomenon is observed when suspension passes through the cavitation device. In earlier works, it has been shown that if the fluid contains solid phase particles, the cavitation bubbles are formed and burst exactly on the moving hard particles.

A powerful pulse of energy, supplied to the hard particles when a bubble bursts, is the very "hammer" which destroys even small particles of solid materials. It is known that the

strength of many materials depends on the particle size, and when the latter reaches a monocrystal size, it increases by two orders of magnitude.

Therefore, when designing the construction of cavitation colloid mill for superfine milling of graphite (95% of the particles should have dimensions less than 1 micron), we have tested about a dozen of different machines constructions with a view of elaborating a cavitator, which would provide the conditions for forming and bursting the maximum number of cavitation bubbles.

The researches that we have jointly conducted with the staff of the Ivanovo Medical Academy and aimed at activation of two licensed drugs for treating diseases of joints (*Tomed and Tomed-Aqua*) in rotary cavitators of type (a) (Fig. 2), showed that death intensity of the various types of bacteria increases significantly, and efficiency of drugs application for treating these diseases (according to medical clinics data for the last 2 years) is growing.

Under the supervision of S. V. Fedosov, T. E. Slizneva (Ivanovo State Polytechnic University) undertook the studies of activation process in rotary-pulsation apparatus in a magnetic field of water solutions of electrolytes [19, 20]. It was shown that their mechano-magnetic treatment contributes to the enhancement of frost resistance of fine-grained concrete for 40 ÷ 50 cycles and provides the increase of the rate of curing at the early stages of hardening and elongation of beginning of setting along with reduction of its finishing, as well as results in enhancing the strength by 15 ÷ 22% compared to the concrete obtained by means of traditional technology. Application of mechano-magnetic activation of liquid mixing allows to save up to 10% of cement.

Mechano-magnetic activation of tempered water containing organic plasticising and water-reducing organic additives promotes mobility of the concrete mixture by up to 100% during 1,5 ÷ 2 hours, i.e. 1.2 ÷ 2.4 times more in comparison with not activated water systems.

Taking into consideration the above-mentioned information, we can conclude that impact pulse loading with a larger momentum energy of solids and water systems allows to intensify significantly many of the heat- and mass-transfer processes, including chemical reactions.

References

[1] Boldyrev W. W., *Eksperimentalnye metody w mehanohimii tberdyh neorganiceskih wescestw*, Nauka, Novosibirsk 1986.

[2] Thiessen P., Meyer K., Heinike Y., *Grundladen der Tribochemie*, Abd. Detsch. Acad. Wiss. Berlin Kl Chem., Ged. Bid., vol. 1, 1966., 194.

[3] Butagin P. U., Kinetika i priroda mehanohimiceskih reakcji, Uspiehi himii, vol. 40, 1971, 1935-1959.

[4] Butagin P. U., Uspiehi himii, vol, 31, 1984, 544-600.

[5] Avvakumov E. G., *Mehaniceskie metody aktivacii himiceskih processov*, Nauka, Novosibirsk 1986.

[6] Avvakumov E. G., Kosova N. U., Senna M., *Magkij mehanohimiceskij sintez – osnova novyh himiceskih tehnologij*, Nauka, Novosibirsk 2000.

[7] Sirokov U. G., *Mehanohimia i tehnologii katalizatorov*, Ivanovo 2005.
[8] Blinicev W. N. and all., *Mnogostupiencataa melnica udarnogo dejstvia*, A.c. № 946651, CCCP 1982.
[9] Blinicev W. N. and all., *Koloidnaa mielnica*, A.c. № 651841, CCCP 1971.
[10] Barambojm N. K., Mehanohimia bysokomolekularnyh soedinenij, Himia, 1971.
[11] Bobkov S. P., Blinicev W. N., Guumdzan P.P., *Wlianie tipa melnicy na energozatraty i mehanohimiceskie avlenia pri tonkom izmelcenii*, Himia i Himic. Tehnologia, vol. 22(3), 1979, 1004-1007.
[12] Balabudkin M. A., *Rotorno-pulsacionnye aparaty v himiko-farmacevticeskoj promyslennosti*, Medicina 1983.
[13] Balabusko A. M., *Rotornye apparaty s modulaciej potoka i ih primenenie v promyslennosti*, Nedra 1992.
[14] Zimin A. I., *Prikladnaa mehanika prerevistyh tecenij*, Foliant 1997.
[15] Promtov M. A., *Pulsacionnye aparaty rotornogo tipa: teoria i praktika*, Masinostroenie, 2001.
[16] Cervakov V. M., Udaev V. F., *Gidrvliceskie i kavitacionnye avlenia v rotornyh apparatah*, Masinostroenie, 2007
[17] Dolinskij A. A., *Nanomasstabnye efekty pri diskretno-impulsnoj transformacii energii*, Inzenerno-fiz. Zurnal, vol. 78(1), 2005, 15-22.
[18] Dolinskij A. A., *Teploobmen i gidrodinamika v parozidkostnyh dipersnyh sredah. Teplofizyceskie osnowy diskretno-impulsnogo vvoda energii*, Nukova dumka, 2008.
[19] Fedosov S. V., Akulova M. V., Slizneva T. E., *Opredelenie tehnologiceskih parametrov mehanomagnitnoj obrabotki vodnyh system s plastifiriuscej dobavkoj*, Stoitelnye materialy, vol. 3, 2010, 49-51.
[20] Fedosov S. V., *Mehanomagnitnaa aktivacia vodnyh rastworov himiceskih dobavok kak sposób modificirovania mielkozernistogo betona*, Himia i Himic. Tehnologia, vol. 57(3), 2014, 111-115.

TECHNICAL TRANSACTIONS | CZASOPISMO TECHNICZNE
MECHANICS | MECHANIKA
2-M/2016

ANETA CELAREK, JAN TALAGA*

A COMPARATIVE ANALYSIS METHODOLOGY OF CALCULATION OF STRENGTH TUBESHEETS BY EUROPEAN STANDARDS AND GUIDELINES FOR UDT

ANALIZA PORÓWNAWCZA METODYKI OBLICZEŃ WYTRZYMAŁOŚCIOWYCH ŚCIAN SITOWYCH WEDŁUG NORM EUROPEJSKICH I WYTYCZNYCH UDT

A b s t r a c t

This paper presents comparison of calculation methods of the required thickness of the tube sheet in the shell and tube heat exchanger compatible with the standards of the European standard PN - EN 13445-3, and the guidelines of the Polish Office of Technical Inspection (UDT). Details of the methods are illustrated by numerical examples – (calculations) for the selected design of the tubesheet.

Keywords: heat exchangers, tubes, tubesheets

S t r e s z c z e n i e

W artykule przedstawiono porównanie metod obliczeniowych wymaganej grubości ściany sitowej w płaszczowo-rurkowym wymienniku ciepła zgodnych ze standardami normy europejskiej PN-EN 13445-3 i wytycznymi polskiego Urzędu Dozoru Technicznego. Szczegóły metod zilustrowano przykładami liczbowymi dla wybranych konstrukcji dna sitowego.

Słowa kluczowe: wymienniki ciepła, rurki, dna sitowe

DOI:

* MSc. Eng. Aneta Celarek, DSc. Eng. Jan Talaga, Institute of Thermal and Process Engineering, Faculty of Mechanical Engineering, Cracow University of Technology.

1. Introduction

The European standard PN-EN 13445-3 shows three primary distinctions in terms of shell and tube heat exchangers. In addition to the above standard PN-EN 13445-3 is Index I, wherein it shows another design solution of a tubesheet. The analysis of strength calculations for the same configurations of tubesheet differs from those described in the Polish guidelines WUDT-UC. Polish guidelines WUDT-UC are treated as mandatory during the design of pressure equipment.

In the norm PN-EN 13445-3: 2002, rules for different types of heat exchangers were shown. According to the norm:

- U-tube heat exchanger (Figure 1);
- Fixed tubesheet heat exchanger (Figure 2);
- Floating head heat exchanger (Figure 3).

Floating head heat exchanger has three different configurations:

a) with an immersed floating head;
b) with an externally sealed floating head;
c) with an internally sealed floating tubesheet [3].

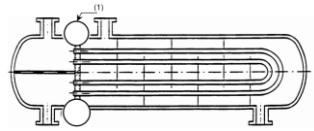

Fig. 1. U-tube heat exchanger [3]

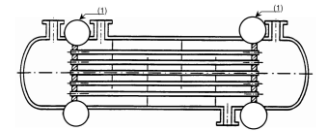

Fig. 2. Fixed tube sheet heat exchanger [3]

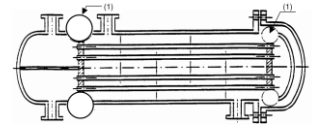

Fig. 3. Floating head heat exchange [3]

Table 1

The characteristic elements in the various types of heat exchangers

Characteristic	U-tube tubesheet heat exchanger	Fixed tubesheet heat exchanger	Floating head heat exchanger
Amount and shape tubesheet	One –flat, circular, uniform thickness	Two – flat, circular and identical (same materials, same connection with shell and channel)	Two – flat, circular, and identical connected by a bundle of straight tubes
Type of tubesheet (moving)	Stationary	Stationary	Stationary attached to the shell and channel Floating
Amount using configurations	6 (see Fig. 4)	6 (see Fig. 4)	6 stationary (Fig. 4) +3 floating (Fig. 5)
Loading conditions	3 cases	7 cases	3 cases
Tubesheet thickness	$e = \frac{D_0}{4\mu(0.8f)}\lvert P_s - P_t\rvert$	$e = \frac{D_0}{4\mu(0.8f)}\lvert P_s - P_t\rvert$	$e = \frac{D_0}{4\mu(0.85f)}\lvert P_e\rvert$

Tab. 1 shows a comparison of the information and characteristics among the types of heat exchangers which are shown in European standards. Tab. 1 also groups the equation on how to calculate the tubesheet thickness and which pressure we have to use in each heat exchanger.

This article shows one of this type – U-tube heat exchanger and different uses of the configurations of tubesheets. According the norm PN-EN 13445-3, the tubesheet may have one of the six configurations (design solutions) shown in Fig 4.

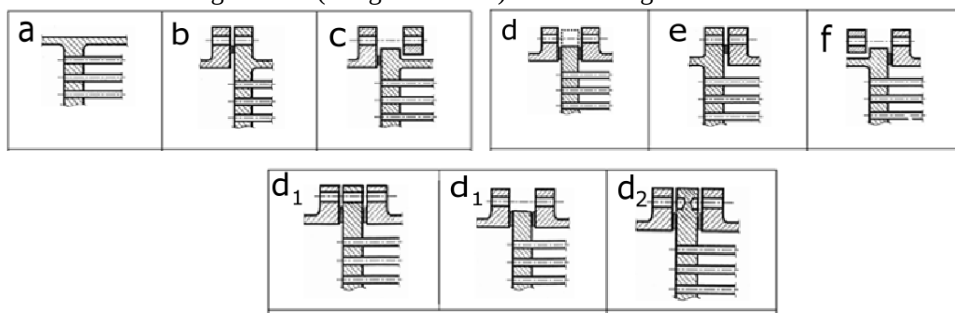

Fig. 4. Various types of configuration tubesheets [3]
a) integral with shell and channel; b) integral with shell and gasketed with channel, extended as a flange; c) integral with shell and gasketed with channel, not extended as a flange; d) gasketed with shell and channel, extended as a flange or not; e) gasketed with shell and integral with channel, extended as a flange; f) gasketed with shell and integral with channel, not extended as a flange

Configuration d covers the cases where the tubesheet is: extended as (d_1 as flange or not d_2)

In the floating tubesheet heat exchangers the floating tubesheet may have one of the 3 configurations shown in Fig 5.

- tubesheet integral (Fig. 5a),
- tubesheet gasketed, extended as a flange (Fig. 5b),
- tubesheet gasketed, not extended as a flange (Fig 5c).

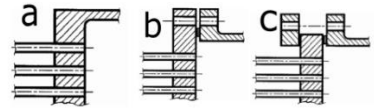

Fig. 5. Various types of configuration floating tubesheets [3]

For each of these types configuration of tubesheet a different method of calculation is used. All of the methods were shown in European standards PE-EN 13445-3.

2. Examples of calculations for U-tube heat exchangers

Below is a numerical example (examples of calculations) of the method of strength calculations for tubesheet contained in European standards PN-EN 13445-3. The calculations were carried out for the tubesheet of configuration b shown in Fig. 6. Tab. 2

presents the type of material and properties which were selected in calculations. The assumed values of tubesheet were shown in Tab. 3 [7, 3].

Table 2

Properties of used material

Tubesheet - material	R_m [MPa]	R_p [MPa]	R_{pt} [MPa]	f [MPa]	f_{20} [MPa]	f_{test} [MPa]	E [MPa]
P280GH (1.0426)	460	280	225	150	186.67	266.67	198610

Table 3

Input date of tubesheet

Input date	Value	Units	Description
e_n	100	mm	Nominal thickness of tubesheet (assume)
c_t	3	mm	Tubesheet corrosion allowance on the tube -side
c_s	3	mm	Tubesheet corrosion allowance on the shell - side
p	34	mm	Tube pitch
d_t	25	mm	Nominal outside diameter of tubes
l_{tx}	80	mm	Expanded length of tube in tubesheet
e_a	94	mm	Analysis thickness
e_t	2.3	mm	Nominal tube wall thickness
E_t	$1.9861 \cdot 10^5$	MPa	Elastic modulus of tube material at design temperature
E	198610	MPa	Elastic modulus of tubesheet material at design temperature
f_t	111.33	MPa	Nominal design stress of tube material at design temperature
f	150	MPa	Nominal design stress of tubesheet material at design temperature
S	178000	mm^2	Total unperforated area of tubesheet
D_0	1163.4	mm	Equivalent diameter of outer tube limit circle
G_S	1255	mm	Diameter of shell gasket load reaction
G_c	1255	mm	Diameter of channel gasket load reaction
W_S	181026	kN	Shell flange design bolt load for the assembly condition
W_c	1097.94	kN	Channel flange design bolt load for the assembly condition

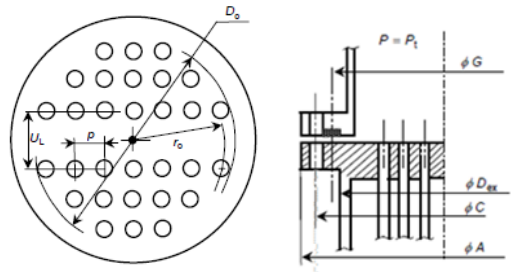

Fig. 6. Tubesheet design for b configuration [3]

The results of calculations on the thickness of the tubesheet are shown in Tab. 4. At this state of calculations, there are no differences in the method of calculation. Despite the following example of the various assumed operating pressures of the tubesheet, the calculation is carried out in the same way [3].

Table 4

The method of calculations concerning size of tubesheet

Equation	Results/ value	Units	Description
$e_a = e_n - c_t - c_s$	94	mm	Analyses thickness tubesheet (initial)
$\mu = \frac{p^* - d^*}{p^*}$	0.2647	–	The basic ligament efficiency for shear
$\rho = \frac{l_{t,x}}{e}$	0.8511	–	The tube expansion depth ratio (0 $\leq \rho \leq$ 1)
$d^* = \max\left\{\begin{bmatrix} d_t - 2\cdot e_t \cdot \left(\frac{E_t}{E}\right)\cdot\left(\frac{f_t}{f}\right)\cdot\rho; \end{bmatrix} \\ [d_t - 2\cdot e_t]\right\}$	22.09	mm	The effective tube hole diameter
$p^* = \frac{p}{\sqrt{1 - 4\frac{\min[(S);(4\cdot D_0\cdot p)]}{\pi\cdot D_0^{\ 2}}}}$	36.85	mm	The effective tube pitch
$\mu^* = \frac{p^* - d^*}{p^*}$	0.4005	–	The effective ligament efficiency of perforated tubesheet for bending
$\frac{E^*}{E} = \alpha_0 + \alpha_1\cdot\mu^* + \alpha_2\cdot\mu^{*2} + \alpha_3\cdot\mu^{*3} + \\ + \alpha_4\cdot\mu^{*4}$	0.414	–	Determination of the graph
$E^* = E\cdot 0414$	82227.64	MPa	The effective elastic modulus of the tubesheet at design temperature
$\vartheta^* = \beta_0 + \beta_1\cdot\mu^* + \beta_2\cdot\mu^{*2} + \beta_3\cdot\mu^{*3} \\ + \beta_4\cdot\mu^{*4}$	0.3106	–	The effective Poisson's ratio of tubesheet (Determination of the graph)
$D^* = \frac{E^*\cdot e^3}{12\cdot(1-\vartheta^{*2})}$	$6.2993\cdot10^9$	Nmm	The equivalent bending rigidity of tubesheet
$\rho_s = \frac{G_s}{D_0}$	1.0787	–	The shell diameter ratio
$\rho_c = \frac{G_c}{D_0}$	1.0787	–	The channel diameter ratio
$K = \frac{A}{D_0}$	1.1174	–	The tubesheet diameter ratio
$F = \frac{1-\vartheta^*}{E^*}\cdot(E\cdot\ln K)$	0.1848	–	The coefficient
$W_{\max} = \max[W_s; W_c]$	181026	kN	The maximum flange design bolt load for the assembly condition

After this stage, for future calculations, pressures operating at the side shell and tube should be selected. In this example, calculations of three types of pressures were carried out. Values of the operating pressure were assumed.

In first load case, the analysed negative pressure operated on the shell – side. In the second load case, the analysed negative pressure operated on the tube – side. In the third case, the negative pressure operating on the shell or the tube side was not taken into consideration.

Table 5

Load cases used in design

ID	Load Case 1	LC2	LC3	Units	Description
P_s	-0.1	1	1	MPa	Shell – Side Pressure
P_t	0.6	-1	0.6	MPa	Tube – Side Pressure

Below, Tab. 6 shows the procedure and the results of calculations carried out of the different load cases described in Tab. 5.

Table 6

Calculation the moment acting at different part of tubesheet [3]

Equation	LC 1	LC 2	LC 3	Units	Description
$M_{TS} = \frac{D_0^{\,2}}{16} \cdot [(\rho_s - 1) \cdot (\rho_s^2 + 1) \cdot P_s - (\rho_c - 1) \cdot (\rho_c^{\,2} + 1) \cdot P_c]$	-10087.73	28822.08	5764.42	Nmm	The moment due to pressures P_s and P_t acting on the unperforated tubesheet rim
$M^* = M_{TS} + \frac{W_{\max}(G_c - G_s)}{2 \cdot \pi \cdot D_0}$	-10087.73	28822.08	5764.42	Nmm	The moment acting on the unperforated tubesheet rim
$M_P = \frac{M^* - \frac{D_0^{\,2}}{32} \cdot F \cdot (P_s - P_t)}{1 + F}$	-3894.83	11128.08	2225.62	Nmm	the moment acting at periphery of tubesheet
$M_0 = M_P + \frac{D_0^{\,2}}{64} \cdot (3 + \vartheta^*) \cdot (P_s - P_t)$	-52905.35	151160	30231.63	Nmm	The moment acting at centre of tubesheet
$M = \max[\lvert M_P \rvert ; \lvert M_0 \rvert]$	52905.35	151160	30231.63	Nmm	The maximum moment acting of tubesheet
$\sigma = \frac{6 \cdot M}{\mu^* \cdot (e_a - h_g')^2}$	97.86	279.59	55.92	MPa	The calculated stress in a component
$\tau = \left(\frac{1}{4 \cdot \mu}\right) \cdot \left(\frac{D_0}{e}\right) \cdot \lvert P_s - P_t \rvert$	-8.18	23.28	4.6756	MPa	The calculated shear stress in a component

Depending on the applied pressure, different torques were obtained. In any case, the strength conditions of the maximum radial bending stress in the tubesheet and the maximum shear stress in the tubesheet have been fulfilled. The designed tubesheet fulfilled strength conditions for pressures assumed in Tab. 5. The material and size of the tubesheet were well selected.

3. Example of calculation for U-tube heat exchanger tubesheet extended as a flange

This section shows a comparison of the results of calculations performed in accordance with the WUDT-UC [2, 4, 8] and European standards. Tab. 7. shows input dates of strength parameters for the material used in the calculations [7, 6]. Tables 9, 10 and 11 were shown the selected results of these calculations. The calculations were carried out for tubesheet extended as a flange [4, 8].

Table 7

Properties of used material

Tubesheet – material	R_m [MPa]	R_p [MPa]	R_{pt} [MPa]	E [MPa]
S235JRG2 (1.0038)	410	235	210	205000

Tab. 8 contains basic information about the value assumed during the design of tubesheet. The input dates of tubesheet were selected from the Polish standards for this project [1, 5].

Table 8

The dimensions and the results of the calculated thickness of the tubesheets depending on the area

WUDT-UC	PN-EN 13445-3	Units	Description
$d_z = 25$	$d_t = 25$	mm	The nominal outer diameter of the pipe
$t = 32$	$p = 32$	mm	The tube pitch
$g = 12$	–	mm	Initial thickness
$l_0 = 12$	$l_{t,x} = 12$	mm	The expanded length of tube in tubesheet
–	$U_L = 32$	mm	The large centre- to- centre distance between adjust tube rows
$f = 533.126$	$S = 533.126$	mm^2	The total unperforated area of tubesheet

Tab. 9 and 10 show the results of calculating assembly and operating the bolts loads, necessary for the appropriate operation of the flange connection.

Table 9

The results of calculations for the assembly in the event of a tubesheet used in connection flange -screw

WUDT-UC	PN-EN 13445-3	Units	Description
D_1 = 1400	d_1 = 1400	mm	The nominal diameter of the tubesheet
D_w = 1426	B = 1426	mm	The inside diameter of the contact face between loose and stub flanges in a lap joint
D_u = 1481	G = 1504.3	mm	The diameter of gasket load reaction
–	b_0 = 26	mm	The basic gasket or joint seating width
U = 54.5	w = *52*	mm	The contact width of gasket or joint seating pressure
U_{cz}= 25.61	b = 12.85	mm	The effective gasket or joint seating width
σ_m = 18.3	y = 26.20	MPa	The minimum required gasket or joint seating pressure
N_{m1} = 2502000	W_A = 104694	**N**	The minimum required bolt load for assembly condition
C = 1.4	–	–	The correction coefficient use in WUDT-UC
N_{m2} = 5618000	–	N	The minimum required bolt load for assembly condition – used correction coefficient

Table 10

The results of calculations for operating in the event of a tubesheet used in connection flange – screw

WUDT-UC	PN-EN 13445-3	Units	Description
D_u = 1481	G = 1504.3	mm	The inside diameter of the contact face between loose and stub flanges in a lap joint
p_0 = 1.6	P = 1.6	MPa	Design pressure
b = 1.5	–	–	The coefficient of hedging against a decline in the strength *S* as a result of creep
σ_r = 4.8	mP = 2.4	MPa	The pressure on the gasket to guarantee tightness of the joint in the operating conditions
U_{cz} = 26.61	b = 12.85	mm	The effective gasket or joint seating width
P = 2754000	H = 2843667	N	The total hydrostatic end force
S = 953200	H_G = 22684	N	The compression load on gasket to ensure tight joint
N_r = 4013000	W_{op} = 2866351	N	The minimum required bolt load for operating condition

Tab. 11 shows the final results for the calculation of the bottom sieve according to WUDT-UC and European standards.

Table 11

Comparison of the results of calculated thickness of the tubesheet

The calculated thickness of the tubesheet	WUDT-UC g_o mm	PN-EN 13445-3 e mm
1. Precinct flange connection	26	32
2. Precinct bundle of tubes	20	12
3. Outside the bundle of tubes	34	12
The thickness of whole tubesheet *	34	32

* Industry seeks to standardise the thickness of the tube sheet for each of its area

4. Conclusion

The European standard PN-EN 13445-3 has procedures for the calculation of tubesheet for more structural solutions than Polish guidelines WUDT-UC. The calculations are dependent on the heat exchanger and the type of tubesheets.

In the case of guidelines WUDT-UC, the amount of these solutions is very limited and reduced to a few cases. However, this greatly facilitates carrying out the calculations. All the values in the design are known.

Large difference were noted when comparing the two methods of calculating algorithms. For calculation algorithm strength WUDT-UC as the minimum thickness of the tube sheet assumes a value equal to 12 mm, regardless of the material from which the tube sheet and the diameter of the heat exchanger and the load applied pressure.

In the European standard PN-EN 13445-3, there is no requirement specifying the minimum size of the tubesheet. The calculation is carried out for the assumed thickness of the tubesheet. It is important only for the thickness to fulfil strength requirements. If these conditions are not fulfilled, the calculations must be repeated by increasing the thickness of the tubesheet.

When comparing the results of calculation for tubesheet extended as a flange, conducted for both of these documents, large differences are noted. The same situation occurs in the event of comparing the dimensions of sealing solutions for the flange connection. They relate to the average diameter of the seal D_u and the inside diameter of the contact face between loose and stub flanges in a lap joint G.

According to the algorithm calculations WUDT-UC thickness of the tubesheet meets the conditions adopted in the project in the precinct flange connection and it is 26 mm. However, according to European standard PN-EN 13445-3, this value is higher, at 32 mm. In the precinct bundle of tubes, higher values in the calculation were obtained for the guidance WUDT-UC equal 20 mm. In the case of the European standard, this value was 12 mm. For the region outside the bundle of tubes, a similar situation was noted. For the European standard PN-EN 13445-3 there was a higher value – 32 mm than for the guidelines WUDT-UC – 12 mm.

Finally, the thickness of tubesheet for European standard PN-EN 13345-3 was equal to 34 mm. The calculations that were carried out for guidelines WUDT-UC amounted to 32 mm.

It was found that the calculations performed according to the European standards PN-EN 13445-3 are more accurate and increase the strength of the structure. Due to the greater thickness of the tubesheet heat exchanger, it meets the requirements of safety and allows safe operation of the device.

In the analysed examples, an analogy on the section of the tubesheet into different areas was noted. Equation determination of tubesheet thickness have been summarised in below Tab. 12.

Table 12

Comparison of formulas used to determine the thickness of the tube sheet in each of its region

Region / Standards	Precinct flange connection	Outside the bundle of tubes	Precinct bundle of tubes
WUDT-UC	$D_z = D_w + 2 \cdot g_s$: - assembly conditions: $\sigma_{km} = 2 \cdot N_m \cdot \frac{D_0 - D_w - 2 \cdot g_s}{\pi \cdot (D_{zk} - 2 \cdot d_0) \cdot h^2}$ - operating conditions: $\sigma_{kr} = 2 \cdot N_r \cdot \frac{D_0 - D_w - 2 \cdot g_s}{\pi \cdot (D_{zk} - 2 \cdot d_0) \cdot h^2}$	$g_0 = 0.45 \cdot \delta \cdot \sqrt{\frac{p_0}{k}}$	$g = \frac{q_{\min}}{m}$
PN-EN 13445-3	- assembly conditions: $e_{fl,a} = \sqrt{\frac{12}{\pi \cdot D_{ex} \cdot \left[(1+\vartheta) + (1-\vartheta) \cdot \left(\frac{D_{ex}}{A} \right)^2 \right]} \cdot \frac{M_A}{f_A}}$ - operating conditions: $e_{fl,op} = \sqrt{\frac{12}{\pi \cdot D_{ex} \cdot \left[(1+\vartheta) + (1-\vartheta) \cdot \left(\frac{D_{ex}}{A} \right)^2 \right]} \cdot \frac{M_{op}}{f}}$	Assumed in the project, checked under the strength conditions and corrected when are not complied.	Assumed in the project, checked under the strength conditions and corrected when are not complied.

References

[1] Pikoń J, *Podstawy konstrukcji aparatury chemicznej. Cz II. Elementy aparatury chemicznej*, PWN, Warszawa 1979.

[2] Warunki Urzędu Dozoru Technicznego, *Urządzenia Ciśnieniowe*, Wydanie 10.2003.

[3] Norma PN-EN 13445-3:2002.

[4] Talaga J, Felkowski Ł, *Obliczenia połączeń kołnierzowych w świetle norm PN-EN 13445 i specyfikacji technicznej WUDT-UC*, Inżynieria i Aparatura Chemiczna, 50, nr 6, 2011, 5-8.
[5] Pikoń J, *Podstawy konstrukcji aparatury chemicznej. Cz I. Tworzywa konstrukcyjne*, PWN, Warszawa 1979.
[6] Materiały firmy Spetech (15.05.2016): http://www.spetech.com.pl.
[7] Norma PN-EN 13445-2:2002.
[8] Celarek A, *Analiza porównawcza metodyki obliczeń wytrzymałościowych ścian sitowych według Norm Europejskich i wytycznych UDT*, Praca magisterska, Politechnika Krakowska, Kraków 2015.

TECHNICAL TRANSACTIONS | CZASOPISMO TECHNICZNE
MECHANICS | MECHANIKA
2-M/2016

PAVEL DITL, ALEXANDER FERNANDO*

SIMULATION OF PROCESS LINES IN MICROSOFT EXCEL - NITRIC ACID PRODUCTION

SYMULACJA LINII TECHNOLOGICZNYCH W PROGRAMIE MICROSOFT EXCEL – PRODUKCJA KWASU AZOTOWEGO

A b s t r a c t

In this contribution, it is explained in the detail how useful Microsoft EXCEL could be for the simulation of process lines. The report contains a manual flowsheet as well as a tutorial case and the results of its application for Nitric acid production can be gained.

Keywords: program Microsoft EXCEL, simulation

S t r e s z c z e n i e

W artykule szczegółowo przedstawiono jak użytecznym narzędziem do symulacji linii procesowych może być program Microsoft EXCEL. Praca zawiera indywidualne arkusze danych, poradniki przydatne w szczególnych przypadkach (tutoriale) oraz wyniki ich zastosowania w produkcji kwasu azotowego.

Słowa kluczowe: program Microsoft EXCEL, symulacja

DOI:

* Prof. PhD. DSc. Eng. Pavel Ditl, MSc. Eng. Alexander Fernando, Department of Process Engineering, Faculty of Mechanical Engineering, Czech Technical University in Prague.

1. Introduction

I already introduced the usage of Microsoft Excel for process line simulation at the 2012 conference in Berlin.

Now, I would like to explain the main principles of this method on the „Boiler“ example, which demonstrates both enthalpy and mass balances.

First of all, we need to understand the basic principles, which are shortly described in this presentation:

1.1. Decision-making

Experience and practice have made us realise that mass and material balances represent effective tools for decision-making. The concept of decision-making shall include the following spheres of action:

- Sizing lines and individual apparatus in designing.
- Adjusting a line to the modified composition of materials.
- Adjusting a line to the modified requirements for quality (composition) of a product.
- Diagnosing failures of operation of lines and locating causes of failure.
- Checking or substituting measured quantities by calculating those quantities and taking advantage of this principle to ensure easier control or to carry out process, or guarantee measurements.
- Optimising operation of a line and searching for alternatives of operation using the method: “What will happen if.....?”
- Training and teaching operating personnel.

This enumeration is certainly not complete; however, it gives us an idea of the content of the concept of decision-making.

1.2. Working tools for decision-making

Decision-making that involves any process requires a quantitative model. This decision-making shall mean either proposing a new process, or modifying a process, or controlling an existing process. Such a model should give us an opportunity to study the behaviour of the system if the initial conditions change. In other words, the model should enable one to study changes of the system behaviour after modifying initial conditions, that is to search for an answer to the question: What will happen if…? Such a model constitutes a prerequisite for an objective quantitative economic analysis of the system. It is necessary to bear in mind at all times that the quantitative model should be exact. This means we receive one and only solution for the selected values of the designating parameters. When using empirical coefficients, such as efficiency, yield, or adjustable constants guaranteed by the provider of the equipment, maximum attention must be paid in order to define these coefficients accurately. The use of empirical coefficients is thus limited to cases where those coefficients include deviations from the ideal behaviour, express efficiency of the process, or adjust the theory to the real behaviour of the equipment. These adjustable parameters often constitute the subject of know-how. In any case, however, exact mass and enthalpy balances constitute the basis of the model. Thereby, a quantitative model of a

process establishes a reliable foundation of the system's economic model, which is the final tool for the management in making decisions.

The law of conservation of mass and the law of conservation of energy can be used as an exact model for processes accompanied by a chemical reaction and heat exchange. On the basis of this model, mass and enthalpy balances can be drawn up for the process in question, and subsequently, complete system characteristic can be acquired.

1.3. Complete system characteristic

Material balances are used for obtaining a complete characteristic for all streams that are present in the process flow chart. This information is essential both for a designer and for the operation control itself. A complete characteristic contains the following details:

- Where the stream comes from and where it goes – that defines the direction of the stream, i.e. its orientation.
- Size of the stream, expressed as weight per time unit ($kg \cdot s^{-1}$) or moles per time unit ($kmol \cdot s^{-1}$).
- What components the stream contains and their part, expressed as a weight or mole fraction of the component in the stream in question. The method of expressing the composition of the stream should be invariant to temperature and pressure.
- Temperature and pressure for each stream are added to the above-mentioned in the case of enthalpy balance.

2. Basic concepts

If we know the composition, temperature and pressure for a stream, we are able to determine:

- any intensive physical property of the stream – such as density, viscosity, or surface tension,
- whether the stream consists of one or more phases and what these phases consist of.

In general, we can say that all intensive physical properties represent a function of composition, temperature and pressure. With liquid and solid phases, the effect of pressure on the value of intensive properties is mostly negligible. As to ideal gases, the change of enthalpy with pressure is null. A more noticeable dependence of enthalpy on pressure is encountered only with streams, the position of which is in the proximity of a two-phase range. This leads to the following conclusions:

- The composition of the stream must serve the purpose of mass balance.
- The temperature of the stream must serve the purpose of enthalpy balance.
- The pressure of the stream does not constitute the object of balance calculations. If we need to know its value (for instance, in order to calculate in what phase the stream is – whether in a gaseous or liquid phase), its value must be determined.

2.1. What is flowsheeting?

Flowsheeting consists of a flow sheet of the process being analysed and the complete system characteristic. It includes neither the dimensions and the structural design of the apparatus, nor the planning of the piping system. Flowsheeting consists in the following steps:

- Drawing up a process flow sheet
- Defining components in individual streams
- Establishing balance equations

By working them out, we obtain the missing information for complete system characteristic. Flowsheeting is a working tool for decision-making.

2.2. What is a balance?

Any extensive property – a property, the numerical value of which changes with the size of the system – can be balanced. This class includes mass, volume, internal energy, entropy, and so forth. On the contrary, intensive properties are properties with their value being independent of the size of the system, such as density, temperature, viscosity, specific heat, colour, hardness, and so forth.

Within the defined boundaries of the system being balanced and the limited time for which the balancing is being performed, the following balance relation holds good for the extensive property being balanced:

$$Accumulation = Input - Output + Source$$

- Input is the quantity of the extensive property being balanced that passes into the system through the balanced system boundaries within the limited time for which the balance is being performed.
- Source is the quantity of the extensive property being balanced that is generated within the system boundaries in the course of the balanced period. Disappearance of the extensive property is expressed as a source with a negative sign.
- Output is the quantity of the extensive property being balanced that gets out of the system through the balanced system boundaries within the limited time, for which the balance is being performed.
- Accumulation is the change in the quantity of the extensive property being balanced within the balanced system boundaries in the course of the balanced period.

The introduction of a source element enables us to balance all extensive properties, even those properties to which the law of conservation does not apply (for instance, entropy, exergy, component subject to a chemical reaction, and so forth). In order to apply a balance relation, it is still necessary to define in greater detail the concepts involved in the balance relation.

At the start of each balancing, three concepts must be defined clearly:

- *Extensive property being balanced*
- *Balanced system boundaries*
- *Limited time for which the balance is being performed*.

2.3. What is a component?

An extensive property being balanced will be hereinafter referred to as a component. Components can be:

- pure chemical compounds, such as methane, sulphuric acid, water, oxygen, to which a specific molar mass can be attributed,
- polymers – chemically pure substances, whose molar mass is not clearly defined,
- substances representing a group of chemical compounds, such as fats, R_2O_3, silicates, hydrocarbons C_{4+},
- substances that cannot be specified chemically, such as water-insoluble residue, substances with density lower than water, substrate in bioreactors.

When defining a component, it is necessary to define in a precise manner the method through which the component is determined. Differences in methods used for determining a component can lead to significant discrepancies. For instance, it is not enough to define a component as water content in a solid phase, it being loose material. Water can be on the surface of particles; in the case of porous particles, it can be bound through adsorption to the inner surface of particles; it can be water of crystallisation if the particles are of crystalline nature, and in the case of some substances it can be chemically bound water. Based on the method of determining the water content, results can differ even in the order of magnitude.

This applies also to a component defined as a particle size. If we determine the proportion of particles of a specific dimension by measuring the particle's largest dimension under the microscope, by separating on sieves, or by measuring the distribution of the particles using the settling method, we will arrive at different results.

2.4. What is a balanced system boundary?

A boundary of the system being balanced must be defined in order so that a component can enter or get out of the system only by crossing the system's boundaries. System boundaries do not have to be identical with the apparatus housing. A system can also be an imaginary volume defined within the apparatus. This method is very often used to define differential volume, it being the system with dx, dy and dz dimensions in rectangular coordinates. Then, the balance relation for the component leads to a partial differential equation.

The system being balanced does not have to be identical with the individual units of apparatus. Units of apparatus can be combined for the purposes of balancing. Admittedly, this reduces the number of input data, required for the performance of the balance calculation, but the possibility of acquiring further information is thereby lost. For instance, if we link, for the purposes of balancing, an evaporating apparatus and crystalliser, we lose the information about the properties of the concentrated solution entering the crystalliser, which is an information necessary for the structural design of the evaporating apparatus. An opposite approach is possible as well. For instance, instead of balancing the whole distillation column, individual levels can be balanced.

2.5. What is a limited time of balance?

If we divide all elements of the balance relation by the limited time of balance, we will obtain the component's quantity per unit of time. This quantity can be termed as stream. Then, the balance relation for any one component can be posted as follows:

Rate of Accumulation = Input Stream -Output Stream + Source per Unit of Time

Source of component per unit of time (rate of source) can be seen as an imaginary (fictive) stream that enters into the system; however, it does not cross its boundaries at the same time. It can have both positive – a component is formed – and negative – a component disappears – value.

Accumulation per unit of time can be designated as the rate of accumulation; it is the change in quantity of the balanced component in the system with time. Therefore, the final form of the balance relation reads as follows:

Input Stream of Component + Fictive Stream of Component = Output Stream of Component + Accumulation Rate of Component.

2.6. What is an amount of component?

In order to substitute into the above-mentioned relation, we need to know the stream of the component, which is the quantity of the component per unit of time. However, we do not usually have the opportunity to measure the component stream directly. In most cases, we measure the overall stream and its composition. The component stream can be calculated from these two pieces of information.

If the component is a differential particle size, the size of the stream of this component can be calculated by multiplying the overall flow of particles by the relative frequency of occurrence of the particles within the monitored interval. When reducing the interval of the particle size to zero, we get a differential and integral description known in literature as population balance.

The numerical value of the flow of the component is required to be invariant to temperature and pressure. This requirement excludes the overall stream to be expressed as volume per unit of time. There remains the possibility of expressing the flows of components as mass or amount (number of pieces) – kilograms of flour and number of eggs per unit of time.

Furthermore, it is required to have the opportunity to convert mass to amount (number of pieces) and vice versa. For it is common practice to weigh small screws instead of counting our thousands of pieces. The approach is accurate only if every piece has exactly the same mass as the other ones. This requirement is satisfied strictly only with molecules. Molecules are too small to be counted out. However, we know that one kmol of any substance contains the same number of molecules, corresponding to the Avogadro's number, which is $6.0221367 \cdot 10^{26}$ $kmol^{-1}$. If we know the molar mass for a component ($kg \cdot kmol^{-1}$), we can convert the amount of substance (kmol) to mass (kg) and vice versa. If a component cannot be attributed molar mass, its quantity can be expressed only as mass in kg.

Consequently, we shall express the fraction of the component present in the stream only as a weight fraction or a mole fraction, depending on whether the overall stream is expressed in $kmol \cdot s^{-1}$ or $kg \cdot s^{-1}$.

2.7. What is a continuous process?

The accumulation of a component in the system is the change in the quantity of the property being balanced (hold-up). If a process is run continuously in a steady state, the change in hold-up and its composition with time is null, and therefore, the rate of accumulation is also null.

The accumulation of mass is usually applied in batch systems. If we choose a limited time of balance exceeding the time of a batch process cycle by a long way, we can accept the assumption of a zero rate of accumulation. If we choose no matter how long balance period, the system accumulation will be given by the level of the system hold-up at the end of the balance period minus the system hold-up at the start of the balance period. This can be the difference between the maximum and the minimum hold-up at the most. If we choose the balance period to be just as long so that the maximum accumulation possible is negligible compared with the input and output streams for the balance period, we can regard also the periodical batch processes to be continuous and deem the rate of accumulation to be zero.

Complete system characteristic does not say anything about the dimensions of individual pieces of equipment, and therefore, the relations we use for balancing do not contain any parameters of the equipment. However, in order to calculate the rate of accumulation, it is necessary to know the hold-up, which constitutes a parameter of the equipment. Therefore, our concern will be focused on continuous and periodical batch processes, where the accumulation rate can be ignored.

2.8. What is a source stream of reaction?

Just as in the case of accumulation, it is necessary to know the hold-up of the equipment in which the chemical reaction takes place in order to calculate the source of a component directly. The rate of generation of the component being balanced is the amount of component generated at the given place in the unit of capacity of the system per unit of time. That means that an intensive property is involved. Since the source in balances is an extensive property, we have to integrate the intensive property through the capacity of the system being balanced. In the case of an ideal stirred tank, where composition and temperature do not constitute functions of the place, we simply multiply the mentioned intensive property by the capacity of the hold-up, which is, however, a parameter of the equipment. In order to avoid this difficulty, we can substitute the source by a fictive stream of reaction.

For every independent reaction, there will be one fictive stream, which will be denominated as nr_k for balances of amount of substance and as mr_k for mass balances, where k is the serial number of reaction in case that more independent reactions are taking place in the block being balanced.

Instead of posting mole and/or weight fractions into the fictive stream column in the specification table for k, we:

- enter the component's stoichiometric coefficient into the component's row, with a positive sign if the component is a product of the reaction (second term on the right side of the stoichiometric equation), or with a negative sign if the component

is a reactant (first term on the left side of the stoichiometric equation) in the case of material balance;

- multiply, in addition, the stoichiometric coefficient (with the appropriate sign) by the component's molar mass in the case of mass balance.

Tutorial Problem:

If we take the stoichiometric equation of formation of sodium hydrogen carbonate in manufacturing soda

$$NaCl + NH_3 + CO_2 + H_2O = NaHCO_3 + NH_4Cl$$

as an example, the column for the fictive stream will read as follows:

Table 1

Stoichiometric coefficients and molecular weight

		for molar balance in kmols/sec	for mass balance in kg/sec
	components	Nr	Mr
1	H_2O	-1	-18.02
2	NaCl	-1	-58.44
3	CO_2	-1	-44.01
4	NH_3	-1	-17.03
5	$NaHCO_3$	1	84.01
6	NH_4Cl	1	53.49

2.9. Why enthalpy balance and not heat balance?

The change in energy of 1 kg of water upon being heated by 0.5°C corresponds to the change in the mass flow rate of the same by 65 $m \cdot s^{-1}$ or raising by 213 m. Such changes in kinetic and potential energy can be hardly encountered in a chemical plant, the exception thereof being power-producing machinery (turbines). For the purposes of balancing, we can therefore ignore potential and kinetic energy of streams and substitute heat balance by enthalpy balance.

This has the same advantage as disregarding the accumulation rate. In order to calculate kinetic and potential energy of a stream at the given place, we need to know the diameter of the piping and its height above the ground, which are parameters of equipment that do not belong into the system characteristic. We do not need this information to calculate the enthalpy of a stream, and therefore, we replace the overall heat balance by enthalpy balance. The mistake that can be thereby caused is negligible in the absolute majority of cases.

2.10. What is the difference between material balance and enthalpy balance?

For a continuous process or a batch process occurring periodically, material balance of a component has the following form:

Accumulation Rate of Component = Input Stream of Component – Output Stream of Component+ Source.

This applies to every component, which means that for a balanced system, we have as many material balances as there are components present in the system.

The dimension of individual parts of the balance equation is $kg \cdot s^{-1}$, or $kmol \cdot s^{-1}$.

The system being balanced can interchange energy with the surroundings not only through the material streams, but also through the exchange across the system boundaries – heat exchangers, or stirrers as the case may be, and so forth.

In this case, the enthalpy balance for a continuous process or a batch process occurring periodically will have the following form:

Enthalpy Accumulation = Input Stream Enthalpy -Output Stream Enthalpy + Interchange of Energy with Surroundings + Source

Individual parts of the balance equation are expressed in kW.

Removal of energy into the surroundings has a plus sign, while power supply has a negative sign. The system in which the interchange of energy with the surroundings is zero, is called *adiabatic*.

Only one enthalpy balance holds good for the balanced block.

2.11. Enthalpy balance

To draw up an enthalpy balance, physical and chemical data of individual components must be available. Various databases can serve as sources of data. Data from individual databases may not be quite consistent, and therefore, it is practical to use only one database if possible and not to take data for various components from different databases. A database adapted for Excel from the book by R.C. Reid, J.M. Prausnitz, and T.K. Sherwood – The Properties of gases and liquids (Mc Graw Hill 1982) is used for the purposes of teaching at the Czech Technical University.

The database of the National Bureau of Standards or the DECHEMA database can be recommended for industrial applications. The respective Internet addresses are provided at the end.

2.12. Formulation of the problem being solved

In order to comply with the law of conservation of mass and enthalpy, the following equations must hold true for every block of the flow sheet:

- material balance for every one component (in order words, the number of balance equations agreeing with the number of different components present in the streams, which pass into or get out of the given block – we take into account both real and fictive streams);
- summation equations for every one stream (in other words, the total of weight or mole fractions of all components in the given stream must equal one);
- other equations, if any, follow from the laws that determine the relations among the composition, pressure, and temperature of individual streams. These are the laws of thermodynamics, chemical and phase balance, or laws of kinetics of processes. These relations are almost always non-linear;

- other equations issue from specifications given by technological regulations (such as yield, selectivity) or in data provided by the producer of the equipment (such as efficiency of machines);
- in the case of changes in temperature, one enthalpy balance is added.

The first two groups form a system of linear equations.
Enthalpy balance is non-linear, which is given by the fact that molar heats represent functions of temperature.

This set of equations forms a mathematical model, for which methods of solving must be established.

2.13. How many equations define the system behaviour in full?

A system is defined in full if the sum of balance equations, summation equations, equations for physical laws, specification equations, and enthalpy balance is equal to the number of unknowns in the equations.

2.14. Solving possibilities of the governing equations

The issue of simplicity of information transmission plays an important role with the model used. There is specialised software available for these models, such as CHEMCAD, PRO, or MAX. In addition, advantage can be taken of mathematical software, such as MATLAB, Mathematica, MATHCAD, and so forth.

This software has two big disadvantages – firstly, it is very expensive, and secondly, to become proficient in the software requires great efforts and a lot of time. It is necessary to bear in mind that a model set up by means of certain software will be used from a certain level of management upwards. At this level, it is possible to encounter the willingness to sacrifice the financial means to buy the software; however, it is an absolute illusion to expect that someone would be willing to sacrifice the time needed in order to become familiar with the software.
However, there is software available with the following advantages:

- It is installed on every computer in an enterprise – one can assume that Microsoft Office is installed on every PC.
- Almost everyone, who is able to use a computer, has a good command of it. And if the manager is not willing to communicate with a computer, his secretary is bound to have a good command of this programme.
- Operating records and source data are stored by means of this programme. Transmitting source data into our model is therefore possible without even one number being retyped using a keyboard.
- All and any economic and statistical analyses are performed by means of this programme. Transferring data for these analyses is also performed through floppy disks, over the net and through other channels, but not by typing the data on the keyboard.
- Tables and diagrams obtained using this programme can be, without the slightest difficulty, transferred into the most widespread Word processor.

We are talking about Excel. Working with Excel may not be as elegant as working with special programmes, but the above-mentioned advantages are significant to such an extent that, for the time being, Excel cannot be replaced with any other tool – exception perhaps being Lotus II, but it is fully compatible with Excel.

3. Methods of setting up and solving a model

The methods of solving have been drawn up to be generally valid and uniform for all types of balance cases. Exactly the same procedure is used for all cases, ranging from the problem of what ratio to use to mix two streams of water with different temperatures so that the resulting stream can have the temperature required, to systems containing dozens of blocks and streams.

These uniform methods have facilitated the elaboration of an exact method of solving, which is available to the engineering public at large, and which consists of the following steps:

The following are required for any process we wish to balance:

1. Process basis and data available with respect thereto.
2. Process flow sheet and definition of balance blocks, incidence matrix.
3. List of components in streams and their definitions.
4. Basis of calculation and conversion of specified flows and compositions.
5. Chemical reactions, determination of number of independent chemical reactions.
6. Specification table and matrix of coefficients.
7. Formulation of additional relations.
8. Conditions of system solvability.
9. Solution of a system of equations using methods of linear algebra, with the advantage of using excel.
10. Table of solutions containing complete system characteristic.

3.1. Solving a system of equations – a model

In general, tasks are not noticeably complicated from the mathematical point of view. Solving a system of equations, most of which are linear, is always involved.

It is important to solve the essential question of whether the system has been overdetermined, that is whether also data that should be the result of the calculation are available for the system characteristic, or whether the system has been determined insufficiently, that means that not enough information is available to enable us to determine the complete system characteristic.

The method of how to proceed from process description to solvable mathematical model has certain logic, which must be adhered to when computing with a calculator as well as when using programmes, such as PRO, MAX, or CHEMCAD. The mentioned programmes obtain the required information from the user using various menus. Formation of and recording in what is known as a specification table is, in fact, making a list of all equations that are available to us to solve the problem.

The methods for EXCEL have exactly the same logical structure as the mentioned programmes, with the difference consisting in that we know exactly why we take the respective steps. Although this method is more laborious, we know the logic and subject-matter of the procedure, and therefore, we are able to eliminate any contingent mistake or error in the specification right at the beginning.

A system can be solved using a calculator only in the cases where it is possible to apply the solution through iterative method by means of substitution.

The following part demonstrates in detail on sample problems the application of the general methods discussed above. Stress is put on the uniform procedure, which must be unconditionally observed for success of the solution to be guaranteed.

3.2. General information

In describing the methods, we will proceed by providing the reader with a standard text and with a solution of the problem being described in EXCEL. This file has been provided with quite a detailed description and numerous commentaries, so that the standard text can serve, after the initial working through, only as reference. In addition, series of problems solved in EXCEL have been attached so that the user can review the methods on other problems as well. This file contains problems ranging from the most simple to the larger-scale ones. Commentaries on these problems do not constitute part of the standard text anymore; the commentary, with which the EXCEL file has been provided, should be sufficient for the user.

Let's discuss the individual phases of the procedure in detail. For example we use problem **Boiler**:

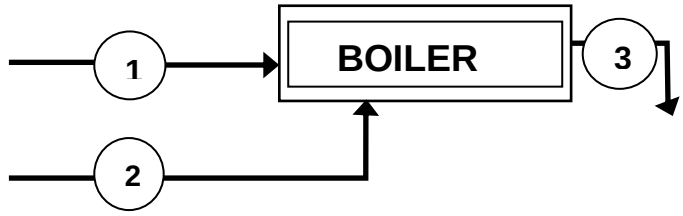

Fig. 1. Input and output flows in a boiler

A pipe oven serves as a source of energy for heating a family house, where power-gas is mixed with air and burned. We assume that power-gas is pure CH_4.
The process of combustion runs according to the following stoichiometric equation

$$CH_4 + 2O_2 = CO_2 + 2H_2O$$

Dry air comes into the oven in surplus compared with the stoichiometry of the process. Combustion occurs under an oxygen surplus and the flue gas contains traces of unburned power-gas.

1. **Process input parameters:**
   R = 8,314 kW·s·Kmol^{-1}·K^{-1}
   T = 273,15 K
   Q = 20 kW
   C_{CH4} in flue gas = 0,004 kmol/∑kmol

C_{O2} in air = 0,21 kmol/∑kmol
Air surplus = 25%
$T_{stream\ 1}$ = 5°C, $T_{stream\ 2}$ = - 15°C, $T_{stream\ 3}$ = 150°C

2. List of components ,streams and process units:

CH_4 = 16,04 kg/kmol
O_2 = 32 kg/kmol
N_2 = 28,01 kg/kmol
CO_2 = 44,01 kg/kmol
H_2O = 18,02 kg/kmol

3. Common basis:

mol flow kg/kmol

4. Reference stream & component flows:

Q = 20 kW

5. Recalculations:

Component concentration in Stream:
Stream 3, Component 4
$C_{3,4}$ = 0,004 kmol/∑kmol
Relation between two Component Flows:
Stream 2, Component 2
$n_{2,2} = 2{,}5 \cdot n_{1,1}$

6. Chemical reactions:

Reactants = Products
$CH_4 + 2\ O_2 = 2\ H_2O + CO_2$
Stoichiometric Coefficients:

Stoichiometric coefficients are defined in the following way:

A) stoichiometric coefficients of reactants have a minus sign and reaction products have a plus sign.
B) stoichiometric coefficients of reactants have a minus sign and reaction products have a plus sign.
C) single stoichiometric coefficients are used in mol balances.
D) In the case of mass balances, we must multiply the stoichiometric coefficients by the corresponding mol masses.

Table 2

Stoichiometric coefficients (S.C)

	Element	S.C	Mass [kg/kmol]	Thermodata indexes
1	CH_4	-1	-16,043	63
2	O_2	-2	-64	34
3	N_2	0	0	31
4	CO_2	1	44,01	48
5	H_2O	2	36,03	22

For the calculation of molar enthalpies of individual components, as a function of temperature, we will use a suitable data-base where we could find the necessary information. For our purposes, we will use the data-base Thermodata.

Now, we have to arrange available data into a suitable form.
As the first step, we put down the **basic parameters.**

Table 3

Basic parameters

number of streams	3
number of chemical reactions	1
number of process units	1
number of components	5

Respecting the recommended form, we put down the **IM** matrix (incidence matrix) and the **TD** matrix (data table):

Table 4

IM

process unit	streams			reactions
	1	2	3	r1
1. Boiler	1	1	-1	1

Table 5

TD

	process unit	streams			reactions
	1. Boiler	1	2	3	r1
1	CH_4	1	0	1	-1
2	O_2	0	1	1	-2
3	N_2	0	1	1	0
4	CO_2	0	0	1	1
5	H_2O	0	0	1	2

Number of unknown parameters:

Scalar product of the matrix TD + number of reactions gives the number of unknowns (**nUKN**):

nUKN = SUMMPRODUCT(TD) + 1

Table 6

Number of mass balance equations can be calculated as the product of TD x IM matrixes

		Number of balances for **Boiler** for each element
1	CH_4	2
2	O_2	2
3	N_2	2
4	CO_2	1
5	H_2O	1

Balance equations = number of non zero elements.

Table 7

Enthalpy of components [kJ/mol], using Termodata.xls:

index values	components	streams			reactions
		1	2	3	r1
63	CH_4	1	0	1	-1
34	O_2	0	1	1	-2
31	N_2	0	1	1	0
48	CO_2	0	0	1	1
22	H_2O	0	0	1	2
T	°C	5	-15	150	Hr1

Table 8

Enthalpy table

index values	components	streams			reactions
		1	2	3	r1
63	CH_4	-0,69989	0	4,88453	74,90181
34	O_2	0	-1,1691	3,73545	0
31	N_2	0	-1,1680	3,65165	0
48	CO_2	0	9	4,96869	-393,768
22	H_2O	0	0	4,26865	-483,99
T	°C	5	-15	150	Hr1
					-802,86

Table 9

Matrix of coefficients “A” and vector of right sides “B”

Element	Process unit	No. of element	Stream; element									
			1	2	2	3	3	3	3	3		
			1	2	3	1	2	3	4	5		
			n1; 1	n2; 2	n2;3	n3; 1	n3; 2	n3; 3	n3; 4	n3; 5	r1	B
CH_4	1	1	1	0	0	-1	0	0	0	0	-1	0
O_2	1	2	0	1	0	0	-1	0	0	0	-2	0
N_2	1	3	0	0	1	0	0	-1	0	0	0	0
CO_2	1	4	0	0	0	0	0	0	-1	0	1	0
H_2O	1	5	0	0	0	0	0	0	0	-1	2	0
	Enthalpy Balance		-0.699	-1.169	-1.168	-4.884	-3.735	-3.651	-4.968	-4.268	802.86	20
	Conc. O_2 in stream 2		0	-0.79	0.21	0	0	0	0	0	0	0
	Conc. CH_4 in stream 3		0	0	0	-0.996	0.004	0.004	0.004	0.004	0	0
	O_2 overflow		2.5	-1	0	0	0	0	0	0	0	0

After, we need to calculate the determinant of Matrix A (blue area) to control if it is solvable

Det A	146,402

And finally, we calculate the mol flows for each stream (vector "**X**") , because $A \cdot X = B$ => $X = B \cdot A^{-1}$

4. Results

Stream	n1,1	n2,2	n2,3	n3,1	n3,2	n3,3	n3,4	n3,5	r1
Flowrate [kmol/sec]	0,028688	0,07172	0,269805	0,001481	0,017306	0,269805	0,027207	0,054414	0,027207

In the same way, we applied this method for simulation of Nitric acid production, where the situation was much more complicated. The matrix of coefficients is the matrix 145 × 145. A block-diagram is shown in the Fig. 2 and a simulation Excel-file can be sent on request- ditl@centrum.cz

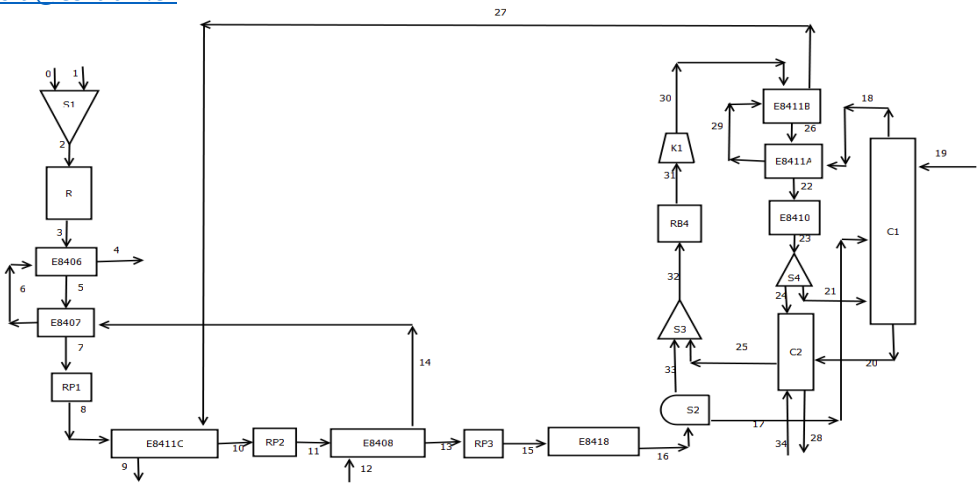

Fig. 2. Block diagram of nitric acid production

For those who are more deeply interested in the methodology we can provide the manual "Flowsheeting in EXCEL" (In Russian, English, German or Czech).

References

[1] http://www.i-programmer.info/ebooks/automating-excel/1264-getting-started.html
[2] https://studium.fs.cvut.cz/studium/u12118/DITL/PPP/ (access only for staff and students, having university ID)
[3] http://4excel.ru/index.php?id=excelbasic

TECHNICAL TRANSACTIONS | CZASOPISMO TECHNICZNE
MECHANICS | MECHANIKA
2-M/2016

EWA DŁUSKA, AGNIESZKA MARKOWSKA-RADOMSKA, AGATA METERA*

MULTIFUNCTIONAL EMULSION STRUCTURES FOR ENCAPSULATION AND MODIFIED RELEASE OF ACTIVE INGREDIENTS

WIELOFUNKCYJNE STRUKTURY EMULSYJNE DO ENKAPSULACJI I MODYFIKOWANEGO UWALNIANIA SKŁADNIKÓW AKTYWNYCH

A b s t r a c t

The paper presents the results of encapsulation of biologically and chemically active ingredients, such as living cells and drugs within multiple emulsions and release co-encapsulated drugs with the rate controlled by physicochemical properties of emulsions. The influence of process parameters in a Couette-Taylor flow bioreactor on the obtained emulsions structures, rate and mechanisms of release and the possibility to modify the release profiles have been discussed and presented.

Keywords: multiple emulsions, encapsulation process, release rate and mechanism

S t r e s z c z e n i e

Praca dotyczy wyników badań enkapsulacji substancji biologicznie i chemicznie czynnych takich jak leki i żywe komórki w emulsjach wielokrotnych oraz procesu ko-uwalniania z szybkością kontrolowaną parametrami fizykochemicznymi emulsji. W pracy przedyskutowano wpływ parametrów procesowych w bioreaktorze z przepływem Couette'a-Taylora na otrzymywane struktury emulsji oraz szybkość i mechanizm procesu uwalniania oraz możliwość modyfikacji krzywych uwalniania.

Słowa kluczowe: emulsje wielokrotne, proces enkapsulacji, szybkość i mechanizm uwalniania

DOI:

* PhD. DSc. Ewa Dłuska, PhD. Agnieszka Markowska-Radomska, MSc. Agata Metera, Faculty of Chemical and Process Engineering, Warsaw University of Technology.

1. Introduction

Multiple emulsions are defined as dispersed systems having structures of droplets in a drop (Fig. 1). The smaller droplets of one liquid (internal phase) within larger drops of a second immiscible liquid (membrane phase) are themselves dispersed in a continuous phase, which has the same composition as the smaller droplet, or a different one. Due to their compartmentalised internal structure, multiple emulsions present many advantages over simple O/W or W/O emulsions for encapsulation, such as the ability to carry both polar and non-polar molecules, and better control in releasing therapeutic molecules [1-5]. They combine the properties of both types of simple emulsions and have the potential to encapsulate a large number of different ingredients e.g. cosmetics, drugs, living cells and incompatible materials, and protect active substances from the environment [1, 4, 6]. These dispersed systems offer a wide range of possible applications for cosmetics, food or the pharmaceutical industries, especially for the encapsulation and controlled release of active ingredients. Double emulsions ($F_1/F_2/F_3$) represent the simplest structures among multiple emulsions, Fig. 1.

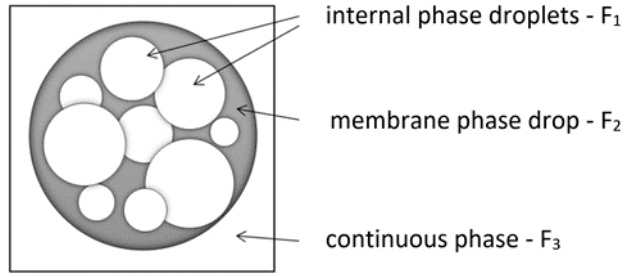

Fig. 1. The structure of double emulsion $F_1/F_2/F_3$

Encapsulation is the process of entrapping biologically/chemically active substances or in general particles of solid or droplets of liquid material or bubbles of gas within a protective membrane to produce capsules/drops in the micro/nanometre to millimetre range. There are two encapsulation processes, matrix in case dispersing active substances within membrane material or core shell when surrounding/coating with a continuous film of polymeric material is considering. The matrix particle allows a manufacturer to encapsulate more than one active ingredient within one particle, while the core shell is ideal for protecting an active ingredient where humidity and moisture or aggressive agents are present. The method of encapsulation can be divided into chemical, physiochemical, electrostatic and mechanical processes. Chemical processes include the interfacial and *in situ* polymerisation methods. Physiochemical processes include coacervation phase separation, multiple emulsion, meltable dispersion and powder bed methods. Mechanical processes include the air-suspension method, pan coating, and spray drying, spray congealing, micro-orifice system and the rotary fluidisation bed granulator method. Material or materials closed can be released for a specified time at a predetermined rate, depending on the process conditions for release-controlled or modified release.

Systems with a modified release of active agents are defined as systems providing a modify rate, profile or place where the release occurs, in comparison to conventional dosage forms of drugs administered through the same route [1, 4, 6]. The main objective of applying modified release systems is to achieve a constant concentration of active ingredients over a therapeutic time. Among systems with a modified profile of release, the following types can be distinguished: delayed, sustained and pulsatile release. The most widespread presentations of modified release drugs include oral, parenteral and transdermal dosage forms. Oral dosage forms are the most commonly used by patients due to their convenient administration. Obtaining drugs with a modified profile of an active agent release involves employing different settings concerning dispersed systems like suspensions, emulsions, aerosols, liposomes or micellar/lamellar structures. However, micro/nanoparticles that have undergone coating or incorporation are most frequently applied to a modified release profile.

Multiple emulsions are an example of a dispersed system applied in the modified release of an active agent. There are two main mechanisms of release: simple or facilitated diffusion or fragmentation of multiple emulsion, i.e. breakage of multiple drops and formation of simple emulsion [6]. In addition, the release process can be controlled by both of the mentioned mechanisms. In majority of drug release systems, the release is limited by mechanisms like dissolution, osmosis, diffusion or chemical reaction [1]. They can take place simultaneously or at different stages of the release process.

A literature overview has shown that the issue of the simultaneous encapsulation of two or more different active ingredients in the multiple emulsion, and their release has not been fully reported and explained yet.

The purpose of the work was to investigate a simultaneous encapsulation of two active ingredients, such as two drugs or living cells within double emulsions and process of release of co-encapsulated drugs.

2. Emulsification and encapsulation process in a Couette-Taylor flow biocontactor

The aim of the experimental research was to examine the process of biological and chemical ingredients encapsulation in double emulsions. Methods: Double emulsions of two types $W_1/O/W_2$ and $O_1/W/O_2$ were prepared by simultaneous emulsification and encapsulation in liquid-liquid Couette-Taylor flow (CTF) bioreactor/biocontactor, Fig. 2 (annular gap width of 1.5 and 2,5 mm and length of 400 mm).

$W_1/O/W_2$ emulsions consisted of alginic acid aqueous solution (inner phase) with living cells (Human Embryonic Kidney – HEK) and a cryoprotectant (sucrose), paraffin (membrane phase), distilled water (outer continuous phase) with appropriate surfactants (Tween and Span) added to each phase. The process parameters included: the rotational frequency of the inner cylinder of the CTF biocontactor: 540 rpm, an annular gap width of 2.5, the ratio of the volumetric flow rates of phases: internal to continuous: 0.25÷0.5 and internal to membrane: 0.5÷1.0, concentration of living cells: one million cells per cm^3.

$O_1/W/O_2$ emulsions contained liquid paraffin as oil phases with an addition of two model active agents (phenyl salicylate and benzoic acid) to inner oil phase and aqueous gelatine solution as a membrane water phase. The process of emulsification and co-

encapsulation of model drugs into $O_1/W/O_2$ has been successfully carried out under conditions corresponding to the rotational frequency of the inner cylinder of the CTF contactor: 1550÷1900 rpm, an annular gap width of 1.5, the ratio of the volumetric flow rates of phases: internal to continuous: 0.1÷0.5 and internal to membrane: 0.2÷0.5, concentration of drugs in the inlet stream for phenyl salicylate: 9.25 and 10 wt%, for benzoic acid: $2 \div 9.1 \cdot 10^{-3}$ wt%.

The details of the preparation technique of multiple emulsions in the CTF contactor and micro-encapsulation procedure were discussed in our earlier publications [6, 7]. The CTF contactor creates suitable hydrodynamic conditions for conducting mass transfer processes in multiphase systems (high interfacial area and mass transfer coefficients) [7÷9].

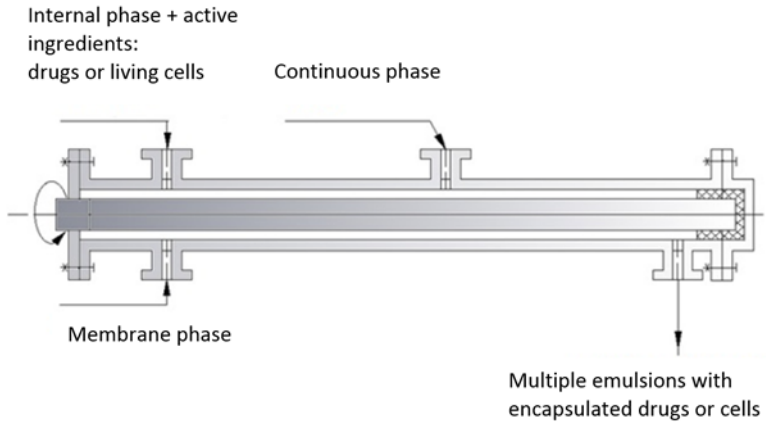

Fig. 2. Liquid-liquid Couette-Taylor flow biocontactor/bioreactor for forming double emulsion $W_1/O/W_2$ and $O_1/W/O_2$ and encapsulating of active ingredients

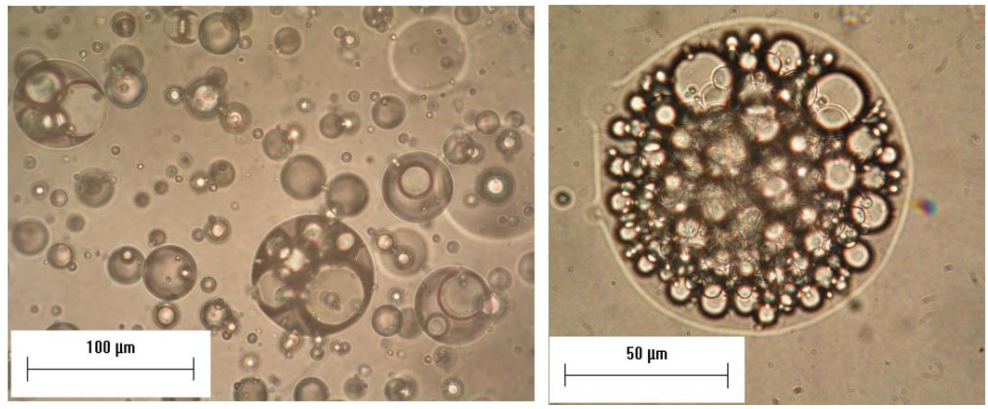

Fig. 3. The representative photos of multiple emulsions $O_1/W/O_2$ with co-encapsulated of two hydrophobic drugs (phenyl salicylate and benzoic acid) within internal paraffin droplets: phenyl salicylate (9.25 wt%) and benzoic acid $2.68 \cdot 10^{-3}$ wt%: left – at time t = 0, right – at t = 46.22 h.

Hydrodynamic conditions in the CTF biocontactor: rotational frequency of inner cylinder: 1622 rpm; flow rates of the liquid phases: internal/membrane/continuous = 50 /15 /100 cm^3/min

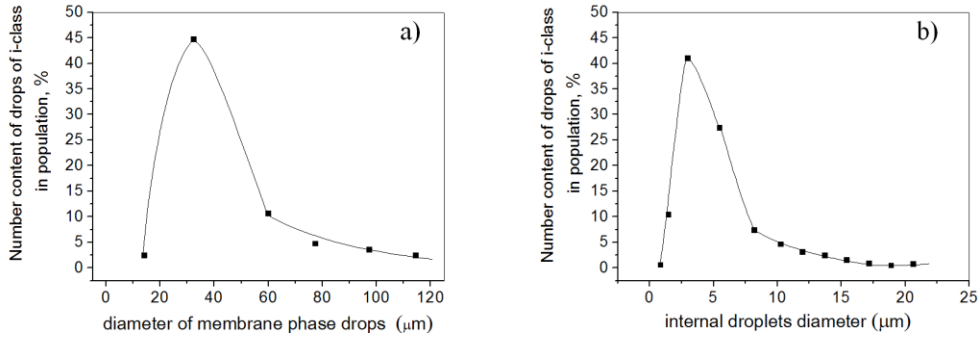

Fig. 4. The drop size distribution of double emulsions $O_1/W/O_2$ with two hydrophobic drugs encapsulated presented in Fig. 3: a) membrane phase drops, b) internal droplets

The shear stresses in a Couette-Taylor Flow apparatus are reduced by one to two orders of magnitude compared to a stirred tank with similar power input per unit volume and stirrer diameter being equal to the rotor of CTF [7]. This is a result of an increase in the area subjected to a constant maximum shear defined by friction drag on the larger surface of cylinder in the CTF device.

The structures of double emulsions with two hydrophobic drugs being encapsulated into internal droplets and drop size distribution are presented in Figs. 3 and 4.

The structures of double emulsions with living cells encapsulated within the internal droplets and the drop size distribution are shown in Figs. 5 and 6.

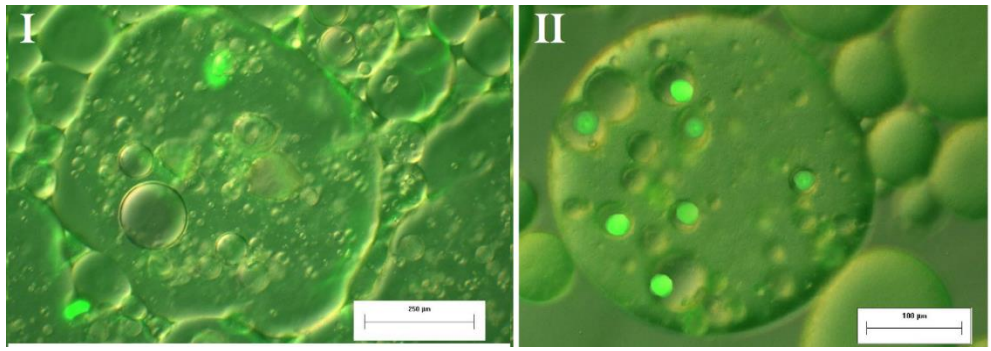

Fig. 5. The fluorescence microscope photos of multiple emulsions $W_1/O/W_2$ with encapsulated of living cells (HEK- Human Embryonic Kidney) within internal alginate droplets – I and additionally with sucrose as a cryoprotectant in the internal droplets – II:
Hydrodynamic conditions in the CTF biocontactor: rotational frequency of inner cylinder: 540 rpm; flow rates of the liquid phases: internal/membrane/continuous = 30 /30 /60 cm^3/min

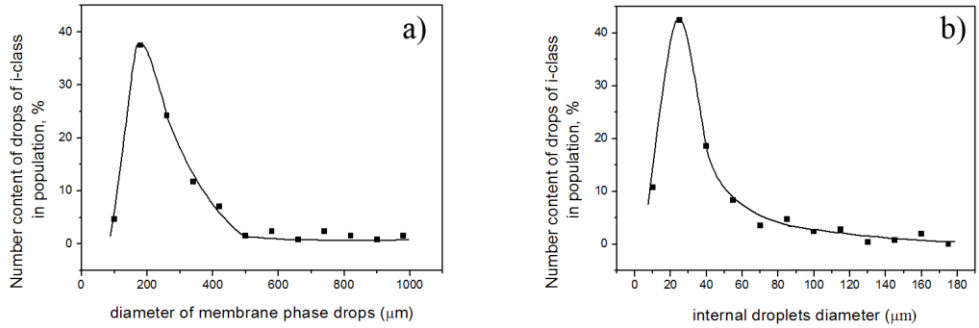

Fig. 6. The drop size distribution of double emulsions $W_1/O/W_2$ with living cells (HEK) encapsulated within internal alginate droplets shown in Fig. 5: a) membrane phase drops, b) internal droplets

3. The rate and mechanism of simultaneous release of two active ingredients

The experimental release study involved the influence of parameters of the emulsification and encapsulation process in a CTF biocontactor and the conditions of the release process (mixing intensity) on the release rates of two entrapped model active agents from internal paraffin droplets to the external paraffin phase of emulsions. The release experiments have been carried out in the stirred tank under a stirring frequency of 150 and 250 rpm at a temperature of 37°C.

The process of simultaneous encapsulation of phenyl salicylate and benzoic acid in the internal phase of $O_1/W/O_2$ double emulsions in the CTF contactor has shown an ability to create modified release by forming different structures of emulsions. The best double emulsions have been those obtained from a solution of drug concentration: 10 wt % of phenyl salicylate and $2.91 \cdot 10^{-3}$ wt % of benzoic acid in a contactor with an internal cylinder frequency of 1802 rpm [10]. These double emulsions $O_1/W/O_2$ with co-encapsulated hydrophobic have been characterised by a high encapsulation efficiency, the highest stability of internal and membrane phase drops and a two-step release profile of phenyl salicylate. The influence of preparation conditions in the CTF contactor, an initial concentration of benzoic acid and the conditions in the release environment on the kinetics of release process are demonstrated in Figs. 7 ÷ 9. The release profiles have been presented in the form of a dependence of cumulative mass fraction of the released ingredient on time.

Simultaneous release of both active substances from double emulsions (prepared under different hydrodynamic and process conditions in the CTF contactor) has shown that the release process occurring in the stirred tank is governed by a diffusion mechanism. The release mechanism has been verified during experiments performed in the stirred tank by comparing change in the drop size using microscopic image analysis. Since the diameter of the membrane phase drops and internal droplets remain unchanged, consequently, the basic release mechanism responsible for the release was unchanged too.

The comparison of the release profiles of emulsions with one (phenyl salicylate) and two (phenyl salicylate + benzoic acid) active agents has shown that the modified pattern, i.e. two-step release kinetics of phenyl salicylate has been a result of the presence of the second ingredient (Figs. 7, 8).

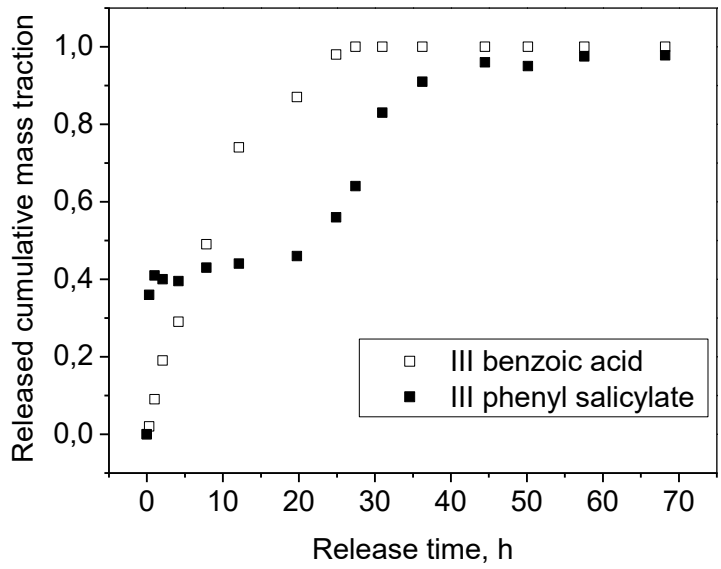

Fig. 7. Release profiles of both encapsulated drugs: benzoic acid and phenyl salicylate from double emulsions III formed under conditions in the CTF contactor: rotational frequency of inner cylinder 1802 rpm, initial concentration of benzoic acid: $9.09 \cdot 10^{-3}$ wt% and phenyl salicylate 10 wt%

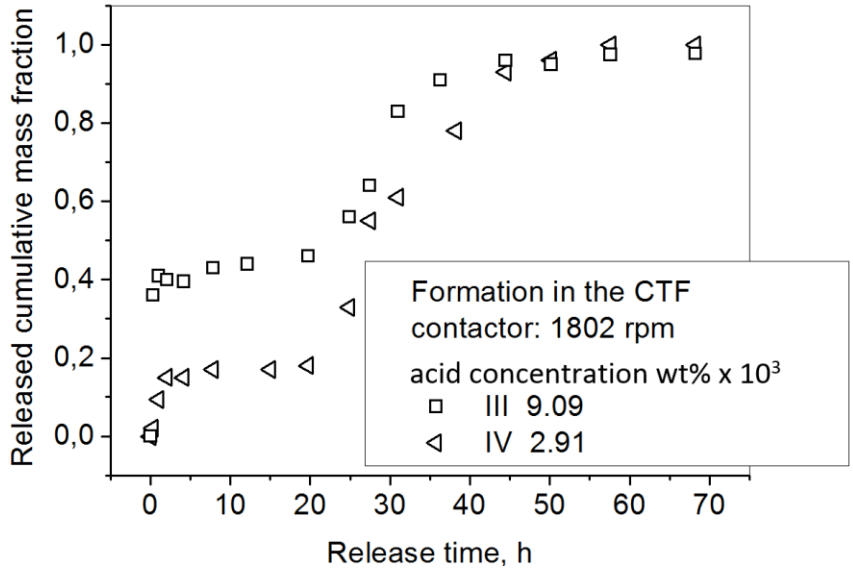

Fig. 8. The influence of an initial benzoic acid concentration on the release rate of phenyl salicylate from double emulsions III and IV formed in the CTF contactor

Addition of the second ingredient affects the time required to completely release the basic encapsulated ingredient, i.e. phenyl salicylate. The longest period of time required for a complete release of phenyl salicylate was observed for emulsions, which have been prepared under the highest rotational frequency of inner cylinder in the CTF contactor. Increasing the mixing intensity of the release medium caused a faster release of the encapsulated drugs (Fig. 9).

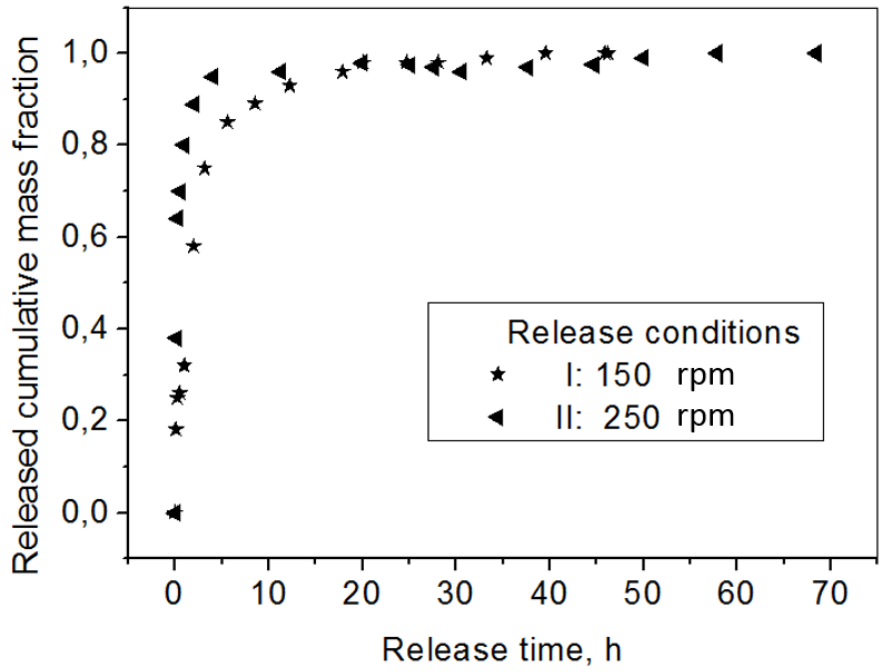

Fig. 9. The influence of the mixing intensity of environment on the release rate of phenyl salicylate from double emulsions I and II formed under conditions in the CTF contactor: rotational frequency of inner cylinder: 1622 rpm; initial concentration of benzoic acid: $2.68 \cdot 10^{-3}$ wt% and phenyl salicylate: 9.25 wt% – emulsions I, initial concentration of benzoic acid: $9.09 \cdot 10^{-3}$ wt% and phenyl salicylate 10 wt% – emulsions II

4. Summary

The study showed that it is possible to encapsulate biologically and chemically active ingredients, such as living cells and two different drugs in double emulsion $W_1/O/W_2$ or $O_1/W/O_2$ using the CTF contactor. Multiple emulsions with living cells can be further considered as carriers of biological material and a microenvironment for banking and storing cells for therapeutic purposes.

The release study involved the simultaneous release of two entrapped model active ingredients (two hydrophobic drugs) from the internal droplets to the external continuous phase of emulsions of

different structures proved that it is possible to modify the release kinetics, i.e. the rate and type of release profiles. The release of active ingredients from multiple emulsions can be controlled through the physicochemical parameters of emulsions and the size of internal droplets and drops forming a liquid-permeable membrane separating the internal droplets from the external environment. A desirable modified type of the release profile would be achieved by adding a few active ingredients into the internal droplets.

Research on simultaneous encapsulation and release of a few substances that have been made until now demonstrates new potential applications of multiple emulsions as systems for controlled/modified drugs release in targeted therapies. However, the issue of simultaneous release of a few active agents from multiple emulsions requires an extension of experimental investigations and mathematical modelling of the process.

References

[1] Aserin A., *Multiple emulsions: Technology and Applications*, J. Wiley & Sons, USA 2008.

[2] Wilson J. L., McDevitt, T. C., *Stem cell microencapsulation for phenotypic control, bioprocessing, and transplantation,* Biotechnology and bioengineering vol. 110(3), 2013, 667-682.

[3] Khopade A. J., Jain N. K., *Concanavalin-A conjugated fine-multiple emulsion loaded with 6-mercaptopurine.*, Drug Delivery, vol. 7(2), 2000, 105-112.

[4] Siepmann J., Siegel R. A., Rathbone M. J. (Eds.), *Fundamentals and applications of controlled release drug delivery*, Springer Science & Business Media, USA 2011.

[5] Hino T., Kawashima Y., Shimabayashi S., *Basic study for stabilization of w/o/w emulsion and its application to transcatheter arterial embolization therapy*, Advanced drug delivery reviews, vol. 45(1), 2000, 27-45.

[6] Markowska-Radomska A., Dluska E., *An evaluation of a mass transfer rate at the boundary of different release mechanisms in complex liquid dispersion,* Chemical Engineering and Processing: Process Intensification, 101, 201656-71.

[7] Dluska E., Markowska-Radomska A., *Regimes of multiple emulsions of W1/O/W2 and O1/W/O2 type in the continuous Couette-Taylor flow contactor,* Chemical Engineering and Technology, vol. 33(1), 2010, 113-120.

[8] Curran S. J., Black R. A., *Oxygen transport and cell viability in an annular flow bioreactor: Comparison of laminar Couette and Taylor-vortex flow regime,* Biotechnology and bioengineering, vol. 89(7), 2005, 766-774.

[9] Dluska E., Hubacz R., *Mass transfer in the two-phase helicoidal contactor,* Inżynieria chemiczna i procesowa, vol. 21(1), 2000, 103-113.

[10] Metera A., *Wytwarzanie aktywnych emulsji wielokrotnych metodą enkapsulacji w przepływie helikoidalnym*, Praca dyplomowa magisterska, Politechnika Warszawska, 2014.

A c k n o w l e d g m e n t s

The authors would like to thank the National Science Centre – Poland for supporting the part of the research regarding the drugs encapsulation and co-release under grant number 2014/13/B/ST8/04274.

TECHNICAL TRANSACTIONS | CZASOPISMO TECHNICZNE
MECHANICS | MECHANIKA
2-M/2016

ANDRZEJ DUDA, JERZY KAMIEŃSKI*

THE CIRCULATION OF LIQUID IN THE MIXING VESSEL EQUIPPED WITH DIFFERENT DUAL IMPELLERS

CYRKULACJA CIECZY W APARACIE Z DWOMA RÓŻNYMI MIESZADŁAMI

Abstract

The aim of the article was the analysis of liquid flow of radial-axial circulation in the mixing vessel equipped with a dual impeller set, of which the lower impeller induces radial-axial liquid stream, while the upper is turbine disc impeller with vertical blades, ejecting the liquid radially. On the basis of measurements of the liquid instantaneous velocity, the circulation flow rate was evaluated and supplemented with the exchange flow rate – occurring between adjacent compartments. The usage of a CMA model allows to describe the cycle of liquid transport.

Keywords: mixing, circulation of liquid,

Streszczenie

W artykule analizowano przepływy strumieni cieczy cyrkulacji promieniowo-osiowej w zbiorniku z dwoma mieszadłami na wale, z których dolne wytwarza promieniowo-osiowy strumień cieczy, górnym zaś jest mieszadło turbinowe tarczowe, z pionowymi łopatkami, wyrzucającymi ciecz promieniowo. W oparciu o pomiary chwilowej prędkości cieczy wyznaczono wydatek jej przepływu cyrkulacyjnego, uzupełniony o przepływy między obszarami cyrkulacyjnymi. Korzystając z modelu CMA opisano cykl przenoszenia cieczy.

Słowa kluczowe: mieszanie, curkulacja cieczy

DOI:

* MSc. Eng. Andrzej Duda, Firma Doradczo-Inżynieryjna EDA, Wieliczka, Prof. PhD. DSc. Eng. Jerzy Kamieński, Institute of Thermal and Process Engineering, Faculty of Mechanical Engineering, Cracow University of Technology.

1. Introduction

This study is dedicated to the flows of liquid streams of the radial-axial circulation in a mixing vessel equipped with different dual impeller sets. In each dual set, the lower impeller induces radial-axial liquid stream, while the upper is a turbine disc impeller with vertical blades, ejecting the liquid radially.

The impellers, rotating in the liquid, spin it as a stream of primary circulation. Whereas the centrifugal force acting on the spinning liquid induces secondary circulation in the entire volume of the vessel. This secondary circulation is known as radial-axial circulation and is related to the pumping process of the impellers. This circulation is crucial for proper and efficient mixing.

In order to achieve the required intensity of the mixing process, two impellers are often assembled on a common drive shaft. Such solution is often used in the mixing of a multiphase systems.

The paper presents the study on three dual impeller sets, located on a common single shaft, at several different distances from each other. During the experiments, the values of the instantaneous velocity of liquid were measured (radial and axial component of the velocity). Then, on the basis of the mean velocities, the circulation flow rate of the liquid was determined.

In the study, the Compartment Model Approach (CMA) was used. The total flow rate values were supplemented by the exchange flow rate of the liquid occurring between circulation compartments. This additional flow rates are caused by fluctuations of liquid velocity. Based on the CMA model, the two-dimensional chart of liquid transport in an apparatus was described. Further use of this model enabled to describe the cycle of liquid transport in an apparatus, the duration of which was related to the mixing time, and could be a measure of the mixing process efficiency when considered it together with energy consumption.

2. Experimental set-up and methodology

The measurements of the instantaneous velocities of liquid were performed using two-channel laser Doppler anemometer (LDA, delivered by the DANTEC Company), operating in the backscattering mode [6]. The experiments were carried out in a cylindrical vessel, with the inner diameter of D = 0.286 m, equipped with four flat baffles, each with the standard width of $0.1 \cdot D$. The cylindrical vessel was built in the rectangular jacket. Both of them were made of the same material, a borosilicate glass of the DURAN type. To eliminate an error of the refraction effect, occurring when the laser beams pass through different materials, the dimethyl sulfoxide, fully transparent liquid, having the same refractive index as DURAN glass, was employed in the experiments. The temperature of the liquid and vessels' walls was controlled by the thermostatic system; the measurements were carried out at the temperature of 22.5°C, wherein the density of the dimethyl sulfoxide was 1100 kg/m^3 and the dynamic viscosity coefficient – of 2.3 mPa.

As the seeding particles, the hollow glass spheres with a silver plated outer surface (trade symbol S-HGS) were used in the experiments. The mean diameter of the particles

was 10 μm, and their average density was 1150 kg/m^3. Both the vessel and the jacket were filled up with liquid to the height of 1.258*D*.

Three different dual impeller sets were examined. The upper impeller was in each case the disc turbine, equipped with six vertical, flat blades – TR-6. The lower impeller was exchanged by three different types: the turbine with six blades inclined at 45° (Pitched Blade Turbine, PBT-6 type), the hydrofoil Chemineer HE-3 impeller [4] and the hydrofoil Lightnin A-315 impeller [12]. The diameter of all examined impellers was of $d = D/3$. The lower impeller was in each case located at the distance of $h = 0.5 \cdot d$ from the vessel's bottom and the value of the impeller spacing Δh was changed in the range of $(0.5 \div 2) \cdot d$.

The liquid velocities were measured in the selected points, located at the vertical middle plane of the vessel, placed between two successive baffles and forming a regular, rectangular grid. The measurement points were spaced by 0.005 m along the radius of the vessel and its height. The two components of the instantaneous velocity of liquid were measured: the radial $u_r(t)$ and the axial $u_z(t)$.

The experiments were carried out within the turbulent flow regime of liquid, at a constant rotational frequency of impellers of 5 [s^{-1}], which corresponded to the Reynolds number for a mixing process, $Re \approx 2.16 \cdot 10^4$. The power consumption was an additional magnitude measured during the experiments.

3. Experimental results

3.1. Mean velocities of liquid

The values of the velocity components: mean $\bar{u}$ and fluctuating u', were calculated on the basis of prior measurement data of the instantaneous velocities, benefiting from the FLOware software.

The components of mean velocity $\bar{u}_i$ were calculated as the weighted averages, with weights corresponding to the residence time $\Delta t_{i,j}$ of seeding particles in the measurement volume [6, 11]:

$$\bar{u}_i = \frac{\sum_{i=1}^{N} u_{i,j} \cdot \Delta t_{i,j}}{\sum_{i=1}^{N} \Delta t_{i,j}} \tag{1}$$

The shape and intensity of the mean flow of liquid in the mixing vessel is determined by the distributions of velocity components and their local values. The primary circulation of liquid, induced during the mixing process by rotating impellers, is partly being converted to the secondary, related to the radial-axial flow. This flow is also directly related to the components of mean velocity: radial and axial.

These radial-axial flows of liquid, occurring in the mixing vessel, depend on the design of applied impellers and their mutual position. They were illustrated in Figs. 1÷3, as distributions of the resultants of mean velocities in the radial and axial direction. They were drawn at the vertical middle plane located between two baffles in the vessel.

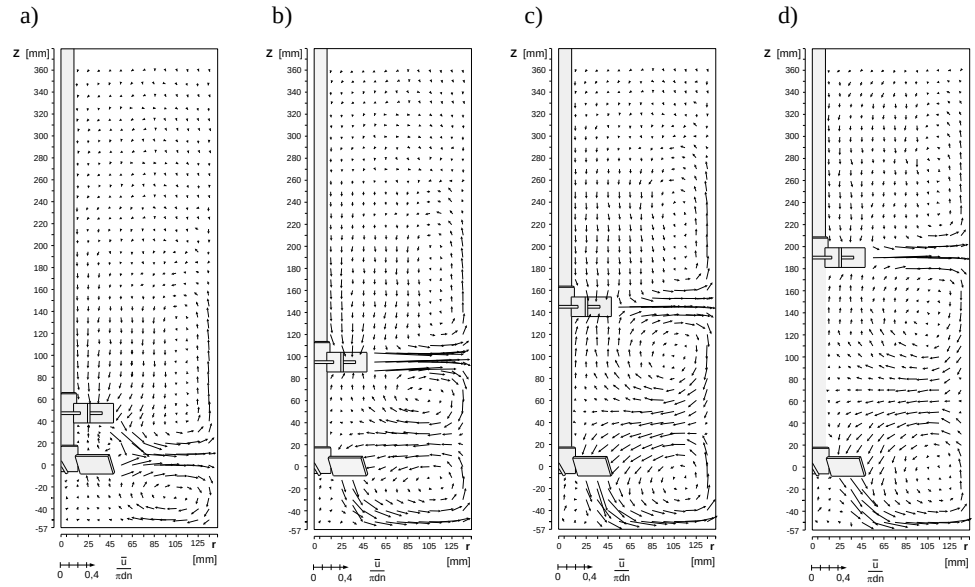

Fig. 1. The distribution of the resultants of mean liquid velocities in the radial and axial direction, in the dual mixing vessel equipped with the upper disc turbine TR-6 and the lower impeller pitched blade turbine PBT-6. The impeller spacing:a) $\Delta h = 0.5d$, b) $\Delta h = d$, c) $\Delta h = 1.5d$, d) $\Delta h = 2d$ [5]

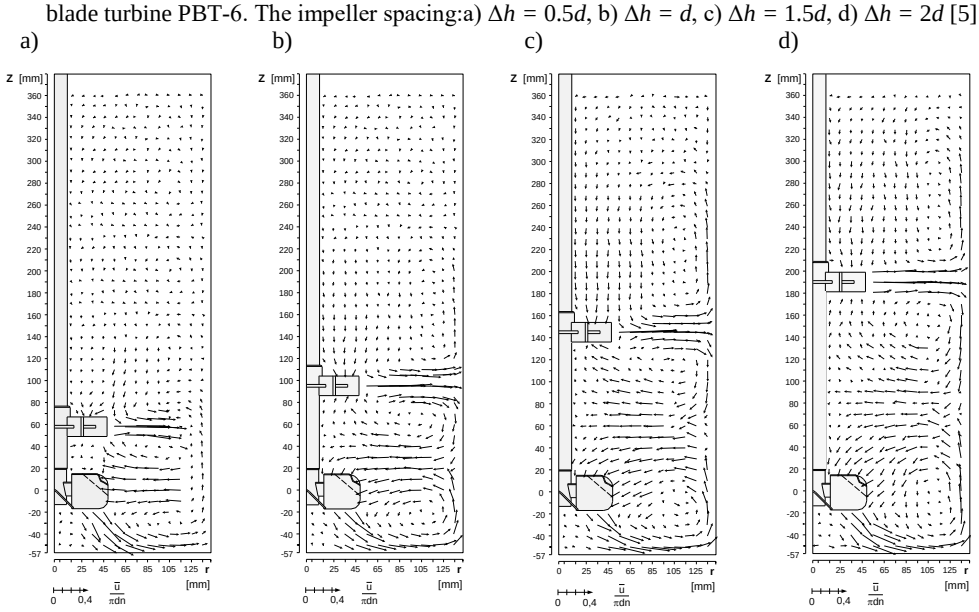

Fig. 2. The distribution of the resultants of mean liquid velocities in the radial and axial direction, in the dual mixing vessel equipped with the upper disc turbine TR-6 and the lower A-315 impeller; the impeller spacing: a) $\Delta h = 0.6d$, b) $\Delta h = d$, c) $\Delta h = 1.5d$, d) $\Delta h = 2d$ [5]

All examined dual impeller sets induce an advantageous structure of the liquid flow in the mixing vessel. When the impellers are at sufficient distance, the flow of liquid is expanded in the entire volume and is sufficiently intense. The flow structure is then composed of several compartments, close to the model structure of a multistage mixing [1, 15, 18]. The circulation flows in the mixing vessel are similar; however, they differ from each other quantitatively, depending on the design of the lower impeller.

The adjacent circulation loops interact only at certain distances between the impellers. If these distances are too small or too large, then the interaction completely disappears. At small values of the spacing, the adjacent circulation loops induced by the upper and the lower impeller coalesce into one common. The shapes of these loops are determined by the resultant streams of the liquid flow, pumped through both of the impellers.

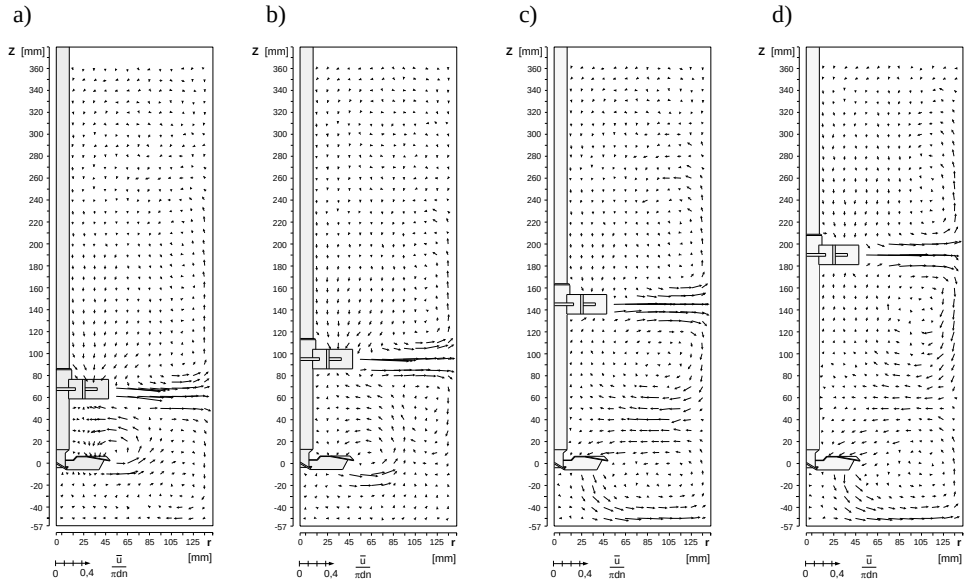

Fig. 3. The distribution of the resultants of mean liquid velocities in the radial and axial direction, in the dual mixing vessel equipped with the upper disc turbine TR-6 and the lower HE-3 Impeller; the impeller spacing: a) $\Delta h = 0.7d$, b) $\Delta h = d$, c) $\Delta h = 1.5d$, d) $\Delta h = 2d$ [5]

It was clearly shown in Figs. 1a, 2a and 3a, illustrating the flows in the mixing vessel equipped with two impellers located at the spacing of $\Delta h = (0.5 \div 0.7) \cdot d$.

In case of dual impeller sets with the lower PBT-6 or HE-3 impeller, the impact of the upper disc turbine is so intense that the lower impeller ejects the liquid radially towards the vessel's wall. While it should induce an axial flow of liquid, taking into consideration its position inside the mixing vessel. In the case of HE-3 impeller, this trend also occurs at greater spacing. It is evident even when $\Delta h = d$. It is different, however, in case of the set with lower A-315 impeller, which induces an intensive axial flow of liquid, directed towards the bottom of the tank, even at a position close to the upper impeller. When the impeller spacing is being increased, a gradual loss of the interaction between the adjacent

liquid streams can be observed, with simultaneous change of the geometry of circulation loops. In case the lower impeller is PBT-6 turbine or A-315, the loops are being spread along the height of the vessel, and for the dual set with the lower impeller of HE-3 type, additionally, a complete change of the geometry of loops and their position in the tank can be noticed.

3.2. Circulation flow rate of liquid

The liquid flow rate Q_C refers to the motion of liquid in the entire volume of the mixing vessel. It is defined as the stream of liquid flowing through the surface, which is located at any cross-section in the tank. Whereby it is considered, both the axial flow rate Q_z, occurring at the horizontal section plane of the tank, at the height of z_i and the radial flow rate Q_r – present at the vertical section plane, at the radius of r_i. Moreover, assuming the circular symmetry of the flow, they are defined as [9]:

$$Q_z(z_i) = \iint_{S_{z_i}} (\bar{u}_z)_{z_i} \, \mathrm{d}S_{z_i} \tag{2}$$

$$Q_r(r_i) = \iint_{S_{r_i}} (\bar{u}_r)_{r_i} \, \mathrm{d}S_{r_i} \tag{3}$$

Furthermore, assuming axial symmetry, the circulation flow rate of liquid in the mixing vessel, Q_C is equal to the maximum value of the flow rates Q_z and Q_r [10]:

$$Q_C = \max\left\{|Q_z|, |Q_r|\right\} \tag{4}$$

The circulation flow rate was calculated on the basis of the components of mean velocity of liquid, evaluated at selected measurement points (Figs. 1÷3).

The quantity and limits of the circulation zones were evaluated on the basis of distributions of resultants of the mean velocity components: radial and axial. The analysis of directions and senses of the mean velocity resultants allowed to evaluate the limits of each zone, by determining the value of z_o height, in around which the real limit of zone can be found. It is exemplified in Fig. 4, where the limits of the respective zones are defined as $z_{o1\text{-}2}$, $z_{o2\text{-}3}$ and $z_{o3\text{-}4}$. The values of the axial components of the mean liquid velocity, measured at the points located the closest to the height coordinate of z_o, just below and above it, were then approximated using a continuous function. Next, it was found by means of standard mathematical procedure that the z value of the height at which this velocity component changed its sign reaching zero.

Thus, the z_g coordinate value of the point on the limit line was obtained, corresponding to a given radius of r. This procedure was repeated for each group of points corresponding to different values of the radius, which was changed every 5 mm. The determination of the limit line, described by the $z_{og} = f(r)$, was based on the approximation of the evaluated z_g values, with usage of the continuous function.

In case the centres of loops (restricted in the respective circulation zones) did not coincide the one straight line corresponding to a certain radius value and parallel to the vessel's axis, it was not possible to evaluate the position of the points of limits, based on

the $\bar{u}_z = f(z)$ function. The vectors of the axial component of the mean velocity took the same sense, near the limit of adjacent circulation zones. In such cases, the points of limit were evaluated using the $\bar{u}_r = f(r)$ function and searching for its zero value corresponding to a certain *r* argument. This function describes alterations of the radial component of the mean velocity versus the radius, at different heights. Then, the points of the circulation zone limit were described using the *rog* radius, which differed depending on the height in the mixing vessel, replacing the dependency of $z_{og} = f(r)$ – with the $r_{og} = f(z)$ function. The circulation flow rate of liquid was evaluated within the limits of each such determined zone. The equations (2), (3) were converted to following form:

$$Q_z(z_i) = 2\pi \int_{r_1}^{r_2} (\bar{u}_z)_{z_i} \, r \, \mathrm{d}r \tag{5}$$

$$Q_r(r_i) = 2\pi r_i \int_{z_{og1}}^{z_{og2}} (\bar{u}_r)_{r_i} \, \mathrm{d}z \tag{6}$$

The procedure described above was illustrated in Fig. 4a. The profiles of $\bar{u}_r$ velocity component drawn along the vessel's height are marked in this figure, for the four selected radiuses, against the real limits of the considered liquid circulation zone. The area covered by this zone is also marked in Fig. 4b, illustrating the mean radial-axial flow of liquid.
In this case, the $\bar{u}_r$ velocity profiles were integrated using the equation (6), within the limits of zone of $|z_{og1\text{-}2}, z_{og2\text{-}3}|$ corresponding to a given radius of the vessel. The liquid flow within the circulation zone was assumed as in closed-circuit. For each velocity profile, there is some part of it in accordance with the direction of coordinate system ($\bar{u}_r^{(+)}$), and its remaining part is opposite of the coordinate system ($\bar{u}_r^{(-)}$). Thus, the two integrals: $Q_r^{(+)}$ and $Q_r^{(-)}$ were calculated. This procedure was repeated for the further values of *ri* radius, and next, all of obtained values were approximated at the end with usage of the continuous function. Similarly, the procedure was carried out using the equation (5). The maximum of these values was the wanted circulation flow rate Q_{Ci}, of the *i*-th zone in the vessel. The liquid flow rate circulating in the total volume of the vessel was evaluated as the sum of the *n* – flow rates from the respective *n*-zones of circulation, which form the total structure of the flow:

$$Q_{C\,\mathrm{sum}} = \sum_{i=1}^{n} Q_{Ci} \tag{7}$$

Finally, it was presented in the form of a dimensionless circulation flow number, of which values were collected in Table 1 and shown in Fig. 5:

$$K_C = \frac{Q_{C\,\mathrm{sum}}}{n \cdot d^3} \tag{8}$$

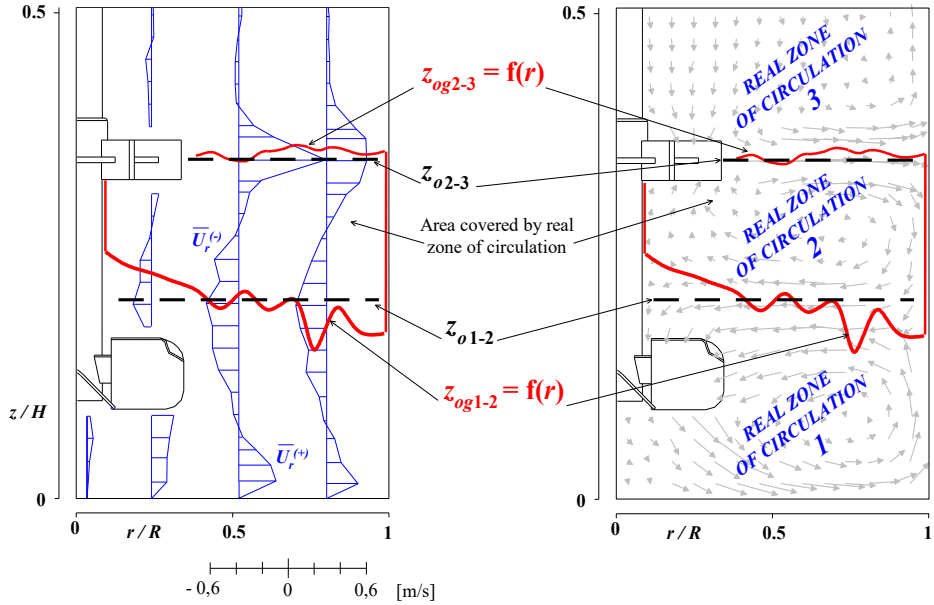

Fig. 4. The location of points of limit z_{og} along the radius of tank. The z_o heights and the real limiting lines of the circulation zones, determined by the procedure of approximation of points z_{oq}. The dual impeller set: TR-6 and A-315, $\Delta h = d$

The greatest values of the circulation flow number can be found for the dual set with A-315 impeller. The set with a pitched blade turbine can induce even a more efficient circulation only at the greatest possible impeller spacing. For the values of $\Delta h \geq d$, the least intense circulation is always induced by the set of lower HE-3 impeller. For each of the examined pair of impellers, the circulation flow rate of liquid takes the greatest values when the impellers are spaced by $\Delta h = 1.5d$.

Table 1

The circulation flow numbers of liquid K_C and $K_{C\,calk}$ for the examined dual impellers, with the upper TR-6 disc turbine

Lower impeller:	PTB-6		A-315		HE-3	
	K_C	$K_{C\,calk}$	K_C	$K_{C\,calk}$	K_C	$K_{C\,calk}$
$\Delta h \cong 0.5d$	2.12	2.93	2.28	3.13	2.15	3.00
$\Delta h = d$	3.09	4.69	3.21	4.53	1.93	3.00
$\Delta h = 1.5d$	3.58	5.19	3.63	4.96	3.08	3.98
$\Delta h = 2d$	3.42	4.57	3.22	4.50	2.83	3.88

The analysis of the flow structure was carried out using the Compartment Model Approach (CMA) [7, 8, 13]. For the flow modelling purposes, the real circulation flows of liquid, determined by the radial and axial components of the mean velocity, were replaced

with the contractual circulation compartments: of the first order - situated above and below each impeller, of the second order – in other zones of the vessel. Thus, the zones of liquid circulation (illustrated in Figs. 1÷3) could be presented in the form of contractual, two-dimensional and rectangular compartments specified in the vertical section of the vessel and located cascaded – one above the other. The compartments illustrate the secondary radial-axial circulation flow of liquid in the dual mixing vessel [7, 17, 18]. The limits of these compartments result from the real limits of the circulation zones, z_{og}. The liquid flow inside the compartment is determined by the Q_{Ci} flow rate. The momentum exchange between adjacent compartments takes place at their limiting line, only in the axial direction. It is correlated to the exchange flow rate, induced by the axial component of fluctuation velocity. This component was determined at the points located on the limiting line of the adjacent circulation zones. The values of u'_z, measured at the points located at certain radius coordinate and at several height coordinates, the closest to the corresponding point of the limiting line, z_g, were compiled as a function of the vessel's height and approximated using the continuous function $u'_z = f(z)$. When this function was known, the value of $u'_{zg} = f(z = z_g)$ could be determined. The RMS values, referred to the axial components of fluctuations of the instantaneous velocity, were assumed in place of the u_z' and u_{zg}'. The RMS values were directly obtained from the LDA measurements.

Then, the liquid velocity components, as a function of radius in the vessel, were processed by another approximation using the $u_{zg}' = f(r)$ relationship. This was carried out in the total volume of the dual mixing vessel, at all of the limits which separate corresponding compartments of the circulation flows. The Q_{Ei} flow rate between the adjacent circulation compartments of liquid was determined by the integration process of the $u_{zg}' = f(r)$ function, within the range of r_g radius values. Due to the symmetry of structure and the continuity of flow, it is assumed that the exchange flow occurs in both directions and is equal from both sides as is:

$$Q_{Ei} = 0.5\left[2\pi \int_{r_{g1}}^{r_{g2}} \left| u'_{zg}(r) \right| r \, \mathrm{d}r \right] \tag{9}$$

The total exchange flow rate $Q_{E\,sum}$ was then defined as a sum of all flows determined on the limiting lines between respective compartments of the circulating liquid:

$$Q_{E\,sum} = \sum_{i=1}^{n} Q_{Ei} \tag{10}$$

Thus, the total, corrected liquid flow rate in the dual mixing vessel $Q_{C\,calk}$ was defined as:

$$Q_{C\,cała} = Q_{C\,\mathrm{sum}} + Q_{E\,\mathrm{sum}} \tag{11}$$

and was presented in the dimensionless form, as the corrected, total flow rate number $K_{c\,calk}$:

$$K_{C\,calk} = \frac{Q_{C\,sum} + Q_{E\,sum}}{n\,d^3} \tag{12}$$

Its values, obtained for the examined dual impeller sets, are collected in Table 1 and shown in Fig. 5.

The corrected flow rate of liquid includes the mean flows within the limits of its circulation compartments, as well as the fluctuation flows – between them. It describes the liquid flow, as if it was an averaged inside each compartment, but considered as instantaneous at its limits. The exchange flows cause quantitative increase of the total flow rate of liquid in the vessel, depending on the total value of flow rate – $Q_{E\,sum}$. This value of flow rate is as various as miscellaneous are the flow structures, in dual mixing vessel.

The results indicate that for the impeller spacing of $\Delta h \geq d$ the greatest values of flow rate number $K_{C\,calk}$ can be found if the lower is pitched blade turbine (PBT-6). Slightly less value (by 1÷4%) can be found if it is A-315 impeller. On the other hand, $K_{C\,calk}$ reaches by far the lowest values in case of HE-3 impeller. The situation is different at close location of the impellers ($\Delta h = d$). Then, the $K_{C\,calk}$ number takes the greatest value for the set of lower A-315 impeller, and is of a few percent lower in case of the rest of examined sets.

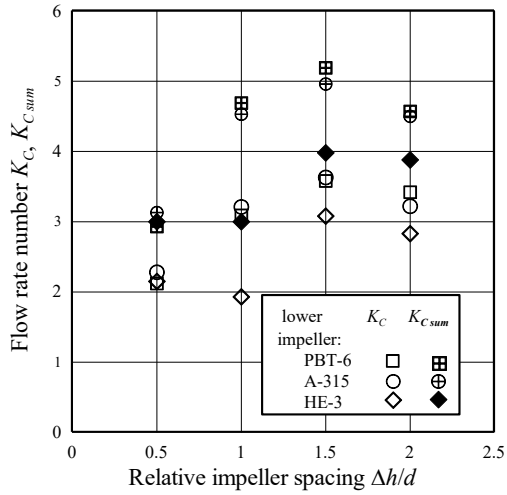

Fig. 5. The flow rate numbers of liquid, K_C and $K_{C\,calk}$ in the dual mixing vessel, versus the relative value of impeller spacing

3.3. Cycle of liquid transport

The flow of liquid is a crucial problem for its mixing. It is related to the transport of liquid elements along the vessel's height, towards the liquid level and reversely. It is possible to describe the liquid transport phenomena in a dual mixing vessel using the assumptions of the CMA model, in the context of momentum exchange within the compartments and between them. The liquid element is successively being moved through the circulation compartments with the velocities of $\bar{u}_r$ and $\bar{u}_z$, and while crossing the compartments' limits, is moving with the velocities of u'_z. An exemplary chart of the trajectories of liquid element is presented in Fig. 6.

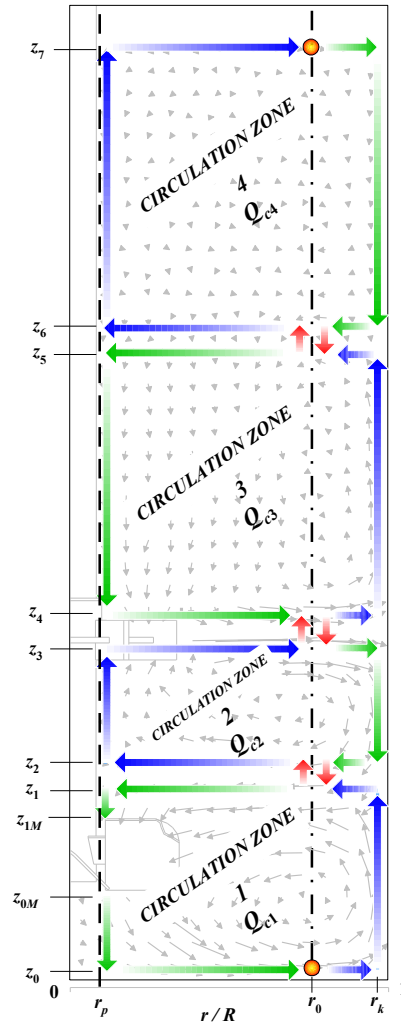

Fig. 6. The chart of liquid element transport in the dual mixing vessel with the lower A-315 impeller and four circulation zones, at $\Delta h = 1d$

Let us assume that the liquid element flows rectilinearly through each length. This element begins its move at the point of coordinates of (r_0, z_0) and flows upward, in the range of [z_0, z_7] and of [r_p, r_k], along the height and radius of the vessel. Once the element reaches one of the above limit coordinates, it changes its direction. Within the compartment, the liquid element flows on the horizontal lengths with the velocity of $\bar{u}_r$, while on the vertical lengths – with the velocity of $\bar{u}_z$. The liquid element traverses each length with different mean velocities. The lengths of element trajectories are set so that they coincide the lines of measurement points, at the middle vertical plane of the vessel. The liquid element crosses the limits of compartments at the points of radial coordinate of r_0, in

which the centres of circulation loops are also located. The crossing velocity of liquid element at these points is u'_z. The calculations were performed for the sets of impellers spaced at $\Delta h = 2d$. The flow structure induced in the mixing vessel, presented in Fig. 6, consists of three compartments of the first order and the fourth – of the second order. The mean velocity values, obtained at the measurement points, were compiled and described with continuous functions, within the respective range: from r_p to r_k and from z_0 to z_7, determining the trajectory of the liquid element. These functions were obtained by the interpolation of discrete values of the velocity, using the MATLAB software and selecting the spline type functions. Thus, to obtain the total transport time of liquid element at the certain length, the numerical integration of the formulas of inversed velocity was performed, according to the equations (13) and (14):

$$\vartheta_j = \int_r \frac{1}{\mathrm{f}_j(r)}\,\mathrm{d}r \tag{13}$$

$$\vartheta_j = \int_z \frac{1}{\mathrm{f}_j(z)}\,\mathrm{d}z \tag{14}$$

where the j-th index refers to the serial number of function, as shown in Table 2.

Table 2

The summary of the functions of liquid element velocity and their intervals of validity (domains)

Lp.	$\bar{u}_i$	r, z
1	$\mathrm{f}_1 = \bar{u}_r(r)$	$r \in \{[r_0, r_k]\} z_0$
2	$\mathrm{f}_2 = \bar{u}_z(z)$	$z \in \{[z_0, z_1]\} r_k$
3	$\mathrm{f}_3 = \bar{u}_r(r)$	$r \in \{[r_k, r_0]\} z_1$
4	$\mathrm{f}_4 = u'_{z1\text{-}2}(z)$	$z \in \{[z_1, z_2]\} r_0$
5	$\mathrm{f}_5 = \bar{u}_r(r)$	$r \in \{[r_0, r_p]\} z_2$
6	$\mathrm{f}_6 = \bar{u}_z(z)$	$z \in \{[z_2, z_3]\} r_p$
7	$\mathrm{f}_7 = \bar{u}_r(r)$	$r \in \{[r_p, r_0]\} z_3$
8	$\mathrm{f}_8 = u'_{z\,2\text{-}3}(z)$	$z \in \{[z_3, z_4]\} r_0$
9	$\mathrm{f}_9 = \bar{u}_r(r)$	$r \in \{[r_0, r_k]\} z_4$
10	$\mathrm{f}_{10} = \bar{u}_z(z)$	$z \in \{[z_4, z_5]\} r_k$
11	$\mathrm{f}_{11} = \bar{u}_r(r)$	$r \in \{[r_k, r_0]\} z_5$
12	$\mathrm{f}_{12} = u'_{z\,3\text{-}4}(z)$	$z \in \{[z_5, z_6]\} r_0$
13	$\mathrm{f}_{13} = \bar{u}_r(r)$	$r \in \{[r_0, r_p]\} z_6$
14	$\mathrm{f}_{14} = \bar{u}_z(z)$	$z \in \{[z_6, z_7]\} r_p$
15	$\mathrm{f}_{15} = \bar{u}_r(r)$	$r \in \{[r_p, r_0]\} z_7$

The numerical integration was performed using the Gaussian quadrature method, and next based on the Newton-Cotes formulas, yielding thereby an exact result of calculations. This way, the functions describing alterations of the radial and axial component of the mean velocity depending on the radius – $\bar{u}_r(r)$ and the vessel's height – $\bar{u}_z(z)$ were obtained. These functions and their intervals were shown in Table 2.

In case the liquid element flowed through the compartments with the velocity values of u'_z, expressed by f_4, f_8 and f_{12} functions, it was assumed that the lengths of $|z_1, z_2|$, $|z_3, z_4|$, $|z_5, z_6|$ were close to zero because the horizontal lengths of the element's trajectory should be located as close to the limits of the adjacent compartments. Therefore, the liquid transport on these lengths could be approximately considered as a pulsing movement, occurring on an infinitely short path, and therefore f_4, f_8, f_{12} functions can be expressed using the limit of a function:

$$\vartheta_j = \lim \frac{z}{\mathrm{f}(u'_z)} \tag{15}$$

These intervals were evaluated considering the most adverse case, the greatest vertical and horizontal flow lengths of the liquid element. Thus, it was stated that the values of r_p and r_k were located as close to the impeller's shaft and the vessel's wall, but far enough, so that neither the boundary layer nor the rotation of the shaft influenced the velocity of the liquid element. Similarly, the values of z_0 and z_7 of height were located as close to the vessel's bottom and to the liquid level, so that the boundary layer and the disturbances on a free liquid surface did not influence the element's velocity.

The duration of cycle of liquid transport was expressed as: $\sum_{j=1}^{m} \vartheta_j$, or in the dimensionless form, as:

$$\Theta = \left(\sum_{j=1}^{m} \vartheta_j \right) \cdot n \tag{16}$$

where m – superscript is the number of lengths (the intervals of integration), which were being traversed by the liquid element while transporting in the tank, wherein: $\{\vartheta_4, \vartheta_8, \vartheta_{12}\} \approx 0$. The results were summarised in Table 3. The energy consumption E during the cycle was also added there.

Table 3

The magnitudes relating to the cycle of liquid transport for the examined dual impeller sets

Lower impeller:	PTB-6			A-315			HE-3		
	$\sum_{j=1}^{m} \vartheta_j$	Θ	E	$\sum_{j=1}^{m} \vartheta_j$	Θ	E	$\sum_{j=1}^{m} \vartheta_j$	Θ	E
	s	–	J	s	–	J	s	–	J
$\Delta h = 2 \cdot d$	19.32	96.6	138.1	21.67	108.4	153.4	37.20	186.0	199.8

4. Conclusions and final remarks

If taking into account the mean liquid flow, the application of the disc turbine combined with the axial impeller yields the beneficial effect of mixing. However, it depends on the design of the lower impeller.

The liquid flow rate in the mixing vessel varies, depending on the relative location of the impellers. The change of the impeller spacing affects the change in the flow structure, which can take different transitional forms as well as thoroughly deformed shapes. In such cases, local reinforcing or suppressing of the liquid streams can occur. It can be seen by an increase or decrease of the K_{ccalk} number. There is the exchange flow rate, occurring on the limit of the respective, adjacent compartments. It was expressed as a function of the axial component of fluctuating velocity. The greatest intensity of the induced liquid flow and beneficial energy consumption can be found for the set of the lower PBT-6 turbine. This magnitude is only slightly lower for the set of A-315 impeller. The situation becomes reversed only at a very close position of the impellers.

Nomenclature

d – impeller diameter, m;
D – vessel diameter, m;
H – lower impeller's clearance in vessel, m;
Δh – impeller spacing, m;
K_C – circulation flow number in total liquid volume;
$K_{C\,calk}$ – corrected flow rate number;
n – rotation frequency of impellers, s^{-1};
Q_C – liquid flow rate general, m^3/s;
$Q_{C\,sum}$ – liquid flow rate in total volume of vessel, m^3/s;
$Q_{C\,calk}$ – liquid flow rate corrected, m^3/s;
Q_E – exchange flow rate of liquid in mixing vessel, general, m^3/s;
$Q_{E\,sum}$ – exchange flow rate of liquid in mixing vessel, total, m^3/s;
Q_r – circulation flow rate in radial direction, within circulation zone, m^3/s;
Q_z – circulation flow rate in axial direction, within circulation zone, m^3/s;
r – radius coordinate, m;
R – vessel diameter, m;
Re – Reynolds number for mixing, –;
R – variable and radial coordinate in vessel, m;
Δt – time residence of liquid in the measuring, s;
u'_{zg} – axial component of fluctuation velocity, at point on limiting line, z_{og}, m/s;
$\bar{u}$, $\bar{u}(t)$ – mean liquid velocity, m/s;
Z – variable and axial coordinate in vessel, m;
z – axial coordinate, m;
z_g – real height of points of limit between compartments, height of point of limit, m;
z_o – estimated height of limits between circulation zones, m;
z_{og} – real limit between compartments (circulation zones), m;
ϑ – transport time of liquid element through certain length, s;

Subscripts

i – general index of component, index of summation;
j – index of summation;
r – index of radial component;
z – index of axial component;

Superscripts

(+) – just drawdown;
(–) – refers to the gas-liquid system conditions;

References

[1] Alves S. S., Maia C. I., Vasconcelos J. M. T., *Experimental and modelling study of gas dispersion in a double turbine stirred tank*, Chemical Engineering Science, vol. 57, 2002, 487-496.

[2] Aubin J., Mavros P., Fletcher D. F., Xuereb C., Bertrand J., *Effect of axial agitator configuration (up-pumping, down-pumping, reverse rotation) on flow patterns generated in stirred vessels*, Transactions of the Institution of Chemical Engineers, vol. 79(A8), 2001, 845-856.

[3] Bader F. G., *Modelling mass transfer and agitator performance in multiturbine fermentors*, Biotechnology and Bioengineering, vol. 30(1), 1987, 37-51.

[4] *Chemineer Bulletin*, Nr 710, homepage: http://www.chemineer.com (date of access: 2008-02-10).

[5] Duda A., *Hydrodynamika mieszania cieczy w aparacie z dwoma mieszadłami*, Rozprawa doktorska, Politechnika Krakowska 2015.

[6] Elsner J. W., Drobniak S., *Metrologia turbulencji przepływów*. *Maszyny Przepływowe*, vol. 18, Wydawnictwo PAN, Wrocław-Warszawa-Kraków 1995.

[7] Fajner D., Magelli F., Pasquali G., *Modelling of non-standard mixers stirred with multiple impellers*, Chemical Engineering Communication, vol. 17, 1982, 285-295.

[8] Jahoda M., Machoň V., *Homogenization of liquids in tanks stirred by multiple impellers*, Chemical Engineering & Technology, vol. 17, 1994, 95-101.

[9] Jaworski Z., Nienow A. W., Koutsakos E., Dyster K. W., Bujalski W., *An LDA study of turbulent flow in a baffled vessel agitated by a pitched blade turbine*, Transactions of the Institution of Chemical Engineers, vol. 69, Part A, 1991, 313-320.

[10] Jaworski Z., Nienow A. W., Dyster K. W., *An LDA study of the turbulent flow field in a baffled vessel agitated by an axial, down-pumping hydrofoil impeller*, Canadian Journal of Chemical Engineering, vol. 74, 1996, 3-15.

[11] Johnson R. W., The *handbook of fluid dynamics*, CRC Press LLC, Boca-Raton, USA, 2000.

[12] *Lightnin Bulletin*, Nr E-120 09/01, homepage: http://www.lightninmixers.com (date of access: 2008-02-15).

[13] Manfredini R. Cavallera V., Marini L., Donati G., *Mixing and oxygen transfer in conventional stirred fermenters*, Biotechnology and Bioengineering, vol. 25(12), 1983, 3115-3131.

[14] MATLAB *Online Documentation*, homepage: http://www.mathworks.com/help/matlab (date of access: 2014-08-03).

[15] Saito F., Nienow A. W., Chatwin S., Moore J. T. J., *Power gas dispersion and homogenisation characteristics of Scaba SRGT and Rushton turbine impellers*, Chemical Engineering Japan, vol. 25(3), 1992, 281-287.

[16] Takenaka K., Takahashi K., Bujalski W., Nienow A. W., Paolini S., Paglianti A., Etchells A. W., *Mixing time for different diameters of impeller at a high solid concentration in an agitated vessel*, Journal of Chemical Engineering of Japan, vol. 38(5), 2005, 309-315.

[17] Vasconcelos J. M. T., Alves S. S., Barata J. M., *Mixing in gas-liquid contractors agitated by multiple turbines*, Chemical Engineering Science, vol. 50(14), 1995, 2343-2354.

[18] Vrábel P., van der Lans R. G. J. M., Luyben K. Ch. A. M., Boon L., Nienow A. W., *Mixing in large-scale vessels stirred with multiple radial or radial and axial up-pumping impellers: modelling and measurements*, Chemical Engineering Science, vol. 55, 2000, 5881-5896.

TECHNICAL TRANSACTIONS | CZASOPISMO TECHNICZNE
MECHANICS | MECHANIKA
2-M/2016

ZYGMUNT DZIECHCIOWSKI, ANDRZEJ CZERWIŃSKI*

NOISE ANALYSIS OF THE LONGITUDINAL PAPER CUTTING MACHINE IN THE CONTEXT OF DECLARATION OF COMPLIANCE OF THE MACHINERY

ANALIZA HAŁASU MASZYNY DO WZDŁUŻNEGO CIĘCIA PAPIERU W KONTEKŚCIE DEKLARACJI ZGODNOŚCI MASZYNOWEJ

Abstract

The paper summarises the noise measurements of a bobbin cutting machine, also referred to as a longitudinal paper cutter machine, taken as a part of the procedure involved in the declaration of compliance of the machinery. Noise measurements were taken with a view to improve the conditions in the work environment. Due to the machine operation, noise level conditions were determined by testing the impulse response inside the machine room. Calculations were carried out in an attempt to improve the working conditions for machine operators.

Keywords: noise analysis, declaration of compliance of machinery, acoustic adjustment

Streszczenie

W artykule przedstawiono wyniki pomiarów i analiz bobiniarki, tj. maszyny do wzdłużnego cięcia roli papieru. Pomiary te były częścią prac związanych ze spełnieniem przez badaną maszynę wymagań deklaracji zgodności maszynowej. W ramach pracy wykonano pomiary hałasu i analizy, których celem była poprawa warunków pracy na stanowisku pracy poddanym ocenie. W ramach pomiarów przeprowadzono tak ocenę warunków akustycznych wywołanych pracą maszyny jak i określono odpowiedź impulsową pomieszczenia, w którym maszyna się znajduje. Wykonano również obliczenia w aspekcie poprawy warunków pracy.

Słowa kluczowe: analiza hałasu, deklaracja zgodności maszynowej, adaptacja akustyczna

DOI:

* DSc. Eng. Zygmunt Dziechciowski, DSc. Eng. Andrzej Czerwiński, Institute of Machine Design, Faculty of Mechanical Engineering, Cracow University of Technology.

1. Introduction

In the context of EU regulations aimed to ensure work safety for machine operators, it is required that all machines designed, manufactured, launched and put to use should ensure the highest possible safety levels. Employers are obligated to ensure that machines are used for what they are intended, in accordance with the manufacturer's recommendations and that all further steps and measures are taken when necessary to improve safety features [1]. This approach is pursued in two basic groups of EU directives on work safety. The first group of documents are those having relevance to design, manufacturing, launching and use of machines and other products, issued to ensure the best safety levels possible. Among those documents, the Directive on Machinery is now of key importance [2]. The other group of EU directives are those specifying the minimum requirements that need to be satisfied when arranging the operators' work and the work environment, such as [3, 4, 5].

The respective requirements as to health and safety and work are applicable as long as the machine operated in the manner specified by the manufacturer still poses a real occupational hazard addressed by the relevant standard requirements, including those relating to noise and mechanical vibration control.

The group of machines covered by the Directive on Machinery [2] includes machines used in the paper industry and the printing industry, for example bobbin cutting machines, which produce high-level acoustic emission when in service. This is caused by the structural design of the machine and its interactions with additional equipment, which are necessary for the process.

As mentioned above, the technological process used in the paper industry and the printing industry makes that they are characterised by the production of high-level acoustic emission when in service. Because of this, they should often be subjected to acoustical adaptation. This adaptation should be preceded by computer simulations. The articles [6] [7, 8, 9] concern the issues of improving the acoustical conditions in the workplace inside of a printing house. In these articles are described, inter alia, the identification process of noise sources, the measurement methodology of acoustic properties of a room (production hall), as well as the results of digital simulation for the selected configuration of acoustic protections.

The purpose of the present study was to determine the potentials of noise reduction in areas in the vicinity of paper cutting machines such that the requirements set forth in the Directive on Machinery should be complied with. Digital simulation procedures were performed to assess the potential benefits of applying a variety of noise reduction strategies (reducing the level of noise produced by machine components, improving the noise absorption capacity of the machine room). The parameters of the calculation model were determined based on sound level measurement data.

2. Test object

The test object was a bobbin cutting machine, i.e. a machine for longitudinal paper cutting. During the cutting process, the roll of paper is spread on the rewinding cylinders, rewound on the roller set and cut longitudinally with circular cutters, followed by winding

of the paper sheet. The machine is located in a room of 12 m in length, 5.7 in width and 3.27/2.88 in height, the ceiling in the room is sloping. The walls and the ceiling are plastered. Up to about 2 m in height, the walls are coated with enamel, and above that- painted with an emulsion paint. The ceiling is painted with an emulsion paint, too. The floor is made of ground concrete. There are two windows in the room (approximately 1 m × 2 m in size) and two gates 2.75 m × 2.75 m. The gates are locked by a sliding door. The layout of the room is shown in Fig 1.

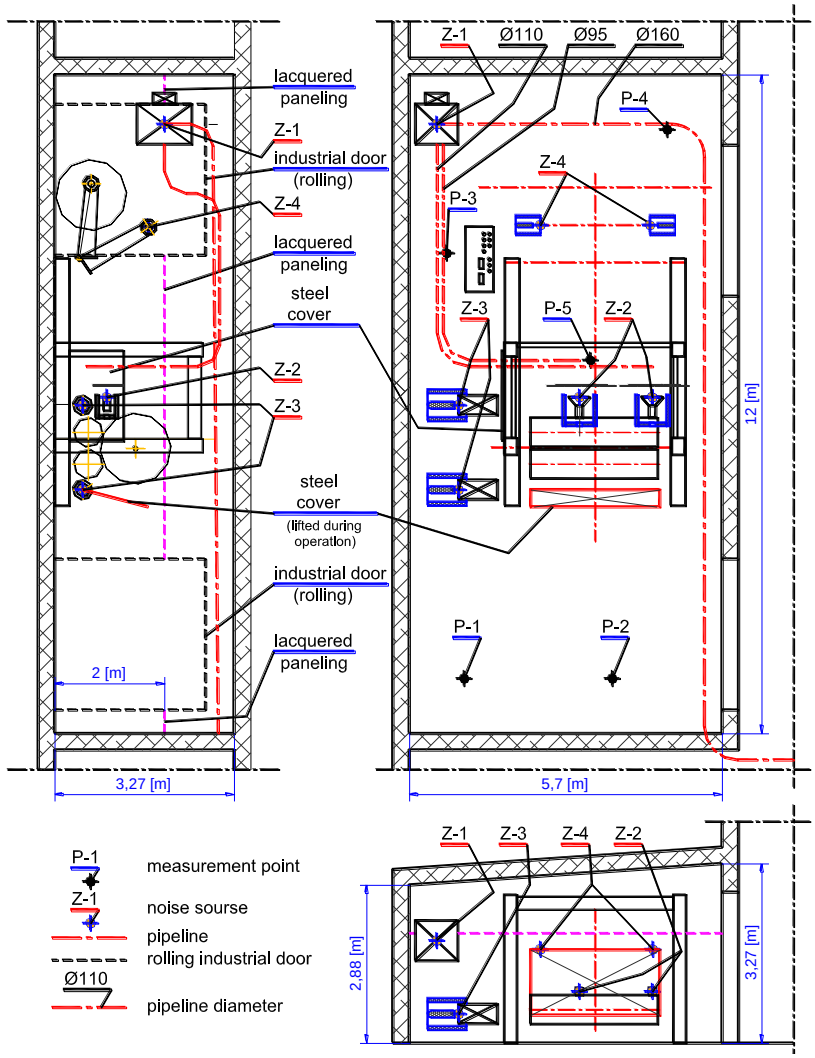

Fig. 1. Test object- position of the bobbin cutting machine inside the room

The bobbin cutting machine has two integral components: the machine for cutting paper sheets on the winding and rewinding end plus the cutting tools and the exhaust system (an exhaust fan with the pipeline, suction nozzles). Key machine components are shown in Fig 1.

Major sources of noise in the investigated area include:

- an exhaust fan (designated as Z-1 in Fig. 1),
- suction nozzles (designated as Z-2 in Fig. 1),
- unwinding cylinder drives (designated as Z-3 in Fig. 1),
- an unwinding roll drive (designated as Z-4 in Fig. 1).

3. The maintenance zone of the operator

When the bobbin cutting machine is in operation, machine operators spend most of their time in zones shown in Fig. 2 and listed in Table 1. During the analyses, attention should mainly be paid to these zones.

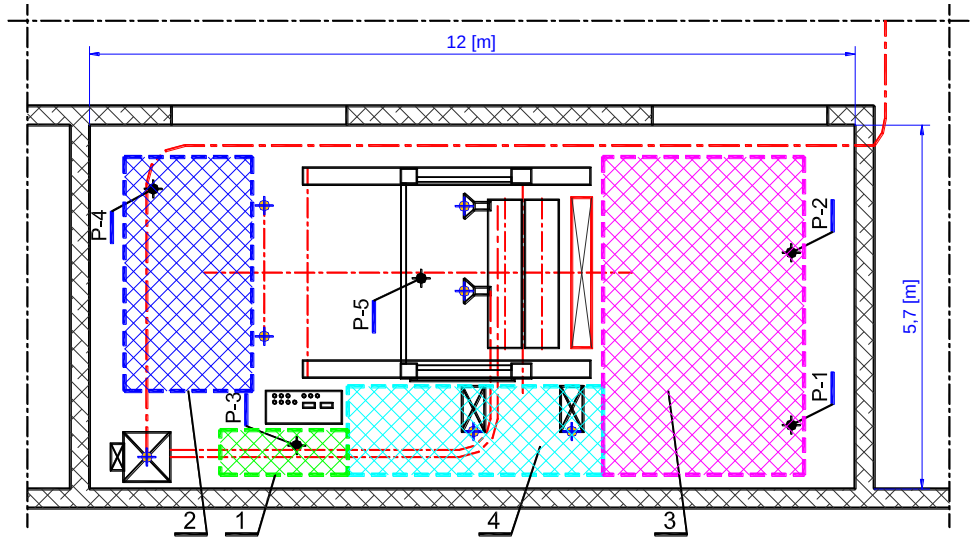

Fig. 2. Investigated area- the workplace operation zones

Table 1

Designation of workplace operation zones (see Fig. 1)

Name of zone	Number of area according to Fig. 2
The operating desktop zone	1
Loading the paper roll zone	2
Receiving the paper roll zone	3
The maintenance zone along the machine	4

4. Results of sound level measurements in workplace operation zones

Sound level measurements were taken to determine the noise levels in particular workplace operation zones (as shown in Fig. 2).

Results of measurements taken in the existing conditions are summarised in Table 2, revealing the exceeded values of equivalent noise levels in relation to the admissible levels during the 8 hours' noise exposure for humans ($L_{EX\ 8h\ perm}$ = 85 dB [10]). Measurements were taken in accordance with the procedure specified in [11, 12].

Table 2

Variability range of the equivalent noise levels in investigated zones- present conditions

Measurement area in accord. with Fig. 2 and Table 2	Mean value for the area $L_{Aeq\ meas\ av}$ [dB]	Exceeding the permissible noise level value for 8 hours' exposure ($L_{EX\ 8h\ perm}$ = 85 dB) $L_{Aeq\ meas\ av}$ - $L_{EX\ 8h\ perm}$ [dB]
[1]	[2]	[3]
1	85.3	0.3
2	87.0	2.0
3	87.1	2.1
4	87.0	2.0

5. Identification of noise sources

To identify the major noise sources inside the machine, sound analyses were performed for various modes of machine operation. Measurements were taken at five points, indicated in Fig 1 and in the vicinity of the selected sources. Specificity of machine operations and processes involved precluded separate measurements of each individual source. Therefore, measurements were repeated for as large as possible number of configurations of operating noise sources.

Table 3

Operating configurations- designations and description

Configuration number	Designation area in accord. with Fig. 3	Description of configuration area in accord. with Fig. 2
Config. No. 1	K-1	Machine stopped; working only source Z-4
Config. No. 2	K-2	Machine stopped; work only noise sources Z-1, Z-2, Z-4
Config. No. 3	K-3	Machine is running; work of sources Z-3, Z-4; without of noise source Z-1, Z-2
Config. No. 4	K-4	Machine is running; work of sources Z-1, Z-3, Z-4; without of noise source Z-2
Config. No. 5	K-5	Machine is running (full operating); work of sources Z-1, Z-2, Z-3, Z-4
Config. No. 6	K-6	Machine stopped; the background noise

Results of 1/3 octave band analysis of the noise levels as given in Fig. 3 as averaged values from 5 measurement points. Plots represent particular configurations of contributing noise sources (summarised in Table 3). Fig. 3 also plots the background noise curve (K-6 curve) and the K-5 curve obtained for all noise sources working, including the cutting process). In Fig. 3 are placed also the summated values of noise level A for the entire frequency band. These values are given in frames where the frame colour and edge pattern correspond to relevant plots.

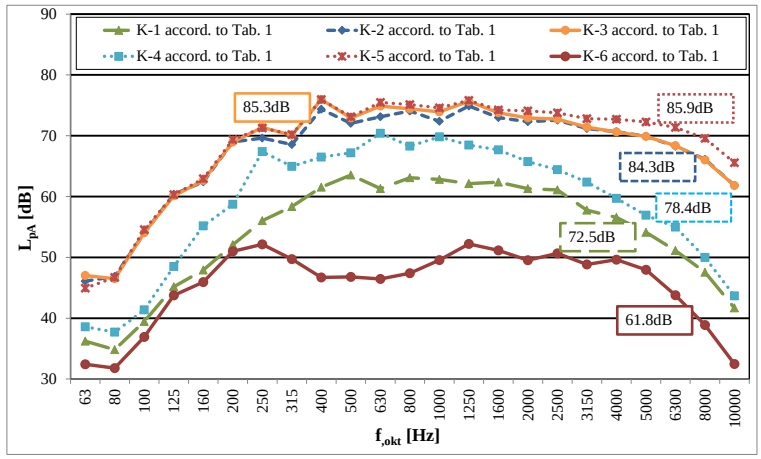

Fig. 3. 1/3 octave band analysis of sound level for the given configuration of operating noise sources – averaged values from 3 measurement points

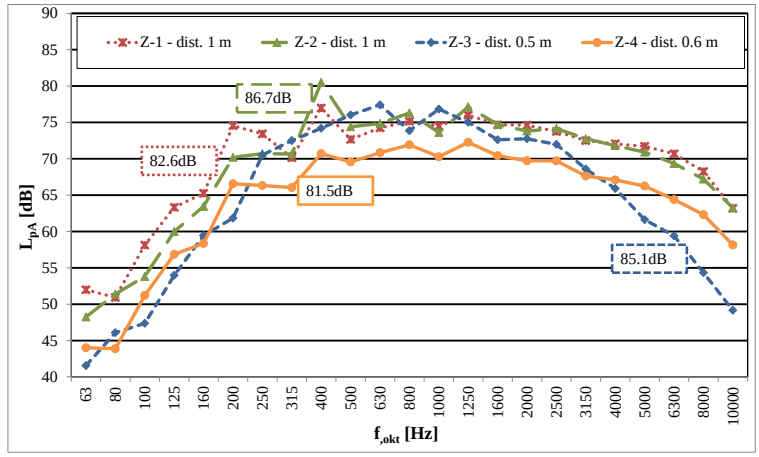

Fig.4. 1/3 octave band analysis of sounds from individual noise sources (Z-1, Z-2, Z-3, Z-4) – near-field measurements

For selected sources, measurements of sound levels were also taken in their close vicinity. Measurement data are summarised in Fig. 4, listing the source number and the distance at which the measurement was taken.

Basing on noise level measurements at selected points near the machine and for various configurations of noise sources, the numerical simulation procedure was applied to identify the sources and establish their sound power levels. To account for sounds reflected in the room, the reverberation time was measured, in accordance with the procedure set forth in [13].

The reverberation time measurement process was also described in [9]. In the room in question, the reverberation time was determined on the basis of the measurement of impulse responses in several points located at a height of 1.2 m above the floor on its overall area. To perform the measurements, measuring equipment shown in Fig. 5 was employed.

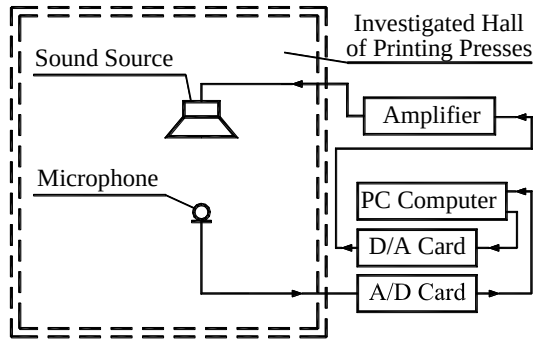

Fig. 5. Measuring equipment

Measured reverberation times are summarised in Fig. 6.

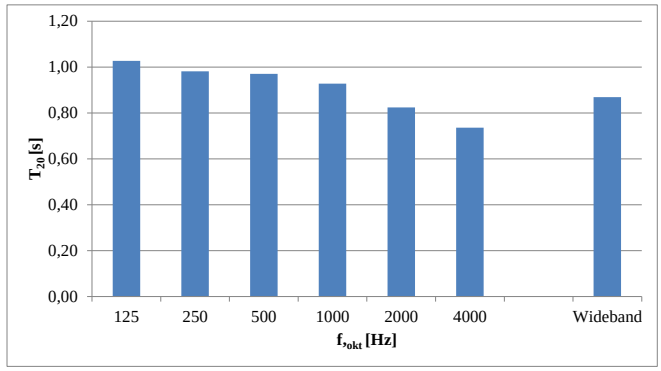

Fig. 6. Values of reverberation time inside the room

Finally, estimated values of sound power level L_{WA} of particular noise sources are summarised in Table 4. The sound power level L_{WA} values were estimated in accordance with the procedure given in [14].

Table 4

Estimated values of sound level L_{WA} from the noise sources

The noise source	Designation in Fig. 1	The number of noise sources	Sound power level L_{WA} [dB]
Exhaust fan	Z-1	1	90
Suction nozzles of paper scrap	Z-2	2	89
Drive of a unwinding cylinders	Z-3	2	86
Drive of a roll unwinding	Z-4	2	79
Pipeline (as a total one)	–	–	71

6. The effects of acoustic adjustments and control on noise distribution in the workplace operation zone

The analysis was conducted to determine the effects of specific sound control and adjustment solutions on the noise levels in the workplace operation zones.

The calculation procedure was applied addressing three aspects: first - adjustments of noise sources, designated with "I", second – acoustic design and adaptation of the room's interior, designated with "II" and third – improvement of working conditions at the control desk, designated with "III". As regards the adjustments of noise sources, several solutions were considered that were aimed at reducing noise emissions to acceptable levels (four options were considered, indicated by numbers 1÷4). In the calculation procedure associated with potential modifications of the machine room, two solutions were considered (II.1, II.2). Further combinations of measures taken to reduce the sound levels were considered too (enhancing the sound absorption capacity of the room and providing a screen near the control desk- designated as "I.4+II.2"), thus yielding 8 options to be handled in calculations.

These options are summarised in Table 5.

Options (I) (designated with "I" in the calculation procedure) involve the modification or adjustments of noise sources, such as fans or driving systems. Four combinations of noise sources were considered (I.1 to I.4), listed in Table 6.

Further calculations were performed to find out how the improvement of sound absorption capacity of the machine room should affect the noise levels. It is suggested that sound absorption capacity of one wall (the wall near the exhaust fan) and of the ceiling should be improved. Average values of the sound absorption coefficients for the walls and the ceiling in the room in the present conditions are taken to be $\alpha = 0.13$ (walls) and $\alpha = 0.11$ (ceiling). The sound absorption coefficient of the used sound absorbent material is $\alpha = 0.5$ [15].

Table 5

Configurations of noise control measures in the considered variants

		Noise control measures						
		Acoustic adjustments of the noise sources in the machine				Acoustic design and adaptation of the machine room		Modification of the control desk
		Exhaust fan Z-1	Suction nozzles of paper scrap Z-2	Drive of a unwinding cylinders Z-3	Drive of a roll unwinding Z-4	Ceiling	Back wall	Screen of a desktop
	Designation	[1]	[2]	[3]	[4]	[5]	[6]	[7]
Variant of calculations	I.1	**x**	**x**					
	I.2	**x**	**x**		**x**			
	I.3	**x**	**x**	**x**				
	I.4	**x**	**x**	**x**	**x**			
	II.1					**x**		
	II.2					**x**	**x**	
	I.4+II.2	**x**	**x**	**x**	**x**	**x**	**x**	
	I.4+III	**x**	**x**	**x**	**x**			**x**

Table 6

Solution options involving adjustment/ no adjustment of selected noise sources

		Characteristics of the calculation variants			
Noise sources	Designation in Fig. 1	I.1	I.2	I.3	I.4
Exhaust fan	Z-1	acoustical adaptation (9 dB) L_{WA} = 81 dB	acoustical adaptation (9 dB) L_{WA} = 81 dB	acoustical adaptation (9 dB) L_{WA} = 81 dB	acoustical adaptation (9 dB) L_{WA} = 81 dB
Suction nozzles of paper scrap	Z-2	a partial acoustic enclosure – absorber R = 15 dB	a partial acoustic enclosure – absorber R = 15 dB	a partial acoustic enclosure – absorber R = 15 dB	a partial acoustic enclosure – absorber R = 15 dB
Drive of a unwinding cylinders	Z-3	Without adaptation L_{WA} = 86 dB	Without adaptation L_{WA} = 86 dB	acoustical adaptation (5 dB) L_{WA} = 81 dB	acoustical adaptation (5 dB) L_{WA} = 81 dB
Drive of a roll unwinding	Z-4	Without adaptation L_{WA} = 79 dB	acoustical adaptation (5 dB) L_{WA} = 74 dB	Without adaptation L_{WA} = 79 dB	acoustical adaptation (5 dB) L_{WA} = 74 dB

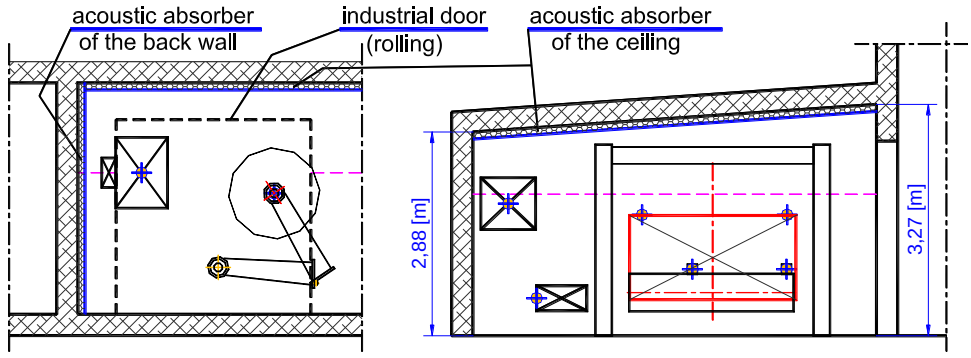

Fig. 7. Positions of acoustical absorbers on the back wall and on the ceiling

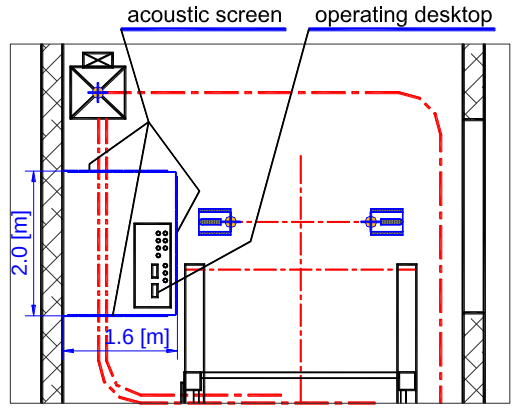

Fig. 8. Position of an acoustic screen protecting the control desk

Surfaces subjected to acoustical adaptation are shown in Fig. 7.

Calculations were also performed to account for the case when a screen was provided to protect the operator from acoustic wave emissions when monitoring the machine. The acoustic screen shall be made of PVC baffles, its position with respect to the control desk is shown in Fig. 8.

Other solutions considered in the procedure were combinations of several sound control measures. Calculations were performed to determine the effectiveness of these sound control measures in relation to particular noise sources (i.e. variant I.4 in Table 3) and to establish the effectiveness of the two sound absorbers (variant II.2 in Table 3). This variant is designated as “I.4+II.2” in Table 3. The effects of acoustic adjustment of all sources and providing the protective screen near the control desk are estimated in the solution variant labelled as “I.4+III”.

7. Calculation results

Measurement data were utilised in computer simulations to investigate both the existing conditions and the 8 variants listed in section 6. Calculation data are presented in the form of sound level distribution maps.

Fig. 9 plots the results obtained in the present conditions. Figs. 10 and 11 show the sound pressure distribution maps for selected variants of room adaptations, illustrating the effectiveness of noise control measures involved in particular solutions.

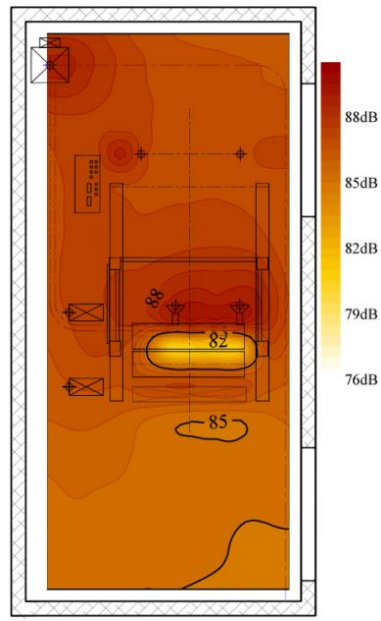

Fig. 9. Sound pressure level distribution inside the room- present state

Analysis of a map in Fig. 9 reveals that among the workplace operation areas, the highest noise levels are registered in the vicinity of sources Z-1 and Z-2, and near the control desk. The sound level registered in these zone approaches 87÷86 dB. Near the point where the paper roll is set, the sound level is as high as 85 dB.

Fig. 10 plots the results obtained when the acoustic adjustments and modifications are made to control the noise level near the major sources (variant I.4). Fig. 10a shows a map of noise distribution around the bobbin cutting machine and the effects of using the noise control measures listed in Fig. 6 are illustrated in Fig. 10b. It is readily apparent that adjustment measures provided in variant I.4 lead to a reduction of sound pressure by 4 or 5 dB.

Noise reduction is more significant when sound absorbers are placed on the wall (variant II.2), which is shown in the map in Fig. 10c. The map plotting the sound pressure reduction levels (Fig. 10d) reveals that in the workplace operation zone, the noise reduction effect is less significant than in the variant I.4 (by 1 or 2 dB).

The effects of simultaneous adjustments and modifications near the major noise sources (I.4) and adaptation and acoustic re-design of selected walls (II.2) are illustrated in Fig. 10a and 10b. In the operation zones the noise level may be reduced by 8÷9 dB.

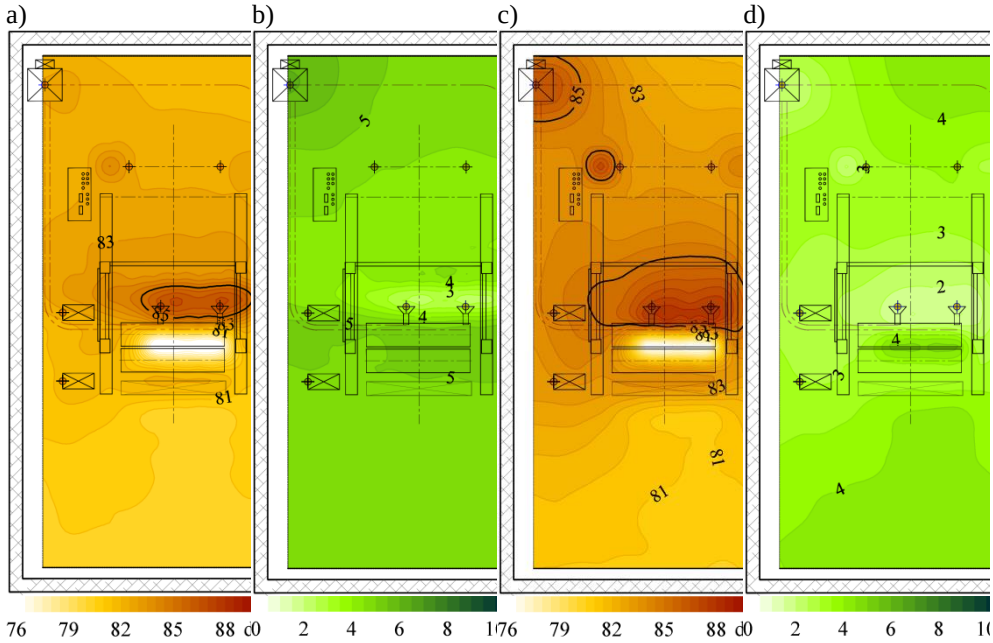

Fig. 10. Calculation results: a) sound pressure level for variant I.4; b) noise reduction for variant I.4; c) sound pressure level for variant II.2; d) noise reduction in variant II.2

Figs. 11a and 11c plot the calculation data obtained for the specific case when the major noise sources were controlled (I.4) and, at the same time, a screen was provided to isolate the control desk zone (III). Noise reduction by 5÷7 dB is sufficient to ensure that the noise levels experienced by the machine operator should be reduced to acceptable levels in the work environment. Distribution of noise reduction values inside the room is presented in Figs. 11c and 11d.

The analysis of results allows for evaluating the potential noise reduction strategies to be implemented in the operation zones (Fig. 2), enabling a preliminary cost analysis of such solutions.

Application of the protective measures listed in variants I.4 (see Table 6), involving the adaptation of the major noise sources and the fan. Providing a transparent screen made of PVC (variant "I.4+III") leads to further noise reduction in the zone I (see Fig. 2).

In order that the noise levels in the workshop operation zones should fall within the admissible limits, it is required that additional flat sound absorbers should be installed on selected walls and on the ceiling (variant "I.4+II.2"). One has to bear in mind, however, that the costs of additional absorbers will be rather high.

Table 7 summarises the estimated noise reduction levels in the zones 1, 2, 3, 4 (see Fig. 2), for the specific solution variants.

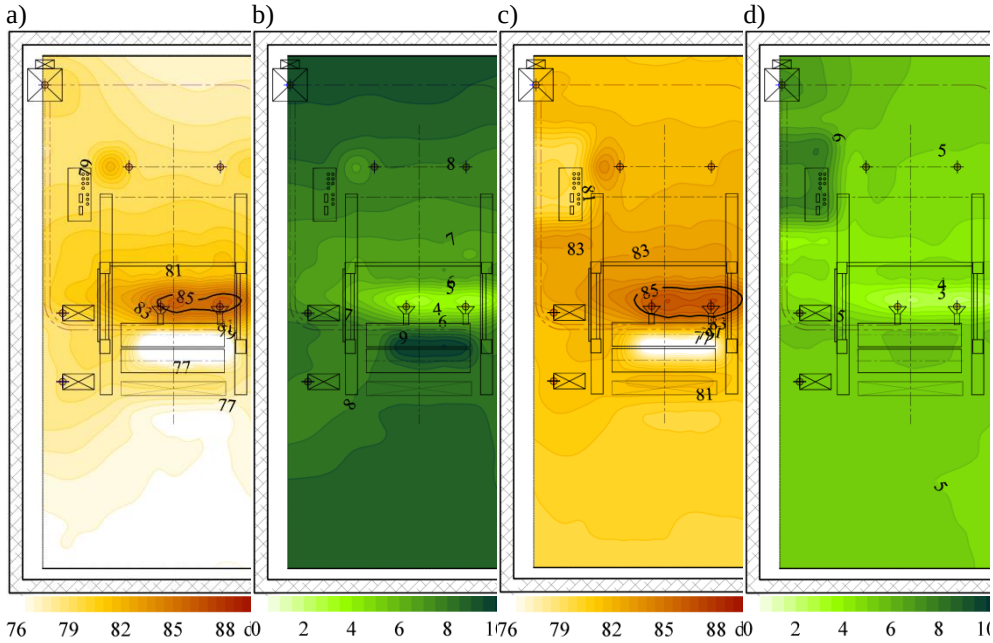

Fig. 11. Calculation results: a) sound pressure level for variant "I.4+II.2"; b) noise reduction for variant "I.4+II.2"; c) sound pressure level for variant "I.4+III"; d) noise reduction in variant "I.4+III"

Table 7

Predicted noise reduction in the workshop operation zone for analysed solutions in relation to the average measured sound level $L_{Aeq\ meas\ av}$ in the area

		Predicted noise reduction in the workshop operation zone for analysed solutions in relation to the average measured sound level $L_{Aeq\ meas\ av}$ in the area $\Delta L_{red\ av}$ [dB] = $L_{Aeq\ meas\ av}$ - $L_{Aeq\ zone\ av}$							
Zone number area in accord. with Fig. 2	Current state Average measured sound level $L_{Aeq\ meas\ av}$ [dB]	I.1	I.2	I.3	I.4	II.1	II.2	I.4+II.2	I.4+III
[1]	[2]	[3]	[4]	[5]	[6]	[7]	[8]	[9]	[10]
1	85.3	2.6	2.8	4.4	4.7	3.3	3.9	8.5	5.1
2	87.0	2.4	2.6	4.2	4.5	2.3	2.9	7.2	4.8
3	87.1	3.1	3.4	4.4	4.8	2.4	3.2	8.2	7.4
4	87.0	3.2	3.7	4.2	4.8	2.6	3.5	8.5	5.4

8. Conclusions

The purpose of the present study was to estimate the effectiveness of the proposed modifications and acoustic adjustments aimed to reduce the noise level in the bobbin machine operation zone. The investigations were undertaken as part of the project aimed to ensure that all relevant requirements set forth in the Directive on Machinery should be complied with [2]. The study considers all potential noise control measures: modification and acoustic adjustment of machine components, re-design and adaptation of the acoustic features of the machine room and providing a transparent screen, made of PVC, around the control desk. Various configurations of sound control measures were duly evaluated. The list of applied noise control measures is given in section 6 and specific options (8) are summarised in Table 5.

The analysis identified the solutions that proved most effective.

The most effective noise reduction in operation zones was registered for the variants "I.4+II.2" and "I.4+III", which involve full adjustment of the noise sources and adaptation (increase the sound absorption coefficient) of the walls and ceiling in the machine room, as well as full acoustic adjustment of major sources of noise plus the screen provided around the control desk. Acoustical adaptation (increase the sound absorption coefficient) of walls and ceiling in the machine rooms with the use of sound absorbers is an expensive solution and found not to be cost-effective despite its excellent performance.

The effectiveness of variant I.4 in noise control is high, too. Even though not in all workshop operation zones could the noise levels be reduced to the admissible levels specified in normative references (below 85 dB), the effectiveness of noise control was found to be satisfactory. This view is fully justified since the normative value involves not only the actual noise level in the zone, but to exposure time as well.

Investigations show that in certain cases the requirements set forth in the Directive on Machinery [2] cannot be fully met through acoustic adjustments of the machine itself (or its components). In many cases, the machine and the machine room have to be treated as one system. Acoustic adjustments of machine components alongside the improvement of acoustic parameters of the machine room will lead to required results. One has to bear in mind the cost-effectiveness of the proposed solutions, which in many cases becomes the major criterion in decision-making.

References

[1] *Ensuring compliance of machinery with the essential requirements in the field of health and safety. Guidelines for producers, suppliers and users of machinery* (in Polish), Centralny Instytut Ochrony Pracy – Państwowy Instytut Badawczy, www.ciop.pl, Warszawa 2010.

[2] Directive 2006/42/EC of the European Parliament and of the Council of 17 May 2006 on machinery.

[3] Directive 89/391/EEC – COUNCIL DIRECTIVE of 12 June 1989 on the *introduction of measures to encourage improvements in the safety and health of workers at work.*

[4] Directive 2009/104/EC – use of work equipment of 16 September 2009 concerning *the minimum safety and health requirements for the use of work equipment by workers at work* (second individual Directive within the meaning of Article 16(1) of Directive 89/391/EEC).
[5] Directive 89/655/EEC - COUNCIL DIRECTIVE of 30 November 1989 concerning the minimum safety and health requirements for the use of work equipment by workers at work (second individual Directive within the meaning of Article 16 (1) of Directive 89/391/EEC).
[6] Czerwiński A., Dziechciowski Z., Krawczyk J., *The concept of reduction of the sound level at workplaces in the printing industry* (in Polish), in: *Teoreticieskie osnowy eniergoriesursosbieriegajuścich priocesow, oborudowania i ekołogicieski biezopasnych proizbodctw*, ISBN 978-5-9616-0377-4, Goubno ИГХТУ (IGChTU), Iwanowo – Rosja, 2010.
[7] Borkowska-Czarnecka K., Czerwiński A., Dziechciowski Z., *Analysis of influence of new printing press installation on a acoustic climate in a press room of a printing house* (in Polish), Czasopismo Techniczne „Mechanika", vol. 2-M, 2012, 55-62.
[8] Czerwiński A., Dziechciowski Z., *Acoustic parameters verification of enclosures of high-performance printing presses* (in Polish), Czasopismo Techniczne „Mechanika", vol. 2-M, 2012, 63-72.
[9] Dziechciowski Z.; Czerwiński A., *Concepts of noise reduction in workplace areas of roll unwinding operators of printing offset press*, Meždunarodnaâ Naučno-Tehničeskaâ Konferenciâ *Problemy resurso- i energosberegaûŝih tehnologij v promyšlennosti i APK* (PRET-2014), monografiâ, Ivanovskij Gosudarstvennyj Himiko-Tehnologičeskij Universitet, tom 2, 2014, 100-113.
[10] Regulation of the Minister of Labour and Social Policy of 6 June 2014 on Maximum Permissible Concentration and Intensity of Agents Harmful to Health in the Working Environment, Journal of Laws of 2014, item 817.
[11] PN-94/N-01307, *Noise – Permissible values of noise in the workplace – Requirements relating to measurements*.
[12] PN EN ISO 9612:2009, *Acoustics – Determination of Occupational Noise Exposure – Engineering Method*.
[13] PN EN ISO 3382-2:2010, *Acoustics – Measurement of Room Acoustic Parameters*, Part 2: *Reverberation Time In Ordinary Rooms*.
[14] PN-EN ISO 3746:2011, *Acoustics – Determination of sound power levels of noise sources using sound pressure – Survey method using an enveloping measurement surface over a reflecting plane*.
[15] Engel Z., *Environmental Noise and Vibration Protection* (in Polish), PWN, Warszawa 1993.

TECHNICAL TRANSACTIONS | CZASOPISMO TECHNICZNE
MECHANICS | MECHANIKA
2-M/2016

TOMÁŠ JIROUT, FRANTIŠEK RIEGER*

MIXING WASTE GYPSUM SUSPENSIONS

MIESZANIE ODPADOWYCH ZAWIESIN GIPSOWYCH

A b s t r a c t

The paper deals with experimental research of the waste suspensions mixing from the energy industry. Mixing experiments were carried out in a transparent baffled vessel with a diameter of 290 mm. Standard pitched six-blade turbine and folded four-blade turbine with diameters of 100 mm in two relative distances from bottom H_2/d = 1 and 0.5 were used in experiments. Measurements were carried out with three volumetric concentrations of suspensions: 16, 31.5 and 47%.

Keywords: m*ixing, suspension, gypsum*

S t r e s z c z e n i e

W pracy przedstawiono badania eksperymentalne mieszania odpadowych zawiesin gipsowych powstających w energetyce. Badania prowadzono w przezroczystym zbiorniku o średnicy 290 mm, z przegrodami. W badaniach stosowano mieszadła osiowe o średnicy 100 mm: standardowe mieszadło sześciołopatkowe oraz mieszadło czterołopatkowe, zakrzywione dla dwóch odległości od dna zbiornika H_2/d = 1 i 0.5. Badania przeprowadzono dla trzech stężeń objętościowych zawiesiny 16, 31.5 i 47%.

Słowa kluczowe: mieszanie, zawiesina, gips

DOI:

* Prof. DSc. Eng. Tomáš Jirout, Prof. PhD. Eng. František Rieger, Department of Process Engineering, Faculty of Mechanical Engineering, Czech Technical University in Prague.

1. Introduction

This paper reports on an experimental study of the waste suspensions mixing from the energy industry. The sedimentation and the rheological behaviour of these suspensions were described in our recent paper [1]. Figs. 1 and 2, reproduced from that paper, show that the settling velocity decreases and the viscosity of these suspensions increases rapidly with increasing particle concentration.

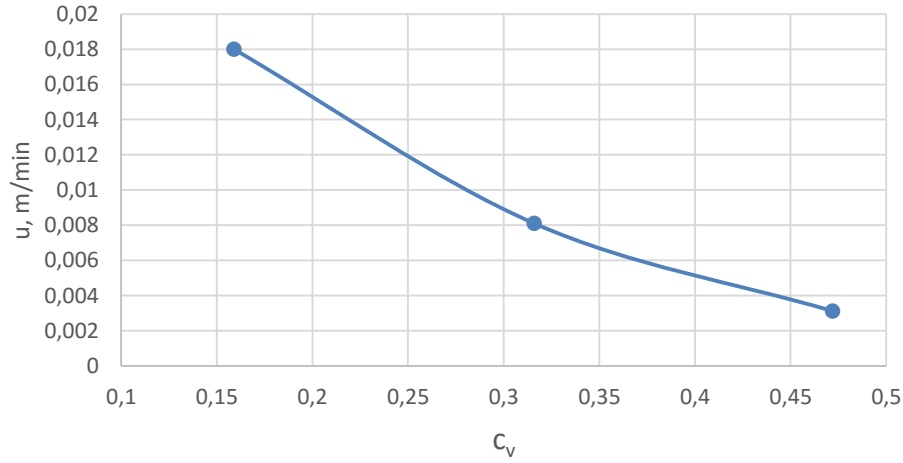

Fig. 1. Dependence of sedimentation velocity on concentration

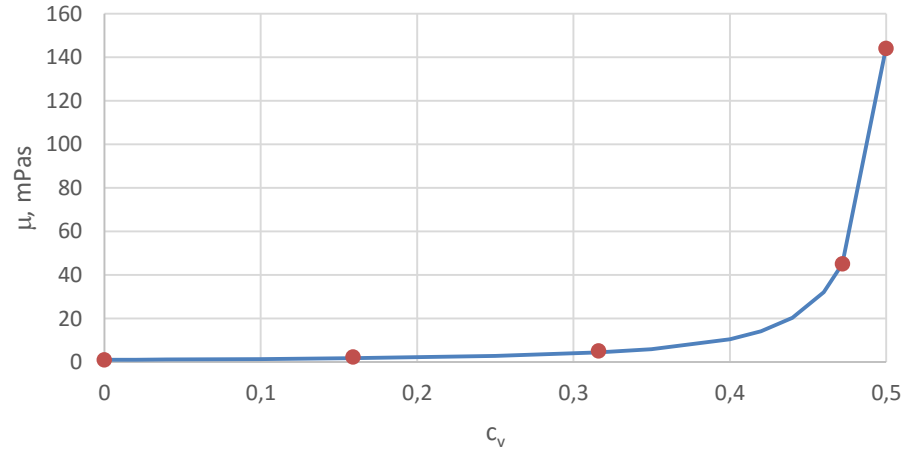

Fig. 2. Dependence of viscosity on volumetric concentration

2. Experimental

Mixing experiments were carried out in a transparent baffled vessel (see Fig. 3) 290 mm in diameter.

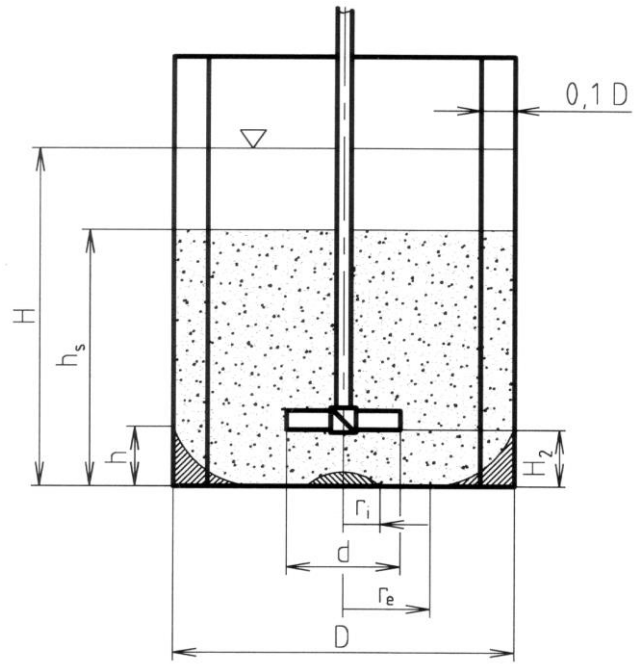

Fig. 3. Experimental vessel, H/D = 1

A standard pitched six-blade turbine (6SL45) and a diagonally folded four-blade turbine (4RLL) 100 mm in diameter, as shown in Fig. 4, at two relative distances from the bottom, H_2/d = 1, 0.75, and 0.5, were used in the experiments. Measurements were carried out with three volumetric concentrations of the suspensions: 16%, 31.5% and 47%.

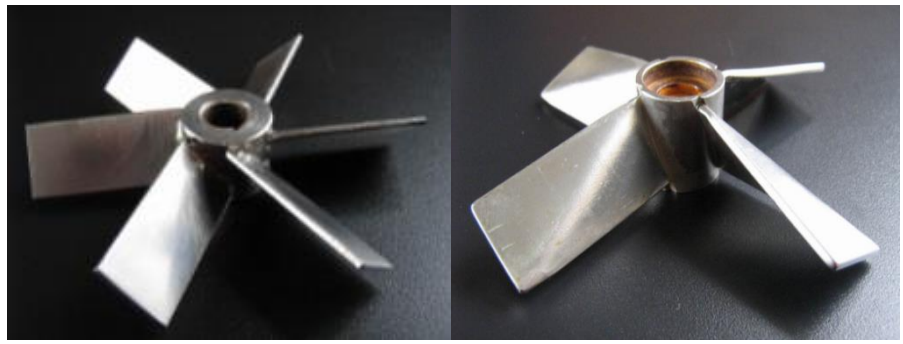

Fig. 4. Agitators used in the experiments

The just suspension speed of the agitator was stated as the speed at which the height of the particle layer h in the bottom corner was zero. The height of the suspension layer h_s and the concentration distribution at the suspension speed were also measured. The concentration distribution was stated on the basis of an analysis of samples taken from the wall of the vessel at various distances from the bottom of the vessel, see Fig. 5. Samples were taken at just-suspension speed and at the speed at which the height of the interface between the suspension and clear water $h_s = H$. An analysette A22 laser analyser was used for sample analysis. The distances z of the places at which samples were taken are specified in Table 1.

Fig. 5. Experimental vessel

Table 1

Sampling point	**1**	**2**	**3**	**4**	**5**	**6**
z [mm]	48	73	97	145	193	242
z/H	0.17	0.25	0.33	0.50	0.67	0.83

3. Experimental results

Analyses of the samples were carried out for a standard pitched six-bade turbine at the lowest concentration of 16%, at which the settling velocity is highest (see Fig. 1). The results for the agitator speed at which $h_s = H$ (see Fig. 5, second photo) are shown in Fig. 6. The results for just-suspension speed (see Fig. 5, third photo) are shown in Figs. 7 and 8. It follows from the results shown in Fig. 6 that at $h_s = H$ there is homogeneity and the particle

size distribution is uniform. From Figs. 7 and 8, when $h_s < H$ at z = 48 mm the concentration is higher, and near the interface at z = 242 mm the concentration is smaller and the particle size distribution is not uniform (the suspension contains only the smallest particles). At the other sampling points (2-5), the suspension is uniform.

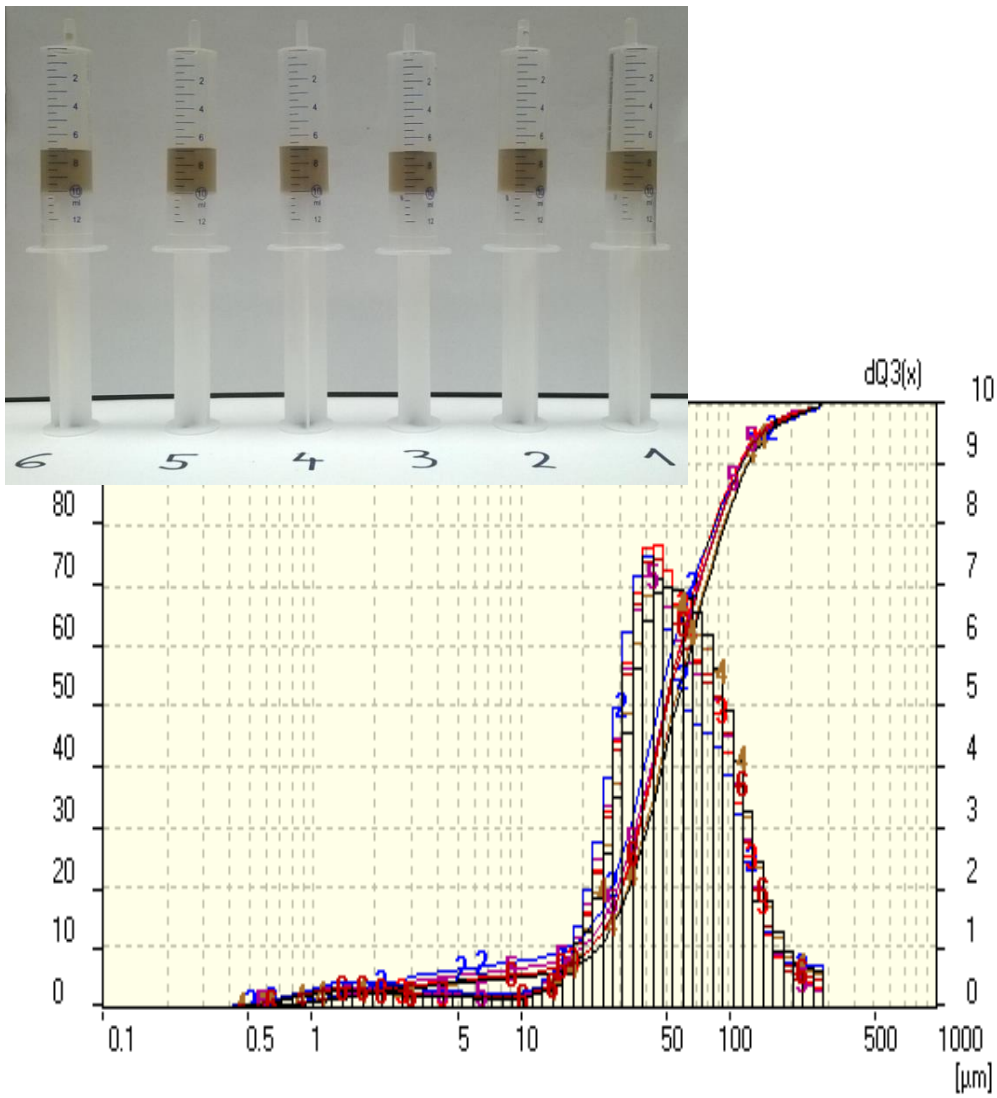

Fig. 6. Analysis of the concentration profile and the particle size distribution at $h_s = H$ (c_v = 16%, pitched blade turbine: H_2/d = 1, n_h = 502 min^{-1})

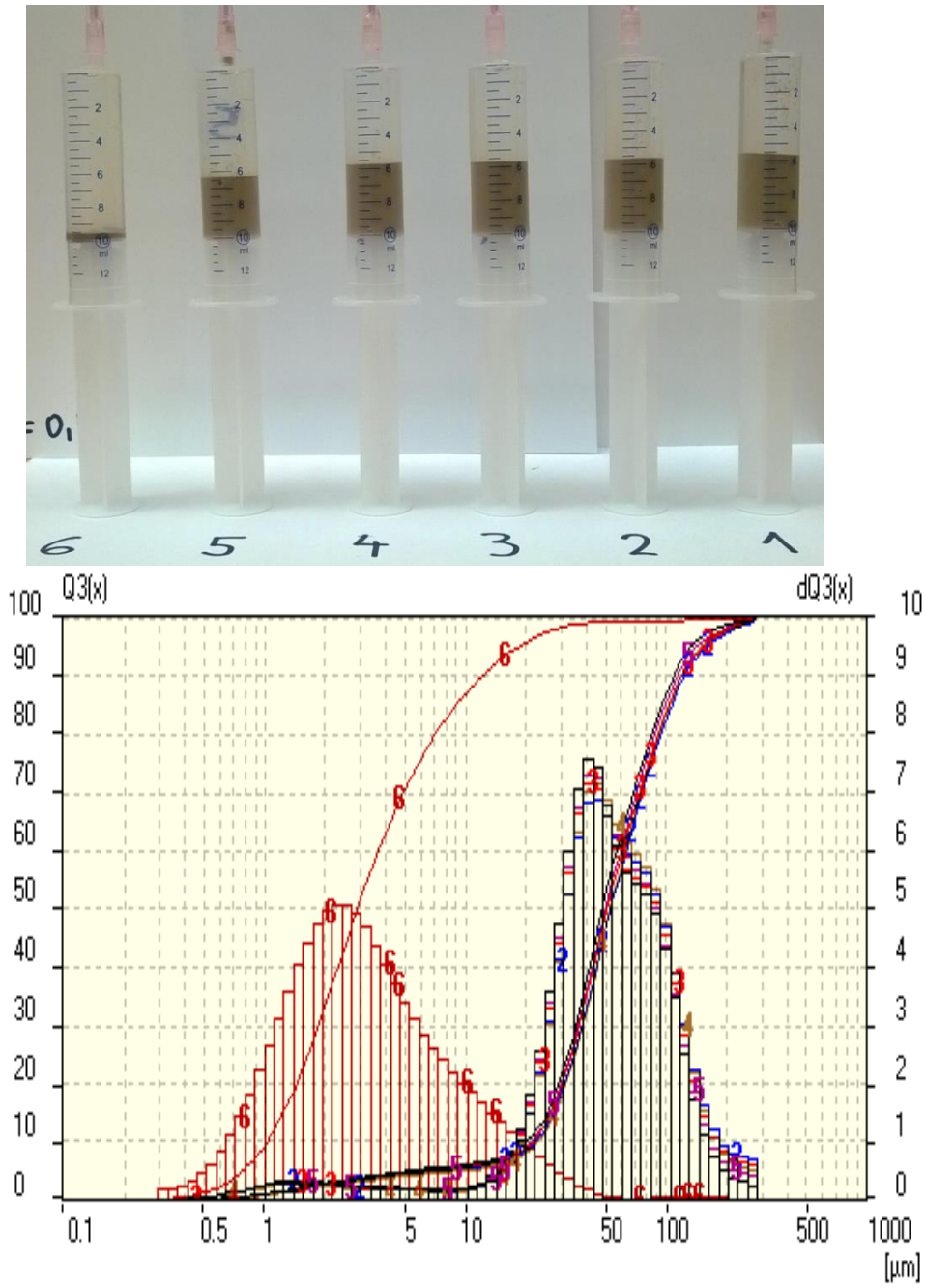

Fig. 7. Analysis of the concentration profile and the particle size distribution at just-suspension speed (c_v = 16%, pitched blade turbine: H_2/d = 0.5, n_{cr} = 226 min^{-1}, h_s/H = 0.724)

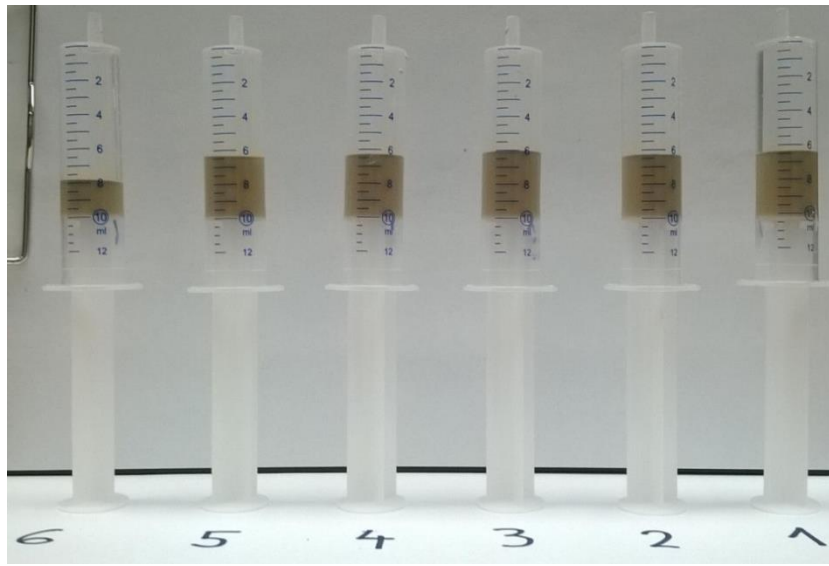

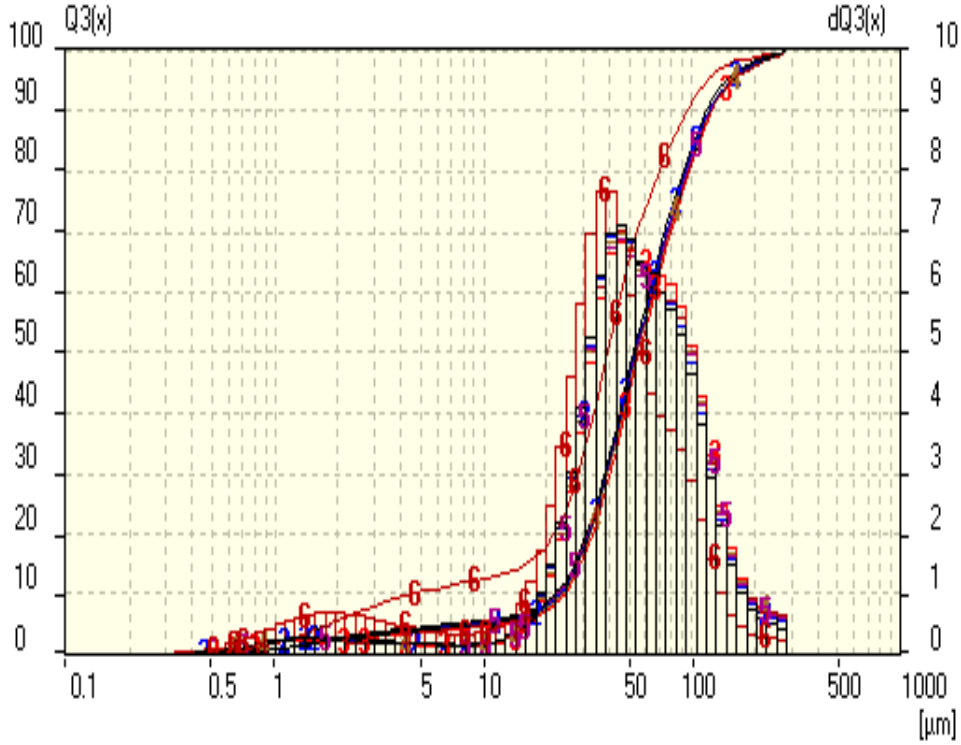

Fig. 8. Analysis of the concentration profile and the particle size distribution at just-suspension speed (c_v =16%, pitched blade turbine: H_2/d = 1, n_{cr} = 330 min^{-1}, h_s/H = 0.879)

The experimental values of just-suspension speed and agitator speed at $h_s = H$ are presented in tables 2 and 3. These tables also contain values for the power consumption and for specific power, calculated from the power number values presented in [2].

Table 2

Values obtained at just-suspension speed

Volumetric particle concentration	*Agitator*	H_2/d	n_{cr} [min^{-1}]	h_s [mm]	h_s/H	*Po*	*P* [W]	ε [$W \cdot m^{-3}$]
16 %	**6SL45**	1	330	255	0.879	1.66	3.31	173
		0.5	226	210	0.724	1.81	1.16	61
	4RLL	1	302	215	0.741	0.78	1.19	62
		0.5	260	195	0.672	0.99	0.97	50
31.5 %	**6SL45**	1	349	270	0.931	1.66	4.57	239
		0.5	245	245	0.845	1.81	1.73	90
	4RLL	1	345	240	0.828	0.78	2.08	108
		0.75	290	240	0.828	0.80	1.26	66
		0.5	280	230	0.793	0.99	1.41	74
47 %	**6SL45**	1	430	290	1.000	1.66	8.55	447
		0.5	390	290	1.000	1.81	6.96	363
	4RLL	1	508	290	1.000	0.78	6.63	346
		0.75	500	285	0.983	0.80	6.48	338
		0.5	480	290	1.000	0.99	7.10	370

Table 3

Values obtained at $h_s = H$

Volumetric particle concentration	*Agitator*	H_2/d	n_h [min^{-1}]	h_s [mm]	h_s/H	*Po*	*P* [W]	ε [$W \cdot m^{-3}$]
16 %	**6SL45**	1	502	290	1	1.66	11.67	609
		0.5	483	290	1	1.81	11.33	592
	4RLL	1	580	290	1	0.78	8.45	441
		0.5	505	290	1	0.99	7.08	370
31.5 %	**6SL45**	1	510	290	1	1.66	14.27	745
		0.5	470	290	1	1.81	12.18	636
	4RLL	1	539	290	1	0.78	7.92	413
		0.75	490	290	1	0.80	6.10	318
		0.5	485	290	1	0.99	7.32	382

It follows from the results presented here that at just-suspension speed for concentrations of 16% and 31.5% $h_s < H$, and for a concentration of 47% $h_s = H$. The just-suspension speeds at the maximum concentration of 47% are significantly higher than at lower concentrations. A comparison of the power consumption shows that a folded blade turbine needs less power than a standard pitched blade turbine.

A comparison of the experimental just-suspension speed values with the values calculated from the relations presented in [3] is shown in Fig. 9. It follows from this figure that there is no significant difference between the experimental values and the calculated values at concentrations of 16% and 31.5%. The experimental values obtained at the maximum concentration of 47% are significantly higher than the calculated values. This is due to the high viscosity of the suspension and the transitional flow in the vessel (the relations presented in [3] hold only for turbulent flow).

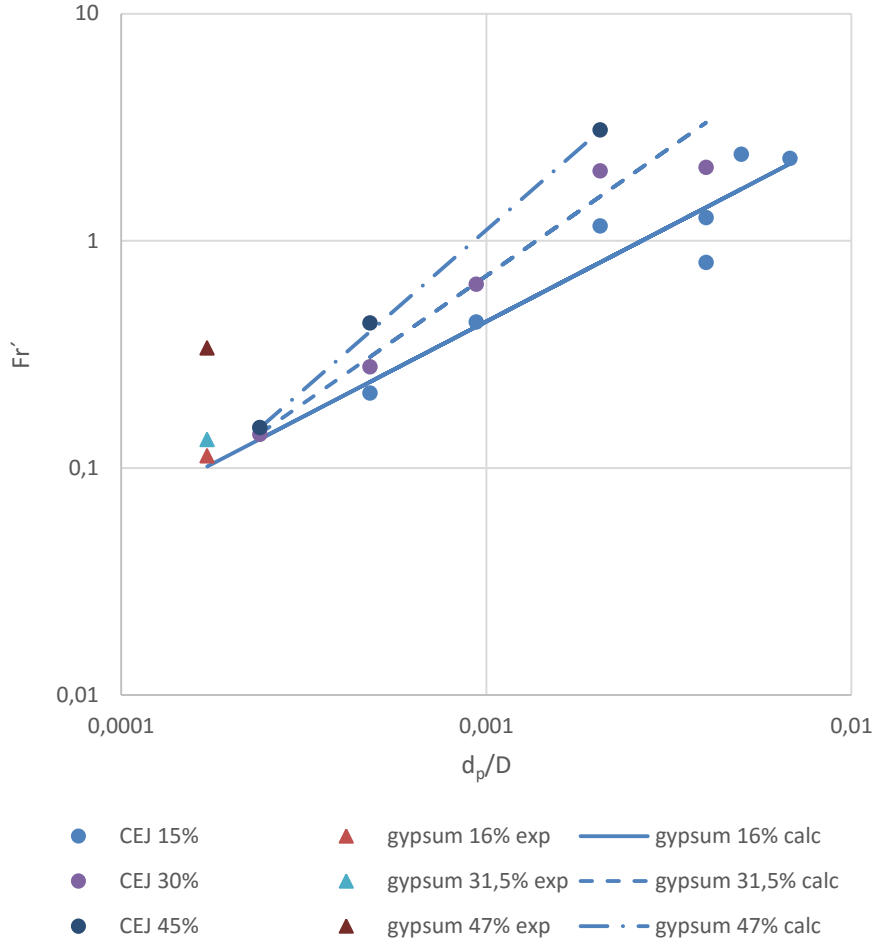

Fig. 9. Comparison of experimental values with results from [3]

List of symbols

c_v – mean volumetric particle concentration
d – agitator diameter
D – vessel diameter
d_p – particle diameter
Fr' – modified Froude number $Fr'=n^2 d\rho/g\Delta\rho$
g – gravity acceleration
h – sediment height
h_s – height of interface between suspension and clear liquid
H – batch height
H_2 – distance between agitator and bottom
n – agitator speed
n_{cr} – just-suspension agitator speed
n_h – agitator speed at which $h_s = H$
$r_{i,e}$ – radii of sediment layer
u – settling velocity
z – distance of sampling point
μ – dynamic viscosity
ρ – suspension density

References

[1] Moravec J., Rieger F., Jirout T., *Viscosity measurements of gypsuzm suspensions*, Proceedings of 22nd Polish Conference of Chemical and Process Engineering, Spala, 5-9 September 2016.
[2] Medek J., *Power characteristics of agitators with flat inclined blades*, Int. Chem. Eng., vol. 20, 1980, 665-672.
[3] Rieger F., *Effect of particle content on agitator speed for off-bottom suspension*, Chem. Eng. J., vol. 79, 2000, 171-175.

TECHNICAL TRANSACTIONS | CZASOPISMO TECHNICZNE
MECHANICS | MECHANIKA
2-M/2016

EVGENY KALININ, SERGEY ERSHOV, SERGEY KOZHEVNIKOV*

REGENERATION AND UTILISATION ROTARY SYSTEMS OF WASTE TECHNOLOGICAL LIQUIDS

WYKORZYSTANIE UKŁADÓW WIRUJĄCYCH DO REGENARACJI ZANIECZYSZCZONYCH PŁYNÓW TECHNOLOGICZNYCH

A b s t r a c t

The article shows prospects of using regeneration and utilisation rotary systems of waste technological liquids in enclosed local water systems.

Keywords: local water systems, waste technological liquids, filtration of disperse solutions.

S t r e s z c z e n i e

W pracy przedstawiono perspektywy wykorzystania układów wirujących do regeneracji zanieczyszczonych płynów technologicznych w zamkniętych, lokalnych systemach

Słowa kluczowe: lokalne systemy wodne, zanieczyszczone płyny technologiczne, filtracja zdyspergowanych roztworów

DOI:

* Prof. PhD. DSc. Eng. Evgeny Kalinin, PhD. DSc. Eng. Sergey Ershov, PhD. DSc. Eng. Sergey Kozhevnikov, Department of Ground Vehicles and Technological Machines, Faculty of Mechanics and Automations, Ivanovo State Polytechnic University.

1. Introduction

In industry, wastewater is formed in treatment processes of different materials in aqueous media, and its quantitative and qualitative composition significantly varies, depending on the purpose of the implemented process.

When using wastewater as a heat carrier, a decisive influence on the efficiency of the heat recovery is had by such features as its pollution, heat capacity and the volume of abduction. Therefore, an analysis of the above wastewater characteristics in different liquid processes is appropriate.

The problem of material resources reusing, for example, in the manufacture of textile finishing industry is of great importance both from the technical and economic point of view, and to ensure optimal production of ecological interaction with the environment. At the same time, the complex problem is solving not only for the regeneration of waste material of technological solutions, but also for the problem of secondary recovery environments with a significant energy potential, by creating technologies and systems operating in a closed loop.

2. Methods

2.1. Local methods of a wastewater treatment

Numerous studies have shown that the wastewater treatment in chemicals and other types of industries is most effective if they are processing directly in the field of contaminants formation before mixing in wastewater sewers. Wastewater technological equipments for the same type of purposes usually contain a significant amount of the same quality contaminants, whose removal can be performed by one method or by combining them, which is economically efficient for cleaning mixtures. A number of pollutions in the wastewater individual equipment can be so large that their discharge into the sewers and further works general constructions is impossible without special pre-treatment means. Thus, local wastewater treatment uses various mechanical, chemical and physico-chemical methods, and the circulating local sewage systems in a number of cases should be a part of an industrial complex.

2.2. Choice of a local method of a wastewater treatment

A local treatment of concentrated effluents allows to recycle valuable components. However, a prerequisite wastewater before entering it into the overall transportation system for biological treatment facilities should consider the necessity of pre-cleaning and preparation at local wastewater treatment plants. Creating reliable automatic quality control systems largely contributes to the execution of the conditions.

Separating the waste water treatment systems plant-wide and locally eliminates the need for costly construction of long-distance pipelines, reservoirs diameters are reduced, simplified communications and water ways post-treatment.

Concentrated waste water after finishing processes advisable to clean by means of various chemicals and oxidation methods extracting from the wastewater components -

extraction, electrochemical, flotation methods, adsorption, filtration, ultrafiltration. Recent methods on the technological characteristics are the most advanced and promising in terms of both the quality of ultrafiltration and capital, and energy costs for wastewater treatment.

The complex technological scheme of wastewater treatment is based on the following principles:

- creation of independent (local) water circulating in each production system with the necessary local treatment facilities and the subsequent use of treated wastewater in the process;
- separation and disposal of waste liquid technological environments, which may be used in a recycling water management;
- construction of facilities for the advanced treatment of biochemical effluent with the return of all recycled water in the production working cycle.

Concentrated wastewater cleared on local technological units can be taken to the biochemical adsorption or filtration systems for the fullest cleaning and then return to the system of water consumption.

Filtration is one of the methods for separating suspended solids from liquids and gases by means of porous walls or special centrifuges.

3. Decisions

3.1. New trends

Today, the development of a membrane filtration unit, in which in order to create the working pressure, a centrifugal force field will be applied, is the most urgent task. This is caused by the fact that besides installing baromembrane, the membrane elements should include: the pump unit, pre-treatment equipment, tanks for feed solution, the permeate and the concentrate, sensors and automatic control and monitoring devices, connection and control valves, frame elements, etc. Centrifugal filtration units, with the diaphragm, have the following advantages: tens of times less power consumption; considerably less space requirements; mobility in mind the small size; relatively low operating pressures due to low contamination of separation surfaces.

It gives even more advantages to bring together multiple stages of membrane separation into one centrifugal set – the combination of macro and micro-filtration process with ultrafiltration. Therefore, expansion of the application scope of membrane technology can only be achieved at the expense of development work on the creation of new and improved existing spacer elements and devices.

The main objective of the developed local treatment systems and the recycling of technological water is to prevent the discharge of waste water into the environment (into the surrounding water). No less important is the problem of collecting valuable chemical components contained in waste solutions with a view to their re-use.

Creating a multi-stage cleaning system running on the wastewater of the whole enterprise requires significant capital expenditures. In this case, mixing sewage processing equipment after different purposes (different from the chemistry of the process) makes it impossible to extract expensive components from working solutions. These components are

irretrievably lost, and in addition to damage to the environment, they increase the costs for companies to resume raw materials.

Saving technological water and preventing the discharge of waste water to a large extent can be achieved through the use of membrane technology. With it, you can select valuable components from spent wash water and send them for recycling. This method allows to avoid a chemical degradation of component molecules in contrast to the method of evaporation and brought to a state in which it becomes possible to reuse by increasing the concentration.

The most promising is using ultrafiltration membranes that provided a high-speed shared solution on its surface, which leads to the possibility of long-term operation of the filtration equipment without intermediate cleaning. Centrifugal devices, in this case, are a key element to create a local waste treatment system of liquid media technology.

A centrifugal membrane device (Fig. 1), as a part of the system, contains three separate levels: macro, microfiltration and ultrafiltration [1]. Performance of the centrifugal membrane device, according to the starting solution, may be chosen in the installation via separation factor value in accordance with the rotor speed. This scheme provides for the recovery and recycling of chemical components process with sufficiently high concentration, and returns to the washing process line the hot cleaned water, which reduces the cost of heat for its subsequent display.

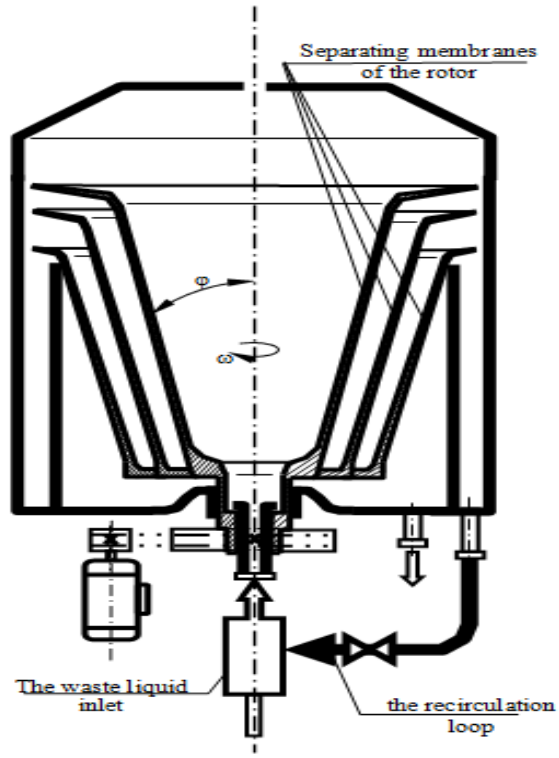

Fig. 1. The design concept of a centrifugal membrane device (CMD)

Equipment of circulating water local system is located directly next to the main process equipment and requires the use of long pipelines and large amounts of storage volume.

Local water recycling system, for example, as a part of the dyeing and drying line, allows achieving the following technical and economic indicators:

- saving technological water, no more than, m^3/h – 6.0;
- saving thermal energy for heating water, no more, Gcal/h (1.3 t/h of normal Pair) – 0.7
- volume reduction of wastewater containing a dye no more than 0.3...0.5 g/l, m^3/h – 6.0.

Thus, the local system of closed water consumption, which included applied centrifugal membrane device, allows to return the purified water effectively into the technological cycle.

3.2. Complete solution

Wastewater of textiles has a high value and high concentration of adsorbed organic halogen compounds as well as intense colour and a significant salt content. Approximately 60% of wastewater in the application of the purification method can be recycled into the production water circulation. The remaining wastewater is treated to such a degree that it can be discharged into the surface water body.

The flow part of the recycled water is desalted by reverse osmosis. Additional demand for industrial water covered by make-up the system of pre-prepared fresh water.

Membrane filtration processes, in particular ultrafiltration and microfiltration, are the separation processes, which take place under pressure using polymeric or porous inorganic materials.

Basic filtration systems consist of two kinds of the same products – filtration devices and filtration modules, which differ mainly by their large-scale indicators (size and weight).

The prospect of the application of multi-stage wastewater treatment system, which comprises: the first stage – pre-cleaning method of macro microfiltration; at the next stage – ultrafiltration separation, realised at higher separation factors (Fig. 2) [2, 3].

4. Conclusions

The possibility of combining all the steps into one system, realised in a centrifugal filtration apparatus, makes it possible to create a highly economical method, implemented on space-saving type of equipment for local systems of circulating water use of technological production.

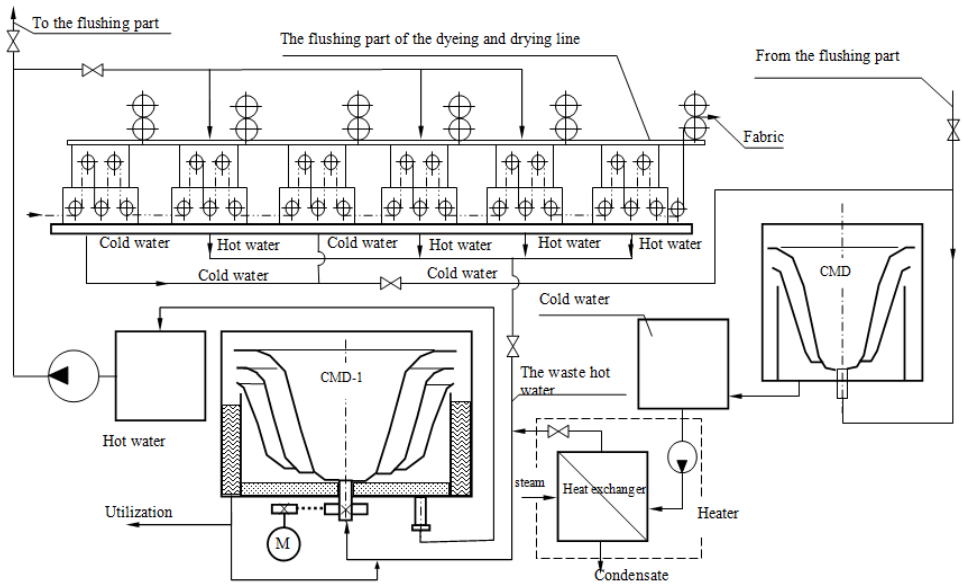

Fig. 2. Technological scheme of the circulating water local system for a dyeing and drying line

References

[1] Ganichev I. V., Kalinin E. N., Kozlov V. V., *The centrifugal device for cleaning the fluid from dispersed impurities: a patent*, Russia, №2226419.

[2] Ganichev I. V., Kalinin E. N., Kozlov V. V., *Experimental and analytical research of centrifugal filtration parameters*, Proceedings of the universities, Technology of textile industry, vol. 6, 2003.

[3] Ganichev I. V., Kalinin E. N., *Identification of the vortex motion dynamic model of membrane fluid flow*, Proceedings of the universities, Technology of textile industry, vol. 2, 2004.

TECHNICAL TRANSACTIONS | CZASOPISMO TECHNICZNE
MECHANICS | MECHANIKA
2-M/2016

RYSZARD KANTOR*, PIOTR SEWERYN**

DYNAMIC MODELING OF OPERATION OF CONTROLLED SOLAR HEATING SYSTEM IN ECOSIMPRO

DYNAMICZNE MODELOWANIE DZIAŁANIA STEROWANEGO GRZEWCZEGO UKŁADU SOLARNEGO W PROGRAMIE ECOSIMPRO

A b s t r a c t

The article describes the structure and operation of virtual one-dimensional dynamic model of the solar heating system using components from the libraries of the EcosimPro program. The model is based on a fragment of a real hybrid sorption-compressor refrigeration system, designed and built in the Laboratory of Thermodynamics and Thermal Machines Measurements at the Faculty of Mechanical Engineering of the Cracow University of Technology. In the second part of the paper, the results of the dynamic simulation are shown along with their comparison to the actual measurement data recorded during one day (and night).

Keywords: dynamic modelling, solar heating system, EcosimPro

S t r e s z c z e n i e

Prezentowany artykuł zawiera opis struktury i działania wirtualnego jednowymiarowego dynamicznego modelu solarnego systemu grzewczego przy użyciu komponentów z bibliotek programu EcosimPro. Model oparty jest na fragmencie rzeczywistego hybrydowego sorpcyjno-sprężarkowego systemu ziębniczego, zaprojektowanego i zbudowanego w Laboratorium Termodynamiki i Pomiarów Maszyn Cieplnych na Wydziale Mechanicznym Politechniki Krakowskiej. W drugiej części artykułu pokazano wyniki dynamicznej symulacji i ich porównanie do rzeczywistych danych pomiarowych, zarejestrowanych w ciągu jednej doby.

Słowa kluczowe: modelowanie dynamiczne, system ogrzewania słonecznego, EcosimPro

DOI:

* DSc. Eng. Ryszard Kantor, Institute of Thermal and Process Engineering, Faculty of Mechanical Engineering, Cracow University of Technology.
** Piotr Seweryn, Faculty of Mechanical Engineering, Cracow University of Technology.

1. Introduction

In the laboratory of Institute of Thermal and Process Engineering seated at the Faculty of Mechanical Engineering of the Cracow University of Technology, there has been designed and assembled a prototype of a two stage hybrid adsorption-compression cooling system [1]. The high temperature stage component of the system is the adsorption chiller driven by the heat generated by the solar collectors. The adsorption chiller works during the summer period as a chiller rejecting the heat from the condenser of the low temperature compressor stage with CO_2 as the cooling agent. Generally, all heating systems driven by solar collectors are characterised by periodic operation and unstable availability of a heat source. This enforces the use of heat accumulators to store the surplus of the heat generated during day and use it during periods of low solar operation (e.g. at nights). The excessive solar heat load to the system may cause a rise of the temperature above limits, thus an additional safety protection system is necessary. There are two possible solutions: a heat rejection system (e.g. by using a cooling tower) or thermally controlled solar blinds blocking the solar radiation.

In the present paper, the structure and operation of a virtual one-dimensional dynamic model of the solar heating system is shown. The model built in the EcosimPro software is based on a fragment of the above-mentioned hybrid refrigeration system.

2. Hybrid sorption-compressor refrigeration system

In Figure 2.1, a general scheme of the hybrid cooling system is shown.

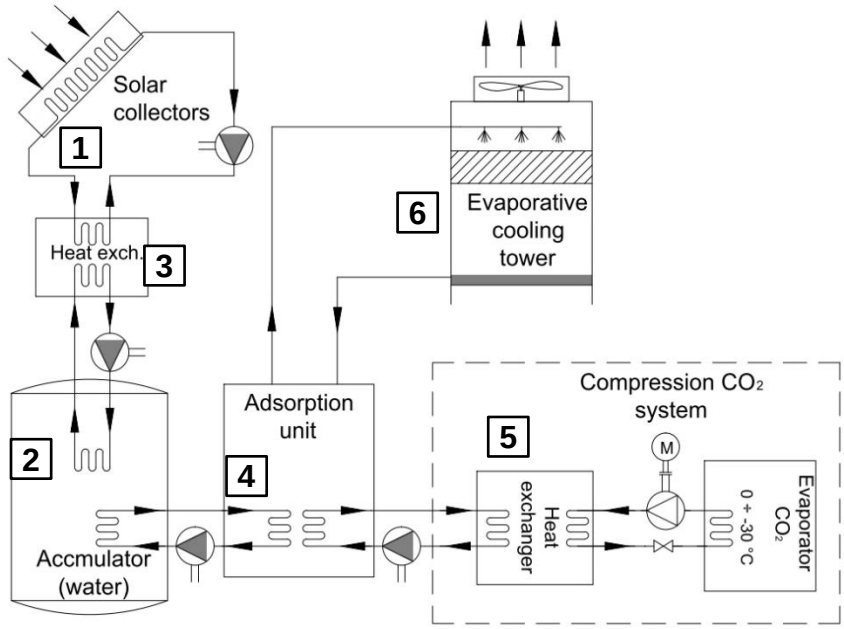

Fig. 2.1. General diagram of the system

The system consists of four main subsystems:

- solar collectors (1) with accumulator (2) coupled by the heat exchanger (3),
- adsorption chiller (4),
- compression CO2 system (5),
- cooling tower (6).

The aim of the present paper is to build a virtual model of one complete subsystem comprising of a set of solar collectors (1), an accumulator (2) and the heat exchanger (3). The model allows to simulate a dynamic behaviour of the solar heating subsystem during a period of several days. A detailed diagram of the solar heating subsystem is shown in Figure 2.2.

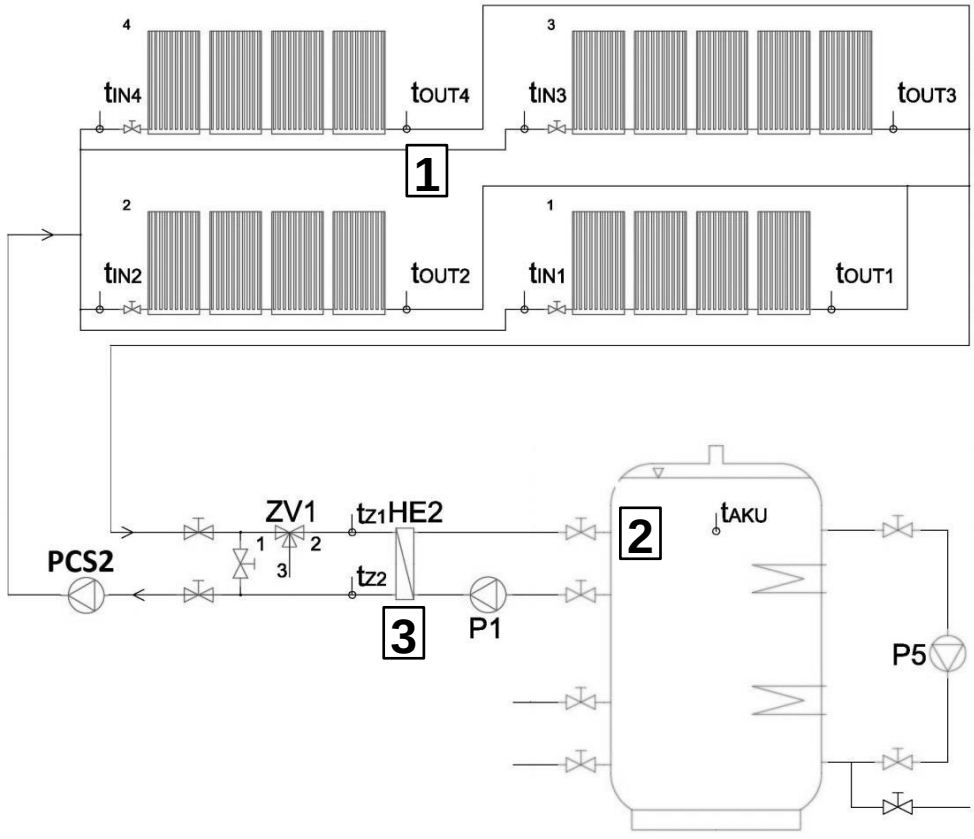

Fig. 2.2. General diagram of the system [2]

3. One-dimensional dynamic modelling in EcosimPro

EcosimPro is a modelling and simulation tool developed by Empresarios Agrupados and used, among others, by ESA[1] and CERN[2]. It allows to build mathematical models of 0D or 1D multidisciplinary continuous-discrete systems and any kind of systems based on differential-algebraic equations (DAE) and discrete events [3].

Models can be created with predefined components from multiple libraries or custom objects written in EL (EcosimPro Language). In order to simulate a schematic model, a mathematical model called partition has to be created. For each partition, the user can define experiments, which contain information about simulation settings, such as time or file name, to save results, initial and boundary conditions.

The greatest advantage of EcosimPro is the possibility of reusing models outside of the software environment in several forms, e.g. standalone C^{++} application. This feature guarantees model reusability by others and further development possibilities like dedicated applications for operator's training, testing models with control programs from real PLC device etc.

The model described below has been created with EcosimPro 5.2.0 by using major components from embedded libraries: Fluidapro, Control, Thermal. The Control and Thermal libraries are standard and free to use, the Fluidapro is a separate library that requires an additional, extra paid, license.

3.1. Virtual model description

In Figure 3.1, a diagram of the created model of solar heating system with the heat storage is shown. The model presents one of the optional states of the system – the heat generated by solar collectors (1) is stored by the accumulator (2).

Fluidapro elements like pipes, tees, valves, volume, heat exchanger, tank and temperature sensors can be distinguished by their symbol shapes. The *Working Fluid* abstract elements (WF) define the working medium (e.g. water). The real pumps are virtually modelled by a simplified component (PCS2, P1).

Elements, which serve to model solar irradiance (G), temperature outside (T_OUT) and mass flow (QM), are imported from the Control library. There are also two Thermal components to simulate the impact of environmental temperature on heat storage.

SolarCollectors element represents a sub-model, which is separately defined in a different file, in order to clarify the scheme view. The *Psolar* element is used to calculate the power gained by solar collectors with given inputs, where the temperature sensor T_MIX registers the current working medium temperature.

In the current *Psolar* model, the measuring point of controlling (feedback) temperature is located after the solar collectors because all solar collectors are identical and thus all are characterised by the same parameters. This workaround simplifies the computational effort and also improves the scheme view. Further simplifications are discussed in the next chapter.

---

[1] European Space Agency

[2] European Organization for Nuclear Research

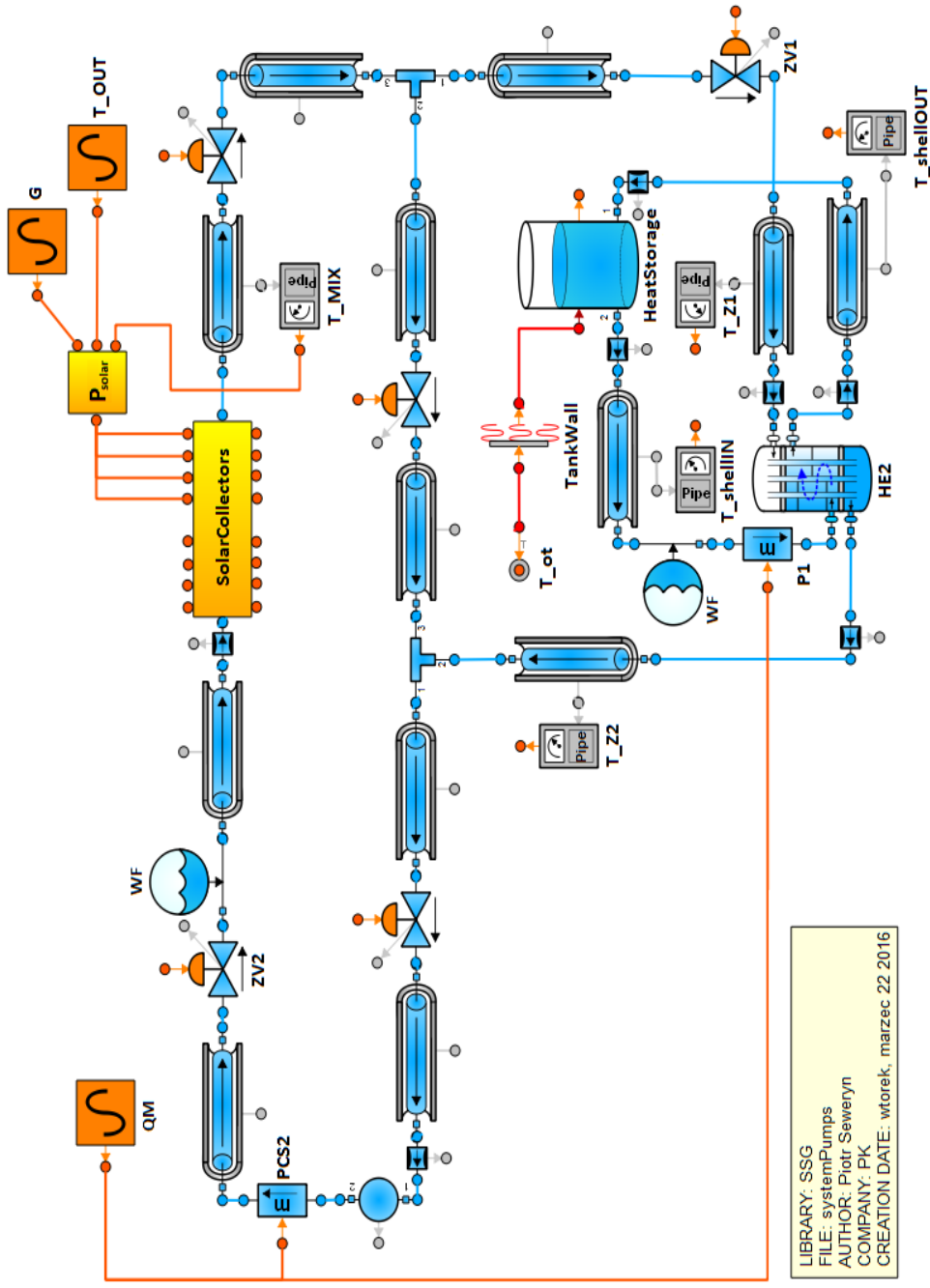

Figure 3.1. Schematic model of solar heating system created in EcosimPro

3.2. Major components of the model

Default parameters of each component have been modified according to the real objects in order to provide as accurate results as possible. The parameters are, e.g. geometrical dimensions, heat exchange coefficients, applied materials etc.

The model of solar heating system in EcosimPro includes some simplifications:

- In order to simplify calculation process, internal boundary conditions (PCS2, P1) are used instead of pumps.
- Working fluid is water instead of glycol mixture, which is not defined in a properties library. It is possible to add it manually in the future.
- In the real solar heating system the brazed plate heat exchangers are used. Due to lack of that element in the library and complexity in custom modelling, a shell-tube heat exchanger (HE2) with appropriately tuned parameters is used instead.

Solar collectors are wrapped in an additional custom component to clarify the scheme view. In Figure 3.2, the model of solar collectors with its distribution pipes, valves and temperature sensors is shown. Heat load from the solar radiation to tube elements is modelled by a heater element from the Thermal library.

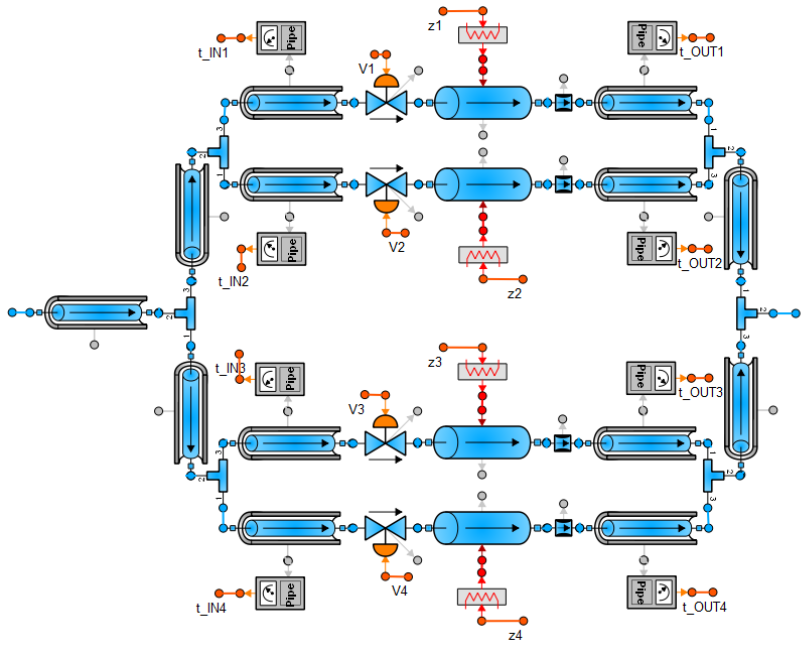

Fig. 3.2. Schematic model of solar collectors

The *Psolar* is a user defined and arranged component that calculates the solar power. It takes into account solar irradiance, ambient temperature and working fluid temperature. It uses the following formula [4]:

$$P = S \cdot (\eta_0 \cdot G - a_1 \cdot (T_m - T_a) - a_2 \cdot (T_m - T_a)^2)$$

where:

S – total aperture area of the collector array, m^2,
η_0 – collector optical efficiency, – ,
G – solar irradiance, W/m^2,
T_m – collector operating temperature (T_MIX), K,
T_a – ambient temperature (T_OUT), K,
a_1, a_2 – temperature difference loss coefficients, W/m^2K, W/m^2K^2 [4].

3.3. Simulation strategy and boundary conditions

In order to carry out the simulation, it is necessary to provide simulation settings, initial and boundary conditions. They are all defined in an experiment file, which is a script written in EL. Regarding initial and boundary conditions, which default values are suggested by the program in each new experiment file, the user may change them by modifying partition file.

All results, presented in the following chapter, have been acquired with the following conditions:

- Initial conditions for the temperature impact on the solar collector's tubes objects are 293.15 K.
- Boundary conditions regarding not fully constrained components are:
  - all valves, except for bypass, are in open state,
  - ambient temperature of heat storage room is 293 K.

Some boundary conditions remain in default values due to their constant character, e.g. gravity acceleration or lack of need to use them in this particular model.

3.4. Simulation results

EcosimPro allows to present and save the simulation results in two ways. The first option is to use an additional application called Monitor to display the results and then save them as images or data files. Another way is to use in the experiment file a function that defines the target file and variables to save in it and then use of acquired data to draw plots in a different application, e.g. Microsoft Excel.

In Figure 3.3, simulation results of the presented model with already defined initial and boundary conditions are shown. The first plot presents a simulated temperature of water in the accumulator (T_AKU) and in the piping located after the solar collectors (T_MIX) and also the ambient temperature T_OUT. The second plot shows the solar irradiance G, with assumption of a warm, sunny and cloudless day in Krakow. Results registered within temperature plots are consistent with preliminary calculations.

The temperature T_AKU of water inside of the heat accumulator (2) is rising consequently, but day by day less effectively. Moreover, during nights, the temperature drops are registered. To reduce this effect, a more complex model with a controlled pump shall be worked out. Switching off the pump during nights and speed control is highly recommended.

In the real system, the collected heat is used not only to charge the heat accumulator (2), but also to drive the adsorption unit (4). Moreover, for safety reason, the wet cooling tower (6) is used for rapid cool down of the overheated working fluid. The presented simplified

model does not include the mentioned safety solutions and in result the overheating (T_MIX above limit of 373 K) of the working fluid is registered during the time of maximal sun irradiation.

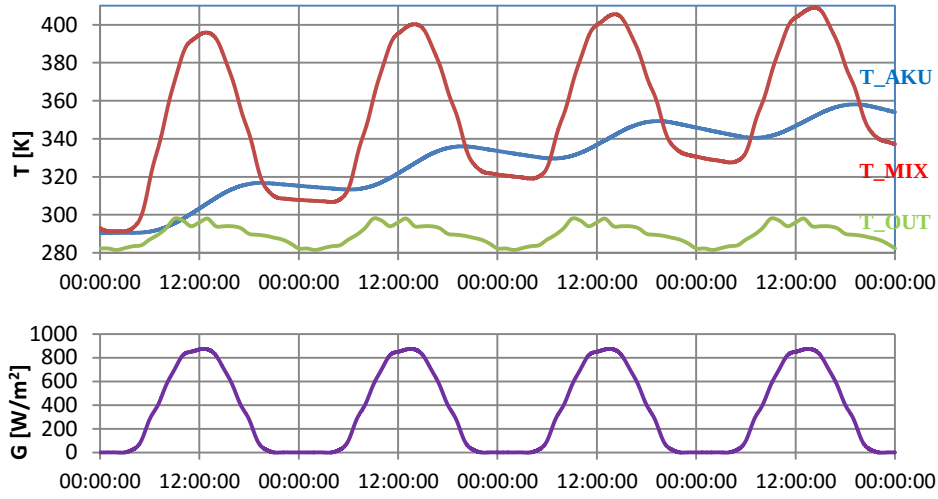

Fig. 3.3. Simulation results – temperature characteristics T_AKU, T_MIX, T_OUT and solar irradiance G

There are two possible solutions to keep the temperature of the working fluid below the limit. The first is a heat rejection system by using a cooling tower, applied in a real installation. The second is a thermally controlled solar blind system, blocking the solar irradiation. For the aim of the present paper, the solar blind system has been modelled. The blinds are being closed on temperature 368 K or above and remain closed until temperature drops to 335 K.

Registered results of the simulation (24 hours) are shown in Figure 3.4. The T_MIX temperature saw-shaped characteristics shows that this is a very efficient method of maximum temperature controlling. The temperature fluctuation span can be narrowed, but in result, this will increase the frequency of the open-close cycle of the solar blind system.

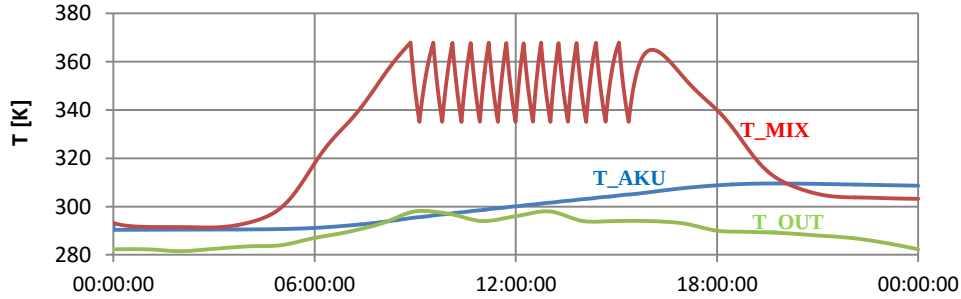

Fig. 3.4. Simulation results for a model with solar collectors covers

4. Experimental verification of the virtual model

The virtual model is based on the real system and there is a certain possibility to compare selected results of the simulation with measurements on the real object in real conditions. It allows to verify the model, performance and effectiveness in comparison to the real installation. However, it is a rare phenomenon characterised by several days of clear unclouded sky, during which one could register quasi-optimal system parameters and the theoretical solar irradiance (Figure 3.3).

4.1. Verification points and parameters

The selected temperatures, presented in Figure 4.1, were registered on 16.06.2015 in the existing system during operation. The temperatures were registered during a sunny day with small rare clouds. It is noticeable on the T_OUT plot that the weather deteriorates from 9 a.m. till 12 a.m. Moreover, during considered time of the year – June, heat accumulator (2) was already charged (T_AKU) and in a stand-by mode. The plot of temperature T_MIX clearly shows the heating process broken by cloudy sky periods. This effect is similar to the mechanical operation of blocking out the solar collectors by the solar blinds during the sunny period of the day.

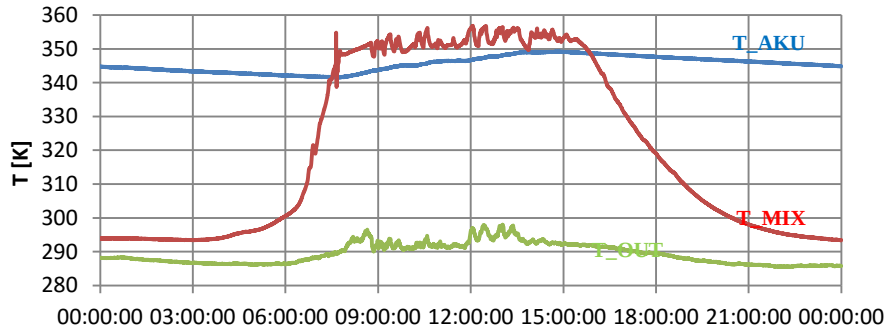

Fig. 4.1. Selected measurements in the real conditions – 16.06.2015 (by courtesy of Roman Duda, Institute of Thermal and Process Engineering)

4.2. Results discussion

In spite of the above-mentioned differences, it is a valuable comparison, showing the performance of the system with both solutions of the maximum temperature control. Although the currently used system is thermally effective, it requires a circulating pump to be frequently switched on during rapid cooling of the overheated working fluid. It is much more effective to use the controlled solar blind system together with the controlled heating medium flow rate (pump speed).

Results of measurements partially resemble those from the simulation. The visible oscillations are the result of cloudy weather. On the other hand, the working fluid temperature measured that day is from 10 to 20 K smaller than on the virtual model with solar blinds, which is mostly caused by ideal solar irradiance applied to the model.

Regarding the heat storage temperature, it is increasing and decreasing in a similar way in all 3 cases and measurements results confirm that during heating process each next day charging is less effective, which mainly is caused by a smaller temperature difference between liquids in the heat exchanger (3).

5. Conclusions

Simulation software, like EcosimPro, is widely used in a modern and innovative industry. It is mostly due to the possibilities of analysing and simulating conceptual solutions without incurring costs of physical implementation. Moreover, it also can be used with existing installations for the purpose of testing new modifications, e.g. the mentioned in this paper system with implemented solar collector blinds.

The virtual model of solar heating system presented in this paper is only a fragment of the much larger and more complex cooling system and any physical difference between the real and the virtual system can have an influence on the results.

The simulation effort allows to save money and time by simulating the virtual experiment. Although to obtain reliable results, it is often required to precisely define the whole system and all of its components.

References

[1] Cyklis P., Kantor R., Ryncarz T., Górski B., *The hybrid compression-sorption system for thermal energy transformation*, 3rd International Conference: Low Temperature and Waste Heat Use in Communal and Industrial Energy Supply Systems. Theory and Practice, October 25th & 26th, 2012, Bremen, Germany, 2012, 44-51.

[2] Cyklis P., Duda R., *Computer driven automatic control of the hybrid two stage refrigeration cycle*, Czasopismo Techniczne. Mechanika, vol. 112(7), 2-M, 2015.

[3] *EcosimPro, system modeling and simulation software*, Empresarios Agrupados [Online: *http://www.ecosimpro.com/products/ecosimpro/*].

[4] *Próżniowy czy płaski - jaki wybrać kolektor słoneczny?*, Hewalex [Online: *http://www.hewalex.pl/pliki/jaki_kolektor.pdf/*].

TECHNICAL TRANSACTIONS | CZASOPISMO TECHNICZNE
MECHANICS | MECHANIKA
2-M/2016

ANN KAPRANOVA, ANTON LEBEDEV, SERGEY SOLOPOV*,
ALEXANDER MELTSER**

THE APPLICATION PROCESS OF THE ORNSTEIN-ULENBEK TO THE FORMATION OF CAVITATION BUBBLES

ZASTOSOWANIE PROCESU ORNSTEIN'A-ULENBEK'A DO OPISU POWSTAWANIA PĘCHERZY KAWITACYJNYCH

A b s t r a c t

In this paper we propose the process of formation of cavitation bubbles in the pilot valve, considered as the steady and homogeneous Markov process.

Keywords: cavitation, formation of bubbles, the Fokker-Planck equation

S t r e s z c z e n i e

W pracy przedstawiono proces powstawania pęcherzy kawitacyjnych w zaworze sterującym jako stabilny i homogeniczny proces Markowa.

Słowa kluczowe: kawitacja, powstawanie pęcherzy, równanie Fokker'a-Planck'a

DOI:

* Prof. DSc. Ann B. Kapranova, Associate Professor DSc. Anton E. Lebedev, MSc Sergey A. Solopov, Mechanical engineering Department, Yaroslavl State Technical University.
** General Director Alexander M. Meltser, ZAO NPO «Regulyator», Yaroslavl.

1. Introduction

The use of regulatory bodies in piping systems allows to perform different technological operations – mixing of liquid streams, maintaining pressure and preventing reverse leakage, etc. The success of the design or modernisation of the elements of the valves depends on the effectiveness of the chosen method of combating undesirable effects of cavitation [1]. To its initial stage in the valves is the formation of bubbles filled with gas and a condensable vapour, arising due to tearing of the liquid in the case of flow in conditions of sharp falling pressure in the flow path of the device.

Application of the stochastic approach for the description of the initial stage of hydrodynamic cavitation as a rule boils down to one of three types of models of education of the nucleons (steam germ) in a liquid environment. In the absence of impurities, an equitable model of homogeneous type [2, 3], and in the presence of suspended particles on or near the surfaces with cracks – heterogeneous type [4, 5]. In addition, the known modifications of the first method of modelling the introduction of an additional coefficient for the number of Gibbs [6], which takes into account the effect of heterogeneity of the environment. However, despite known attempts, the postulation of the relevant law of the distribution of heterogeneous nuclei [7], as shown by the analysis of literary sources [8], the question of the formation of the distribution functions of the cavitation bubbles according to their sizes remains open.

2. The application of the Fokker-Planck equation for the process of formation of cavitation bubbles

In this paper, the process of formation of cavitation bubbles in the regulatory valve, considered as steady and homogeneous Markov process, is presented. In the case when the description of the probability distribution of events, the stationarity implies the possibility of shifting the origin of time, and the uniformity is dependent on time intervals. Note that the main feature of the given random process is that the transition to the subsequent state of the system is determined by its instantaneous condition.

Modelling the process of formation of cavitation bubbles is a stochastic way, including in the formalism of a process of Ornstein-Ulenbek when this bubble macro system is energetically closed from the Gibbs ensemble. Microscopic parameters of this ensemble can serve as the selected coordinates and impulses of Hamilton for each of the similar subsystems, for example, cavitation bubbles are spherical. In the process, the principle of maximum entropy runs, which is in its growth for closed macrosystem and then saving at equilibrium condition [9, 10]. For the process of bubble formation in the conditions of hydrodynamic cavitation will set in the phase space a set of variables, consisting of two variables: the radius of the spherical bubble r, and the velocity of its centre of mass v. The Fokker-Planck equation with drift and diffusion terms of the types corresponding to the process of the Ornstein-Ulenbek is recorded relative to the equilibrium distribution function condition generated spherical cavitation bubbles

$$\frac{\partial F(t,r,v)}{\partial t} = D_1 \frac{\partial^2 F}{\partial r^2} + D_2 \frac{\partial^2 F}{\partial v^2} + \varepsilon_1 \frac{\partial (rF)}{\partial r} + \varepsilon_2 \frac{\partial (vF)}{\partial v} \tag{1}$$

where in the set of phase space coordinates r and velocity v

D_1, D_2 – the diffusion coefficients,
ε_1, ε_2 – the frequency of bubble formation,
F – the equilibrium distribution function of the system condition.

3. Description of stochastic cavitation energy sphere

It is believed that when cavities formed after the rupture of liquids under conditions of rapid pressure drop are filled with gas and a condensable vapour, there is an internal vortex motion in the cavitation bubbles. Then, according to [10], the element dΩ of the phase space is defined as

$$\mathrm{d}\Omega = v\,\mathrm{d}v\,\mathrm{d}r \tag{2}$$

Description of stochastic cavitation bubble energy E with respect to its radius r and the speed of the centre of mass of v implies taking into account the kinetic energies of motion of the bubble in the liquid flow and the internal motion of the system of gas-steam, the energies of formation of the free surface and cavity fill energy due to the condensation of vapour, energy of the hydrodynamic interaction of bubble and liquid. Consequently, introducing coefficients c_1 and c_2

$$c_1 = q_1 \cdot \bar{r}^3 + q_2 \cdot \bar{r}^{-1} \tag{3}$$

$$c_2 = \frac{5 \cdot q_1 \cdot M^2 \cdot \bar{r}^{-7}}{8} + q_3 \cdot \bar{r} + q_4 \tag{4}$$

depending on the structural and regime parameters of flow area control valve and physico-mechanical characteristics of the transported medium, the simulated stochastic energy takes the form

$$E = c_1 \cdot r^2 + c_2 \cdot v^2 \tag{5}$$

where

$\bar{r}$ – the average value of the radius of the bubble,
M – the random component of angular momentum.

Expression (3) and (4) contain the constants q_i, $i = \overline{1,4}$ when asked by the formulas

$$q_1 = \frac{2 \cdot \pi \cdot (\alpha_g \cdot \rho_g + \alpha_s \cdot \rho_s)}{3} \tag{6}$$

$$q_2 = \frac{k_\varsigma \cdot \varsigma_{12} \rho_1}{4}, \quad q_3 = \frac{8 \cdot \pi \cdot P_s}{3} \tag{7}$$

$$q_4 = 4 \cdot \pi \cdot \sigma \tag{8}$$

where

α_g, α_s – the volume fraction of filling bladder with gas and steam,

ρ_g, ρ_s, ρ_l – the density of the gas, steam and liquids,

k_ζ – the parameter of proportionality in the expression for the energy of hydrodynamic interaction $E_{hi} = k_\zeta \cdot \Delta P/(2 \cdot r)$ when calculating the pressure drop in the valve by the formula of Weisbach $\Delta P = \zeta_{12} \cdot \rho_i \cdot v^2/2$,

ζ_{12} – the coefficient of hydraulic resistance of the transition zone for movement of liquid medium, which corresponds to the limit of variation of the Reynolds number $10 < Re < 10^4$, according to [1],

P_s – the saturated vapour pressure,

σ – e surface tension of the liquid.

Note that the value of ζ_{12} is determined by the sum of the coefficients of hydraulic resistance for two zones of laminar and turbulent flows of fluids in the flow part of the valve, which are calculated according to the principle of superpositions of local losses taking into account design and operating parameters of the regulating device and the physical properties of the surfaces of the channels. For example, such parameters include: the diameters of conditional passes and various sections of the spool, the length of the straight channels and the throttle passages, a square cross-section entrance of the (conditional, before and after sudden expansion), gap width of the throttle passage, the degree of roughness of the internal surfaces of the valve, etc.

4. Representation of the kinetic equation of the equilibrium process in the formalism of stochastic energy of the cavitation bubble

The representation (1) of the kinetic equation for $F(t, r, v)$ is the sought distribution function over the States relative to one set of variables (time, radius, velocity the centre of mass of the bubble) to the Fokker-Planck equation with a different set of (stochastic time and energy bubble from the expression (5)) when $\tilde{F}(t, E)$

$$\frac{\partial \tilde{F}(t,E)}{\partial t} = \frac{\mathrm{d}E_0}{\mathrm{d}t} \cdot \left(E \cdot \frac{\partial^2 \tilde{F}}{\partial E^2} + \frac{\partial \tilde{F}}{\partial E} \right) + \frac{1}{E_0} \cdot \frac{\mathrm{d}E_0}{\mathrm{d}t} \cdot \left(E \cdot \frac{\partial \tilde{F}}{\partial E} + \tilde{F} \right) \tag{9}$$

where

E_0 – the energy of the system at the time of stochastic according to [9, 10].

In particular, during the transition from the representation (1) to the form (9) for a given kinetic equation the equilibrium state of the system, it is assumed that the ratios are

$$c_1 \cdot D_1 = c_2 \cdot D_2 \tag{10}$$

$$\varepsilon_1 = \varepsilon_2 \tag{11}$$

where

c_1, c_2 – the coefficients of the expressions (3).

Then taking into account (5) the energy of the system at the time of stochastic E_0 and its flow $\mathrm{d}E_0/\mathrm{d}t$ when $j = \overline{1,2}$ can be specified in the form

$$E_0 = \left(2 \cdot \varepsilon_j\right)^{-1} \frac{\mathrm{d}E_0}{\mathrm{d}t} \tag{12}$$

$$\frac{\mathrm{d}E_0}{\mathrm{d}t} = 4 \cdot c_j \cdot D_j \tag{13}$$

Therefore, taking into account the expressions (3) and (12), we obtain

$$\varepsilon_1 = \varepsilon_2 = \left(2 \cdot E_0\right)^{-1} \frac{\mathrm{d}E_0}{\mathrm{d}t} \tag{14}$$

$$D_1 = \left[4 \cdot \left(q_1 \cdot \bar{r}^{\,3} + q_2 \cdot \bar{r}^{\,-1}\right)\right]^{-1} \frac{\mathrm{d}E_0}{\mathrm{d}t} \tag{15}$$

$$D_2 = \left[4 \cdot \left(\frac{5 \cdot q_1 \cdot M^2 \cdot \bar{r}^{\,-7}}{8} + q_3 \cdot \bar{r} + q_4\right)\right]^{-1} \frac{\mathrm{d}E_0}{\mathrm{d}t} \tag{16}$$

where

q_i – constants defined by formulas (6 ÷ 8) when $i = \overline{1,4}$.

The Fokker-Planck equation (6) has a reduced representation [9]

$$\frac{\partial \tilde{F}(t,E)}{\partial t} = \frac{\mathrm{d}E_0}{\mathrm{d}t}\left[\frac{\partial}{\partial E}\left(E\frac{\partial \tilde{F}}{\partial E}\right) + \frac{1}{E_0}\frac{\partial\left(E\tilde{F}\right)}{\partial E}\right] \tag{17}$$

with the solution according to the described way of modelling a stochastic energy of the cavitation bubble (5) in the form of the representation of the equilibrium distribution function on the system condition

$$\tilde{F}\left(t, E\left(t,r,v\right)\right) = A \cdot \exp\left[-\frac{E\left(t,r,v\right)}{E_0}\right] \tag{18}$$

where

A – normalisation constant, defined with an input element of the phase space $d\Omega$ according to (2) from the relation

$$\int_{\Omega} \tilde{F}\left(t, E\left(t, r, v\right)\right) d\Omega = 1 \tag{19}$$

5. The main results and conclusions

Thus, this operation of transition from the representation of the kinetic equation (1) to the form (9) for the equilibrium state of the system leads to the relations (14 ÷ 16) for connection between the diffusion coefficients D_1, D_2, the frequency of formation of cavitation bubbles ε_1, ε_2 and the energy of the system at the time of randomisation E_0.

Note that the General form of the obtained expressions (12) for the energy characteristics of the process of bubble formation coincides with the given parameters for the process of disintegration of the liquid jet from the work [10]. The equilibrium distribution function for the states of the system in the form (18) with normalisation of the ratio (19) and formed of stochastic energy of the cavitation bubble (5) can be used to determine the differential distribution function of bubbles on radiuses.

References

[1] Arzumanov E. S., *Cavitation in local hydraulic resistances*, Energy, Moscow, 1978.

[2] Frenkel J. I., *Kinetic theory of liquids*, Nauka, Leningrad 1959.

[3] Lienhard J H., Karimi A., *Homogeneous nucleation and the spinodal line*, Journal of Heat Transfer, vol. 103(1), 1981, 61-64.

[4] Shin T .S., Jones O. C., *Nucleation and flashing in nozzles-1. A distributed nucleation model*, Int. J. Multiphase Flow, vol. 19(6), 1993, 943-964.

[5] Hsu Y. Y., *On the size range of active nucleation cavities on a heating surface*, Journal of Heat Transfer, vol. 94, 1962, 207–212.

[6] Ellas E., Chambre P. L., *Bubble transport in flashing flow*, Int J. Multiphase Flow, vol. 26, 2000, 191-206.

[7] Kumzerova E. J., Schmidt A. A., *Numerical modeling of nucleation and bubble dynamics with the rapid loss of fluid pressure*, Journal of Engineering. Physics, vol. 2(7), 2002, 36-40.

[8] Kapranova A. B., Lebedev A. E., Melzer A. M., Nekludov S. V., Serov E. M., *On the methods of modeling the main stages of development of hydrodynamic cavitation*, Fundamental Research, vol. 3(2), 2016, 268-273.

[9] Klimontovich Y. L., *Turbulent motion and structure of Chaos: A new approach to the statistical theory of open systems*, LENAND, Moscow 2014.

[10] Zaitsev A. I., Bytev D. O., *Impact processes in the dispersion-film systems*, Chemistry, Moscow 1994.

TECHNICAL TRANSACTIONS | CZASOPISMO TECHNICZNE
MECHANICS | MECHANIKA
2-M/2016

ANN KAPRANOVA, IVAN VERLOKA, ANTON LEBEDEV, ANATOLIJ ZAITSEV*

THE MODEL OF DISPERSION OF PARTICLES DURING THEIR FLOW FROM CHIPPING THE SURFACE

MODELOWANIE ROZKŁADU WIELKOŚCI CZĄSTEK PO UDERZENIU O PŁASZCZYZNĘ

Abstract

We propose a method for forming differential of the distribution functions of the number of particles of bulk materials on the angle of reflection from bumper (baffle) plate.

Keywords: mixing, brush elements, the bumper, the granular mixture, model

Streszczenie

Zaproponowano metodę wyznaczania różniczkowych funkcji rozkładu wielkości cząstek stałych w zależności od kąta odbicia od płaszczyzny.

Słowa kluczowe: mieszanie, elementy szczotkowe, zderzak, mieszanina cząstek, model

DOI:

* Prof. DSc. Ann B. Kapranova, MSc. Ivan I. Verloka, Associate Professor DSc. Anton E. Lebedev, PhD. DSc. Anatolij I. Zaitsev, Mechanical Engineering Department, Yaroslavl State Technical University.

1. Introduction

The problem of obtaining a homogeneous particle mixture containing unequal volume fractions of particulate components, for example, in routine ratio 1:10 or more, remains relevant and can be successfully achieved using a gravity type mixer [1]. In the designed device of special purpose for the formation sparse streams offered to apply mixing drums with brush elements above the tray, which serves the working materials. In order to improve the quality of the granular mixture obtained in the gravity apparatus, bumper plates (baffle plates) may be used, which are established after drums with brush elements. Shock interaction between the baffle plate and the arrive flows of loose components that are gripped by end of brush elements, resulting in the formation of reflected flow of mixture, which is sliding on the tray located under the drum.

The development of engineering methods of calculating gravity mixer involves choosing the most efficient ranges for changing its design and operational parameters. In connection with this, a special interest is had in the evaluation of the angles of reflection streams of loose components, which are formed after the shock interaction with the flat baffle plate. It is believed that these reflection angles are angles in which the average speed of particle of i-th component (i = 1, ..., n_k) is directed perpendicular to the plane of impingement. Such modelling of the dispersion of particles in the process of reflection stream of i-th material from the baffle plate can be made on the basis of a stochastic approach [2, 3].

2. Geometric features of ways of moving sparse flows of loose components in the working volume of a gravity mixer

The tray, which is under the mixing drum (with brush elements) and on which there are vertically fed n_k particle ingredients in a volume ratio that given by the technological regulations, is at an angle μ_0 to the vertical direction. In the gap, which is had by the height h_0, between this tray and rotating drum, there is a deformation of brush elements and gripping by them portions of layers working loose materials. The number of deformed brush elements – n_b. Baffle plate is located behind the drum at an angle ψ to it tray. Arrive on the baffle plate, flow of bulk component i formed after gripping of particles by brush elements (j = 1, ..., n_b), mounted on a cylindrical surface of the mixing drum along helical lines in opposite directions, starting from its ends. Step of helical winding –h_s; Length of brush element – l_b; the radius and the length of the mixing drum – r_b and L_b; the angular speed of rotation ω. The expressions for the relationship between constructive-regime parameters of the mixing drum and characteristic angles λ_{ij}, α_{ij}, φ_{ij}, β_{ij} and averaged by the number of deformed brush elements values λ_i, α_i, φ_i, β_i for the arriving on the baffle plate flow of i-th component after gripping by brush element j according to [4] are of the form

$$\lambda_{ij} = \alpha_{ij} + \varphi_{ij} - \beta_{ij}, \quad \lambda_i = \frac{\alpha_i}{n_b} + \varphi_i - \beta_i, \quad \alpha_i \equiv \sum_{j=1}^{n_b} \alpha_{ij} \tag{1}$$

$$\beta_{ij} = \operatorname{arctg}\left[\frac{2\cdot h_s\cdot\left(l_b - h_0\right)}{L_b\left\{r_b + h_0 + \left(l_b - h_0\right)\cdot\left[1 - \frac{2\cdot h_s\cdot\left(\alpha_{ij} + \varphi_{ij}\right)}{L_b}\right]\right\}}\right], \quad \beta_i \equiv n_b^{-1}\sum_{j=1}^{n_b}\beta_j \tag{2}$$

$$\varphi_{ij} = \frac{\pi}{2} + \alpha_{ij} - \frac{\arcsin\left(\left\{\left(r_b\cdot\sin\sigma_{ij}\right)^2 + \left(r_b + h_0\right)^2\right\}\cdot\frac{\cos\sigma_{ij}}{r_b + h_0}\right)}{1 + \frac{d_0\cdot\left\{2\cdot h_s\cdot\left(l_b - h_0\right)/L_b\right\}^2}{d_1^{1/2}}}, \quad \varphi_i \equiv n_b^{-1}\sum_{j=1}^{n_b}\varphi_{ij} \tag{3}$$

where

λ_{ij}, α_{ij} – angle spreading by brush element j for material *i*, respectively, from the vertical and the horizontal directions;

φ_{ij} – central angle relative to the drum rotation axis, describing the bending of brush element that have number *j* depending on the position on it occupied portions of component *i*;

β_{ij} – characteristic angle between the direction of the material flow rate *i* and vector tangent to the helical path of end of brush element *j* in section plane of the drum*;*

σ_{ij}, d_0, d_1 – constants depending on the values of these parameters of the mixing element.

By introducing the concept of the coefficient of restitution ($k_{Vi} = \sin\gamma_{1i} / (\sin\gamma_{2i})$) for the average velocities of the move of arriving on the baffle plate, loose flow of *i*-th component and reflected from it respectively at angles γ_{1i} and γ_{2i}, can similarly [5] to obtain the functional dependence $k_{Vi} = f_i(\mu, \psi, L_i, h_i)$, where μ – characteristic angle between the perpendiculars to the baffle plate and to the tray under the mixing drum; ψ – angle between the tray and the baffle plate; L_i – spreading width of the *i*-th material along a tray; h_i – height between tray and baffle plate to shock point for average speed of arriving flow of component *i*. Then, the average value of spreading angle α by the number of deformed brush elements from (1) with considering (2) and (3) and the expression $\psi = \psi_1 + \mu_0 - \pi/2$ takes the form of functional dependence

$$\alpha_i\left(\gamma_{2i}\right) = n_b\cdot\left\{\pi - \left[\frac{\psi_1 + \mu_0 + \gamma_{2i}}{f_i\left(\mu, \psi, L_i, h_i\right)}\right] - \varphi_i + \beta_i\right\} \tag{4}$$

where

ψ_1 – the angle between baffle plate and horizontal direction;

μ_0 – the angle of the tray under the drum to the vertical direction.

3. Determination of differential distributions of particles of flow reflected from baffle plate depending on the angle of reflection

Stochastic modelling of process dispersion of particles of mixed components after reflection from the rectilinear baffle plate inclined at a predetermined angle to the vertical can be accomplished using complete differential distribution function of particles of each material on the angle of spreading after interaction with brush elements [6]

$$S_i^{(np)}\left(\alpha_{ij}\right)=\prod_{j=1}^{n_b} S_{ij}^{(np)}\left(\alpha_{ij}\right) \tag{5}$$

$$\begin{aligned} S_{ij}^{(np)}\left(\alpha_{ij}\right)=\varsigma_{ij}\cdot\left\{\left[\operatorname{erf}\left(\frac{\eta_{ij}\left(\tilde{\alpha}_{ij}\right)\cdot\left[1+\varepsilon_0\cdot\varepsilon_{3i}\cdot\left(\alpha_{ij}+\varphi_{ij}\right)\right]^2}{\varepsilon_{3i}}\right)-\operatorname{erf}\left(\frac{\eta_{ij}\left(\tilde{\alpha}_{ij}\right)}{\varepsilon_{3i}}\right)\right]\times\right. \\ \left.\times\left[\eta_{ij}\left(\tilde{\alpha}_{ij}\right)\right]^{-1}\cdot\exp\left\{-\frac{\left[\eta_{ij}\left(\tilde{\alpha}_{ij}\right)\right]^2\cdot\varepsilon_4\cdot\varepsilon_0{}^2\cdot\left(\alpha_{ij}+\varphi_{ij}\right)^2}{\varepsilon_{1i}\cdot\varepsilon_{2i}}\right\}\right\} \end{aligned} \tag{6}$$

These functions are non-equilibrium and correspond to the kinetic equations for the energetically open macrosystem with macroscale fluctuations of states [1] caused by the influx of outside material (energy) and leading to the ordering of macrosystem in unstable conditions. For example, such as fluctuations in [6] are collisions between particles arriving streams of loose components, which are formed after the gripping by symmetrically arranged brush elements in the form of helical winding with different ends of the mixing drum. Wherein this modelling of stochastic energy $E_{ij}^{(np)}$ for a particle i of bulk material when gripped by brush element j, which is part of the expression to determine the number of particles of component i

$$\mathrm{d}N_{ij}^{(np)}=A_{ij}^{(np)}\cdot\exp\left[-\frac{E_{ij}^{(np)}}{E_{0ij}^{(np)}}+\frac{\left(E_{ij}^{(np)}\right)^2}{2\cdot E_{fij}{}^2}\right]\mathrm{d}\Omega_{ij} \tag{7}$$

in the element of phase volume $\mathrm{d}\Omega_{ij} = -\omega^2 r_{ij}\mathrm{d}r_{ij}\mathrm{d}\Theta_{ij}$ for polar coordinate system in the cross-section of the drum with centre on its axis of rotation allows for translational movement of bulk materials particles, the random nature of their angular momentum when gripping by deformed brush element j and the interaction with the brush element having angular stiffness. Parameters $E_{0ij}^{(np)}$ and $E_{fij}^{(np)}$ included in the expression (7) have the meaning, respectively, of a macrosystem energy at the moment of its randomisation and the energy loss of the macrosystem at macroscale fluctuations of its condition; $A_{ij}^{(\mathrm{np})}$ – normalization parameter.

Geometric relationship (1) in (4) between the angles of spreading flows of particles arriving on the baffle plate and the angle of inclination according to expressions (5) and (6) allows to create full differential distribution function of particles of loose components $\chi_{ij}^{(\mathrm{np})}(\gamma_{2i})$ on the angle of reflection from the baffle surface taking into account the coefficient of restitution $k_V = k_V(\gamma_{2i})$

$$\chi_i^{(np)}(\gamma_{2i}) = \prod_{j=1}^{n_b} \xi_{ij}^{(np)}(\gamma_{2i}) \tag{8}$$

$$\xi_{ij}^{(np)}(\gamma_{2i}) = \varsigma_{ij} \cdot \left\{ \left[\operatorname{erf}\left(\frac{\eta_{ij}(\tilde{\alpha}_{ij}) \cdot \left\{ 1 + \varepsilon_0 \cdot \varepsilon_{3i} \cdot \left[\alpha(\gamma_{2i}) + \varphi_{ij} \right] \right\}^2}{\varepsilon_{3i}} \right) - \operatorname{erf}\left(\frac{\eta_{ij}(\tilde{\alpha}_{ij})}{\varepsilon_{3i}} \right) \right] \times \right.$$
$$\left. \times \left[\eta_{ij}(\tilde{\alpha}_{ij}) \right]^{-1} \cdot \exp\left\{ - \frac{\left[\eta_{ij}(\tilde{\alpha}_{ij}) \right]^2 \cdot \varepsilon_4 \cdot \varepsilon_0{}^2 \cdot \left[\alpha(\gamma_{2i}) + \varphi_{ij} \right]^2}{\varepsilon_{1i} \cdot \varepsilon_{2i}} \right\} \right\} \tag{9}$$

where the functional dependence of $\alpha_i(\gamma_{2i})$ has the following form

$$\alpha_i(\gamma_{2i}) = n_b \cdot \left(\beta - \varphi_i + \frac{B_1 \cdot B_3 - B_2 + \left[(B_1 \cdot B_3 + B_2)^2 - 4 \cdot B_3 \cdot \gamma_{2i} \right]^{1/2}}{2 \cdot B_3} \right) \tag{10}$$

$$B_1 = \frac{\pi}{2} - \psi + \mu_0, \quad B_2 = P_{1i} \cdot \left[(\pi - \psi) \cdot \cos\mu - P_{2i} \right], \quad B_3 = (\pi - \psi) \cdot P_{1i} \cdot \sin\mu \tag{11}$$

$$P_{1i} = \frac{1 - (\pi - \psi) \cdot \left(\frac{L_i}{h_i} - \operatorname{ctg}\psi \right)}{2 \cdot \left(\frac{L_i}{h_i} - \operatorname{ctg}\psi \right) \cdot \left(1 + \frac{L_i}{h_i} - \operatorname{ctg}\psi \right)}, \quad P_{2i} = \left(\pi - \psi + \frac{L_i}{h_i} - \operatorname{ctg}\psi \right) \cdot \operatorname{ctg}\psi \tag{12}$$

4. The main results of modelling and conclusions

We illustrate the results obtained for functions $\chi ij^{(np)}(\gamma_{2i})$ and $\xi_{ij}^{(np)}(\gamma_{2i})$ from expressions (8) and (9) on the example of the reflection natural sand GOST 8736-93 (i = 1) from the baffle plate. The dependence presented by the graphs in Fig. 1 allow us to estimate the maximum value of the reflection angle γ_{21} of the flow of loose ingredient (i = 1), after interaction with brush elements j = 1, 2, 3. In particular, the sparse stream of particles arriving on the baffle plate, formed after gripping of natural sand by brush elements, which first was captured by the layers of material from the clearance with the tray (Fig. 1, curve *3*, j = 3, with n_b = 3), is discarded from the baffle plate on angle greater by 2.6 times than a similar flow formed after interaction with brush elements (Fig. 1, curve *1*, j = 1), which came out of the gap tray-drum last. The maximum value of the angle of reflection that characterises the dispersion of the full arriving flow of natural sand flow after hitting the baffle plate (Fig. 1, curve 4), close to the value of the angle for the flow relating to gripping by brush elements with a number j = 2 (Fig. 1, curve 2).

Thus, hereinafter depending $\chi_{ij}^{(np)}(\gamma_{2i})$ and $\xi_{ij}^{(np)}(\gamma_{2i})$ from the expressions (8) and (9) may be used for calculating the weight fraction of the mixed components of the resulting mixture, and for assessing it quality for selected criteria.

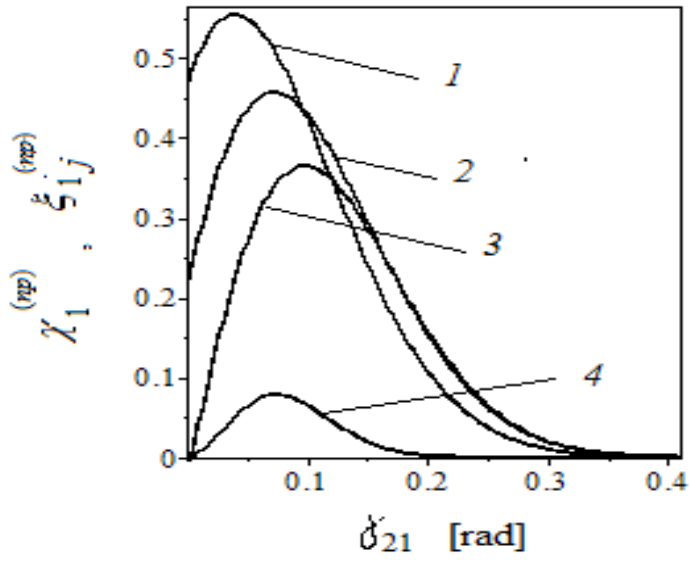

Fig. 1. Dependencies $\chi_1^{(np)}(\gamma_{21})$ and $\xi_{1j}^{(np)}(\gamma_{21})$ for differential non-equilibrium distribution functions of the number of particles of natural sand GOST R 8736-93 ($i = 1$) in the angle of reflection γ_{21} from the baffle plate: $L_b = 1{,}85\ 10^{-2}$ m; $l_b = 4{,}5 \cdot 10^{-2}$ m; $r_b = 3{,}0 \cdot 10^{-2}$ m; $h_s = 1{,}6 \cdot 10^{-2}$ m; $h_0 = 3{,}0 \cdot 10^{-2}$ m; $\omega = 52{,}36$ s^{-1}; $n_b = 3$; $\mu_0 = 1{,}3089$ rad; $\Psi_1 = 0{,}9599$ rad; $\mu = 0{,}7071$ rad; $L_1 = 2{,}8 \cdot 10^{-1}$ m; $h_1 = 8{,}0 \cdot 10^{-2}$ m; 1-3 – $\xi_{1j}^{(np)}(\gamma_{21})$; 1 – $j = 1$; 2 – $j = 2$; 3 – $j = 3$; 4 – $\chi_{1(}^{np)}(\gamma_{21})$

References

[1] Kapranova A. B., Bakin M. N., Verloka I. I., Zaitsev A. I., *Ways to describe the motion of the solid dispersed mediums in different planes for the cross sections of the mixing drum*, Transactions of the TSTU, vol. 21(2), 2015, 296-304.

[2] Klimontovich Y. L., *Turbulent motion and structure of Chaos: A new approach to the statistical theory of open systems*, LENAND, Moscow 2014.

[3] Zaitsev A. I., Bytev D. O., Impact processes in the dispersion-film systems, Chemistry, Moscow, 1994.

[4] Bakin M. N., Kapranova A. B., Verloka I. I., *Investigation of the distribution of bulk components in the working volume of the drum-ribbon mixer*, Fundamental Research, vol. 5(5), 2014, 928-933.

[5] Kapranova A. B., Bakin M. N., Lebedev A. E., Zaitsev A. I., *Parameter estimation of recovery shock interacting streams of particulate media with a sloping baffle plate*, Chemistry and Chemical Technology, vol. 56 (8), 2013, 111-113.

[6] Kapranova A. B., Verloka I. I., Zaitsev A. I., *Comparative analysis of equilibrium and nonequilibrium distribution functions of granular media mix*, XXVIII – International Scientific Conference on Mathematical Methods in Technics and Technologies - MMTT- 28, Yaroslavl, Russia, 2 – 4 june 2015, 223-227.

TECHNICAL TRANSACTIONS | CZASOPISMO TECHNICZNE
MECHANICS | MECHANIKA
2-M/2016

TADEUSZ KOMOROWICZ*, KONRAD NERING, STANISŁAW WALCZAK**

ANALYSIS OF THE FLOW OF CRYSTALLISING WATER SLURRIES IN PIPELINES

ANALIZA PRZEPŁYWU SZLAMÓW WODNYCH KRYSTALIZUJĄCYCH W RUROCIĄGACH

A b s t r a c t

The paper presents a method for monitoring the flow conditions in pipelines in the case of transport of crystallising water slurries forming scale. The method's core is the ability to calculate the equivalent pipeline diameter under varying flow conditions in industrial practice. The method was successfully tested in the laboratory and employed in an industrial plant.

Keywords: hydrotransport, formation of scale in pipelines, flow monitoring

S t r e s z c z e n i e

W artykule przedstawiono metodę monitorowania warunków przepływu w rurociągach w przypadku transportu krystalizujących szlamów wodnych tworzących osady. Sedno metody to przedstawienie sposobu obliczania średnicy zastępczej rurociągu w warunkach zmiennego przepływu w praktyce przemysłowej. Metoda została z powodzeniem przetestowana w laboratorium i wdrożona w jednym z zakładów przemysłowych.

Słowa kluczowe: hydrotransport, tworzenie się osadów w rurociągach, monitoring przepływu

DOI:

* DSc. Eng. Tadeusz Komorowicz, Chair of Chemical and Process Engineering, Faculty of Chemical Engineering and Technology, Cracow University of Technology.
** DSc. Eng. Konrad Nering, DSc. Eng. Stanisław Walczak, Institute of Thermal and Process Engineering, Faculty of Mechanical Engineering, Cracow University of Technology

1. Introduction

Many branches of industry employ long distance pipeline hydraulic transport of waste powder solids. Because of a complex chemical composition of the transported solids, a partial solubility in water of individual components of the mixture, possible chemical reactions between them in the water environment and varying transport conditions caused by the weather, scale on the internal pipeline surface grows as a result of the crystallisation effect (Fig. 1). The problem of solid's deposition in pipelines is also discussed in the literature [1, 2, 3].

Fig. 1. A view of a pipeline cross-section – the formed scale decreases the free cross sectional area

As a result of the scale formation, the pipeline throughput decreases. In order to keep the flow rate of slurry at a constant level, it is necessary to gradually raise the inlet pressure generated by the pumps by increasing their rotational speed. In order to do this, a problem of gradual increase of the current intensity and a simultaneously higher consumption of power by pumps appears. It results in higher operational costs. Because of this, a lot of effort is put in industry to prevent the crystallisation and formation of scale in pipelines by adding carefully selected chemical agents.

In order to prove the effectiveness of the applied chemical additives, it is necessary to develop a continuous method for monitoring the flow conditions. But in industrial practice, the streams of transported slurries often vary in time intervals, which results in difficulties in making an appraisal. The authors made an effort to find a parameter to appraise the flow conditions in pipelines, i.e. an actual diameter, independent of the stream quantity. As a result of the investigations, an equivalent pipeline diameter derived on the basis of the Darcy-Weisbach equation has been introduced.

2. Analysis of flow conditions in an industrial plant

The analysis was carried out in an industrial hydrotransport plant susceptible to scale formation. The analysing operational parameters were:

- the discharge pressure values at the inlets to individual pipelines,
- the current intensity values received by pumps,
- the volume flow rate values of pumped slurry.

The analysis was based on a large range of data. They were systemised and averaged to cause their clarity.

The exemplary plots of pressure vs. time in a selected pipeline inlet, and the current intensity consumed by pumps vs. the time to keep a constant pump capacity in time in this pipeline are presented respectively in Figs. 2-4.

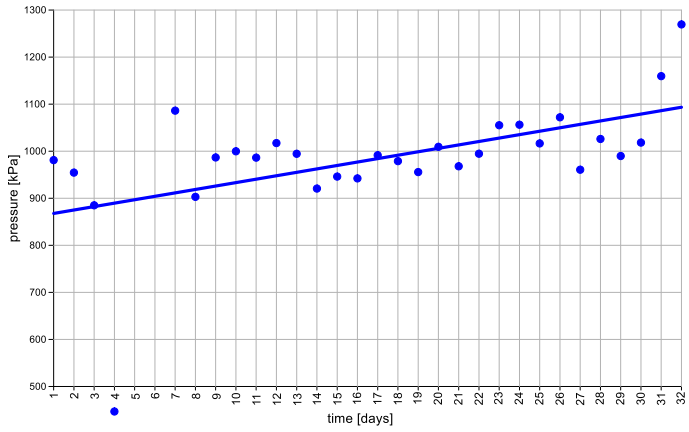

Fig. 2. Pressure vs. time for a selected pipeline

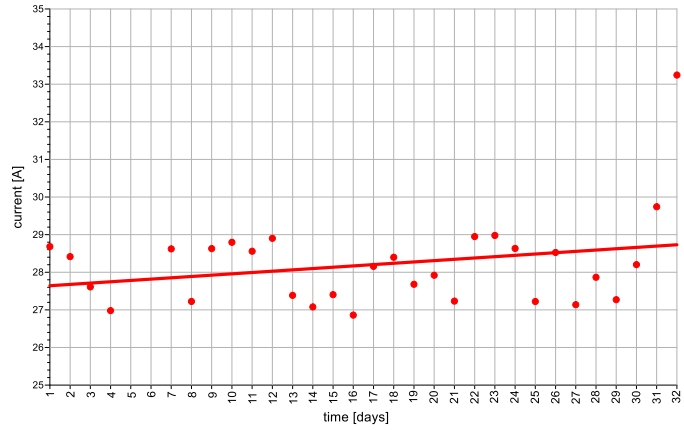

Fig. 3. Current intensity vs. time for a selected pipeline

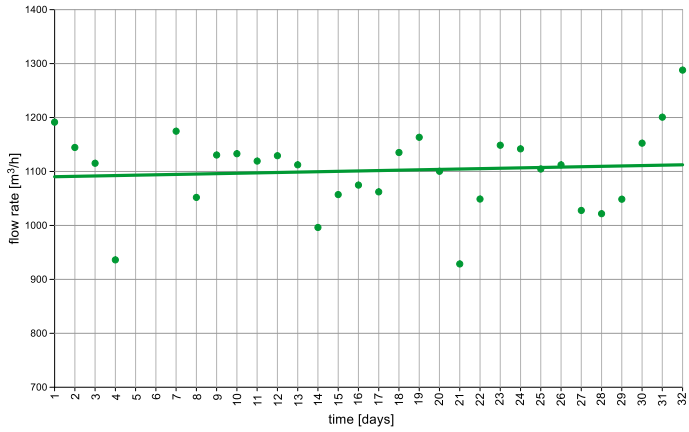

Fig. 4. Pump capacity vs. time for a selected pipeline

3. Rheological studies of examined slurry

Monitoring the hydrotransport pipeline, especially under conditions of various flow rates, demands the determination of the parameter unambiguously describing the pipeline's state, regardless of the flow conditions, such as the flow rate and the pressure drop. This parameter could be the dimensionless equivalent pipeline diameter.

To determine the dimensionless equivalent pipeline diameter using the Darcy-Weisbach equation, it is necessary to identify the rheological parameters of the flowing slurry, including the curves describing the flow resistance [4].

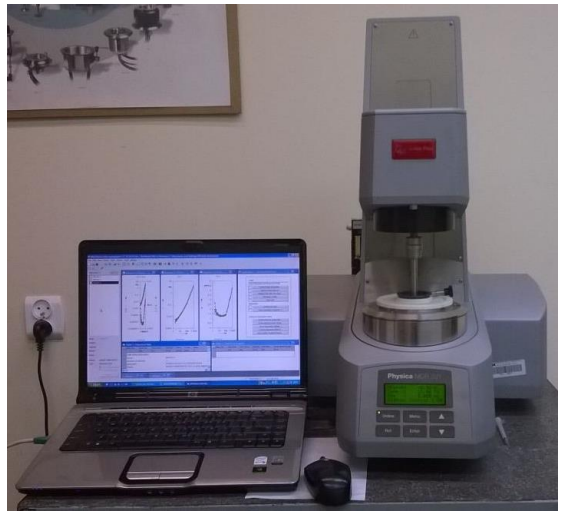

Technical Data	Unit	MCR 302
Bearing		Air
EC motor		Yes
Maximum torque	mNm	200
Min. torque, rotation	nNm	1
Min. torque, oscillation	nNm	0.5
Angular deflection (set value)	µrad	0.05 to ∞
Min. angular velocity	rad/s	10^{-9}
Max. angular velocity	rad/s	314
Max. speed	1/min	3000
Min. angular frequency	rad/s	10^{-7}
Max. angular frequency	rad/s	628
Normal force range	N	0.005-50
Normal force resolution	mN	0.5

Fig. 5. MCR301 rheometer with basic technical data

In order to identify the rheological parameters of the flowing slurry, the rheological studies were carried out with the application of a rotational rheometer (MCR 301 type) available at the Department of Fluid Mechanics. The rheometer and its basic technical data are presented in Fig. 5.

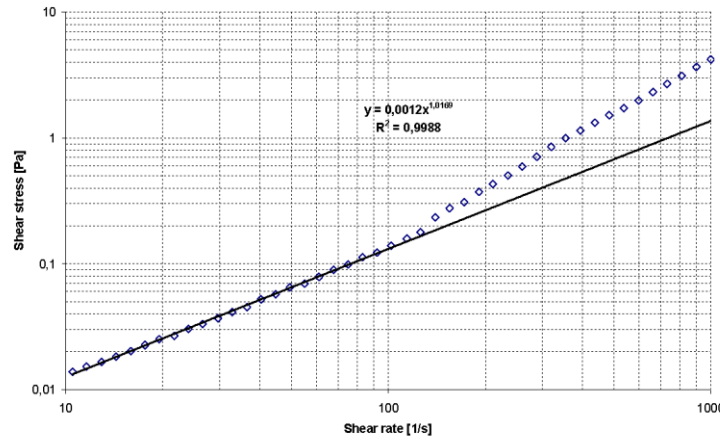

Fig. 6. Flow curve of slurry flowing through the examined pipeline

The prepared slurry was subjected to a preliminary rheological examination in order to determine the characteristics of its rheological parameters. The resulting flow curve with regression is shown in Fig. 6. This curve describes a relationship between the tangential stress and the shear rate. The values of the flow behaviour index *n* and the flow consistency index *K* according to Ostwald - de Waele rheological model were determined by linear regression of the experimental data and presented in the logarithmic scale.

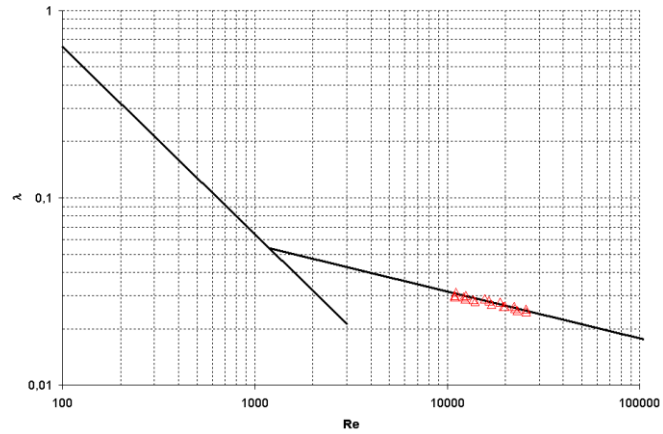

Fig. 7. Comparison of friction factor λ (measured – red, Blasius formula – black) in turbulent flow using a capillary-pipe rheometer

The obtained results of the flow behaviour index *n* for the tested slurry are close to 1, so the tested slurry can be treated as a Newtonian liquid and the flow resistance can be presented in classic Reynolds number (*Re*)-lambda (λ) layout.

The aim of further research was to determine the curve of flow resistance of the slurry flowing through the examined pipeline. The studies were carried out in a tube of an inner diameter D = 13.04 mm. The measurements were made with the application of a capillary-pipe rheometer built at the Division of Fluid Mechanics [5]. This setup allows to conduct a comprehensive identification of the rheological properties of complex rheological fluids in the laboratory. The test results are shown in Fig. 5.

4. Derivation of formula for calculating the equivalent pipeline diameter

The formula for calculating the dimensionless equivalent pipeline diameter can be derived on the basis of the Reynolds number formula and the Darcy-Weisbach equation:

$$Re = \frac{D \cdot u}{\nu} \tag{1}$$

$$\lambda = \frac{D \cdot \Delta p}{2 \cdot \rho \cdot u^2 \cdot L} \tag{2}$$

where

D – the nominal pipeline diameter,
u – the mean flow velocity,
ρ – the density of slurry,
ν – the kinematic viscosity coefficient of the slurry,
Δp – the pressure drop in the pipeline,
L – the pipeline length.

Basing on the resistance curve, it can be found that the Darcy friction factor λ in the turbulent flow can be approximated with the Blasius formula:

$$\lambda = \frac{0.3164}{\sqrt[4]{\frac{D \cdot u}{\nu}}} = \frac{0.3164}{\sqrt[4]{\frac{4 \cdot Q}{\pi \cdot D \cdot \nu}}} \tag{3}$$

where

Q – the volume flow rate.

When replacing the mean velocity with the volume flow rate, the Darcy-Weisbach equation can be written as follows:

$$\Delta p = \lambda \cdot \frac{8 \cdot L}{D^5} \cdot \frac{\rho \cdot Q^2}{\pi^2} \tag{4}$$

Then, the friction factor λ can be described by the relation:

$$\lambda = \frac{\pi^2 \cdot \Delta p}{8 \cdot L \cdot \rho} \cdot \frac{\cdot d^5}{Q^2} \tag{5}$$

where

d – the actual pipeline diameter related to the free cross-sectional area.

When equalising (3) and (5) and taking into account the actual diameter, a following relation can be obtained:

$$d = \left(3.398 \cdot 10^{-3} \cdot L^4 \cdot \rho^4 \cdot \nu \cdot \frac{Q^7}{\Delta p^4} \right)^{\frac{1}{19}} \tag{6}$$

For a fluid flowing through a pipeline, it can be assumed that the values in equation (6) are constant, except for the volume flow rate Q and the pressure drop Δp. Hence, the dependence (6) can be represented as:

$$d = B \cdot \left(\frac{Q^7}{\Delta p^4} \right)^{\frac{1}{19}} \tag{7}$$

where

B – the constant describing the liquid and the pipeline parameters.

The dimensionless equivalent pipeline diameter d_e has been defined as a ratio of the actual pipeline diameter d to the nominal pipeline diameter D (it is a relative quantity):

$$d_e = \frac{d}{D} \tag{8}$$

5. Results and discussion

The developed method for determining the dimensionless equivalent pipeline diameter has been applied for monitoring the bore of a selected industrial pipeline. An additional object of monitoring was a verification of the effectiveness of the action of chemical additive preventing crystallisation and scale deposition in the pipeline. The composition of the chemical additive is confidential. Earlier, during the hydrotransport, the examined pipeline grew over with scale and it was necessary to clean it periodically.

The tests proved the correctness of the developed method of pipeline monitoring: it indicated a gradual decrease of the dimensionless equivalent pipeline diameter (Fig. 6 left – a declined line with time) in normal operation. The application of the mentioned chemical additive caused a set-back of the crystallisation and scale deposition in the pipeline (Fig. 6 right – the horizontal line, a constant value of the dimensionless equivalent pipeline diameter).

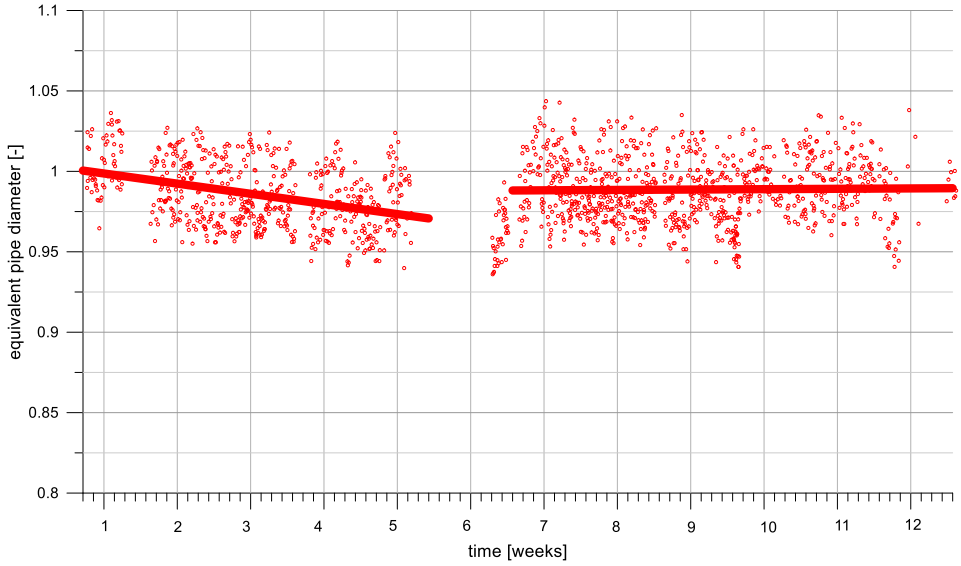

Fig. 6. The results of tests of the hydrotransport pipeline dimensionless equivalent diameter (a linear approximation)

The presented method can be applied in industrial practice for monitoring the bores ofpipelines in case of varying flow rates.

References

[1] Kaushai D. R., *Solids concentration profiles and pressure drop in pipeline flow of multisized particulate slurries,* International Journal of Multiphase Flow, vol. 28(10), 2002, 1697-1717.

[2] Kaushai D. R., *Concentration at the pipe bottom at deposition velocity for transportation of commercial slurries through pipeline,* Powder Technology, vol. 125(1), 2002, 89-101.

[3] Bednarski S., Komorowicz T., Pabiś A., *Sposób hydraulicznego transportu na duże odległości materiałów poliziarnistych i urządzenie do wyprowadzania frakcji grubej z rurociągu hydrotransportu*, Patent RP Nr 205676 z dn. 31.05.2010 (WUP 05/10)

[4] Matras Z., *Metoda identyfikacji reologicznej cieczy*, Inżynieria i Aparatura Chemiczna, Nr 4-5, 2007, 83-86.

[5] Matras Z., Walczak S., *Reometr kapilarno-rurowy,* Czasopismo Techniczne, Z. 5-M, 2003, 359-370.

TECHNICAL TRANSACTIONS | CZASOPISMO TECHNICZNE
MECHANICS | MECHANIKA
2-M/2016

JANUSZ KRAWCZYK*, ANDRZEJ HERYAN, ŁUKASZ WAWSZCZAK**

ENVIRONMENTAL INTERACTION ASSESSMENT OF VOC'S EMISSION FROM PRINTING PLANT HOT ROTARY HEAT-SET

OCENA ODDZIAŁYWANIA NA ŚRODOWISKO EMISJI LZO W PROCESIE DRUKU GORĄCY OFFSET ROTACYJNY (HEAT-SET)

Abstract

The paper presents an analysis of gaseous emissions arising from the operations of printing using a printing process hot offset rotary. The first part presents the general characteristics of the process and the paint used. The following part shows the results of modelling the emission of pollutants according to the efficiency of the cleaning system, as well as depending on other parameters influencing the dispersion process impurities.

Keywords: modelling of emissions, printing industry, rotary offset (heat-set)

Streszczenie

W pracy przedstawiono analizę emisji zanieczyszczeń (LZO) powstających w wyniku działalności zakładu poligraficznego wykorzystującego w procesie druku gorący offset rotacyjny. Część pierwsza prezentuje ogólną charakterystykę procesu oraz wykorzystywanych farb. W dalszej części przedstawiono wyniki modelowanie emisji zanieczyszczeń w zależności od sprawności układu oczyszczającego, a także w zależności od innych parametrów wpływających na proces dyspersji zanieczyszczeń.

Słowa kluczowe: modelowanie emisji zanieczyszczeń, gorący offset rotacyjny

DOI:

* PhD. DSc. Eng. Janusz Krawczyk, prof. CUT, Institute of Thermal and Process Engineering, Faculty of Mechanical Engineering, Cracow University of Technology.

** DSc. Andrzej Heryan, MSc. Łukasz Wawszczak, Department of Scientific Research "Eko-Hera", Cracow.

1. Introduction

From the time of Johannes Gutenberg, who is considered to be one of the precursors of industrial printing method, printing processes have undergone many changes and modifications. Constant competition forces the use of ever newer solutions to optimise printing costs, while maintaining appropriate quality parameters. In the case of multi-format printing, a frequently used technique is the process of printing by hot rotary heat-set, which enables to print significant amounts of paper in a relatively short time. Multi-format printing implies the use of the equipment of printing machines that are significant sources of emissions of dust and gas pollutants, mainly organic compounds.

The paper presents an analysis of the emission of dust and gas emitted by modern offset printing, in which a large part of printing is done on automatic thermoforming machines.

2. Analysis of the sample printing offset in the context of emissions of dust and gas into the atmosphere

2.1. The object of the study

The object of the analysed company is printing activity.

The printing plant prints colour magazines, newspapers, advertising catalogues and leaflets, etc. A flat indirect (offset) printing technique with the fixation of paint at elevated temperature (*heat-set*) applies in the production process.

The printing plant is located in one of the outlying districts of the city in an area planned for the activities of production and services. The immediate surroundings of the plant are the lands used for the purposes of business production and service.

2.2. Printing technology

Web offset printing is a relatively cheap and quick way to obtain a large number of prints. Lightweight aluminium matrix formed on the drum printing sends an image on an intermediate drum with a rubber coating, which in turn transfers the image to paper. Hence, there is the second important definition of this technique – *indirect* print. This printing unit is capable of rotation at high speed.

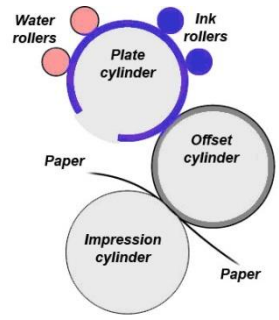

Fig. 1. Offset printing

Common use of colour web offset printing in addition to speed arises from the variety of possible use of media, i.e.: from coated paper (*non-absorbent* surface), the newsprint to cardboard (substrate *absorbent*).

2.3. Raw materials used in the printing process

Due to the volume of raw materials, which are used and the characteristics of the fusing mechanisms of printing inks in the process of web offset printing, determination of the characteristics of used inks is essential in order to assess the impact of the installation on the atmospheric air. Fusing mechanisms of inks of the type of *heat-set* occur due to the influence of the delivery of significant amounts of heat (blow heat, drying tunnels, which are heated by gas burning, etc.). Depending on the drying system, the paper has a temperature ranging from 90 to 150°C, which corresponds to a temperature of 200÷300°C of the drying agent. At these high temperatures, it evaporates mineral oil, which is a solvent for paints of *heat-set* type and water (moisture) from paper and wetting agents.

For the production of *heat-set* paints, adhesives containing the composition of phenol-formaldehyde resins and alkyd resins, polymerised linseed oil, mineral oil (fraction with a boiling point of 240÷300°C), colorants, tinters and excipients are used. Mineral oils used for the production of paints of the type *heat-set* are special species usually of naphthenic mineral oils. They are refined in such a way that they are almost odourless and colourless. Depending on the distillation, the boiling point is in the range of 240÷270°C, 260÷290 and 270÷300°C. In the *halftone* paints, mineral oils vary in their boiling points because paints of different colours are to be traversed in the printing path of different distances. Therefore, a black colour which has the longest distance to go, has in its composition an oil having the lowest volatility. The yellow ink goes in turn the shortest possible route and, therefore, contains mineral oil with high volatility [1].

2.4. Characteristics of emerging emissions

For the production of *heat-set* paints, mineral oils containing aromatic compounds are used. In addition, wetting agents containing alcohol, iso-propyl or organic alternatives are used in the printing process. Depending on the drying system, it evaporates mineral oil, in varying amounts, which is a solvent of *heat-set* paint and water (moisture) from paper and wetting agents. The main pollution are therefore volatile organic compounds (VOCs) emitted in the installation in the amount of approx. 30 kg/h of VOC.

Furthermore, due to the demand on the substantial amount of thermal energy for the drying process of the paper, the fuel is typically used for natural gas, in which the products of combustion (mainly nitrogen oxides, carbon monoxide, carbon dioxide) also flow to the atmosphere.

2.5. Legal requirements relating to the issue of emerging contaminants

Legal requirements for environmental protection regulate the Framework Law of 27 April 2001. Environmental Protection Law (Polish Journal of Laws of 2013 item. 1232, as amended.) and implementing acts to the above Law. According to the Regulation of the Minister of Environment of 26 January 2010 on reference values for certain substances in the air (Polish Journal of Laws of 2010 no. 16 item. 87) [2] plant, which leads pollution in

an organised manner to the atmosphere is obliged to use solutions that will not exceed the permissible reference value, ice. appropriate normative values concerning excess emissions will be saved.

Moreover, in the case of large printing plants, which consume large quantities of raw materials (this translates into considerable use of VOC), additional requirements apply for the protection of atmospheric air as defined in the Regulation of the Minister of Environment of 4 November 2014 on emission standards for certain types of installations, combustion plants and equipment incineration or co-incineration of waste [3]. The processes carried out in the system used in this printing plant include (in accordance with Annex 7 to the above regulation to hot offset rotary process, which identified the following emission standards (Annex 8 point 1):

For VOC usage> 25 Mg / year
S1 = 20 mg / m^3 VOC
(counted on organic carbon).

2.5. Methods of reducing emissions of pollutants

Systems of injecting air containing solvents are usually designed to maintain an adequate atmosphere within the workspaces and equipment significantly below the permissible concentrations of pollutants. Deriving solvents from the key sources can lead to disposal system of waste gases because of the need to comply with regulations on environmental protection. When designing injecting systems, some things must be taken into account:

- the amount of the discharged air,
- level of solvent,
- type of utilisation, its cost-effectiveness and impact on the environment,
- number of working hours per year.

When injecting a large amount of air relative to the solvent increases the size of reduction system, and may increase the amount of energy required as drive, which supports combustion. In the case of large printing plants using web offset printing generally used methods are based on oxidation of pollutants through the use of thermal afterburners. In certain cases, it is reasonable to use catalytic afterburners, which through the use of a catalyst operate at lower temperatures than thermal afterburners (this translates into energy savings).

Moreover, in the case of large printing plants, there are also solutions in which every single print line may have a dedicated system of waste gas treatment. For example, if it is integrated into the dryer(s), the system allows for easy use of heat or exhaust gases for heating the air in the dryer. Printing presses in such a case depend on the central system of waste gases.

2.6. Sources of emissions in the tested offset printing plant

When injecting pollutants into the air is related to the functioning of the basic technological processes (sources of emissions from the production equipment). Vapours produced during drying of the printed paper web are extracted on machines and routed to a

thermal afterburner, which reduces pollution. Burners with the installed thermal capacity in the range 850÷1600 kW function for particular drying tunnels of web offset printing machines for drying the printed paper.

2.7. Maps of the distribution of concentrations of selected pollutants around the premises

Simulations of the changes of individual pollutants concentrations in the atmosphere were made using modelling software a steady-state Gaussian plume model on the basis of measurements of pollutants emissions carried out by an accredited laboratory according to Polish reference methodology [2]. The resulting simulations are expressed as map of spatial concentration distribution and demonstrated in Figs. 2 a and b to show the greatest concentration of major pollutants in the vicinity of the plant.

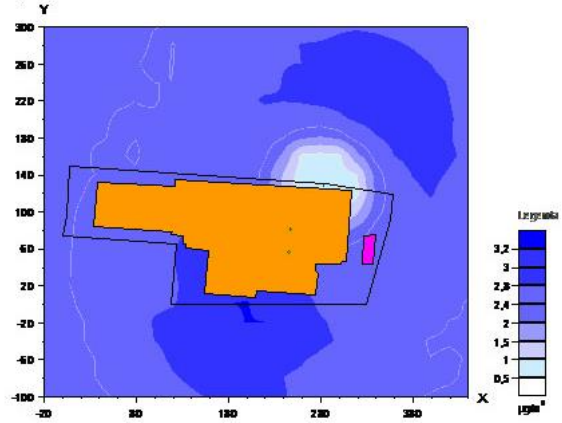

Fig. 2a. The map showing isolines of the peak concentrations of selected pollutants (aromatic hydrocarbons)

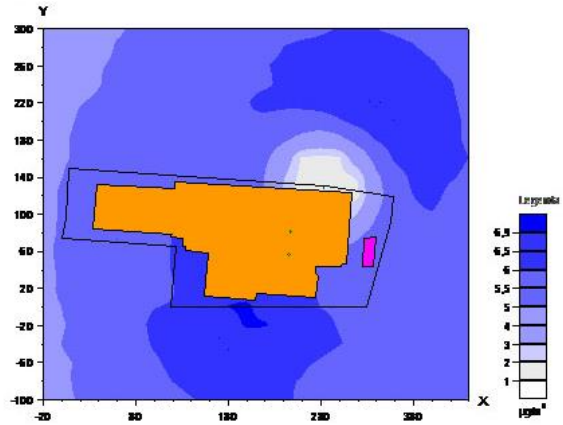

Fig. 2b. The map showing isolines of the peak concentrations of selected pollutants (aliphatic hydrocarbons)

3. Calculation of the concentrations of dust and gas pollutants emitted into the atmosphere depending on changes of selected technical parameters of the installation

According to the measurements carried out by the accredited laboratory, the afterburner efficiency in the test plant is approx. 99% of VOC. The tables 1 and 2 show how the change in volume would have affected the maximum concentration of emitted pollutants (VOC) by using afterburner with a different efficiency, as well the change of peak levels when choosing the other technical characteristics of the emitter (height, diameter) was presented.

This simulation was performed to investigate whether the use of relatively cheap and fast to carry out technical solutions (change in height or diameter of the emitter) instead of afterburners with extremely high efficiency, can significantly reduce the impact of printing plant on the atmospheric air.

Table 1

The average increase in the concentrations of pollutants compared to the actual afterburner efficiency

Pollution	**Maximum concentration of impurities (depending on the efficiency of the afterburner) [mg/m^3]**				
	95%	**96%**	**97%**	**98%**	**99%**
Benzene [1]	2.03	1.84	1.64	1.44	1.24
Xylene [2]	2.08	1.74	1.39	1.04	0.69
Styrene[3]	1.09	0.90	0.70	0.50	0.30
Toluene [4]	1.69	1.41	1.12	0.84	0.56
Aromatic hydrocarbons [5]	14.42	11.71	8.99	6.28	3.57
Ethylbenzene [6]	1.21	1.02	0.82	0.62	0.42
Aliphatic hydrocarbons [7]	31.34	25.43	19.53	13.63	7.72
The average increase in the concentrations of pollutants compared to the actual afterburner efficiency [%]	+ 218.28	+ 163.67	+ 109.10	+ 54.52	–

When changing the performance of an afterburner from 99% to 95%, we can observe up to 218% average increase in the concentration of pollutants in the air. Even in the case of restriction of performance of afterburner from 99% to 98% we can observe up to 50% average increase in peak concentrations in the atmosphere. A summary of calculation results is also presented graphically in the chart below:

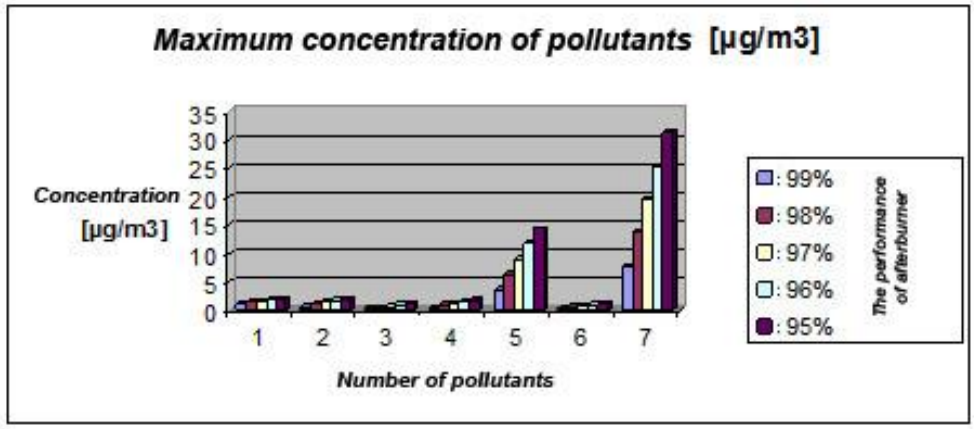

Fig. 3. A graph showing maximum concentration of selected impurities depending on the performance of afterburner

The change of the height of the emitter can affect the concentration pollutants as follows:

Table 2

The average decrease in the concentrations of pollutants depending on the height of emitter of afterburner

	Maximum concentration of impurities (depending on the amount of boost emitter) [m]				
	14	**16**	**18**	**20**	**22**
The average decrease in the concentrations of pollutants depending on the height of emitter of afterburner [%]	–	- 6.05	- 11.32	- 14.36	- 18.31

When changing the diameter of the emitter, concentrations of pollutants can achieve the values as follows:

Table 3

The average decrease in the concentrations of pollutants depending on the diameter of emitter of afterburner

	Maximum concentration of impurities (depending on the diameter of emitter) [m]				
	1,4	**1,3**	**1,2**	**1,1**	**1,0**
The average decrease in the concentrations of pollutants depending on the diameter of emitter of afterburner [%]	–	- 2.46	- 4.96	- 6.30	- 9.18

4. Conclusions

- From the presented analysis of emissions (VOC) resulting from the operations of the printing plant using hot offset, in a printing process, we can conclude that the concentrations of VOCs are within the range of permissible emission standards.
- Change of the performance of afterburner to a varying degrees results in the maximum concentration of each pollutant.
- Change of performance of afterburner from 99% to 98% causes – according to modelling, which was carried out – more than 50% increase in peak concentrations of impurities.
- Change of the diameter of the emitter by about 0.2÷0.4 meter or change of the height of the emitter by 2 to 6 meters allows for a reduction of the maximum concentrations of pollutants by approx. 5 to 15%.
- In the case of small deviations from the normative reference values of pollutants in ambient air can be considered as a method to reduce nuisance on a change of parameters of emitter (height, diameter).

References

[1] Jakucewicz S., *Farby drukowe*, Michael Huber Polska Sp. z o.o., Wrocław 2001.
[2] Regulation of the Minister of Environment of 26 January 2010 on *reference values for certain substances in the air*, Polish Journal of Laws of 2010, no. 16, item 87.
[3] Regulation of the Minister of Environment of 4 November 2014 on *emission standards for certain types of installations, combustion plants and equipment incineration or co-incineration of waste*, Polish Journal of Laws of 2014, vol. 1, item 1546.

TECHNICAL TRANSACTIONS | CZASOPISMO TECHNICZNE
MECHANICS | MECHANIKA
2-M/2016

ANDREY A. LIPIN, ALEKSANDR G. LIPIN*, RYSZARD WÓJTOWICZ**

MODELLING THE COMBINED POLYMERISATION AND DRYING OF POLYACRYLAMIDE PREPOLYMER

MODELOWANIE ŁĄCZONEGO PROCESU POLIMERYZACJI I SUSZENIA DLA PREPOLIMERU POLIAKRYLOAMIDOWEGO

Abstract

In the paper, the mathematical model of combined polymerisation and drying of polyacrylamide prepolymer is presented. It allows to predict the change of monomer conversion degree, polymer moisture content, the temperatures of gas and polymer in the dryer as well as dryer sizes. Using a developed model, values of technological parameters were established, providing faster polymerisation than in the case of drying.

Keywords: *acrylamide, polyacrylamide, polymerization, aqua solution, drying, combined process, mathematical model, belt dryer*

Streszczenie

W ramach pracy stworzono model matematyczny dla łączonego procesu polimeryzacji i suszenia prepolimeru poliakryloamidowego. Proponowany model umożliwia wyznaczenie zmiany stopnia konwersji monomeru, zawartość wilgoci polimeru, temperatury gazu i polimeru w suszarce oraz wymiary suszarki. Z użyciem modelu wyznaczono wartości parametrów technologicznych procesu, umożliwiając szybszy proces polimeryzacji w porównaniu z suszeniem w aparacie.

S*łowa kluczowe:* *akryloamid, poliakryloamid, polimeryzacja, roztwór wodny, suszenie, proces łączony, model matematyczny, suszarka taśmowa*

DOI:

* PhD. DSc. Eng. Andrey A. Lipin, DSc. Eng. Aleksandr G. Lipin, Faculty of Chemical Engineering and Cybernetics, Ivanovo State University of Chemistry and Technology.

** DSc. Eng. Ryszard Wójtowicz, Institute of Thermal and Process Engineering, Faculty of Mechanical Engineering, Cracow University of Technology.

1. Introduction

Polyacrylamide is a water soluble polymer. Owing to the unique combination of properties, it is widely used as thickener, film former, stabiliser of suspensions, sizing agent in the textile industry, coagulant and flocculant, agent reducing of hydraulic resistance, soil builder as well as protective reagent in the drilling technique [1]. This necessitates a significant increase in the production efficiency of polyacrylamide.

One way of improving polyacrylamide production technology is to combine prepolymer polymerisation to high conversion degree with drying [2]. In the laboratory scale, this process was implemented in the belt drier with radiation-convective heat supply. For industrial production of polyacrylamide with the use of this method, it is necessary to design the apparatus of industrial-scale. A suitable tool for the calculation and prediction of technological and constructional parameters of industrial-scale apparatus is the mathematical modelling method. Therefore, developing a mathematical model of the combined polymerisation and drying is an important goal.

2. Mathematical model

The combined process of polymerisation and drying of polyacrylamide prepolymer is carried out in a belt drier with radiation-convective heat supply. Infrared drying is used because it allows to provide high values of the specific heat flow. It is necessary due to a high moisture content of prepolymer (about 60%). As a source of infrared radiation, it is advisable to use gas-fired panels. Flue gases move inside these panels, heating them. Air serves to remove water vapour and it moves in the dryer by natural convection. The prepolymer is fed into the dryer as a gel. It moves by belt countercurrent to air. The diagram of dryer is shown in Fig. 1.

The mathematical model of the combined process includes a system of equations (1 - 5), complemented by equations of chemical kinetics (6 - 10) with closing relations (11 - 19).

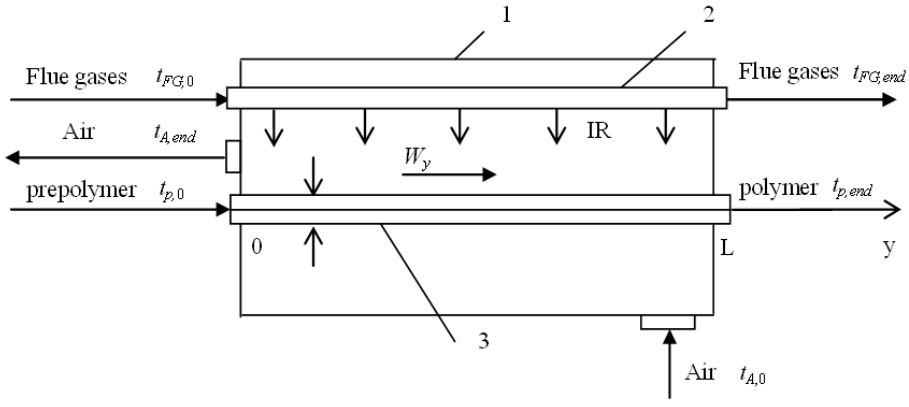

Fig.1. The diagram of dryer: 1 – the shell; 2 – heat-radiating panel; 3 – material

Changes of heat-radiating panel temperature T_{IR}, flue gases temperature T_{FG}, moisture content U and drying polymer temperature T_p upon the dryer length are calculated by solving the system of equations (1 - 5).

$$\alpha_{FG}\left(T_{FG}-T_{IR}\right)=c_{12}\left[\left(\frac{T_{IR}}{100}\right)^4-\left(\frac{T_p}{100}\right)^4\right] \tag{1}$$

$$\frac{\mathrm{d}t_{FG}}{\mathrm{d}y}=-\frac{\alpha_{FG}\cdot B\cdot\left(t_{FG}-t_{IR}\right)}{G_{FG}\cdot c_{FG}} \tag{2}$$

$$\frac{\mathrm{d}t_p}{\mathrm{d}y}=\frac{c_{12}\cdot\left[\left(\frac{T_{IR}}{100}\right)^4-\left(\frac{T_p}{100}\right)^4\right]\cdot B+r^*\frac{\mathrm{d}U}{\mathrm{d}y}\cdot G_p+\alpha_A\cdot\left(t_A-t_p\right)\cdot B+\Delta H\cdot\left(\frac{\mathrm{d}C_M}{\mathrm{d}y}\right)\cdot W_y\cdot B\cdot h}{G_p\cdot\left(c_p+c_w\cdot U\right)} \tag{3}$$

$$\frac{\mathrm{d}U}{\mathrm{d}y}=\frac{\beta\cdot B\cdot\left(p_p-p_A\right)}{G_p} \tag{4}$$

$$p_p=p_s\left(t_p\right)\cdot\psi\left(U\right) \tag{5}$$

where: $\psi(U)$ – empirical coefficient considering reduction of water vapour partial pressure by reducing the moisture content of the prepolymer.

Initial conditions for equations (2)-(4) are as follows: $t_{FG}(0) = t_{FG,0}$, $t_p(0) = t_{p,0}$, $U(0)=U_0$.

The polymerisation kinetics was described in [3]. Free radical-forming reaction, growth and chain termination reactions were considered having simulated of the acrylamide radical polymerisation kinetics, initiated by a redox system.

The system of kinetic equations for concentrations of redox system compounds (oxidant and reductant), monomer concentration, and initial moments of the molecular weight distribution of both active and inactive chains, is as follows:

$$\frac{\mathrm{d}I}{\mathrm{d}y}=-\frac{a\cdot k_i\cdot I^a\cdot J^b}{W_y} \tag{6}$$

$$\frac{\mathrm{d}J}{\mathrm{d}y}=\frac{-b\cdot k_i\cdot I^a\cdot J^b}{W_y} \tag{7}$$

$$\frac{\mathrm{d}C_M}{\mathrm{d}y}=\frac{-k_p\cdot C_M\cdot\mu_0}{W_y} \tag{8}$$

$$\frac{d\mu_0}{dy} = \frac{f_i \cdot k_i \cdot I^a \cdot J^b - k_{td} \cdot \mu_0^{\ 2}}{W_y} \tag{9}$$

$$\frac{d\lambda_0}{dy} = \frac{k_{td} \cdot \mu_0^{\ 2}}{W_y} \tag{10}$$

Initial conditions for the system of differential equations (6 - 10) are as follows: $\mu_0(0) = \lambda_0(0) = 0$, $C_M(0) = C_{M,0}$, $I(0) = I_0$, $J(0) = J_0$.
The average value of the polymer molecular weight was predicted by:

$$\overline{M}\ n = \frac{M_M \cdot \left(C_{M,0} - C_M\right)}{\mu_0 + \lambda_0} \tag{11}$$

Constants of elementary reactions rates were calculated by following equations:

$$k_i = 1.039 \cdot 10^8 \cdot \exp\left(-\frac{42000}{R \cdot T}\right) \tag{12}$$

$$k_p = 0.8 \cdot 10^7 \cdot \exp\left(-\frac{11700}{R \cdot T}\right) \tag{13}$$

$$k_{td}^0 = 6.8 \cdot 10^{11} \cdot \exp\left(-\frac{11700}{R \cdot T}\right) \tag{14}$$

Laws of change of growth and chain termination rate constants with conversion increasing are approximated by the following dependencies:

$$\frac{k_{td}}{k_{td}^0} = \frac{1}{1 + 122.2 \cdot X^2} \tag{15}$$

$$\frac{f_i}{f_i^0} = \frac{1}{1 + s \cdot X^m} \tag{16}$$

$$m = 4 + 0.2 \cdot t \tag{17}$$

$$s = 121767 + 0.395 \cdot t^3 - 23202 \cdot t^{0.5} + 7.418 \cdot 10^{14} \cdot e^{-t} \tag{18}$$

$$X = 1 - \frac{C_M}{C_{M,0}} \tag{19}$$

The system of equations (1 - 19) was solved numerically by means of the Mathcad software. Runge-Kutta 4th order numerical method was used. Mesh with step Δy = 0.001 m was used along the dryer length.

Proposed model has been practically validated. In the laboratory scale experiments two technological parameters were measured: the temperature and moisture content of the polymer. The relative error for temperature was 5.5%, for moisture content it was 7%. The relative error in both cases did not exceed 10%, so we can make a conclusion about the adequacy of the proposed mathematical model.

3. Results and discussion

Computation of the dryer was performed using the developed mathematical model. Initial conditions of the processes occurring in the prepolymer for the drying step are characteristic of the reaction mass obtained under isothermal conditions at temperature of 30°C. The initial moisture content is 1 kg/kg, degree of conversion is 50%. Calculations were performed for a 2 mm thickness of the prepolymer layer.

Figure 2 presents the change of prepolymer temperature t, air temperature t_A, heat-radiating panel temperature t_{IR} and flue-gases temperature t_{FG} along the dryer length. The model considers the inconstancy of flue gases temperature t_{FG} inside of heat-radiating panels. Flue gases move inside these panels heating them; therefore, the temperature of radiation surface t_{IR} changes also. The prepolymer is heated by a stream of infrared radiation. Its temperature changes from 25°C to 95°C. The air moves counter current to prepolymer and heats from 20°C till 93°C (Fig. 2).

Figure 3 shows the change of prepolymer moisture content U and the degree of monomer conversion X during time of combined polymerisation and drying processes. The initial stage of the process is characterised by rapid growth of the prepolymer temperature (see curve 1 in Fig. 2), which leads to a reduction of diffusion limitations on the initiation reaction and chain growth reaction, and hence to an increase of the polymerisation rate. Water is a required component of the reaction mass. The prepolymer moisture content decreases rapidly, but it is sufficient to complete the polymerisation. Thus, at a conversion of 99%, the polymer moisture content is about 0.2 kg/kg. Figure 3 shows that the monomer conversion increases rapidly and achieves 99.5% conversion degree on the 2/3 of dryer length. It corresponds to 4 meters. The prepolymer moisture content reaches the required value only at 6 meters. So, we can conclude that for the chosen range of parameters, the

polymerisation proceeds faster than drying. This is achieved due to drying being carried out by natural air convection. Heating the material is provided by IR radiation sources.

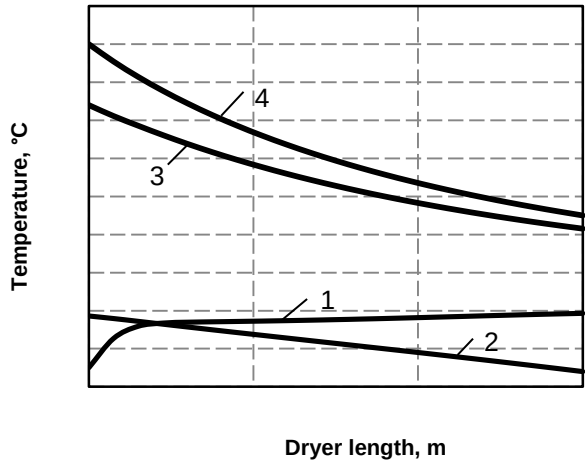

Fig. 2. The temperature upon the dryer length
1 – polymer temperature; 2 – air temperature; 3 – heat-radiating panel temperature; 4 – flue gases temperature

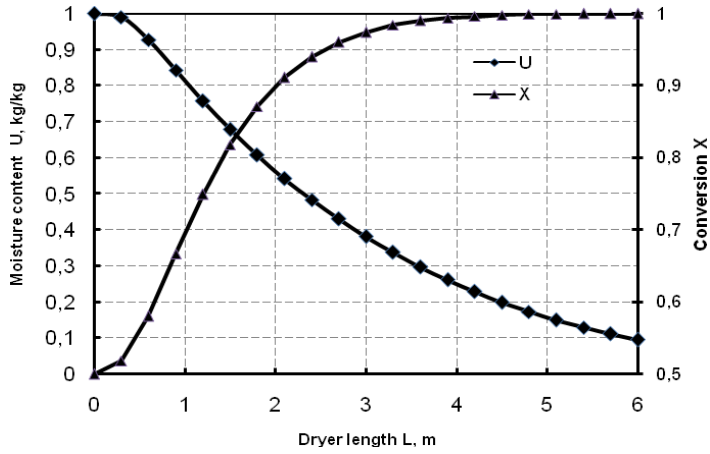

Fig. 3. The polymer moisture content *U* and monomer conversion *X* upon the dryer length *L*

Thus, the developed mathematical model describes the kinetic laws of combined polymerisation and drying as well as the influence of polymerisation kinetics on the heat and mass transfer. It allows to predict the change of monomer conversion degree, moisture content of polymer, temperatures of gas and polymer in the dryer as well as dryer sizes.

In a practical industrial scale application the combined polymerisation and drying of polyacrylamide prepolymer can be carried out in existing commercial IR dryers. But these dryers should be upgraded for new product.

N o m e n c l a t u r e

- a, b – stoichiometric factors, – ;
- B – belt length, m;
- c_{12} – mutual emissivity coefficient, W m^{-2} K^{-4};
- C_M – monomer concentration, [mole l^{-1};
- c – heat capacity, J kg^{-1} K^{-1};
- f_i – initiation efficiency, – ;
- G – mass flow, kg s^{-1};
- h – gel layer thickness, m;
- I – oxidant concentration, mole l^{-1};
- J – reductant concentration, mole l^{-1};
- k_p – chain growth rate constant, l $mole^{-1}$ s^{-1};
- k_{td} – chain termination rate constant, l $mole^{-1}$ s^{-1};
- k_i – initiation rate constant, l^{a+b-1} $mole^{1-a-b}$ s^{-1};
- m – empirical coefficient, – ;
- p – pressure, [Pa;
- R – universal gas constant, J $mole^{-1}$ K^{-1};
- r^* – vaporisation heat, J kg^{-1};
- s – empirical coefficient – ;
- t – temperature, °C;
- T – temperature, °K;
- U – moisture content, kg kg^{-1};
- W_y – velocity of the prepolymer, m s^{-1};
- X – degree of monomer conversion, – ;
- y – coordinate along the dryer length, m;
- α_{FG} – heat-transfer coefficient from flue gases to heat radiating panel, W m^{-2} K^{-1};
- α_A – heat-transfer coefficient from polymer to air, W m^{-2} K^{-1};
- β – mass transfer coefficient, kg m^{-2} s^{-1} Pa^{-1};
- ΔH – heat of reaction, J $mole^{-1}$;
- μ_0 – initial moment of the molecular weight distribution of active chains, mole l^{-1};
- λ_0 – initial moment of the molecular weight distribution of inactive chains, mole l^{-1};

Subscripts

- A – air
- FG – flue gases

IR – infrared radiation
w – water
0 – initial value
end – end value

References

[1] Abramova L. I., *Polyacrylamide*, Khimiya, Moscow 1992.
[2] Lipin A. A., Lipin A. G., Shibashov A. V. *Polyacrylamide synthesis using polymerisation-desorption process*, Izv. Vyssh. Uchebn. Zaved. Khim., Khim. Tekhnol. 2015. Vol. 58(1), 2015, 51-53.
[3] Lipin A. A., Shibashov A. V., Lipin A. G. *Modelling of acrylamide polymerization in the concentrated water solutions*, Izv. Vyssh. Uchebn. Zaved. Khim., Khim. Tekhnol., vol. 57(12), 2014, 85-87.

TECHNICAL TRANSACTIONS | CZASOPISMO TECHNICZNE
MECHANICS | MECHANIKA
2-M/2016

ZBIGNIEW MATRAS, BARTOSZ KOPICZAK*

THE POLYMER-MICELLAR AGGREGATES AS AN EFFICIENT REDUCER OF THE ENERGY LOSSES IN PIPE FLOW

AGREGATY POLIMEROWO-MICELARNE JAKO EFEKTYWNY REDUKTOR STRAT ENERGETYCZNYCH W PRZEPŁYWACH RUROWYCH

Abstract

The paper presents polymer-micellar aggregates as efficient drag reducers of the energy losses in straight pipe flow. A small amount of high molecular polymers: Polyethylene Oxide, Cetyltrimetyl Ammonium Bromide surfactant and Sodium Salicylate salt additives, are applied to obtain polymer-micellar aggregates formation. An analysis of how polymer-micellar additives influence the shape and character of flow resistance curves has been performed. It is documented that for polymer-micellar solutions the stable transitional zone between, the laminar and the turbulent flows are **extended** toward higher values of the Reynolds number. Occurrence of the third turbulent zone of drag reduction is also observed.

Keywords: Energy losses, pipe flow, flow laminarisation, aggregate

Streszczenie

W artykule przedstawiono agregaty polimerowo-micelarne jako efektywny reduktor strat energetycznych w przepływach rurowych. Do procesu formowania agregatów wykorzystano niewielkie ilości wielkocząsteczkowego politlenku etylenu i substancji powierzchniowo czynnej bromku heksadecylotrójmetyloamoniowego z dodatkiem salicylanu sodu. Dokonano analizy wpływu roztworu polimerowo-micelarnego na kształt i charakter krzywych oporów przepływu. Dla analizowanych roztworów zaobserwowano rozszerzenie stabilnej strefy przejściowej w kierunku większych wartości liczby Reynoldsa. Zaobserwowano również trzecią, turbulentną strefę redukcji oporów przepływu.

Słowa kluczowe: Straty energetyczne, przepływ rurowy, laminaryzacja przepływu, agregat

DOI:

* Prof. PhD. DSc. Eng. Zbigniew Matras, MSc. Eng. Bartosz Kopiczak, Institute of Thermal and Process Engineering, Faculty of Mechanical Engineering, Cracow University of Technology.

1. Introduction

Drag reducers have been widely investigated for more than 60 years, since the first observations of drag reduction in turbulent flows was documented by Toms [1] and Mysels [2]. Since then, the abnormal flow drag reduction by surfactant or polymer additives has been intensively examined and described in the subject literature [3, 4, 5, 6, 7, 8]. This phenomenon allows for a significant increase of the flow rate without increasing power demand, or vice versa – to reduce power demand, while maintaining a constant flow rate. It provides large potential possibilities for the application of this effect in different industry branches, particularly in the oil industry [7, 9] or in heating [8], firefighting [10], transport of slurries [7], sludge and brines [8, 11]. Causes of the described drag reduction have been perceived in the existence of a new internal solution structure, which is formulated at the moment when the special additives are introduced into the solution. Addition of high molecular weight polymer agents into the solvent results in macromolecule formation, which has a crucial influence on turbulence structure in the flow [4, 7, 12, 13,]). Although, there is still strong debate on whether a single polymer molecule or clusters of polymer molecules are responsible for the drag reduction effect, experimental results clearly prove that even a dozen of the ppm polymer concentration in solvent induces an efficient drag reduction effect in turbulent range of flow [7, 8, 14].

In case of application of surfactants as drag reducing additives, formation of micelle structures is observed [8, 12]. In order to improve the micellarisation process effectiveness in a surfactant solution, small amounts of electrolytes are applied (e.g. sodium salicylate or sodium bromide). At no motion condition, the mentioned structures are chaotic. Only during fluid flow shearing do both macromolecules and micelles start to arrange in a characteristic orientation, in accordance with the principle of minimum resistance. In both surfactant and polymer induced experiments on the drag reduction effect, a hypothetical mechanism of the phenomenon is widely accepted to be found in the interaction between polymer or surfactant molecules with the flow turbulence structure. On the basis of advanced measurement techniques, such as Particle Image Velocimetry (PIV), it is observed that the analysed polymer additives can lead to reduction or elimination of the ejections of low-momentum fluid from the wall region to the outer velocity region [14]. It is also observed that the presence of polymers leads to a decrease in the frequency and the intensity of large-scale ejections when compared to a Newtonian solvent and to the reduction of the magnitude and frequency of the small-scale eddies [15]. Usually, elongational viscosity or elasticity of polymer chain [5, 7] are proposed to explain hypothetical polymer drag reduction mechanics. On the other hand, for a surfactant aqueous solution, which reveals neither viscoelastic properties nor presence of elongational viscosity is observed [8, 13], a local shear-thickening hypothesis is proposed [8, 16].

The novel and poorly recognised effect is a phenomenon of fluid flow drag reduction by the simultaneous addition into the solvent of both high molecular polymer and surfactant with salt. In the published works related to this subject [17, 18, 19], the internal structure formation and chemical reaction process in polymer-micellar solutions are mainly highlighted. First attempts at experimental examination of turbulent wall shear stress and drag reduction effect have been performed [20, 21, 22, 23, 24, 25]. The results confirmed that simultaneous addition into the solvent of the analysed additives combines and intensifies positive features of their purely polymer and micellar analogues, providing

additional extension of drag reduction zones. Moreover, the researchers indicate that this new effect requires a comprehensive experimental study to gain a deeper knowledge of this phenomenon.

Presence of polymer macromolecules in the surfactant solution enhances micelles structures formation ability. It leads to the formation of micellar structure at a lower concentration. The newly formed macromolecules are called aggregates [21, 24]. Adding a slight amount of salt (e.g. NaCl or NaSal) to the high molecular polymer and surfactant solution causes micelles size growth. The number of micelles linked with polymer chains also increases. Furthermore, the addition of the salt can increase the solution viscosity.

The aim of this paper is to perform an analysis of the drag reduction efficiency by simultaneous addition to the solvent both surfactants and high molecular polymer, comparing to the drag reduction effect obtained by addition of pure polymer or pure surfactant agents. The paper presents polymer-micellar aggregates as efficient drag reducers of the energy losses in straight pipe flow

2. Characteristic of polymer-micellar solution aggregates structure

A simultaneous addition of small amounts of polymer and surfactant additives to the solvent triggers an initiation of the micellarisation process at much a lower concentration, comparing to the critical micelle concentration (CMC) [8, 25, 27]. This concentration at which micelles formation initiation occurs in the presence of polymer macromolecules is called the critical aggregation concentration (CAC). Most of experimental studies have shown that a simultaneous addition of small amounts of polymer and surfactant agents to the solvent cause initiation of the micellarisation process at lower concentration, compared to CMC [18, 21]. The newly formed polymer-micelle macromolecules are called aggregates [21, 26, 27]. Upon the experimental study of polymer-micellar aqueous solutions [21, 24, 26], the mechanism of aggregates formation process can be described. Initially, polymer and surfactants molecules occur in the solution independently. The situation significantly changes when a small amount of salt is introduced into the solution. According to the [17, 18, 21, 27], as a result of electrostatic or hydrophobic interaction, the micelles are combined with the polymer chains by coiling around them. The final state of the mixture has single threadlike micelles with a part of polymer macromolecule chain coiled around rigid micelles, forming aggregates.

Consequently, it increases the solution's viscosity values. It should be pointed out that salt additive causes a significant viscosity decrease. It is justified by the more intensive interaction between polymer chains.

3. Material and measurments set-up

Having analysed the level of difficulty of the planned experimental tests and taking into account the type of physical quantities to be measured, the experiment was performed using a modern capillary-pipe rheometer, designed and constructed in the Division of Fluid Mechanics laboratory at the Cracow University of Technology [28]. The device allows the

operator to conduct a comprehensive identification of rheological characteristics of the examined liquid in laboratory conditions.

The versatility of the described capillary-pipe rheometer allows the operator to assign not only classical experimental flow curves in the laminar range of flow, but also to examine and interpret properly the flow characteristics of fluids, which behave differently when compared with purely viscous non-Newtonian fluids in the turbulent flow region. This applies primarily to the solutions of polymers and surfactants, which are the subject of research in this work, as well as to the fluids, which can be considered on the border between the physical continuum and multi-phase system, e.g. rheostable (purely viscous) or viscoelastic suspensions. A schematic diagram of the capillary-pipe rheometer is illustrated in Figure 1.

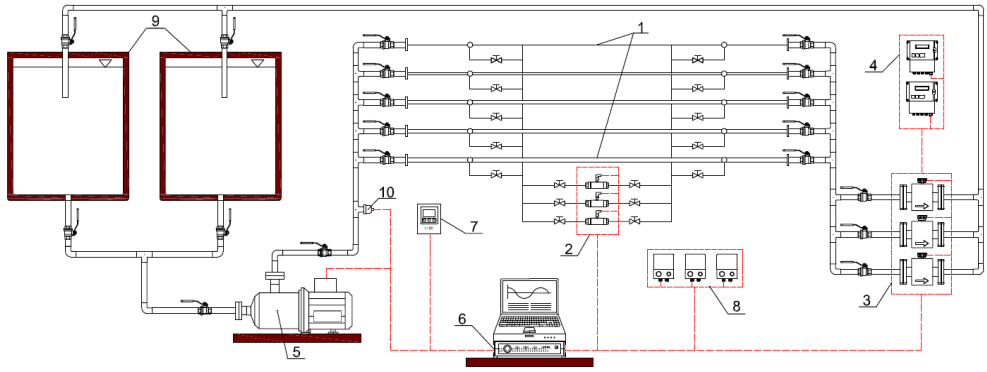

Fig. 1. Diagram of the multifunction capillary-pipe rheometer:
1 – straight capillaries and pipes with circular cross-section; 2 – differential pressure drop sensors PD1 and PDF, 3 – electromagnetic flowmeters; 4 – flowmeter controllers; 5 – Multistage rotodynamic pumps with triple-phase electrical engine; 6 – data acquisition system; 7 – microprocessor frequency converter L100; 8 – amplifiers WP-01A; 9 – tanks; 10 – temperature sensors PT 100

The basic elements of the device are straight copper and stainless steel capillaries and pipes with a circular cross-section (1). They are used for the measurement of fluid flow pressure loss at pipe distance L. Static pressure holes were spotted at distances $L_{inl} = L_{out} \approx 150d$ from the pipe inlet and outlet. This ensures stable flow conditions and eliminates the influence of the so-called "entrance effect."

The fluid flow in the capillary-pipe rheometer is forced by hermetic multistage rotodynamic pumps (5), which suck in the fluid from one of the tanks (9) and then pump it into one of the eight horizontal pipes of different diameters (1). After passing through the electromagnetic flowmeters (3), the fluid returns to the storage tank. The measurements of the pressure losses were performed using PD1 or PDF differential pressure drop sensors (2).

For the current temperature control (possibility of maintaining a constant temperature in the measuring system was provided), a resistive temperature sensor (10) was placed in the fluid supply pipe.

Pumps can work in either series or parallel arrangements, depending on the required flow rate or pressure loss value. This allows the operator to obtain a wide range of Reynolds number reaching the value of 3×10^5 for the measurement system pressure value up to 10 bar, without the loss of fluid continuity (no foaming of the solution or air bubbles).

A microprocessor frequency converter (7) was used to control the pump frequency and consequently the volumetric flow rate. The main element supporting the action of the capillary-pipe rheometer is a multi-channel data acquisition system SPIDER 8 (Hottinger Baldwin Messtechnik), arranged to measure the electrical signals from the different sensors (tension, force, pressure, displacement, acceleration and temperature sensors).

Additionally, large volume tanks (1 m^3) were used to eliminate the effect of foaming of micellar and polymer-micellar solutions and to minimise the influence of the unavoidable degradation of the polymer-micellar aggregates or macromolecular structures on measurement results.

During the preparation of the polymer-surfactant solutions, pH of the chosen drag reducing additives should be particularly considered. Incorrect selection of pH may result in an undesired chemical reaction.

Anionic surfactants cannot be used, while aqueous solutions of certain polymers can have an acidic reaction. Cationic and anionic surfactants can be combined with non-ionic polymer solutions.

After the preliminary study, the following drag reducers have been used for the experimental analysis:

- Poly(ethylene oxide) $[CH_2\ CH_2\ O]_n$ (PEO) – non-ionic polymer with viscosity-based high molecular weight given by the manufacturer equal to $8\cdot10^6$ g/mol^{-1}, purchased from Sigma-Aldrich, Inc.
- Cetyltrimetyl ammonium bromide $[CH_3(CH_2)i_5N(CH_3)_3]+Br\sim$ (CTAB) – cationic surfactant purchased from Sigma-Aldrich, Inc.

In order to lower the CAC value, salt $C_7H_5NaO_3$ (NaSal) sodium salicylate has been used. Different compositions of polymer, surfactant and salt mass fraction in solvent were used in order to analyse the chemical additive concentration effect. Distilled water was used as a solvent. Polna, Inc. Electrical Distillatory Type DE20 was used to purify tap water. The conductivity of the solvent was of the order of 1μS/cm.

After the addition of the appropriate drag reducers to the solvent, the solutions were mixed gently so as not to cause mechanical degradation of polymer chains. The first mixing was performed in cylindrical vessels, by the use of our own designed roller mixer with very a low rotational speed equal to 1÷5 rpm. Then, the solution was diluted in the main tanks. Before measurements, the mixtures were left to rest for 24 hours.

Adiabatic steady flow of homogenous solutions was examined in 8 different straight pipes with diameters between 1.8mm and 21mm, all with a temperature of 27˚C.

4. Rheological characteristics and flow resistance measurements results

In order to identify the rheological characteristics of the analysed solutions, each of the experimental/pipe flow curves have been drawn in form of functional relationship described by the Equation (1):

$$\tau_w = f(\Gamma) \tag{1}$$

where: $\tau_w = \dfrac{D\Delta P}{4L}$ – shear stress on pipe wall,

$\Gamma = \dfrac{8v_m}{D}$ – pipe shear rate (value of shear rate on pipe wall).

An interpretation of experimental results presented in form of function (1) indicates that the analysed solutions can be successfully approximated with the Ostwald de Waele power-law fluid model. Representative rheological characteristics in form of experimental/pipe flow curves are illustrated in Figure 2.

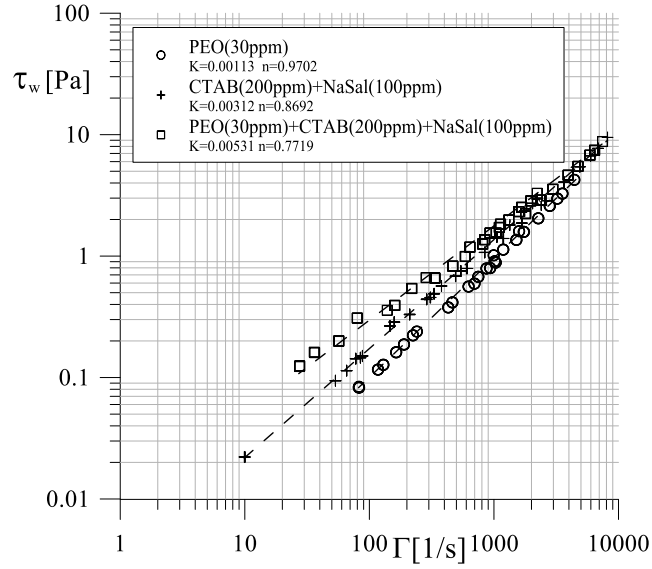

Fig. 2. Representative experimental flow curves for polymer, surfactant and polymer-surfactant solutions

Additionally, representative diagram of the shear viscosity curves vs. shear rate for the analysed solutions, which correspond to Figure 2, are presented in Figure 3.

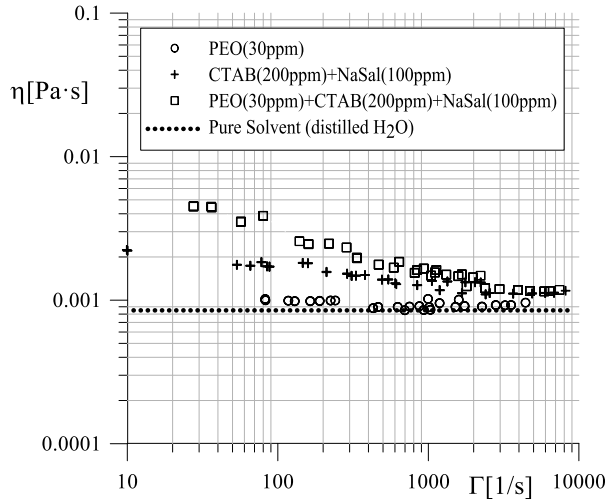

Fig. 3. Representative shear viscosity curves as a function of shear rate for polymer, surfactant and polymer-surfactant solutions

The mass fraction of individual additives, composing rheologically complex polymer-micellar solution, affects the value of the n flow index. This parameter characterises non-Newtonian properties of a fluid. There is no way to predict a priori, its value for a solution composed is arbitrarily and having different mass frictions of particular drag reducers. It was only observed that the increase of both CTAB and NaSal concentration in the examined solution having a constant polymer concentration leads to the intensification of non-Newtonian properties of the fluid, i.e. to the increase of the value of fluid consistency constant K and the decrease of the n flow index.

The interpretation of experimental data and the assessment of the respective solution additives' influence on the increase or reduction of the flow resistance and the shape and location of resistance curves depend significantly on the adopted coordinate system in which these data is presented. Firstly, experimental results of flow resistance are presented in the classical system of dimensionless numbers [Re_s, c_f] described by formulas (2) and (3):

$$Re_S = \frac{v_m \cdot \rho_S \cdot d}{\eta_S} \tag{2}$$

$$c_f = \frac{d \cdot D \cdot P}{2 \cdot r \cdot v_m^{\,2} \cdot L} \tag{3}$$

and additionally, in the form of drag reduction coefficient *DR*, defined as a function of the Reynolds number (2), and described in percentage term:

$$DR = \left(1 - \frac{c_f}{c_{fS}}\right) \cdot 100\% \tag{4}$$

Figure 4 presents the flow resistance curves of polymer, surfactant and polymer-surfactant water solutions, defined in the system of dimensionless numbers (2) and (3).

Analyses of flow resistance curves reveal that in any of analysed flow ranges measurement points do not correspond to the theoretical functions, which describe Newtonian fluid flow. The simultaneous addition of even small amounts of high molecular polymers and surfactants causes an increase of flow resistance in the laminar range of flow.

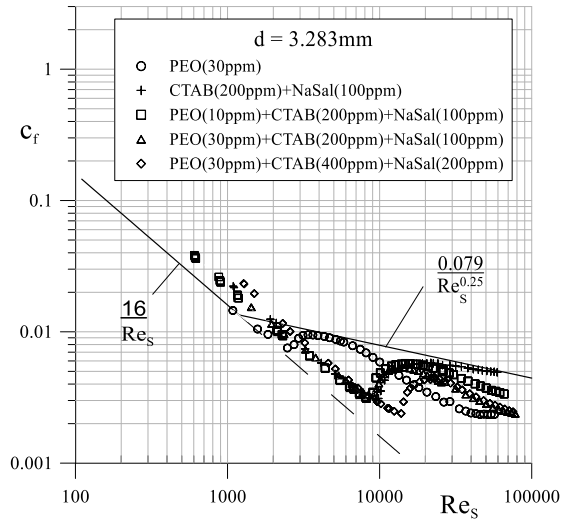

Fig. 4. The flow resistance curves of polymer, surfactant and polymer-micellar water solutions, defined in the system of dimensionless numbers (2) and (3)

The drag reduction coefficient curves (4) are illustrated in Figure 5. It is observed that in case of the turbulent flow simultaneous application of analysed chemical additives produces the drag reduction effect.

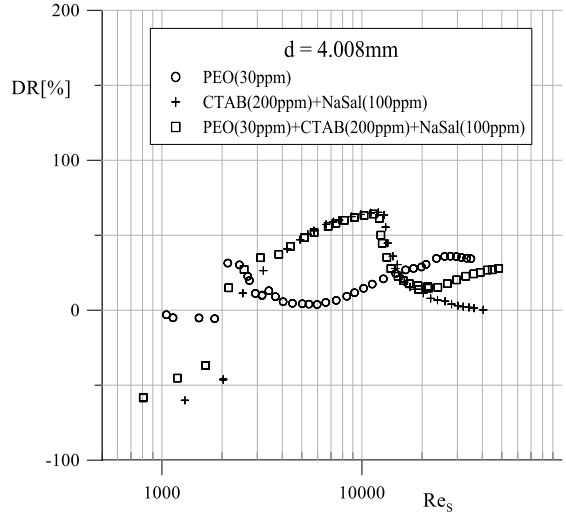

Fig. 5. The drag reduction coefficient curves *DR = f(Re)*

Due to the difficulty in unambiguous determination of the critical value the Reynolds number Re_s, the *DR* values presented in Figure 5 are calculated in such a way that it was assumed that $c_{fs} = 16/Re_s$ in the range of the Reynolds number $Re_s < 2100$, whereas the formula $c_{fs} = 0.079/Re_s^{-0.25}$ was used in the range of Reynolds number $Re_s \geq 2100$. Therefore, a sharp increase of the DR value observed in the transition zone, particularly in the polymer solution (see in Figure 5), does not reflect the actual degree of drag reduction in this range of flow. In case of the polymer solution flow, in the initial stage of the turbulent flow, no noticeable reduction of flow resistance is observed. Only after exceeding certain characteristic Reynolds number $Re_s \approx 1.5 \cdot 10^4$, the onset of the drag reduction effect occurs and the phenomenon increases with the increase in the value of the Reynolds number. A similar increase in the reduction of the shear resistance in rotating disc apparatus for the turbulent flow range, induced with PEO additive, was observed in the drag reduction effect obtained by the use of a rotating-disk apparatus [22].

Furthermore, the value of the critical Reynolds number, for which transition from the laminar flow to the turbulent flow is observed, takes various values, which depend on pipes' diameters, type and concentration of chemical additives introduced to the solvent.

A better interpretation of the simultaneous addition of the polymer and surfactant with salt effect on drag reduction, in comparison with adequate addition of pure polymer or pure surfactant with salt, can be achieved by presentation of the same measurement date in modified system of "pseudorheostable" numbers [Re_M, c_{fM}]. The modified system on dimensionless numbers used in the analysis is described correspondingly by formulas (5) and (6):

$$Re_M = \frac{d^n \cdot v_m^{2-n} \cdot \rho_S}{K \cdot \left(\frac{3 \cdot n + 1}{4 \cdot n}\right) 8^{n-1}} \cdot \left[\frac{2 \cdot (n+1)}{3 \cdot n + 1}\right]^{-2,5} \tag{5}$$

$$c_{fM} = \frac{d \cdot \Delta P}{2 \cdot \rho_S \cdot v_m^2 \cdot L} \cdot \left[\frac{2 \cdot (n+1)}{3 \cdot n + 1}\right]^{2,5} \tag{6}$$

As one knows [5], in such defined dimensionless numbers system flow resistance curves of rheostable (purely viscous) non-Newtonian fluids are transformed to a single curve – in the whole range of modified Reynolds numbers (5) – identical to the classical Newtonian curve described in the laminar range by Fanning equation and in the turbulent flow by Blasius formula. Selection of such a coordinate system was dictated additionally by the fact that it facilitates identification and description of the characteristic drag reduction flow zones. In this modified system of pseudorheostable dimensionless numbers [Re_M, c_{fM}], each deviation of experimental flow resistance curve, which indicates abnormal drag reduction from pseudorheostable Blasius curve, allows for the identification of the influence of specific additives (polymers or/and surfactants with salt) on the range of analysed drag reduction effect. Figure 6 presents comparison of flow resistance curves in the modified dimensionless number system (5) and (6) for 3 types of solutions with different internal structures.

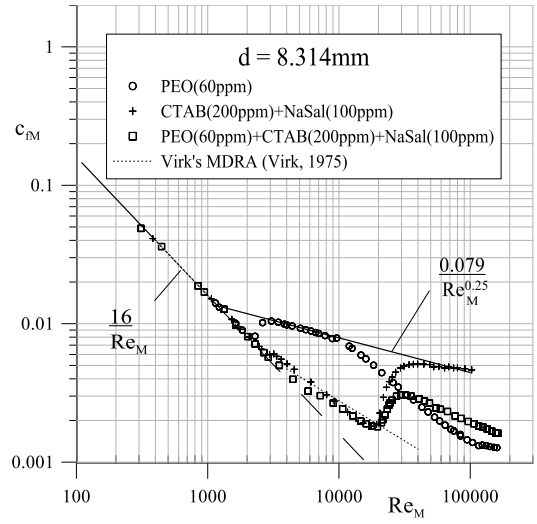

Fig. 6. The flow resistance curves of polymer, surfactant and polymer-surfactant water solutions, defined in the system of cardinal numbers (5) and (6).

The results of experimental data analysis indicate that polymer-surfactant-salt additives cause significant drag reduction in a wider range of flow in comparison with pure polymer or pure surfactant-salt solutions. Surfactant and salt additives (micellar solution) induce appearance of the stable transitional zone B (compare Figure 6 and Figure7), in which spectacular reduction of flow resistance is observed – usually greater when compared to the same effect achieved with polymer additives.

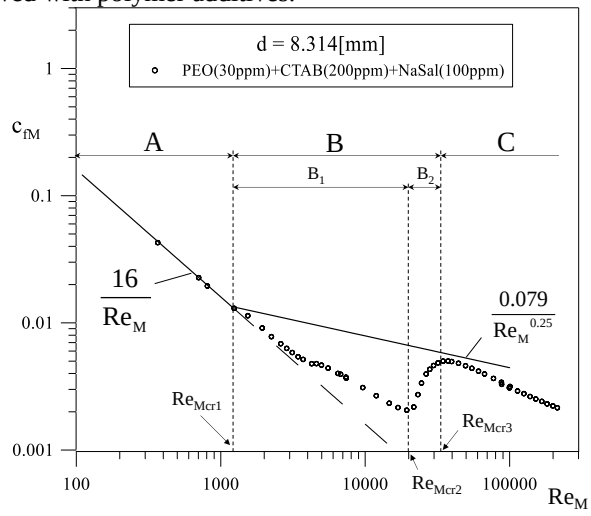

Fig. 7. The scheme of characteristic flow resistance curve zones for representative polymer-micellar solution: A – laminar zone, B – extended transitional zone (B_1 – stable transitional zone, B_2 – unstable transitional zone), C – turbulent zone.

It is observed that in the stable transitional zone B_1, the loss of the stability of the laminar flow increases very softly when the Reynolds number values grow. In this range, relative drag reduction is the greatest. Beyond a certain second critical value of the Reynolds number Re_{Mcr2} the occurrence of an unstable transitional zone B_2 is observed. It is especially well-illustrated in Figure 7. In this range of flow, a rapid loss of drag reduction effect occurs.

From Figure 6, it is documented that for polymer-micellar solutions, beyond a certain third critical value of the Reynolds number Re_{Mcr3}, the fluid starts to behave like a classical rheostable non-Newtonian fluid.

However, in comparison with pure micellar solution, an additional abnormal drag reduction zone C (see Figure 7) in the turbulent range of flow is observed in case of analysed polymer-micellar solution. The viscoelastic properties of the solution are a dominant factor in this zone of flow. This effect is also well-illustrated in Figure 8.

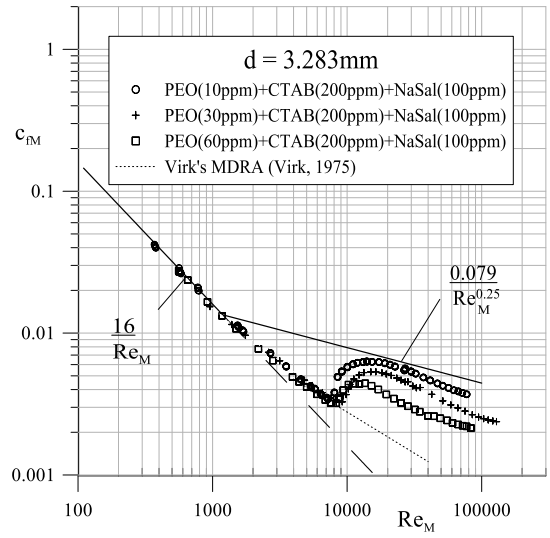

Fig. 8. Polymer concentration effect on the flow resistance curves of polymer-surfactant aqueous solutions

It should also be pointed out that addition to the micellar solution of even small amounts of high molecular weight polymer (about 10 ppm) causes a reduction of the non-Newtonian properties of the solution.

Experiment results indicate the influence of NaSal additive on drag reduction effect. Figure 9 presents a comparison of flow resistance curves of the pure polymer solution, the polymer-surfactant solution and the polymer-surfactant-salt solution.

It is clearly evident that with the addition of a small amount of electrolytes (e.g. salts or alcohols), a reformation of spherical micelles into threadlike micelles must proceeded. It leads to significant extension of the transitional zone B_1. Efficient drag reduction effect is observed within this zone of flow

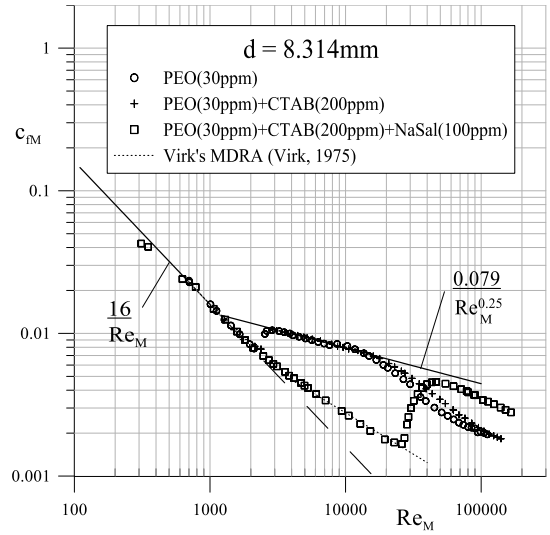

Fig. 9. The effect of NaSal additive on polymer-surfactant flow resistance curve

The results of drag reduction measurements analysis indicate the effect of pipe diameter influence on the drag reduction efficiency. Figure 10 illustrates the pipe diameter effect on the flow resistance curves of polymer-surfactant aqueous solutions.

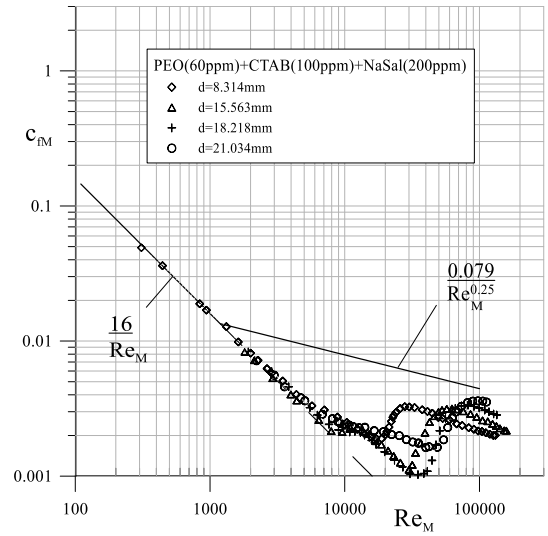

Fig. 10. Pipe diameter effect on the flow resistance curves of polymer-surfactant aqueous solutions

Increasing the pipe diameter d results in a clear extension of the stable transitional zone B_1 towards higher values of the Reynolds number. Moreover, decreasing the pipe diameter

value d results in an increase of the drag reduction effect in the third additional turbulent range of flow C.

The experimental results reveal that polymer-micellar solution can be characterised by a lower susceptibility to mechanical degradation during flow or that its degradation can be almost unnoticeable in the analysed range of flow. Figure 11 illustrates a shift of the collapse of drag reduction effect toward greater values of Reynolds number caused by application of polymer and polymer-surfactant additives.

A pure PEO solution degrades very fast when it goes under high shearing conditions. A collapse of the drag reduction is gradually observed in such a case. Experimental results show a considerable increase of the Reynolds number value for which mechanical degradation of polymer and collapse of DR effect is observed in polymer-micellar solution.

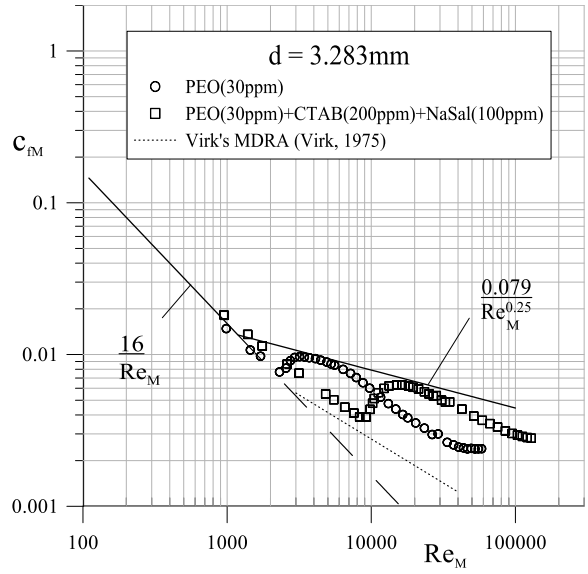

Fig. 11. Shift of the collapse of drag reduction effect toward greater values of Reynolds number caused by application of polymer and polymer-surfactant additives

5. Conclusions

Experimental study of drag reduction process induced by co-addition of polymer and surfactant with salt indicates that polymer-micellar aggregates are efficient drag reducers of the energy losses in straight pipe flow. Analyses of experimental data document that the simultaneous addition of surfactants and salt, together with high molecular polymers, causes a minor increase of flow resistance in the laminar range of flow compared to the analogue flow of pure solvent. It produces, however, a significant extension of the stable transitional zone between the laminar flow and the turbulent flow. The surfactant with salt additives has a major influence on the efficiency of the drag reduction in this zone.

Experimental results prove that the simultaneous addition of surfactant, salt and high molecular polymer leads to the occurrence of third significantly extended drag reduction zone in the turbulent range of flow. The dominant factors in that zone are the viscoelastic properties of the solution caused by the presence of polymer macromolecules, wherein an increase of the mass fraction of the polymer additive increases the efficiency of the drag reduction effect only in the turbulent range of flow.

The performed comparative studies presented that the analysed polymer-micellar solutions combine and intensify positive features of their purely polymer or purely micellar analogues, providing a more efficient drag reduction effect in a wider range of flow.

Under the experimental data, it can be hypothesised that aggregates, subjected to the shear stress, take orientation consistent with the aforementioned principle of minimum resistance. With an increasing value of the Reynolds number, internal friction forces stretch and extend the aggregates, leading to the laminarisation of the initial phase of the turbulent flow.

Therefore, it can be presumed that the rigid rod like/threadlike micelles, which create the core of the aggregates, are responsible for reducing the flow resistance in the extended transitional zone between the laminar and the turbulent flow.

The aggregates and micelles are responsible for the transmission of internal friction within the liquid. The value of the critical Reynolds number for which the transition to the turbulent zone is observed is greater for polymer-micellar solutions. This means that the stable transition zone is extended. The reason for such behaviour can be the partial disintegration of aggregates to original forms, i.e. micelles (formed from the surfactant) and macromolecules (formed from the polymer) due to a significant increase of the shear rate. From this moment, both micelles and macromolecules interact separately on the transported solution, causing a further drag reduction effect. Passing further in the turbulent range of flow micelles lose their orientation and no longer have a major impact on the drag reduction. A key role in this zone is played by the polymer. Not having undergone an earlier degradation, the polymer macromolecules still cause the flow reduction.

In drag reduction caused by the use of polymer-micellar solution, one cannot talk about the so-called *collapse of the drag reduction.* It occurs permanently over a wide range of Reynolds numbers. Nevertheless, in the turbulent zone, polymer macromolecules undergo a certain mechanical degradation. Decreasing the shear rate leads to the reconstruction of the internal structure of the solution. As a result of electrostatic or hydrophobic interaction, the recreated micelles are combined with the polymer chains by coiling around them. These chains are somewhat shorter and such newly created aggregates do not have the same rheological properties as the original ones. This results in a slight increase of the flow resistance in comparison with a freshly prepared solution.

Thee presented experimental results of the drag reduction effect are consistent in terms of qualitative analysis with proposed hypothesis, and confirm the described mechanism of the phenomenon in an indirect way.

References

[1] Toms, B. A., *Some Observations on the flow of linear polymer solutions through straight tubes at large Reynolds numbers*. Proceedings of the International Congress of Rheology, Holland, North-Holland, Amsterdam, Section II, 1948, 135-141.

[2] Mysels, K. J., *Flow of thickened fluid*. December 27, US Patent 2, 492:173, 1949.

[3] Virk P. S., *Drag reduction fundamentals*, AIChE Journal, vol. 21, Issue 4, 1975, 625-656.

[4] Sellin, R. H. J., Hoyt, J. W., Poliert, J., Scrivener, O., *The effect of drag reducing additives on fluid flows and there industrial applications part II: present applications and futures proposals*. Journal of Hydraulic Research, vol. 20, 1982, 235-292.

[5] Matras Z., *Przepływ cieczy Tomsa w przewodach kołowych*, Politechnika Krakowska, Monografia 29, 1984.

[6] Gyr A., Bewersdorff H. W., *Drag reduction of turbulent flows by additives*, vol. 32, Kluwer Academic Publishers, P.O. Box 17, 3300 AA, 1995.

[7] White, C. M., Mungal, M. G., *Mechanics and Predictions of Turbulent Drag Reduction with Polymer Additives*, Annular Review of Fluid Mechanics, no. 40, 2008, 235-256.

[8] Wang Y., Yu B., Zakin J. L., Shi H., *Review on Drag reduction and Its Heat Transfer by Additives*, Advances in Mechanical Engineering, no. 10,2011, 17.

[9] Dujmovich T. and Gallegos A., *Drag reducers improve throughput, cut costs*, Offshore, vol. 65, no. 12, 2005, 55-58.

[10] Fabula, A. G., *Fire-fighting benefits of polymeric friction reduction*. Trans ASME J Basic Engng, 1971, 93-453.

[11] Motier, J. F., Chou L. C., Kommareddi N. S., *Commercial drag reduction: past, present, and future*, Proceedings of the ASME Fluids Engineering Division Summer Meeting, San Diego, Calif, USA 1996.

[12] Tamano S., Ito M., Kato K. and Yokota K., *Turbulent drag reduction in nonionic surfactant solutions*, Physics of Fluids, vol. 22(5), 2010, 055102.

[13] Cai S.-P., *Drag reduction of a cationic surfactant solution and its shear stress relaxation*, Jurnal of Hydrodynamics, vol. 24(2), 2012, 202-206.

[14] Warholic M. D., Heist D. K., Katcher M., Hanratty T. J., *A study with particle- image velocimetry of the influence of drag-reducing polymers on the structure of turbulence*, Exp. Fluids, vol. 31, 2001, 474-483.

[15] Liberatore M. W., Baik S., Mchugh A. J., Hanratty T. J., *Turbulent drag reduction of polyacrylamide solutions: effect of degradation on molecular weight distribution*. J. Non-Newtonian Fluid Mech., vol. 123, 2004, 175-183.

[16] Hadri F., Besq A., Guillou S., Makhloufi R., *Drag reduction with an aqueous solution of CTAC-NaSal: Study of the wall slip with a Couette geometry*, Comptes Rendus Mécanique, vol. 338, Issue 3, 2010, 152-157, ISSN 1631-0721.

[17] Minatti E., Zanette D., *Salt effects on the interaction of poly(ethylene oxide) and sodium dodecyl sulfate measured by conductivity*, Colloids Surfaces A: Phisicochem Eng Aspects, 1996, 113:237.

[18] Hou Z., Li Z., Wang H., *Interaction between poly(ethylene oxide) and sodium dodecyl sulfonate as studied by surface tension, conductivity, viscosity, electron spin resonance and nuclear magnetic resonance*, Colloid Polym. Sci., vol. 277, 1999, 1011-1018.
[19] Goddard E. D., *Polymer/Surfactant Interaction: Interfacial Aspects*, Journal of Colloid and Interface Science, vol. 256, 2002, 228-235.
[20] Suksamranchit S., Sirivat A., Jamieson A. M., *Polymer–surfactant complex formation and its effect on turbulent wall shear stress*, Journal of Colloid and Interface Science, vol. 294, Issue 1, 2006, 212-221, ISSN 0021-9797.
[21] Matras Z., Malcher T., Gzyl-Malcher B., *The influence of polymer-surfactant aggregates on drag reduction*, Thin Solids Films, vol. 516, 2008, 8848-8851.
[22] Kim J. T., Kim C. A., Zhang K., Jang C. H., Choi H. J, *Effect of polymer–surfactant interaction on its turbulent drag reduction*, Colloids and Surfaces A: Physicochemical and Engineering Aspects, vol. 391, Issues 1-3, 2011, 125-129, ISSN 0927-7757.
[23] Mohsenipour A. A., Pal R., *The Role of Surfactants in Mechanical Degradation of Drag-Reducing* Polymers, Ind. Eng. Chem. Res., vol. 52 (3), 2013, 1291-1302.
[24] Mohsenipour A. A., Pal R., Prajapati K., *Effect of cationic surfactant addition on the drag reduction behaviour of anionic polymer solutions*, The Canadian Journal of Chemical Engineering, vol. 91, Issue 1, 2013, 181-189.
[25] Matras Z. and Kopiczak B., *Intensification of drag reduction effect by simultaneous addition of ,surfactant and high molecular polymer into the solvent*, Chemical Engineering Research and Design, vol. 96, 2015, 35-42.
[26] Jönsson B., Lindman B., Holmberg K., Kronberg B., *Surfactants and polymers in aqueous solution*, John Wiley & Sons, Chichester, UK 1998.
[27] Diamant H., Andelman D., *Onset of self-assembly in polymer-surfactant systems*, Europhysics Letters, vol. 48(2), 1999, 170-176.
[28] Matras Z., Walczak S., *The capillary-pipe rheometer for the identification of complex properties of multiphase non-Newtonian fluids*, Inżynieria i Aparatura Chemiczna, No. 6,2006, 150-151.

TECHNICAL TRANSACTIONS | CZASOPISMO TECHNICZNE
MECHANICS | MECHANIKA
2-M/2016

MATEUSZ MUSIK*, JAN TALAGA**

INVESTIGATION OF FLUID DYNAMICS IN AN UNBAFFLED STIRRED VESSEL WITH AN ECCENTRICALLY LOCATED RUSHTON TURBINE

BADANIA HYDRODYNAMIKI MIESZANIA W MIESZALNIKU BEZ PRZEGRÓD Z NIECENTRYCZNIE USYTUOWANYM MIESZADŁEM TURBINOWYM

A b s t r a c t

The paper presents the results of experimental investigation of the hydrodynamics in unbaffled stirred vessel with eccentric Rushton turbine configuration. Basing on flow visualisation. the main flow features were determined. Laser Doppler Anemometry measurements provided radial and axial components of the mean flow velocity vectors. The obtained data of power consumption allowed to determine the impact of the impeller eccentricity ratio *e*/*R* on the power number *Ne*.

Keywords: agitation, eccentrically located impeller, unbaffled vessel, LDA measurements

S t r e s z c z e n i e

W artykule przedstawiono wyniki badań doświadczalnych hydrodynamiki mieszania w zbiorniku bez przegród z niecentrycznie usytuowanym mieszadłem turbinowym tarczowym. Dokonano wizualizacji przepływu. W oparciu o wyniki pomiarów z wykorzystaniem anemometru laserowego wyznaczono rozkłady promieniowej i osiowej składowej średniej prędkości przepływu cieczy. Określono doświadczalnie wpływ niecentryczności *e*/*R* usytuowania mieszadła na liczbę mocy mieszania *Ne*.

Słowa kluczowe: mieszanie, niecentryczne mieszadło, mieszalnik bez przegród, pomiary LDA

DOI:

* MSc. Eng. Mateusz Musik, Avio Aero GE Aviation business, Turbine Unit Department, Bielsko-Biała, Poland.

** DSc. Eng. Jan Talaga, Institute of Thermal and Process Engineering, Faculty of Mechanical Engineering, Cracow University of Technology.

1. Introduction

Mechanical mixing is commonly used in many processes in chemical, food, pharmaceutical or biotechnology industries. A typical design solution of stirred tank is a vertical vessel with a centrically located shaft. Most often, the stirred tank is equipped with four vertical baffles, fixed to the vessel wall, which deter vortex formation and intensify mixing by increasing the axial flow rate [1]. However, in some processes, baffles may cause an undesired effect creating dead zones behind baffles where sludge can accumulate. It can occur especially in stirred tanks with a flat bottom and during multiphase fluid mixing [2]. In such case, it is an alternative solution as unbaffled mixing [3, 4] with eccentrically located impeller. What is more, the design also eliminates unfavourable central vortex formation.

This paper presents an experimental investigation of hydrodynamics and power consumption of mixing in unbaffled stirred tank with eccentrically located Rushton impeller.

2. Experimental

Research was performed in a vertical tank (Fig. 1a) made of *Duran* glass with inside diameter D = 0,286 m and flat bottom. Liquid level were equal to tank inside diameter ($H = D$). The standard Rushton turbine was used. The impeller diameter was $d = 1/3D$ and the blade thickness to diameter ratio was 0,01. The off-bottom clearance was $h = d$. Dimethyl sulfoxide (DMSO) (η = 0,0023 Pa·s, ρ = 1100 kg/m^3) was used as the working fluid.

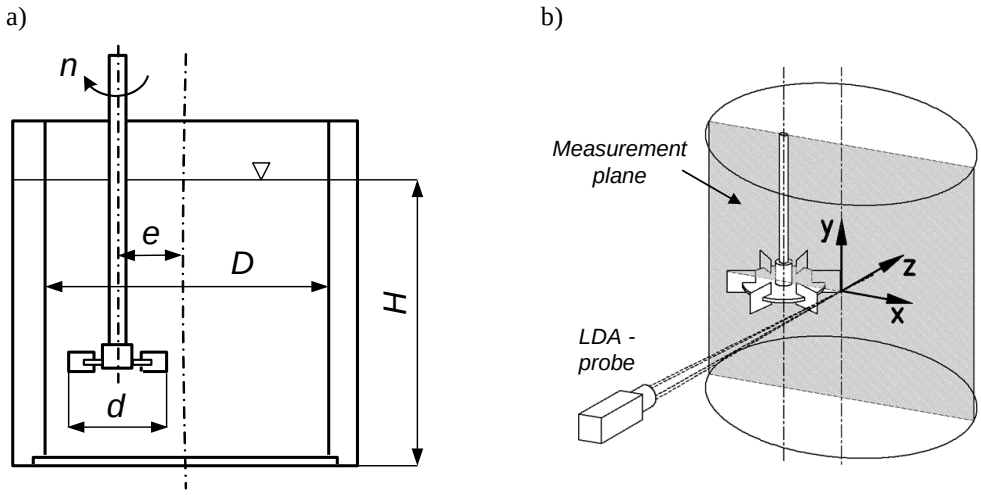

Fig. 1. Stirred vessel with an eccentrically located Rushton turbine;
a) geometric characteristics of stirred vessel, b) scheme of measuring system

The hydrodynamics investigation involved a visualisation of the liquid flow in the stirred tank and an analysis of the components of the mean flow velocity vectors. Temporary flow velocity measurements were carried out using two-component Laser Doppler Anemometry (LDA) operating in back scatter mode [5]. Argon-Ion laser provided a pair of blue beams with λ = 488 nm and a pair of green beams with λ = 514,5 nm. The obtained measurement data were processed by a *Dantec Burst Spectrum Analyser*. The working fluid was seeded with silver coated hollow glass spheres with a mean diameter of 10 μm and a density of 1150 kg/m^3. Liquid flow visualisation was carried out using a digital camera.

The power consumption ($P = M \cdot 2\pi n$) was determined from torque measurements M performed on the shaft using torquemeter (*Vibrometer)*. At the same time, the impeller rotational speed n had been measured.

Research was performed for 3 different positions of the impeller shaft from the tank axis: central position (e = 0) and two off-axis positions (e = 0,25R, e = 0,5R), where $R = D/2$.

The flow velocity measurements were performed in plane through tank axis and impeller shaft axis (Fig. 1b). The mixing intensity was controlled by impeller rotational speed changes, and ranged from 200 to 600 *rpm*, corresponding to full turbulent flow in stirred tank and impeller Reynolds number $Re = (1{,}44 \div 4{,}32) \cdot 10^4$.

3. Results and discussion

Fig. 2 shows an example of the impact of the impeller's shaft eccentricity on the liquid flow in an unbaffled stirred tank for a rotational impeller speed of n = 250 rpm. When the impeller is located in the axis of the tank (e = 0, Fig. 1a), one centrically vortex can be observed. The vortex depth increases with the impeller rotational speed increase. For n = 502 rpm, the vortex departs from the top of the vessel above the impeller. From that moment, some air from above the liquid surface starts to be entrained into the flow. The air was dispersed in the tank by the impeller blades. Displacement of the shaft from tank axis towards the wall causes the formation of the vortex in the field between tank wall and impeller shaft (Fig. 2b). Low rotational speed characterises the presence of a vortex in the upper part of the tank, bellow the liquid surface. With a rotational speed increase, the vortex reaches more into the bottom of the tank and at a sufficiently rate of rotation, it reaches the impeller blades. The formation of that vortex in the stirred vessel with eccentrically located impeller were also documented in experimental studies [6, 7], as well as in CFD simulations [2]. Authors of the study [6] also observed the creation of the second vortex departing from the impeller blades towards the vessel bottom. In this paper, such results were not observed. The difference can be explained by the fact that in [6], the stirred tank was equipped with an cover, which was located just above the liquid level and prevented air to be entrained into the flow from the above of liquid surface.

The increase of eccentricity changes the location of the forming vortex, which moves toward the tank wall. Equally higher eccentricity corresponds to a higher vortex inclination to the vertical axis of the tank. For e = 0,5R eccentricity, inclination is 29°±4°. A similar observation has been found in other studies. In paper [6], the upper vortex was inclined by

15°, whereas paper [7] presents an inclination between 16° and 23°. For [7], the root cause of these differences may be explained by a different impeller off-bottom clearance (where $h = 0{,}5D$), and in case of [6], providing closing cover. No changes of the vortex inclination due to rotational speed were observed.

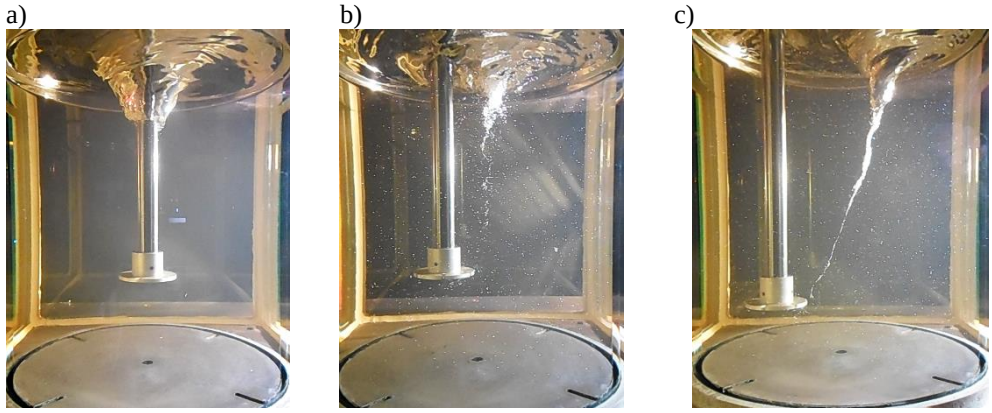

Fig. 2. Flow visualisations with the impeller rotational speed n = 250 rpm for various eccentricity; a) $e = 0$, b) $e = 0{,}25R$, c) $e = 0{,}5R$

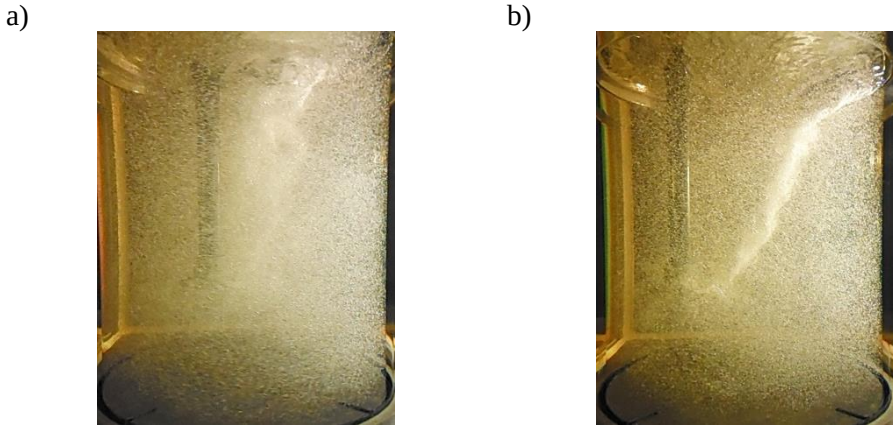

Fig. 3. Air dissipation throughout the volume of the vessel; a) $e = 0{,}25R$ and n = 354 rpm, b) $e = 0{,}5R$ and n = 302 rpm

The vortex created by the eccentrical location of the impeller causes entraining of the gas from the surface into the flow. The intensity of that phenomenon strengthens with an increase of the impeller rotational speed increase and the eccentricity. Fig. 3 shows an example of gas dissipation throughout the volume of the tank for two different e values. For $e = 0{,}25R$ eccentricity, such effect is achieved at rotational speed n = 354 rpm (Fig. 3a), and for $e = 0{,}5R$ eccentricity at lower rotational speed n = 302 rpm (Fig. 3b).

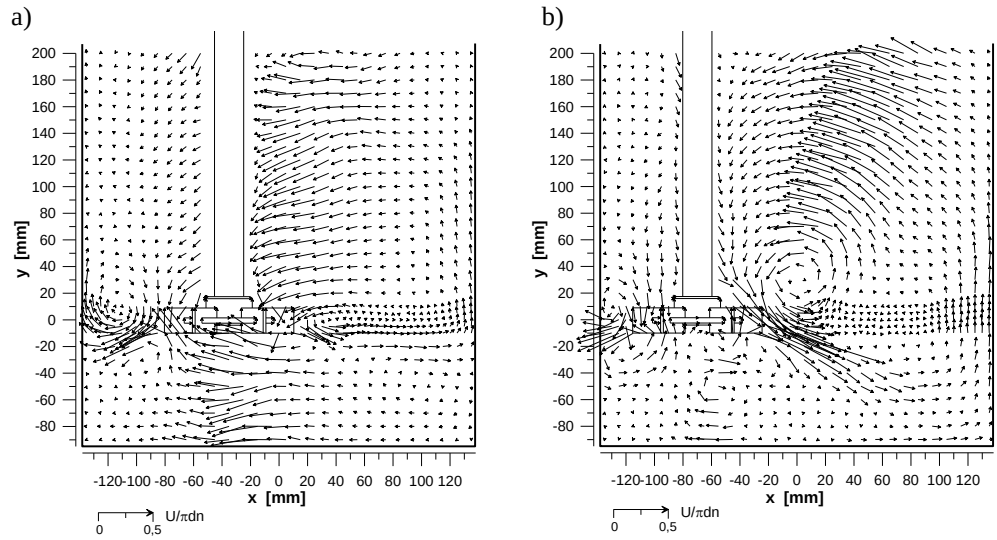

Fig. 4. Vector plot of liquid flow in a stirred vessel with an eccentrically positioned Rushton turbine for various impeller eccentricity: a) $e = 0{,}25R$, b) $e = 0{,}5R$

Fig. 4 shows the results of the measurement of the radial and axial components of the mean flow velocity for two different eccentricities: $e = 0{,}25R$ (Fig. 4a) and $e = 0{,}5R$ (Fig. 4b). Fig. 1b presents the measuring plane. Velocity data determined during mixing with rotational speed n = 225 rpm are presented in dimensionless form, i.e. normalised with respect to the impeller blade tip velocity, $(U/\pi \cdot d \cdot n)$. Based on the results, it can be stated that for mixing with eccentrically positioned impeller, the flow pattern is not axisymmetric as it is for central position of the impeller [8]. For the eccentricity $e = 0{,}25R$ (Fig. 4a), the largest values of the radial component occur in the vortex area from impeller blades towards the top of the vessel. Large radial component values are also observed under Rushton turbine. For the eccentricity $e = 0{,}5R$ (Fig. 4b), velocities are much lower, while in the vortex area values of radial velocity components increase. Higher eccentricity also causes significant variation of velocity profiles in the impeller discharge stream. In $e = 0{,}5R$ (Fig. 4b) case, the formed vortex affects the flow of the pumped by impeller blades liquid. It results in a significant increase of the radial component of velocity at the side where the distance between the impeller and the tank wall is the largest. In this case, maximum radial velocities are about 2 ÷ 2,5 larger in comparison with $e = 0{,}25R$ case. The axial components also increase, which cause the flow stream to be pumped towards the vessel bottom. At the area where the impeller is closest to the vessel wall, the velocity profile changes due to the impeller discharge stream-wall interaction.

The measurement of the power consumption for the stirred vessel without baffles is presented in Fig. 5 as the power characteristic $Ne = f(Re)$ for different eccentricities e/R of the impeller shaft. All power characteristics $Ne = f(Re)$ are found to be independent of the Re number for the range of the performed experiments. The similar independence was found in [9] for impellers type HE 3 and for propeller stirrer. Marked in Fig 5 by dashed line decrease of power number Ne for large Reynolds numbers Re, for eccentric impeller

position, is the result of the increase of aeration of mixing liquid caused by formed in the stirred vessel vortex. The aeration of the liquid increases with the impeller rotational speed increase, which results in mixing liquid density decrease, and therefore, with a decrease of the power number.

The results of the experimental analysis allow to conclude that for the liquid stirring in the unbaffled tank with an eccentrically located impeller, the power number is always larger than for the stirring with centrically located impeller (e = 0). Fig. 5 presents also power numbers *Ne* for the conventional stirring with four baffles (J = 4) and centrically located Rushton turbine (e = 0). According to analysis of changes in eccentricity (e = 0 ÷ 0,5R) it can be concluded that power number *Ne* for mixing with eccentrically located impeller in the unbaffled stirred tank is always larger than for centric agitation (*Ne* = 0,74) and always lower than for conventional stirred vessel with baffles (*Ne* = 3,75).

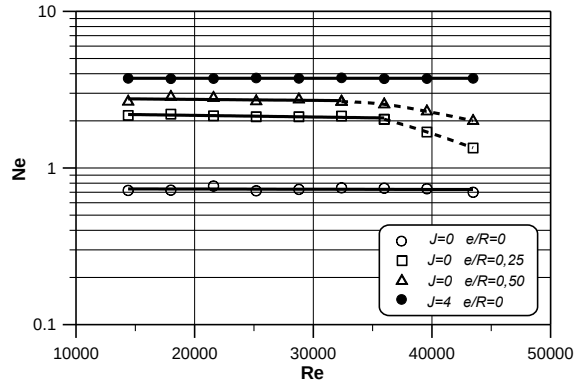

Fig. 5. Power characteristics *Ne = f (Re)* for the stirred tank with the Rushton turbine: J = 0 and e/R = 0; 0,25; 0,5 or J = 4 and e/R = 0

The experimentally proven effect of the stirrer eccentricity ratio e/R on the power number *Ne* in the stirred tank without baffles and with the Rushton turbine is depicted in Fig. 6. The obtained results of the measurements were described mathematically and were approximated by the following correlation:

$$Ne = 0{,}74 \cdot \left[-6{,}89 \cdot \left(\frac{e}{R} \right)^2 + 9{,}04 \cdot \left(\frac{e}{R} \right) + 1 \right] \tag{1}$$

with the maximal relative error ±5,6%, within the ranges of the $Re \in \langle 1{,}44 \cdot 10^4;\ 4.32 \cdot 10^4 \rangle$ and eccentricity $e/R \in \langle 0;\ 0{,}6 \rangle$.

Equation (1) describes the evaluated impact of impeller eccentricity e/R as a quadratic function, which is in agreement with experimental results for Rushton turbine, which were reported in [8, 10]. In [9], the linear relationship $Ne = f(e/R)$ was estimated; however, it concerned different impeller types (HE 3 and propeller stirrer), which operate as axial pumping impellers. As the conclusion, it can be estimated that the impact of eccentricity on the power number can be presented as a quadratic function for radial pumping impellers, such as the Rushton turbine, and as a linear function for axial pumping impellers.

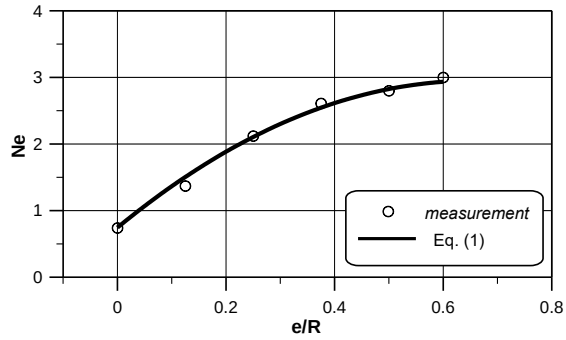

Fig. 6. The dependence $Ne = f(e/R)$ for the unbaffled stirred tank with the Rushton turbine

4. Conclusions

Displacement of the shaft from tank axis towards the wall causes the formation of the vortex in the field between tank wall and the impeller shaft (Fig. 2b). Low rotational speed characterises the presence of vortex in the upper part of the tank, bellow the liquid surface. With a rotational speed increase, the vortex reaches closer into the bottom of the tank and at a sufficiently rate of rotation reaches the impeller blades. The increase of eccentricity changes the location of the forming vortex, which moves toward the tank wall. Equally, higher eccentricity corresponds to a higher vortex inclination to the vertical axis of the tank. For $e = 0{,}5R$ eccentricity, the inclination is 29°±4°. No changes of the vortex inclination due to rotational speed were observed.

Based on the results of the measurement of the mean flow velocity, it can be stated that for mixing with eccentrically positioned impeller, the flow pattern is not axisymmetric as it is for central position of the impeller. The largest values of the radial component occur in the vortex area from impeller blades towards the top of the vessel. At the area where the impeller is closest to the vessel wall, the velocity profile changes due to the impeller discharge stream-wall interaction.

According to analysis of changes in eccentricity ($e = 0 \div 0{,}5R$), it can be concluded that the power number Ne for mixing with eccentrically located impeller in the unbaffled stirred tank is always larger than for centric agitation ($Ne = 0{,}74$) and always lower than for conventional stirred vessel with baffles ($Ne = 3{,}75$).

The experimentally determined effect of the stirrer eccentricity ratio e/R on the power number Ne in the stirred tank without baffles and with the Rushton turbine describes equation (1). That correlation estimates that for radial pumping impeller, the impact of eccentricity on power number is a quadratic dependence.

S y m b o l s

d	impeller diameter, m,
D	tank inner diameter, m,

e eccentricity, i.e., distance of the shaft from the vessel axis, m,
h off-bottom clearance of the stirrer, m,
H liquid height in the tank, m,
M torque, N·m,
n impeller rotational speed, s^{-1},
P power consumption, W,
R radius of the stirred tank, $R = D/2$, m,
U mean velocity, $m \cdot s^{-1}$,
Ne power number, $Ne = P/(n^3 d^5 \rho)$, –,
Re impeller Reynolds number, $Re = (n \cdot d^{2\cdot} \rho)/\eta$, –,
η dynamic viscosity of the liquid, Pa·s,
ρ liquid density, $kg \cdot m^{-3}$.

References

[1] Kamieński J., *Mixing of multiphase systems*, WNT, Warszawa 2004 (in Polish).
[2] Wójtowicz R., Lipin A. A., *The computational-fluid-dynamics study of an unbaffled stirred vessel with eccentrically positioned impeller*, Technical Transactions, series Chemistry, vol. 17(1), 2015, 99-108.
[3] Rieger F., Ditl P., Novák V., *Vortex depth in mixed unbaffled vessels*, Chemical Engineering Science, vol. 34, 1979, 397-403.
[4] Ciofalo M., Brucato A., Grisafi F., Torraca N., *Turbulent flow in closed and free-surface unbaffled tanks stirred by radial impellers*, Chemical Engineering Science., vol. 51, 1996, 3557-3573.
[5] Talaga J., *Measurements of tutbulent-flow parametres in a stirred mixer*, Chemical and Process Engineering, vol. 22, 3E, 2001, 1387-1392 (in Polish).
[6] Galletti C., Brunazzi E., *On the main flow features and instabilities in an unbaffled vessel agitated with an eccentrically located impeller*, Chemical Engineering Science, vol. 63, 2008, 4494-4505.
[7] Montante G., Bakker A., Paglianti A., Magelli F., *Effect of the shaft eccentricity on the hydrodynamics of unbaffled stirred tanks*, Chemical Engineering Science, vol. 61, 2006, 2807-2814.
[8] Galleti C., Pintus S. Brunazzi E., *Effect of shaft eccentricity and impeller blade thickenes on the vortices features in an unbaffled vessel*, Chemical Engineering Research and Design, vol. 87, 2009, 391-400.
[9] Karcz J., Cudak M., Szoplik J., *Stirring of a liquid in a stirred tank with an eccentrically located impeller*, Chemical Engineering Science, vol. 60, 2005, 2369-2380.
[10] Karcz J., Cudak M., *An effect of the type of an eccentrically located impeller on the efficiency of heat transfer process*, In Proceedings of the 12th European Conference on Mixing, 27-30 June 2006, Bologna, Italy, 727-734.

TECHNICAL TRANSACTIONS | CZASOPISMO TECHNICZNE
MECHANICS | MECHANIKA
2-M/2016

STANISLAV RUDOBASHTA[*], GALINA ZUEVA[**], VJACHESLAV DMITRIEV[***]

THEORETICAL AND EXPERIMENTAL BACKGROUNDS OF OSCILLATING INFRARED DRYING DISPERSED MATERIALS

TEORETYCZNE I EKSPERYMENTALNE PODSTAWY OSCYLACYJNEGO SUSZENIA PROMIENNIKOWEGO MATERIAŁÓW SYPKICH

Abstract

The research on the influence of the initial moisture content of seeds, of the duration of IR drying, of temperature regime on the effect of stimulation and keeping the effect with time, was carried out. A mathematical model for the dynamics of heating a seed layer, taking into account the moisture evaporation, is developed. Paper presents experimental data on mass conductivity properties for a dried layer of seeds, the recommendations for process equipment design are given.

Keywords: drying, kinetic calculation, zone method, dispersed materials

Streszczenie

W pracy analizowano wpływ początkowej zawartości wilgoci w nasionach, czasu trwania suszenia IR oraz zakresu temperatur na stymulację jakości nasion oraz utrzymywanie efektu stymulacji. Zaproponowano model matematyczny dynamiki ogrzewania warstwy nasion uwzgledniający odparowanie wilgoci. Przedstawiono dane eksperymentalne przewodności masowej dla warstw suszonych nasion oraz wytyczne projektowania urządzeń.

Słowa kluczowe: suszenie, obliczenia kinetyczne, metoda strefowa, materiały sypkie

DOI:

[*] Prof. PhD. Stanislav Rudobashta, Department of Heat Engineering, Hydraulics and Enterprises Energy Supply, Russian State Agrarian University.

[**] Prof. PhD. Galina Zueva, Department of Higher and Applied Mathematics, Ivanovo State University of Chemistry and Technology.

[***] Prof. PhD. Vjacheslav Dmitriev, Department of Security and Legal Order, Tambov State Technical University.

1. Introduction

Infrared drying of various materials is frequently used in practice [1-4], thus for drying heat-sensitive materials in order to prevent overheating, an oscillating mode in temperature must be used. It was found in [5] that the oscillating IR drying of the vegetable seeds carried out under conditions of the temperature range from t_{min} = 34°C till t_{max} = 40°C causes significant seeds stimulation. Research on the influence of the initial moisture content of seeds, of the duration of the IR drying on the effect of stimulation, were carried out in [6], as well as the research on keeping with time the stimulating effect. The mathematical model, which allows to calculate the dynamics of the heating material layer irradiated by an oscillating electromagnetic field – taking into account the evaporation of moisture from it is developed in [7], numerical experiments to study on the basis of the model the influence of technological parameters on the dynamics of layer heating are carried out in [8, 9]. They showed the possibility of the model in the organisation of the drying process. The calculations have been done in [8, 9] for a monolayer of seeds, but with mass conductivity data for isolated seeds. However, to reduce the size of the dryer for oscillating IR drying, the seeds must be dried in the bed. There are no data on mass conductivity of seeds in a layer, so the aim of this work is to obtain experimental data on mass conductivity of seeds in a layer, to describe these data with a function of moisture content and temperature of material, to compare the results for a layer with the data on mass conductivity of individual seeds, to develop an engineering method for calculating the kinetics of seeds oscillating infrared drying using these data and to calculate the industrial machine on its base.

2. Experimental study of seed layer mass conductivity

The mass conductivity of a seed layer was investigated with the zonal method – by receiving the drying curves with the exclusion of external diffusion resistance, and their processing by the method of splitting into a number of concentration zones and defining the value of mass conductivity coefficient for each of them by the solution of a linear differential equation of mass conductivity in a regular process mode. Drying curves were obtained when the drying agent (air) at velocity of 5 m/s had three different temperatures: 40, 50 and 60°C. As the object of the study "Stuttgarter Risen" onion seeds have been chosen because there are data on mass conductivity for a single seed, which could be compared to the results of the research.

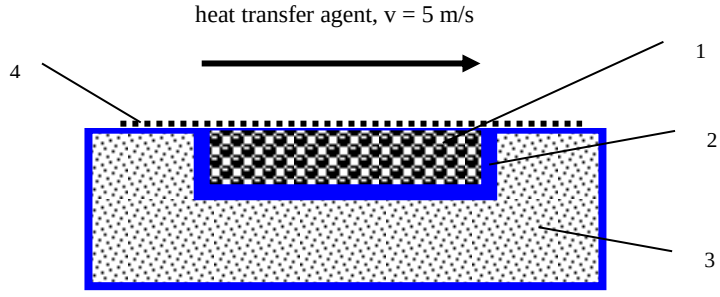

Fig. 1. Measuring cell for studying the kinetics of drying the seed layer
1 – layer of seeds; 2 – cell; 3 – thermal insulation; 4 – mesh

The measuring cell was designed as a cell filled with seeds, 5 mm high and 50 mm in diameter, situated in a substrate of foamed polyurethane (Fig.1).

The top layer was covered with a thin brass mesh (wire thickness of 0.12 mm, cell size of 1.5 mm), which prevents seeds from being blown-off by the air flow. A single "Stuttgarter Risen" onion seed is a limited cylinder with a diameter d = 1.7 mm and a length l = 0.9 mm (equivalent diameter d_{eq} = 1.57 mm). Thermocouples HC with 0.08 mm diameter electrodes were placed into three seeds, which measure the changes in seeds' temperature while drying. The seeds with embedded thermocouples were placed in three basic layers: the upper, middle and lower (bottom layer) (Figure 2.).

A measuring cell was placed into a working chamber of a dryer (Fig. 1), which was an air thermostat with air circulating inside it and driven by a fan. Air in the thermostat is dried by means of silica gel, which allowed to maintain a low moisture content that is close to zero. The set-up was equipped with an electric air heater, with TRM202 temperature regulators working HC with thermocouple. The air temperature was measured and maintained with an accuracy of ±0.1°C. A layer weight in the drying process was measured by AB 210-01 EDO electronic balance with accuracy of 1 mg cell without extraction of cell with seeds from a drying chamber, measuring time should not exceed 10 seconds.

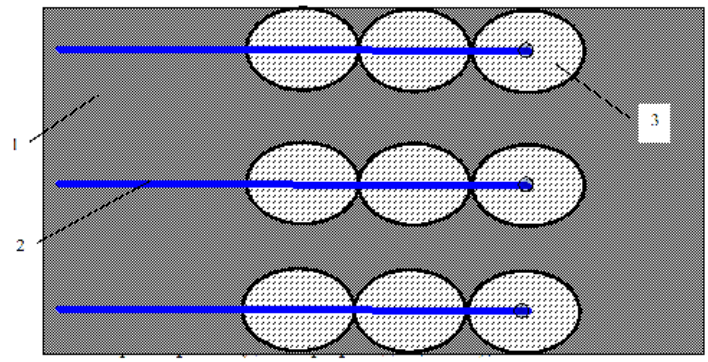

Fig. 2. The layout of thermocouples in the layer of seeds:
1 – a layer of seeds; 2 – thermocouple; 3 – seed

The analysis of drying curves of onion seed layer, obtained at different air velocities, showed that at velocity of 5 m/s external diffusion resistance is completely eliminated and the drying process is limited by the internal diffusion resistance, which makes it possible to determine the dependence of the mass conductivity ratio on the seeds' moisture content from drying curve by zonal method [10].

Fig. 3 illustrates the drying curves obtained when the velocity of the drying agent is 5 m/s, and Fig. 4 shows the experimental heating thermogram of elementary layers of seeds, obtained for drying agent at 50°C (at other temperatures of the drying agent, they have a similar form).

Consideration of the thermograms allows to come to two conclusions: 1) the temperature in each layer varies throughout the process of drying, so the drying is characterised by non-isothermal internal mass transfer; 2) heating curves for different

elementary layers of a material, despite the small thickness of the entire layer (5 mm), differ substantially. The values of mass conductivity coefficient k, m^2s^{-1} according to each concentration zone were calculated by a zonal method using drying curves, shown in Fig. 3 [10]. The changes in the value of the mass conductivity coefficient during the process calculated by zones are shown in Fig. 5.

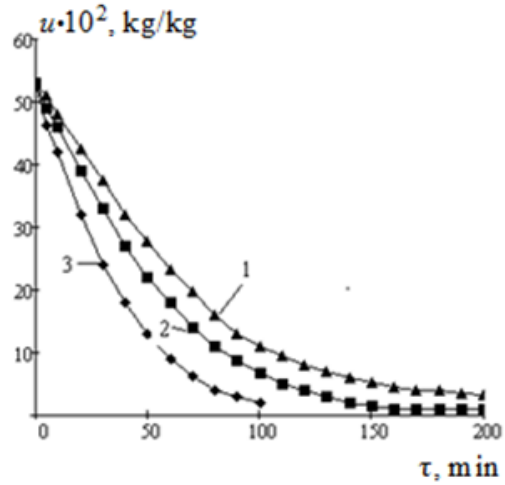

Fig. 3. The convective drying curves of a wet dense layer of "Stuttgarter Risen" onion seeds $u \cdot 10^2$, kg/kg (air velocity 5 m/s; 1 – $t_{d.a}$ = 40°C; 2 – $t_{d.a}$ = 50°C; 3 – $t_{d.a}$ = 60°C)

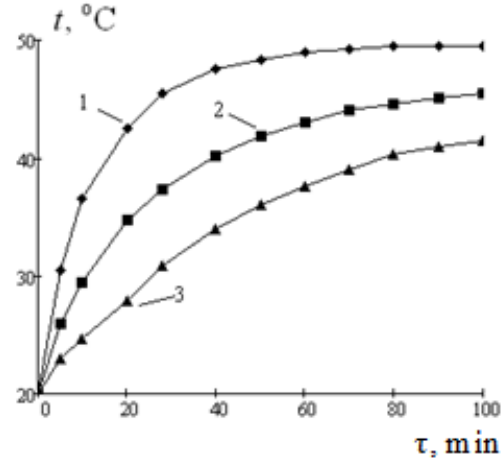

Fig. 4. Heating thermograms of elementary seeds layers at $t_{d.a}$ = 50°C:
1 – top layer; 2 – middle layer; 3 – bottom layer

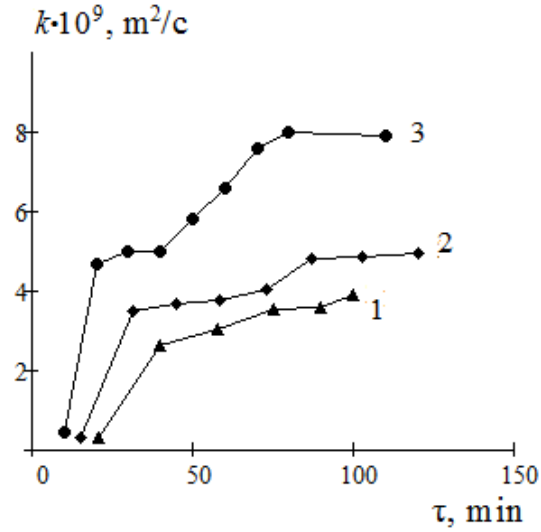

Fig. 5. Changing with time mass conductivity ratio while drying at air temperature:
1 – 40°C; 2 – 50°C; 3 – 60°C

3. The analysis and mathematical processing the data obtained

Examination of Fig. 5 allows to conclude the following: 1) the mass conductivity coefficient *k* changes significantly during drying, thus the calculation of drying kinetics at a constant value of *k* would result in significant errors in the determination of the drying time (estimation error arising from negligence of the change is given in [10]); 2) change in the coefficient k in the investigated drying process is due to its dependence on both moisture content and the temperature, but the effect of temperature on the coefficient k prevails over the effect of moisture, so the mass conductivity coefficient increases as the temperature of the seeds rises while drying; 3) coefficient *k* has the order of 10^{-9}, while its order is equal to 10^{-11} in drying single seed [11]. The difference in orders of mass conductivity coefficient while drying a unit seed and a seed layer is caused by the fact that during drying, a layer of vapour diffusion in areas between individual seeds plays an important role, while in a unit seed drying, vapour diffusion in spaces between individual seeds as a type of mass transfer is absent.

Since the mass conductivity coefficient *k* as the physical parameter is a function of the moisture content and temperature of the material $k = f(u,t)$, it is advisable in experimental data obtained for this coefficient to untie affecting parameters, thus it gives an opportunity to present this coefficient as a physical quantity, and not as a regime parameter, and to use it for engineering calculations. This problem was solved with the use of multidimensional (two-dimensional) function approximation procedures using the Cobb-Douglas model in the MATHCAD system [12]. As a result, the following functional dependence of the mass conductivity on the moisture content and temperature of the material was obtained, which

can be used in the calculation of convective drying kinetics of a dense layer of "Stuttgarter Risen" onion seeds, blown over the surface

$$k = a_0 \cdot u^{a1} \cdot t^{a2} \cdot f(t_{d.a}/50), \tag{1}$$

where

$$a_0 = 4.12 \cdot 10^{-15};\ a_1 = 6.19 \cdot 10^{-2};\ a_2 = 3.73;$$

$$f(t_{d.a}/50) = 9.59 - 15.15 \cdot (t_{d.a}/50) + 6.50 \cdot (t_{d.a}/50)^2;$$

t – temperature of the material, °C,

$t_{d.a}$ – temperature of drying agent, °C,

U – local moisture content, kg/(kg of dry material).

Equation (1) was used to calculate the drying kinetics of onion seed layer during oscillating IR drying at layer thickness h = 5 mm, at oscillation of seeds' temperature between t_{min} = 34°C to t_{max} = 40°C, at continuous blowing of the seeds' surface by atmospheric air with temperature $t_{d.a}$ = 20°C. The calculation is performed under the condition that the temperature of the material to be dried is constant and equal to $t = (t_{min} + t_{max})/2 = (34° + 40°)/2 = 37°C$. The results of calculation and their comparison with experimental drying curve are shown in Fig. 6.

As it can be seen in the figure, the calculation of the drying curve using data on mass conductivity described by equation (1) gives a satisfactory agreement with the experiment. The same figure shows the comparison between experimental and calculated drying curves for a monolayer of onion seeds, in this calculations data on mass conductivity for individual seeds, shown in [11] are used. In this case, the calculated and experimental drying curves have satisfactory agreement, and the drying curve for a monolayer of seeds passes, as would be expected, more steeply than for the layer.

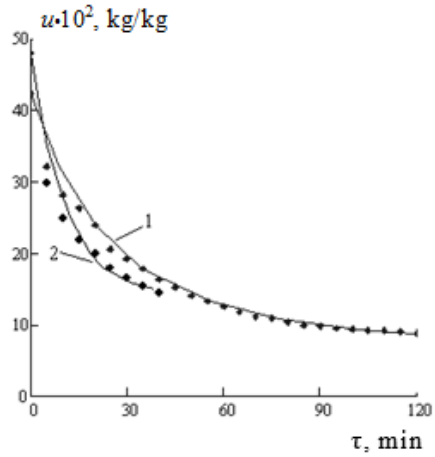

Fig. 6. Comparison of experimental and calculated drying curves of "Shtutgarer Risen" onion seeds at oscillating infrared energy supply (the line – calculation, points - experiment):
1 – dense blown layer; 2 – monolayer; t_{min} = 34°C; t_{max} = 40°C, $t_{d.a}$ = 20°C.

4. Recommendations for hardware design of oscillating infrared seeds drying and kinetic calculation of the process

The studies performed have shown that the data on mass conductivity of seeds in a layer are reliable and can be used for calculating drying kinetics. The absence of oscillations in the moisture content of seeds on the drying curve in the oscillating seeds layer IR drying, carried out in the temperature range of the material t_{min} = 34°C ... t_{max} = 40°C (Fig. 6), suggest the possibility of calculating the kinetics of this process on the basis of the solution of mass conductivity differential equation written for layer blown up on the surface, under appropriate boundary conditions of the problem – using the data in terms of mass conductivity for a layer. The calculation methods are described in [10]. To implement this method in practice, is necessary to obtain data on the mass conductivity of dried seeds, which can be obtained in the same way as it was done in this work for onion seeds.

The infrared dryer for continuous oscillating infrared drying can be carried out on the basis of a typical conveyor dryer with IR emitters located over the dried material (e.g. based on a commercial IR dryer, such as an infrared belt dryer of Russian production model UTZ-4). Equipping a corresponding dryer by automatic control system will implement an oscillating mode of infrared drying. The technique of engineering kinetic calculation has been proposed for the apparatus of this type on the basis of a developed mathematical model, using the data of mass conductivity coefficient for a layer. The aim of the calculation is to determine the necessary residence time for the seeds in the apparatus, thus providing the specified productivity, and at the same time, it allows to find the device dimensions on the stage of its design.

References

[1] Ratti C., Mujumdar A. S., *Infrared drying*, in *Handbook of Industrial Drying*, 3-rd edition. A. S. Mujumdar (Ed), CRC Press, Boca Raton, FL. 2007.

[2] Mujumdar A. S. (Ed)., *Drying'92*, Proceedings of 8-th International Drying Symposium, Elsevier, Amsterdam, 1992, 667-729.

[3] Supmoon N., Noomhorm, A. *Influence of combined hot air impingement and infrared drying on drying kinetics and physical properties of potato chips*, Drying Technology, vol. 31(1), 2013, 24-31.

[4] Bon J., Kudra T,. *Enthalpy-driven optimization of intermittent drying*, Drying Technology, vol. 25 (4), 2007, 523-532.

[5] Rudobashta S. P., Grigoriev I. V., *Impulse infrared drying the seeds of vegetables, nontraditional and rare plants*, Industrial Heat Engineering, vol. 33 (8), 2011, 85-90 (in Russian).

[6] Rudobashta S. P., Zueva G. A.; Zuev N. A., S*eeds stimulation by oscillating infrared heat treatment*, Industrial Heat Engineering, vol. 35 (7), 2013, 218-222 (in Russian).

[7] Rudobashta S. P., Kartashov E. M., Zuev N. A., *Heat-and Mass Transfer in Drying in an Oscillating Electromagnetic Field*, Theoretical Foundations of Chemical Engineering, vol. 45 (6), 2011, 830-837.
[8] Rudobashta, S., Zueva G., Zuev N., *Mathematical Modelling and Numerical*, Analysis of Oscillating Infrared Seeds Drying Process, XIII Polish Drying Symposium, Kołobrzeg, 5-6 September, 2013, 1-6.
[9] Rudobashta, S., Zueva G., Zuev N., *Mathematical modeling and numerical simulation of seeds drying under oscillating infrared irradiation*, Drying Technology, vol. 32 (11), 2014, 1352-1359.
[10] Rudobashta, S. P., *Mass transfer in the solid phase systems*, Chemistry, Moscow 1980 (in Russian).
[11] Rudobashta S. P., Zueva G. A., Dmitriev V. M., Zuev N. A., *Mass conductivity when drying colloidal capillary-porous materials*, Proceedings of the Higher Educational Institutions. Chemistry and Chemical Engineering, vol. 57 (1), 2014, 103-107 (in Russian).
[12] Ohorzin V. A., *Applied mathematics in MATHCAD system*: Schoolbook, Lany, St. Petersburg 2009 (in Russian).

TECHNICAL TRANSACTIONS | CZASOPISMO TECHNICZNE
MECHANICS | MECHANIKA
2-M/2016

WIESŁAW SZATKO*, ŁUKASZ WAWSZCZAK**

WORK SAFETY INTERACTION ASSESSMENT OF VOC'S EMISSION UNDER EMERGENCY WORK OF IPPC INSTALLATION

OCENA ODDZIAŁYWANIA NA ŚRODOWISKO PRACY EMISJI LZO W WARUNKACH AWARYJNEJ PRACY INSTALACJI IPPC

A b s t r a c t

The study evaluated the impact of emissions (VOCs) as a result of the operation of the printing of plant at working positions of those performing their tasks outdoors or in buildings next door. The first part of the paper presents the general characteristics of the process and materials used for printing. The further part shows the results of the modelling of emissions, depending on the operating state of purification (emission in normal conditions and emission in failure state of the afterburner).

Keywords: *modelling of emissions, printing industry, heat-set rotary offset, working under emergency conditions, failure of afterburner*

S t r e s z c z e n i e

W pracy oceniono wpływ emisji zanieczyszczeń (LZO) przez zakład poligraficzny na stanowiskach pracy usytuowanych na wolnym powietrzu lub w budynkach sąsiadujących. Część pierwsza prezentuje charakterystykę procesu oraz materiałów wykorzystywanych do druku. W dalszej części przedstawiono wyniki modelowania emisji zanieczyszczeń w zależności od stanu pracy układu oczyszczającego (normalna praca oraz awaria dopalacza).

Słowa kluczowe: *modelowanie emisji zanieczyszczeń, przemysł poligraficzny, gorący offset rotacyjny (heat-set), praca w warunkach awaryjnych, awaria dopalacza*

DOI:

* Dr Wiesław Szatko, Institute of Thermal and Process Engineering, Faculty of Mechanical Engineering, Cracow University of Technology.
** MSc. Eng. Łukasz Wawszczak, Eco-HERA, Cracow.

1. Introduction

As part of this work, concentrations of pollutants in ambient air emitted during technological processes were calculated (based on the measurements of emissions of pollutants):

a) under normal conditions (operation of all equipment is compatible with the assumptions of technological process and the conditions, which are set out in the applicable decision – permission for the introduction of pollutants into the air (i.e. the integrated and sectoral permission)
b) during fault conditions of the thermal afterburner and emissions of emitters of emergency in accordance with the conditions, which are set out in the applicable decision – permission for the introduction of pollutants into the air (i.e. the integrated permission):
   - in the case of "normal weather conditions";
   - in the case of "very unfavourable weather conditions".

The publication presents a comparison of the calculated concentrations of pollutants in the air to the limit values for specific workplaces by the applicable Ordinance of the Minister of Labour and Social Policy with the maximum concentrations of pollutants.

2. The analysis in the context of emissions of dust and gas in various operating conditions of the flue gas purification

2.1. Research object

The object of the analysed company is printing activity. The installation that is classified as an IPPC installation (web offset machines) is covered by an integrated permission defined in the Regulation of the Minister of the Environment of the 27th of August 2014 on the types of installations, which may cause significant pollution of individual elements of nature or the environment as a whole (Journal of Laws of 2014 item 1169), i.e. installation for offset printing, classified as an installation for the surface treatment of substances, objects or products using organic solvents, solvent consumption of 150 kg per hour or more than 200 tonnes per year.

The plant area has an approximately rectangular shape with dimensions of 340×120 m. Other industrial plants outweigh in the vicinity of the plant. Wastelands, fields, meadows, groves, etc. prevail from the northern side. The nearest residential buildings (low, dispersed buildings) are located approximately 500 meters from the plant.

2.2. Emission of contaminants

Emission is the act of an operation, which involves the transfer of any element to its surroundings. Emission of contaminants to the environment involves the introduction of pollution (the products of human activity) to the environment, and in particular:

- substances (e.g. solid contaminants, liquid or gaseous contaminants),
- energy (e.g. noise, vibration, electromagnetic fields) to the air, water, soil or earth.

The definition of emission in ecological importance is given in the Act of the 27th of April 2001 on Environmental Protection Law. By emissions, legislator determines the introduction, directly or indirectly, of substances or energy, such as heat, noise, vibration and electromagnetic fields to the air, water, soil or earth as a result of human activity. Importantly, substances are chemical elements and their compounds, mixtures or solutions appearing in the environment or elements, which are the results of human activity. A hazardous substance is one or more substances or mixtures of substances, which, because of their chemical, biological or radioactive characteristics, in the event of improper handling, cause risk to the life or health of humans or the environment; a hazardous substance may be a raw material, product, intermediate waste, as well as a substance, which arises as a result of a failure.

The type and quantity of the introduced substances or energy at a given time and the concentration or levels of substances or energy, in particular in waste gases, sewage and waste generated, is defined as the amount of emissions.

In this paper, we analysed the emissions of solid, liquid and gas contaminants into the air. Emission unit is kg/h (or their derivatives – mg/s, Mg/year).

As a result of the emission of pollutants, the concentration of the pollutant increases in the air. This concentration is dependent on the amount of emissions, characteristics of the emitted gases, the emission process and mainly on the meteorological conditions. Distribution of concentrations of the contaminants in the air is called immission pollution, and the area under study – immission field. The unit of immission is $\mu g/m^3$, determined for the following conditions (temperature 293 K, pressure 101.3 kPa).

Table 1

The list of pollutants emitted into the atmosphere

No	Pollution
1	Benzene
2	Methylethylketon
3	Nitrogen dioxide
4	Sulphur dioxide
5	Ethylbenzene
6	Xylene
7	Sulphuric acid
8	entire dust
9	PM10 dust
10	PM2.5 dust
11	Styrene
12	Carbon monoxide
13	Toluene
14	aliphatic hydrocarbons
15	aromatic hydrocarbons

2.3. Types of emitted pollutants

All the pollution associated with both the functioning of the basic technological processes, as well as the auxiliary processes, were taken into account. The table below lists

all the contaminants identified in the measurements of emissions performed by specialised companies dealing with the measurement of emissions, as well as listed in material safety data sheets of used raw materials.

2.4. Legal requirements relating to the issue of emerging contaminants

The permissible concentrations of pollutants on the health requirements defined in the Regulation of the Minister of Labour and Social Policy of the 6th of June 2014 on the maximum permissible concentration and intensity of harmful factors in the work environment (Journal of Laws 2014/817 of the 23rd of June 2014) according to the above Regulation pursuant to Art. 228 § 3 of the Act of the 26th of June 1974 – Labour Code (Journal of Laws of 1998. No. 21, item 94, as amended):

§ 1.1. The values of maximum concentrations of chemicals and dust of harmful factors in the work environment are specified in the list attached as Annex 1 to the Regulation.

§ 2. The values referred to in § 1.1, determine the maximum permissible concentrations of harmful factors, determined as:

1) The maximum allowable concentration (MAC) – the value weighted average concentration, the impact on the employee during an 8-hour daily and average weekly working time, as defined in the Act of the 26th of June 1974 – the Labour Code, the period of its activity should not cause negative changes in the state of health and the health of the future generations;

2) The maximum instantaneous concentration (MIC) – average value of concentration, which should not cause negative changes in the health of the worker, whether in the workplace no longer than 15 minutes and not more than 2 times during a work shift, at an interval of less than 1 hour;

3) maximum threshold concentration (MTC) – the concentration that due to the risk of health or life of the employee cannot be exceeded in the work environment at any time.

Note the differences in the definition of pollution in the environmental protection legislation and the regulations on permitted values of contamination at workplaces.

2.5. Assumptions about the calculations of the spread of contamination

To realise this objective work, three variants (variant I variant IIA and IIB variant) were established, for which the analysis of the spread of pollutants was performed:

- Variant I – normal operation of all installations and equipment reducing emissions. In this variant of pollution, arising printing presses are collected in one conduit and carried to catalytic afterburner where they are burned. The purified exhaust gas is emitted into the atmosphere.
- Variant II – failure of the catalytic afterburner. In this variant of pollution, the arising printing presses are discharged by the individual emergency emitters to the atmosphere. There is no purification of impurities.

Due to the fact that the aim of the study was to determine the concentrations of pollutants in the grid of receptors and in free points, and as we know, this concentration

will be a function of the emission and meteorological conditions, two variants: IIA and IIB variant were separated for the second variant.

- Variant IIA is characterised by normal meteorological conditions.
- Variant IIB is characterised by very bad weather.

Thus, the size of the air pollution will vary discretely;

- the lowest contamination to the conditions described in Option I, which will occur approximately 75% of the time during the year,
- high contamination for conditions described in Variant IIA, which will be present to 7.5% of the time during the year,
- very high contamination for conditions described in the variant IIB, which will occur to 2.5% of the time during the year,
- lack of contamination, when the system does not work – about 15% per year.

Normal meteorological conditions mean meteorological data containing meteorological statistics for given area and the different seasons (winter, summer and year).

The nuisance of sources of emissions to the environment depends, to a large extent, on meteorological parameters, of which the most important are: speed and wind direction, the equilibrium of the atmosphere, the air temperature and precipitation. Factors affecting speed and intensity of the spread of contamination are: atmospheric stability conditions characterised by the possibility of atmospheric diffusion and the frequency and speed of the winds. There are 6 classes of atmospheric stability, and 36 found in the atmosphere of a combination of equilibrium states and wind speed.

- Class I – highly unstable,
- Class II – moderately unstable,
- Class III – weak instability,
- Class IV – indifferent balance,
- Class V – poor durability,
- Class VI – constant and firmly fixed equilibrium,

The occurrence of class balance I ÷ III proves favourable dispersion (taking out the emissions outside the region of their emittance). The occurrence of states V and VI proves unfavourable spread of contamination and the possibility of their concentration in the area of emissions.

Class IV is an indifferent class, but its occurrence while large wind speed favours a beneficial spread of contamination.

Due to the fact that computer programs used for modelling the emission calculate the distribution of contaminants for the annual meteorological values, there was no possibility to introduce in the program the conditions, which occurred in the small amount of time (about several to several tens of hours). For this reason, when trying to grasp the impact of very adverse weather conditions, after a full analysis of the data resulting from our own research and literature data, it was found that it is possible to do this indirectly by increasing the size of the emission with the ratio, which presents the hindered spread of pollutants in the air.

2.6. Tables of distribution of concentrations of selected pollutants around the premises

Distribution maps of concentrations of individual pollutants (according to Polish reference methodology for performing the analysis) were made on the basis of knowledge of the emission of pollutants (developed on the basis of measurements carried out by an accredited laboratory). The results in the following tables allow you to determine where the greatest concentration of major pollutants is in the vicinity of the plant and to compare them with the maximum concentrations of pollutants in the workplace:

Working conditions in offices

Table 2

Working conditions – normal operation of afterburner

No	No*	Pollution	MAC µg/m^3	STEL µg/m^3	Maximum concentration µg/m^3	The ratio of maximum concentration to MAC
1.	1	The dust containing free silica >50 % inhalable fraction	**2 000**	**---**	***8,175*** **11,443**	***0,0041*** **0,0057**
2	1	The dust containing free silica >50 % respirable fraction	**300**	**---**	***8,175*** **11,443**	***0,0272*** **0,0381**
3	37	Benzene	**1600**	**---**	***1,817*** **1,650**	0,0011 **0,0010**
4	448	Styrene	**50 000**	**100 000**	***0,871*** **0,780**	***0,0001*** **0,0001**
5	67	Methylethylketon	**450 000**	**900 000**	***9,918*** **17,021**	***0,0001*** **0,0001**
6	220	Ethylbenzene	**200 000**	**400 000**	***0,919*** **0,841**	***0,0001*** **0,0001**
7	301	Xylene	**100 000**	**---**	***1,530*** **1,412**	***0,0001*** **0,0001**
8	479	Toluene	**100 000**	**200 000**	***1,282*** **1,174**	***0,0001*** **0,0001**
9	188	Nitrogen dioxide	**700**	**1500**	***68,840*** **157,177**	***0,0983*** **0,2245**
10	190	Sulphur dioxide	**1300**	**2700**	***8,925*** **6,902**	***0,0069*** **0,0053**
11	320	Sulphuric acid	**50**	**---**	***0,110*** **0,074**	***0,0022*** **0,0015**
12	475	Carbon monoxide	**23 000**	**117 000**	***202,712*** **172,499**	***0,0088*** **0,0075**
13	---	aliphatic hydrocarbons	---	---	***24,586*** **21,915**	---
14	---	aromatic hydrocarbons	---	---	***11,277*** **10,055**	---

Table 3

Operating conditions: failure of afterburner – favourable weather conditions

No	No*	Pollution	MAC µg/m^3	STEL µg/m^3	Maximum concentration µg/m^3	The ratio of maximum concentration to MAC
1.	1	The dust containing free silica >50 % inhalable fraction	**2 000**	---	***8,194*** **9,706**	***0,0041*** **0,0048**
2	1	The dust containing free silica >50 % respirable fraction	**300**	---	***8,194*** **9,706**	***0,0273*** **0,0323**
3	37	Benzene	**1600**	---	***22,951*** **16,859**	***0,0143*** **0,0105**
4	448	Styrene	**50 000**	**100 000**	***24,305*** **17,868**	***0,0005*** **0,0004**
5	67	Methylethylketon	**450 000**	**900 000**	***9,938*** **17,221**	***0,0001*** **0,0001**
6	220	Ethylobenzene	**200 000**	**400 000**	***24,337*** **17,911**	***0,0001*** **0,0001**
7	301	Xylene	**100 000**	---	***40,406*** **29,585**	***0,0004*** **0,0003**
8	479	Toluene	**100 000**	**200 000**	***34,174*** **25,020**	***0,0004*** **0,0003**
9	188	Nitrogen dioxide	**700**	**1500**	***146,415*** **236,042**	***0,2092*** **0,3372**
10	190	Sulphur dioxide	**1300**	**2700**	***10,987*** **8,799**	***0,0084*** **0,0068**
11	320	Sulphuric acid	**50**	---	***0,110*** **0,074**	***0,0022*** **0,0015**
12	475	Carbon monoxide	**23 000**	**117 000**	***210,548*** **180,460**	***0,0091*** **0,0078**
13	---	aliphatic hydrocarbons	---	---	***700,524*** **514,828**	---
14	---	aromatic hydrocarbons	---	---	***321,060*** **235,955**	---

Table 4

Operating conditions: failure of afterburner – adverse weather conditions

No	No*	Pollution	MAC µg/m^3	STEL µg/m^3	Maximum concentration µg/m^3	The ratio of maximum concentration to MAC
1.	1	The dust containing free silica >50 % inhalable fraction	**2 000**	**---**	***8,220*** **9,709**	***0,0041*** **0,0048**
2	1	The dust containing free silica >50 % respirable fraction	**300**	**---**	***8,220*** **9,709**	***0,0274*** **0,0323**
3	37	Benzene	**1600**	**---**	***78,976*** **50,401**	***0,0494*** **0,0315**
4	448	Styrene	**50 000**	**100 000**	***84,308*** **53,688**	***0,0017*** **0,0011**
5	67	Methylethylketon	**450 000**	**900 000**	***9,952*** **17,454**	***0,0001*** **0,0001**
6	220	Ethylobenzene	**200 000**	**400 000**	***84,340*** **53,714**	***0,0001*** **0,0001**
7	301	Xylene	**100 000**	**---**	***140,024*** **89,177**	***0,0014*** **0,0009**
8	479	Toluene	**100 000**	**200 000**	***118,450*** **75,438**	***0,0012*** **0,0007**
9	188	Nitrogen dioxide	**700**	**1500**	***429,360*** **361,463**	***0,6134*** **0,5164**
10	190	Sulphur dioxide	**1300**	**2700**	***17,298*** **11,643**	***0,0133*** **0,0090**
11	320	Sulphuric acid	**50**	**---**	***0,124*** **0,086**	***0,0025*** **0,0017**
12	475	Carbon monoxide	**23 000**	**117 000**	***218,732*** **189,409**	***0,0095*** **0,0082**
13	---	aliphatic hydrocarbons	---	---	***2430,695*** **1547,808**	---
14	---	aromatic hydrocarbons	---	---	***1114,013*** **709,378**	---

The results for office space in the building number 1 are presented by the green colour (italics), while the results for office space in building number 2 are presented by the blue colour.

3. Conclusion

1. The amount of pollutant concentrations at workplaces (points free) is dependent on the emission of pollutants.
2. An increase in the concentrations of pollutants, which are burnt by the afterburner in the event of a failure of the afterburner and adverse weather conditions, is 10,000% (assuming normal operation of the afterburner for 100%).
3. The size of the concentrations in free points is the smallest at the normal operation of the afterburner and the largest in the failure of afterburner and adverse weather conditions,
4. The volume of concentrations in free points is the lowest for the level of an area ($Z = 0$) and increases with the increasing Z and reaches maximum values at $Z = 11$ m.
5. The analysed work of the plant does not pose a threat to life and health of office workers; however during the failure of the afterburner, temporarily onerous conditions may occur, but they are not harmful.
6. It should be noted that the exposure limits for the workplace environment are about 1,000 times higher than those resulting from environmental regulations. For this reason, the STEL and TWA are expressed in mg/m^3, while the reference values are set out in the environmental protection legislation in $\mu g/m^3$.

TECHNICAL TRANSACTIONS | CZASOPISMO TECHNICZNE
MECHANICS | MECHANIKA
2-M/2016

MAŁGORZATA ŚRODULSKA-KRAWCZYK*, JERZY ROSIŃSKI**

WET DUST COLLECTION IN SUB-ZERO TEMPERATURES

ODPYLANIE MOKRE W TEMPERATURACH UJEMNYCH

A b s t r a c t

The results of experimental studies confirm the suitability of non-freezing liquids for use as dust collecting liquids in equipment working at low temperatures. Based on the completed studies, the hypothesis regarding the impact of liquid viscosity on the effect of releasing the surface collecting the dust particles and, therefore, on the efficiency of the dust collection process cannot be clearly verified. Decreasing the efficiency of dust collection correlated with the increase of liquid viscosity is likely an effect of changing the conditions for the formation of liquid dust collectors.

Keywords: wet dedusting, dedusting efficiency, dedusting in sub-zero temperatures

S t r e s z c z e n i e

Wyniki badań eksperymentalnych potwierdzają przydatność płynów niezamarzających do wykorzystania urządzeniach pracujących w niskich temperaturach. Hipoteza dotycząca wpływu lepkości cieczy na uwolnienie powierzchni wychwytu cząstek pyłu, a w związku z tym skuteczność procesu odpylania nie może być jednoznacznie zweryfikowana. Zmniejszenie skuteczności odpylania związane ze wzrostem lepkości cieczy może być efektem zmiany warunków tworzenia ciekłych kolektorów.

Słowa kluczowe: mokre odpylanie, skuteczność odpylania, odpylanie w temperaturach ujemnych

DOI:

* Chair of Chemical and Process Engineering, Faculty of Chemical Engineering and Technology, Cracow University of Technology.

** Department of Industrial Apparatus, Institute of Thermal and Process Engineering, Cracow University of Technology.

The operation of wet dust collection equipment, especially periodic operation, in sub-zero temperatures is problematic and expensive. It requires the use of additional equipment, maintaining an above-zero temperature within the unit or the use of non-freezing liquids for dust collection. The literature regarding wet dust collection lacks the assessment of possibilities and results of tests in the field of dust collection from gas using non-freezing liquids. Despite the fact that the proposed method is expensive, it should be mentioned that in certain conditions, it may be the only solution available. This pertains in particular to the equipment located outside buildings and operating in winter conditions. This equipment, frequently for the lack of indoor installation, operates directly adjacent to industrial systems. Often, their function is a short-term, periodic operation in case of system failure. It is, therefore, vital to maintain their permanent stand-by status by the use of types of liquids, which do not freeze in sub-zero outdoor temperatures as the dust collecting liquid.

In the process of operation, the temperature of the collection liquid can be changed in the course of direct contact heat exchange inside the unit. Temperature changes are accompanied by alterations in the physical properties of the dust collection liquid, in particular – viscosity.

There are no descriptions of theoretical or experimental studies determining the effect of the viscosity of the dust collection liquid on the efficiency of the dust collection process. The reason seems to be the fact that water is the most prominent dust collection liquid and the units most frequently operate in stable temperature conditions.

Discussions substantiating the possibility of the effect of liquid viscosity on the efficiency of the dust collection process can be related both to the analysis of basic mechanisms affecting the deposition of particles on liquid collectors and the conditions of generating said collectors. The transmission of dust particles from gas to the liquid occurs for the most part as a result of inertial effects, catching effect and diffusion. Dust particles are separated in liquid collectors – depending on the type of the wet dust collector: droplets of liquid moving in a stream of aerosol, layers of liquid formed in the unit, surfaces of gas bubbles formed in the barbotage process or wet surfaces of the walls of the unit. One of the tendencies in the development of wet dust collection systems is the introduction of intensive operation units with a large gas phase flow capacity, which would entail an advantageous decrease in the size of the units. In these cases, due to the high relative velocity of the gas and liquid phases, the inertial and direct catching mechanisms have a decisive impact on the dust collection process.

The Warych's monograph [1] contains an extensive description of individual mechanisms on the dust particles deposition on liquid collectors. Descriptions of the mechanisms and their impact on the efficiency of the dust collection process can be found in virtually all monographs, e.g. Warych's [2] or Löffler's [3] addressing the issues of wet dust collection from gas. The literature assigns less significance to the description of the conditions of the generation of liquid collectors and their impact on the efficiency of the dust collection process.

When discussing the mechanism of inertial effects independent from the dust collector, it is generally assumed that in the case of hydrophilic dusts, dust contact with the surface of the liquid is equal to immediate absorption of the dust by the liquid and therefore – immediate release and renewal of the liquid surface for further collisions. In the case of hydrophobic (poor wettability) dusts, the time required for the absorption of the particle by

the liquid may be longer than the time after which the next particle comes into contact with the surface of the liquid. The reduction of the dust collection capacity of the liquid is therefore probable – due to the deflection of the particle approaching the surface of the liquid from the deposited particle. This effect can be considered particularly probable because, in the wet dust collection conditions, more dust collides with each liquid surface element than is required to coat the surface once. Therefore, the rate of particle absorption can be critical in the efficiency of the dust collection process [4]. The rate of particle absorption can be affected not only by the energy required to overcome the surface tension forces, but also the velocity of the particle in a liquid medium, depending on its viscosity.

The efficiency of the dust collection process can be correlated [4] with the rate of binding of dust and liquid, defined as the mass m_s penetrating the liquid surface unit A into the liquid as a result of the collision of dust particles with the surface in a unit of time:

$$r = \frac{m_s}{A \cdot \tau} \tag{1}$$

The rate of binding of dust and liquid depends on the physical and chemical properties of the dust and its susceptibility to wetting, physical and chemical properties of the gas and the dust collection liquid as well as the concentration of the aerosol. In order to verify his hypothesis, Kabsch [4] carried out studies regarding the effect of aerosol concentration on the rate of binding of dust and liquid. The increase in the concentration of dust in gas resulted in an increase of the rate of binding; however, to a lesser degree than would result from linear relationship.

The hypothesis that wettability is significant in the case of inertial particle deposition and rate of penetration of the liquid seems to be justified. The confirmation is the Weber's experiment [5] – shooting 1 mm water droplets with glass and silicone balls. Wettable dust balls immediately penetrated inside the droplets, silicone balls accumulated on the surface.

The analysis of basic wet dust collection models by Semrau, Barth and Calvert [3], no effect of the viscosity of the suspension on the dust collection process was found. Pemberton [6] found that in the case of deposition of particles with poor wettability on droplets, their penetration inside the liquid is necessary and their movement in the liquid is determined by Stokes' law. The rate of movement depends on the medium resistance coefficient and also the dynamic liquid viscosity index. The efficiency of dust particles deposition on droplets as a result of the simultaneous effects of three mechanisms – inertial, impaction, interception and diffusion – is described by a semi-empirical Slinn's formula [7], taking into account the relation between liquid viscosity and gas viscosity.

It is generally believed that there is a specific droplet diameter [8], for which optimum conditions are achieved for the deposition of specific size dust particles, and the efficiency of dust particles deposition on the droplet quickly decreases together with the decrease in particle size.

Upon their analysis of the circulating dust collector operation, Jarzębski and Głowiak [9] found that the inertial dust collision with water droplets is key to the dust collection process. The efficiency of dust particles deposition decreases with the increase in the size of droplets generated in the deposition area. In the case of droplet population with compressed air, the size of the droplets is determined by the Nukijama and Tanasawa formula [10], which indicates that droplet size is positively correlated with the viscosity of the liquid

phase. An increase in the viscosity can therefore result in a decrease of the dust collection efficiency.

The height of the dynamic foam layer created in the dust collection at a given relative difference between the gas and liquid phase velocities is reduced with the increase in the liquid viscosity [11], resulting in decreasing effectiveness of the dust collection system.

It should follow that a similar effect also applies to the layer of intensive barbotage and the droplet–splash layer often occurring in dust collection systems.

In summary, it can be said that the literature describes cases, which could warrant conclusions regarding the effect of liquid viscosity on the efficiency of the dust collection process. This effect can be observed when considering the inertial effects as well as variables, together with the change in viscosity, generation conditions and sizes of the created collectors.

Since, in the case of wet dust collection in intensive operation units, the inertial mechanism is key to the efficiency of the process, it was decided to conduct model tests on a modified circulating system. The construction of the model unit was simplified compared to classic circulating dust collectors. The two-chamber structure was abandoned, the "dirty" chamber was included in the guide channel. In this case, all dust particles are captured in one unit volume. The separation of dust particles in the unit occurs on droplets generated in the guide, in the intensive barbotage zone formed near the aerosol outlet from the guide, on the wetted surfaces of the guise, in the layer of liquid flowing from the guide (water curtain) and in the droplet-splash layer. In the conditions of developed unit operation, there is a possibility of generating almost all types of liquid collectors occurring in wet dust collection processes.

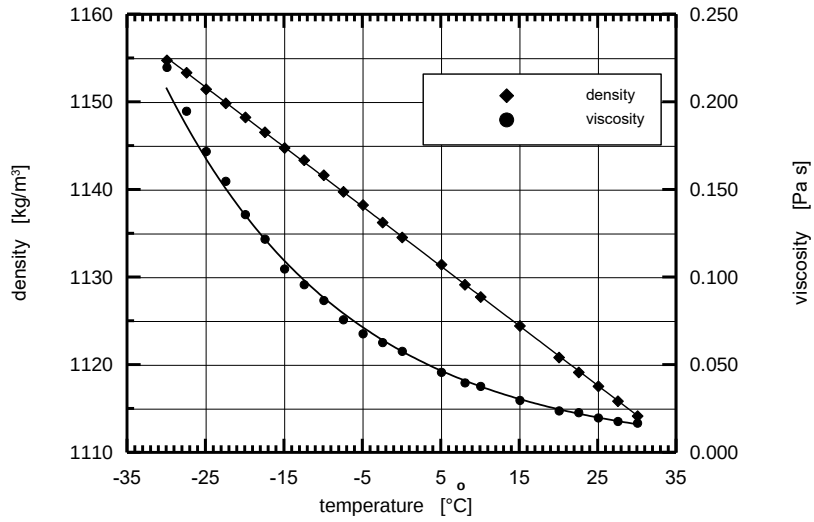

Fig. 1. Relationship between density / non-freezing liquid dynamic viscosity index and temperature

The tests were conducted using a non-freezing liquid with viscosity strongly reacting to changes in the temperature. The relationship between density / non-freezing liquid dynamic

viscosity index and the temperature is presented in the diagram – figure 1. Due to the high dynamic viscosity, the liquid was mixed with water in a 1:1 ratio. This decreased the dynamic viscosity of the solution, which in the temperature range of: - 10°C to 15°C changed between 0.004 and 0.00081 Pa·s. At this concentration, the crystallisation temperature for the liquid is - 37°C, which is important for use in actual industrial conditions.

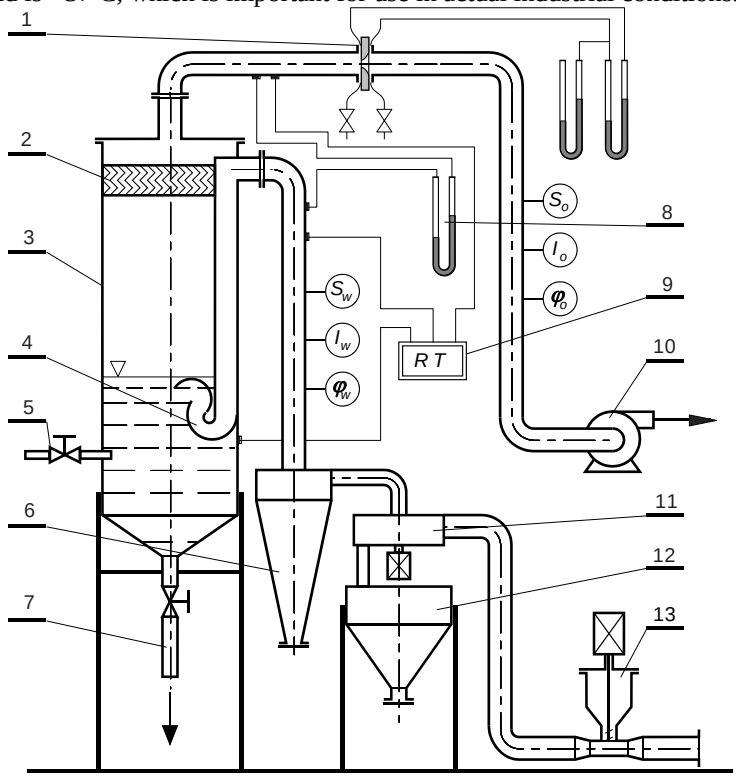

Fig. 2. Testing unit setup
1 – measuring orifice, 2 – liquid trap, 3 – rotoclone, 4 – guide, 5 – water supply, 6 – sorter discharge cyclone, 7 – suspension discharge from the rotoclone, 8 – measurement of the pressure drop on the rotoclone, 9 – thermometer, 10 – exhaust fan, 11 – sorter, 12 – tank for oversize particles separated in the sorter, 13 – dust batcher, S_w, S_o – dust concentration measurement system, I_w, I_o – grade composition measurement system, φ_w, φ_o – gas moisture content measurement system

A testing unit presented in figure 2 was constructed in order to conduct the tests. The main component of the unit is the rotoclone–type circulating dust collector /3/. The aerosol was created by introducing dust to the inlet pipeline with a batcher /13/. The application of a batcher with efficiency adjustment enabled the creation of the desired dust concentration on the dust collector inlet. Since talc was used as test dust, a pneumatic sorter /11/ was installed on the inlet pipeline to stop dust grades over 20 μm. The dusty gas travelled via the inlet pipeline through the guide /4/ into the process area of the unit. From there, purified gas was exhausted by the outlet pipeline, through the liquid trap /2/. The flow of the gas

was generated by the exhaust fan /10/, its expenditure was measured by a quadrant measuring orifice /1/. The expenditure of the gas flowing through the system was adjusted by changing the amount of "false" air introduced to the pipeline directly before the exhaust fan. A pressure gauge /8/ enabled the measurement of the drop in the pressure of gas flowing through the unit and the thermometer /9/ indicated the temperatures of gas in inlet and outlet pipelines as well as the temperature of liquid in the unit. Similar system for the measurement of dust concentration /S_w, S_o/, grade composition /I_w, I_o/ and gas moisture content /φ_w, φ_o/.

The overall efficiency of the dust collection process was calculated based on the measurements of dust concentrations in specific cross-sections of the inlet and outlet pipelines. The concentrations both in the inlet and outlet pipelines were determined based on the collected gas samples from which the dust was separated through filtration.

In order to determine the grade-based efficiency of the dust collection process for the tested unit, the grade composition of the aerosol was measured before and behind the dust collector. Cascade impactors [12] were used to determine the grade composition. This method enabled measurements by sampling the aerosol directly from the pipeline, without the need to separate the required amount of liquid beforehand.

The results of talc collection tests using non-freezing liquid, i.e. the overall efficiency and grade-based efficiency, are presented as a table and on diagrams – figures 4 and 5. Testing was conducted at three temperatures: t = -10°C, t = 0°C and t = 15°C, with the corresponding viscosities of: μ = 0.004 Pa·s, μ = 0.0056 Pa·s, μ = 0.0081 Pa·s.

Table 1

Changes in dust collection liquid viscosity and overall efficiency in relation to temperature measurement

measurement temperature	dynamic viscosity coefficient	overall efficiency
°C	Pa·s	%
- 10	0.0081	97.8
0	0.0056	98.8
15	0.0040	99.5

Very high overall talc collection efficiencies of 97.8%, 98.8% and 99.5% were obtained in testing conditions. The achieved efficiencies of talc separation in ambient temperatures were higher than in the case of dust collection with the use of pure water only [13]. It can be said that the high efficiency was a result of low, compared to water, surface tension of the liquid of $61.4 \cdot 10^{-3}$ N/m in t = 15°C. As the temperature rises, the viscosity of the liquid and its surface tension decrease. The assessment of the effects of individual physical and chemical properties on the dust collection process efficiency was impossible. An instrument capable of measuring the surface tension of liquids in sub-zero temperatures was not available. According to table data, the surface tension for water changes by $4 \cdot 10^{-3}$ N/m when the temperature changes by 20°C. Based on that, it can be expected that the effect of temperature on the surface tension of the liquid applied in the tests would be rather minor –

this, unfortunately, was not confirmed with an experiment. Following this assumption, obtaining such minute changes in overall efficiency with doubling the dynamic viscosity index questions the previously stated hypothesis regarding the effect of viscosity on the efficiency of particle absorption inside collectors and releases their surface. Also small are the changes in the efficiency of capturing particles smaller than 2 micrometres in the efficiency range of 97.1% to 85.6% as presented in figures 4 and 5. Decreasing the efficiency of dust collection correlated with the increase of liquid viscosity is likely an effect of changing the hydrodynamic conditions of the system, which affects the formation of liquid dust collectors. The hypothesis, however, applied to particles with poor dynamic wettability and the wettability properties of dust could have improved together with the decrease in the surface tension of the liquid.

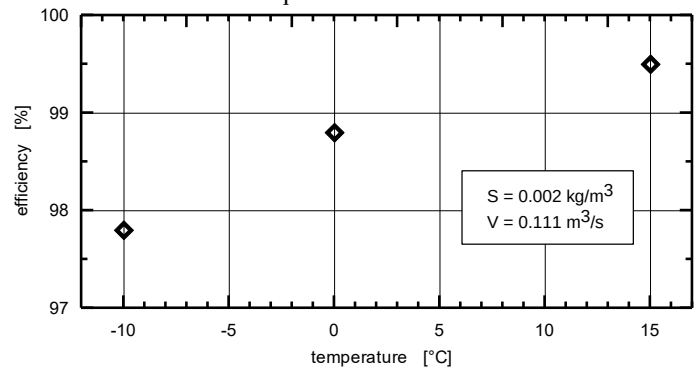

Fig. 4. Relationship between the overall efficiency of the dust collection process in non-freezing liquid and temperature

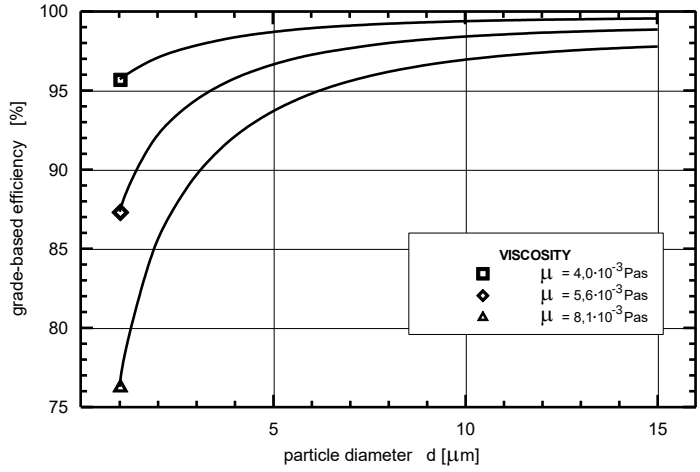

Fig. 5. Relationship between the grade-based efficiency of the dust collection process in non-freezing liquid and temperature

Therefore, based on the completed studies, the hypothesis regarding the impact of liquid viscosity on the effect of releasing the surface collecting the dust particles and, therefore, on the efficiency of the dust collection process cannot be clearly verified. The results confirm the suitability of non-freezing liquids for use as dust collecting liquids in equipment working at low temperatures.

References

[1] Warych J., *Odpylanie gazów metodami mokrymi*, Warsaw, WNT, 1979.
[2] Warych J., *Oczyszczanie przemysłowych gazów odlotowych*, WNT, Warszawa 1994.
[3] Löffler F., *Staubabscheiden*, Georg Thieme Verlag, Stuttgart, New York, 1988.
[4] Kabsch M., *Metody badania zwilżalności pyłów*, Prace naukowe Instytutu Inżynierii Ochrony Środowiska, nr 28 (7), Wrocław 1976.
[5] Weber E., Broche W., *Aparate und Ferfahren der industriellen Gasreinigung*, Oldenbourg – Verlag, 1973.
[6] Pemberton C. S., *Scavening Action of Rain on Non – Wettable Particle Matter Suspended in the Atmosphere*, Aerodynamic Capture of Particles, Pergamon Press 1960.
[7] Slinn W., Water, Air and Soil Poll., vol. 7, 1977, 513.
[8] Wicke M., *Aufbau, Leistung und Betriebsverhalten von Naßentstaubern Fortschritt*, Berichte der VDI, v. 3, nr 33.
[9] Jarzębski L., Głowiak B., Arch. Ochrony Środ., nr 1, 1977, 11.
[10] Hobler T., *Dyfuzyjny ruch masy i absorbery*, WNT, Warszawa 1976.
[11] Użow B. N., Waldberg A. Y., *Oczistka gazow mokrymi filtrami*, Himiâ, Moscow 1972.
[12] Dyląg M., Maszek L., Roszak Z., Rosiński J., *Impaktory kaskadowe – przegląd oraz podstawy konstrukcji*, Mat. konf. *Rozdzielanie zawiesin ciał stałych w płynach*, Warszawa 1990.
[13] Kasz J., Krawczyk J., Filtration and Separation, Nov/Dec. 1988.

TECHNICAL TRANSACTIONS | CZASOPISMO TECHNICZNE
MECHANICS | MECHANIKA
2-M/2016

JUSTYNA WIŚNIOWSKA*, STANISŁAW WITCZAK, MARCIN PIETRZAK**

MULTI-PHASE FLOW MIXTURE THROUGH A SUDDEN CHANGE IN CHANNEL CROSS-SECTION

PRZEPŁYW MIESZANINY WIELOFAZOWEJ PRZEZ NAGŁĄ ZMIANĘ PRZEKROJU KANAŁU

Abstract

The paper presents the results of a study involving the impact of sudden change of cross-sectional area on the flow patterns and local pressure drops for flow of multi-phase mixture. The experiment was conducted in the conditions of a horizontal and vertical flow through a measuring channel. Pressure drops calculated on the basis Kawahara and Lottes methods are compared with experimental data. A system of two interconnected pipes with internal diameters of 40 and 22 mm as well as 46 and 16 mm and a total length of 7 m formed the measurement channel. The experiments involved air, water and oil.

Keywords: multi-phase flow, contraction, expansion, flow patterns, pressure drops

Streszczenie

W pracy przedstawiono wyniki badań dotyczących wpływu gwałtownej zmiany pola przekroju poprzecznego kanału na struktury przepływu oraz miejscowe straty ciśnienia w przepływie mieszaniny wielofazowej. Porównano spadki ciśnienia obliczone na podstawie metod Kawahary i Lottesa z wartościami eksperymentalnymi. Badania prowadzono w warunkach poziomego i pionowego przepływu przez kanał pomiarowy z przeszkodą lokalną. Kanał pomiarowy stanowił układ dwóch rur o średnicach wewnętrznych 40 i 22 mm oraz 46 i 16 mm i całkowitej długości 7 m. Fazę gazową stanowiło powietrze, a fazę ciekłą olej maszynowy i woda.

Słowa kluczowe: przepływ wielofazowy, przewężenie, rozszerzenie, struktury przepływu, opory przepływu

DOI:

* Justyna Wiśniowska, Wakro Sp. z o.o.

** Prof. PhD. DSc. Eng. Stanisław Witczak, DSc. Eng. Marcin Pietrzak, Department of Chemical and Process Engineering, Faculty of Mechanical Engineering, Opole University of Technology.

1. Introduction

Multi-phase flow of gas-liquid mixtures takes place in a variety of installations in the chemical, oil, gas, or food industries, to mention just a few. The local obstacles, such as sudden expansions and contractions of the pipe, are inherent components in a number of flow-through systems. As pressure, volume fraction and flow pattern regimes are considerably affected by the design of such systems, it is important to understand the impact of existing elements on the parameters of multi-phase flow. The knowledge of the type of multi-phase flow patterns plays a fundamental role in the calculations of flow parameters [1]. However, the ability to forecast the type of flow pattern is very difficult due to the very nature of multi-phase flow. An additional difficulty is associated with the existence of certain areas of flow pattern disturbance caused by a change in the cross-section of the pipe.

Despite the bulk of research into multi-phase flow in straight channels reported to this date, there is a scarcity of works concerned with the subject of multi-phase flow in the channels including a sudden contraction or expansion of the cross sectional area of a pipe. Only a few methods for calculating the local pressure drop of two-phase flow through a sudden contraction and expansion are available in the literature. However, even the existing methods do not account for all parameters that affect the value of the pressure drop during such flow including, in particular, a study of the impact of flow pattern disturbances. For this reason, experimental research was carried out and is reported by the authors.

To complement and expand the description of the phenomena of the gas-liquid flow resulting from a sudden change in the diameter of a channel, new experiments and studies work were carried out.

2. Experiment

The experimental setup was designed and built according to recommendations available in the literature. For clarification purposes, the diagram presents the design of the flow-through system for the case of horizontal flow in Figure 1. The main element of the installation was a measurement channel, which consisted of two interconnected pipes with two internal diameters of D = 40 mm and d = 22 mm in a horizontal layout and a total length of 7 m. An experiment involving flow through a sudden expansion or contraction of the channel was conducted for this purpose. The pipes were made of transparent PMMA, as it enabled the authors to visually assess two-phase flow patterns and their disturbance areas. The length of these areas was determined using a millimetre scale placed along the pipes.

Multi-phase mixture consisted of a mixture of water or low viscosity oil and air. The volumetric flow rates of phases were measured by flowmeters of oil, water and air (V_{oil} = 5.0÷20.0 dm^3/min, V_{water} = 2.0÷20.0 dm^3/min and V_{air} = 1.6÷509.0 dm^3/min). The observations of the flow patterns were performed on a 1 m test section, which was located at a distance of 50 diameters from the inlet to the test section. This made it certain that the flow structure is fully developed and it is not affected by the installation of a local obstacle. In addition, the flow patterns were also observed directly before and after the local obstacle. A series of pressure transducers were installed behind the control section, used for the

measurement of the pressure drops due to the existence of a sudden pipe contraction or expansion. The system of pressure transducers locations used for the measurement along the pipe is the same before and after a local obstacle. The data regarding the local pressure drops was collected by a measurement card, coupled with a computer, which recorded data at a high frequency (i.e. 100 measurements per 1 second) followed by averaging the measured values over time.

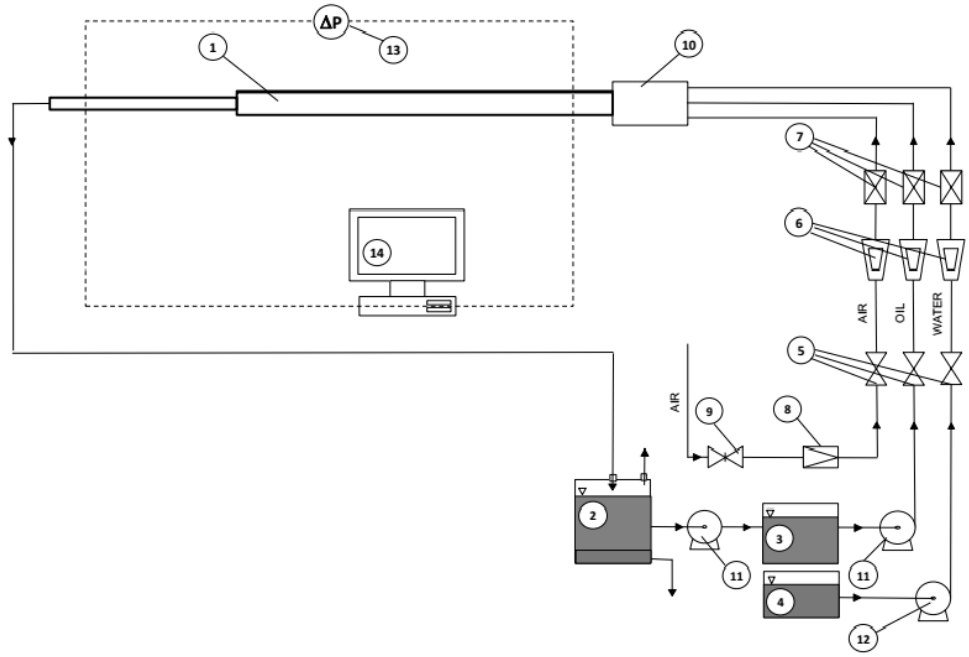

Fig. 1. Experimental set-up
1 – measurement channel with sudden expansion, 2 – separator, 3 – oil tank, 4 – water tank, 5 – shut-off valves, 6 – flowmeter of oil, water, air, 7 – one-way valves, 8 – pressure regulation valve, 9 – air control valve, 10 – agitator, 11 – oil pump, 12 – water pump, 13 – pressure transducers, 14 – measurement card coupled with a computer

3. Results

During the next stage of research, flow conditions corresponding to the two-phase flow patterns identified during the experiment were subsequently compared with the areas of these patterns found in the flow pattern map created by Ulbrich and Troniewski [1] (Fig. 2). Figure A shows the flow pattern map for a pipe before the local obstacle (D = 40 mm) where the types of flow patterns were marked. In Figure B, the type of flow pattern was marked for the smaller pipe diameter (d = 22 mm).

The figures show that in both cases the observed flow patterns were approximately in conformity with the corresponding areas shown in the Troniewski and Ulbrich map.

However, it was observed that the decrease of the pipe diameter during the flow of gas – liquid results in a change in the flow pattern.

For demonstration purposes, figure 3 shows several photographs taken during the experiment involving oil-air and air-water flow through a sudden expansion. Figure 4 shows several photographs taken during the experiment involving oil-air and air-water flow through a sudden contraction. As can be seen, the presence of a local obstacle always leads to a change in the flow patterns both before and after the pipe contraction. The photographs found above indicate the changes in the flow patterns caused by a sudden increase in pipe diameter. The distances where the flow pattern was not fully developed can be clearly discerned there. Such a length, also known as the length of the disturbance area, is defined here as the distance from an obstacle to the location where a uniform flow pattern is formed again. Beyond this area, the mean square root of the deviation of the local void fraction profile is constant and less than 5%, as reported by the authors of the study in [2].

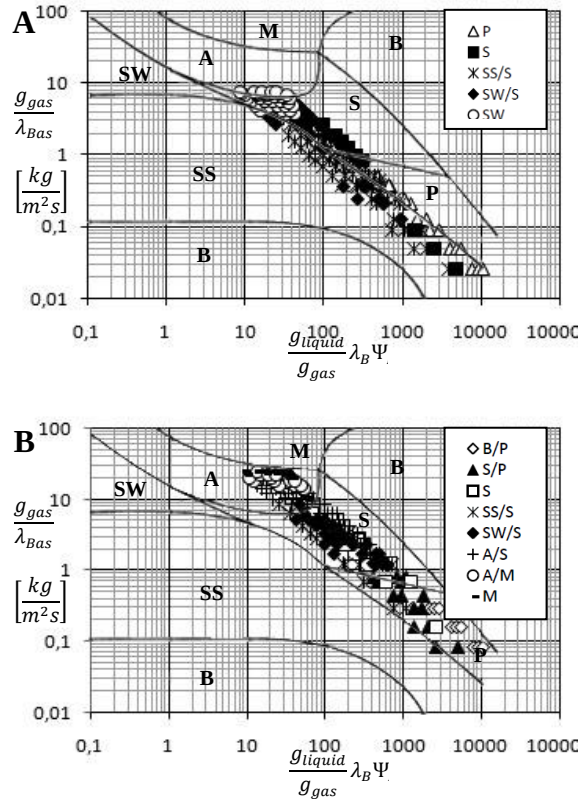

Fig. 2. The flow patterns observed in a pipe before the contraction (A) and after the contraction (B): B – bubble flow, P – plug flow, S – slug flow, SS – stratified flow, SW – stratified-wavy flow, A – annular flow, M – mist flow.

Figure 5 shows one example of the measured change of pressure in two-phase oil-air and water-air flow along the measuring channel. Pressure profiles in the case of flow through a sudden expansion of the channel may vary significantly due to the length of the disturbance zone of flow patterns followed by the area in which the system can recover pressure to its initial value. The pressure recovery due to the sudden expansion is defined as the difference in the pressure when the fully developed pressure gradient lines upstream and downstream of the expansion are extrapolated to a point where a change in the area occurs[3].

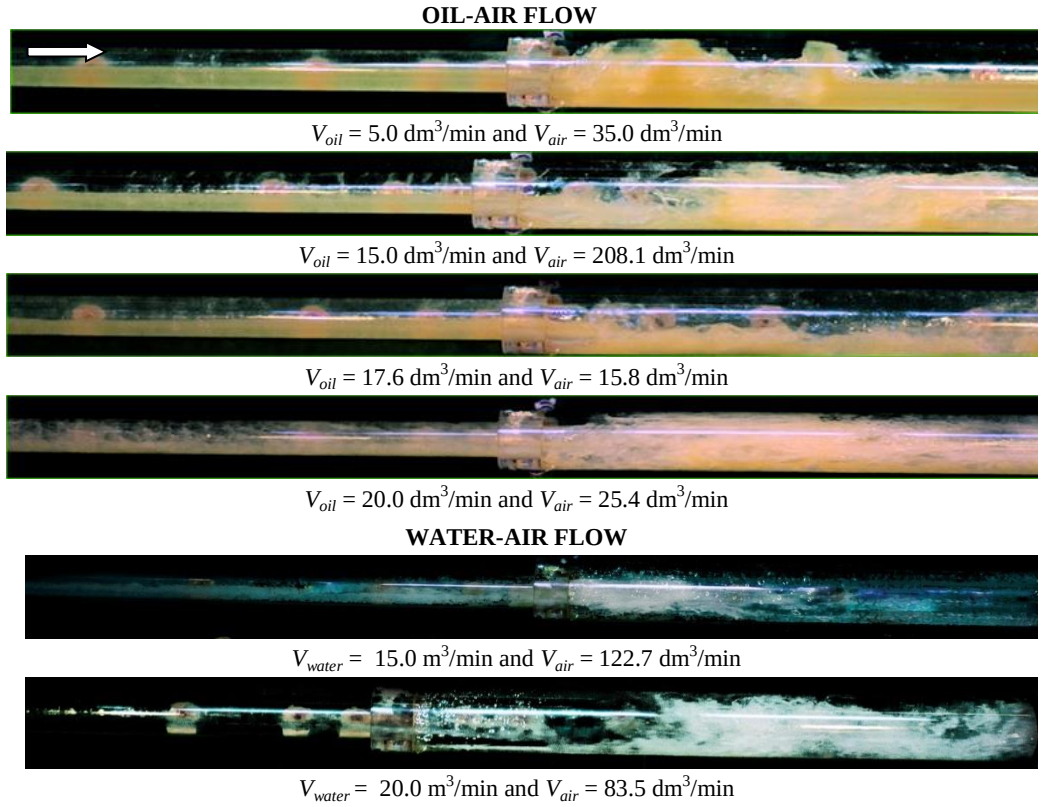

Fig. 3. Flow pattern development during flow of oil-air and water-air mixtures through a sudden expansion

The graphs above (Fig. 6) show the flow patterns developing along the pipe after its sudden expansion. The analysis of the resulting images clearly indicates that the correlations used for calculating the disturbance zones should take into account both the parameters of the liquid phase and the gas phase. If the impact of any of them is disregarded, an adequate assessment of the length of these zones for the sudden expansion will not be possible [4].

On the other hand, during the two-phase flow through sudden contraction of the pipe immediately before this obstacle, the local static pressure decreases due to a sudden acceleration of the flow. After the sudden contraction, the pressure in the pipe gains its minimum value and then increases slightly to the point where a fully developed gradient line of the pressure is achieved. The pressure drop during flow through a sudden contraction is defined as the difference in the pressure in the local obstacle, based on the fully developed pressure gradients upstream and downstream of the contraction.

Figure 7 contains several photographs derived from the research of the characteristics of two-phase oil-air flow through a sudden contraction. Figure 8 is meant to show the areas of flow pattern disturbance in the channel before the contraction.

By analogy to two-phase flows, the pressure drop noted during the three-phase flow is relative to the relations between the volume rates of the components in the flow. On the basis of the data shown in Fig. 9, we can see that an increase in pressure drop occurs for a constant volumetric flow rate of the air accompanied by an increase in volume flow rate of liquid.

OIL-AIR FLOW

V_{oil} = 7.5 dm^3/min and V_{air} = 55.0 dm^3/min

V_{oil} = 9.5 dm^3/min and V_{air} = 280.0 dm^3/min

V_{oil} = 17.6 dm^3/min and V_{air} = 172.5 dm^3/min

WATER-AIR FLOW

V_{water} = 9.5 dm^3/min and V_{air} = 475.1 dm^3/min

V_{water} = 17.5 dm^3/min and V_{air} = 314.9 dm^3/min

V_{water} = 20.0 dm^3/min and V_{air} = 122.7 dm^3/min

Fig. 4. Changes of flow patterns of oil-air and water-air flow through a sudden contraction

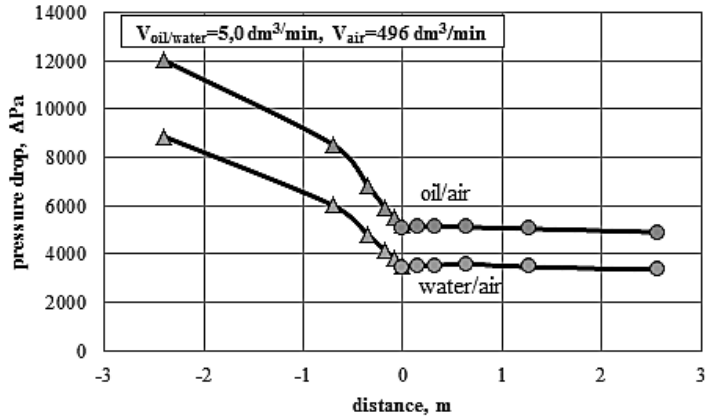

Fig. 5. Pressure drop profiles during the two-phase gas-liquid flow through a sudden expansion

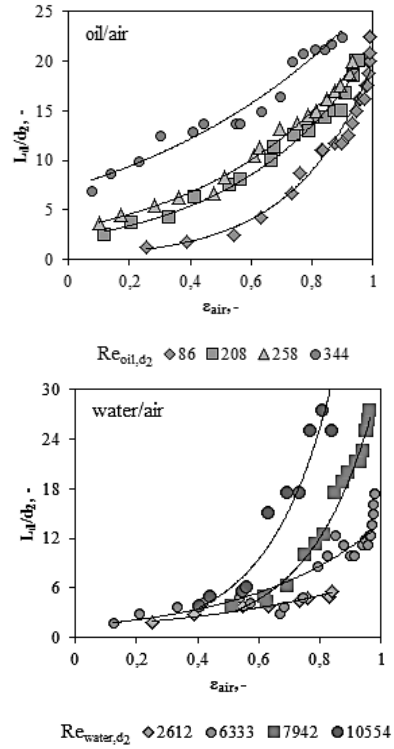

Fig. 6. Developing lengths of flow patterns in the pipe after a sudden expansion

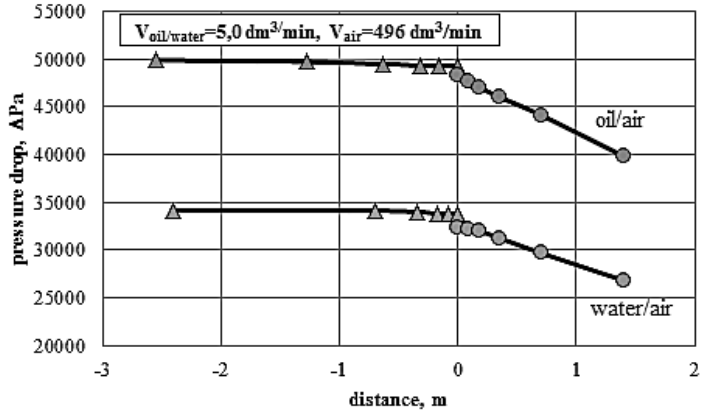

Fig.7. Pressure profiles during the two-phase gas-liquid flow across the channel with a sudden contraction

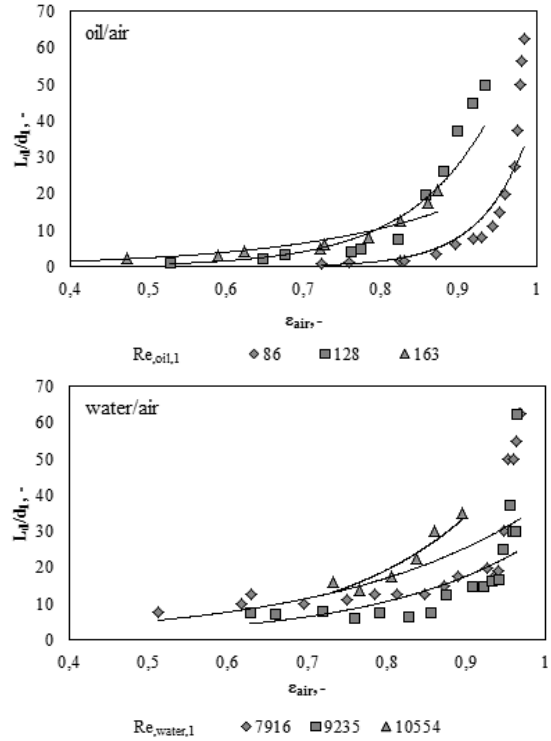

Fig. 8. Developing lengths of flow patterns in the pipe before a sudden contraction

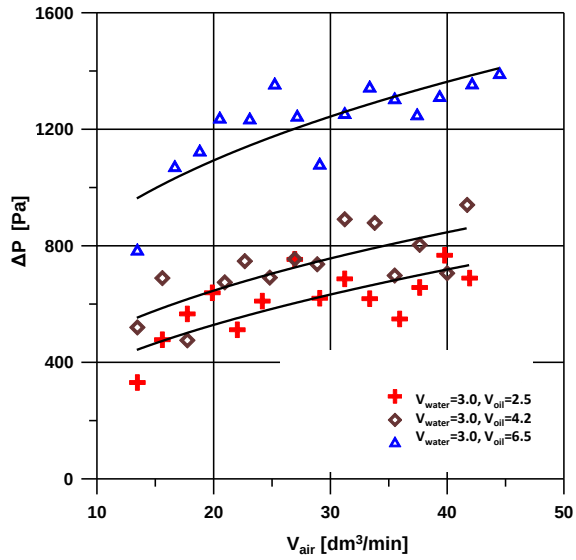

Fig. 9. Pressure drop profiles during gas-liquid-liquid three-phase flow through a sudden contraction

4. Calculation of pressure drops in air-water-oil three-phase flow

The results of statistical tests indicate that the pressure drops for the sudden contraction should be calculated by the use of the Kawahara [5] method, to be equal to:

$$\Delta P_T = \frac{g_T^2}{2 \cdot \rho_{liquid}} \cdot \left[\left(\frac{1}{C_c} - 1 \right)^2 + 1 - \sigma_A^2 \right] \cdot \left[1 + x \cdot \left(\frac{\rho_{liquid}}{\rho_{air}} - 1 \right) \right] \tag{1}$$

$$\rho_{liquid} = \rho_{water} \cdot \alpha_{water} + \rho_{oil} \cdot \alpha_{oil} \tag{2}$$

$$\alpha_{water} = (\varepsilon_{water})^{0.8} \tag{3}$$

$$\alpha_{oil} = 1 - \alpha_{water} \tag{4}$$

$$C_c = \frac{1}{0.639 \cdot (1 - \sigma_A)^{0,5} + 1} \tag{5}$$

$$\sigma_A = \left(\frac{d}{D} \right)^2 \tag{6}$$

where:
ΔP_T – total pressure drop, Pa
g_T – total mass flux density, kg/(m^{2}s)
ρ_{liquid} – liquid density, kg/m^3
ρ_{air} – gas density, kg/m^3
x – mass quality, -
α_{water} – water volume fraction, -
α_{oil} – oil volume fraction, -
σ_A – area ratio, -
ρ_{water} – water density, kg/m^3
ρ_{oil} – oil density, kg/m^3
d, D – internal diameter (contraction, expansion), m.

For gas-liquid flow conditions through expansion, the highest accuracy ensured by application of the Lottes [6] method:

$$\Delta P_T = \frac{g_T^2}{2 \cdot \rho_{liquid}} \cdot \frac{\sigma_A \cdot (1-\sigma_A)}{(1-\alpha_{air})^2} \tag{7}$$

$$\alpha_{air} = \frac{\varepsilon_{air}^{0.37}}{1+\left(\frac{1}{\varepsilon_{air}}-1\right)^{0.5}} \cdot \left(\frac{1-\varepsilon_{water}}{1+\varepsilon_{oil}}\right)^{0.43} \tag{8}$$

$$\varepsilon_{air} = \frac{V_{air}}{V_{air}+V_{water}+V_{oil}}, \tag{9}$$

$$\varepsilon_{water} = \frac{V_{water}}{V_{air}+V_{water}+V_{oil}} \tag{10}$$

$$\varepsilon_{oil} = \frac{V_{oil}}{V_{air}+V_{water}+V_{oil}} \tag{11}$$

where:
α_{air} – mean real void fraction, -
ε_{air} – inlet void fraction, -
ε_{water} – inlet water volume fraction, -
ε_{oil} – inlet oil volume fraction, -.

The values obtained on the basis of calculations were compared with data obtained in experimental studies, as shown in Figures 10 and 11. The result of less than ±40% of relative error was obtained for both correlations.

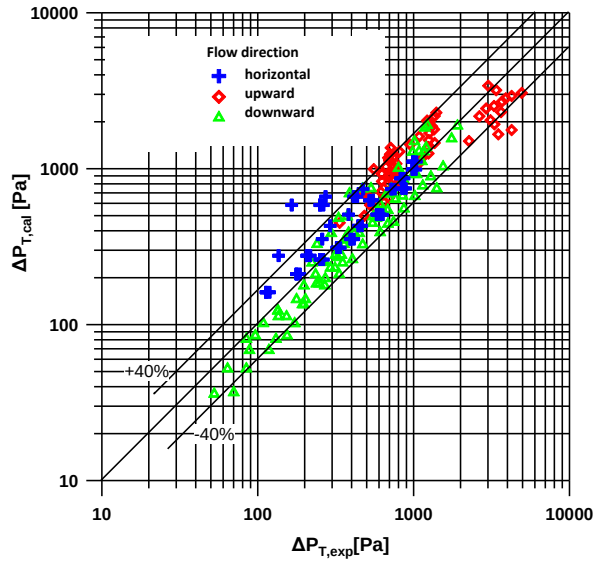

Fig. 10. Comparison of measured pressure drop $\Delta P_{T,exp}$ of three-phase flow with the calculated value $\Delta P_{T,cal}$ on the basis of the Kawahara method (1)

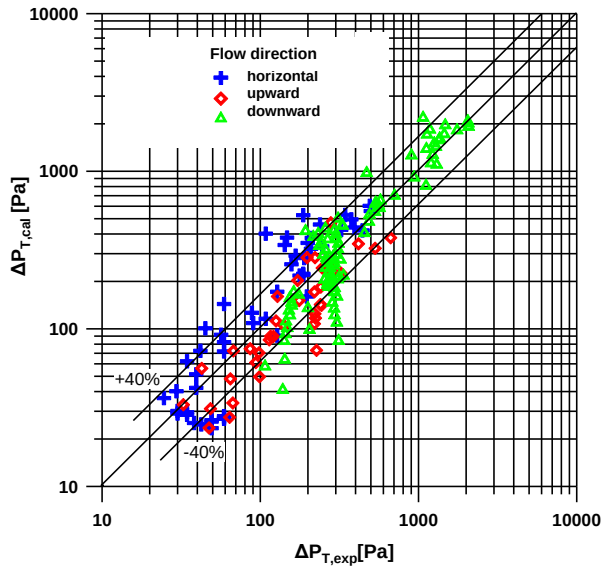

Fig. 11. Comparison of measured pressure drop $\Delta P_{T,exp}$ of three-phase flow with the ones calculated $\Delta P_{T,cal}$ on the basis of the Lottes method (4)

5. Conclusions

The following general conclusions could be derived from the analysis of the results and review of the literature:

1. Flow pattern disturbances of a multi-phase mixture occur during flow through a sudden change in the cross-section of the pipe.
2. The disturbances of flow pattern form the reason for the local change in the void fraction of the phases, and consequently, properties of the mixture are affected by them.
3. Due to the presence of local disturbances caused by the change in the cross-section of pipe, local pressure drop, it is difficult to calculate the local pressure drop.
4. The current methods of calculating the developing lengths in the two-phase flow of gas-liquid mixture through sudden expansion of the channel are not always effective as they do not enable all flow parameters to be taken into account.
5. Further analysis of the results should be aimed at the development of a mathematical equation used to describe the impact of the length of disturbance of flow pattern on the pressure drop in the multi-phase flow in a channel with a sudden change in the cross sectional area.

References

[1] Dziubiński M., *Hydrodynamika mieszanin dwufazowych ciecz-gaz*, Wyd. Politechniki Łódzkiej, Łódź 2005.
[2] Ahmed W. H., Ching C. Y., Shoukri M., International Journal of Heat and Fluid Flow, vol. 29, 2008, 194-206.
[3] Ahmed W. H., Ching C. Y., Shoukri M., International Journal of Multi-phase Flow, vol. 33, 2007, 575-594.
[4] Wiśniowska J, Zeszyty Naukowe Politechniki Opolskiej, seria: Mechanika z. 98, nr 341, 2011, 97-98.
[5] Kawahara, A., Chung, P., Kawaji, M.: *Investigation of two-phase flow pattern, void fraction and pressure drop in a microchannel*, International Journal of Multi-phase Flow, vol. 28, 2002, 1411-1435.
[6] Lottes P. A., *Expansion losses in two-phase flow*, Nuclear Science Engineering, vol. 9, 1961, 26-31.

TECHNICAL TRANSACTIONS | CZASOPISMO TECHNICZNE
MECHANICS | MECHANIKA
2-M/2016

RYSZARD WÓJTOWICZ*, PAWEŁ WOLAK**

PERFORMANCE OF A CYCLONE WITH AN ASLANT SHAPED INLET

ANALIZA PRACY ODPYLACZA CYKLONOWEGO Z UKOŚNIE UKSZTAŁTOWANYM KANAŁEM WLOTOWYM

A b s t r a c t

This paper presents an analysis of selected operating parameters of a cyclone with a modified inlet. The modification consisted in an angular arrangement of an inlet channel wall. This can result – in view of previously conducted experiments – in a faster insertion of a dusty gas into a swirl motion, an improvement of particles separation process. The analysis was carried out using numeric CFD simulations. The results were compared to those obtained from simulations and lab-measurements for a cyclone with standard inlet.

Keywords: dedusting, cyclone, pressure drop, dedusting efficiency, CFD simulations

S t r e s z c z e n i e

W pracy przedstawiono analizę wybranych parametrów pracy odpylacza cyklonowego ze zmodyfikowanym wlotem. Modyfikacja polegała na kątowym usytuowaniu ścianki kanału wlotowego, co – w świetle prowadzonych wcześniej badań własnych – może skutkować szybszym wprowadzeniem strumienia zapylonego gazu w ruch wirowy i w jego efekcie poprawą efektywności procesu separacji cząstek. Analizę przeprowadzono wykonując symulacje numeryczne CFD. Uzyskane wyniki porównano z wynikami symulacji i pomiarów laboratoryjnych wykonanymi dla cyklonu ze standardowym wlotem.

Słowa kluczowe: odpylanie, odpylacz cyklonowy, spadek ciśnienia, skuteczność odpylania, symulacje CFD

DOI:

* DSc. Eng. Ryszard Wójtowicz, Institute of Thermal and Process Engineering, Faculty of Mechanical Engineering, Cracow University of Technology.
** M.Sc. Eng. Paweł Wolak, Mechanical Equipment Department, Air Liquide Global E&C Solutions Poland S.A.

1. Introduction

The cyclones are commonly used in industry, process engineering and environmental protection for separation of solid particles from dusty gases, and also as a separation device in pneumatic transport systems [1, 2]. It is worth noting that apparatuses of this kind – despite a seemingly simple design – are characterised by complex and difficult-to-describe gas flow, resulting from simultaneously coexistence two opposite directed gas streams. The performance of a cyclone (its dedusting efficiency, pressure drop, reliability, etc.) is strongly influenced by its geometry and dimensions. Even a slight change of these parameters may result in a change of the dedusting efficiency and the creation of undesirable phenomena, e.g. a gas flow directly from an inlet channel to the outlet (short circuit) or unfavourable for dust removal process transferring of gas motion to a dust chamber.

A useful tool for cyclone design and optimisation seem to be simulation packages, based on codes of Computational Fluid Dynamics (CFD) [3]. They allow preliminary quick analysis of gas flow inside a cyclone and easy modification of its dimensions and geometry, without having to build costly prototypes and to conduct time-consuming experimental investigations.

This work verifies an idea [4] concerning the improvement of cyclone performance by an angular arrangement of a wall of the inlet channel. It should result in directing the dusty gas stream closer to a cyclone wall, putting it faster in a swirl motion, reduction of particles bouncing from a wall and unfavourable particles entrainment by a clean gas in an outflow. Analysis was carried out using CFD modelling. The results were compared to those obtained from simulations and lab-measurements for a cyclone with a standard inlet.

2. Experimental

Cyclones used in numerical investigations are shown in Figure 1. The diameter of the cylindrical part was always D = 0.192 m and the total height of the cyclone H = 0.745 m. The height of the cylindrical part was h = 0.242 m. The diameter and length of the vortex finder were D_e = 0.09 m and s = 0.140 m, respectively. The diameter of the cyclone at the end of the conical part was chosen to be B = 0.045 m. Three different gas inlets were tested. One of them was a standard, square cross-sectional with dimensions $a = b$ = 0.042 m (Fig. 1b), two modified by an angular arrange of the inlet channel wall at an angle $\alpha = 2°$ (Fig. 1c) and $\alpha = 4°$ (Fig. 1d). Other cyclones dimensions are presented in Fig.1. Gas flowing through the cyclone was air (ρ_c = 1.225 kg/m^3, $\mu_c = 1.7894 \cdot 10^{-5}$ Pa·s). Its velocity at the inlet of the cyclone was u = 15 m/s. The density of solid particles was ρ_s = 2700 kg/m^3. The dispersed phase volume fraction was relatively low, less than 5%. During simulations, it was assumed that particle size distribution is characterised by the Rosin-Rammler theoretical distribution. The analysis of flow was performed based on results of numerical modelling, using as a pre-processor the mesh generator *Gambit 2.4* and as a solver *Ansys Fluent 14.0*. Turbulent gas flow in the cyclone was described using the Navier-Stokes equations of mass and momentum transport, averaged by Reynolds method (RANS) [5]. As a closing method, the RNG (Renormalisation Group) [3, 6] k-ε turbulence

model was selected with an additional option of the Swirl Modification [7], taking into account a vorticity nature of flow inside the cyclone. To simulate the motion of the discrete phase (particles), the Euler-Lagrange (EL) [8] approach was used.

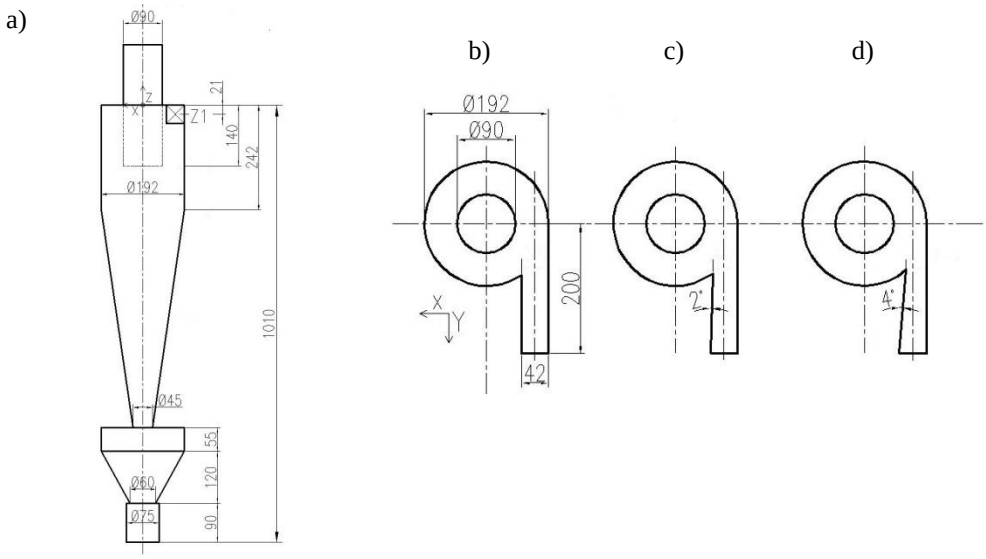

Fig. 1. The cyclone examined a) a view, b) standard inlet $\alpha = 0°$, c) modified inlet $\alpha = 2°$, d) modified inlet $\alpha = 4°$

Detailed information on the cyclone design and methodology of simulations is presented elsewhere [9, 10]. These papers also present comparisons of the standard cyclone simulations with theoretical models and measurements, which confirm that the used numerical model is correct.

3. Results and discussion

Figure 2 presents contour and vector maps of the flow pattern in the cyclone. An angular arrangement of a cyclone inlet makes that a gas delivered is inclined toward a cyclone wall with a sudden narrowing of a stream. Dusty gas starts to rotate with high tangential velocities, of which maximum values for an inlet channel angle $\alpha = 0°$ (Fig. 2a), $\alpha = 2°$ (Fig.2b) and $\alpha = 4°$ (Fig.2c) are higher in comparison with an inlet velocity (u = 15 m/s) by 30%, 42% and 65%, respectively. This tendency observed already in a cyclone with a standard inlet [9, 10] is significantly intensified by an angular arrangement of an inlet. It can cause an increase of cyclone dedusting efficiency. Besides, in a cyclone with an aslant shaped inlet, solid particles are supplied closer to the cyclone wall and they are faster introduced into rotational motion. It largely reduces their bouncing from a wall and eliminates their flow directly to the gas outlet stream.

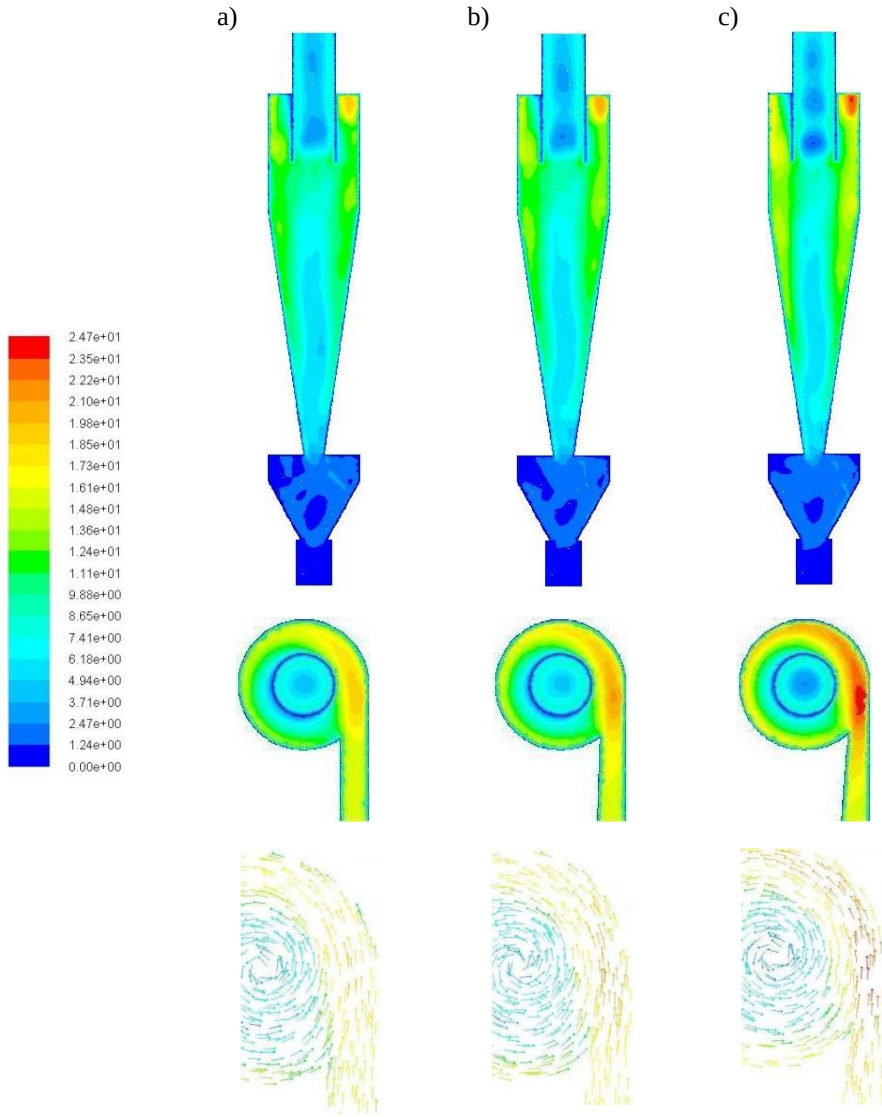

Fig. 2. Contour and vector maps of flow pattern: a) standard inlet $\alpha = 0°$, b) modified inlet $\alpha = 2°$, c) modified inlet $\alpha = 4°$

Figure 3 presents the trajectory of the selected particle (d_p = 2 μm), which is supplied to the cyclone with a dusty gas stream. In the cyclone with a standard inlet (Fig. 3a), a particle of this size will not be dedusted. After several rotations in a swirl gas stream, a particle enters an outflow and leaves the cyclone. In cyclones with modified inlets (Fig. 3b and Fig. 3c), trajectories of particle in the cyclone upper part are larger in diameter. Polluted gas in this part has a proper velocity and particles are separated.

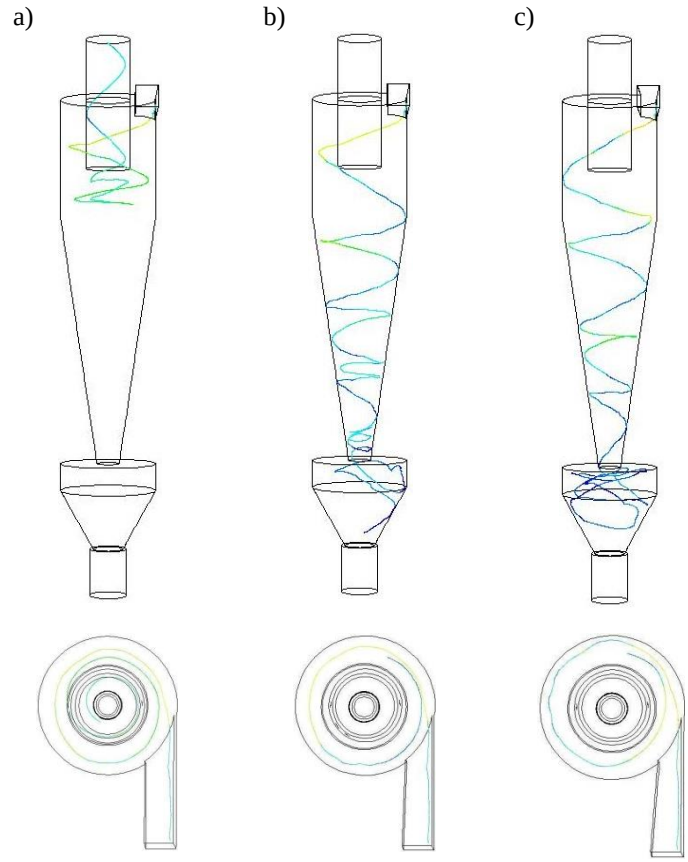

Fig. 3. Trajectories of a dust particle (d_p = 2 μm): a) standard inlet α = 0°, b) modified inlet α = 2°, c) modified inlet α = 4°

The above-described phenomena and mechanisms are confirmed by data presented in Table 1. Predicted cyclone efficiency, estimated on the basis of a classic relation:

$$\eta = \frac{m_s}{m_i} \cdot 100\% \tag{1}$$

(m_s is a mass dedusted (collected) particles, and m_i is the mass of all particles supplied to a cyclone with a polluted gas) increases for both modified inlets (α = 2° and α = 4°) by 1.3 % and 3% respectively.

On the other hand, it should be noted that for cyclone performance estimation, a second parameter – the pressure drop – should be taken into account. This parameter, in addition to efficiency, also decides on the cost-effectiveness of the process and its expenditures. In Table 1, predicted pressure drops are also presented. With respect to the cyclone with a standard inlet, they increase by 20 % (α = 2°) and 32.6% (α = 4°).

Table 1

Pressure drop and dedusting efficiency for examined cyclones

Cyclone	Pressure drop [Pa]	Dedusting efficiency [%]
Standard inlet ($\alpha = 0°$)	313	86.3
Modified inlet ($\alpha = 2°$)	376	87.4
Modified inlet ($\alpha = 4°$)	415	88.9

In the literature, there are not any uniform criterion linking these two parameters and evaluating of cyclone efficiency together. In general, the leading parameter determining the cyclone choice is the dedusting efficiency. These CFD simulations show that modification of a cyclone inlet by an angular arrangement of its wall is fully justified.

References

[1] Hoffmann A. C., Stein L. E., *Gas cyclones and swirl tubes – principles, design and operation*, Springer - Verlag, Berlin 2008.

[2] Warych J., *Gas cleaning*, WNT, Warsaw 1998 (in Polish).

[3] Jaworski Z., *Computational fluid dynamics in chemical engineering*, Exit, Warsaw 2005 (in Polish).

[4] Mieszkowski A., Roszak Z., *Environment protection systems*, Cracow University of Technology, Cracow 2010 (in Polish).

[5] Pope S.B., *Turbulent flows*, Cambridge University Press, Cambridge 2013.

[6] Wójtowicz R., Lipin A.A., Talaga J., *On the possibility of using of different turbulence models for modeling flow hydrodynamics and power consumption in mixing vessels with turbine impellers*, Theoretical Foundations of Chemical Engineering, 48, (4), 2014, 360-375. DOI: 10.1134/S0040579514020146

[7] Ansys Inc., Ansys Fluent theory guide, Canonsburg 2011.

[8] Andersson B., Andersson R., Hakansson L., Mortensen M., Sudiyo R., van Wachem B., *Computational fluid dynamics for engineers*, Cambridge University Press, Cambridge 2012.

[9] Wójtowicz R., Wolak P., *Identification of multiphase flow in a cyclone separator*, International Scientific and Technical Conference "Problems of Resources and Energy Saving Technologies in the Industry and Agricultural Complex (PRET-2014)" (Monograph, W.N. Bliniczew, edt.), ISUCT, Iwanowo, Russia 2014, p. 252-264 (ISBN 978-5-9616-0494-8).

[10] Wójtowicz R., Wolak P., *An example of the use of computational-fluid-dynamics analysis for simulation of two-phase flow in a cyclone with a tangential inlet*, Environment Protection Engineering, 4, 2016 (in press).

CONTENTS

TREŚĆ